



UNIVERSITY OF
LIVERPOOL

Development of Small-Molecule Anti-*Wolbachia* Agents for the Treatment of Filariasis.

Paul McGillan

Supervisors: Prof. Paul M O'Neill Dr Neil G. Berry

2017

Thesis submitted in accordance with the requirements of the University of Liverpool
for the degree of Doctor in Philosophy by Paul McGillan
September 2017



PGR Policy on Plagiarism and Dishonest Use of Data
PGR CoP Appendix 4 Annexe 1

PGR DECLARATION OF ACADEMIC INTEGRITY

NAME (Print)	Paul McGillan
STUDENT NUMBER	200661002
SCHOOL/INSTITUTE	Department of Chemistry
TITLE OF WORK	Development of Small-Molecule Anti-<i>Wolbachia</i> Agents for the Treatment of Filariasis

This form should be completed by the student and appended to any piece of work that is submitted for examination. Submission by the student of the form by electronic means constitutes their confirmation of the terms of the declaration.

Students should familiarise themselves with Appendix 4 of the PGR Code of Practice: PGR Policy on Plagiarism and Dishonest Use of Data, which provides the definitions of academic malpractice and the policies and procedures that apply to the investigation of alleged incidents.

Students found to have committed academic malpractice will receive penalties in accordance with the Policy, which in the most severe cases might include termination of studies.

STUDENT DECLARATION

I confirm that:

- I have read and understood the University's PGR Policy on Plagiarism and Dishonest Use of Data.
- I have acted honestly, ethically and professionally in conduct leading to assessment for the programme of study.
- I have not copied material from another source nor committed plagiarism nor fabricated falsified or embellished data when completing the attached material.
- I have not copied material from another source, nor colluded with any other student in the preparation and production of this material.
- If an allegation of suspected academic malpractice is made, I give permission to the University to use source-matching software to ensure that the submitted material is all my own work.

SIGNATURE.....

DATE.....

Contents

Abbreviations.....	6
Abstract	12
1 – Introduction	15
1.1 Lymphatic filariasis (LF).....	15
1.1.1 Global prevalence of LF.....	15
1.1.2 Life cycle of <i>Wuchereria bancrofti</i>	16
1.1.3 Diagnosis of LF	17
1.2 Onchocerciasis	18
1.2.1 Global prevalence of onchocerciasis.....	18
1.2.2 <i>Onchocerca Volvulus</i> Life Cycle.....	19
1.2.3 Diagnosis of Onchocerciasis	20
1.3 Existing Anti-Filarial Treatments	20
1.3.2 Control programs	24
1.3.3 Drug Resistance.....	24
1.4 Wolbachia – A Common Target for LF and Onchocerciasis.....	26
1.4.1 Wolbachia as obligate mutualists with filarial nematodes.....	26
1.4.2 Potential drug targets for the development of anti-Wolbachia agents.....	27
1.4.3 Treatments to remove Wolbachia bacteria from hosts	28
1.5 Aims	31
1.6 Identification of small molecule anti-Wolbachia agents	32
1.6.1 Target Vs Phenotypic screening	32
1.6.2 In vitro assay development	33
1.6.3 HTS: Chemotype identification	33
1.7 Strategy for the discovery of small molecule anti-Wolbachia agents	36
1.7.1 Screening cascade	36
1.7.2 Drug-metabolism and Pharmacokinetics (DMPK)	38
1.7.3 Development of synthetic methodology and biological relevance of Pyrazolopyrimidines.....	40
1.7.3 Initial pyrazolopyrimidine target selection.....	43
1.8 References	46
Chapter 2 Initial SAR studies: 2-pyridyl ring and linker modifications.....	58
2.1 R ⁴ - & R ⁵ - Substituted Pyrazolopyrimidines	58
2.11 Series 1 Target selection and development of a synthetic route	58
2.12 Biological Evaluation of initial targets R ⁴ & R ⁵ substituted pyrazolopyrimidines	60
2.2 Further R ⁴ - & R ⁵ - Substituted Pyrazolopyrimidines.....	62

2.21 Series two target selection and synthesis	64
2.22 Further R ⁴ & R ⁵ SAR exploration – in vitro DMPK and potency results	67
2.3 Series 3: 3-(R ¹) 4-F Ph, R ⁴ - & R ⁵ - Substituted Pyrazolopyrimidines:	70
2.31 Design and Synthesis.....	70
2.32 Series 3 in vitro DMPK and Potency	71
2.4 6 (R ³)- Substituted Pyrazolopyrimidines.....	75
2.41 Target Design and Synthesis	75
2.42 (R ³) Pyrazolopyrimidines Biological Evaluation	78
2.5 Conclusion.....	79
2.6 Experimental.....	83
2.7 References	101
Chapter 3 Pyrazolopyrimidines - R ¹ exploration	106
3.1 Early lead optimisation	106
3.2 Development of synthetic strategies for analogues with diverse R ¹ substituents	108
3.3 R ¹ Mono-substituted phenyl ring systems	110
3.4 R ¹ position biaryl ring systems	115
3.5 Small R ¹ substitutions - Aryl-Removed analogues.....	118
3.6 Bioisosteric replacement of the R ¹ phenyl ring	122
3.7 Conclusion.....	126
3.8 Experimental.....	129
3.8 References	166
Chapter 4 Lead Optimisation & Advanced Biological Evaluation	172
4.1 Early-Lead Optimisation Summary (Chapter 3).....	172
4.2 Lead optimisation	173
4.2.1 R ¹ position optimisation; saturated heterocyclic rings.....	173
4.2.2 3-(R), 5-(H), 6-(R), Pyrazolopyrimidine	179
4.3 Advanced Biological Evaluation	183
4.3.1 In vitro Brugia malayi microfilariae studies	183
4.3.2 Assessment of permeability, efflux ratio, in vitro toxicity and CYP inhibition of selected frontrunners.....	186
4.3.3 In vivo assays.....	191
4.4 Conclusions	196
4.5 Future Work.....	197
4.6 Experimental.....	199
4.7 References	210
Appendix 1 WuXi App Tech Experimental.....	214

Acknowledgements

Firstly, I would like to thank my supervisors for their support and guidance in the past 4 years – Prof Paul O’Neill, Dr Neil Berry and Dr David Hong.

I would like to thank all past and present members of the 4th floor labs within the Department of Chemistry for all their help throughout my studies.

I am extremely grateful to the biology team at the Liverpool School of Tropical Medicine and to our collaborators within AstraZeneca, WuXi App Tech and Eisai who have provided essential information presented throughout this work.

Finally, I would like to extend my gratitude to the many friends I have gained during my time at the University for all of their help during my time at the University.

Abbreviations

ABZ	Albendazole
ADL	Acute adenolymphangitis
ADMET	Absorption, distribution, metabolism, excretion and toxicity
APOC	African programme for onchocerciasis control
APOD	Acute papular onchodermatitis
AUC	Area-under curve
AWOL	<i>Anti-Wolbachia</i>
AZ	AstraZeneca
BZD	Benzimidazole
CDK-2	Cyclin-dependent kinase-2
CNS	Central nervous system
CPOD	Chronic papular onchodermatitis
CRF-1	Corticotrophin releasing factor -1
CRO	Contract research organisation
DALY's	Disability-adjusted life years
DEC	Diethylcarbamazine
DHODH	Dihydroorotate dehydrogenase
DMPK	Drug-Metabolism and Pharmacokinetics
DMSO	Dimethyl sulfoxide
DNA	Deoxyribonucleic acid
DOXY	Doxycycline
EC ₅₀	Concentration of a drug required to produce a half-maximal response
ELISA	Enzyme-linked Immunosorbent assay
FAO	Food and agriculture organisation
FDA	Food and drug administration
Fig	Figure
FMN	Flavin mononucleotide
Fts	Filamenting temperature sensitive protein
GPELF	Global programme to eliminate lymphatic filariasis
GST	Glutathione S-transferase
HepCl	Hepatic clearance
hERG	Human ether-a-go-go-gene
HIV	Human immunodeficiency virus
HPLC	High performance Liquid chromatography
HTS	High-throughput screen
IC ₅₀	Inhibitory concentration 50
IVM	Ivermectin
LCMS	Liquid chromatography-mass spectrometry
LF	Lymphatic filariasis
LOD	Lichenified onchodermatitis

LSTM	Liverpool School of Tropical Medicine
MDA	Mass drug administration
MDR	Multi-drug resistance
MEL	Melasormine
Mf	Microfilariae
Mics.Cl	Microsomal Clearance
Min	Minocycline
MMV	Medicines for malaria venture
mRNA	Messenger Ribonucleic acid
Mrp-1	Multi-drug resistance protein -1
OCP	Onchocerciasis control programme
OEPA	Onchocerciasis elimination programme for the Americas
OSD	Onchocercal skin disease
PCR	Polymerase chain reaction
PD	Pharmacodynamics
PEG300	Polyethylene glycol 300; (55% polyethylene glycol, 25% propylene glycol, 20% water)
Pgp	Permeability glycoprotein
Pgp-1	Phagocytic glycoprotein -1
PK	Pharmacokinetics
PPDK	Pyruvatephosphate dikinase
SAR	Structure-activity relationship
SCID	Severe-combined immunodeficient
SER	Spot edge ridge
SPF	Specific pathogen-free
SSV	Standard suspension vehicle (0.5% sodium carboxymethyl cellulose, 0.5% benzyl alcohol, 0.4% Tween80, 0.9% NaCl)
T _{1/2}	Half-life
TB	Tuberculosis
THP	Tetrahydropyran
TPE	Tropical pulmonary eosinophilia
UNDP	United nations development program
UPLC	Ultra-performance liquid chromatography
WHO	World-health organisation
Wsp	<i>Wolbachia</i> Surface protein
WT	Wild-type
ZipA	Z-interaction protein A

List of Figures

Chapter 1

Fig 1.1 Map displaying LF global prevalence with endemic countries and state of MDA programmes displayed (2016).¹

Fig 1.2 Life-cycle of the nematode *W. bancrofti*.²

Fig 1.3 Map displaying global prevalence of Onchocerciasis distribution map (2013).

Fig 1.4 Flow diagram depicting the different stages of the *Onchocerca volvulus* parasite life cycle.³

Fig 1.5 Structure of diethylcarbamazine (DEC), macrocyclic lactone Ivermectin (IVM) and benzimidazole compound Albendazole (ABZ)

Fig 1.6 Structure of the macrocyclic lactone moxidectin

Fig. 1.7 Structure of Melasormine, the arsenical drug with adulticidal properties.

Fig 1.8 Structure of the antibiotics doxycycline (DOXY) and minocycline (MIN) respectively

Fig 1.9 Microscopic images displaying the anti-*Wolbachia* efficacy of doxycycline after 18 months; Image B: untreated female worm cells, Image D: doxycycline treated cells. Figure adapted from the work of Hoerauf *et al.*⁴

Fig 1.10 Doxycycline's clinical efficacy against LF after 6 weeks of treatment and following an 18-month observation period.

Fig 1.11 Structure of the antibiotic rifampicin

Fig 1.12 HTS screening cascade for 3 screens of the MMV library

Fig 1.13 Six templates generated from screening the BioFocus Diversity Library

Fig 1.14 Four templates generated from the MMV Diversity Library

Fig 1.15 Initial hit for the pyrazolopyrimidine template and a General structure

Fig 1.16 Screening cascade for the design, synthesis and testing of new compounds.

Fig 1.17 Operetta fluorescence imaging and SER texture scoring readout for *Wolbachia* infected cells.

Fig 1.18 Optimisation of a series of CRF-1 receptor antagonists

Fig 1.19 Optimisation of a series of selective CDK-2 inhibitions

Fig 1.20 Results obtained from whole-cell assays for the pyrazolopyrimidine template

Fig 1.21 SmartCyp scoring information for the initial hit **AWF911**.

Chapter 2

Fig 2.1 General scaffold for pyrazolopyrimidine core.

Fig 2.2 Results obtained from whole-cell assays for the commercially available pyrazolopyrimidines.

Fig 2.3 DMPK predictions for early analogues designed for synthesis.

Fig 2.4 Low-energy conformer analysis of **9151702** in Spartan.

Fig 2.5 Low-energy conformer analysis of **AWF904** in Spartan.

Fig 2.6 Comparison of **AWF905** with the 6-Me parent analogue which possesses greater anti-*Wolbachia* activity.

Fig 2.7 Introduction of ethyl oxime to alleviate the metabolic liability of the benzylic position

Fig 2.8 Predicted DMPK properties for methylation of the linker and replacement of the 2-pyridyl ring with a saturated 2-pyrrolidyl ring system.

Fig 2.9 Metabolism-driven optimisation of HIV protease inhibitors through introduction of a thiazole.

Fig 2.10 Low-energy conformer analysis of analogue **AWF915**

Fig 2.11 *in vitro* potency and DMPK properties of methylated and 4-F Ph analogues.

Fig 2.12 Predicted DMPK values for analogues containing an amide and methyl alcohol linker moiety.

Fig 2.13 *N*-methylation of the amine linker within pyrazolopyrimidine analogues

Fig 2.14 Structure of the initial hit **AWF911** with the 4-pyridyl regio-isomer.

Fig 2.15 Predicted DMPK properties for analogues with various R³ positions

Fig 2.16 SmartCyp predictions for trifluoroethyl analogue **AWZ9067** and 5,6 dimethyl **AWF918**.

Fig 2.17 Structures of analogues with varied 5-(R³) positions with *in vitro* Biological and DMPK results.

Fig 2.18 Summary of hit to early lead optimisation discussed in the previous chapter.

Fig 2.19 Summary of the SAR understood from the analogues studied so far.

Chapter 3

Fig 3.1 Summary of hit to early lead optimisation discussed in the previous chapter.

Fig 3.2 Pyrazolopyrimidine core with the general scaffold for the focus of SAR study and initial HTS hits.

Fig 3.3 Structure of the palladium catalyst dppf (diphenylphosphinoferrocene)

Fig 3.4 Introduction of a 4-Cl Ph at the 3-(R¹) position

Fig 3.5 Predicted DMPK properties used in the design of a variety of aryl ring systems for the R¹ position

Fig 3.6 Structure of the palladium catalyst dtbpf (ditertiarybutylphosphino ferrocene).

Fig 3.7 General structure for compounds with varied R¹ positions.

Fig 3.8 Predicted solubility changes upon incorporation of a terminal heterocyclic ring.

Fig 3.9 Structure and measured biological activity for **AWF930** with an unsubstituted at the R¹ position.

Fig 3.10 Potential metabolism pathway for drugs containing aromatic ring systems

Fig 3.11 Optimization towards cholesterol absorption inhibitor ezetimibe (Zetia).

Fig 3.12 Structures of electrophilic halogenating agents, used for installing halogens at the R¹ position

Fig 3.13 Replacement of a 4-Cl Ph ring with a THP to lower LogD

Fig 3.14 Optimisation of various compound series involving the replacement of phenyl ring with a cyclopropyl moiety.

Fig 3.15 Predicted DMPK properties for analogues **AWZ9035** and **AWZ9036** containing the cyclopropyl and THP analogues respectively.

Fig 3.16 Summary of early lead optimisation discussed in this chapter.

Fig 3.17 SAR summary from study of the R¹ position of the pyrazolopyrimidine core.

Chapter 4

Fig 4.1 Early-lead optimisation as discussed throughout **Chapter 3**.

Fig 4.2 DMPK properties and whole-cell anti-*Wolbachia* activity for **AWZ9035** and **AWZ9036**.

Fig 4.3 Reducing ring size from a tetrahydropyran to an oxetane ring to improve compound metabolic stability.

Fig 4.4 Reduction in 4-fluoro piperidine ring size to improve the oral bioavailability in a series of aurora kinase inhibitors.

Fig 4.5 Introduction of a morpholine ring to greatly improve compound half-life when incubated with human liver microsomes.

Fig 4.6 Incorporation of various saturated nitrogen heterocycles during optimisation of cannabinoid receptor 2 agonists.

Fig 4.7 Pyrazolopyrimidines with saturated heterocycles at the R¹ position designed for synthesis.

Fig 4.8 Comparison of 5-H analogues with their 6-Me parents.

Fig 4.9 Structure of the lead tetrahydropyran analogue **AWZ9100** with the pure stereoisomers.

Fig 4.10 *In vitro* mf screening results for selected analogues 5 μ M

Fig 4.11 Structure of **AWZ9014** studied for *in vivo* PK PD profile with measured *in vitro* whole-cell activity and DMPK properties

Fig 4.12 Summary of lead optimisation (Chapter 2 - 4)

Fig 4.13 Summary of the hit to lead optimisation carried out during this work

Fig 4.14 General pyrazolopyrimidine core for future optimisation.

Abstract

Filarial nematodes are an important group of human pathogens that affect more than 157 million people worldwide and contribute to serious public health and socio-economic problems. These parasites are responsible for the neglected tropical diseases lymphatic filariasis (LF) and onchocerciasis and taken together, these diseases are a leading cause of global morbidity. Currently, treatment of LF relies on diethylcarbamazine plus albendazole in areas which are not co-endemic for onchocerciasis and ivermectin which is used to treat onchocerciasis in areas which are co-endemic. The current anthelmintic therapies have undesirable adverse effects, activity restricted to the immature worm stage and contraindicated patient groups. In addition to these drawbacks, drug resistance is another important factor that is driving research efforts to identify and generate safer alternative drugs with novel mechanisms of action. *Wolbachia* is an essential endosymbiotic bacterium that lives inside the cells of the filarial worms. As the filariae are dependent on *Wolbachia* for survival and fertility, eliminating the bacteria with antibiotic drugs cures patients, blocks transmission and delivers a new strategy for eradicating lymphatic filariasis and onchocerciasis while avoiding the severe adverse effects with current therapies. Doxycycline is the current gold standard for anti-*Wolbachia* activity, but requires treatment for at least 4 weeks and is contraindicated in children less than 9 years of age and pregnant women. The anti-*Wolbachia* (AWOL) drug discovery and development consortium, which is funded by the Bill & Melinda Gates foundation, aims to identify alternative drugs that are suitable for a wider patient range and require a shorter treatment regimen. The work presented is focused on the identification and development of novel small-molecule therapies for these diseases. Initially, a brief introduction to Lymphatic Filariasis and Onchocerciasis will be presented followed by current therapies before discussion of the target bacteria *Wolbachia*. A phenotypic screen of the Medicines for Malaria venture diversity library revealed many hits that showed promising anti-*Wolbachia* activity. Chemoinformatic analysis of these hits identified the most promising chemical scaffolds to enter a medicinal chemistry optimization phase. This thesis primarily focuses on the establishment of SAR for molecules containing a pyrazolopyrimidine core, with subsequent optimization of metabolic stability and solubility profiles in line with our target candidate profile. Several synthetic pathways have been explored that allow for modification at key positions around the pyrazolopyrimidine core. These pathways have enabled extensive functionalization, generating a large library of over 190 compounds where many analogues possess nanomolar activity against *Wolbachia in vitro* and display greatly improved *in vitro* DMPK parameters over the initial hit. The 2-pyridyl ring seen in the initial hit appears essential for anti-*Wolbachia* activity and SAR studies focused on reducing ClogP revealed that bioisosteric replacement of the phenyl ring seen with a tetrahydropyran group was tolerated in terms of anti-*Wolbachia* potency with an improvement in measured DMPK properties. Data on the most advanced molecule in this series shows similar efficacy to that of the current gold-standard doxycycline. Based on the work contained in this thesis, there are several options available for further modification of both the pyrazolopyrimidine core and substituents that could allow for further improvement of both DMPK properties and compound potency.

Chapter 1

Introduction

Contents

Abbreviations	6
Abstract	12
Chapter 1 – Introduction	15
1.1 Lymphatic filariasis (LF)	15
1.1.1 Global prevalence of LF	15
1.1.2 Life cycle of <i>Wuchereria bancrofti</i>	16
1.1.3 Diagnosis of LF	17
1.2 Onchocerciasis	18
1.2.1 Global prevalence of onchocerciasis.....	18
1.2.2 <i>Onchocerca Volvulus</i> Life Cycle	19
1.2.3 Diagnosis of Onchocerciasis	20
1.3 Existing Anti-Filarial Treatments	20
1.3.2 Control programs	24
1.3.3 Drug Resistance	24
1.4 <i>Wolbachia</i> – A Common Target for LF and Onchocerciasis.....	26
1.4.1 <i>Wolbachia</i> as obligate mutualists with filarial nematodes	26
1.4.2 Potential drug targets for the development of anti- <i>Wolbachia</i> agents.....	27
1.4.3 Treatments to remove <i>Wolbachia</i> bacteria from hosts	28
1.5 Aims.....	31
1.6 Identification of small molecule anti- <i>Wolbachia</i> agents	32
1.6.1 Target Vs Phenotypic screening	32
1.6.2 <i>In vitro</i> assay development	33
1.6.3 HTS: Chemotype identification	33
1.7 Strategy for the discovery of small molecule anti- <i>Wolbachia</i> agents.....	36
1.7.1 Screening cascade	36
1.7.2 Drug-metabolism and Pharmacokinetics (DMPK)	38
1.7.3 Development of synthetic methodology and biological relevance of Pyrazolopyrimidines	40
1.7.3 Initial pyrazolopyrimidine target selection.....	43
1.8 References	46

1 – Introduction

1.1 Lymphatic filariasis (LF)

1.1.1 Global prevalence of LF

The parasitic disease filariasis is a vector-borne disease caused by a range of nematodes which are able to infect a number of diverse environments within a human host.⁵ Filariasis can be divided into three categories; lymphatic filariasis (LF), subcutaneous filariasis and serous cavity filariasis. In 2012 greater than 120 million people suffered from these diseases with a further 1.3 billion people at risk of infection in over 72 endemic countries. Currently these cases have been reduced to an estimated 40 million people suffering from lymphatic filariasis who experience serious incapacitation or disfigurement.⁶ Due to control programmes initiated by the WHO over 350 million people no longer require prophylactic chemotherapy. However, 947 million people are still at risk of infection in over 54 countries, many of whom live within Africa, Asia or Brazil (**Fig. 1.1**).^{1,6} Filarial diseases contribute to a further decline in health in patients suffering from life-threatening infections such as HIV, TB or malaria.⁷ Filariasis is responsible for significant losses to productivity within the agricultural industry attributed to the loss of livestock and additional cost incurred in the treatment measures required to preserve remaining livestock, this is estimated at an annual loss of US\$1.3 billion.^{8–10}

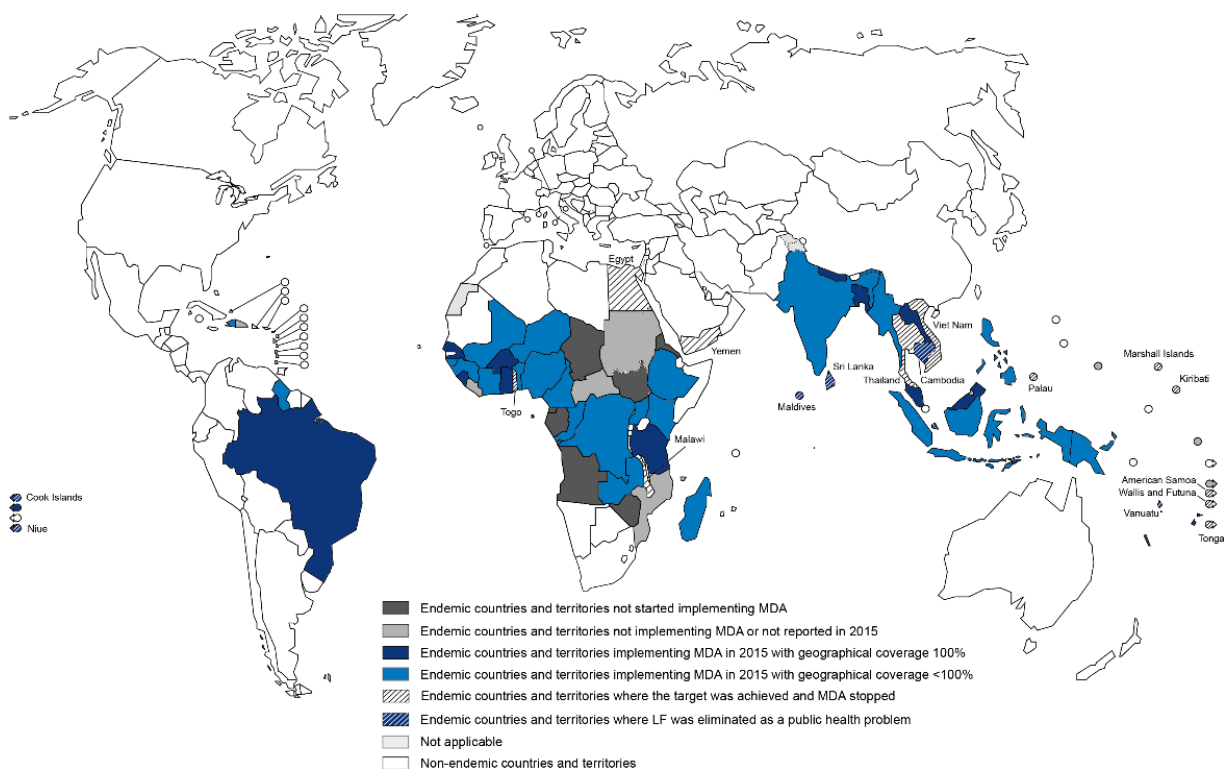


Fig. 1.1 Map displaying LF global prevalence with endemic countries and state of MDA programmes displayed (2016).¹

The causative agents for LF are the group of nematodes; *Wuchereria bancrofti*, *Brugia malayi* and *Brugia timor*, with the majority (~90%) of cases due to *W. bancrofti* infection.⁶ A wide range of mosquitoes are responsible for the transmission of LF while mosquitoes of the *Culex* genus, which are spread around urban or semi-urban areas, are generally the most efficient for transmitting *W. bancrofti*.¹¹ Chronic cases of LF can lead to a condition known as elephantiasis, which is characterised by the swelling and disfiguring of the lower extremities. This condition significantly decreases the number of able-bodied workers in populations experiencing a high incidence of transmission; in severe cases, healthy individuals are forced to become full-time carers for incapacitated family members with severe conditions. This produces huge socio-economic issues within areas of high incidence where the burden of the disease is related to the intensity and duration of the infection therefore LF has a greater impact on older age groups when the disease has had a greater time to develop.¹²

1.1.2 Life cycle of *Wuchereria bancrofti*.

The life cycle of the *W. bancrofti* nematode is displayed in Fig. 1.2, this cycle initiates with the transfer of the infectious stage larvae (L3) onto a host's skin during a the bite of an *Anopheles* or *Culex* mosquito.¹³ Once within the human host the infectious larvae migrate around the body within the bloodstream until they reach the lymphatic system where they develop into adult worms. Once capable, the adult worms form nests and begin to reproduce; this forms many immature worms in the form of microfilariae (mf) which then circulate the body within the blood.

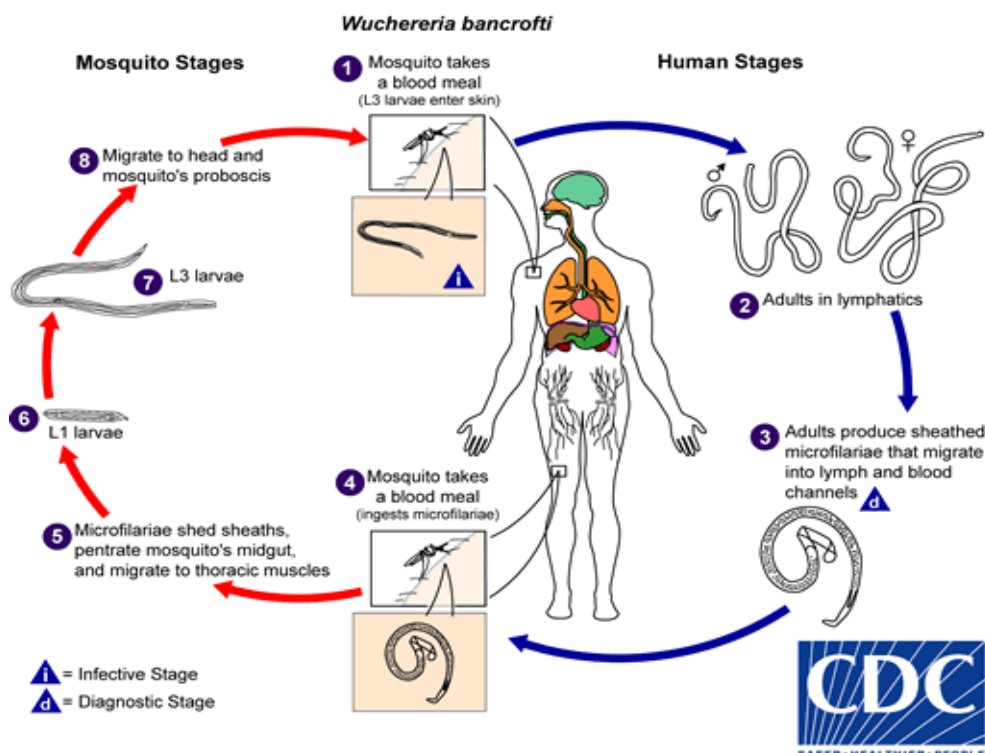


Fig 1.2 Life-cycle of the nematode *W. bancrofti*.²

Microfilariae can be transferred from the blood to a feeding mosquito to again develop into immature (L1) larvae and subsequently infectious larvae (L3) which remain within the thoracic muscles of the mosquito and are primed for retransmission.⁵

Female adult worms can grow up to 10 cm in length and typically live for five to seven years, while the smaller male worms will grow to approximately 2-4 cm in length.² It is possible for these adult worm nests to grow large enough to cause fluid blockages within human lymph nodes, resulting in fever due to swelling of the lymphatic system. The first classified manifestation of LF is termed acute adenolymphangitis (ADL). Symptoms of ADL are characterised by the sudden onset of fever and inflammation of the lymphatic system. Tropical pulmonary eosinophilia (TPE) is a syndrome that develops in some suffers of LF, normally in people aged between 30 to 40 and is about four times more likely to affect males than females. Symptoms of TPE include excessive coughing and asthma attacks which can occasionally be mistaken for tuberculosis, if left untreated TPE can result in lung disease.¹⁴ The World Health Organisation (WHO) has published a grading system to classify the severity of lymphatic filariasis cases within the clinic. Grade 1 cases display pitting oedema that is reversible upon elevation of the leg while Grade 2 indicates non-pitting oedema that is not reversible by elevating the leg. A Grade 3 category indicates non-pitting oedema with increased swelling relative to Grade 2 cases. Additionally, grade 3 cases are associated with sclerosis and papillomatous changes to the skin surface and many of grade 2 and grade 3 patients suffer from elephantiasis.¹⁵

1.1.3 Diagnosis of LF

Diagnosis of LF is difficult. Traditional diagnostic methods involve the use of microscopy to detect mf within the blood; however, since mf exhibit a marked periodicity the time of specimen collection is important. Microfilariae of the *Brugia* or *Wuchereria* species primarily circulate at night which results in added difficulty to obtain appropriate blood samples for analysis.¹⁶ There are assays available which detect the presence of *W. bancrofti* antigens within the blood. The enzyme-linked immunosorbent assay (ELISA) and the immunochromatographic card tests are the primary methods used for detection of LF. These tests are very specific for the condition with almost 100 percent reliability.¹⁷ They are however subject to some disadvantages; the tests only detect for *W. bancrofti*, therefore overlooking the other causative species of *Brugia*, they are expensive costing US\$ 2-4 per person which makes them unsuitable for programmes which screen over 380 million people per year and it is also possible for these tests to produce false-positives due to the detection of antigens present after worm death.¹⁷ The identification of adult worms within the scrotum of males or the breasts of females is possible using high frequency ultrasound imaging to detect for worm movement.¹⁸ These techniques are necessary as diagnosis of adult worms present within the nodes of the lymphatic system is extremely difficult. The implementation of these techniques is expensive and therefore is unsuitable for use in endemic areas.

1.2 Onchocerciasis

1.2.1 Global prevalence of onchocerciasis

Onchocerciasis (or river blindness) is caused by the parasitic nematode *Onchocerca Volvulus* (*O. Volvulus*) and is the world's second leading infectious cause of blindness.¹⁹ There are 120 million people at risk of Onchocerciasis, 96% of which are located in Africa as shown in **Fig. 1.3**. The disease however also exists in Yemen and throughout a number of Latin American nations.¹⁰ Individuals who are at greatest risk of contracting onchocerciasis are those who live near to suitable river habitats for the vectors, Simulium blackflies, which transmit the parasite *O. Volvulus* to its host. The most efficient vector of *O. Volvulus* throughout Africa is *Simulium damnosum sensus lato*, whilst within the Western hemisphere there are many important vectors including *S. ochraceum* and *S. metallicum*. At present, approximately 37 million humans are infected with *O. Volvulus* although symptoms may not appear until several months after initial infection once the mf count within the human host has increased to a sufficient level.

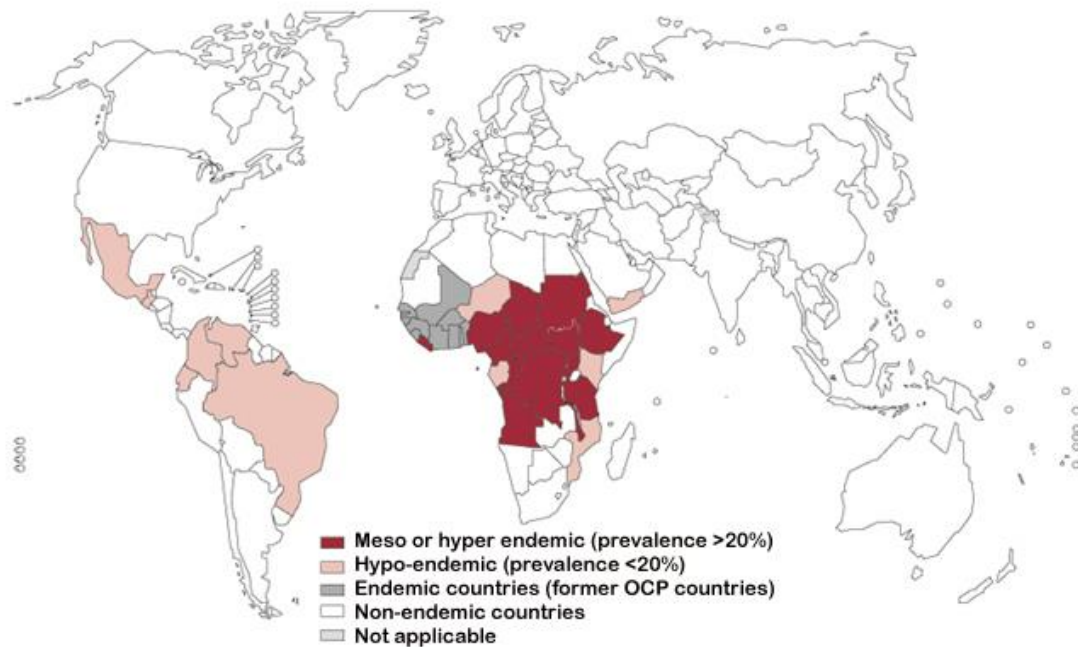


Fig. 1.3 Map displaying global prevalence of Onchocerciasis distribution map (Figure adapted from WHO, Onchocerciasis distribution map - 2013).²⁰

Onchocerciasis is responsible for the suffering of over 6.5 million people with associated skin-conditions, a further half a million people suffering from visual impairments and almost 300,000 of these individuals are blind.²¹ The abnormal skin conditions are known as localized and chronic papular onchodermatitis, these account for 60% of the disease burden or Disability-adjusted life-years (DALYS), the number of years those afflicted lose due to ill-health caused by onchocerciasis.¹⁹ Food shortages and a struggling economy resulting from insufficient able-bodied workers has forced people residing within endemic regions to abandon their

homes, leaving fertile river valleys in order to move to areas which experience reduced transmission. These forested areas are generally difficult to farm and further contribute to food shortages and a struggling economy.¹⁹ Therefore, the impact of these infectious diseases goes far beyond the impairment of health by compromising working societies in affected regions.

1.2.2 *Onchocerca Volvulus* Life Cycle

The infective larvae of *O. Volvulus* are transmitted onto the skin of humans during the bite of an infected blackfly. Larvae enter the human body by penetrating the wound inflicted by the fly bite then migrate to subcutaneous tissues and slowly develop into adult worms.¹⁹ Female adult worms can measure up to 40 cm in length and remain in nodules; male adult worms measure ~20 cm in length and can migrate between nodules fertilising the larger female worm.²² This results in the production of approximately 1600 mf per day which are then released into the bloodstream and surrounding tissue. Female worms remain fertile for up to nine years and the average life-expectancy of adult worms is 15 years. Mf are primarily found near the surface of the skin where it is possible for them to be ingested by feeding blackflies and allows for diagnosis of the condition. Immature forms of the worm cannot mature into infective larvae without transmission to feeding blackflies; therefore, the adult worm count within an individual can be associated with the number of infectious bites incurred. Once transmitted to a black-fly the immature larvae penetrate the stomach wall of the black fly and move towards the thoracic muscles where they remain and develop into infectious larvae over the next seven days, after which larvae are now primed for transmission to further humans.²² The life cycle of *O. Volvulus* is summarised in Fig. 1.4³ and is divided into the human and blackfly stages of the nematode life cycle with the infectious larvae and diagnostic mf worm stages labelled.

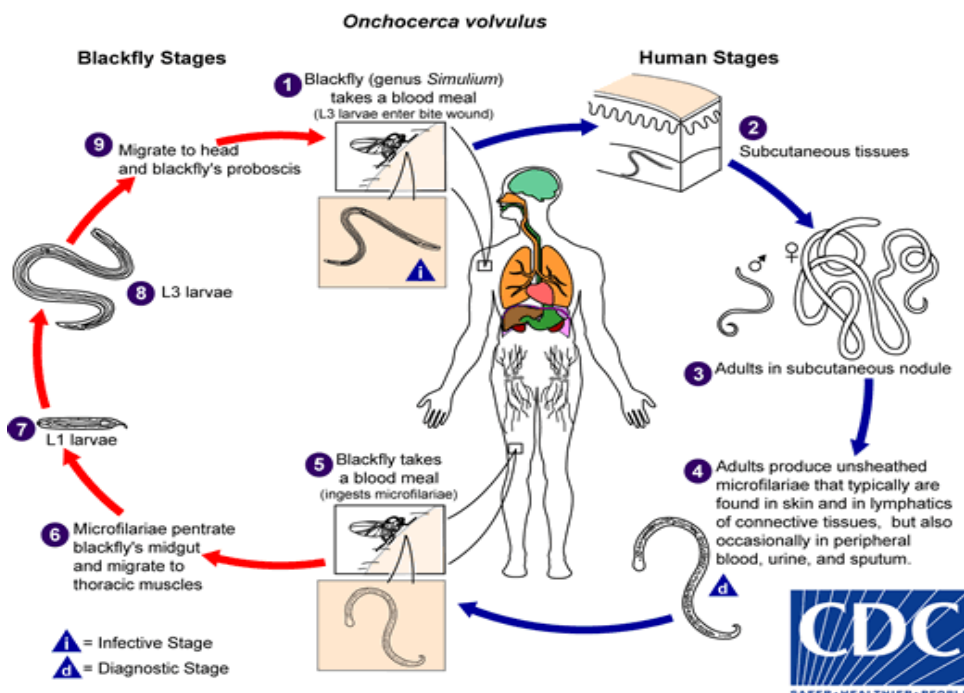


Fig 1.4 Flow diagram depicting the different stages of the *Onchocerca volvulus* parasite life cycle.³

Microfilariae (mf) typically live for one to two years and are responsible for the disease pathology of onchocerciasis including inflammatory reactions within the skin, lymph nodes and eyes. The majority of this inflammation can be associated with dead or dying mf which causes the release of endogenous substances into surrounding tissue.¹⁹ This poses an issue with the use of filaricidal therapies that act directly on the worm and result in the release of further harmful substances into the body at the sites of worm death. Onchocercal skin disease (OSD) is caused by mf migration throughout the body allowing continuous secretion of enzymes such as collagenase which cause damage to skin collagen and elastin, resulting in the loss of skin elasticity ultimately causing disfigurement.²³ Visual impairment is caused by mf invasion of the eyes, exposing these organs to harmful enzymes on worm death resulting in serious inflammation. Inflammatory reactions within the eye produce opaque spots on the cornea which can later develop into a permanently cloudy cornea causing loss of vision and potentially, blindness.¹⁹ In addition to the symptoms of blindness, dermatitis, skin atrophy and inflammation, a high mf load has been identified as a factor which reduces the life span of infected people. Those afflicted with OSD can suffer from significant psychological trauma contributing to a number of negative socio-economic effects such as productivity losses in the agricultural industry and decreased school attendance.^{24–28}

1.2.3 Diagnosis of Onchocerciasis

There are several techniques that are used to diagnose individuals infected with onchocerciasis, the most common of which is the skin snip test which is used to detect the presence of mf within the skin. This can be a challenging method of diagnosis since the time when mf are present within the skin (the optimum time for skin snip diagnosis) occurs between 3 and 15 months following initial infection. The removed skin sample is placed in a saline solution causing any mf to emerge therefore allowing detection. It is also possible to use polymerase chain reaction (PCR) to diagnose patients with low levels of infection; however, this technique is relatively expensive compared to other diagnostic methods and is therefore unsuitable to administer in large-scale programs within developing countries.²⁹ Mf within the eye can be detected using a slit-lamp (microscope and a lamp) with skin nodules being surgically removed to detect for adult worms. It is also possible to test for circulating antigens of *O. Volvulus* within the blood through the use of Ov16 card tests which are employed within the onchocerciasis elimination program for the Americas (OEPA) as a means of determining if transmission has been eliminated.²⁹

1.3 Existing Anti-Filarial Treatments

Currently the treatment of filariasis involves drugs such as diethylcarbamazine (DEC), ivermectin (IVM) and albendazole (**Fig 1.5**).³⁰ DEC is a synthetic piperazine derived anthelmintic (compound efficacious against parasitic worms, helminths) used for the treatment of filarial infections in humans and animals which displays activity against both microfilariae and macrofilariae (the adult worm).

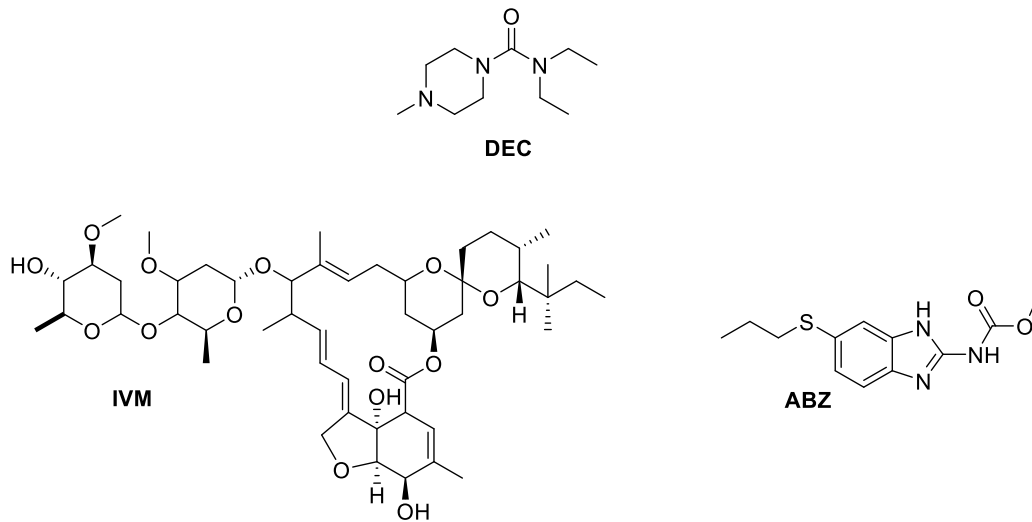


Fig. 1.5 Structure of diethylcarbamazine (DEC), macrocyclic lactone Ivermectin (IVM) and benzimidazole compound Albendazole (ABZ)

DEC is thought to exert its anti-filarial activity *via* a number of mechanisms including inhibition of arachidonic acid synthesis³¹ and induction of cellular immune responses by up-regulating the activity of lymphocytes,³² eosinophils, macrophages³³ and other natural killer cells.³⁴ DEC's efficacy has also been linked with an accumulation of mf in the liver, lung, kidney and spleen, therefore serving to expose mf to a greater concentration of immune cells. This mechanism can cause issues with DEC therapy when worm death in these organs expels harmful substances resulting in serious inflammatory reactions. In addition to systemic inflammatory responses, localised reactions are known to occur at the site of adult worm infections following treatment with diethylcarbamazine. The Mazzotti reaction, first described in 1948,³⁵ is characterized by fever, tachycardia, hypotension, adenitis, pruritus and arthralgia following the treatment of onchocerciasis with DEC. Such severe inflammatory reactions and adverse effects preclude the use of DEC for patients with Onchocerciasis. In addition, DEC therapy is not suitable for patients residing within areas which are co-endemic with loiasis, another form of filariasis caused by the parasitic worm *L.loa*, as they are at risk of potentially fatal adverse effects upon treatment with DEC. It is therefore essential that this category of patients are not treated with DEC and this presents a huge issue with the mass drug administration of DEC.

The orally administered benzimidazole compound, albendazole (ABZ) is an anthelmintic with proven efficacy against many intra and extraluminal parasites, ABZ can be considered a prodrug with the active form being the bioactivated albendazole sulfoxide. Albendazole in combination with diethylcarbamazine is the recommended treatment for LF in areas that are not co-endemic with onchocerciasis.³⁶ The intrinsic anthelmintic action of benzimidazoles relies on a progressive disruption of basic cell functions which arises from binding of the drug to parasite tubulin and causing depolymerisation of microtubules.³⁷ The lipophilicity of benzimidazole anthelmintics enables passive diffusion through cell membranes into the intestinal cells of nematodes.³⁸ benzimidazoles have also been shown to inhibit glucose uptake in nematodes, causing the depletion of glycogen stores and ATP formation, representing a plausible mechanism by which ABZ causes parasite death. One major issue with ABZ treatment is poor absorption which results in reduced drug exposure; however,

administration with a fatty meal can increase ABZ absorption up to five-fold.³⁹ ABZ is rapidly metabolised *via* CYP1A2 and CYP3A4 P450 enzymes with repeated dosing of ABZ known to up-regulate its own metabolism by induction of metabolising enzymes.^{40,41}

Another existing anti-filarial treatment is Ivermectin (IVM), a potent anthelmintic discovered from the actinomycete bacteria *Streptomyces avermitilis*, exhibiting broad spectrum activity against gastrointestinal and lung nematodes however; is not macrofilaricidal.^{34,35} IVM targets mf *via* binding to glutamate-gated chloride channels, increasing the permeability of nerve and muscle cells to chloride ions which results in paralysis, and ultimately death of the immature worms within the blood and any present within adult worms.^{7,19} Some observations have been made which support the possibility of an active involvement of the immune system in the mechanism of action of IVM, although further investigation is required.⁴⁵ Depletion of microfilariae serves to prevent disease progression, providing relief from severe itching and visual impairment which are associated with Onchocerciasis. Depletion of mf also decreases the possibility of parasite transmission to vectors. Therefore, treatment with IVM once a year remains a standard prophylactic approach although in practice it is common to treat infected people up to three times a year with IVM.¹⁹ Whilst IVM has no known significant drug-drug interactions it is necessary to screen communities that may be at risk of contracting another form of filariasis, loiasis, since these people would be at risk of severe, potentially fatal, adverse reactions on treatment with IVM.⁴⁶ Since IVM has no efficacy against adult worms and as the adult *Onchocerca Volvulus* parasite can live for up to 15 years, it is necessary to continue patient treatment for this prolonged time period. Other contraindications with IVM treatment involve conditions associated with impaired blood-brain barrier penetration, since penetration of the drug into the CNS can cause lethargy, tremors and death. Consequently, IVM is not approved for children weighing less than 15 kg, pregnant women or mothers nursing infants during the first week of life.¹⁹ Despite requiring such a long treatment period and a number of contraindicated patient groups, IVM remains the current recommended treatment for onchocerciasis and for LF in areas which are co-endemic with onchocerciasis.

It has been recommended that IVM is given in combination with albendazole for treatment in areas experiencing a high risk of both LF and onchocerciasis. It is necessary to use such a treatment regimen in these areas due to the severe adverse reactions associated with treating onchocerciasis patients with DEC.⁴⁷ Co-administration of two drugs acting against LF which have different molecular targets has the advantage of halting the development of resistance which remains a concern with single drug treatment programs.

Natural product research has led to the discovery of some outstanding new drugs including moxidectin (**Fig. 1.6**) a semisynthetic macrocyclic lactone derived from nemadectin, a milbemycin produced from fermentation of *Streptomyces cyanogriseus*.⁴⁸ Moxidectin results in the paralysis and death of parasites as it binds to glutamate-gated chloride ion channels which are essential for neurotransmission within muscle cells and has been shown to result in the sterilisation of female adult worms.⁷ Moxidectin is commonly used in veterinary medicine for treatment of and prophylactic measures against heartworm infections.^{7,48} Some studies assessing the efficacy of moxidectin in controlling filariae as a therapeutic alternative to IVM displayed

promising results however further evaluation is required to determine if moxidectin is safe for introduction into the clinic.⁴⁹

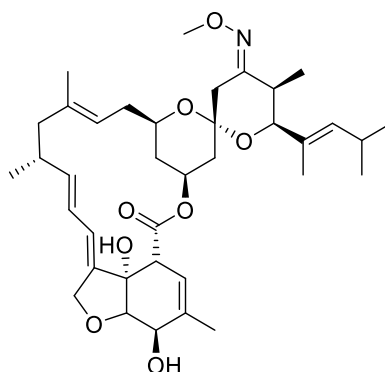


Fig 1.6 Structure of the macrocyclic lactone moxidectin

Arsenical drugs have been the mainstay in heart-worm adulticidal therapy for the past four to five decades, Melasormine (MEL) (**Fig. 1.7**), a key example and is the only drug approved in the USA by the food and drug administration (FDA) which is an adulticide. Melasormine is a trivalent arsenical compound, like melarsoproll, which can penetrate the CNS of the host. However, patients may therefore be exposed to the adverse associated with CNS penetration such as encephalopathy. While the mechanism of action of melasormine is not fully understood, it is possible that it is involved in blocking glycolysis in worms through inhibiting the activity of phosphopyruvate kinase, known to be sensitive to trivalent arsenicals.⁵⁰ The exacerbated inflammatory reactions associated with rapid worm death, as discussed previously, impose a high risk associated with MEL treatment and therefore encourage the use of alternative therapies for heartworm infection which pose fewer risks to the patient.⁵¹

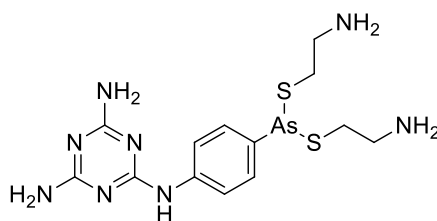


Fig. 1.7 Structure of Melasormine, the arsenical drug with adulticidal properties.

1.3.2 Control programs

In the 1970s the investigation of onchocerciasis in endemic villages and districts of West Africa began. Studies discovered that within endemic areas, more than 60% of the population carried the parasite with 10% of the adult population suffering from blindness, with half of those afflicted being males above the age of 40.^{52,53} Within affected countries, the 'river blindness partnership' was formed by the agencies of the World Bank, the World Health Organisation (WHO), the Food and Agriculture Organization (FAO) and the United Nations Development Program (UNDP). This partnership was responsible for the work of the Onchocerciasis Control Program (OCP) (1974 - 2002) and more recently, the African Programme for Onchocerciasis Control (APOC) (1996 - 2015). Prevention of blindness was the major goal for the OCP and this programme was established to cover zones endemic for onchocerciasis. This covered 11 countries in total, with the objective being to eliminate onchocerciasis as a disease of public health and socio-economic importance. The program utilised vector control strategies using seven different insecticides in addition to IVM (Mectizan) which was donated by Merck.⁵⁴ Since the initiation of the OCP, a number of countries have been verified as free from infection with over 25 million hectares of land now primed for resettlement. This accounts for the prevention of approximately 600,000 cases of blindness and over 16 million children born into areas where onchocerciasis is not considered a disease of concern.⁵⁵ Furthermore, widespread control programmes using more specialised therapies for areas co-endemic for various filarial diseases, will allow further progress towards the ultimate goal of elimination of filarial infections as a disease of public-health concern. The APOC covers a larger area of 19 countries and intends to treat over 90 million people, protecting an at-risk population of 115 million people by annual treatment with IVM.

The Global Programme to Eliminate Lymphatic Filariasis (GPELF)⁵⁶ is based on mass drug administration (MDA), comprising either a single annual dose of DEC with ABZ, or ABZ with IVM where onchocerciasis is also endemic. Vector control efforts for GPELF include residual indoor spraying and insecticide treated nets like control strategies used for other diseases such as malaria. These efforts serve to minimise and then restrict the transmission of infection, managing morbidity and prevent disability. Since initiation of this programme, 18 countries have carried out the necessary interventions and are currently reviewing the success of these efforts to confirm elimination of the disease; a further 22 countries are progressing towards the stage of elimination. The control of these diseases involves the combined use of IVM, DEC and ABZ over long time periods, therefore creating a growing concern for the development of resistance against these current front-line therapies. This has promoted research into alternative drugs which are suitable for wider patient ranges and exhibit novel mechanisms of action in the on-going pursuit for treatment of these conditions.

1.3.3 Drug Resistance

Ivermectin

Selective pressure from the mass administration of IVM as a single drug, in addition to the need for decades of sustained treatment during the OCP and APOC (Section 1.4), has resulted in resistance development to IVM in a number of parasites including *Onchocerca volvulus*.⁵⁷ Such resistance has been documented in a number of nematodes and arthropods resulting from insensitivity of the glutamate-gated chloride channel (GluCl) receptors which prevents efficient drug binding.^{58,59} In the nematode *Caenorhabditis elegans*, IVM resistance has been associated with the over-expression of the multi-drug resistance protein (mrp-1), permeability glycoprotein-1 (pgp-1),⁶⁰ which is also observed in the IVM resistant mites *Sarcoptes scabiei*.⁶¹

Benzimidazoles

Mutations to benzimidazole binding sites within the homologous tubulin genes in parasites have been associated with benzimidazole resistance. It has also been proposed that up-regulated catalase activity effectively protects *Haemonchus contortus* from benzimidazole action.^{62,63} Glutathione S-transferase (GST) is an important enzyme involved in the detoxification of potentially harmful substances including reactive oxygen species, lipid peroxidation products and electrophilic compounds.⁶³ It has been proposed that increased GST activity may participate in benzimidazole drug resistance which is seen in the triclabendazole (TCBZ) resistant strain of *Fasciola hepatica*. In the bodies of nematodes, higher amounts of ABZ glucosides were found in benzimidazole-resistant strains relative to BDZ-sensitive strains, suggesting that increased glucuronidation promotes benzimidazole resistance. Meanwhile, peroxidase activity has been shown to be significantly diminished in resistant strains compared to susceptible strains, suggesting the involvement of peroxidase in the bioactivation of benzimidazole compounds.

The main treatment options which are available for LF and onchocerciasis, DEC, ABZ and IVM respectively each possess undesirable adverse effects and lead to contraindicated patient groups; DEC's effects on onchocerciasis patients and the complications of IVM and DEC in Loaasis patients (see Section 1.3). Coupled with concerns of resistance development, these factors are driving current research efforts to identify and generate safe therapeutic alternatives which are suitable for all patient groups and which ideally possess unique mechanisms of action to avoid the risk of resistance development that exists with current treatments.

1.4 *Wolbachia* – A Common Target for LF and Onchocerciasis

1.4.1 *Wolbachia* as obligate mutualists with filarial nematodes

A large number of the nematodes responsible for causing filarial diseases share an endosymbiotic relationship with the bacterium *Wolbachia*.^{51,64,65} *Wolbachia* is a highly common and a widely distributed gram-negative bacterium which infects a large number of insect species and nematodes of the arthropod phylum.⁶⁶ *Wolbachia* are intracellular alpha-proteobacteria that are divided into seven groups.^{67–70} Two groups of *Wolbachia* infecting nematodes are classified into two sub groups (C and D), while four supergroups (A, B, E, H) infect exclusively arthropods and finally an additional group of *Wolbachia* (F) which are capable of infecting both nematodes and arthropods.⁷¹ The *Wolbachia* which infect the nematodes responsible for Onchocerciasis and LF are the most distantly related strains, *Wolbachia pipientis* which are estimated to have diverged 60-100 million years ago.⁷²

Wolbachia are maternally transmitted from mother nematodes to offspring as they are present within oocytes and developing embryos in the female reproductive tract,^{73,74} in contrast infected males produce sperm that does not contain *Wolbachia*. Cytoplasmic incompatibility is a term which describes the inability of infected males to mate with uninfected females, while eggs produced by infected females are compatible with unmodified sperm and with sperm produced by males infected with the same strain of *Wolbachia*. Infected females therefore have a more significant impact on the *Wolbachia* presence within the next generation of nematodes, whereas the presence of infected males within a population prevents the reproduction of uninfected females which also results in an increased percentage of *Wolbachia*-containing nematodes within the population.⁷² *Wolbachia* infection causes the death of a number of male nematodes during larval development which allows for a greater ratio of female worms to develop through a process termed male-killing. In addition, it is possible for male nematodes to develop as females through a process known as feminisation; this is another technique by which *Wolbachia* distorts the sex ratio within a population to further raise its own prevalence within a population. The presence of *Wolbachia* within nematodes does not appear to activate an immune response during any phase of the host's lifecycle, this is likely due to stealth on the part of *Wolbachia*, as there is presently no evidence suggesting *Wolbachia* to actively suppress host immunity.⁷⁵

The specific endosymbiotic relationship that *Wolbachia* shares with infected filariae is unclear, it has however been observed that the bacteria are important during the process of embryo development, embryogenesis, in infected filariae.^{76–78} It has been suggested that *Wolbachia* can provide their host with additional detoxification pathways, as it has been previously observed that insecticide-resistant mosquitoes harbour higher densities of *Wolbachia* than insecticide susceptible mosquitoes. Similar observations suggest that *Wolbachia* are responsible for the synthesis of detoxification enzymes such as catalase,⁷⁹ while other research suggests that *Wolbachia* may have a pivotal role in nutrition for the nematodes.⁸⁰ Gene sequencing of *Wolbachia pipientis*

has shown that a limited number of amino acids can be synthesised by the bacteria while the remainder must be imported from their hosts. It has also become apparent that *Wolbachia* has incomplete pathways for the biosynthesis of various enzymes and cofactors such as NAD, biotin, lipoic acid, ubiquinone, folate, pyridoxal phosphate and Coenzyme A⁷¹ which could serve as tractable pathways for small-molecule anti-*Wolbachia* drug development. The work of Sharma and Kumar has revealed 61 potential drug targets within *Brugia malayi* *Wolbachia* which could be further validated experimentally through drug discovery pipelines for programmes exploring the treatment opportunities for lymphatic filariasis.¹³ These targets are presented in a database named the FiloBase which may be used for further research and drug development against filariasis.⁸¹

1.4.2 Potential drug targets for the development of anti-*Wolbachia* agents

Wolbachia have been validated as a tractable target for the treatment of filarial infections such as LF and Onchocerciasis as they are necessary for oogenesis, embryogenesis and the correct development of adult worms.⁸² Heme is an iron-containing tetrapyrrole which is an essential cofactor for many proteins such as cytochromes, haemoglobins, peroxidases and catalases. Data suggests that the heme biosynthetic pathway in *Wolbachia* is a potential anti-filarial drug target due to its requirement for the survival of both *Wolbachia* and its filarial host. All but one heme biosynthetic gene, ferrochelatase, which encodes proteins that are essential in the final step of the biosynthesis of heme are absent in the *B.malayi* genome.⁸³ This implies that filarial nematodes are incapable of *de novo* heme biosynthesis, a condition that is characteristic of all or most nematodes, including *Caenorhabditis*.⁸⁴ Although heme biosynthesis is a proposed drug target, it remains unknown how heme and heme intermediates might be transferred from *Wolbachia* to the filarial host. Two inhibitors of heme biosynthesis with distinct biological targets (aminolevulinic acid dehydratase and ferrochelatase, succinyl acetone and *N*-methyl mesoporphyrin respectively) have been shown to have negative effects on adult worms and mf.⁸⁵ This suggests that these enzymes are indeed viable targets for the development of anti-*Wolbachia* agents.

Fortunately, there is a larger evolutionary distinction between *Wolbachia* and mammals than between nematodes and mammals which presents a good opportunity for the development of selective therapies. A number of potential targets have been identified by genomic analysis including membrane proteins, ankyrins, lipoprotein biosynthesis, enzymes of lipid II biosynthesis and the glycolytic enzymes, all of these could be utilised in the development of anti-*Wolbachia* therapies.⁸⁶⁻⁸⁹ Two enzymes which are essential for glycolysis are absent within the *Wolbachia* genome, 6-phosphofructokinase and pyruvate kinase, are replaced with the gluconeogenic enzyme, fructose-1,6-biphosphate, and by pyruvatephosphate dikinase (PPDK). As PPDK is absent within mammals this enzyme presents a promising target for chemotherapeutic intervention for the treatment of filarial infections through *Wolbachia* removal.⁷¹

Filamenting temperature sensitive proteins play a central role during bacterial cytokinesis, while Z-interacting protein is a membrane-anchored protein in gram negative bacteria which forms the septal ring, a collection of these proteins (FtsZ) which localise at the site of cell division and regulate this process.⁹⁰ FtsZ which is the

most highly conserved protein present in all bacteria, except *Chlamydia spp*, and is essential for cell division.⁸⁶ FtsZ is responsible for recruiting and coordinating more than a dozen other proteins required for cell division.⁹⁰⁻⁹² In *E. coli*, temperature sensitive mutations in the FtsZ gene inhibit cell division therefore limiting cell growth. Up-regulation of *Wolbachia* FtsZ gene expression is found in fourth-stage larvae and adult female worms containing mf which could prove a promising target for anti-*Wolbachia* drug development, with several small molecule inhibitors of FtsZ having been identified.⁹³⁻⁹⁵ ZipA is also recognised as a new target for antimicrobial drug development, with a number of potential hits which have been identified through high-throughput screening (HTS).⁹⁶

1.4.3 Treatments to remove *Wolbachia* bacteria from hosts

Treatment of *Wolbachia*-infected nematodes with antibiotics has been shown to result in sterility and eventually death of nematodes.^{4,97} Typically long-term sterilization, as well as adult-killing of *O. volvulus* and lymphatic filarial nematodes (*B. malayi* and *W. bancrofti*), occurs using three to eight-week courses of antibiotic treatment.⁹⁸⁻¹⁰³ Treatment of filarial diseases with antibiotics can avoid the adverse effects associated with filaricidal therapies which causes severe inflammatory reactions at the site of worm death due to the release of *Wolbachia* bacterium and other endogenous substances, as discussed previously.^{104,105} Testing the effects of tetracycline's, both doxycycline and minocycline (**Fig. 1.8**), on *Wolbachia*-containing filarial nematodes has suggested that antibiotics have the potential to be macrofilaricidal in humans which presents a potential new approach for the treatment of a range of filarial infections.

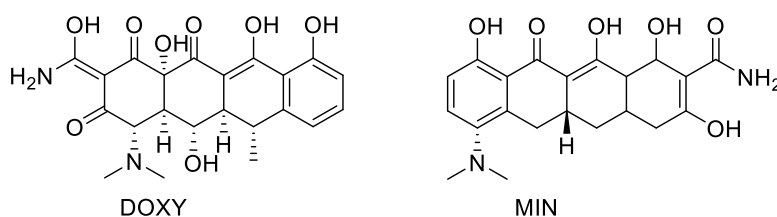


Fig 1.8 Structure of the antibiotics doxycycline (DOXY) and minocycline (MIN) respectively.

A microscopic image displaying the effects of doxycycline on female adult worms following 18 months of treatment with doxycycline is displayed in **Fig. 1.9**; *Wolbachia* cells are shown in red and microfilariae contained within oocytes are coloured blue,⁴ this figure shows reduced *Wolbachia* burden within the female worm cells following treatment with doxycycline. Female nematodes have proven to be more sensitive to tetracycline antibiotics than males nematodes^{30,106} which is likely due to increased *Wolbachia* levels in female worms due to the positive effects that *Wolbachia* bacteria has on embryogenesis.

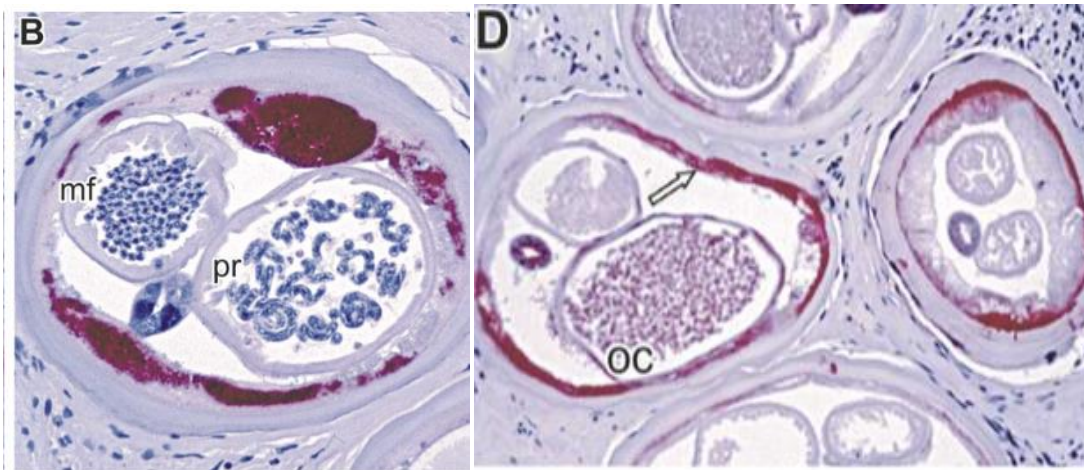


Fig 1.9 Microscopic images displaying the anti-*Wolbachia* efficacy of doxycycline after 18 months; Image B: untreated female worm cells, Image D: doxycycline treated cells. Figure adapted from the work of Hoerauf *et al.*⁴

The macrofilaricidal effects observed with antibiotic therapy have been associated with the depletion of *Wolbachia* which leads to the degeneration and sterility of adult worms.^{59,65} **Fig. 1.10** provides a pictorial representation of doxycycline's efficacy within a clinical setting. The images depict the effects of a six-week treatment plan following an 18-month observation period



Fig 1.10 Doxycycline's clinical efficacy against LF after 6 weeks of treatment and following an 18-month observation period. (Unpublished, personal communication from Mark Taylor).

Tetracycline antibiotics have been used for over half a century and act *via* inhibition of protein synthesis during amino acid translation through binding to the 30S ribosomal subunit in the mRNA translation complex of gram-positive and gram-negative bacteria. Doxycycline completely suppresses normal early-stage embryonic development of *Wolbachia* in nematodes which is followed by a progressive loss of intact sperm-cell formation, spermatogenesis. The effects of doxycycline on mf densities were found to be slow compared to that of IVM and DEC,⁴ this is a benefit of antibiotic-mediated therapy since the inflammation which is often seen with rapid acting filaricidal treatments, is avoided.

Doxycycline has been shown to have negative effects on the development of bones and teeth in infants and babies when taken by woman during pregnancy;¹⁰⁷ consequently the use of doxycycline is contraindicated in infants and pregnant women. As with all tetracycline antibiotics, doxycycline is also known to cause skin photosensitivity and drug induced lupus. Also, to gain sufficient efficacy against *Wolbachia*, long treatment periods, of at least 4 weeks are required. To efficiently treat conditions such as LF and onchocerciasis, it is necessary to shorten these treatment periods and is therefore necessary to find alternative drugs which require shorter treatment plans. It is also possible that 'resting' bacteria may begin to multiply in worms 3-15 years following doxycycline treatment.⁴ These dormant organisms are thought to represent a persistent non-replicating form of the bacteria with greatly reduced antibiotic susceptibility which could explain the difficulties in achieving complete *Wolbachia* depletion. Similar observations have been reported for other parasites infected with intracellular bacteria such as chlamydia,³⁰ anaplasma¹⁰⁸ and mycobacterium.¹⁰⁹

As has been discussed earlier, *Wolbachia* expulsion at the site of worm-death contributes to the inflammatory responses associated with filaricidal therapies. There is however evidence to suggest that the anti-filarial effects exhibited by antibiotics is a consequence of dead or dying *Wolbachia* cells that have been expelled from the worm and are toxic to the surrounding nematode tissues.¹¹⁰ Accelerated *Wolbachia* clearance from nematodes is observed following drug withdrawal which could be associated with a greater capacity of the host cells to eliminate the damaged bacteria.¹¹¹ This observation could also be a result of the high concentrations of tetracycline therapy which inhibits mitochondrial lipid metabolism resulting in a toxic effect associated with abnormal lipid retention within cells termed steatosis.¹¹²

Minocycline has been shown to have similar anti-*Wolbachia* activity to doxycycline *in vitro* with improved *in vivo* efficacy, therefore making it an ideal candidate for further pharmacokinetic and pharmacodynamic (PK and PD) investigation.¹¹³ At bioequivalent exposures, minocycline was found to deplete *Wolbachia* levels by more than 99% after a 28-day treatment regimen in a *Brugia malayi* murine model. Although this data is promising, minocycline is subject to a risk of more severe adverse effects than doxycycline¹¹⁴ and further work is therefore required to evaluate the efficacy of minocycline within a clinical setting.

Rifampicin (**Fig 1.11**) is a bactericidal antibiotic which is the second most commonly used for anti-*Wolbachia* therapy and acts *via* inhibition of DNA-dependent RNA polymerase, causing the inhibition of DNA synthesis.^{115,116} Rifampicin has been shown to deplete mf release from adult female worms with low concentration therapies and is known to kill both adult worms and mf with higher-concentration treatment plans.¹¹⁷ Longer observation periods following rifampicin treatment have shown a less pronounced effect on *Wolbachia* depletion than is seen with doxycycline therapy which can result in greater than 90% depletion of *Wolbachia* from *B. malayi* adult worms and mf.¹⁰³

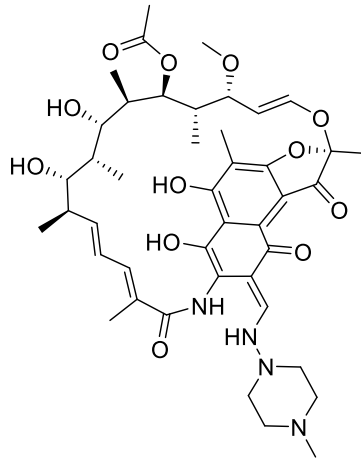


Fig 1.11 Structure of the antibiotic rifampicin

Rifampicin is known to cause hepatotoxicity and is also responsible for the up-regulation of many CYP450 enzymes which can cause a number of adverse effects when taken with other drugs.^{118,119}

In summary, *Wolbachia* is an essential endosymbiotic bacterium within filarial worms which offers a novel target for chemotherapeutic intervention. Drugs targeting *Wolbachia* will be prophylactic, curative and macrofilaricidal. Due to its high efficacy; well understood mechanism of action, minimal associated adverse effects when compared to rifampicin and minocycline and finally proven clinical efficacy, doxycycline is considered the current gold-standard for anti-*Wolbachia* therapy. However, doxycycline requires a long treatment plan of at least 4 weeks and is contraindicated in pregnant women and children. This is problematic within MDA programs and therefore hampers transmission blocking and limits efforts towards disease eradication.

Having highlighted the urgent need for improved therapies to treat LF and onchocerciasis. The main aims of this research project will now be covered, followed by results and associated discussions.

1.5 Aims

Anti-*Wolbachia* therapy delivers safe macrofilaricidal activity with superior therapeutic outcomes compared to all standard anti-filarial treatments. In principle, this treatment can be achieved with currently registered drugs such as doxycycline which is both affordable and available to endemic communities. The main barriers to doxycycline use are the required long treatment period (4-6 weeks) and contraindication in children under eight years of age and pregnant women. Therefore, the primary goal of the Anti-*Wolbachia* drug discovery and development programme is to identify alternate drugs that are suitable for a wider patient range and require shorter treatment regimens (7 days or less). A secondary goal is to refine and develop regimens of existing antibiotics suitable for a more restricted use that is compatible with MDA prior to the availability of a new

regimen resulting from the discovery project. This developed regimen could serve as a successful treatment in individuals with high loiasis co-infection at risk of severe adverse effects upon ivermectin treatment.

The objective of this current work is to optimise small molecule Anti-*Wolbachia* agents to provide novel chemotherapeutic molecules that are also suitable for clinical development or that can behave as a suitable series of drug compounds to support other candidate compounds selected from within the program. The selected molecular candidate will ideally possess an excellent DMPK profile which translates to good exposure and activity within the *in vivo* Severe-combined immunodeficient (SCID) mouse model. The Target candidate profile for a suitable lead should be able to deplete >99% of the *Wolbachia* within the *in vivo* model during seven days of treatment. Identification of such a compound will involve a rigorous discovery, lead optimization and candidate selection process from work within the AWOL II: Macrophilicidal drug discovery program.

1.6 Identification of small molecule anti-*Wolbachia* agents

1.6.1 Target vs Phenotypic screening

Structure-based drug discovery usually starts with the identification of a target of interest for a disease state. This can normally be elucidated through clinical observations of patient phenotypes or screening of chemical libraries against specific enzymes or cells. Knowledge of the molecular target can assist the development of SAR in new drug compounds.^{120,121,121} Known natural substrates of targets can offer insight into the pharmacophores that are essential for biological activity. Target-based assays can sometimes express higher concentrations of the target protein than the native biological system which may lead to inaccurate efficacy readouts.¹²² These assays unfortunately limit the identification of drugs with novel targets to those which act against targets with target-based assays available.¹²³ Finally, hit compounds resulting from target-based screening need to be tested in cell-based or phenotypic assays containing a range of targets and complexes which can interact with the optimised candidate to discover if translation is seen from the target-based screen.

^{124,125}

Consequently, phenotypic drug discovery is carried out without knowledge of the drug target, using a whole-cell based assay approach. This encompasses greater complexity as cells are expressed in their native environment making the assay generally more physiologically relevant. Phenotypic screening is useful in identifying new targets for the treatment of diseases which can occur through screening large libraries of compounds or repurposing known drugs for new indications. Repurposing known and well understood drugs for new indications can save time and resources during compound development.^{126,127} Cell viability assays are one of the most common phenotypic assays where active compounds are identified which kill cells, these assays are commonly used in the search for anti-cancer and bactericidal agents.

1.6.2 *In vitro* assay development

Early in this research project, the AWOL consortium developed a cell-based assay containing the whole *Wolbachia* organism as the primary *in vitro* screen. This allowed rapid and sensitive screening of chemical libraries, where a mosquito (*Aedes albopictus*) cell line was infected with the *Wolbachia* bacteria.¹²⁸ Following incubation with compounds, the remaining *Wolbachia* surface protein (*wsp*) is measured using a quantitative PCR readout with each viable *Wolbachia* cell containing one *wsp*.¹²⁹ More recently, the primary assay has been enhanced to allow for higher throughput by using an Operetta imaging system to image fluorescently stained non-viable *Wolbachia* cells following compound incubation, which removes the need for quantitative PCR. This assay now forms the primary screen in our anti-*Wolbachia* screening cascade within the project which is carried out by the Liverpool School of Tropical Medicine.

1.6.3 HTS: Chemotype identification

Similarity searching is a procedure which was described over 20 years ago, by which it is possible to scan through the chemical space of a large library of compounds and rank the compounds by their similarity to a reference compound or user defined set of queries representing a collection of compounds.¹³⁰ These queries, from a medicinal chemistry standpoint, are usually the most common attributes that a set of known bioactive molecules possess. It has therefore become a valuable tool for identifying novel bioactive molecules. Searching through a chemical library for compounds with similar chemical properties should elucidate several compounds which possess similar activity at a biological target. 1D Molecule descriptors are numerical values which represent a property that the compound possesses such as; molecular weight, heteroatom count, number of rotatable bonds, logP etc. 2D descriptors are more complex and can be used as queries, searching for size and degrees of branching.¹³⁰

An initial screen of 10,000 compounds from the BioFocus diversity library yielded 50 actives (hit rate of 0.5%) which were then used as queries in a range of similarity searches of the 500,000 compounds from within the Medicines for Malaria Venture (MMV) library, this HTS cascade is summarised in **Fig.1.12**. Following the initial screen, there was sufficient knowledge of active and inactive molecules to develop machine learning models with the hits and misses from Screen one informing the similarity searching for Screen two and these results then informed the second screen of the MMV library (Screen

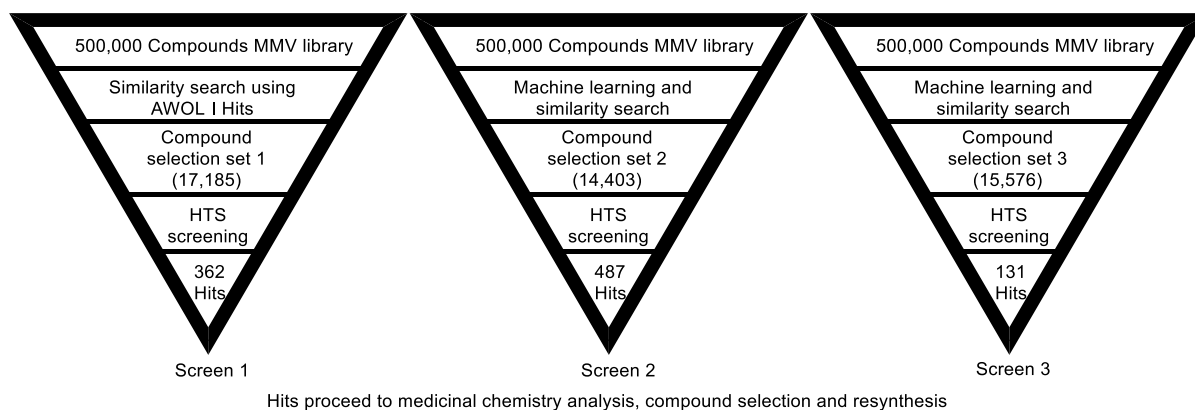


Fig 1.12 HTS screening cascade for three screens of the MMV library

The screening resulted in several templates suitable for medicinal chemistry optimisation, identifying compounds suitable for candidate selection and subsequent pre-clinical studies. The initial screen of the BioFocus diversity library generated several hits within six possible templates which are suitable for further investigation (**Fig 1.13**). Hits were defined as active if they possessed > 50% of doxycycline activity and potent hits if they possessed > 90% of doxycycline's activity.

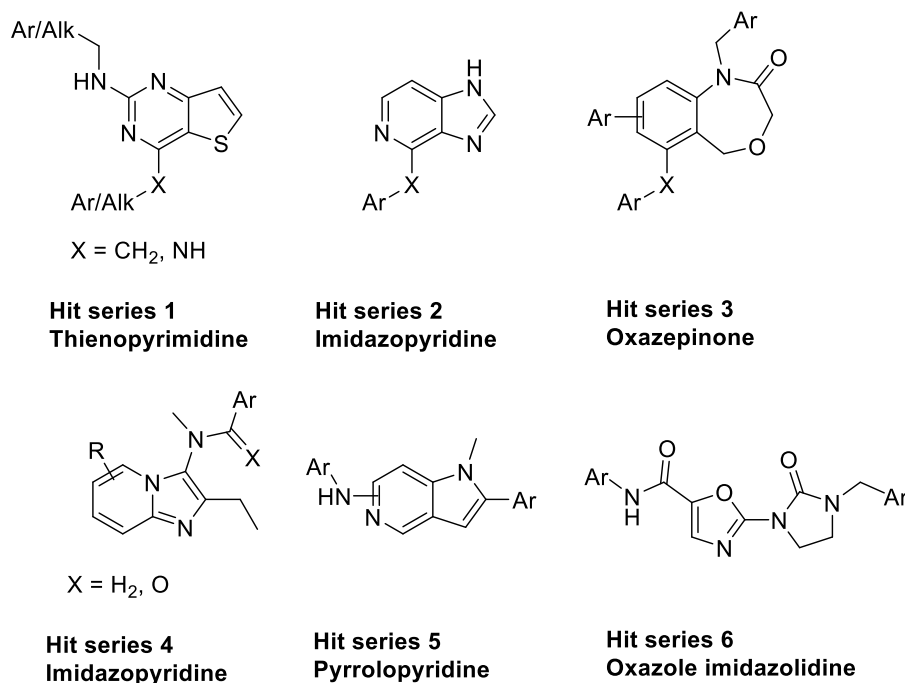


Fig. 1.13 The six templates identified from screening the BioFocus Diversity Library

These six templates were then investigated by medicinal chemists at the University of Liverpool or by external partners WuXi App Tech. Screening of the MMV library also identified several additional templates as starting points for medicinal chemistry optimisation (**Fig. 1.14**), these templates were also investigated at the University of Liverpool or WuXi App Tech.

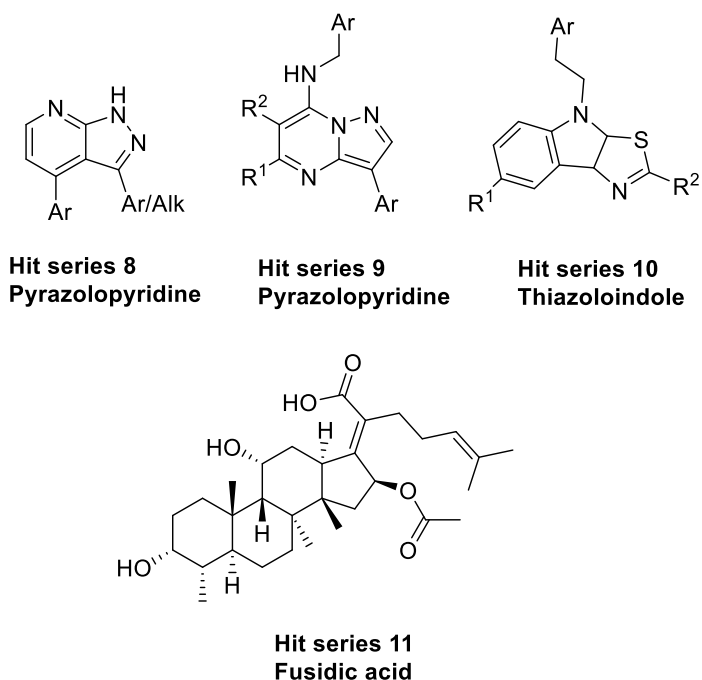


Fig. 1.14 The four templates generated from the MMV Diversity Library

Phenotypic screening of the MMV library identified 45 hits within the pyrazolopyrimidine template (Hit series 9 **Fig. 1.14**) which displayed potent anti-*Wolbachia* activity. One of the most promising hits from this chemotype is displayed in **Fig. 1.15**. It contained the 7-(2-pyridylmethanamine) motif, an allyl group at the 6-position and a phenyl ring at the 3-position of the pyrazolopyrimidine core. A generalised structure for this template is depicted in **Fig. 1.15** with the numbering system for the core scaffold displayed.

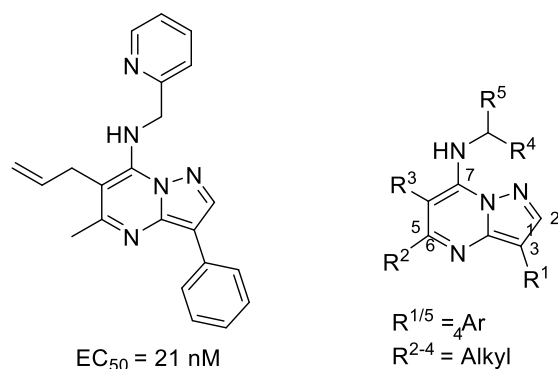


Fig 1.15 Initial hit for the pyrazolopyrimidine template and a General structure

1.7 Strategy for the discovery of small molecule anti-*Wolbachia* agents

1.7.1 Screening cascade

The overall screening cascade used for our medicinal chemistry optimisation is presented in **Fig 1.16** where the experimental read-outs were used to drive and inform the molecular design highlighted. Target compound design was guided by Drug-Metabolism and Pharmacokinetics (DMPK) predictions, carried out by AstraZeneca, since the primary objective of this work was to improve DMPK properties as the potency of this chemotype was demonstrated in the initial hit. Evaluation of *in vitro* potency was performed in parallel to *in vitro* DMPK analysis on all synthesised compounds.

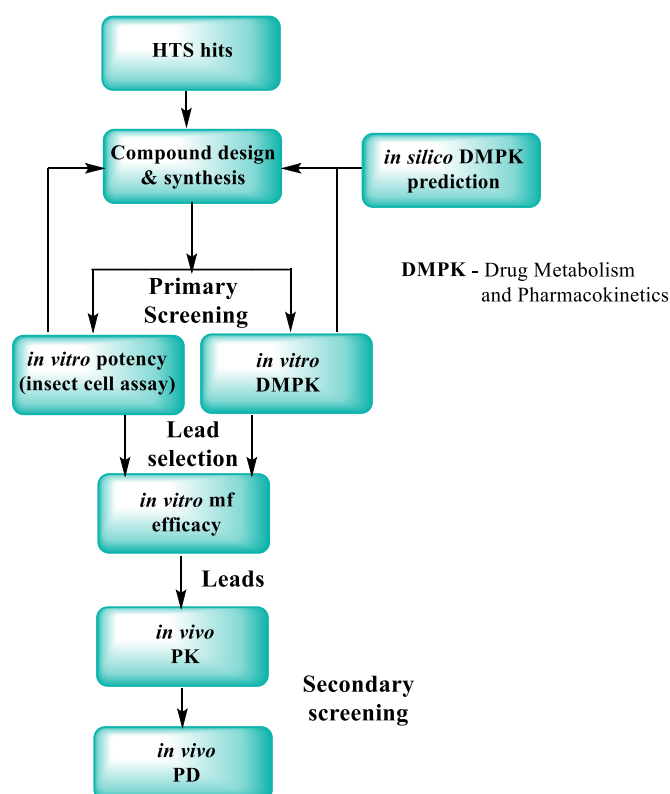


Fig. 1.16 Screening cascade for the design, synthesis and testing of new compounds.

In vitro potency evaluation was carried against a C6/36 (wALbB) cell line which has been described previously.¹³¹ Briefly, this is a mosquito (*Aedes albopictus*) derived cell-line which has been stably infected with *Wolbachia pipientis* (wALbB). Small molecule anti *Wolbachia* agents were dissolved in DMSO with each compound added to two wells of a 384-well plate (assayed in duplicate) giving a final concentration of 5 μ M. Control samples in each plate consisted of 12 wells of vehicle control (DMSO) and 6 wells of the following controls: 5 μ M doxycycline (positive control— the gold standard for *Wolbachia* reduction; SigmaAldrich) and a suboptimal 50 nM doxycycline concentration. After seven days of sterile incubation at 26 °C, DNA staining media was added to each well which caused staining of the host cell nucleus and the *Wolbachia*. The Operetta

high-content automated imaging system (PerkinElmer) and the Perkin Elmer software Harmony were used to measure the fluorescence resulting from 6 fields (6 pictures) per well. The system locates the nucleus, then the cytoplasm and uses an algorithm to determine how 'spotty' the remaining cytoplasm appears, cytoplasm containing a large amount of *Wolbachia* will have a high spot edge ridge (SER) texture score but doxy treated cells with no *Wolbachia* will have a low score (Fig 1.17).

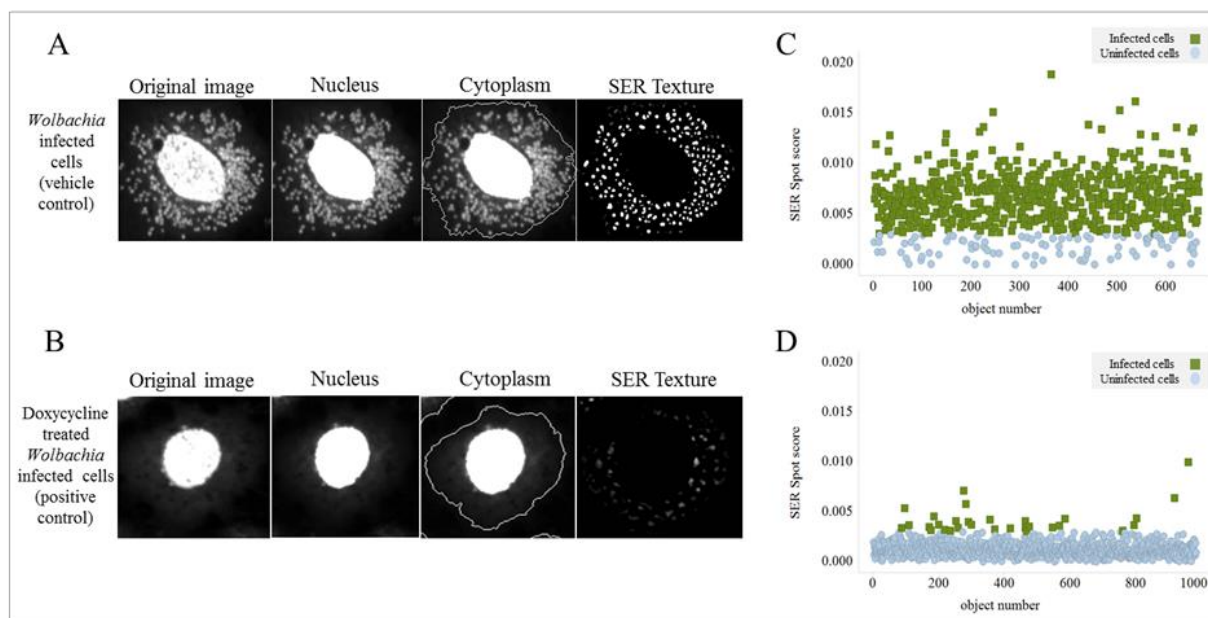


Fig 1.17 Operetta fluorescence imaging and SER texture scoring readout for *Wolbachia* infected cells.

Images C and D in Fig 1.17 represent the readout from each well with each dot representing one cell, a threshold is set on the texture score and all cells above that score are classified as infected and below the score classified as uninfected. From this readout, each well has a % number of infected cells calculated, where DMSO control cells will have infection levels of >70% and DOXY or hit-treated cells will have <20% infection level. Some of the best compounds with a good balance of activity and DMPK properties were then advanced into the *in vitro* *Brugia malayi* mf efficacy screens.

The *in vitro* mf assay was developed to provide a link between the *in vitro* insect cell-based assay and *in vivo* *B. malayi* screening, to enable greater throughput whilst actively seeking compounds with the ability to reduce *Wolbachia* load in the targeted parasite. The compounds were incubated in five wells with 8000 *B. malayi* mf for six days before DNA extraction and performing qPCR to calculate the ratio of *Wolbachia* Surface Protein (*wsp*) copy number to Glutathione S-Transferase (*GST*) copy number, which is used as a worm-size biomarker in drug treated wells versus control wells. This gives a good indication of the remaining *Wolbachia* load accounting for larger worms which would initially possess a higher *Wolbachia* count. The most optimal compounds which emerge from secondary screening were advanced to the *in vivo* PK and PD study within SCID mouse model infected with larvae of *B. malayi* (See Chapter 4).

The anti-*Wolbachia* activities observed from the two *in vitro* assays may differ slightly due to differences in strains and biomass of *Wolbachia* in these two assays. In general, tested compounds show higher EC₅₀ in the Mf assay than in the insect cell line assay, and the translation of anti-*Wolbachia* potency from the mf assay to

in vivo efficacy is clearer than the one from insect cell line assay.¹³² This may demonstrate the increased difficulty that compounds have diffusing across multiple membranes into bacteria which reside within the internal organs of nematodes.¹³³ In order to obtain sufficient exposure within a biological system it is essential that our compounds possess suitable DMPK properties.

1.7.2 Drug-metabolism and Pharmacokinetics (DMPK)

For over a decade, medicinal chemists have been aware of desirable molecular properties which constitute promising drug compounds. Lipinski *et al.*, published a set of guidelines which molecules should ideally fall within if they are likely to possess good oral bioavailability.¹³⁴ This 'rule of five' predicts that poor absorption or permeation is more likely to occur for a compound that fails two or more of the guidelines: possesses greater than 5 H-bond donors, 10-H bond acceptors, a molecular weight of 500 or a ClogP value of 5. Hansch *et al.*, stated in 1987, that prospective drug compounds should be as hydrophilic as possible without compromising efficacy.¹³⁵ This has been further explained as a measure of lipophilic ligand efficiency.^{136,137} More recently, the GlaxoSmithKline 4/400 rule has been proposed to provide a more accurate set of guidelines to highlight promising drug-like space.¹³⁸ The 4/400 rule states that compounds with a molecular mass between 250-400 and a CLogP value between 2-4, will more likely have a favourable absorption, distribution, metabolism, excretion and toxicity (ADMET) profile.¹³⁸⁻¹⁴⁰ These early property design efforts allow the development of SAR to be directed towards designing compounds with good oral bioavailability by setting specific goals and using predictive computational methods prior to synthesis.¹⁴¹ During work on this project, *in silico* DMPK predictions were carried out as discussed above (**Fig. 1.16, Chapter 1.9.1**) by our collaborators, AstraZeneca, and used to direct compound design to prioritise synthesis.

Following compound synthesis, *in vitro* DMPK analysis was also performed by AstraZeneca, including logD determination, an aqueous solubility, metabolic stability assessment and plasma protein binding studies.

A thermodynamic solubility assay was performed using a stock solution of DMSO where a known amount of compound can be dried and dissolved in phosphate buffer. After shaking for 24 hours the solution was then filtered and the resulting concentration analysed by LCMS and HPLC.

Lipophilicity (LogD_{7.4}) was measured using a shake flask method by adding a stock solution of DMSO to a 1:1 mixture of octanol and phosphate buffer solution to give a 10 µM compound concentration. The solutions were shaken for three hours to equilibrate before separating the layers and diluting them several times. The ratio of the compound concentration was analysed within the diluted samples by UPLC-MS/MS and used to calculate the LogD values.

Human plasma protein binding (PPB) was measured by addition of compounds (10 µM) to phosphate buffered saline and incubated for 3 hours, proteins were then precipitated by the addition of acetonitrile and the centrifuged supernatant analysed by LC-MS/MS. The percentage human plasma protein binding as expected to be seen following compound dosing was determined by $(\text{total plasma concentration} - \text{free concentration}) / (\text{total plasma} + \text{buffer concentration}) \times 100$.

Rat hepatocyte clearance (*R.Heps.CL*) and human microsomal clearance (*H.Mic.CL*) were measured by equilibration of substrate with hepatocyte cells or microsomal proteins before activation of the metabolic reactions by addition of 1-aminobenzotriazole or β -NADPH respectively. At eight time points, ranging up to 120 minutes, aliquots were removed and quenched with methanol before sedimentation of precipitated proteins and quantification of remaining substrate using HPLC/MS. Microsomes retain activity of key metabolising enzymes that reside in the smooth endoplasmic reticulum, such as cytochrome P450s (CYPs), flavin monooxygenases and glucuronosyl-transferases. Hepatocytes offer a valuable insight into a broader scope of enzyme reactions than microsomal studies including reticular systems, cytosolic and mitochondrial enzymes.

A traffic light system will be used within the results chapters of this thesis to document and visualise desirable, acceptable and poor *in vitro* potency and DMPK properties where favourable properties are coloured green, acceptable parameters are coloured amber while poor/unacceptable properties are shown in red. The boundaries for these different properties are documented below in **Table 1.1** which are supported by a number of analyses carried out recently on tractable chemical space and DMPK properties.^{139,142}

	EC₅₀ (nM)	LogD 7.4	Aq.Sol (μM)	H.M.Cl (μL/min/mg)	R.HepsCl (μL/min 10⁻⁶)	Human PPB (%)
Desired	<100	1-4	>50	<20	<20	<99
Acceptable	100-300	0-1,4-5	20-50	20-60	20-60	<99.5
Poor	300+	<0, >5	<20	>60	<60	>99.5

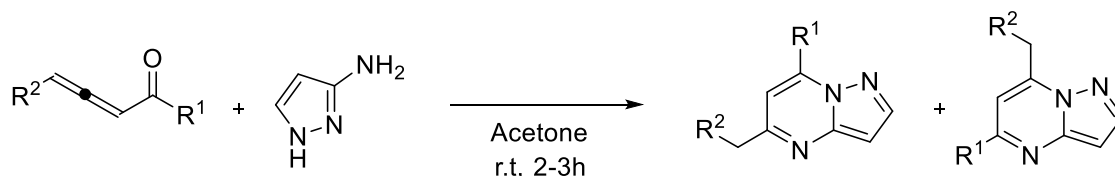
Aq.Sol – Aqueous solubility, **H.M.Cl** – Human microsomal clearance, **R.HepsCl**– Rat hepatocyte clearance, **Human PPB** – Human plasma protein binding

Table 1.1 Appropriate and inappropriate potency and DMPK values and margins.

These potencies and DMPK parameters will be optimised throughout the studies on this pyrazolopyrimidine chemotype. There are many advantages to prospective drug compounds possessing enhanced metabolic stability; the increased bioavailability and longer half-life ($t_{1/2}$) should allow for less frequent dosing and improve patient compliance of any resulting candidate. Improvement of metabolic stability should also reduce intra-patient variability in drug exposure as this is majorly affected by differences in patient drug metabolising capacity.¹⁴³ Reduction in clearance from different species should allow for better extrapolation of animal data and in turn, more accurate PK prediction in humans.¹⁴⁴ Finally, improving aqueous solubility (reducing overall lipophilicity/logD) will improve absorption and should also improve the metabolic stability since the binding sites of metabolising enzymes are lipophilic in nature and readily accept more lipophilic molecules.¹⁴⁵

1.7.3 Development of synthetic methodology and biological relevance of Pyrazolopyrimidines

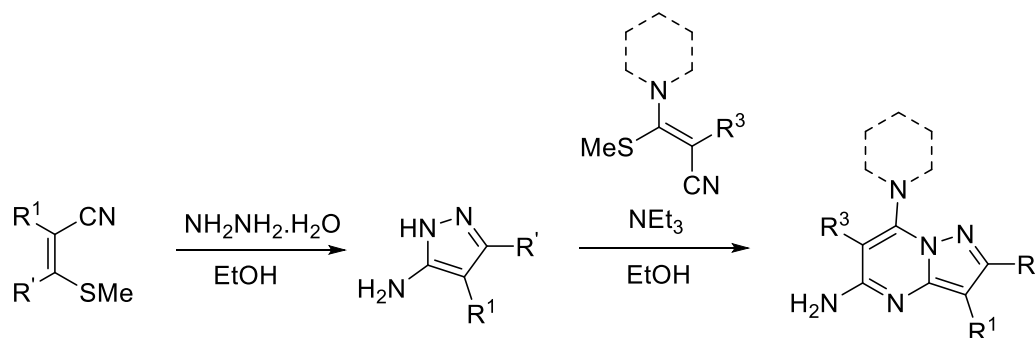
Synthesis of pyrazolopyrimidines is commonly achieved by the condensation of 3-amino pyrazole with either; a 1,3 dicarbonyl compound¹⁴⁶, 1,2 allenic ketones¹⁴⁷, enamines¹⁴⁸ or enamine nitriles.¹⁴⁹ The use of 1,2 allenic compounds has its advantages including the use of mild reaction conditions (**Scheme. 1.1**) and for the substrates studied by the authors F.Xuesen *et al.*, high yielding (75-95%) reactions.¹⁴⁷



Scheme 1.1 Synthesis of pyrazolopyrimidines by condensation of 3-amino pyrazole with 1,2 allenic compounds.

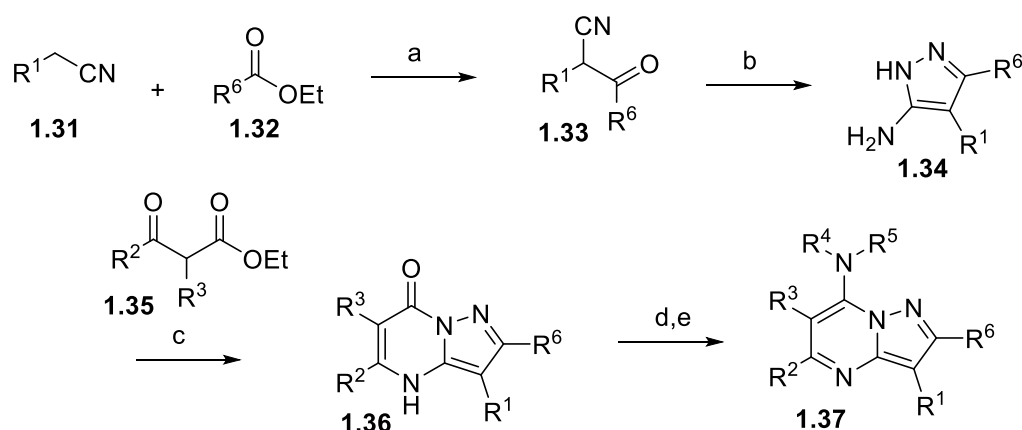
The described reaction proceeds efficiently in a variety of polar aprotic solvents by reaction of the amine with the central allene carbon, allowing the pyrazole to react at the ketone carbonyl group. This gives the major product with the R² group adjacent to the pyridine nitrogen, along with trace amounts of the regio isomer.¹⁴⁷ This reaction is useful for the introduction of a variety of aliphatic or aryl groups at the 5- and 7- positions and has been successfully applied to produce pyrazolopyrimidine nucleoside analogues.¹⁴⁷ To introduce an amine at the 7-position of the pyrazolopyrimidine core, an alternative strategy would be needed as the amide starting material would most likely be much more difficult to react *via* the above procedure.

Another possible approach would induce the condensation of a 3-amino pyrazole with an enamine nitrile. These pyrazole starting materials can be produced by reaction of the necessary nitrile with hydrazine (**Scheme. 1.2**).¹⁵⁰ the resulting intermediate can then be reacted with the enamine nitrile to give a secondary amine opposite the pyrimidine nitrogen of the pyrazolopyrimidine core.¹⁴⁹



Scheme 1.2 Synthesis of various pyrazole starting materials and pyrazolopyrimidines

These reactions allow for the installation of an amine adjacent to the pyridine nitrogen at the 5-position, with various secondary amines at the 7-position of the pyrazolopyrimidine core. To produce pyrazolopyrimidines comparable to the hit molecule (**Fig. 1.15**), it is necessary to install a primary amine at the 7-position. The synthesis of similar pyrazolopyrimidine compounds have been reported with a number of pharmacological implications including their behaviour as kinase inhibitors, K⁺ channel blockers and anti-depressants.^{151–161} More specifically, pyrazolopyrimidines can act as anxiolytics *via* antagonism of the human corticotrophin releasing factor-1 (CRF-1) receptor¹⁶¹ and as anti-cancer agents by inhibition of the cyclin-dependent kinase-2.¹⁵⁹ A robust method by which 7-aminopyrazolo pyrimidines can be generated has been reported by the group of J.Y Hwang *et al.*, during optimisation of analogues as hepatitis C virus inhibitors. Throughout their work, J.Y Hwang *et al.*, synthesised many compounds with various groups in the R^{1–6} positions, a general scheme for this synthesis is outlined in **Scheme.1.3**.¹⁵³



Scheme. 1.3 Reagents: (a) Na, EtOH, reflux; (b) N₂H₄, EtOH, reflux; (c) beta-ketoester, AcOH, 110°C, 3h (d) POCl₃, 100°C, 1h (e) R⁴R⁵NH, DIPEA, DMF, rt, overnight.¹⁵³

The amino pyrazole **1.34** is formed by reaction of the necessary nitrile **1.31** with the substituted ethyl ester **1.32** and the formed alpha cyano-ketone **1.33** can be treated with hydrazine before subsequent cyclocondensation with the dicarbonyl compound **1.35** to give the pyrazolopyrimidine core. Chlorination of the intermediate **1.36** and subsequent substitution with various amines can provide many target compounds.

The authors found that ortho-chlorination of the phenyl ring at the R¹ position resulted in over a 30-fold increase in binding affinity for the CRF-1 receptor over the unsubstituted phenyl analogue **10a** (**Fig 1.18**). The 4-chlorophenyl derivative also possessed improved binding affinity and combination of these beneficial modifications resulted in compound **10d** with high affinity for the CRF-1 receptor. Finally, modification of the R⁴ and R⁵ positions from the initial ethyl and butyl group to a propyl and the cyclopropyl methyl side chain in **10j** further improved compound potency.

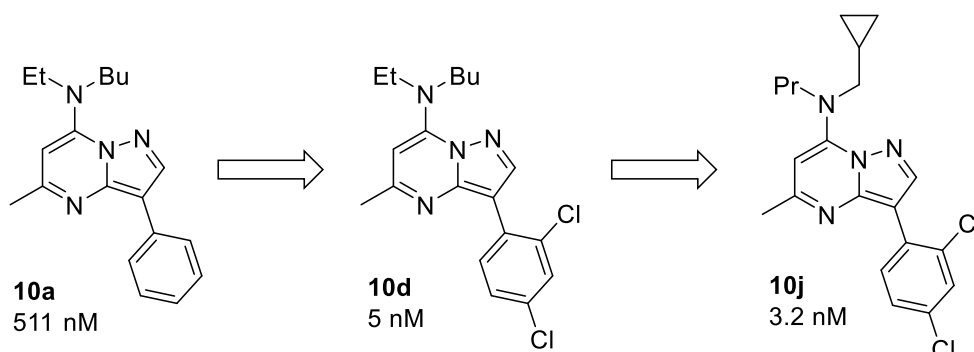
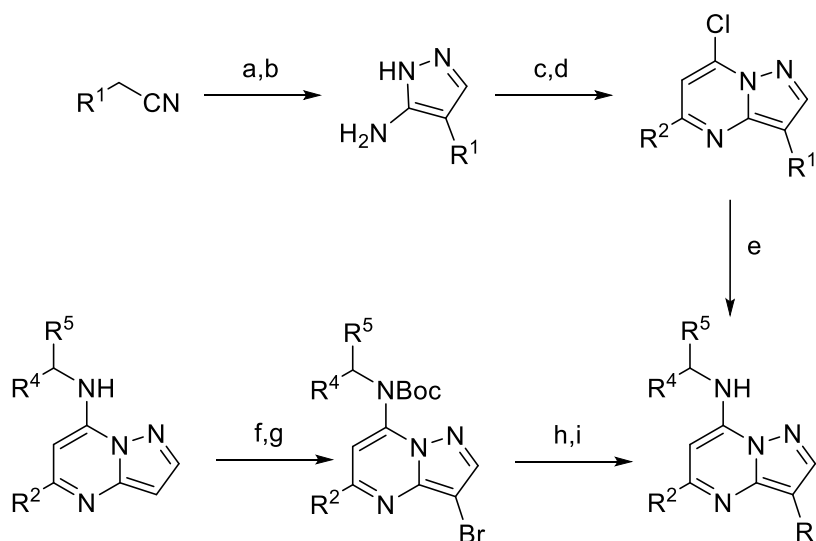


Fig 1.18 Optimisation of a series of CRF-1 receptor antagonists

During their studies, a variety of pyrazolopyrimidines with high affinity for the CRF-1 receptor were characterised. Further studies detailing the consequences of their antagonistic effects towards the CRF-1 receptor *in vitro* and *in vivo* are underway. Pyrazolopyrimidines have also been designed as cyclin-dependent kinase inhibitors, synthesised by K.Paruch *et al.*, using a more diverse synthetic route which allows for easier customisation of the R¹ position: their synthesis is depicted below in **Scheme. 1.4**.¹⁶²



Scheme. 1.4 Reagents: (a) HCO₂Et *t*-BuOK, THF; (b) N₂H₄, AcOH, EtOH; (c) R²COCH₂CO₂Me, PhCH₃; (d) POCl₃, *N,N*-dimethylaniline; (e) R⁴R⁵NH₂, DIPEA, dioxane, (f) Boc₂O, DMAP, CH₂Cl₂; (g) NBS, CH₃CN; (h) R¹B(OH)₂, Pd(PPh₃)₄, Na₂CO₃, DME:H₂O; (i) TFA, CH₂Cl₂¹⁶³

This synthesis enables late-stage functionalisation of the R¹ position *via* coupling with various aryl boronic acids, which represents an attractive design route concerning study of this position.

Some of the most promising analogues resulting from this body of work are displayed below in (**Fig 1.19**) alongside the initial hit. The authors elucidate that substitution at the R¹ position is important for promoting potent inhibition of CDK-2 (**14j**) as is halogenation of the phenyl ring at the R² position (compounds **5** and **14j** as named by the authors). The 3-pyridyl methanamine side chain at the 7 position of the pyrazolopyrimidine core provides the most potent inhibitors, forming the N-oxide of this ring in forming **15j** allows for greater selectivity against CDK-2 over other CDK's.

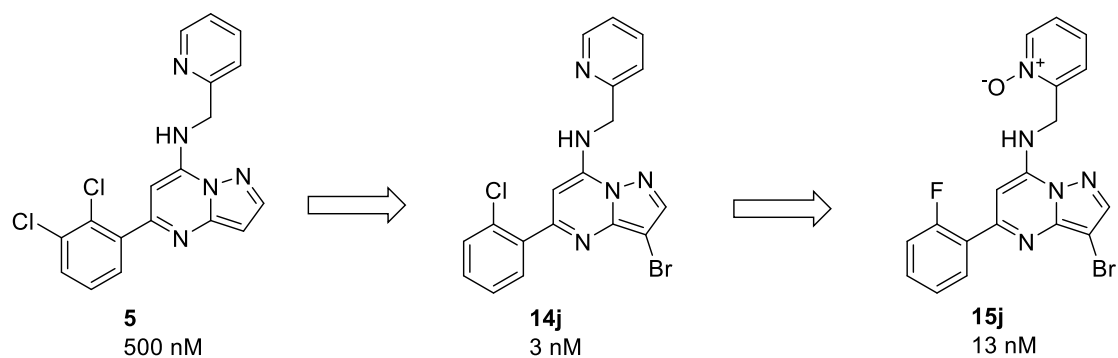


Fig 1.19 Optimisation of a series of selective CDK-2 inhibitors¹⁶²

Compound **15j** was screened against a panel of 50 kinases without observing any CDK cross-reactivity demonstrating its selective potency against CDK-2. This compound was moderately protein-bound in 17 different tumour cell-lines demonstrated clonogenic IC_{50} values in the range 120-390 nM. **15j** was orally bioavailable and demonstrated efficacy in a tumour xenograft model in a mouse study at 40 mpk, PO for 10 days observing a 96% tumour growth inhibition. This demonstrates that properly substituted pyrazolopyrimidines can serve as orally bioavailable efficacious CDK2 inhibitors. These results offer encouragement that compounds containing this pyrazolopyrimidine core could be optimised to produce drugs that are orally bioavailable and possess high activity against the *Wolbachia* bacteria.

1.7.3 Initial pyrazolopyrimidine target selection

In the interest of validating the potency of the chemotype identified in original hit (**Fig 1.15**), compounds which were commercially available and contained this template, with the addition of the relevant substituents for our SAR studies, were purchased and tested against *Wolbachia in vitro* (**Fig. 1.20**)

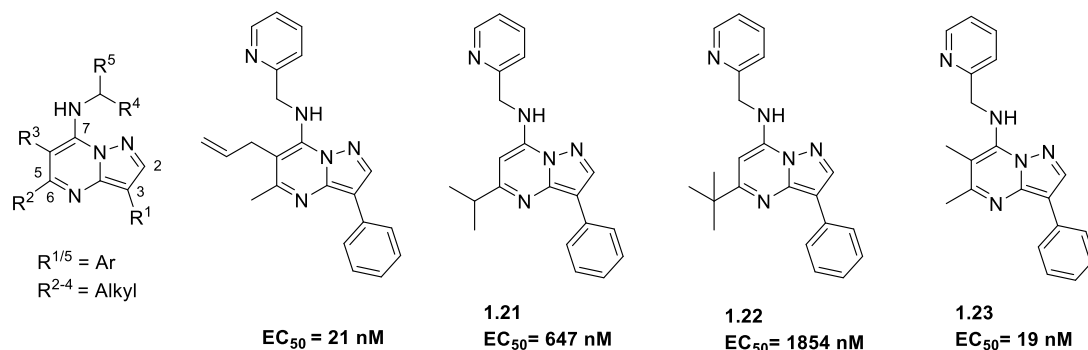


Fig. 1.20 Results obtained from whole-cell assays for commercially available pyrazolopyrimidines

These results validated the high anti-*Wolbachia* activity that this template possesses, with EC_{50} values from the *in vitro* assay measured in the range of 19 nM to 1854 nM (**Fig. 1.20**). One early SAR observation resulting from these compounds, is that extension or branching of the alkyl group at the 5-position appears to result in a significant decrease in anti-*Wolbachia* activity.

The methylene linker at the 7-position of the pyrazolopyrimidine core and allyl group displayed in the initial hit are predicted to be metabolic hot spots. SmartCyp is an online tool used for predicting the CYP450-related metabolic stability of the many different functionalities within a compound. Displayed in **Fig 1.21** are the results calculated for analysing the initial hit using this tool.^{164–168}

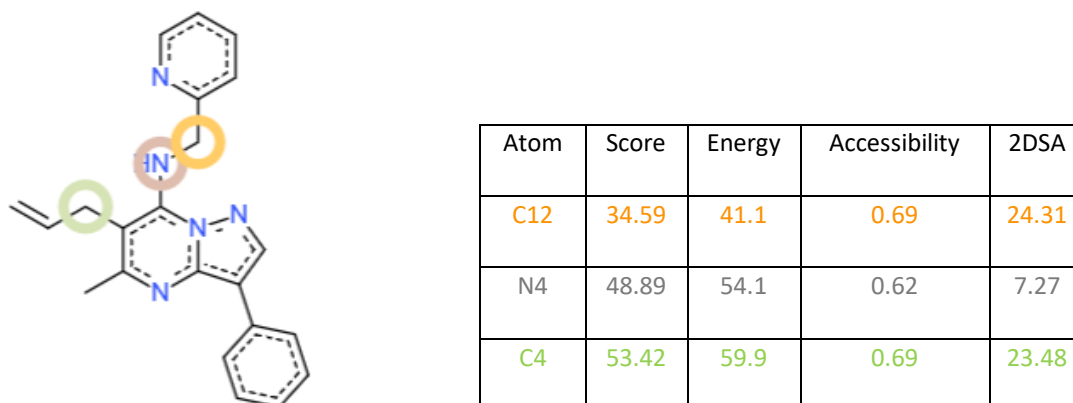


Fig 1.21 SmartCyp scoring information for the initial hit **AWF911**.^{164–168}

The software scores all atoms within a compound, considering their susceptibility to metabolising enzymes, with the three most metabolically labile atoms displayed in the figure and highlighted on the chemical structure. The value ranges from 0 to 998, with lower scores representing less stable atoms. This score is calculated using many parameters including an approximate activation energy for the catalytic site of various CYP450 enzymes with the molecule at specific atoms, the accessibility of an atom to these enzymes, which is the relative measure of topological distance of an atom from the centre of the molecule is (always between 0.5 (atom at the centre) and 1 (atom at the end)) and the solvent accessible surface area (2DSA) which represents the local accessibility of an atom.^{164–168}

These positions were the focus of SAR studies with the specific aim of improving the overall stability of our template. Organic synthesis at the University of Liverpool and WuXi App Tech has enabled extensive functionalization at key positions of the pyrazolopyrimidine core primarily at the 3 and 7 positions (R^1 and $R^{4/5}$ - **Fig. 1.15**), generating over 200 compounds with more than 80 analogues possessing nanomolar activity against *Wolbachia in vitro*, with improved DMPK parameters compared to the initial hit.

Having discussed synthetic strategies towards similar pyrazolopyrimidine compounds, the chosen routes for synthesis of selected compounds and subsequent biological activities will be discussed. Initially the 2-pyridyl ring displayed in the initial hit was modified and study commenced towards modification of the 7-position (R^4/R^5) at the pyrazolopyrimidine core.

All compounds presented within the chapters to follow which are defined by an **AWZ9** compound code were synthesised by the CRO WuXi App Tech while the **AWF9** analogues were synthesised in-house. The detailed experimental and analytical data for these **AWZ9** compounds are contained within **Appendix 1**. To provide a clear justification of the rationale for compound design throughout this work, several of these compounds

have been included and discussed. Mainly, discussions of these compounds centre around biological data however, when relevant for the validation of new chemistry, brief synthetic schemes are presented and discussed during the pyrazolopyrimidine optimisation in the chapters to follow. The SAR studies discussed in the following chapter (Chapter 2) will focus on the 2-pyridyl ring and methylene linker displayed in the initial hit, followed by extensive analysis of the lower phenyl ring at the 3-position of the pyrazolopyrimidine core (Chapter 3). Finally, the current leads from this work are evaluated in Chapter 4 and the advanced biological evaluation of these compounds is displayed and discussed here.

1.8 References

- (1) WHO. WHO map of LF prevalence and MDA status http://gamapserver.who.int/mapLibrary/Files/Maps/LF_2015.png.
- (2) CDC. Biology - Life Cycle of *Wuchereria bancrofti* - 2017 https://www.cdc.gov/parasites/lymphaticfilariasis/biology_w_bancrofti.html.
- (3) Abegunde, A. T.; Ahuja, R. M.; Okafor, N. J. Doxycycline plus Ivermectin versus Ivermectin Alone for Treatment of Patients with Onchocerciasis. *Cochrane database Syst. Rev.* **2016**, No. 1, CD011146.
- (4) Hoerauf, A.; Mand, S.; Volkman, L.; Buttner, M.; Marfo-Debrekyei, Y.; Taylor, M.; Adjei, O.; Buttner, D. W. Doxycycline in the Treatment of Human Onchocerciasis: Kinetics of *Wolbachia* Endobacteria Reduction and of Inhibition of Embryogenesis in Female *Onchocerca* Worms. *Microbes Infect* **2003**, *5* (4), 261–273.
- (5) Fox, L. M.; King, C. L. 110 - Lymphatic Filariasis A2 - Magill, Alan J.; Hill, D. R., Solomon, T., Ryan, E. T. B. T.-H. T. M. and E. I. D. (Ninth E., Eds.; W.B. Saunders: London, 2013; pp 815–822.
- (6) WHO - 2017. Lymphatic filariasis <http://www.who.int/mediacentre/factsheets/fs102/en/>.
- (7) Rana, A. K.; Misra-Bhattacharya, S. Current Drug Targets for Helminthic Diseases. *Parasitol Res* **2013**, *112* (5), 1819–1831.
- (8) Gasbarre, L. C. Effects of Gastrointestinal Nematode Infection on the Ruminant Immune System. *Vet Parasitol* **1997**, *72* (3–4), 327–337.
- (9) Rapsch, C.; Dahinden, T.; Heinzmann, D.; Torgerson, P. R.; Braun, U.; Deplazes, P.; Hurni, L.; Bar, H.; Knubben-Schweizer, G. An Interactive Map to Assess the Potential Spread of *Lymnaea truncatula* and the Free-Living Stages of *Fasciola hepatica* in Switzerland. *Vet Parasitol* **2008**, *154* (3–4), 242–249.
- (10) WHO. Working to Overcome the Global Impact of Neglected Tropical Diseases. *First WHO Report on neglected Tropical Diseases* **2010**.
- (11) Brockarie, M.; Kazura, J.; Alexander, N.; Dagoro, H.; Bockarie, F.; Perry, R.; Alpers, M. Transmission Dynamics of *Wuchereria bancrofti* in East Sepik Province, Papua New Guinea. *Am. J. Trop. Med. Hyg.* **1996**, *54* (6), 577–581.
- (12) Cooper, P. J.; Nutman, T. B. Onchocerciasis. *Hunter's Trop. Med. Emerg. Infect. Dis.* **2013**, 827–834.
- (13) Sharma, O. P.; Kumar, M. S. Essential Proteins and Possible Therapeutic Targets of *Wolbachia* Endosymbiont and Development of FiloBase-a Comprehensive Drug Target Database for Lymphatic Filariasis. **2016**, *6*, 19842.
- (14) Lobos, E.; Ondo, A.; Ottesen, E. A.; Nutman, T. B. Biochemical and Immunological Characterization of a Major Ige-Inducing Filarial Antigen of *Brugia malayi* and Implications for the Pathogenesis of Tropical Pulmonary Eosinophilia. *J. Immunol.* **1992**, *149* (9), 3029–3034.
- (15) WHO. Fourth Report of the WHO Expert Committee on Filariasis. *World Health Organisation Tech Rep Ser* **1984**, 3–112.
- (16) CDC. CDC Laboratory Identification of Parasitic Diseases of Public Health Concern <https://www.cdc.gov/dpdx/diagnosticProcedures/blood/specimencoll.html>.
- (17) WHO. Progress Report of 2000-2009 and Strategic Plan 2010-2020 of the Global Programme to Eliminate Lymphatic Filariasis. **2010**.
- (18) Noroes, J.; Addiss, D.; Amaral, F.; Coutinho, A.; Medeiros, Z.; Dreyer, G. Occurrence of Living Adult *Wuchereria bancrofti* in the Scrotal Area of Men with Microfilaraemia. *Trans. R. Soc. Trop. Med. Hyg.* **1996**, *90* (1), 55–56.

- (19) Cooper, P. J.; Nutman, T. B. 112 - Onchocerciasis. In *Hunter's Tropical Medicine and Emerging Infectious Disease (Ninth Edition)*; Magill, A. J., Hill, D. R., Solomon, T., Ryan, E. T., Eds.; W.B. Saunders: London, 2013; pp 827–834.
- (20) WHO. Onchocerciasis distribution map http://www.who.int/onchocerciasis/distribution/Distribution_onchocerciasis_2013.pdf?ua=1.
- (21) WHO. Onchocerciasis and Its Control. *Technical Report Series* **1995**, 852.
- (22) CDC. Onchocerciasis (River Blindness) <https://www.cdc.gov/parasites/onchocerciasis/biology.html>.
- (23) WHO. The Importance of Onchocercal Skin Disease. **1995**.
- (24) Benton, B. Economic Impact of Onchocerciasis Control through the African Programme for Onchocerciasis Control: An Overview. *Ann. Trop. Med. Parasitol.* **1998**, 92, S33–S39.
- (25) Amazigo, U. Onchocerciasis and Women's Reproductive Health: Indigenous and Biomedical Concepts. *Trop. Doct.* **1993**, 23 (4), 149–151.
- (26) Oladepo, O.; Brieger, W. R.; Otusanya, S.; Kale, O. O.; Offiong, S.; Titiloye, M. Farm Land Size and Onchocerciasis Status of Peasant Farmers in South-Western Nigeria. *Trop. Med. Int. Heal.* **1997**, 2 (4), 334–340.
- (27) Vlassoff, C.; Weiss, M.; Ovuga, E. B. L.; Eneanya, C.; Nwel, P. T.; Babalola, S. S.; Awedoba, A. K.; Theophilus, B.; Cofie, P.; Shetabi, P. Gender and the Stigma of Onchocercal Skin Disease in Africa. *Soc. Sci. Med.* **2000**, 50 (10), 1353–1368.
- (28) Aehyung Kim, A. T. and A. H. Health and Labor Productivity: The Economic Impact of Onchocercal Skin Disease. *World Bank Policy Research Working Paper 1836. Work. Pap. 1836* **1999**.
- (29) Richards, F. O.; Boatin, B.; Sauerbrey, M.; Seketeli, A. Control of Onchocerciasis Today: Status and Challenges. *Trends Parasitol.* **2001**, 17 (12), 558–563.
- (30) Cross, H. F.; Haarbrink, M.; Egerton, G.; Yazdanbakhsh, M.; Taylor, M. J. Severe Reactions to Filarial Chemotherapy and Release of Wolbachia Endosymbionts into Blood. *Lancet* **2001**, 358 (9296), 1873–1875.
- (31) El-Shahawi, G. A.; Abdel-Latif, M.; Saad, A. H.; Bahgat, M. Setaria Equina: In Vivo Effect of Diethylcarbamazine Citrate on Microfilariae in Albino Rats. *Exp. Parasitol.* **2010**, 126 (4), 603–610.
- (32) Piessens, W. F.; Beldekas, M. Diethylcarbamazine Enhances Antibody-Mediated Cellular Adherence to Brugia Malayi Microfilariae. *Nature* **1979**, 282 (5741), 845–847.
- (33) Ottesen, E. A.; Weller, P. F. Eosinophilia Following Treatment of Patients with Schistosomiasis Mansoni and Bancroft's Filariasis. *J. Infect. Dis.* **1979**, 139 (3), 343–347.
- (34) Pedersen, B. K.; Bygbjerg, I. C.; Svenson, M. Increase in Natural Killer Cell Activity during Diethylcarbamazine Treatment of Patients with Filariasis. *Acta Trop.* **1987**, 44 (3), 353–355.
- (35) Mazotti, L. Onchocerciasis in Mexico. *4th Internat. Congr. Trop. Med. Malar.* **1948**, 3–8.
- (36) Bockarie, M. J.; Tisch, D. J.; Kastens, W.; Alexander, N. D. E.; Dimber, Z.; Bockarie, F.; Ibam, E.; Alpers, M. P.; Kazura, J. W. Mass Treatment to Eliminate Filariasis in Papua New Guinea. *N. Engl. J. Med.* **2002**, 347 (23), 1841–1848.
- (37) Lacey, E. Mode of Action of Benzimidazoles. *Parasitol. Today* **1990**, 6 (4), 112–115.
- (38) Loffler, M.; Jockel, J.; Schuster, G.; Becker, C. Dihydroorotat-Ubiquinone Oxidoreductase Links Mitochondria in the Biosynthesis of Pyrimidine Nucleotides. *Mol Cell Biochem* **1997**, 174 (1–2), 125–129.
- (39) Pawluk, S. A.; Roels, C. A.; Wilby, K. J.; Ensom, M. H. H. A Review of Pharmacokinetic Drug–Drug Interactions with the Anthelmintic Medications Albendazole and Mebendazole. *Clin. Pharmacokinet.* **2015**, 54 (4), 371–383.

- (40) Li, X.-Q.; Björkman, A.; Andersson, T. B.; Gustafsson, L. L.; Masimirembwa, C. M. Identification of Human Cytochrome P450s That Metabolise Anti-Parasitic Drugs and Predictions of in Vivo Drug Hepatic Clearance from in Vitro Data. *Eur. J. Clin. Pharmacol.* **2003**, *59* (5), 429–442.
- (41) Dayan, A. D. Albendazole, Mebendazole and Praziquantel. Review of Non-Clinical Toxicity and Pharmacokinetics. *Acta Trop.* **2003**, *86* (2–3), 141–159.
- (42) Egerton, J. R.; Ostlind, D. A.; Blair, L. S.; Eary, C. H.; Suhayda, D.; Cifelli, S.; Riek, R. F.; Campbell, W. C. Avermectins, New Family of Potent Anthelmintic Agents: Efficacy of the B1a Component. *Antimicrob Agents Chemother* **1979**, *15* (3), 372–378.
- (43) Renz, A.; Trees, A. J.; Achukwi, D.; Edwards, G.; Wahl, G. Evaluation of Suramin, Ivermectin and Cgp-20376 in a New Macroparasitocidal Drug Screen, Onchocerca-Ochengi in African Cattle. *Trop. Med. Parasitol.* **1995**, *46* (1), 31–37.
- (44) Tchakoute, V. L.; Bronsvort, M.; Tanya, V.; Renz, A.; Trees, A. J. Chemoprophylaxis of Onchocerca Infections: In a Controlled, Prospective Study Ivermectin Prevents Calves Becoming Infected with O-Ochengi. *Parasitology* **1999**, *118*, 195–199.
- (45) Ali, M. M. M.; Mukhtar, M. M.; Baraka, O. Z.; Homeida, M. M. A.; Kheir, M. M.; Mackenzie, C. D. Immunocompetence May Be Important in the Effectiveness of Mectizan (R) (Ivermectin) in the Treatment of Human Onchocerciasis. *Acta Trop.* **2002**, *84* (1), 49–53.
- (46) Gardon, J.; GardonWendel, N.; DemangaNgangue, D.; Kamgno, J.; Chippaux, J. P.; Boussinesq, M. Serious Reactions after Mass Treatment of Onchocerciasis with Ivermectin in an Area Endemic for Loa Loa Infection. *Lancet* **1997**, *350* (9070), 18–22.
- (47) Molyneux, D. H.; Bradley, M.; Hoerauf, A.; Kyelem, D.; Taylor, M. J. Mass Drug Treatment for Lymphatic Filariasis and Onchocerciasis. *Trends Parasitol.* **2003**, *19* (11), 516–522.
- (48) Tagboto, S.; Townson, S. Antiparasitic Properties of Medicinal Plants and Other Naturally Occurring Products. In *Advances in Parasitology*; Academic Press, 2001; Vol. 50, pp 199–295.
- (49) Specht, S.; Hoerauf, A.; Adjei, O.; Debrah, A.; Büttner, D. W. Newly Acquired Onchocerca Volvulus Filariae after Doxycycline Treatment. *Parasitol. Res.* **2009**, *106* (1), 23–31.
- (50) Frayha, G. J.; Smyth, J. D.; Gobert, J. G.; Savel, J. The Mechanisms of Action of Antiprotozoal and Anthelmintic Drugs in Man. *Gen. Pharmacol. Vasc. Syst.* **1997**, *28* (2), 273–299.
- (51) McCall, J. W.; Genchi, C.; Kramer, L.; Guerrero, J.; Dzimianski, M. T.; Supakorndej, P.; Mansour, A. M.; McCall, S. D.; Supakorndej, N.; Grandi, G.; Carson, B. Heartworm and Wolbachia: Therapeutic Implications. *Vet. Parasitol.* **2008**, *158* (3), 204–214.
- (52) WHO Expert Committee on Onchocerciasis. Third Report. *World Heal. Organ Tech Rep Ser* **1987**, *752*, 1–167.
- (53) WHO. PAG Mission: Controle de l’Onchocercose Dans La Région Du Bassin de La Volta: *Rapp. la Mission d’Assistance Prep. aux Gouv. Côte d’Ivoire, Dahomey, Ghana, Haute-Volta, Mali, Niger, Togo. Geneva WHO* **1973**.
- (54) Benton, B.; Bump, J.; Seketeli, A.; Liese, B. Partnership and Promise: Evolution of the African River-Blindness Campaigns. *Ann. Trop. Med. Parasitol.* **2002**, *96*, 5–14.
- (55) WHO. Onchocerciasis control program http://www.who.int/blindness/partnerships/onchocerciasis_OCP/en/.
- (56) Evans, D. S.; Unnasch, T. R.; Richards, F. O. Onchocerciasis and Lymphatic Filariasis Elimination in Africa: It’s about Time. *Lancet (London, England)*. England May 2015, pp 2151–2152.
- (57) Dadzie, Y.; Neira, M.; Hopkins, D. Final Report of the Conference on the Eradicability of Onchocerciasis. *Filaria J* **2003**, *2* (1), 2.
- (58) Dent, J. A.; Smith, M. M.; Vassilatis, D. K.; Avery, L. The Genetics of Ivermectin Resistance in

- Caenorhabditis Elegans. *Proc Natl Acad Sci U S A* **2000**, *97* (6), 2674–2679.
- (59) McCavera, S.; Rogers, A. T.; Yates, D. M.; Woods, D. J.; Wolstenholme, A. J. An Ivermectin-Sensitive Glutamate-Gated Chloride Channel from the Parasitic Nematode *Haemonchus Contortus*. *Mol. Pharmacol.* **2009**, *75* (6), 1347–1355.
- (60) James, C. E.; Davey, M. W. Increased Expression of ABC Transport Proteins Is Associated with Ivermectin Resistance in the Model Nematode *Caenorhabditis Elegans*. *Int. J. Parasitol.* **2009**, *39* (2), 213–220.
- (61) Mounsey, K. E.; Pasay, C. J.; Arlian, L. G.; Morgan, M. S.; Holt, D. C.; Currie, B. J.; Walton, S. F.; McCarthy, J. S. Increased Transcription of Glutathione S-Transferases in Acaricide Exposed Scabies Mites. *Parasit. Vectors* **2010**, *3*.
- (62) Kotze, A. C.; McClure, S. J. *Haemonchus Contortus* Utilises Catalase in Defence against Exogenous Hydrogen Peroxide in Vitro. *Int. J. Parasitol.* **2001**, *31* (14), 1563–1571.
- (63) Torres-Rivera, A.; Landa, A. Glutathione Transferases from Parasites: A Biochemical View. *Acta Trop.* **2008**, *105* (2), 99–112.
- (64) Ji, H. Le; Qi, L. Da; Hong, X. Y.; Xie, H. F.; Li, Y. X. Effects of Host Sex, Plant Species, and Putative Host Species on the Prevalence of *Wolbachia* in Natural Populations of *Bemisia Tabaci* (Hemiptera: Aleyrodidae): A Modified Nested PCR Study. *J. Econ. Entomol.* **2015**, *108* (1), 210–218.
- (65) Hoerauf, a; Volkmann, L.; Hamelmann, C.; Adjei, O.; Autenrieth, I. B.; Fleischer, B.; Büttner, D. W. Endosymbiotic Bacteria in Worms as Targets for a Novel Chemotherapy in Filariasis. *Lancet* **2000**, *355* (9211), 1242–1243.
- (66) Kurz, M.; Iturbe-Ormaetxe, I.; Jarrott, R.; Cowieson, N.; Robin, G.; Jones, A.; King, G. J.; Frei, P.; Glockshuber, R.; O’Neill, S. L.; Heras, B.; Martin, J. L. Cloning, Expression, Purification and Characterization of a DsbA-like Protein from *Wolbachia Pipientis*. *Protein Expr. Purif.* **2008**, *59* (2), 266–273.
- (67) Bordenstein, S. R.; Paraskevopoulos, C.; Dunning Hotopp, J. C.; Sapountzis, P.; Lo, N.; Bandi, C.; Tettelin, H.; Werren, J. H.; Bourtzis, K. Parasitism and Mutualism in *Wolbachia*: What the Phylogenomic Trees Can and Cannot Say. *Mol. Biol. Evol.* **2009**, *26* (1), 231–241.
- (68) Baldo, L.; Werren, J. H. Revisiting *Wolbachia* Supergroup Typing Based on WSP: Spurious Lineages and Discordance with MLST. *Curr. Microbiol.* **2007**, *55* (1), 81–87.
- (69) Lo, N.; Casiraghi, M.; Salati, E.; Bazzocchi, C.; Bandi, C. How Many *Wolbachia* Supergroups Exist? *Molecular biology and evolution*. United States March 2002, pp 341–346.
- (70) Casiraghi, M.; Bordenstein, S. R.; Baldo, L.; Lo, N.; Beninati, T.; Wernegreen, J. J.; Werren, J. H.; Bandi, C. Phylogeny of *Wolbachia Pipientis* Based on *gltA*, *groEL* and *ftsZ* Gene Sequences: Clustering of Arthropod and Nematode Symbionts in the F Supergroup, and Evidence for Further Diversity in the *Wolbachia* Tree. *Microbiology* **2005**, *151* (12), 4015–4022.
- (71) Slatko, B. E.; Taylor, M. J.; Foster, J. M. The *Wolbachia* Endosymbiont as an Anti-Filarial Nematode Target. *Symbiosis* **2010**, *51* (1), 55–65.
- (72) McGraw, E. A.; O’Neill, S. L. Evolution of *Wolbachia Pipientis* Transmission Dynamics in Insects. *Trends Microbiol.* **1999**, *7* (7), 297–302.
- (73) Bandi, C.; Trees, A. J.; Brattig, N. W. *Wolbachia* in Filarial Nematodes: Evolutionary Aspects and Implications for the Pathogenesis and Treatment of Filarial Diseases. *Vet. Parasitol.* **2001**, *98* (1–3), 215–238.
- (74) Taylor, M. J.; Bandi, C.; Hoerauf, A. *Wolbachia*. Bacterial Endosymbionts of Filarial Nematodes; J.R. Baker; Academic Press, 2005; Vol. Volume 60, pp 245–284.
- (75) McGraw, E. A.; O’Neill, S. L. *Wolbachia Pipientis*: Intracellular Infection and Pathogenesis in *Drosophila*. *Curr. Opin. Microbiol.* **2004**, *7* (1), 67–70.

- (76) Townson, S.; Hutton, D.; Siemienska, J.; Hollick, L.; Scanlon, T.; Tagboto, S. K.; Taylor, M. J. Antibiotics and Wolbachia in Filarial Nematodes: Antifilarial Activity of Rifampicin, Oxytetracycline and Chloramphenicol against *Onchocerca Gutturosa*, *Onchocerca Lienalis* and *Brugia Pahangi*. *Ann. Trop. Med. Parasitol.* **2000**, *94* (8), 801–816.
- (77) Hoerauf, A.; Nissen-Pähle, K.; Schmetz, C.; Henkle-Dührsen, K.; Blaxter, M. L.; Büttner, D. W.; Gallin, M. Y.; Al-Qaoud, K. M.; Lucius, R.; Fleischer, B. Tetracycline Therapy Targets Intracellular Bacteria in the Filarial Nematode *Litomosoides Sigmodontis* and Results in Filarial Infertility. *J. Clin. Invest.* **1999**, *103* (1), 11–18.
- (78) Bandi, C.; McCall, J. W.; Genchi, C.; Corona, S.; Venco, L.; Sacchi, L. Effects of Tetracycline on the Filarial Worms *Brugia Pahangi* and *Dirofilaria Immitis* and Their Bacterial Endosymbionts Wolbachia. *Int. J. Parasitol.* **1999**, *29* (2), 357–364.
- (79) Henkle-Duhrsen, K.; Eckelt, V. H.; Wildenburg, G.; Blaxter, M.; Walter, R. D. Gene Structure, Activity and Localization of a Catalase from Intracellular Bacteria in *Onchocerca Volvulus*. *Mol Biochem Parasitol* **1998**, *96* (1–2), 69–81.
- (80) Howells, R. E.; Chen, S. N. *Brugia Pahangi*: Feeding and Nutrient Uptake in Vitro and in Vivo. *Exp Parasitol* **1981**, *51* (1), 42–58.
- (81) Kumar, S. &. No Title url: <http://filobase.bicpu.edu.in>.
- (82) Taylor, M. J.; Hoerauf, A. Wolbachia Bacteria of Filarial Nematodes. *Parasitol Today* **1999**, *15* (11), 437–442.
- (83) Ghedin, E.; Wang, S.; Spiro, D.; Caler, E.; Zhao, Q.; Crabtree, J. Draft Genome of the Filarial Nematode Parasite *Brugia Malayi*. *Science* (80). **2007**, *317* (5845), 1756–1760.
- (84) Rao, A. U.; Carta, L. K.; Lesuisse, E.; Hamza, I. Lack of Heme Synthesis in a Free-Living Eukaryote. *Proc Natl Acad Sci U S A* **2005**, *102* (12), 4270–4275.
- (85) Wu, B.; Novelli, J.; Foster, J.; Vaisvila, R.; Conway, L.; Ingram, J.; Ganatra, M.; Rao, A. U.; Hamza, I.; Slatko, B. The Heme Biosynthetic Pathway of the Obligate Wolbachia Endosymbiont of *Brugia Malayi* as a Potential Anti-Filarial Drug Target. *PLoS Negl. Trop. Dis.* **2009**, *3* (7), e475.
- (86) Holman, A. G.; Davis, P. J.; Foster, J. M.; Carlow, C. K.; Kumar, S. Computational Prediction of Essential Genes in an Unculturable Endosymbiotic Bacterium, Wolbachia of *Brugia Malayi*. *BMC Microbiol* **2009**, *9* (243), 1471–2180.
- (87) Raverdy, S.; Foster, J. M.; Roopenian, E.; Carlow, C. K. S. The Wolbachia Endosymbiont of *Brugia Malayi* Has an Active Pyruvate Phosphate Dikinase. *Mol. Biochem. Parasitol.* **2008**, *160* (2), 163–166.
- (88) Ghedin E, Daehnel K, Foster J, Slatko B, L. S. The Symbiotic Relationship between Filarial Parasitic Nematodes and Their Wolbachia endosymbionts—A Resource for a New Generation of Control Measures. *Symbiosis.* **2008**.
- (89) Pfarr K, Foster J, S. B. It Takes Two: Lessons from the First Nematode Wolbachia Genome Sequence. **2007**.
- (90) Weiss, D. S. Bacterial Cell Division and the Septal Ring. *Mol Microbiol* **2004**, *54* (3), 588–597.
- (91) Bi, E. F.; Lutkenhaus, J. FtsZ Ring Structure Associated with Division in *Escherichia Coli*. *Nature* **1991**, *354* (6349), 161–164.
- (92) Margolin, W. FtsZ and the Division of Prokaryotic Cells and Organelles. *Nat Rev Mol Cell Biol* **2005**, *6* (11), 862–871.
- (93) Lappchen, T.; Hartog, A. F.; Pinas, V. A.; Koomen, G. J.; den Blaauwen, T. GTP Analogue Inhibits Polymerization and GTPase Activity of the Bacterial Protein FtsZ without Affecting Its Eukaryotic Homologue Tubulin. *Biochemistry* **2005**, *44* (21), 7879–7884.
- (94) Lappchen, T.; Pinas, V. A.; Hartog, A. F.; Koomen, G. J.; Schaffner-Barbero, C.; Andreu, J. M.;

- Trambaiolo, D.; Lowe, J.; Juhem, A.; Popov, A. V.; den Blaauwen, T. Probing FtsZ and Tubulin with C8-Substituted GTP Analogs Reveals Differences in Their Nucleotide Binding Sites. *Chem Biol* **2008**, *15* (2), 189–199.
- (95) Vollmer, W. The Prokaryotic Cytoskeleton: A Putative Target for Inhibitors and Antibiotics? *Appl Microbiol Biotechnol* **2006**, *73* (1), 37–47.
- (96) Slayden, R. A.; Knudson, D. L.; Belisle, J. T. Identification of Cell Cycle Regulators in Mycobacterium Tuberculosis by Inhibition of Septum Formation and Global Transcriptional Analysis. *Microbiology* **2006**, *152* (Pt 6), 1789–1797.
- (97) Hoerauf, A.; Volkmann, L.; Hamelmann, C.; Adjei, O.; Autenrieth, I. B.; Fleischer, B.; Buttner, D. W. Endosymbiotic Bacteria in Worms as Targets for a Novel Chemotherapy in Filariasis. *Lancet* **2000**, *355* (9211), 1242–1243.
- (98) Hoerauf, A.; Specht, S.; Buttner, M.; Pfarr, K.; Mand, S.; Fimmers, R.; Marfo-Debrekyei, Y.; Konadu, P.; Debrah, A. Y.; Bandi, C.; Brattig, N.; Albers, A.; Larbi, J.; Batsa, L.; Taylor, M. J.; Adjei, O.; Buttner, D. W. Wolbachia Endobacteria Depletion by Doxycycline as Antifilarial Therapy Has Macrofilaricidal Activity in Onchocerciasis: A Randomized Placebo-Controlled Study. *Med. Microbiol. Immunol.* **2008**, *197* (3), 295–311.
- (99) Hoerauf, A.; Mand, S.; Adjei, O.; Fleischer, B.; Buttner, D. W. Depletion of Wolbachia Endobacteria in Onchocerca Volvulus by Doxycycline and Microfilaridermia after Ivermectin Treatment. *Lancet (London, England)* **2001**, *357* (9266), 1415–1416.
- (100) Turner, J. D.; Tendongfor, N.; Esum, M.; Johnston, K. L.; Langley, R. S.; Ford, L.; Faragher, B.; Specht, S.; Mand, S.; Hoerauf, A.; Enyong, P.; Wanji, S.; Taylor, M. J. Macrofilaricidal Activity after Doxycycline Only Treatment of Onchocerca Volvulus in an Area of Loa Loa Co-Endemicity: A Randomized Controlled Trial. *PLoS Negl. Trop. Dis.* **2010**, *4* (4), e660.
- (101) Mand, S.; Pfarr, K.; Sahoo, P. K.; Satapathy, A. K.; Specht, S.; Klarmann, U.; Debrah, A. Y.; Ravindran, B.; Hoerauf, A. Macrofilaricidal Activity and Amelioration of Lymphatic Pathology in Bancroftian Filariasis after 3 Weeks of Doxycycline Followed by Single-Dose Diethylcarbamazine. *Am. J. Trop. Med. Hyg.* **2009**, *81* (4), 702–711.
- (102) Supali, T.; Djuardi, Y.; Pfarr, K. M.; Wibowo, H.; Taylor, M. J.; Hoerauf, A.; Houwing-Duistermaat, J. J.; Yazdanbakhsh, M.; Sartono, E. Doxycycline Treatment of Brugia Malayi-Infected Persons Reduces Microfilaremia and Adverse Reactions after Diethylcarbamazine and Albendazole Treatment. *Clin. Infect. Dis.* **2008**, *46* (9), 1385–1393.
- (103) Specht, S.; Mand, S.; Marfo-Debrekyei, Y.; Debrah, A.; Konadu, P.; Adjei, O.; Büttner, D.; Hoerauf, A. Efficacy of 2- and 4-Week Rifampicin Treatment on the Wolbachia of Onchocerca Volvulus. *Parasitol Res* **2008**, *103* (6), 1303–1309.
- (104) Taylor, M. J.; Cross, H. F.; Bilo, K. Inflammatory Responses Induced by the Filarial Nematode Brugia Malayi Are Mediated by Lipopolysaccharide-like Activity from Endosymbiotic Wolbachia Bacteria. *J Exp Med* **2000**, *191* (8), 1429–1436.
- (105) Saint André, A. V.; Blackwell, N. M.; Hall, L. R.; Hoerauf, A.; Brattig, N. W.; Volkmann, L.; Taylor, M. J.; Ford, L.; Hise, A. G.; Lass, J. H.; Diaconu, E.; Pearlman, E. The Role of Endosymbiotic Wolbachia Bacteria in the Pathogenesis of River Blindness. *Science* (80). **2002**, *295* (5561), 1892–1895.
- (106) Brattig, N. W.; Bazzocchi, C.; Kirschning, C. J.; Reiling, N.; Büttner, D. W.; Ceciliani, F.; Geisinger, F.; Hochrein, H.; Ernst, M.; Wagner, H.; Bandi, C.; Hoerauf, A. The Major Surface Protein of Wolbachia Endosymbionts in Filarial Nematodes Elicits Immune Responses through TLR2 and TLR4. *J. Immunol.* **2004**, *173* (1), 437–445.
- (107) Mylonas, I. Antibiotic Chemotherapy during Pregnancy and Lactation Period: Aspects for Consideration. *Arch Gynecol Obs.* **2011**, *283* (1), 7–18.
- (108) Casiraghi, M.; McCall, J. W.; Simoncini, L.; Kramer, L. H.; Sacchi, L.; Genchi, C.; Werren, J. H.; Bandi, C.

- Tetracycline Treatment and Sex-Ratio Distortion: A Role for Wolbachia in the Moulting of Filarial Nematodes? *Int. J. Parasitol.* **2002**, 32 (12), 1457–1468.
- (109) Fenn, K.; Blaxter, M. Quantification of Wolbachia Bacteria in *Brugia Malayi* through the Nematode Lifecycle. *Mol. Biochem. Parasitol.* **2004**, 137 (2), 361–364.
- (110) MJ, T. Wolbachia Bacterial Endosymbionts. *Kluwer Acad. Publ.* **2002**, 143–155.
- (111) Sacchi, L.; Corona, S.; Kramer, L.; Calvi, L.; Casiraghi, M.; Franceschi, A. Ultrastructural Evidence of the Degenerative Events Occurring during Embryogenesis of the Filarial Nematode *Brugia Pahangi* after Tetracycline Treatment. *Parasitologia* **2003**, 45 (2), 89–96.
- (112) Amacher, D. E.; Martin, B. A. Tetracycline-Induced Steatosis in Primary Canine Hepatocyte Cultures. *Fundam. Appl. Toxicol.* **1997**, 40 (2), 256–263.
- (113) Johnston, K. L.; Ford, L.; Umareddy, I.; Townson, S.; Specht, S.; Pfarr, K.; Hoerauf, A.; Altmeyer, R.; Taylor, M. J. Repurposing of Approved Drugs from the Human Pharmacopoeia to Target Wolbachia Endosymbionts of Onchocerciasis and Lymphatic Filariasis. *Int. J. Parasitol. Drugs Drug Resist.* **2014**, 4 (3), 278–286.
- (114) Smith, K.; Leyden, J. J. Safety of Doxycycline and Minocycline: A Systematic Review. *Clin. Ther.* **2005**, 27 (9), 1329–1342.
- (115) Masters Anthony J.; Katzung, Bertram G, S. B. . T. Katzung & Trevor's Pharmacology. **2005**.
- (116) Sensi, P.; Margalith, P.; Timbal, M. T. Rifomycin, a New Antibiotic; Preliminary Report. *Farm. Sci* **1959**, 14 (2), 146–147.
- (117) Rao, R.; Well, G. J. In Vitro Effects of Antibiotics on *Brugia Malayi* Worm Survival and Reproduction. *J Parasitol* **2002**, 88 (3), 605–611.
- (118) Askgaard, D. S.; Wilcke, T.; Dossing, M. Hepatotoxicity Caused by the Combined Action of Isoniazid and Rifampicin. *Thorax* **1995**, 50 (2), 213–214.
- (119) Graham, R. A.; Downey, A.; Mudra, D.; Krueger, L.; Carroll, K.; Chengelis, C.; Madan, A.; Parkinson, A. In Vivo and in Vitro Induction of Cytochrome P450 Enzymes in Beagle Dogs. *Drug Metab Dispos* **2002**, 30 (11), 1206–1213.
- (120) Darvas, F.; Dormán, G.; Krajcsi, P.; Puskás, L. G.; Kovári, Z.; Lörincz, Z.; Ürge, L. Recent Advances in Chemical Genomics. *Curr. Med. Chem.* **2004**, 11 (23), 3119–3145.
- (121) Vogt, A.; Lazo, J. S. Chemical Complementation: A Definitive Phenotypic Strategy for Identifying Small Molecule Inhibitors of Elusive Cellular Targets. *Pharmacol. Ther.* **2005**, 107 (2), 212–221.
- (122) Wedler, F. C. Enzyme Kinetics: Behavior and Analysis of Rapid Equilibrium and Steady-State Enzyme Systems. Author: Irwin H. Segal (University of California, Davis). Published by Wiley-Interscience, New York, 1975. Price: \$24.50. No. of Pages: 957. *Int. J. Chem. Kinet.* **1976**, 8 (1), 159.
- (123) Rask-Andersen, M.; Almén, M. S.; Schiöth, H. B. Trends in the Exploitation of Novel Drug Targets. *Nat. Rev. Drug Discov.* **2011**, 10 (8), 579–590.
- (124) Arrowsmith, J. Trial Watch: Phase II Failures: 2008-2010. *Nat. Rev. Drug Discov.* **2011**, 10 (5), 328–329.
- (125) Arrowsmith, J. Trial Watch: Phase III and Submission Failures: 2007-2010. *Nat. Rev. Drug Discov.* **2011**, 10 (2), 87.
- (126) Ashburn, T. T.; Thor, K. B. Drug Repositioning: Identifying and Developing New Uses for Existing Drugs. *Nat Rev Drug Discov* **2004**, 3 (8), 673–683.
- (127) Reaume, A. G. Drug Repurposing through Nonhypothesis Driven Phenotypic Screening. *Drug Discov. Today Ther. Strateg.* **2011**, 8 (3–4), 85–88.
- (128) Turner, J. D.; Langley, R. S.; Johnston, K. L.; Egerton, G.; Wanji, S.; Taylor, M. J. Wolbachia Endosymbiotic Bacteria of *Brugia Malayi* Mediate Macrophage Tolerance to TLR- and CD40-Specific

- Stimuli in a MyD88/TLR2-Dependent Manner. *J. Immunol.* **2006**, *177* (2), 1240–1249.
- (129) Johnston, K. L.; Wu, B.; Guimaraes, A.; Ford, L.; Slatko, B. E.; Taylor, M. J. Lipoprotein Biosynthesis as a Target for Anti-Wolbachia Treatment of Filarial Nematodes. *Parasit. Vectors* **2010**, *3*, 99.
- (130) Willett, P.; Barnard, J. M.; Downs, G. M. Chemical Similarity Searching. *J. Chem. Inf. Comput. Sci.* **1998**, *38* (6), 983–996.
- (131) Clare, R. H.; Cook, D. A. N.; Johnston, K. L.; Ford, L.; Ward, S. A.; Taylor, M. J. Development and Validation of a High-Throughput Anti-Wolbachia Whole-Cell Screen: A Route to Macroparasiticidal Drugs against Onchocerciasis and Lymphatic Filariasis. *J. Biomol. Screen.* **2015**, *20* (1), 64–69.
- (132) Hermans, P. G.; Hart, C. A.; Trees, A. J. In Vitro Activity of Antimicrobial Agents against the Endosymbiont Wolbachia Pipientis. *J. Antimicrob Chemother* **2001**, *47* (5), 659–663.
- (133) Pohl, P. C.; Klafke, G. M.; Carvalho, D. D.; Martins, J. R.; Daffre, S.; Vaz, I. D.; Masuda, A. ABC Transporter Efflux Pumps: A Defense Mechanism against Ivermectin in *Rhipicephalus* (Boophilus) *Microplus*. *Int. J. Parasitol.* **2011**, *41* (13–14), 1323–1333.
- (134) Lipinski, C. A.; Lombardo, F.; Dominy, B. W.; Feeney, P. J. Experimental and Computational Approaches to Estimate Solubility and Permeability in Drug Discovery and Development Settings. *Adv. Drug Deliv. Rev.* **1997**, *23* (1), 3–25.
- (135) Hansch, C.; Björkroth, J. P.; Leo, A. Hydrophobicity and Central Nervous System Agents: On the Principle of Minimal Hydrophobicity in Drug Design. *J. Pharm. Sci.* **2017**, *76* (9), 663–687.
- (136) Hopkins, A. L.; Keseru, G. M.; Leeson, P. D.; Rees, D. C.; Reynolds, C. H. The Role of Ligand Efficiency Metrics in Drug Discovery. *Nat. Rev. Drug Discov.* **2014**, *13* (2), 105–121.
- (137) Leeson, P. D.; Springthorpe, B. The Influence of Drug-like Concepts on Decision-Making in Medicinal Chemistry. *Nat. Rev. Drug Discov.* **2007**, *6* (11), 881–890.
- (138) Gleeson, M. P. Generation of a Set of Simple, Interpretable ADMET Rules of Thumb. *J. Med. Chem.* **2008**, *51* (4), 817–834.
- (139) Hann, M. M.; Keserü, G. M. Finding the Sweet Spot: The Role of Nature and Nurture in Medicinal Chemistry. *Nat. Rev. Drug Discov.* **2012**, *11* (5), 355–365.
- (140) Gleeson, M. P.; Hersey, A.; Montanari, D.; Overington, J. Probing the Links between in Vitro Potency, ADMET and Physicochemical Parameters. *Nat Rev Drug Discov* **2011**, *10* (3), 197–208.
- (141) Cumming, J. G.; Davis, A. M.; Muresan, S.; Haeberlein, M.; Chen, H. Chemical Predictive Modelling to Improve Compound Quality. *Nat Rev Drug Discov* **2013**, *12* (12), 948–962.
- (142) Hughes, J. P.; Rees, S.; Kalindjian, S. B.; Philpott, K. L. Principles of Early Drug Discovery. *Br. J. Pharmacol.* **2011**, *162* (6), 1239–1249.
- (143) Nassar, A.-E. F.; Kamel, A. M.; Clarimont, C. Improving the Decision-Making Process in the Structural Modification of Drug Candidates: Enhancing Metabolic Stability. *Drug Discov. Today* **2004**, *9* (23), 1020–1028.
- (144) Ariens, E.J. and Simonis, A. . Optimization of Pharmacokinetics, an Essential Aspect of Drug Development, by “Metabolic Stabilization”. in *Strategy in Drug Research. Pharmacochem. Libr. Elsevier* **1982**, 165–178.
- (145) Dragovich, P. S.; Prins, T. J.; Zhou, R.; Johnson, T. O.; Hua, Y.; Luu, H. T.; Sakata, S. K.; Brown, E. L.; Maldonado, F. C.; Tuntland, T.; Lee, C. A.; Fuhrman, S. A.; Zalman, L. S.; Patick, A. K.; Matthews, D. A.; Wu, E. Y.; Guo, M.; Borer, B. C.; Nayyar, N. K.; Moran, T.; Chen, L.; Rejto, P. A.; Rose, P. W.; Guzman, M. C.; Doval Santos, E. Z.; Lee, S.; McGee, K.; Mohajeri, M.; Liese, A.; Tao, J.; Kosa, M. B.; Liu, B.; Batugo, M. R.; Gleeson, J.-P. R.; Wu, Z. P.; Liu, J.; Meador, J. W.; Ferre, R. A. Structure-Based Design, Synthesis, and Biological Evaluation of Irreversible Human Rhinovirus 3C Protease Inhibitors. 8. Pharmacological Optimization of Orally Bioavailable 2-Pyridone-Containing Peptidomimetics. *J. Med. Chem.* **2003**, *46* (21), 4572–4585.

- (146) Compton, D. R.; Sheng, S.; Carlson, K. E.; Rebacz, N. A.; Lee, I. Y.; Katzenellenbogen, B. S.; Katzenellenbogen, J. A. Pyrazolo[1,5-A]pyrimidines: Estrogen Receptor Ligands Possessing Estrogen Receptor Beta Antagonist Activity. *J. Med. Chem.* **2004**, *47* (24), 5872–5893.
- (147) Zhang, X.; Song, Y.; Gao, L.; Guo, X.; Fan, X. Highly Facile and Regio-Selective Synthesis of pyrazolo[1,5-A]pyrimidines via Reactions of 1,2-Allenic Ketones with Aminopyrazoles. *Org. Biomol. Chem.* **2014**, *12* (13), 2099–2107.
- (148) Ahmetaj, S.; Velikanje, N.; Groselj, U.; Sterbal, I.; Prek, B.; Golobic, A.; Kocar, D.; Dahmann, G.; Stanovnik, B.; Svete, J. Parallel Synthesis of 7-Heteroaryl-pyrazolo[1,5-A]pyrimidine-3-Carboxamides. *Mol. Divers.* **2013**, *17* (4), 731–743.
- (149) Al-Adiwish, W. M.; Tahir, M. I. M.; Siti-Noor-Adnalizawati, A.; Hashim, S. F.; Ibrahim, N.; Yaacob, W. A. Synthesis, Antibacterial Activity and Cytotoxicity of New Fused pyrazolo[1,5-A]pyrimidine and pyrazolo[5,1-c][1,2,4]triazine Derivatives from New 5-Aminopyrazoles. *Eur. J. Med. Chem.* **2013**, *64*, 464–476.
- (150) Kuwayama, Y.; Kataoka, S. Reactions of Ketenethioacetals. I. *Yakugaku Zasshi* **1965**, *85* (5), 387–390.
- (151) Perdona, E.; Costantini, V. J.; Tessari, M.; Martinelli, P.; Carignani, C.; Valerio, E.; Mok, M. H.; Zonzini, L.; Visentini, F.; Gianotti, M.; Gordon, L.; Rocheville, M.; Corsi, M.; Capelli, A. M. In Vitro and in Vivo Characterization of the Novel GABAB Receptor Positive Allosteric Modulator, 2-[1-[2-(4-Chlorophenyl)-5-methylpyrazolo[1,5-A]pyrimidin-7-Yl]-2-Piperidinyl]eth Anol (CMPPE). *Neuropharmacology* **2011**, *61* (5–6), 957–966.
- (152) Ali, S.; Heathcote, D. A.; Kroll, S. H.; Jogalekar, A. S.; Scheiper, B.; Patel, H.; Brackow, J.; Siwicka, A.; Fuchter, M. J.; Periyasamy, M.; Tolhurst, R. S.; Kanneganti, S. K.; Snyder, J. P.; Liotta, D. C.; Aboagye, E. O.; Barrett, A. G.; Coombes, R. C. The Development of a Selective Cyclin-Dependent Kinase Inhibitor That Shows Antitumor Activity. *Cancer Res* **2009**, *69* (15), 6208–6215.
- (153) Hwang, J. Y.; Windisch, M. P.; Jo, S.; Kim, K.; Kong, S.; Kim, H. C.; Kim, S.; Kim, H.; Lee, M. E.; Kim, Y.; Choi, J.; Park, D.-S.; Park, E.; Kwon, J.; Nam, J.; Ahn, S.; Cechetto, J.; Kim, J.; Liuzzi, M.; No, Z.; Lee, J. Discovery and Characterization of a Novel 7-aminopyrazolo[1,5-A]pyrimidine Analog as a Potent Hepatitis C Virus Inhibitor. *Bioorg. Med. Chem. Lett.* **2012**, *22* (24), 7297–7301.
- (154) Tye, H.; Mueller, S. G.; Prestle, J.; Scheuerer, S.; Schindler, M.; Nosse, B. Novel 6,7,8,9-Tetrahydro-5H-1,4,7,10a-Tetraaza-Cyclohepta[f]indene Analogues as Potent and Selective 5-HT(2C) Agonists for the Treatment of Metabolic Disorders. *Bioorg Med Chem Lett* **2011**, *21* (1), 34–37.
- (155) Kamouchi, M.; Kajioka, S.; Sakai, T.; Kitamura, K.; Kuriyama, H. A Target K⁺ Channel for the LP-805-Induced Hyperpolarization in Smooth Muscle Cells of the Rabbit Portal Vein. *Naunyn Schmiedebergs Arch Pharmacol* **1993**, *347* (3), 329–335.
- (156) Griffith, D. A.; Hargrove, D. M.; Maurer, T. S.; Blum, C. A.; De Lombaert, S.; Inthavongsay, J. K.; Klade, L. E.; Mack, C. M.; Rose, C. R.; Sanders, M. J.; Carpino, P. A. Discovery and Evaluation of pyrazolo[1,5-A]pyrimidines as Neuropeptide Y1 Receptor Antagonists. *Bioorg Med Chem Lett* **2011**, *21* (9), 2641–2645.
- (157) Arita, M.; Kojima, H.; Nagano, T.; Okabe, T.; Wakita, T.; Shimizu, H. Phosphatidylinositol 4-Kinase III Beta Is a Target of Enviroxime-like Compounds for Antipoliiovirus Activity. *J Virol* **2011**, *85* (5), 2364–2372.
- (158) Shiota, T.; Yamamori, T.; Sakai, K.; Kiyokawa, M.; Honma, T.; Ogawa, M.; Hayashi, K.; Ishizuka, N.; Matsumura, K.; Hara, M.; Fujimoto, M.; Kawabata, T.; Nakajima, S. Synthesis and Structure-Activity Relationship of a New Series of Potent Angiotensin II Receptor Antagonists: pyrazolo[1,5-A]pyrimidine Derivatives. *Chem Pharm Bull* **1999**, *47* (7), 928–938.
- (159) Williamson, D. S.; Parratt, M. J.; Bower, J. F.; et al. Structure-Guided Design of pyrazolo[1,5-A]pyrimidines as Inhibitors of Human Cyclin-Dependent Kinase 2. *Bioorg. Med. Chem. Lett.* **2005**, *15* (4), 863–867.

- (160) Mukaiyama, H.; Nishimura, T.; Kobayashi, S.; Komatsu, Y.; Kikuchi, S.; Ozawa, T.; Kamada, N.; Ohnota, H. Novel pyrazolo[1,5-A]pyrimidines as c-Src Kinase Inhibitors That Reduce IKr Channel Blockade. *Bioorg. Med. Chem.* **2008**, *16* (2), 909–921.
- (161) Wustrow, D. J.; Capiris, T.; Rubin, R.; Knobelsdorf, J. A.; Akunne, H.; Davis, M. D. Pyrazolo[1,5-A]pyrimidine CRF-1 Receptor Antagonists. *Bioorg Med Chem Lett* **1998**, *8* (16), 2067–2070.
- (162) Paruch, K.; Dwyer, M. P.; Alvarez, C.; Brown, C.; Chan, T.-Y.; Doll, R. J.; Keertikar, K.; Knutson, C.; McKittrick, B.; Rivera, J.; Rossman, R.; Tucker, G.; Fischmann, T. O.; Hruza, A.; Madison, V.; Nomeir, A. A.; Wang, Y.; Lees, E.; Parry, D.; Sgambellone, N.; Seghezzi, W.; Schultz, L.; Shanahan, F.; Wiswell, D.; Xu, X.; Zhou, Q.; James, R. A.; Paradkar, V. M.; Park, H.; Rokosz, L. R.; Stauffer, T. M.; Guzi, T. J. Pyrazolo[1,5-A]pyrimidines as Orally Available Inhibitors of Cyclin-Dependent Kinase 2. *Bioorg. Med. Chem. Lett.* **2007**, *17* (22), 6220–6223.
- (163) Guzi, T. J.; Paruch, K.; Dwyer, M. P.; Parry, D. A. Pyrazolo[1,5-A]pyrimidine Compounds as Protein Kinase Inhibitors and Their Preparation, Pharmaceutical Compositions and Their Use in the Treatment of Protein Kinase-Mediated Diseases, 2007.
- (164) Rydberg, P.; Gloriam, D. E.; Olsen, L. The SMARTCyp Cytochrome P450 Metabolism Prediction Server. *Bioinformatics* **2010**, *26* (23), 2988–2989.
- (165) Rydberg, P.; Gloriam, D. E.; Zaretski, J.; Breneman, C.; Olsen, L. SMARTCyp: A 2D Method for Prediction of Cytochrome P450-Mediated Drug Metabolism. *ACS Med. Chem. Lett.* **2010**, *1* (3), 96–100.
- (166) Rydberg, P.; Jørgensen, M. S.; Jacobsen, T. A.; Jacobsen, A.-M.; Madsen, K. G.; Olsen, L. Nitrogen Inversion Barriers Affect the N-Oxidation of Tertiary Alkylamines by Cytochromes P450. *Angew. Chemie Int. Ed.* **2013**, *52* (3), 993–997.
- (167) Rydberg, P.; Olsen, L. Ligand-Based Site of Metabolism Prediction for Cytochrome P450 2D6. *ACS Med. Chem. Lett.* **2012**, *3* (1), 69–73.
- (168) Rydberg, P.; Rostkowski, M.; Gloriam, D. E.; Olsen, L. The Contribution of Atom Accessibility to Site of Metabolism Models for Cytochromes P450. *Mol. Pharm.* **2013**, *10* (4), 1216–1223.

Chapter 2

**Initial SAR studies: 2-pyridyl ring and
linker modifications**

Contents

Chapter 2 Initial SAR studies: 2-pyridyl ring and linker modifications.....	Error! Bookmark not defined.
2.1 R ⁴ and R ⁵ - Substituted Pyrazolopyrimidines	Error! Bookmark not defined.
2.11 Series 1 Target selection and development of a synthetic route	Error! Bookmark not defined.
2.12 Biological Evaluation of initial targets R ⁴ & R ⁵ substituted pyrazolopyrimidines	Error! Bookmark not defined.
2.2 Further R ⁴ and R ⁵ Substituted Pyrazolopyrimidines	Error! Bookmark not defined.
2.21 Series two target selection and synthesis	Error! Bookmark not defined.
2.22 Further R ⁴ & R ⁵ SAR exploration – <i>in vitro</i> DMPK and potency results.....	Error! Bookmark not defined.
2.3 Series 3: 3-(R ¹) 4-F Ph, R ⁴ - & R ⁵ - Substituted Pyrazolopyrimidines:	Error! Bookmark not defined.
2.31 Design and Synthesis.....	Error! Bookmark not defined.
2.32 Series 3 <i>in vitro</i> DMPK and Potency	Error! Bookmark not defined.
2.4 6 (R ³)- Substituted Pyrazolopyrimidines.....	Error! Bookmark not defined.
2.41 Target Design and Synthesis	Error! Bookmark not defined.
2.42 -(R ³) Pyrazolopyrimidines Biological Evaluation	Error! Bookmark not defined.
2.5 Conclusion.....	Error! Bookmark not defined.
2.6 Experimental.....	Error! Bookmark not defined.
2.7 References	Error! Bookmark not defined.

Chapter 2 Initial SAR studies: 2-pyridyl ring and linker modifications

2.1 R⁴ and R⁵- Substituted Pyrazolopyrimidines

2.1.1 Series 1 Target selection and development of a synthetic route

The general scaffold for series 1 is displayed in **Fig 2.1** with the numbering system used for the core also displayed. Early SAR studies focused on exploring the chemical space around the 2-pyridyl ring which is present in the initial hit from the MMV library, DT2009-0128388, defined here as **AWF911** (**Fig 2.1**). In this chapter, the chemical modification will focus on the methylene linker and the C-6 allyl group present in the initial hit molecule. Both sites were predicted to be prone to rapid P450 metabolism (**Chapter 1 Section 7.3**). Analogues were designed for synthesis incorporating alternative aryl rings and halogenated pyridyl rings at the R⁵ position which could also serve to deteriorate the metabolic liability of the linker and pyridine nitrogen to metabolism.

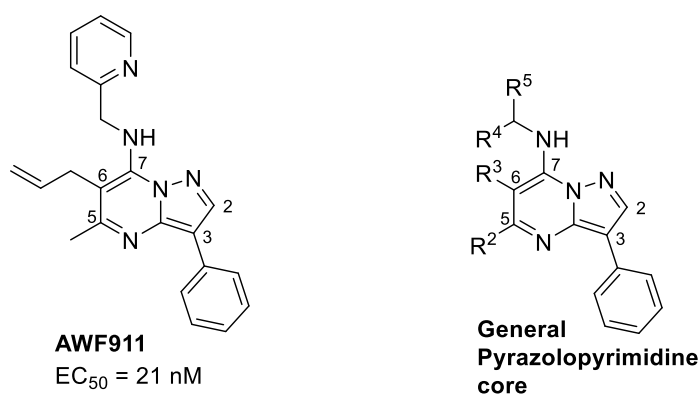


Fig. 2.1 General scaffold for pyrazolopyrimidine core.

One early SAR observation from biological evaluation of the initial hit and the commercially available compounds discussed earlier in **Fig 1.21** (**Chapter 1 Section 7.3**) and displayed again below (**Fig 2.2**), suggest that the 6-position (R³) can be modified without abolishing compound potency. The commercially available analogues (**Fig 2.2**) demonstrated that a methyl substituent is tolerated at this R³ position in terms of anti-*Wolbachia* potency. Removal of the allyl functionality of **AWF911** was explored to mitigate the potential metabolic instability with this functionality, which is highlighted by the SmartCyp predictions (**Fig 1.21 Chapter 1 Section 7.3**) and *in silico* DMPK predictions carried out by AstraZeneca (AZ) (**Fig. 2.3**).

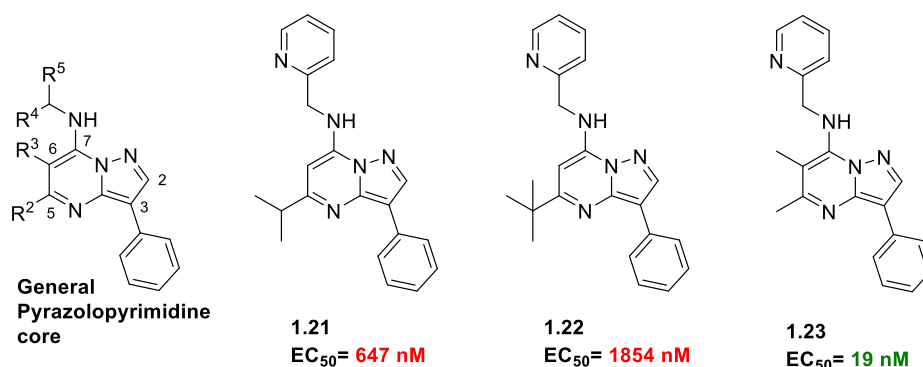


Fig. 2.2 Results obtained from whole-cell assays for the commercially available pyrazolopyrimidines.

These initial screening results suggest that extension or branching of the alkyl substituent at the R² position results in decreased anti-*Wolbachia* activity. Our first series of analogues examined the effect of removal of this 6-methyl group on potency, DMPK predictions carried out by AstraZeneca also suggest this chemical modification might improve the overall metabolic stability of our compounds (**Fig 2.3**).

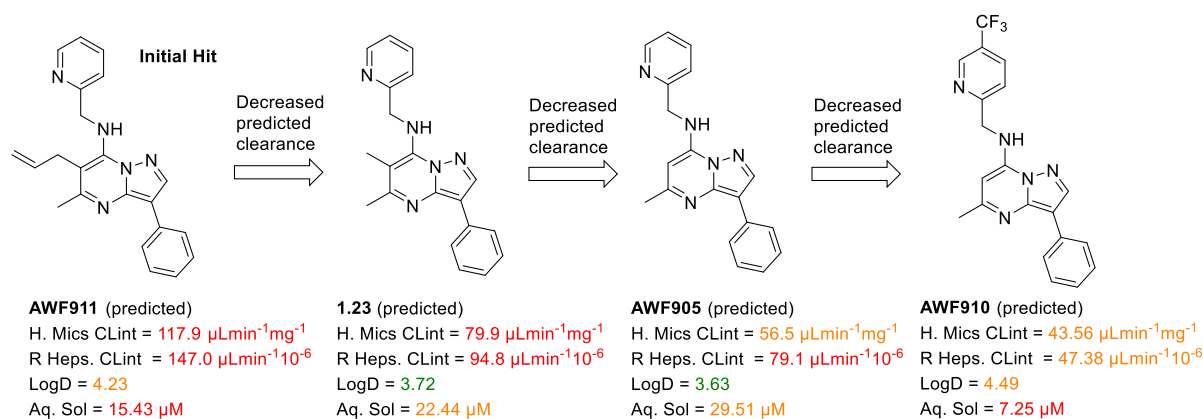
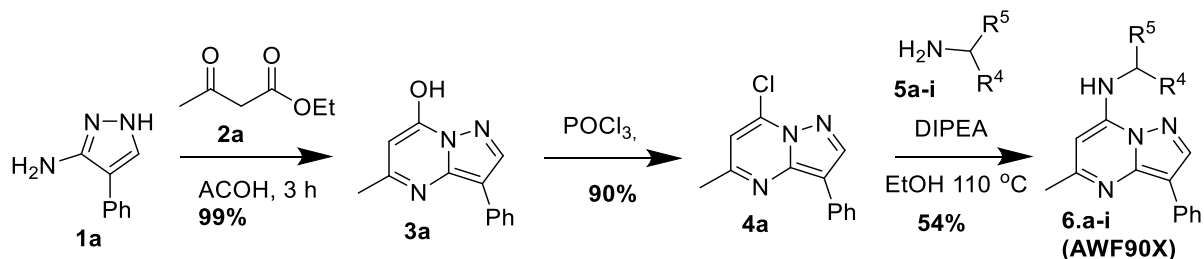


Fig. 2.3 DMPK predictions for early analogues designed for synthesis.

In addition to removal of the methyl group at the 6-(R³) position, a range of analogues were selected for synthesis and biological evaluation which modified the 2-pyridyl ring seen in the initial hit with various aryl ring systems including halogenated pyridyl and phenyl rings. The DMPK predictions displayed above in **Fig. 2.3** support removal of the methyl and incorporation of a 2-pyridyl 4-CF₃ ring as a promising approach to improve compound stability. The synthetic route (**Scheme 2.1**) was established to provide a point of divergence at the final product forming step. This synthesis was adopted by the work previously published from the groups of J.Y Hwang *et al.*,¹ and K. Paruch *et al.*² and their approach allows multiple analogues to be accessed from a common intermediate. To probe the chemical space surrounding the R^{4/5} position, the initial targets maintained the R¹ phenyl and R² methyl substitution. The R¹ phenyl ring was chosen as an appropriate starting point due to promising activity in the initial hit and the commercial availability of **1a**, the 3-amino 4-phenyl pyrazole starting material (£12/g – Fluorochem, United Kingdom).

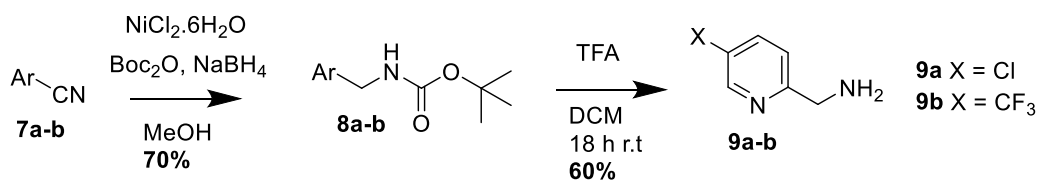


Scheme 2.1 Synthetic pathway to pyrazolopyrimidine analogues with modified R^{4/5} positions

The pyrazolopyrimidine ring was formed in near quantitative yields by a condensation reaction between 3-amino, 4-phenyl pyrazole **1a** and the 1,3-dicarbonyl compound **2a**. Subsequent chlorination of the 7-hydroxy pyrimidine (**3a**) provided very high yields of the important 7-chloro intermediate **4a** which granted access to multiple analogues (**AWF90X** – see **Table 2.1**) with various R⁴ & R⁵ positions upon substitution with the necessary amines (**5a-i**).

While most of the yields in the final product forming step were ~40%, there was some variations depending on the substituent at the R⁵ position as for this set of analogues the R⁴ groups was remained constant (R⁴ = H). These various yields for the first compounds synthesised are documented below in **Table 2.1** alongside the biological evaluation results. Most of these reactions gave similar yields of 37-40%, while the 2-pyridyl 4-trifluoromethyl methanamine (**9b**, **Scheme 2.2**) resulted in the isolation of a greater amount of the desired product (58%).

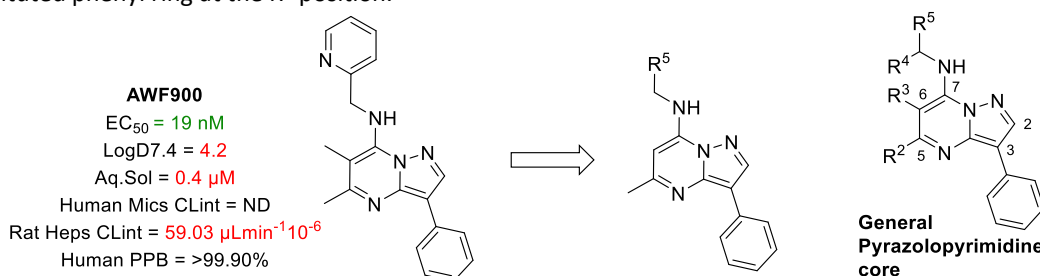
Where possible the amine side chain (**5a-i**) used in the product forming steps (**Scheme 2.1**) were purchased. For more complex amines that were unavailable or expensive (2-pyridyl 3 CF₃ £690/g – Apollo Scientific), they were synthesised by reduction of the corresponding nitrile derivative. Reduction of the nitrile compounds was first attempted utilising LiAlH₄ as the reducing agent following the work of Yang *et al.*³ This procedure did not prove very successful due to poor yields which further complicated the difficult purification of the desired amines which resulted in impure material being isolated. Due to these problems, an alternative reduction procedure following the work of Caddick *et al.*, was utilised (**Scheme 2.2**). Within this procedure the nitriles **7a-b** are reduced by Nickel borohydride prepared from nickel(II)chloride hexahydrate and sodium borohydride to afford the free amines which are then Boc-protected *in situ*.⁴ This allowed for simpler purification of the amine precursors **8a-b** which forms the desired methanamine intermediates **9a-b** by Boc-deprotection using TFA.



Scheme 2.2 Two-step reduction of nitriles to their corresponding aryl-methanamines.

2.12 Biological Evaluation of initial targets R⁴ & R⁵ substituted pyrazolopyrimidines

The *in vitro* *Wolbachia* activity and DMPK measurements obtained for the first series of pyrazolopyrimidine analogues with various R⁵ aryl rings are all shown in **Table 2.2**, as noted these analogues contain an unsubstituted phenyl ring at the R¹ position.



Compound code	R ⁵	Reaction Yield (%)	EC ₅₀ (nM)	LogD 7.4	Aq.Sol (μM)	H.MicsCl (μLmin ⁻¹ mg ⁻¹)	R.HepsCl (μLmin ⁻¹ 10 ⁻⁶)	Human PPB (%)
AWF901		40	3012	4.6	0.06	80.1	77.2	99.95
AWF902		39	5176	2.9	0.08	34.5	30.9	99.95
AWF903		13	1384	3.8	4.00	78.9	91.3	99.43
AWF904		37	NA	3.6	2.00	41.5	55.2	98.00
AWF905		39	145	3.6	ND	23.6	54.8	98
AWF906		40	NA	3.5	2.00	67.7	83.2	99.03
AWF907		54	NA	4.3	0.20	14.0	38.1	99.82
AWF908		11	NA	4.3	0.60	ND	40.7	99.93

NA – No activity at highest concentration (5 μM) ND – Not determined

Table 2.2 First series of analogues with modified aromatic side-chains at the R⁵ position, *in vitro* potency and calculated DMPK data

Introduction of a more hydrophobic phenyl ring (**AWF901-2** aq. Sol = 0.06 μM) reduces the aqueous solubility over the pyridyl analogues **AWF904-6** (Aq. Sol = 2.00 μM) and produces analogues with very weak anti-*Wolbachia* activity (**AWF901-2** EC_{50} = >2500 nM) over the 2-pyridyl analogue **AWF905** (EC_{50} = 145 nM). There is a notable improvement in aqueous solubility through the incorporation of 3 or 4 pyridyl rings (**AWF904** & **AWF906**) (2.00 μM) over the parent 2-pyridyl analogue **AWF900** (0.4 μM) however these regio-isomers possess no anti-*Wolbachia* activity at the highest tested concentration (5 μM). It is possible that an intramolecular hydrogen bonding interaction may occur within the 2-pyridyl analogue between the pyridine nitrogen and amine linker. This will increase molecular planarity and may be essential for entry of the analogues into the active site of the drug target. This interaction will also, bring the 2-pyridyl ring more in plane with the pyrazolopyrimidine core increasing crystal packing energy and may ultimately reduce the aqueous solubility of our analogues.⁵

Studies of a range of strong and weak intramolecular hydrogen bonds in a variety of different solvent systems have determined that the distance and angle around the hydrogen bond provides a good indication of the directionality of such interactions. This is an essential characteristic of a hydrogen bonds with angles near to 180° and distances between 1.2–1.5 Å corresponding to very strong hydrogen bonds. Hydrogen bonds can occur over larger distances were 1.5–2.2 Å would be found in strong interactions and 2.0–3.0 Å would correspond to a weak hydrogen bond.³¹

Analysis of **AWF900** in Spartan16⁶ were each compound was energy minimised using the MMFF94 force field and a conformational energy searches were performed using default settings allows the lowest energy conformers for the 6-methyl, 2-pyridyl compound to be studied. These conformers with low relative energy between 5 and 7 kJmol^{-1} (**Fig 2.4**) are absent in the analysis of analogues not containing the 2-pyridyl nitrogen such as the modelled 6-Methyl 3-pyridyl analogue (**AWF904**, **Fig 2.5**). Also, this model depicts 2 to 2.6 angstroms between the amine hydrogen and 2-pyridyl functionalities which suggests that there is an intramolecular hydrogen bond present at this position (**Fig 2.4**). This interaction is displayed in the 3D model in **Fig 2.4** which brings the 2-pyridyl ring in plane with the pyrazolopyrimidine core.

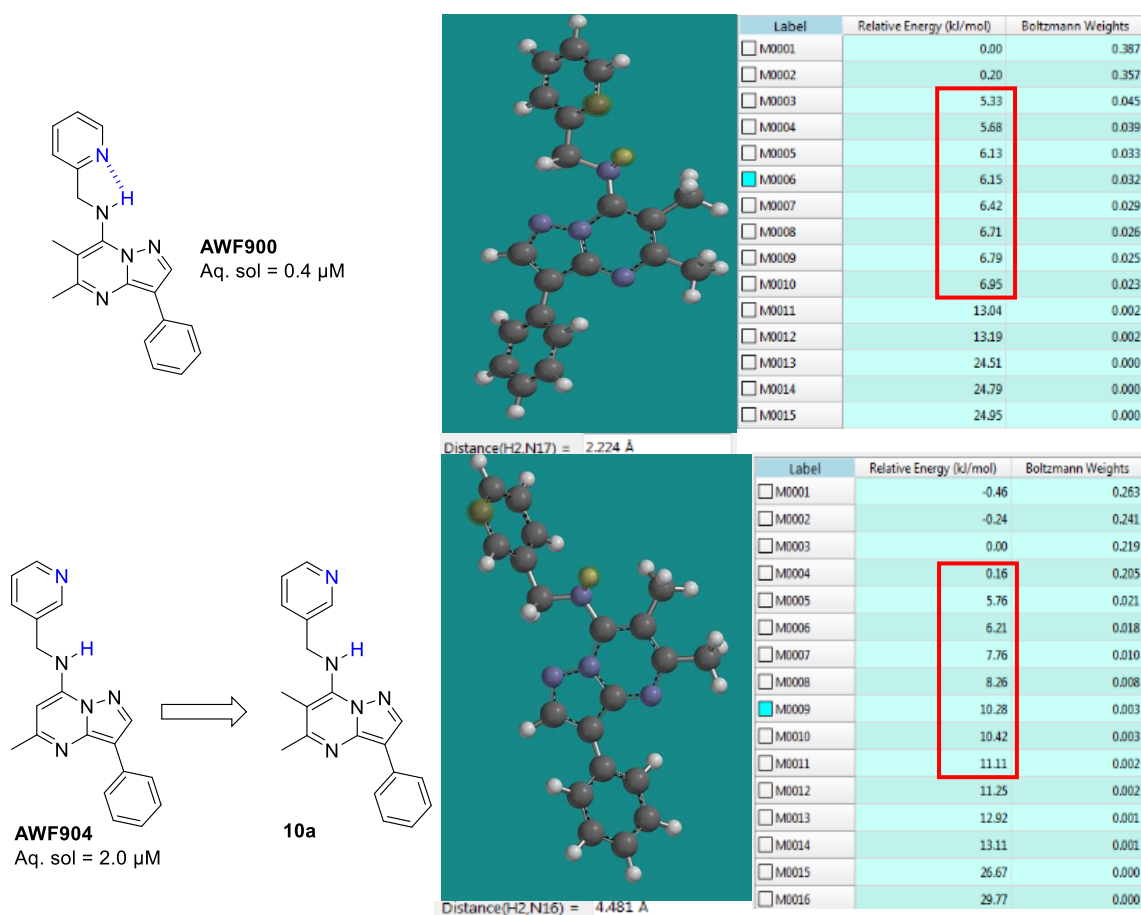


Fig 2.4 Low-energy conformers (M0006-8) displayed by analysis of **AWF900** in Spartan. And corresponding conformers in **10d**

Some of these lower energy conformers (5-7 kJmol⁻¹ – **Fig 2.4**) within **AWF900** are absent in the 3-pyridyl structure **10a** (**Fig. 2.5**) when subjected to the same analysis. This supports the hypothesis that the intramolecular hydrogen bond between the 2-pyridyl and the amine linker promotes low energy planar conformations in that part of the molecule which may result in the reduced aqueous solubility of the 2-pyridyl analogue seen during DMPK analysis.²

According to the work of Bader³², a bond or interaction between a pair of atoms can be characterized by the properties of electron density at a point, known as the bond critical point (BCP). This BCP corresponds to a centre point in the electron density surface between these atoms.

The analysis displayed below was carried out by Isabel Rozas³³ were the structure was optimized at DFT level using the functional M06-2X³⁴ and the basis set 6-311++G(d,p)³⁵ with the Gaussian09 package³⁶. This figure highlights the intramolecular bond angles and distances between the pyrazole and pyridine nitrogen's and the hydrogen of the amine linker. The bond distances (2.18 Å & 2.32 Å) and the bond angles (~100°) suggest that moderately strong hydrogen bonds will be present at these positions with the bond critical point highlighted in green. Finally, the package also picked out another potential hydrogen bond present between the pyridine of

the pyrazolopyrimidine core and an ortho-hydrogen of the lower R¹ phenyl ring. All this evidence supports the argument that intramolecular hydrogen bonding will have an impact on the resultant aqueous solubility of these pyrazolopyrimidine compounds and therefore disrupting this molecular planarity could serve as a viable approach to improve the aqueous solubility of later analogues.

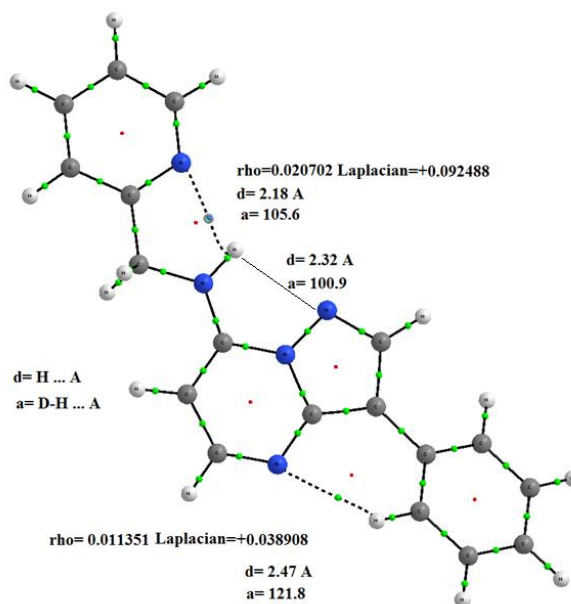


Fig 2.6 Modelling of the hydrogen bond interactions present within **AWF900** using the Gaussian 09 package.

The improvement in aqueous solubility with a 3 or 4 pyridyl ring system could be explained by disruption of this intramolecular interaction however unfortunately these compounds proved entirely inactive against *Wolbachia* at the highest tested concentration (5 μ M). Also, the nitrogen atom within the 3 and 4-pyridyl ring systems will be more exposed to an aqueous environment and this will also increase aqueous solubility.

The 2-pyridyl 3-CF₃ analogue **AWF907** exhibits reduced clearance compared to the 2-pyridyl parent analogue when incubated with rat hepatocyte cells and human microsomal protein. This suggests that the carbon adjacent to the pyridine nitrogen may be prone to metabolism and blocking this position would improve the stability of our compounds. However, these results did not elucidate any successful modifications that the R⁵ position tolerated in terms of anti-*Wolbachia* activity. Small modifications such as the introduction of a 4-F (**AWF903**) or 4-Cl (**AWF908**) caused a significant decrease or complete removal of activity. These results suggest that the 2-pyridyl nitrogen is a crucial moiety within this chemotype, perhaps forming an essential H-bond with the putative target.

2.2 Further R⁴ and R⁵- Substituted Pyrazolopyrimidines

2.21 Series two target selection and synthesis

The R³ position (6-position of the pyrazolopyrimidine ring – Fig 2.6) also appears to play an important role in driving anti-*Wolbachia* activity, comparison of results from **AWF905** (145 nM) and that of methyl containing substituent **AWF900 (1.23)** (Fig 2.6) (19 nM) indicate a significant seven-fold difference in potency.

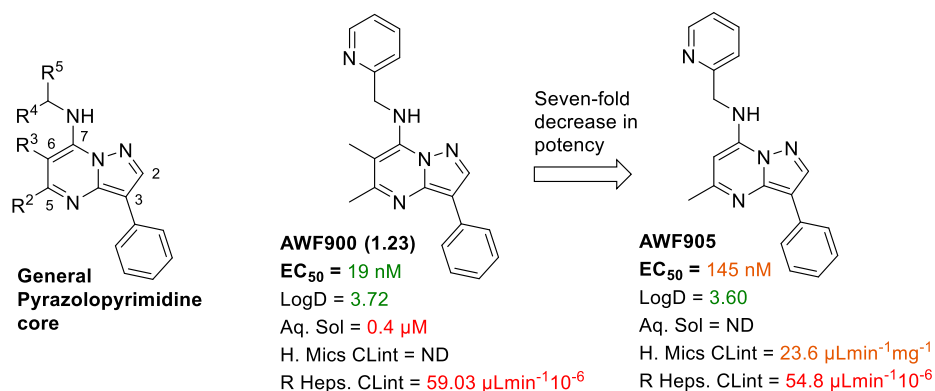
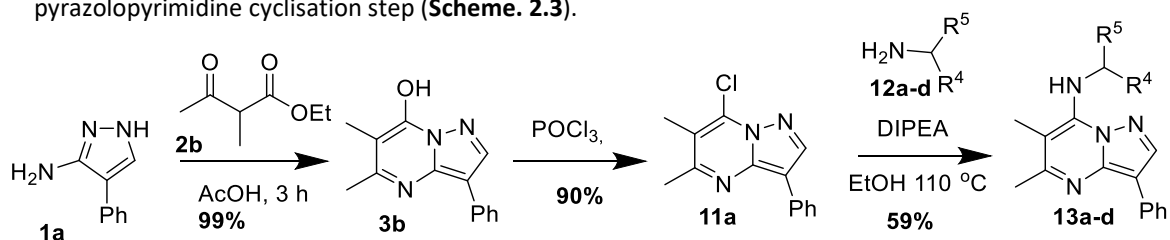


Fig 2.6 Comparison of **AWF905** with the 6-Me parent analogue which possesses greater anti-*Wolbachia* activity.

We incorporated this beneficial substitution into our core scaffold during the study of the R^{4/5} positions by incorporation of the methylated carbonyl compound, ethyl 2-methyl-3-oxobutanoate (**2b**) into the pyrazolopyrimidine cyclisation step (**Scheme. 2.3**).



Scheme. 2.3 Synthetic pathway to pyrazolopyrimidine analogues with modified R^{4/5} positions

This second series of analogues were designed to increase the metabolic stability through modification of the benzylic position to block metabolism at this position. There are many successful examples in the literature where removal or blocking a benzylic position has served to improve the metabolic stability of potential drug candidates. Palani *et al.*,⁷ introduced an oxime at the benzylic position of compound **14a** to produce the more stable **14b** during their metabolism-driven optimisation of CCR5 antagonists (**Fig 2.7**) which resulted in greater drug exposure (AUC_{0-6h}).⁷

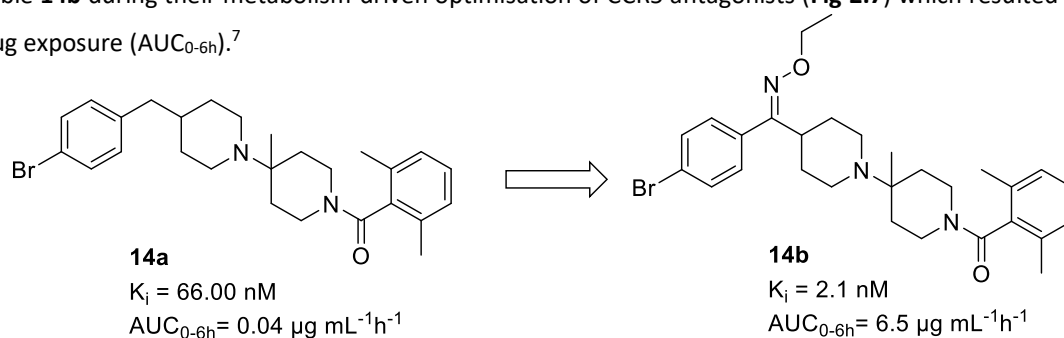


Fig 2.7 Introduction of ethyl oxime to alleviate the metabolic liability of the benzylic position

Initially we considered the incorporation of a single methyl substituent on the benzylic carbon atom. DMPK predictions from AZ supported the hypothesis that this modification would improve the metabolic stability of these compounds (**Fig 2.8**).

Substitution of heteroaromatics with more hydrophilic saturated heterocyclic ring systems is an established medicinal chemistry strategy for the improvement of aqueous solubility and metabolic stability. Such a strategy has been employed successfully by Morwick *et al.*,⁸ in their development of bisbenzimidazole Rho kinase inhibitors which possess multiple therapeutic opportunities including; neuropathic pain,⁹ cancer,¹⁰ bronchial asthma,¹¹ and glaucoma.¹² Reduction in unsaturated heterocycle ring size or substitution with a saturated heterocyclic ring systems are useful strategies for improving aqueous solubility.¹³ Furthermore, the *in silico* DMPK predictions carried out by AZ, concerning the replacement of a 2-pyridyl ring system with a 2-pyrrolidyl ring suggests that such a modification would greatly improve aqueous solubility and metabolic stability (**Fig. 2.8**).

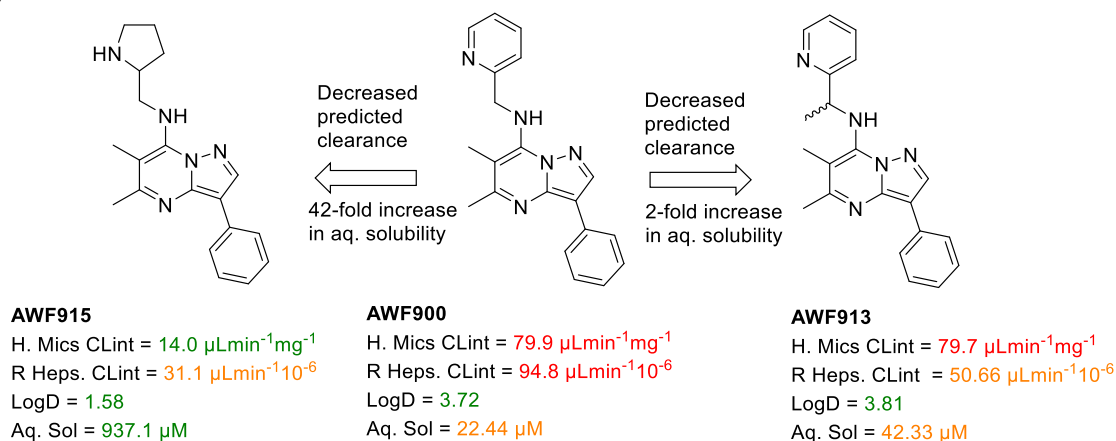


Fig 2.8 Predicted DMPK properties for methylation of the linker and replacement of the 2-pyridyl ring with a saturated 2-pyrrolidyl ring system.

Drug compounds containing pyridyl ring systems can often be exposed to *N*-oxidation as a primary route of metabolism.¹³ There are several ways to reduce this liability within analogues such as removal of the nitrogen or substitution of the pyridyl ring system to make the nitrogen less accessible to oxidation. As previous studies demonstrated that the replacement of the pyridyl ring with a phenyl ring or small substitutions to the pyridyl ring system completely removed anti-*Wolbachia* activity therefore as removal of the nitrogen was not a viable option (**Table 2.1**), alternative bioisosteres were sought. During the work to synthesise the potent HIV protease inhibitor ritonavir, Kempf and colleagues successfully replaced two pyridyl ring systems in the compound **15a** to eliminate pyridyl *N*-oxidation as a primary route of metabolism which resulted in a **15b** which experienced a near twofold improvement in bioavailability (**Fig 2.9**).¹⁴

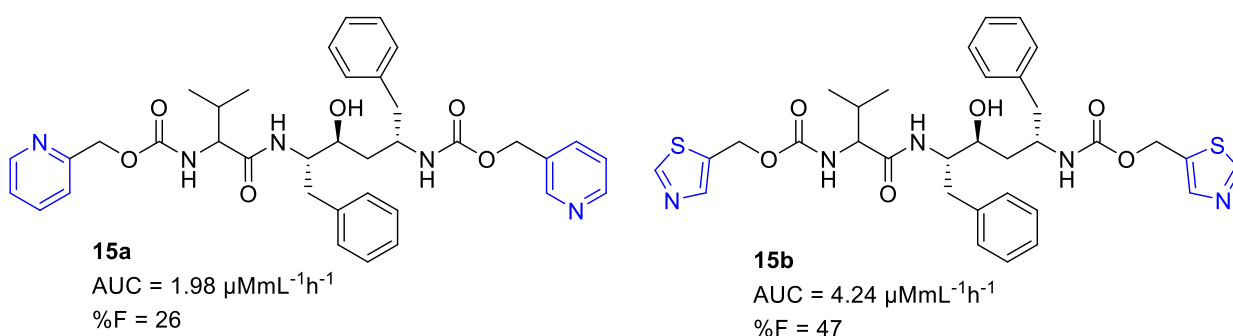
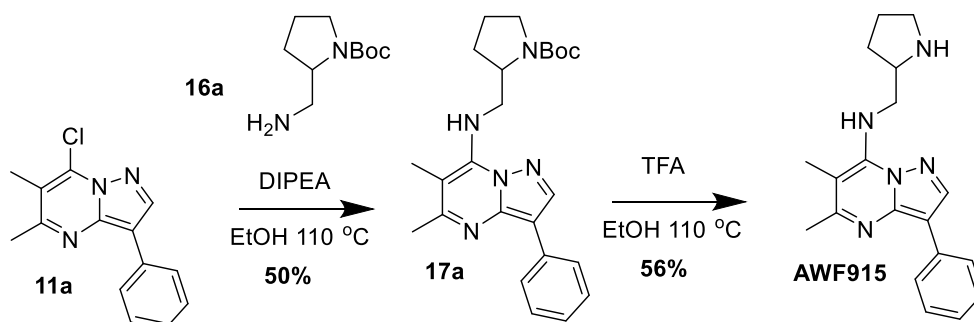


Fig 2.9 Metabolism-driven optimisation of HIV protease inhibitors through introduction of two thiazole rings.

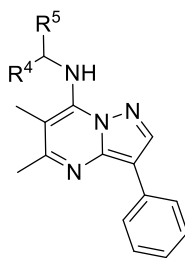
This improvement in stability resulted in greater drug exposure demonstrated by a larger Area-under curve (AUC) and greater bioavailability following oral dosing.

2.22 Further R⁴ and R⁵ SAR exploration – *in vitro* DMPK and potency results

In addition to examining the hydrophilic pyrrolidine ring and methylated linker, installation of a thiazole was also considered. These analogues were reached by chemistry discussed above in **Scheme 2.4**, the results for these analogues with various R^{4/5} functionalities are displayed in **Table 2.3**. The pyrrolidyl analogue **AWF915** was reached by reaction of the Boc-protected commercially available derivative **16a** with **11a** which gives the desired product upon Boc-deprotection. (**Scheme 2.4**)



Scheme 2.4 Synthesis of **AWF915** with the unsaturated 2-pyrrolidyl ring.



Code	R ⁴	R ⁵	EC ₅₀ (nM)	LogD 7.4	Aq.Sol (μM)	H.M.Cl ($\mu\text{Lmin}^{-1}\text{mg}^{-1}$)	R.HepsCl ($\mu\text{Lmin}^{-1} 10^{-6}$)	Human PPB (%)
AWF900		H	19	4.2	0.40	ND	59.0	>99.90
AWF913		Me (Racemic)	90	4.3	6.00	60.6	163.7	99.91
AWF914		H	>2500	4	0.60	54.2	138.6	99.64
AWF915		H	NA	10.0	511	10.05	133.9	ND

NA – No activity at highest concentration (5 μM) ND – Not determined

Table 2.3 Further analogues with modified R^{4/5} positions containing a 6-Me with *in vitro* potency and measured DMPK data

Replacement of the 2-pyridyl ring with the 2-pyrrolidyl or thiazole rings both proved unsuccessful in terms of anti-*Wolbachia* activity; however, the 2-pyrrolidyl ring did prove to have greatly enhanced aqueous solubility (511 μM) and reduced clearance when incubated with human microsomes (10.1 $\mu\text{Lmin}^{-1}\text{mg}^{-1}$) in line with *in silico* prediction.

AWF913 with a methylated linker (R⁴=Me) was tested as a racemic mixture and despite a notable decrease in compound potency (EC₅₀ = 19 nM to 90 nM) an increase in aqueous solubility (from 0.4 μM to 6.0 μM) was observed. This could again be attributed to disruption of any H-bonding between the 2-pyridyl nitrogen and amine linker.

Spartan analysis of the compound **AWF913** (Fig 2.10) containing the methylated linker displayed five fewer low energy conformers (between 3-7 kJmol^{-1}) than the parent analogue **AWF900** which experiences reduced solubility. This is likely to be due to the presence of the methyl group within the linker which interferes with the intramolecular hydrogen bonding capacity of **AWF915** resulting in fewer low energy conformations where the hydrogen bond is present. The most stable conformation to form this hydrogen bond (M0011 Relative energy to lowest energy conformer found = 39.97 kJmol^{-1} – Fig 2.10) within the methylated analogue is

predicted to be of much higher energy compared to the benzylic linker variant (Relative energy = 6.35 kJmol^{-1}

Fig 2.5)

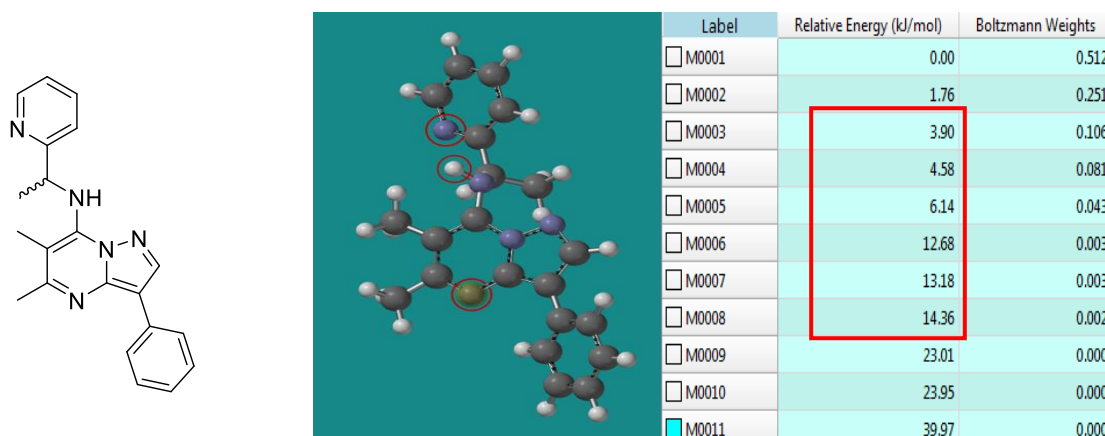


Fig 2.10 Low-energy conformer analysis of analogue **AWF915**.

Work conducted on the pyrazolopyrimidine template in parallel to the study of the R^4 and R^5 positions elucidated a beneficial modification to the lower phenyl ring at the $3/R^1$ position. We found that incorporation of a 4-F Ph group at this position was tolerated in terms of potency and could promote a large improvement in metabolic stability (Fig 2.11).

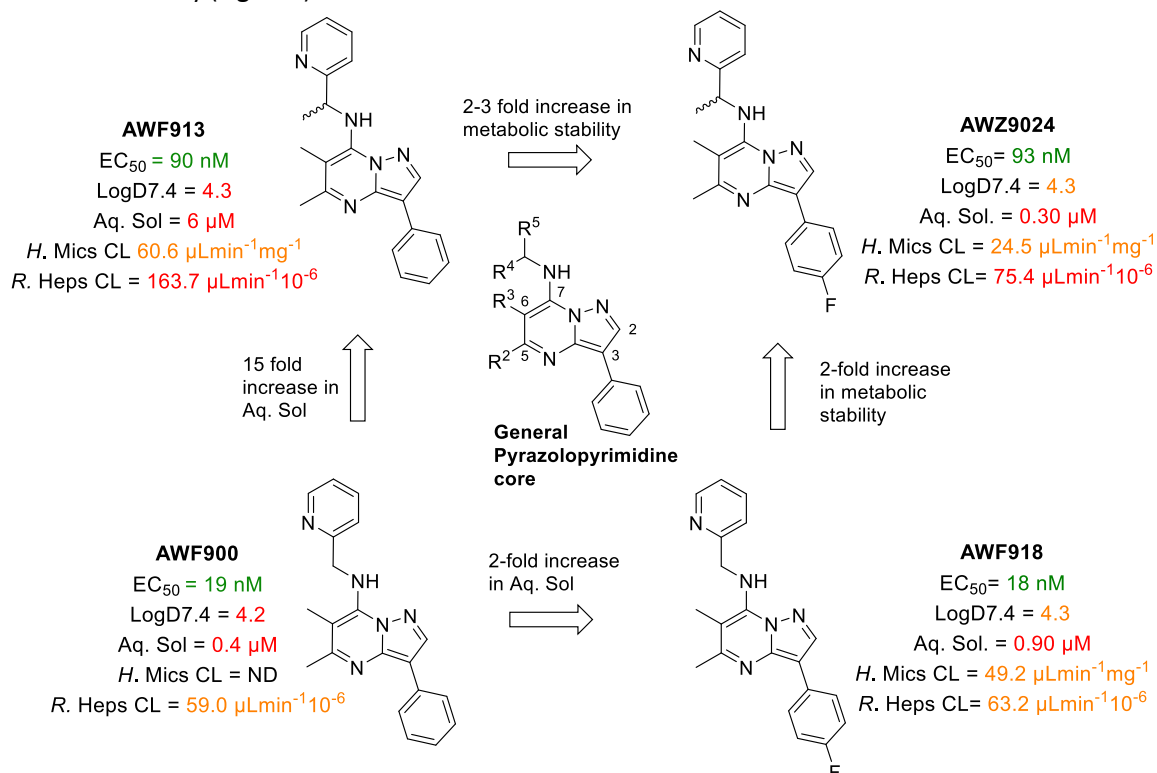


Fig 2.11 *in vitro* potency and DMPK properties of methylated and 4-F Ph analogues.

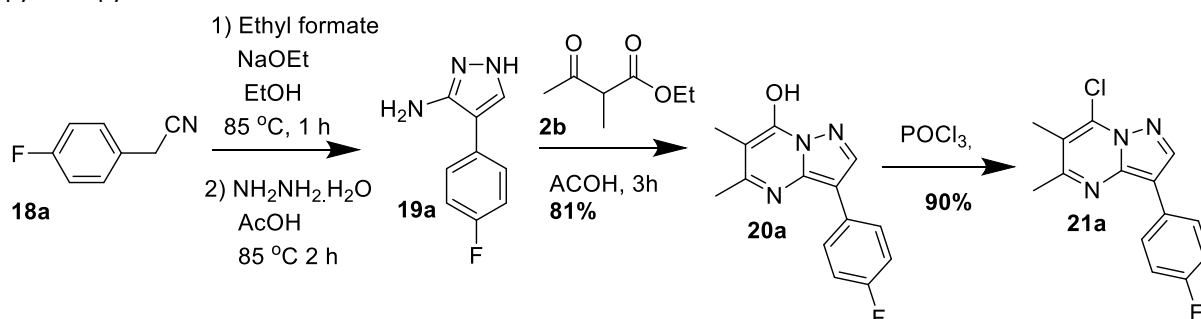
While the *in vitro* DMPK analysis for the methylated analogues **AWF913** and **AWZ9024** suggest that the 4-fluoro phenyl ring results in a decrease in aqueous solubility ($6.0 \text{ }\mu\text{M}$ to $0.3 \text{ }\mu\text{M}$) this appears to be molecule

dependent as many other analogues such as **AWF900** and **AWF918** (0.4 μM to 0.9 μM) do not suffer this decreased solubility (**Fig 2.11**).

2.3 Series 3: 3-(R^1) 4-F Ph, R^4 - and R^5 - Substituted Pyrazolopyrimidines:

2.31 Design and Synthesis

The first analogue in this series **AWF918** was synthesised by a more diverse route in respect to altering the R^1 position of the chemotype which is discussed later (Chapter 3 3-aryl pyrazolopyrimidines). However, during further assessment of the $\text{R}^{4/5}$ positions the 4-F Ph modification was adopted into the core scaffold. To simplify the synthesis of these compounds, a 4-F substituted phenyl ring was installed into the initial pyrazole starting material **19a** (**Scheme 2.5**). This was performed by the reaction of the nitrile compound 2-(4-Fluorophenyl)acetonitrile (**18a**) with ethyl formate to form the aldehyde intermediate which cyclises upon reaction with hydrazine to give **19a** (**Scheme 2.5**). This 4-F Ph 5-amino pyrazole could then be used within the synthesis discussed previously and presented here in **Scheme 2.5** to give the important 7-chloro pyrazolopyrimidine **21a**.



Scheme 2.5 – Procedure for the synthesis of substituted pyrazole intermediates.

Further modifications to the linker functionality were designed for synthesis during the next series of analogues following promising DMPK predictions (**Fig 2.12**). Introduction of an amide linker (**AWF959**) was predicted to improve metabolic stability despite a predicted three-fold drop in aqueous solubility. Incorporation of a methyl alcohol linker is predicted to offer a four-fold improvement to aqueous solubility and a predicted two-fold decrease in human microsomal clearance.

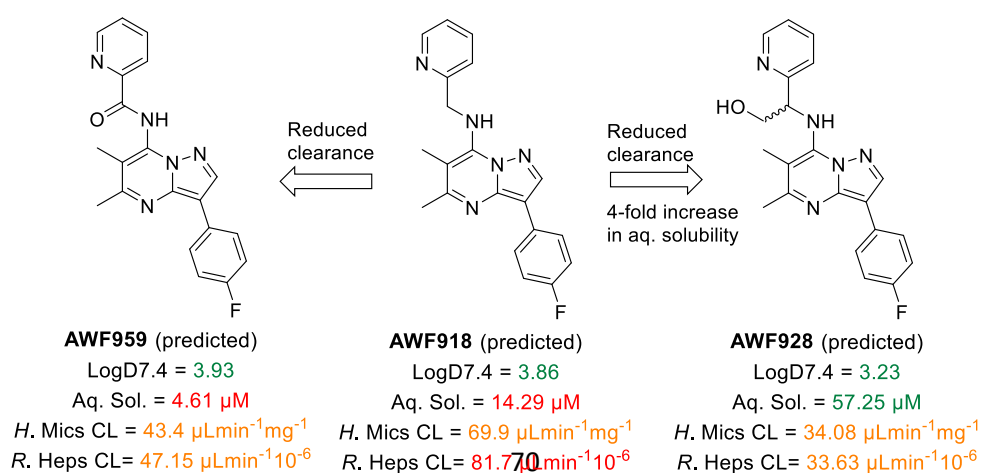
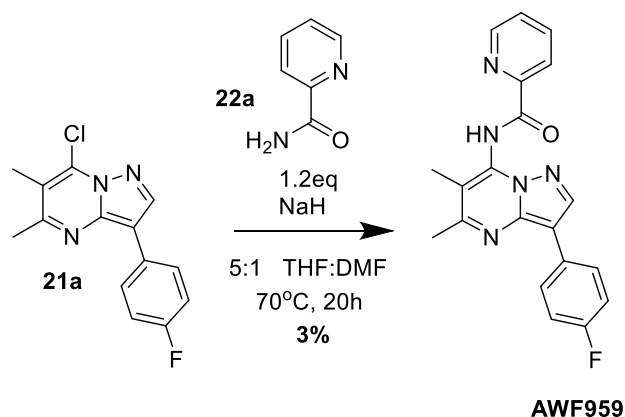


Fig 2.12 Predicted DMPK values for analogues containing an amide and methyl alcohol linker moiety.**Scheme 2.6** Installation of an amide linker between the pyrazolopyrimidine core and 2-pyridyl ring.

Compounds designed following these predictions included a methyl alcohol linker and a cyclopropyl linker (**AWZ9066**) which were synthesised by previously discussed chemistry (**Scheme 2.3**). An amide linker was installed by the reaction of the 7-chloro intermediate **21a** (**Scheme 2.6**) and picolinamide (**22a**). Pre-mixing picolinamide (**22a**) with sodium hydride allowed for reaction with the 7-chloro pyrazolopyrimidine **21a** to form the desired product **AWF959** (**Scheme 2.6**). The yield for this reaction was very low however enough of **AWF959** was isolated for *in vitro* biological evaluation.

2.32 Series 3 *in vitro* DMPK and Potency

Series three molecules involved several analogues without the methylene linker and a variety of aliphatic side-chains at the R^{4/5} positions since DMPK predictions (data not shown here) looked promising. These analogues were synthesised by our chemistry partner WuXi and the results from the *in vitro* biological and DMPK evaluation for this series of compounds are displayed in **Table 2.4**.

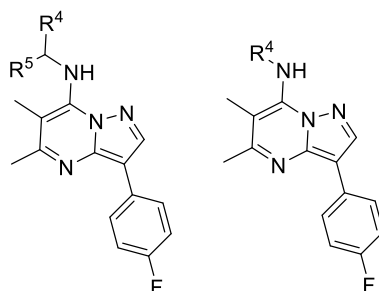
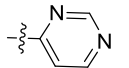


Table entries: 1-11, 14-17 12, 13

Table entry	Compound	R ⁴	R ⁵	EC ₅₀ (nM)	LogD 7.4	Aq. Sol (μM)	Human Mics Clint (μL/min/mg)	Rat Heps Clint (μL/min - 10 ⁻⁶)	Human PPB (%)
1	AWF918		H	17	4.3	0.90	49.2	67.7	99.8
2	AWZ9003		H	>2500	3.2	37.0	9.03	217.4	94.5
3	AWZ9027		H	>2,500	1.8	54	<3.0	62.5	93.4
4	AWZ9028		H	>2500	ND	ND	ND	ND	ND
5	AWF934		H	NA	2.55	49.0	1.7	6.7	95
6	AWZ9001		H	> 2,500	3.9	0.50	65.3	128.9	98.9
7	AWZ9002		H	>2500	3.10	148	15.52	57.49	96.2
8	AWF963		H	NA	4.9	0.10	48.0	67.0	>99.96
9	AWF937		H	33	3.3	0.50	48.9	41.3	99
10	AWF933		H	183	3.4	2.00	35.68	95.85	99

11	AWF935		H	518	3.15	1.00	27.32	68.6	98
----	--------	---	---	-----	------	------	-------	------	----

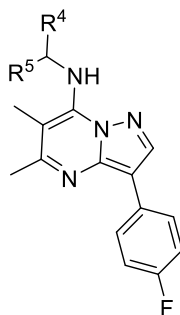
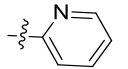
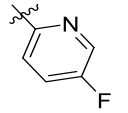
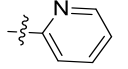
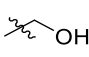
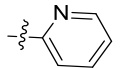
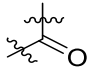
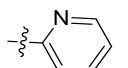

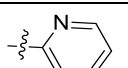


Table entry	Compound	R ⁴	R ⁵	EC ₅₀ (nM)	LogD 7.4	Aq. Sol (μM)	Human Mics Clint (μL/min/mg)	Rat Heps Clint (μL/min 10 ⁻⁶)	Human PPB (%)
12	AWZ9007		R ⁴ directly attached	>2,500	ND	ND	ND	ND	ND
13	AWZ9008		R ⁴ directly attached	>2,500	ND	ND	ND	ND	ND
14	AWF928			>2500	3.8	25.0	12.6	56.5	99.08
15	AWF959			456	4.1	0.80	53.6	13.1	99.6
16	AWZ9066			>2500	>5.00	ND	14.3	29.3	>99.95
17	AWZ9024		Me	93	4.3	0.3	24.5	75.4	ND

NA – No activity at highest concentration (5 μM) ND – Not determined

Table 2.4 Continued R^{4/5} exploration with a 4-F Ph ring at the R¹ position

Compounds containing hydrophilic aliphatic amines (**AWZ9003**, **AWZ9027-8**) in **Table 2.4** (entries **2-4**) were synthesised by our chemistry partner WuXi App Tech and served to greatly improve the aqueous solubility of these pyrazolopyrimidine compounds (**AWZ9003** Aq. Sol = 37 μM, **AWZ9027** Aq. sol = 54 μM) over **AWF918** (Table entry **1**, Aq. sol = 0.9 μM) however such modifications removed anti-*Wolbachia* potency. The aromaticity of the R⁴ group also appeared to be essential for activity due to the complete loss of activity seen in compound **AWF934** (table entry **5**) with the saturated 2-piperidyl ring losing activity as seen earlier in the saturated 2-pyrrolidyl analogue **AWF915**. This lack of potency is also seen upon incorporation of the morpholine and piperidine heterocyclic systems (**AWZ9001** and **AWZ9002**), table entries **6** and **7** respectively despite a large increase in aqueous solubility and reduced clearance in the piperidyl analogue **AWZ9002** compared to the 2-pyridyl parent analogue (entry **1**). Introduction of the 2-oxetane ring system (**AWF963** – entry **8**) was also detrimental to anti-*Wolbachia* potency. The only tolerated change at this position in terms

of potency was the 2,6-pyrimidine ring (**AWF937** – table entry **9**) which provided a negligible increase in metabolic stability at the cost of a near two-fold drop in potency compared to **AWF918** (entry **1**) (18 to 33 nM). Other pyrimidine regio-isomers, **AWF933** and **AWF935** (tables entries **10** and **11**) resulted in a major decrease in compound potency (EC_{50} = 185 and 518 nM) respectively despite a small reduction in clearance from a metabolic system.

Removal of the methylene linker functionality by insertion of various substituted amino pyridines proved to completely remove anti-*Wolbachia* activity seen by the analysis of **AWZ9007-8** (table entries **12** and **13**). Analysis of entry **14** containing a methyl alcohol substituent within the linker supports previous observations that modification of this position results in a major decrease in compound potency (EC_{50} = >2500 nM). Introduction of the amide linker group (**AWF959** – entry **15**) did not seem to positively benefit any of the assessed DMPK parameters compared to the parent analogue **AWF918** and caused a significant drop in anti-*Wolbachia* efficacy (18 nM to 456 nM). Introduction of a cyclopropyl ring system into the linker functionality (**AWZ9056** – entry **16**) increased logD compared with **AWF918**, which should lead to improved the aqueous solubility. Also, blocking the benzylic position should reduce clearance from both rat hepatocyte and human microsomes (clearance values < 30); however, completely removed anti-*Wolbachia* activity. This supports the theory that modification of the linker can distort intramolecular H-bonding to promote better solubility and that the specific modification of the benzyl linker can modulate metabolism. Further examination of a methylated linker in **AWZ9024** (entry **17**) displayed a notable 4-fold decrease in activity compared to **AWF918** (18 nM to 93 nM). Analogues synthesised by our chemistry partners demonstrated that *N*-methylation of the linker was also not tolerated in terms of compound potency (**Fig 2.13**); at this point methylation of the benzyl position was the only tolerated modification of the linker that maintains suitable potency.

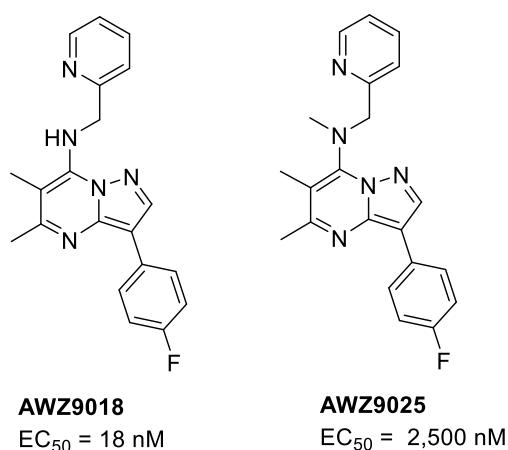


Fig 2.13 *N*-methylation of the amine linker within pyrazolopyrimidine analogues

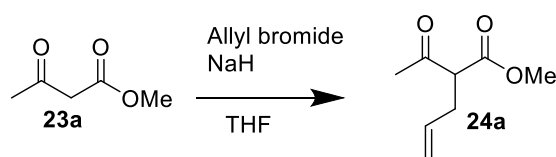
In summary, further variations to the R^4 position underlined the essential nature of the 2-pyridyl ring. These results support the idea that the NH linker is also an essential moiety, presumably as a H-bond donor at the drug target, while the 2-pyridyl nitrogen is an essential H-bond acceptor. Additionally, it is plausible that an intramolecular H-bond interaction between these two functionalities which is important for the compound conformation upon entering the necessary binding site. This could be an explanation for the complete loss of

activity seen upon modification of either functionality as opposed to a partial loss of activity which could be expected if both interactions were independently important for promoting good activity.

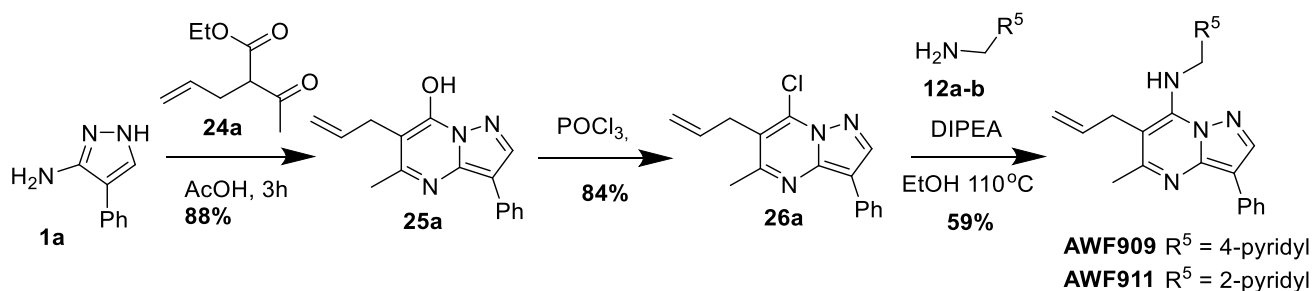
2.4 6 (R^3)- Substituted Pyrazolopyrimidines

2.41 Target Design and Synthesis

The initial hit **AWF911** with the 6-(R^3) allyl group was synthesised via previously discussed chemistry with the necessary allyl substituted beta-keto ester **24a** which was produced in-house from methyl 3-oxobutanoate **23a** using sodium hydride and allyl bromide (**Scheme 2.7**). Synthesis of the initial hit was carried out in parallel to the corresponding 4-pyridyl regio-isomer (**Scheme 2.8**), this was to verify the observations made thus far during analysis of the R^5 position that alterations to this position are not only restricted but almost entirely prohibited to produce molecules with potent anti-*Wolbachia* activity.



Scheme 2.7 Synthesis of methyl 2-acetylpent-4-enoate.



Scheme 2.8 Re-synthesis of the initial hit **AWF911** and the 4-pyridyl regio isomer **AWF909**

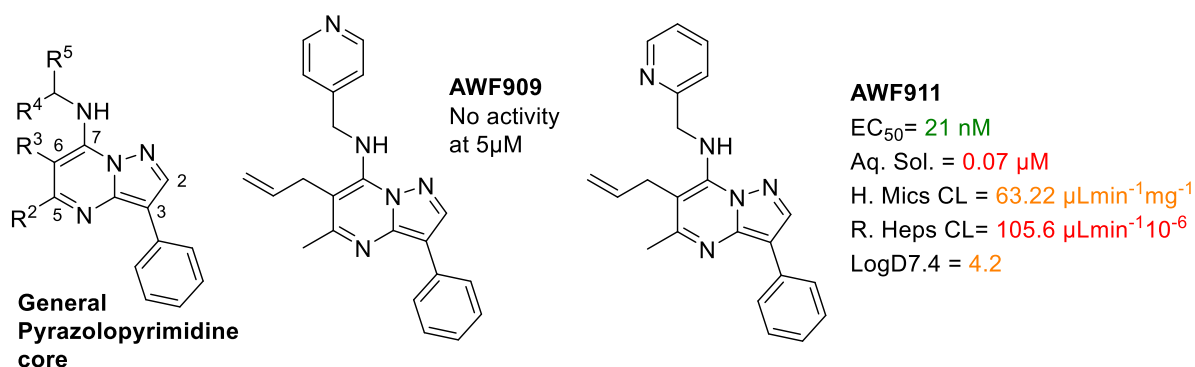


Fig. 2.14 Structure of the initial hit **AWF911** with the 4-pyridyl regio-isomer.

The resultant anti-*Wolbachia* activity of **AWF911** and lack of in the regio-isomer **AWF909** (Fig 2.14) confirmed the requirement of a terminal 2-pyridyl group for high activity whilst simultaneously displaying that lipophilic substituents are tolerated at the R² position and promote good activity. **AWF911** displayed increased human microsomal clearance, compared to the 6-H analogue **AWF905** (63.2 Vs 23.6 $\mu\text{Lmin}^{-1}\text{mg}^{-1}$). A 6-methyl substituent was tolerated in terms of anti-*Wolbachia* activity and had improved metabolic stability over the allyl displayed in the initial hit.

Following the successful incorporation of a few groups at the C6 (R³) position (Me, H, allyl) additional analogues were designed for synthesis with modified R³ positions to further evaluate the SAR surrounding this position and to determine the optimum substituent in terms of potency and DMPK properties. DMPK predictions were carried out for a variety of analogues and the most promising selected for synthesis (Fig 2.15).

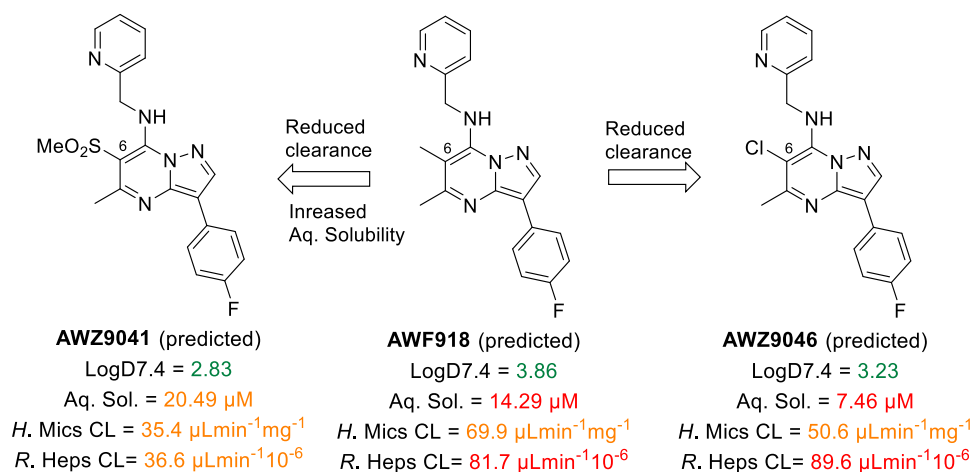
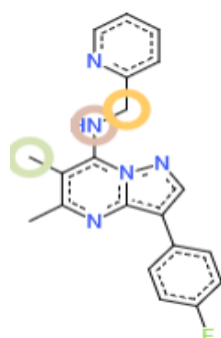


Fig 2.15 Predicted DMPK properties for analogues with various R³ positions

Incorporation of a sulfonyl methyl substituent at the R³ position (**AWZ9041**) (Fig 2.15) is predicted to be more stable than the methyl-containing pyrazolopyrimidine compounds demonstrated by the reduced predicted clearance values. A chlorine atom at the R³ (**AWZ9046**) position is expected to at least maintain the stability and was selected for synthesis to study the effect that a halogen at this position has on the anti-*Wolbachia* activity of these analogues. Another analogue designed for synthesis by our chemistry partners contained a trifluoroethyl at the position (**AWZ9067**). SmartCyp predictions used previously to examine the predicted metabolic stability of the initial hit **AWF911** (Chapter 1) were used to examine **AWZ9067** containing the fluorinated alkyl chain and the parent analogue **AWF918** (6-Me) (Fig 2.16)



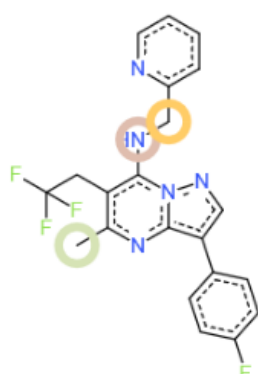
AWF918

Standard CYP2C CYP2D6

1: Molecule from ChemDoodle Web Components

Rank Atom Score Energy Accessibility 2DSASA

1	C.14	34.41	41.1	0.71	24.31
2	N.13	48.63	54.1	0.64	8.09
3	C.10	58.53	66.4	0.71	53.78



AWZ9067

Standard CYP2C CYP2D6

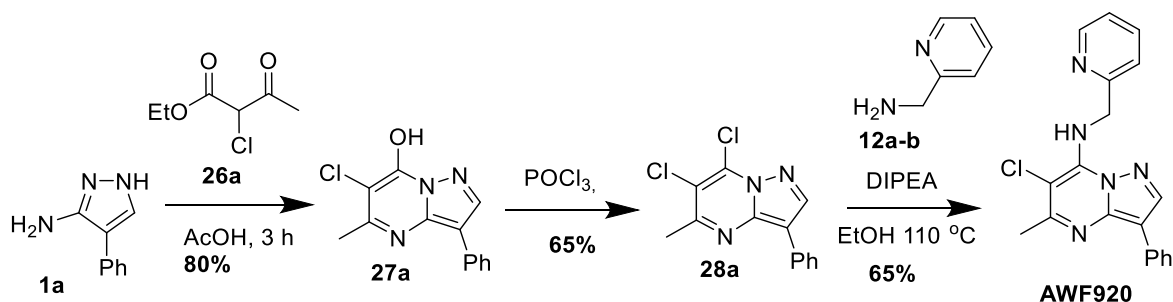
1: Molecule from ChemDoodle Web Components

Rank Atom Score Energy Accessibility 2DSASA

1	C.24	34.41	41.1	0.71	24.31
2	N.23	48.67	54.1	0.64	7.27
3	C.11	59.08	66.4	0.64	54.42

Fig. 2.16 SmartCyp predictions for trifluoroethyl analogue **AWZ9067** and 5,6 dimethyl **AWF918**.

These predictions suggest that the 6-position of the pyrazolopyrimidine core will be less susceptible to metabolism when a trifluoroethyl substituent is incorporated (**AWZ9067**) when compared to the 6-Me analogue **AWF918**. Albeit the predicted values only indicate a small increase in metabolic stability as the next most susceptible atom is the terminal methyl group at the 5-position of the core; however, this analogue was selected for synthesis to measure the difference to *in vitro* stability compared with DMPK data measured for **AWF918** once the potential metabolism to the 6-position had been suitably blocked.

**Scheme 2.9** Synthesis of **AWF920** containing a 6-chloro substituent

The various structures and biological activities of analogues within the first series of compounds exploring the R³ position are documented below in **Fig 2.17** alongside the *in vitro* DMPK properties.

2.42 (R³) Pyrazolopyrimidines Biological Evaluation

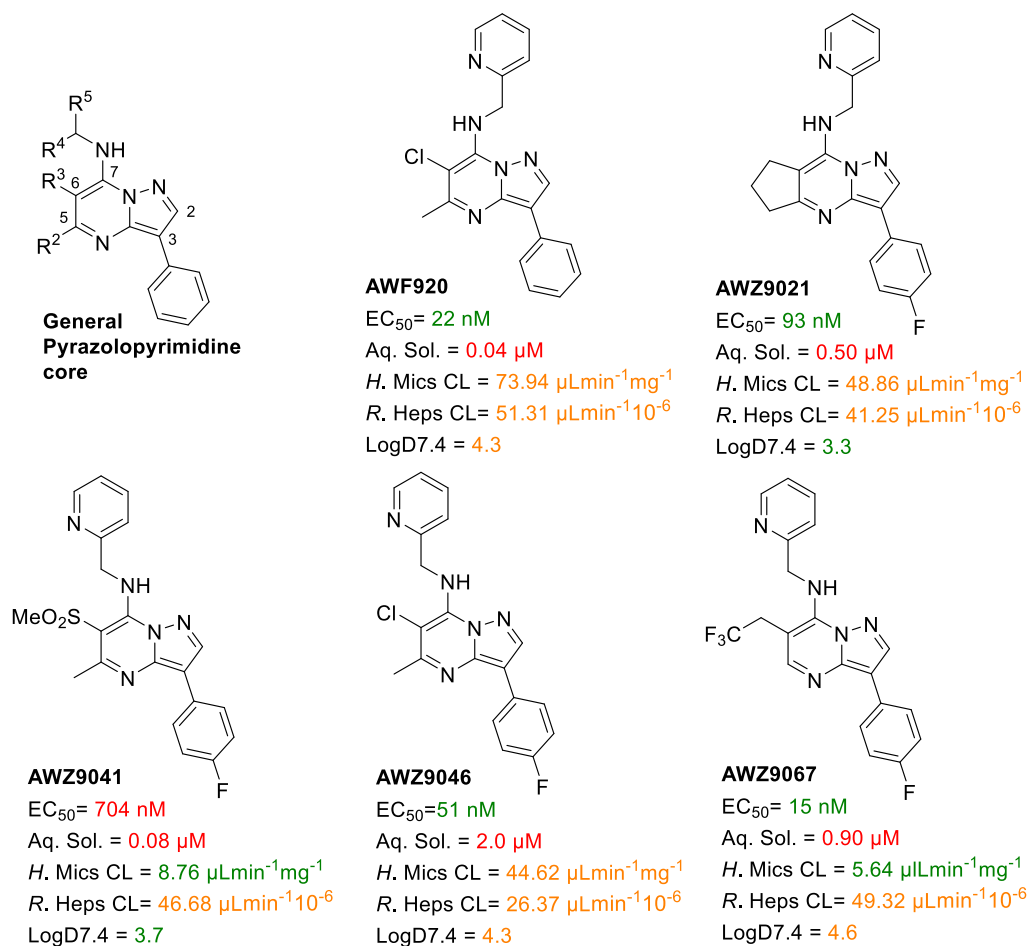


Fig. 2.17 Structures of analogues with varied 5-(R³) positions with *in vitro* Biological and DMPK results.

These **AWZ** compounds were synthesised using the reactions discussed extensively throughout this chapter and are displayed above in **Scheme 2.9**, using the necessary di-carbonyl compounds (See Appendix 1). Analogues which were unsubstituted at the R² position such as **AWZ9067** required a base catalysed pyrazolopyrimidine ring formation (Appendix 1) which is discussed later (Ch. 4) during further study of this position when this reaction was utilised in-house. Incorporation of a fused cyclopentyl ring at the R² and R³ positions (**AWZ9021**) was well-tolerated in terms of anti-*Wolbachia* activity (EC₅₀ = 93 nM) and displayed that both positions could be varied without a significant loss of activity. This modification did not increase aqueous solubility; however, by removal of the two metabolically labile terminal methyl groups the metabolic stability increased as shown by a decreased rat hepatic clearance (41.3 μLmin⁻¹10⁻⁶) compared to the parent analogue **AWZ918** (67.7 μLmin⁻¹10⁻⁶). Incorporation of a polar SO₂Me group at the R³ position in **AWZ9041**, whilst

promoting improved human microsomal stability, was not a suitable modification in terms of potency, producing a 35-fold drop in anti-*Wolbachia* efficacy ($EC_{50} = 704$ nM). The bioisosteric incorporation of chlorine is a suitable substitution at the R³ position in terms of potency (**AWF920** $EC_{50} = 22$ nM) and in some analogues resulted in decreased human microsomal clearance in comparison to the corresponding 6-methyl analogues. Introduction of the trifluoromethyl substituent at the 6/R³ position in compound **AWZ9067** alongside removal of the 5-methyl provided good anti-*Wolbachia* activity ($EC_{50} = 15$ nM) and greatly reduced human microsomal clearance ($5.64 \mu\text{Lmin}^{-1}\text{mg}^{-1}$). However, all analogues containing halogen substituents in the R³ position (chlorine, trifluoromethyl, trifluoroethyl) synthesised thus far were shown to produce undesired worm toxicity in the *in vitro* *Brugia malayi* mf assay. (See Ch.4 *in vitro* analysis section). As discussed earlier in Ch.1 it is essential that any compounds targeting *Wolbachia* act purely by targeting the bacteria and possess no direct efficacy against the worm to avoid the inflammatory reactions associated with filaricidal therapies. For this reason, it was decided that these modifications were unsuitable at this point; however, would be revisited in optimized analogues and tested for direct-worm toxicity.

2.5 Conclusion

Key modifications that improved the overall properties of this template are summarised in **Fig 2.18**. The allyl group which was present within the initial hit **AWF911** was associated with metabolic instability and following its removal (R³ = H) there was improvement to stability but a decrease in compound potency. Several modifications were tolerated at this 6-(R³) position in terms of producing compounds which demonstrate acceptable *in vitro* anti-*Wolbachia* activity while the methyl group proved to offer the best balance of potency and DMPK properties. The 2-pyridyl group was essential for compound potency and whilst methylation of the linker generally offers a small improvement to stability when compared to other analogues and boosts the aqueous solubility this modification reduces compound potency.

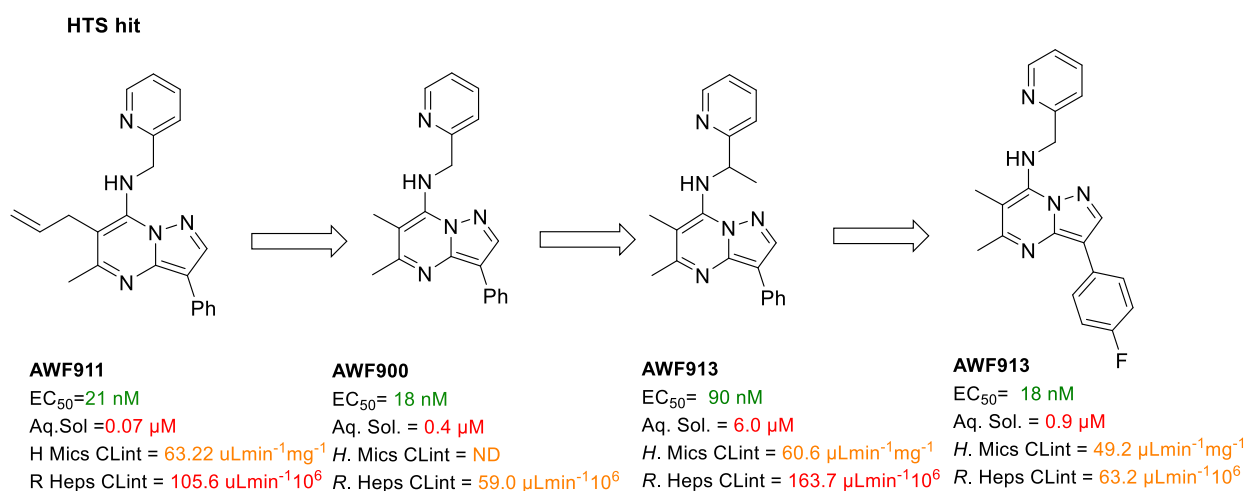


Fig 2.18 Summary of hit to early lead optimisation discussed in this chapter.

Compound optimisation by modification of the 2-pyridyl ring or methylene linker is limited by few suitable alterations being tolerated in terms of potency. One main success during the work discussed in this chapter concerning the optimisation of these pyrazolopyrimidine compounds is the over 85-fold improvement in aqueous solubility seen from the initial hit **AWF911** to **AWF913**. Despite such a notable improvement to aqueous solubility it was still necessary to enhance DMPK properties of these analogues. Functionalisation of the lower phenyl ring offers further opportunities to improve the potency and DMPK properties of our pyrazolopyrimidines. The next chapter will focus on pyrazolopyrimidines containing various modifications to the phenyl ring system displayed in the initial hit **AWF911**.

Of the analogues synthesised so far, the majority fall within the guidelines of promising chemical space for drug candidates set out by the GlaxoSmithKline 4/400 rule explained earlier in Ch. 1.7.2, these analogues are highlighted in green on **Chart 2.1**. While the outliers which are highlighted in orange are slightly outside this range they are compliant with Lipinski's rule of 5,¹⁵ demonstrating suitable properties to potentially possess promising oral bioavailability. During the future optimisation of this template more analogues containing properties which fall within the 4/400 guidelines^{16,17} will be sought to maximise the opportunity of producing analogues with suitable ADMET properties.

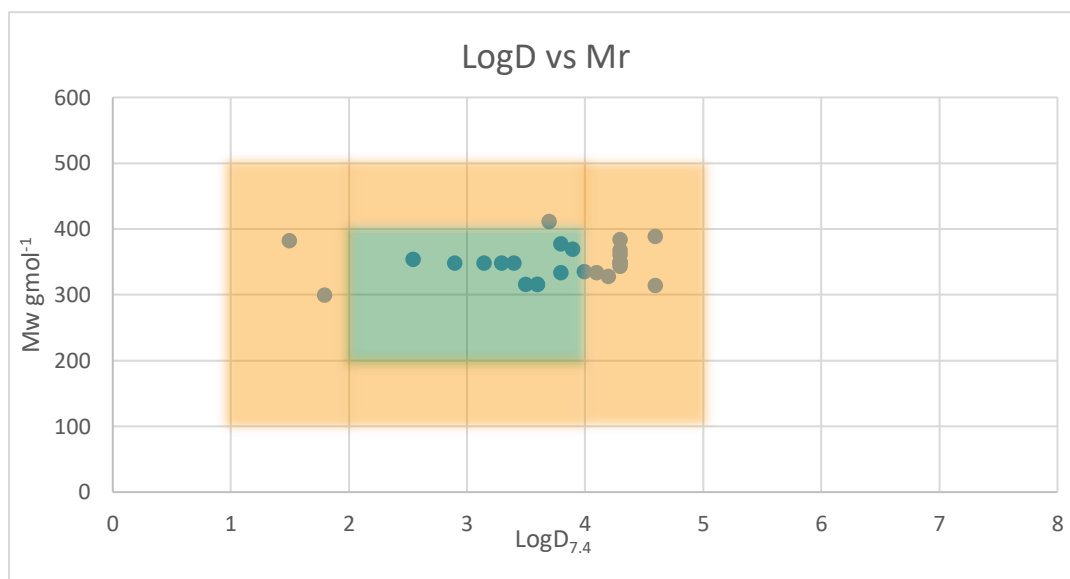


Chart 2.1 A plot of LogD against molecular weight for the pyrazolopyrimidines in this series.

As expected during the design of these analogues, the reduction in LogD has enhanced the aqueous solubility throughout the optimisation of this series of analogues which is demonstrated in **Chart 2.2**. Improvement of aqueous solubility will remain a priority throughout the synthesis of a new series of analogues to ultimately produce pyrazolopyrimidines which are suitable for oral dosing.

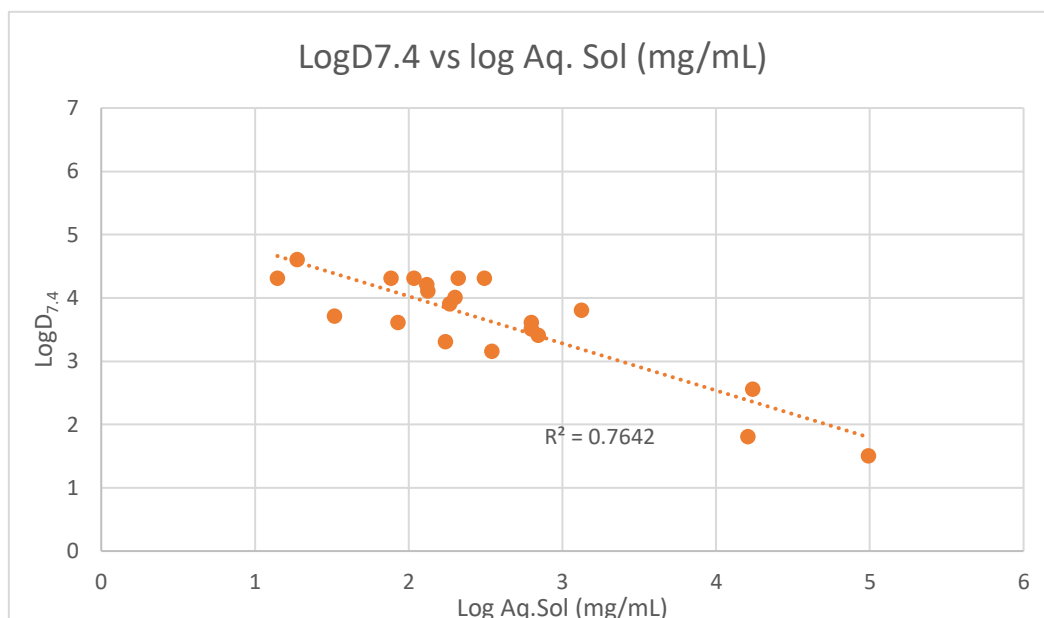


Chart 2.2 Plot of log Aq.sol against LogD for pyrazolopyrimidine analogues in this chapter.

Finally, there appears to be a weak correlation ($R^2 = 0.64$) between LogD and log Rat hepatocyte clearance, as LogD decreases (or Aq. Solubility increases) the metabolic stability of our compounds increases as demonstrated by the reduced clearance values (**Chart 2.3**). It could be suggested that this increase in stability is due to the binding-pockets within enzymes which are responsible for metabolising the pyrazolopyrimidine compounds are lipophilic and less readily available for the more hydrophilic compounds.¹⁸ This correlation further supports the design of compounds with greater aqueous solubility which could also serve to boost the stability of our analogues within a metabolic system.

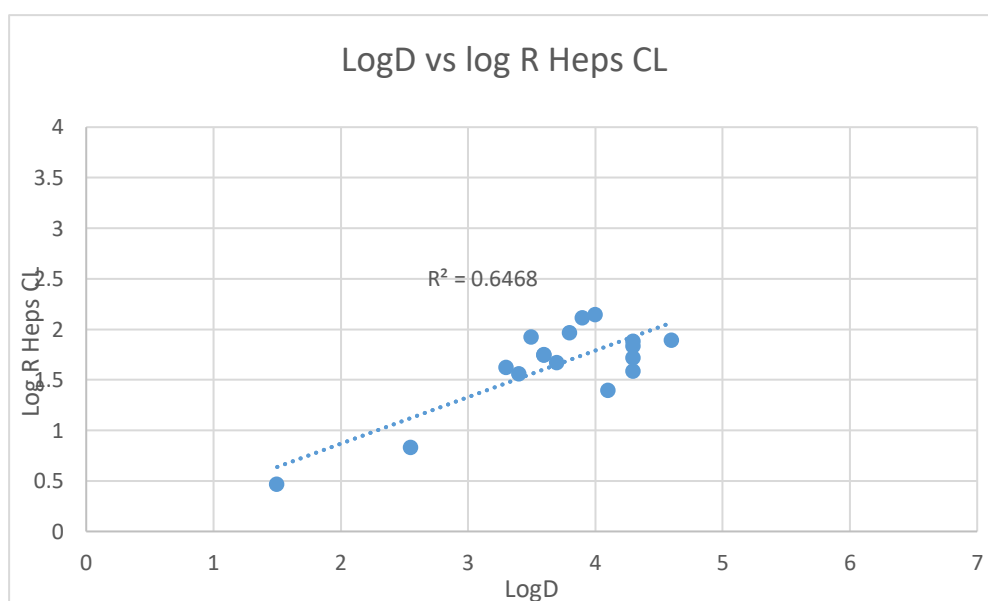


Chart 2.3 Plot of LogD versus the log R.Hepatocyte clearance of pyrazolopyrimidines in chapter 1.

A summary of the SAR derived from this part of work is displayed in **Fig.2.19**

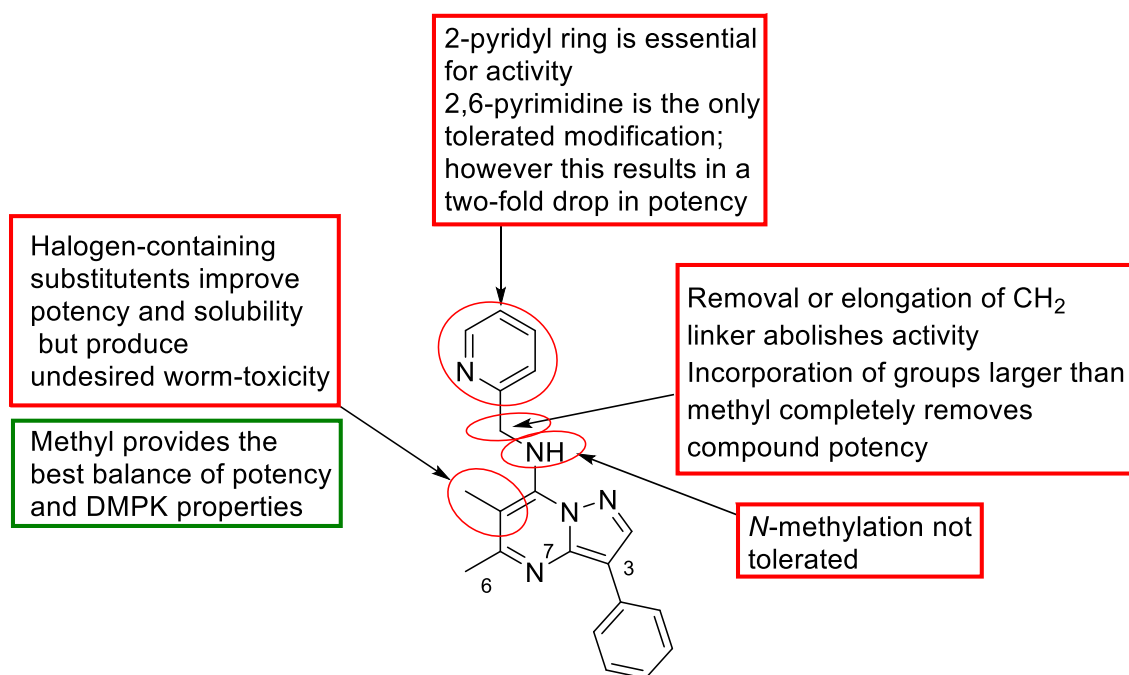


Fig 2.19 Summary of the SAR understood from the analogues studied so far.

With the SAR restricted in terms of the 2-pyridyl ring and linker functionalities, our next series of analogues within chapter 3 will focus on the chemical space surrounding the phenyl ring at the 3-position (R^1) of the pyrazolopyrimidine core. As demonstrated within this chapter, modification of the 6-position (R^3) offers an opportunity to quite drastically alter compound potency and therefore future analogues will continue to probe this area to determine the optimum group at this position in terms of potency and DMPK properties.

2.6 Experimental

Biological Evaluation (See Chapter 4 experimental for screening materials and methods)

General

Air- and moisture-sensitive reactions were performed in oven dried glassware sealed with rubber septa under an atmosphere of nitrogen from a manifold or balloon. Anhydrous solutions and sensitive liquids were transferred via syringe or stainless-steel cannula. Reactions were stirred using Teflon-coated magnetic stir bars. Organic solutions were concentrated using a Buchi rotary evaporator with a diaphragm vacuum pump.

Purification of solvents and reagents

Anhydrous solvents were either purchased from Sigma Aldrich or dried and distilled immediately prior to use under a constant flow of dry nitrogen. Tetrahydrofuran was distilled from Na, dichloromethane and Et₃N were distilled from CaH₂. All reagents were purchased from Sigma Aldrich, Alfa Aesar, Frontier Scientific, Apollo Scientific, Fluorochem and were used without any purification unless otherwise indicated.

Purification of products

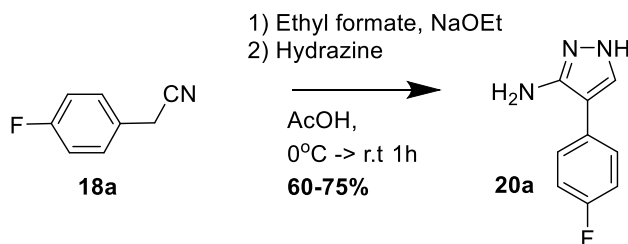
Thin layer chromatography (TLC) was performed on 0.25 mm Merck silica gel 60 F254 plates and visualised by ultraviolet light. U.V. inactive compounds were visualised using iodine, p-anisaldehyde solution, ninhydrin or potassium permanganate followed by gentle heating. Flash column chromatography was performed on ICN ecochrom 60 (32-63 mesh) silica gel eluting with various solvent mixtures and using an airline to apply pressure.

Analysis

Melting points were determined by a Gallenkamp apparatus and are uncorrected. ¹H NMR spectra were recorded on Bruker AMX 400 (400 MHz) spectrometer and reported as chemical shift on parts per million (ppm, δ) relative to tetramethylsilane as the internal reference, integration, multiplicity (s = singlet, br s = broad singlet, d = doublet, t = triplet, q = quartet, sex = sextet, m = multiplet), coupling constant (J, Hz), assignment. ¹³C NMR spectra were recorded on Bruker AMX400 (101 MHz) spectrometer and reported in terms of chemical shift (ppm, δ) relative to residual solvent peak. Mass spectra (MS) and high-resolution mass spectra (HRMS) were recorded on a VG analytical 7070E machine, Fisons TRIO spectrometers using electron ionisation (EI) and chemical ionisation (CI), and Micromass LCT mass spectrometer using electron spray ionisation (ESI). All mass values are within error limits of ± 5 ppm. Elemental analyses (%C, %H, %N) were either determined by the

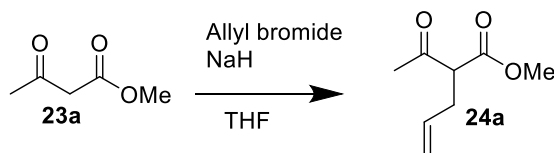
University of Liverpool Microanalysis Laboratory or the London Metropolitan University Elemental Analysis Service. Reported percentages are within error limits of $\pm 0.5\%$.

Synthesis of 4-(4-Fluorophenyl)-1H-pyrazol-3-amine¹⁹

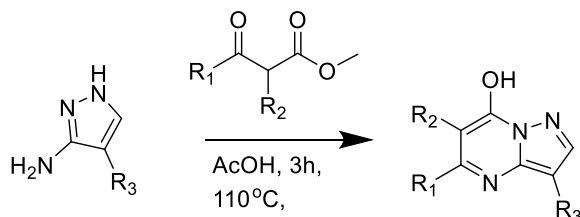


To a mixture of NaOEt (6.04 g, 88.7 mmol) and EtOH (100 ml) was added 2-(4-Fluorophenyl)acetonitrile (**18a**) (8.87 ml, 82.56 mmol) and the mixture was allowed to stir at 0°C for 5 minutes. Ethyl formate (14.88 ml, 1.85 mmol) was added to the reaction which was then heated to 85°C and stirred for one hour. Volatiles were removed under reduced pressure and the residue formed was diluted with H₂O and 2M HCl to adjust to pH 3-4. The aqueous layer was extracted with EtOAc (3x 50 ml) and washed with brine (40 ml). Organics were dried using Na₂SO₄ and evaporated to dryness. To crude 2-(4-Fluorophenyl)-3-oxo-propane nitrile in EtOH (100 ml) was added NH₂NH₂·H₂O (7.12 ml, 147.12 mmol) followed by AcOH (6 ml, 104.92 mmol). The reaction was allowed to stir at 85°C for 2 hours before cooling to room temperature and evaporating to dryness, to afford the desired product **20a**. (10.62 g, 73%); ¹H NMR (400 MHz, DMSO-*d*₆) δ 11.69 (s, 1H), 7.65 (s, 1H), 7.52 (dd, *J* = 8.6, 5.6 Hz, 2H), 7.15 (t, *J* = 8.9 Hz, 2H), 4.73 (s, 2H); ¹³C NMR (101 MHz, DMSO-*d*₆) δ 160.3 (d, *J* = 240.9 Hz), 156.1 (s), 130.6 (s), 131.0 (d, *J* = 3.0 Hz), 127.7 (d, *J* = 7.1 Hz, 2C), 119.7 (s), 115.7 (d, *J* = 21.0 Hz, 2C); MS (CI+ CH₄): *m/z* (rel. Intensity) [M+H] 178.1 (100), HRMS (CI+) calcd for [(C₉H₈FN₃)+H]: 178.0700 found: 178.0780

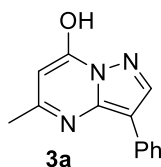
Synthesis of Methyl 2-acetylpent-4-enoate²⁰



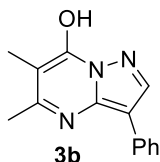
To Methyl acetoacetate **23a** (5.4 ml, 50 mmol) in THF (15 ml) at 0°C was added NaH (1.32 g, 55 mmol) and the reaction was allowed to stir for 30 minutes. Allyl bromide (6.6 g, 55 mmol) was then added to the reaction mixture before allowing the reaction to warm to room temperature and stirring overnight. The reaction was evaporated to dryness, diluted with EtOAc and washed with water. Organic layer was dried with MgSO₄ and evaporated to dryness to give the crude product which was purified by column eluting with 20% EtOAc:Hexane to afford the product **24a** as a colourless oil in good yield (4.96 g, 64%); ¹H NMR (400 MHz, CDCl₃) δ 5.86 – 5.64 (m, 1H), 5.10 (dd, *J* = 17.1, 1.41 Hz, 1H), 5.06 (dd, *J* = 10.2 Hz, 1.41 Hz, 1H), 3.74 (s, 3H), 3.55 (t, *J* = 7.4 Hz, 1H), 2.60 (m, 2H), 2.24 (s, 3H); MS (ES+): *m/z* (rel. Intensity) 157.1 (100)

General procedure 2.1 for the synthesis of 5-methyl pyrazolo[1,5-a]pyrimidin-7-ol¹

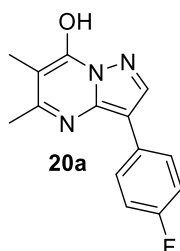
To the 3-Amino, 1,2-pyrazole (5.16 mmol) in AcOH (8 ml) was added the appropriate beta-keto ester (20.64 mmol) and the reaction was allowed to stir at 110°C for 3 hours. The reaction was cooled to room temperature and diluted with Et₂O causing precipitation of the desired product which was filtered and washed with further Et₂O.

5-Methyl-3-phenylpyrazolo[1,5-a]pyrimidin-7-ol¹ **3a**

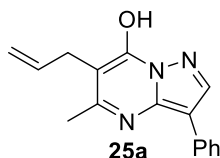
General procedure 2.1 to give **3a** as a white solid (3.46 g, 92%); ¹H NMR (400 MHz, DMSO-d₆) δ 11.91 (s, 1H), 8.11 (s, 1H), 7.57 (dd, *J* = 8.2, 1.1 Hz, 2H), 7.47 (dd, *J* = 10.6, 4.9 Hz, 2H), 7.39 – 7.28 (m, 1H), 5.67 (s, 1H), 2.35 (s, 3H); MS (Cl⁺ CH₄): *m/z* (rel. Intensity) [M+H] 226.1 (100)

5,6-Dimethyl-3-phenylpyrazolo[1,5-a]pyrimidin-7-ol **3b**

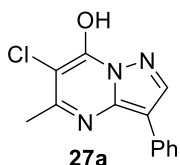
General procedure 2.1 to give **3b** as a white solid (2.54 g, 84%); ¹H NMR (400 MHz, DMSO-d₆) δ 11.66 (s, 1H), 8.09 (s, 1H), 7.57 (d, *J* = 7.3 Hz, 2H), 7.46 (t, *J* = 7.7 Hz, 2H), 7.31 (t, *J* = 7.4 Hz, 1H), 2.38 (s, 3H), 2.00 (s, 3H); ¹³C NMR (101 MHz, DMSO-d₆) δ 157.3, 147.4, 142.3, 137.3, 131.4, 129.2 (2C), 127.8, 126.8 (2C), 103.9, 102.0, 17.7, 10.9; MS (Cl⁺ CH₄): *m/z* (rel. Intensity) [M+H] 240.1135 (100), HRMS (Cl⁺) calcd for [(C₁₄H₁₃N₃O)+H]:240.1131; found: 240.1135

3-(4-Fluorophenyl)-5,6-dimethylpyrazolo[1,5-a]pyrimidin-7-ol **20a**

General procedure 2.1 to give **20a** as an off-white solid (9.46 g, 81%); $^1\text{H NMR}$ (400 MHz, DMSO- d_6) δ 11.65 (s, 1H), 8.06 (s, 1H), 7.59 (dd, $J = 8.7, 5.5$ Hz, 2H), 7.29 (t, $J = 8.9$ Hz, 2H), 2.37 (s, 3H), 2.00 (s, 3H); $^{13}\text{C NMR}$ (101 MHz, DMSO- d_6) δ 172.5, δ 161.4 (d, $J = 243.2$ Hz), 157.3, 147.4, 142.3, 137.3, 129.8 (d, $J = 8.0$ Hz 2C), 127.8 (d, $J = 3.0$ Hz), 116.0 (d, $J = 21.4$ Hz 2C). 101.9, 21.5, 10.8; **MS** (CI+ CH_4): m/z (rel. Intensity) [M+H] 258.1 (100), HRMS (CI+) calcd for [(C₁₄H₁₂N₃O)+H]:258.1030; found: 258.1035

6-Allyl-5-Methyl-3-phenylpyrazolo[1,5-a]pyrimidin-7-ol **25a**

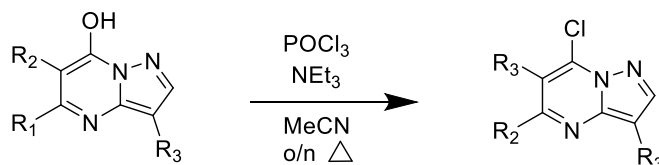
General procedure 2.1 to give **25a** as an off-white solid (2.34 g, 88%); $^1\text{H NMR}$ (400 MHz, DMSO- d_6) δ 11.75 (s, 1H), 8.11 (s, 1H), 7.64 – 7.52 (m, 2H), 7.46 (t, $J = 7.7$ Hz, 2H), 7.32 (t, $J = 7.4$ Hz, 1H), 5.86 (ddt, $J = 16.0, 10.1, 5.9$ Hz, 1H), 5.10 – 4.93 (m, 2H), 3.27 (d, $J = 5.9$ Hz, 2H), 2.38 (s, 3H); $^{13}\text{C NMR}$ (101 MHz, DMSO- d_6) δ 156.9, 148.4, 142.5, 137.3, 136.0, 131.3, 129.2 (2C), 127.8, 126.9 (2C), 115.3, 104.2, 104.1, 29.1, 17.2; **MS** (ES+): m/z (rel. Intensity) [M+H] 266.1 (100)

5-Methyl 6-chloro-3-phenylpyrazolo[1,5-a]pyrimidin-7-ol **27a**

General procedure 2.1 to give **27a** as an off-white solid (2.46 g, 79.5%); $^1\text{H NMR}$ (400 MHz, DMSO- d_6) δ 12.37 (s, 1H), 8.17 (s, 1H), 7.57 (d, $J = 7.6$ Hz, 2H), 7.48 (t, $J = 7.6$ Hz, 2H), 7.35 (t, $J = 7.3$ Hz, 1H), 2.52 (s, 3H); $^{13}\text{C NMR}$ (101 MHz, DMSO- d_6) δ 153.4, 149.1, 143.3, 136.9, 130.8, 129.3 (2C), 128.1, 127.2 (2C), 105.2, 102.5, 18.4; **MS**

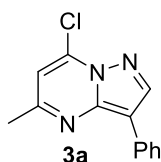
(Cl⁺ CH₄): m/z (rel. Intensity) [M+H] 258.1 (100), HRMS (Cl⁺) calcd for [(C₁₄H₁₂ClN₃O)+H]:258.1037; found: 258.1042

General procedure 2.2 for the synthesis of 7-Chloro-5-Methyl-pyrazolo[1,5-a]pyrimidines²



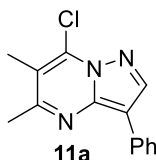
To the pyrazolo-pyrimidine compound (1 equiv) and NEt₃ (2 equiv) in MeCN was added POCl₃ (3 equiv) and the solution stirred under reflux overnight. The reaction was cooled to room temperature, volatiles removed under reduced pressure before pouring onto crushed ice. Basified with 2M NaOH and aqueous extracted with EtOAc, combined organic extracts washed with brine, dried with MgSO₄ and evaporated to dryness to give the product.

7-Chloro-5-methyl-3-phenylpyrazolo[1,5-a] pyrimidine^{1,21}

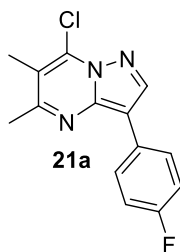


General procedure 2.2 to give **3a** as a yellow solid (0.21 g, 83%); ¹H NMR (400 MHz, DMSO-d₆) δ 8.79 (s, 1H), 8.13 (d, *J* = 7.1 Hz, 2H), 7.44 (t, *J* = 7.1 Hz, 2H), 7.38 (s, 1H), 7.26 (t, *J* = 7.1 Hz, 1H), 2.60 (s, 3H); MS (Cl⁺ CH₄): m/z (rel. Intensity) [M+H] 244.1 (100) , [M+H] 246.1 (28)

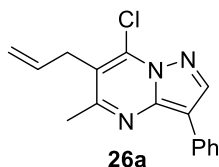
7-Chloro-5,6-dimethyl-3-phenylpyrazolo[1,5-a] pyrimidine (11a)



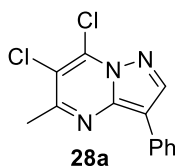
General procedure 2.2 to give **11a** as a yellow solid. (2.55 g, 97%); ¹H NMR (400 MHz, DMSO-d₆) δ 8.71 (s, 1H), 8.14 (d, *J* = 7.3 Hz, 2H), 7.44 (t, *J* = 7.7 Hz, 2H), 7.25 (t, *J* = 7.4 Hz, 1H), 2.61 (s, 3H), 2.38 (s, 3H); ¹³C NMR (101 MHz, DMSO-d₆) δ 172.3, 160.3, 150.6, 143.8, 142.2, 136.1, 132.3 (2C), 129.3, 126.5 (2C), 112.8, 21.4, 14.8; MS (Cl⁺ CH₄): m/z (rel. Intensity) [M+H] 182.0 (100), [M+H] 184.0 (26) HRMS (Cl⁺) calcd for [(C₈H₉ClN₃)+H]:182.0480; found: 182.0488

7-Chloro-3-(4-fluorophenyl)-5-methylpyrazolo[1,5-a]pyrimidine 21a

General procedure 2.2 to give **21a** as a yellow solid; $^1\text{H NMR}$ (400 MHz, DMSO- d_6) δ 8.68 (s, 1H), 8.15 (dd, J = 8.9, 5.6 Hz, 2H), 7.27 (t, J = 8.9 Hz, 2H), 2.60 (s, 3H), 2.37 (s, 3H); $^{13}\text{C NMR}$ (101 MHz, DMSO- d_6) δ 161.1 (d, J = 242.9 Hz), 160.0, 143.6, 142.2, 135.0, 128.8 (d, J = 3.1 Hz), 127.8 (d, J = 7.8 Hz, 2C), 116.8, 115.9, (d, J = 21.3 Hz, 2C), 108.9, 24.6, 14.8; **MS (ES+)**: m/z (rel. Intensity) [M+H] 276.1 (100), [M+H] 278.1 (32) HRMS (ES+) calcd for [(C₁₄H₁₂N₃F₃Cl)+H]:276.0704; found: 276.0700. calcd for [(C₁₄H₁₂N₃F₃Cl)+H]:278.0674; found: 278.0681

6-Allyl-7-chloro-5-methyl-3-phenylpyrazolo[1,5-a] pyrimidine 26a

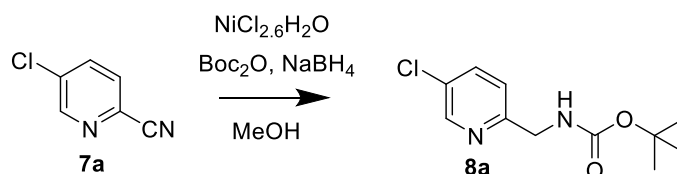
General procedure 2.2 to give **26a** as a yellow solid (2.05 g, 84%); $^1\text{H NMR}$ (400 MHz, DMSO- d_6) δ 8.81 (s, 1H), 8.20 (d, J = 8.3 Hz, 2H), 7.50 (t, J = 7.8 Hz, 2H), 7.31 (t, J = 7.4 Hz, 1H), 6.03 (ddt, J = 17.1, 10.2, 5.6 Hz, 1H), 5.19 (dd, J = 10.2, 1.5 Hz, 1H), 5.09 (dd, J = 17.2, 1.6 Hz, 1H), 3.66 (d, J = 5.6 Hz, 2H), 2.69 (s, 3H); $^{13}\text{C NMR}$ (101 MHz, DMSO- d_6) δ 159.7, 144.0, 142.9, 137.2, 133.8, 132.1, 129.1 (2C), 126.6, 126.1 (2C), 117.8, 117.1, 110.0, 32.6, 24.0; **MS (ES+)**: m/z (rel. Intensity) [M+H] 284.1 (100), [M+H] 286.1 (27)

7-chloro-5,6-dimethyl-3-phenylpyrazolo[1,5-a] pyrimidine 28a

General procedure 2.2 to give **28a** as a yellow solid (1.23 g, 88%); $^1\text{H NMR}$ (400 MHz, DMSO- d_6) δ 8.81 (s, 1H), 8.11 (d, J = 7.3 Hz, 2H), 7.45 (t, J = 7.7 Hz, 2H), 7.28 (t, J = 7.4 Hz, 1H), 2.70 (s, 3H); $^{13}\text{C NMR}$ (101 MHz, DMSO- d_6) δ 152.0, 133.2, 128.8, 123.1, 119.6, 117.4, 117.3, 107.8, 102.02, 88.4, 14.8; **MS (CI+ CH₄)**: m/z (rel.

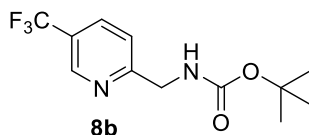
Intensity) [M+H] 278.0 (100), [M+H] 280.0 (58.59) HRMS (CI+) calcd for [(C₈H₉ClN₃)+H]:278.0246; found: 278.0256

Procedure for the synthesis of *Tert*-butyl ((5-chloropyridin-2-yl) methyl) carbamate **8a^{4,22}**



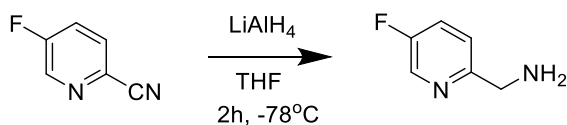
To 2-Cyano-5-chloropyridine **7a** (0.6 g, 4.33 mmol) in MeOH (20 ml) at 0 °C was added NiCl₂·6H₂O (0.05g, 0.43 mmol) and Boc₂O (1.89, 8.66 mmol). NaBH₄ (0.85 g, 30.31 mmol) was added in portions over 25 minutes with vigorous stirring, the resultant black reaction mixture was warmed to room temperature and stirred for 5 hours. The reaction was evaporated to dryness, diluted with EtOAc and washed with NaHCO₃. Organic layer was dried with MgSO₄ and concentrated under pressure, the crude product was purified by column eluting with 20% EtOAc in Hexane to give **8a**. (0.54 g, 51.7%); ¹H NMR (400 MHz, CDCl₃) δ 8.47 (d, *J* = 2.2 Hz, 1H), 7.62 (dd, *J* = 8.3, 2.3 Hz, 1H), 7.26 (d, *J* = 8.4 Hz, 1H), 6.01 (br s, 1H), 4.41 (d, *J* = 5.8 Hz, 2H), 1.46 (s, 9H); **MS (ES+)**: *m/z* (rel. Intensity) 243.1 (3) 187.0 [M-*t*-Bu] (24.74), 143.1 [M-Boc] (100)

Tert*-butyl ((5-(trifluoromethyl)pyridin-2-yl)methyl)carbamate **8b*



Synthesised according to the procedure to reach **8a** to give **8b** (0.77 g, 48%); ¹H NMR (400 MHz, MeOD) δ 8.81 (s, 1H), 8.12 (d, *J* = 8.1 Hz, 1H), 7.57 (d, *J* = 8.2 Hz, 1H), 4.45 (s, 2H), 1.49 (s, 9H); ¹³C NMR (101 MHz, MeOD) δ 163.5, 157.1, 145.4 (q, *J* = 4.2 Hz), 134.2 (q, *J* = 3.2 Hz), 124.9 (q, *J* = 33.0 Hz). 122.4, 120.8, 79.2, 45.2, 27.3; **MS (ES+)**: *m/z* (rel. Intensity) [M-*t*-Bu] (3), 177.1 [M-Boc] (100)

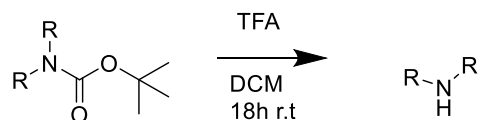
Synthesis of (5-Fluoropyridin-2-yl) methanamine^{23,24}



To 2-Cyano-5-fluoropyridine (1 g, 7.4 mmol) in THF (10 ml) was added LiAlH₄ (0.55 g, 14.7 mmol) and the resultant dark brown solution was allowed to stir at -78°C under a nitrogen atmosphere for 2 hours. The reaction

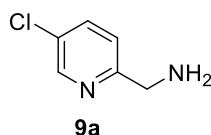
was quenched with water (0.5 ml), diluted with 2M NaOH (0.5 ml) and water (3 ml). To the mixture was added EtOAc then this was filtered through a pad of celite and MgSO₄ washing with EtOAc. The crude product was evaporated to dryness and used directly within the next step without further purification. (0.42 g, 41%)

General procedure 2.3 for Boc-removal.



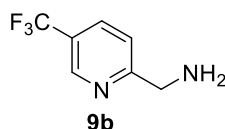
To the Boc-protected amine (2.23 mmol) in DCM (5 ml) was added TFA (21.8 mmol) and the reaction was allowed to stir at room temperature for 18 hours. Upon completion of the reaction the volatiles were removed under pressure, resultant residue was diluted with EtOAc and washed with NaHCO₃.

(5-Chloropyridin-2-yl)methanamine **9a**²⁵



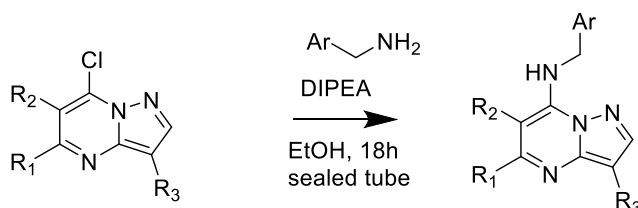
General procedure 2.3. Organics dried with MgSO₄ and evaporated to dryness to give the crude amine which was used directly in the next step (0.21 g, 66%); **MS (ES+)**: m/z (rel. Intensity) 143.0 (16)

(5-(Trifluoromethyl)pyridin-2-yl)methanamine **9b**²⁶



General procedure 2.3. Organics dried with MgSO₄ and evaporated to dryness to give the crude amine product which was used directly in the next step (71 mg, 17%); **MS (ES+)**: m/z (rel. Intensity) 177.0 (100)

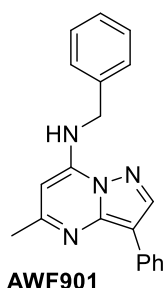
General procedure 2.4 for amine substitution of 5-methyl pyrazolo[1,5-a]pyrimidines²⁷



To the chlorinated pyrazolo-pyrimidine **20** (0.85 mmol) in EtOH (10 ml) was added the aryl-amine (0.85 mmol) and DIPEA (1.02 mmol). The yellow solution was allowed to stir at 110 °C in a sealed tube overnight, once

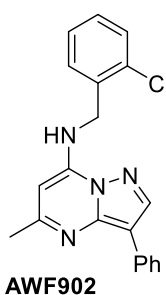
completed the reaction was evaporated to dryness and the crude product loaded to silica. Purification by flash chromatography eluting with 40% to 80% EtOAc in hexanes allowed isolation of the desired products.

***N*-Benzyl-5-methyl-3-phenylpyrazolo[1,5-*a*]pyrimidin-7-amine (AWF901)²⁸**

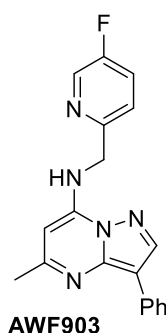


General procedure 2.4 to give **AWF901** as an off-white solid (0.19 g, 40%) ; ¹H NMR (400 MHz, DMSO-*d*₆) δ 8.60 (s, 1H), 8.58 (m, 1H), 8.16 (d, *J* = 7.4 Hz, 2H), 7.38 (m, 6H), 7.26 (t, *J* = 7.2, 1H), 7.16 (t, *J* = 7.2, 1H), 6.10 (s, 1H), 4.63 (d, *J* = 6.5 Hz, 2H), 2.41 (s, 3H); **Melting point:** 154-155 °C ¹³C NMR (101 MHz, DMSO-*d*₆) δ 159.7, 147.0, 145.5, 141.8, 138.7, 133.4, 129.0(2C), 128.9, 127.6, 127.5(2C), 125.6, 125.4, 106.9, 86.5, 44.9, 25.4; **MS (Cl⁺ NH₄):** *m/z* (rel. Intensity) [M+H] 315.2 (100), [M+H] 225.1 (20) HRMS (ES⁺) calcd for [(C₂₀H₁₉N₄)+H]:315.1600; found: 315.1604; **CHN analysis:** Calculated: C:76.41%, H:5.77%, N:17.82% Found C:75.58%, H:5.73%, N:17.60%

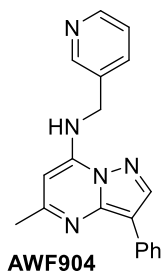
***N*-(2-Chlorobenzyl)-5-methyl-3-phenylpyrazolo[1,5-*a*]pyrimidin-7-amine (AWF902)**



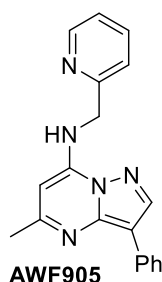
General procedure 2.4 to give **AWF902** as an off-white solid (0.11 g 39%); **Melting point:** 152-153 °C ¹H NMR (400 MHz, DMSO-*d*₆) δ 8.63 (s, 1H), 8.51 (s, 1H), 8.17 (d, *J* = 7.9 Hz, 2H), 7.57 – 7.46 (m, 1H), 7.40 (t, *J* = 7.7 Hz, 2H), 7.33 (m, 3H), 7.18 (t, *J* = 7.4 Hz, 1H), 6.07 (s, 1H), 4.71 (s, 2H), 2.42 (s, 3H); ¹³C NMR (101 MHz, DMSO-*d*₆) δ 159.9, 147.0, 145.4, 141.9, 135.4, 133.5, 132.4, 129.9, 129.4, 128.9 (2C), 128.3, 127.9, 125.6 (2C), 125.5, 107.1, 86.4, 43.1, 25.5; **MS (Cl⁺ NH₄):** *m/z* (rel. Intensity) [M+H] 349.1 (100), [M+H] 351.1 (26) HRMS (Cl⁺) calcd for [(C₂₀H₁₈ClN₄)+H]:349.1215; found: 349.1215; **CHN analysis:** Calculated: C:68.66%, H:4.91%, N:16.06%. Found C:68.88%, H:4.94%, N:15.86%;

***N*-((5-Fluoropyridin-2-yl)methyl)-5-methyl-3-phenylpyrazolo[1,5-*a*]pyrimidin-7-amine (AWF903)**

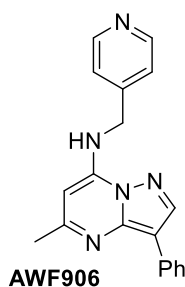
General procedure 2.4 (75 mg, 13%); **Melting point:** 183-184 °C **¹H NMR (400 MHz, DMSO-*d*₆)** δ 8.61 (s, 1H), 8.57 (d, *J* = 2.8 Hz, 1H), 8.50 (t, *J* = 6.2 Hz, 1H), 8.16 (d, *J* = 7.6 Hz, 2H), 7.73 (td, *J* = 8.8, 2.8 Hz, 1H), 7.49 (dd, *J* = 8.8, 4.4 Hz, 1H), 7.39 (t, *J* = 7.6 Hz, 2H), 7.17 (t, *J* = 7.6 Hz, 1H), 6.11 (s, 1H), 4.73 (d, *J* = 6.2 Hz, 2H), 2.43 (s, 3H); **¹³C NMR (101 MHz, DMSO-*d*₆)** δ 159.8, 158.9 (d, *J* = 251 Hz) 153.9 (d, *J* = 3.6 Hz), 147.0, 145.5, 141.8, 137.4 (d, *J* = 23.7 Hz), 133.5, 128.9 (2C), 125.6 (2C), 125.5, 124.5 (d, *J* = 18.6 Hz), 123.2 (d, *J* = 4.5 Hz), 107.0, 86.6, 46.2, 25.5; **MS (CI+ NH₄):** *m/z* (rel. Intensity) [M+H] 332.0 (100), HRMS (CI+) calcd for [(C₁₉H₁₅FN₅)+H]:332.1307; found: 332.1306; **CHN analysis:** Calculated: C:68.46%, H:4.84%, N:21.01%. Found C:68.25%, H:4.81%, N:20.94%;

***N*-((3-pyridyl)methyl)-5-methyl-3-phenylpyrazolo[1,5-*a*]pyrimidin-7-amine (AWF904)**

General procedure 2.4 to give **AWF904** as an off-white solid (0.15 g, 37%); **Melting point:** 174-175 °C **¹H NMR (400 MHz, CDCl₃)** δ 8.67 (d, *J* = 1.8 Hz, 1H), 8.64 (t, *J* = 6.6 Hz, 1H), 8.59 (s, 1H), 8.47 (dd, *J* = 4.8, 1.8 Hz, 1H), 8.15 (dd, *J* = 8.0, 1.0 Hz, 2H), 7.82 (dt, *J* = 8.0, 1.8 Hz, 1H), 7.42 – 7.31 (m, 3H), 7.15 (t, *J* = 7.4 Hz, 1H), 6.19 (s, 1H), 4.66 (d, *J* = 6.6 Hz, 2H), 2.42 (s, 3H); **¹³C NMR (101 MHz, CDCl₃)** δ 164.7, 153.9, 153.7, 151.6, 150.3, 146.5, 140.3, 139.1, 138.1, 133.5(2C), 130.3, 130.2, 128.9 (2C), 111.8, 91.2, 47.5, 30.2; **MS (CI+ NH₄):** *m/z* (rel. Intensity) [M+H] 316.0(100), HRMS (ES+) calcd for [(C₁₉H₁₈N₅)+H]:316.1562; found: 316.1557; **CHN analysis:** Calculated: C:72.36%, H:5.43%, N:22.21%. Found C:71.95%, H:5.41%, N:22.10%;

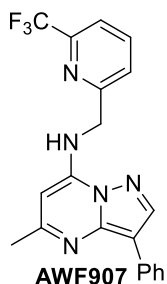
5-Methyl-3-phenyl-*N*-(pyridin-2-ylmethyl)pyrazolo[1,5-*a*]pyrimidin-7-amine (AWF905)^{29,30}

General procedure 2.4 to give **AWF905** as an off-white solid (0.155 g, 39%); **Melting point:** 144-146 °C **¹H NMR (400 MHz, DMSO-*d*₆)** δ 8.62 (s, 1H), 8.58 (d, *J* = 4.4 Hz, 1H), 8.49 (t, *J* = 6.1 Hz, 1H), 8.17 (d, *J* = 7.6 Hz, 2H), 7.79 (t, *J* = 7.6 Hz, 1H), 7.45 – 7.35 (m, 3H), 7.35 – 7.27 (dd, *J* = 6.7, 5.4 Hz 1H), 7.17 (t, *J* = 7.3 Hz, 1H), 6.10 (s, 1H), 4.74 (d, *J* = 6.1 Hz, 2H), 2.43 (s, 3H); **¹³C NMR (101 MHz, DMSO-*d*₆)** δ 159.9, 157.4, 149.6, 147.1, 145.4, 141.8, 137.6, 133.5, 128.8(2C), 125.6, 125.5 (2C), 123.1, 121.6, 106.9, 86.6, 46.5, 25.4; **MS (ES+):** *m/z* (rel. Intensity) [M+H] 316.2 (100), HRMS (ES+) calcd for [(C₁₉H₁₈N₅)+H]:316.1562; found: 316.1569; **CHN analysis:** Calculated: C:72.36%, H:5.43%, N:22.21%. Found C:71.96%, H:5.36%, N:22.17%;

5-Methyl-3-phenyl-*N*-(pyridin-4-ylmethyl)pyrazolo[1,5-*a*]pyrimidin-7-amine (AWF906)

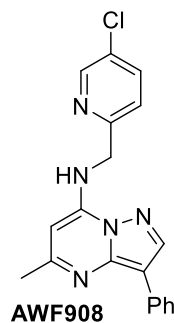
General procedure 2.4 to give **AWF906** as an off-white solid (0.15 g, 39%); **Melting point:** 151-155 °C **¹H NMR (400 MHz, DMSO-*d*₆)** δ 8.66 (t, *J* = 6.6 Hz, 1H), 8.63 (s, 1H), 8.53 (d, *J* = 5.6 Hz, 2H), 8.17 (d, *J* = 7.7 Hz, 2H), 7.39 (m, 4H), 7.17 (t, *J* = 7.3 Hz, 1H), 6.07 (s, 1H), 4.68 (d, *J* = 6.5 Hz, 2H), 2.41 (s, 3H); **¹³C NMR (101 MHz, DMSO-*d*₆)** δ 159.9, 150.2(2C), 147.7, 147.0, 145.5, 141.9, 133.6, 129.1(2C), 125.6, 125.5 (2C), 122.4(2C), 107.1, 86.6, 43.8, 25.4; **MS (ES+):** *m/z* (rel. Intensity) [M+H] 316.2 (100), HRMS (ES+) calcd for [(C₁₉H₁₈N₅)+H]:316.1562; found: 316.1560 **CHN analysis:** C: Calculated: C:72.36%, H:5.43%, N:22.21%. Found 71.57%, H:5.43%, N:22.02%.

5-Methyl-3-phenyl-*N*-((6-(trifluoromethyl)pyridin-2-yl)methyl)pyrazolo[1,5-*a*]pyrimidin-7-amine (AWF907)

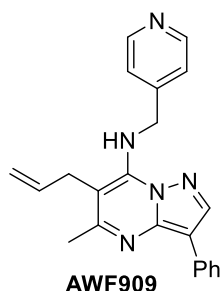


General procedure 2.4 (0.21 g, 54%); **Melting point:** 167-169 °C $^1\text{H NMR}$ (400 MHz, DMSO-d_6) δ 8.87 (s, 1H), 8.75 (t, $J = 6.6$ Hz, 1H), 8.63 (s, 1H), 8.16 (d, $J = 7.7$ Hz, 2H), 8.09 (d, $J = 8.1$ Hz, 1H), 7.90 (d, $J = 8.1$ Hz, 1H), 7.39 (t, $J = 7.7$ Hz, 2H), 7.17 (t, $J = 7.3$ Hz, 1H), 6.24 (s, 1H), 4.79 (d, $J = 6.5$ Hz, 2H), 2.43 (s, 3H); $^{13}\text{C NMR}$ (101 MHz, DMSO-d_6) δ 160.0, 149.8, 146.8, 145.8 (d, $J = 33.9$ Hz), 145.5, 141.9, 138.5 (d, $J = 0.7$ Hz), 137.2, 133.5, 128.9 (2C), 125.6 (2C), 125.5, 122.17 (q, $J = 273$ Hz), 121.2 (d, $J = 2.8$ Hz), 107.1, 86.4, 42.3, 25.4; **MS (ES+):** m/z (rel. Intensity) $[\text{M}+\text{H}]$ 384.1 (100), HRMS (ES+) calcd for $[(\text{C}_{20}\text{H}_{17}\text{N}_5\text{F}_3)+\text{H}]$:384.1436; found: 384.1446; **CHN analysis:** Calculated: C:62.66%, H:4.21%, N:18.27%. Found C:62.36%, H:4.14%, N:18.13%;

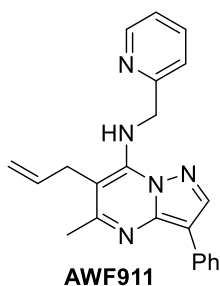
***N*-((5-Chloropyridin-2-yl)methyl)-5-methyl-3-phenylpyrazolo[1,5-a]pyrimidin-7-amine (AWF908)**



General procedure 2.4 (55 mg, 11%); **Melting point:** 198-199 °C $^1\text{H NMR}$ (400 MHz, DMSO-d_6) δ 8.63 (m, 2H), 8.53 (t, $J = 6.3$ Hz, 1H), 8.17 (d, $J = 7.8$ Hz, 2H), 7.92 (dd, $J = 8.4, 2.2$ Hz, 1H), 7.44 (d, $J = 8.4$ Hz, 1H), 7.33 (t, $J = 7.7$ Hz, 2H), 7.17 (t, $J = 7.3$ Hz, 1H), 6.10 (s, 1H), 4.74 (d, $J = 6.3$ Hz, 2H), 2.42 (s, 3H); $^{13}\text{C NMR}$ (101 MHz, DMSO-d_6) δ 159.9, 156.4, 148.1, 147.0, 145.5, 141.9, 137.3, 133.5, 130.2, 128.9 (2C), 125.6 (2C), 125.5, 123.1, 107.0, 86.6, 46.1, 25.4; N:19.39%; **MS (ES+):** m/z (rel. Intensity) $[\text{M}+\text{H}]$ 350.1 (100), HRMS (ES+) calcd for $[(\text{C}_{19}\text{H}_{17}\text{N}_5\text{Cl})+\text{H}]$:350.1172; found: 350.1173; **CHN analysis:** Calculated: C:65.24%, H:4.61%, N:20.02%. Found C:64.99%, H:4.53%,

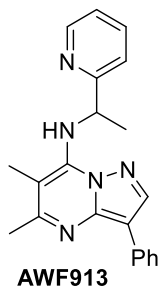
6-Allyl-5-methyl-3-phenyl-N-(pyridin-4-ylmethyl)pyrazolo[1,5-a]pyrimidin-7-amine (AWF909)

General procedure 2.4 to give **AWF909** as an off-white solid (0.20 g, 52%); **Melting point:** 132-133 °C **¹H NMR (400 MHz, DMSO-*d*₆)** δ 8.55 (s, 1H), 8.49 (d, *J* = 5.9 Hz, 2H), 8.16 (d, *J* = 7.4 Hz, 2H), 7.79 (t, *J* = 7.1 Hz, 1H), 7.38 (t, *J* = 7.7 Hz, 2H), 7.28 (d, *J* = 5.8 Hz, 2H), 7.16 (t, *J* = 7.4 Hz, 1H), 6.00 (ddt, *J* = 15.2, 10.0, 4.9 Hz, 1H), 5.13 – 5.06 (m, 3H), 4.91 (dd, *J* = 17.2, 1.4 Hz, 1H), 2.46 (s, 3H); **¹³C NMR (101 MHz, DMSO-*d*₆)** δ 159.9, 150.1(2C), 150.1, 146.3, 144.8, 141.3, 136.1, 133.4, 128.9(2C), 125.5, 125.5 (2C), 121.9(2C), 115.8, 106.3, 98.1, 46.9, 30.0 23.9; **MS (ES⁺):** *m/z* (rel. Intensity) [M+H] 356.2 (100), HRMS (ES⁺) calcd for [(C₂₂H₂₂N₅)+H]:356.18752; found: 356.1877; **CHN analysis:** Calculated: C:74.34%, H:5.96%, N:19.70%. Found C:73.87%, H:5.89%, N:19.71%

6-Allyl-5-methyl-3-phenyl-N-(pyridin-2-ylmethyl)pyrazolo[1,5-a]pyrimidin-7-amine (AWF911)

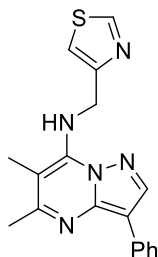
General procedure 2.4 to give **AWF911** as an off-white solid (0.28 g, 75%); **Melting point:** 158-160 °C **¹H NMR (250 MHz, DMSO-*d*₆)** δ 8.56 (s, 1H), 8.55 (s, 1H), 8.18 – 8.11 (m, 2H), 8.03 (t, *J* = 6.0 Hz, 1H), 7.77 (td, *J* = 7.7, 1.7 Hz, 1H), 7.37 (m, 3H), 7.29 (dd, *J* = 6.9, 5.4 Hz, 1H), 7.14 (t, *J* = 7.4 Hz, 1H), 6.05 (ddt, *J* = 15.0, 9.8, 4.8 Hz, 1H), 5.11 (m, 1H) 5.11 (d, *J* = 6.4 Hz, 2H), 4.92 (dd, *J* = 17.2, 1.5 Hz, 1H), 3.49 (d, *J* = 4.6 Hz, 2H), 2.46 (s, 3H); **¹³C NMR (101 MHz, DMSO-*d*₆)** δ 160.1, 158.2, 149.3, 146.0, 144.4, 141.2, 137.5, 136.8, 133.5, 128.9(2C), 125.5, 125.4, 122.9, 121.7(2C), 116.1, 106.6, 97.6, 48.7, 30.2, 24.0; **MS (ES⁺):** *m/z* (rel. Intensity) [M+H] 356.2 (100), HRMS (ES⁺) calcd for [(C₂₂H₂₂N₅)+H]:356.1875; found: 356.1879; **CHN analysis:** Calculated: C:74.34%, H:5.96%, N:19.70%. Found C:74.10%, H:5.92%, N:19.40%.

5,6-Dimethyl-3-phenyl-N-(1-(pyridin-2-yl)ethyl)pyrazolo[1,5-a]pyrimidin-7-amine (AWF913)



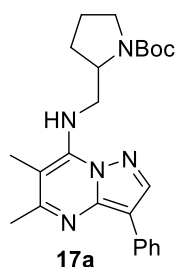
General procedure 2.4 to give **AWF913** as an off white solid (0.47 g, 59%); **Melting point:** 111-113 °C **¹H NMR (400 MHz, DMSO-*d*₆)** δ 8.61 (d, *J* = 4.3 Hz 1H), 8.55 (s, 1H), 8.14 (d, *J* = 7.4 Hz, 2H), 7.79 (td, *J* = 7.7, 1.6 Hz, 1H), 7.50 (d, *J* = 7.8 Hz, 1H), 7.45 (d, *J* = 8.9 Hz, 1H), 7.38 (t, *J* = 7.7 Hz, 2H), 7.31 (dd, *J* = 7.0, 5.2 Hz, 1H), 7.15 (t, *J* = 7.4 Hz, 1H), 5.76 (dq, *J* = 13.5 6.7 Hz 1H), 2.50 (s, 3H), 2.31 (s, 3H), 1.54 (d, *J* = 6.7 Hz, 3H); **¹³C NMR (101 MHz, DMSO-*d*₆)** δ 162.1, 159.9, 149.4, 145.1, 144.1, 141.1, 137.7, 133.5, 128.9(2C), 125.5, 125.5, 123.1, 121.5(2C), 106.8, 98.0, 54.6, 24.8, 24.5, 13.3; **MS (ES+):** *m/z* (rel. Intensity) 344.2 (100), 345.2 (23) HRMS (ES+) calcd for (C₂₁H₂₁N₅):336.1283; found: 336.1279; **CHN analysis:** Calculated: C:73.44%, H:6.16%, N:20.39%. Found C:73.19%, H:6.16%, N:20.07%.

5,6-Dimethyl-3-phenyl-*N*-(thiazol-4-ylmethyl)pyrazolo[1,5-*a*]pyrimidin-7-amine (AWF914)



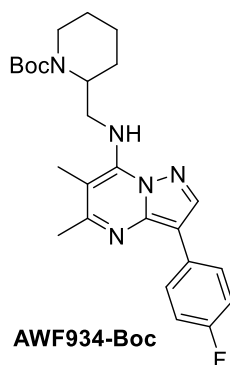
General procedure 2.4, product purified by column chromatography eluting with 20% EtOAc:DCM (0.34 g, 46%); **Melting point:** 144-146 °C **¹H NMR (400 MHz, DMSO-*d*₆)** δ 9.07 (s, 1H), 8.52 (s, 1H), 8.15 (d, *J* = 7.4 Hz, 2H), 7.55 (t, *J* = 6.7 Hz, 1H), 7.44 (s, 1H), 7.38 (t, *J* = 7.7 Hz, 2H), 7.15 (t, *J* = 7.4 Hz, 1H), 5.22 (d, *J* = 6.7 Hz, 2H), 2.50 (s, 4H), 2.27 (s, 3H); **¹³C NMR (101 MHz, DMSO-*d*₆)** δ 159.5, 156.2, 155.1, 155.1, 145.9, 144.3, 141.1, 140.9, 133.6, 128.9, 125.4, 115.7, 115.6, 106.3, 97.4, 44.9, 24.6, 13.0; **MS (ES+):** *m/z* (rel. Intensity) 336.1 (100), 337.1 (23) HRMS (ES+) calcd for (C₈H₁₈N₅):344.1875; found: 344.1873; **CHN analysis:** Calculated: C:64.45%, H:5.11%, N:20.88%, S:9.56% Found C:64.26%, H:5.10%, N:20.86%, S:9.61%.

Tert-butyl 2-(((5,6-dimethyl-3-phenylpyrazolo[1,5-a]pyrimidin-7-yl)amino)methyl)pyrrolidine-1-carboxylate(17a)



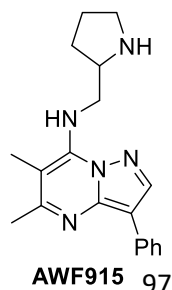
General procedure 2.4 (0.59 g, 46%); $^1\text{H NMR}$ (400 MHz, DMSO-d_6) δ 8.50 (s, 1H), 8.15 (d, $J = 7.4$ Hz, 3H), 7.38 (t, $J = 7.7$ Hz, 3H), 7.15 (t, $J = 7.4$ Hz, 1H), 7.06 (br s, 1H), 4.04 (br s, 1H), 3.96 – 3.80 (m, 2H), 3.27 – 3.13 (m, 2H), 2.50 (s, 7H), 2.29 (s, 4H), 1.92 – 1.75 (m, 5H), 1.37 (s, 7H); $^{13}\text{C NMR}$ (101 MHz, DMSO-d_6) δ 158.6, 154.2, 146.3, 145.3, 141.3, 133.8,, 128.8(2C), 125.4(2C), 125.2, 105.7, 78.3, 67.1, 43.7, 28.1, 28.0, 26.6, 25.6, 24.7, 19.4, 13.0(3C); **MS (ES+)**: m/z (rel. Intensity) 422.3 (100), 423.3 (23) HRMS (ES+) calcd for ($\text{C}_{24}\text{H}_{32}\text{N}_5\text{O}_2$):422.2556; found: 422.2556

Tert-butyl 2-(((3-(4-fluorophenyl)-5,6-dimethylpyrazolo[1,5-a]pyrimidin-7-yl)amino)methyl)piperidine-1-carboxylate



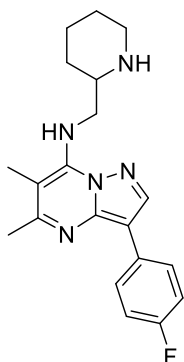
General procedure 2.4 The crude product was purified by column chromatography eluting with 30%EtOAc:Hexane (50%); $^1\text{H NMR}$ (400 MHz, DMSO-d_6) δ 8.48 (s, 1H), 8.18 (d, $J = 2.4$ Hz, 2H), 7.30 – 7.14 (m, 2H), 6.96 (br s, 1H), 4.36 (br s, 1H), 4.16 (br s, 1H), 4.03 (br s, 1H), 3.88 (br s, 1H), 2.96 (t, $J = 11.6$ Hz, 1H), 2.47 (s, 3H), 2.20 (s, 3H), 1.56 (t, $J = 28.9$ Hz, 5H), 1.02 (s, 9H). $^{13}\text{C NMR}$ (101 MHz, DMSO-d_6) δ 160.4 (d, $J = 241.5$ Hz), 158.7, 154.5, 146.3, 144.8, 141.0, 130.3 (d, $J = 3.0$ Hz), 127.0 (d, $J = 7.6$ Hz, 2C), 115.6 (d, $J = 21.0$ Hz, 2C), 104.8, 96.9, 78.2, 623.0, 43.7, 28.0, 26.6, 25.6, 24.7, 19.4, 13.0; **MS (ES+)**: m/z (rel. Intensity) 454.3 (100), 455.3 (22) HRMS (ES+) calcd for ($\text{C}_{25}\text{H}_{33}\text{N}_5\text{O}_2\text{F}$):454.2618; found: 454.2609.

5,6-Dimethyl-3-phenyl-N-(pyrrolidin-2-ylmethyl)pyrazolo[1,5-a]pyrimidin-7-amine (AWF915)



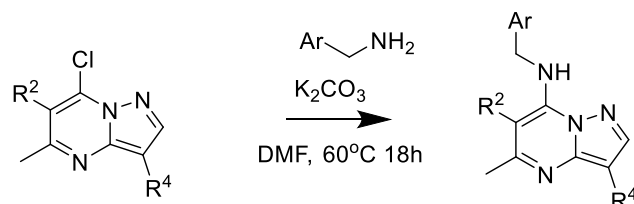
General procedure 2.4 (0.22 g, 50%); **Melting point:** 140-141 °C $^1\text{H NMR}$ (400 MHz, DMSO-d_6) δ 8.51 (s, 1H), 8.15 (d, $J = 7.4$ Hz, 2H), 7.38 (t, $J = 7.7$ Hz, 2H), 7.15 (t, $J = 7.4$ Hz, 1H), 7.02 (t, $J = 5.5$ Hz, 1H), 3.82 – 3.52 (m, 2H), 2.87 – 2.74 (m, 3H), 2.50 (s, 3H), 2.31 (s, 3H), 1.87 – 1.67 (m, 3H), 1.65 - 1.55 (m, 1H), 1.47 – 1.32 (m, 1H); $^{13}\text{C NMR}$ (101 MHz, DMSO-d_6) δ 159.6, 146.2, 144.1, 140.9, 133.7, 128.9 (2C), 125.4 (2C), 125.3, 106.4, 96.6, 58.3, 49.0, 46.3, 29.2, 25.9, 24.8, 13.5; **MS (ES+):** m/z (rel. Intensity) 322.2 (100), 323.2 (23) HRMS (ES+) calcd for ($\text{C}_{19}\text{H}_{24}\text{N}_5$):322.2032; found: 322.2029; **CHN analysis:** Calculated: C:71.00%, H:7.21%, N:21.79%. Found C:70.39%, H:7.15%, N:21.61%.

5,6-Dimethyl-3-phenyl-N-(piperidin-2-ylmethyl)pyrazolo[1,5-a]pyrimidin-7-amine (AWF934)

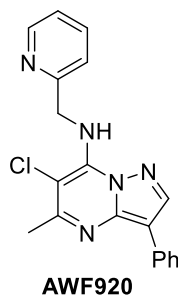


General procedure 2.4 The crude product was purified by column chromatography eluting with 60% EtOAc:Hexane, NEt_3 (56%); **Melting point:** 157-160 °C $^1\text{H NMR}$ (400 MHz, DMSO-d_6) δ 8.51 (s, 1H), 8.19 (dd, $J = 8.4, 5.7$ Hz, 2H), 7.22 (t, $J = 8.8$ Hz, 2H), 7.05 (br s, 1H), 3.87 – 3.60 (m, 2H), 3.35 (s, 2H), 2.99 (d, $J = 11.7$ Hz, 1H), 2.74 (s, 1H), 2.49 (s, 3H), 2.29 (s, 3H), 1.73 (s, 1H), 1.55 (dd, $J = 35.4, 7.7$ Hz, 2H), 1.31 (s, 2H), 1.16 (dd, $J = 17.4, 9.6$ Hz, 1H); $^{13}\text{C NMR}$ (101 MHz, DMSO-d_6) δ 160.4 (d, $J = 241.5$ Hz), 159.7, 146.2, 144.0, 140.8, 130.2 (d, $J = 2.9$ Hz), 127.0 (2C d, $J = 7.5$ Hz), 115.7 (2C d, $J = 21.0$ Hz), 105.4, 96.6, 56.8, 50.1, 46.3, 29.8, 26.4, 24.8, 24.35, 13.4; **MS (ES+):** m/z (rel. Intensity) 354.2 (100), 355.2 (24) HRMS (ES+) calcd for ($\text{C}_{20}\text{H}_{25}\text{N}_5\text{F}$):354.2094; found: 354.2085; **CHN analysis:** Calculated: C:67.97%, H:6.84%, N:19.82%. Found C:67.06%, H:6.77%, N:19.19%.

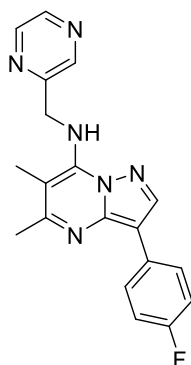
General procedure 2.5 for the synthesis of 5,6-Dimethylpyrazolo[1,5-a]pyrimidin-7-amines¹



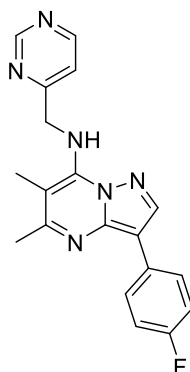
To the chlorinated pyrazolo-pyrimidine (1 equiv) in DMF (1ml/0.1mmol) was added the aryl-amine (1 equiv) and K_2CO_3 (1.2 equiv). The solutions were stirred at 60°C in overnight, once completed the reactions were evaporated to dryness, diluted with EtOAc before washing with water and brine. Organics were dried over MgSO_4 before loading the crude product to silica gel and purifying by column chromatography.

6-Chloro-5-methyl-3-phenyl-N-(pyridin-2-ylmethyl)pyrazolo[1,5-a]pyrimidin-7-amine (AWF920)

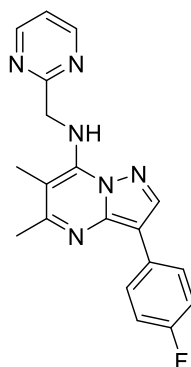
General procedure 2.5 The crude product was washed with water and the grey precipitate triturated with Et₂O to afford **AWF920**. (0.37 g, 65%); **Melting point:** 170-171 °C **¹H NMR (400 MHz, DMSO-d₆)** δ 8.61 (s, 1H), 8.54 (d, *J* = 4.5 Hz, 1H), 8.41 (br s, 1H), 8.13 (d, *J* = 7.4 Hz, 2H), 7.79 (td, *J* = 7.7, 1.6 Hz, 1H), 7.40 (m, 3H), 7.30 (dd, *J* = 6.9, 5.3 Hz, 1H), 7.19 (t, *J* = 7.4 Hz, 1H), 5.39 (s, 2H), 2.56 (s, 3H); **¹³C NMR (101 MHz, DMSO-d₆)** δ 158.0, 157.1, 149.2, 144.3, 143.9, 142.3, 137.4, 132.9, 129.0 (2C), 125.9, 125.7 (2C), 122.8, 121.5, 107.3, 96.6, 48.8, 24.4; **MS (ES⁺):** *m/z* (rel. Intensity) 350.1 (100), 352.1 (32) HRMS (ES⁺) calcd for (C₁₉H₁₇N₅35Cl):350.1172; found: 350.1169. calcd for (C₁₉H₁₇N₅37Cl):352.1143; found: 352.1148; **CHN analysis:** Calculated: C:65.24%, H:4.61%, N:20.02%. Found C:64.24%, H:4.54%, N:19.86%.

3-(4-Fluorophenyl)-5,6-dimethyl-N-(pyrazin-2-ylmethyl)pyrazolo[1,5-a]pyrimidin-7-amine (AWF933)

General procedure 2.5 The crude product was purified by column chromatography eluting with 60% EtOAc:Hexane,NEt₃ to afford **AWF933** as an off-white solid. (29%); **Melting point:** 151-153 °C **¹H NMR (400 MHz, DMSO-d₆)** δ 8.70 (s, 1H), 8.58 (s, 1H), 8.53 (s, 1H), 8.48 (s, 1H), 8.17 (d, *J* = 3.7 Hz, 2H), 7.69 (s, 1H), 7.21 (d, *J* = 5.6 Hz, 2H), 5.30 (s, 2H), 2.50 (s, 3H), 2.28 (s, 3H); **¹³C NMR (101 MHz, DMSO-d₆)** δ 160.1 (d, *J* = 120.8 Hz), 159.5, 154.8, 146.1, 144.3, 144.2, 143.9, 143.7, 141.0, 130.0 (d, *J* = 3.0 Hz), 127.1 (2C, d, *J* = 7.6 Hz), 115.6 (2C d, *J* = 21.1 Hz), 105.3, 97.4, 47.6, 24.7, 13.0; **MS (ES⁺):** *m/z* (rel. Intensity) 349.2 (100), 350.2 (22) HRMS (ES⁺) calcd for (C₁₉H₁₈N₆F):349.1577; found: 349.1571; **CHN analysis:** Calculated: C:65.50%, H:4.92%, N:24.12%. Found C:64.91%, H:4.83%, N:23.58%.

3-(4-Fluorophenyl)-5,6-dimethyl-N-(pyrimidin-4-ylmethyl)pyrazolo[1,5-a]pyrimidin-7-amine (AWF935)

General procedure 2.5 The crude product was purified by column chromatography eluting with 60% EtOAc:Hexane, NEt_3 to 80% EtOAc:Hexane, NEt_3 afford **AWF935** as an off-white solid. (20%); **Melting point:** 157-159 °C **$^1\text{H NMR}$ (400 MHz, DMSO-d_6) δ** 9.13 (s, 1H), 8.73 (d, $J = 5.2$ Hz, 1H), 8.47 (s, 1H), 8.17 (dd, $J = 8.8$, 5.6 Hz, 2H), 7.75 (t, $J = 6.5$ Hz, 1H), 7.50 (d, $J = 5.1$ Hz, 1H), 7.21 (t, $J = 8.9$ Hz, 2H), 5.26 (d, $J = 6.5$ Hz, 2H), 2.50 (s, 3H), 2.26 (s, 3H). **MS (ES+):** m/z (rel. Intensity) 349.2 (100), 350.2 (21) HRMS (ES+) calcd for ($\text{C}_{19}\text{H}_{18}\text{N}_6\text{F}$):349.1577; found: 349.1576; **CHN analysis:** Calculated: C:65.50%, H:4.92%, N:24.12%. Found C:64.85%, H:4.83%, N:23.81%.

Synthesis of 3-(4-Fluorophenyl)-5,6-dimethyl-N-(pyrimidin-2-ylmethyl)pyrazolo[1,5-a]pyrimidin-7-amine (AWF937)

General procedure 2.5 The crude product was purified by column chromatography eluting with 60% EtOAc, NEt_3 to afford **AWF937** as an off-white solid. (24.5%); **Melting point:** 181-183 °C **$^1\text{H NMR}$ (400 MHz, DMSO-d_6) δ** 8.8 (d, $J = 4.9$ 2H), 8.47 (s, 1H), 8.18 (dd, $J = 8.8$, 5.6 Hz, 2H), 7.78 (t, $J = 5.9$ Hz, 1H), 7.42 (t, $J = 4.9$ Hz, 1H), 7.21 (t, $J = 8.9$ Hz, 2H), 5.35 (d, $J = 5.9$ Hz, 2H), 2.50 (s, 3H), 2.30 (s, 3H); **$^{13}\text{C NMR}$ (101 MHz, DMSO-d_6) δ** 160.1 (d, $J = 120.7$ Hz), 159.4, 159.2, 158.0, 146.2, 144.2, 140.9, 130.1 (d, $J = 3.0$ Hz), 127.0 (2C d, $J = 7.6$ Hz), 120.4, 115.7 (2C d, $J = 21.1$ Hz), 105.1, 96.8, 50.1, 24.8, 13.0; **MS (ES+):** m/z (rel. Intensity) 349.2 (100), 350.2 (21) HRMS (ES+) calcd for ($\text{C}_{19}\text{H}_{18}\text{N}_6\text{F}$):349.1577; found: 349.1568; **CHN analysis:** Calculated: C:65.50%, H:4.92%, N:24.12%. Found C:63.76%, H:4.74%, N:23.43%.

2.7 References

- (1) Hwang, J. Y.; Windisch, M. P.; Jo, S.; Kim, K.; Kong, S.; Kim, H. C.; Kim, S.; Kim, H.; Lee, M. E.; Kim, Y.; Choi, J.; Park, D.-S.; Park, E.; Kwon, J.; Nam, J.; Ahn, S.; Cechetto, J.; Kim, J.; Liuzzi, M.; No, Z.; Lee, J. Discovery and Characterization of a Novel 7-aminopyrazolo[1,5-A]pyrimidine Analog as a Potent Hepatitis C Virus Inhibitor. *Bioorg. Med. Chem. Lett.* **2012**, *22* (24), 7297–7301.
- (2) Paruch, K.; Dwyer, M. P.; Alvarez, C.; Brown, C.; Chan, T.-Y.; Doll, R. J.; Keertikar, K.; Knutson, C.; McKittrick, B.; Rivera, J.; Rossman, R.; Tucker, G.; Fischmann, T. O.; Hruza, A.; Madison, V.; Nomeir, A. A.; Wang, Y.; Lees, E.; Parry, D.; Sgambellone, N.; Seghezzi, W.; Schultz, L.; Shanahan, F.; Wiswell, D.; Xu, X.; Zhou, Q.; James, R. A.; Paradkar, V. M.; Park, H.; Rokosz, L. R.; Stauffer, T. M.; Guzi, T. J. Pyrazolo[1,5-A]pyrimidines as Orally Available Inhibitors of Cyclin-Dependent Kinase 2. *Bioorg. Med. Chem. Lett.* **2007**, *17* (22), 6220–6223.
- (3) Du, B. D. J.; Elworthy, T. R.; Hendricks, R. T.; Kondru, R. K.; Lou, Y.; Owens, T. D.; Park, J.; Smith, D. B.; Soth, M.; Yang, H. Pyrrolopyrazine Kinase Inhibitors. US7902197 (B2) — 2011-03-08.
- (4) Caddick, S.; Judd, D. B.; Lewis, A. K. de K.; Reich, M. T.; Williams, M. R. V. A Generic Approach for the Catalytic Reduction of Nitriles. *Tetrahedron* **2003**, *59* (29), 5417–5423.
- (5) Ishikawa, M.; Hashimoto, Y. Improvement in Aqueous Solubility in Small Molecule Drug Discovery Programs by Disruption of Molecular Planarity and Symmetry. *J. Med. Chem.* **2011**, *54* (6), 1539–1554.
- (6) Spartan 16, Wavefunction Inc. <http://www.wavefun.com/>.
- (7) Palani, A.; Shapiro, S.; Josien, H.; Bara, T.; Clader, J. W.; Greenlee, W. J.; Cox, K.; Strizki, J. M.; Baroudy, B. M. Synthesis, SAR, and Biological Evaluation of Oximino-Piperidino-Piperidine Amides. 1. Orally Bioavailable CCR5 Receptor Antagonists with Potent Anti-HIV Activity. *J. Med. Chem.* **2002**, *45* (14), 3143–3160.
- (8) Morwick, T.; Büttner, F. H.; Cywin, C. L.; Dahmann, G.; Hickey, E.; Jakes, S.; Kaplita, P.; Kashem, M. A.; Kerr, S.; Kugler, S.; Mao, W.; Marshall, D.; Paw, Z.; Shih, C.-K.; Wu, F.; Young, E. Hit to Lead Account of the Discovery of Bisbenzamide and Related Ureidobenzamide Inhibitors of Rho Kinase. *J. Med. Chem.* **2010**, *53* (2), 759–777.
- (9) Mueller, B. K.; Mack, H.; Teusch, N. Rho Kinase, a Promising Drug Target for Neurological Disorders. *Nat Rev Drug Discov* **2005**, *4* (5), 387–398.
- (10) Yin, L.; Morishige, K.-I.; Takahashi, T.; Hashimoto, K.; Ogata, S.; Tsutsumi, S.; Takata, K.; Ohta, T.; Kawagoe, J.; Takahashi, K.; Kurachi, H. Fasudil Inhibits Vascular Endothelial Growth Factor-Induced Angiogenesis in Vitro and in Vivo. *Mol. Cancer Ther.* **2007**, *6* (5), 1517–1525.
- (11) Kobayashi, M.; Kume, H.; Oguma, T.; Makino, Y.; Ito, Y.; Shimokata, K. Mast Cell Tryptase Causes Homologous Desensitization of β -Adrenoceptors by Ca²⁺ Sensitization in Tracheal Smooth Muscle. *Clin. Exp. Allergy* **2008**, *38* (1), 135–144.
- (12) Rao, V. P.; Epstein, D. L. Rho GTPase/Rho Kinase Inhibition as a Novel Target for the Treatment of Glaucoma. *BioDrugs* **2007**, *21* (3), 167–177.
- (13) St. Jean, D. J.; Fotsch, C. Mitigating Heterocycle Metabolism in Drug Discovery. *J. Med. Chem.* **2012**, *55* (13), 6002–6020.
- (14) Kempf, D. J.; Sham, H. L.; Marsh, K. C.; Flentge, C. A.; Betebenner, D.; Green, B. E.; McDonald, E.; Vasavanonda, S.; Saldivar, A.; Wideburg, N. E.; Kati, W. M.; Ruiz, L.; Zhao, C.; Fino, L.; Patterson, J.; Molla, A.; Plattner, J. J.; Norbeck, D. W. Discovery of Ritonavir, a Potent Inhibitor of HIV Protease with High Oral Bioavailability and Clinical Efficacy. *J. Med. Chem.* **1998**, *41* (4), 602–617.
- (15) Lipinski, C. A.; Lombardo, F.; Dominy, B. W.; Feeney, P. J. Experimental and Computational Approaches to Estimate Solubility and Permeability in Drug Discovery and Development Settings. *Adv. Drug Deliv. Rev.* **1997**, *23* (1), 3–25.

- (16) Gleeson, M. P. Generation of a Set of Simple, Interpretable ADMET Rules of Thumb. *J. Med. Chem.* **2008**, *51* (4), 817–834.
- (17) Gleeson, M. P.; Hersey, A.; Montanari, D.; Overington, J. Probing the Links between in Vitro Potency, ADMET and Physicochemical Parameters. *Nat Rev Drug Discov* **2011**, *10* (3), 197–208.
- (18) Klebe, G. The Foundations of Protein–Ligand Interaction BT - From Molecules to Medicines: Structure of Biological Macromolecules and Its Relevance in Combating New Diseases and Bioterrorism; Sussman, J. L., Spadon, P., Eds.; Springer Netherlands: Dordrecht, 2009; pp 79–101.
- (19) Gregg, B. T.; Tymoshenko, D. O.; Razzano, D. A.; Johnson, M. R. Pyrazolo[1,5-A]pyrimidines. Identification of the Privileged Structure and Combinatorial Synthesis of 3-(hetero)arylpyrazolo[1,5-A]pyrimidine-6-Carboxamides. *J. Comb. Chem.* **2007**, *9* (3), 507–512.
- (20) Keraenen, M. D. Sequential Hydroformylation, Aldol Reactions: Stereochemical Control towards the Synthesis of the Labdane Diterpenoid Forskolol and Related Terpenoid Natural Products., Dortmund Universitätsbibliothek Technische Universität Dortmund 2004.
- (21) Senga, K.; Novinson, T.; Wilson, H. R.; Robins, R. K. Synthesis and Antischistosomal Activity of Certain pyrazolo[1,5-A]pyrimidines. *J. Med. Chem.* **1981**, *24* (5), 610–613.
- (22) Edgar, M. T.; Pettit, G. R.; Krupa, T. S. Synthesis of L-(5-Chloro-2-Pyridyl)glycine. *J. Org. Chem.* **1979**, *44* (3), 396–400.
- (23) Allen, J. G.; Briner, K.; Cohen, M. P.; Galka, C. S.; Hellman, S. L.; Martinez-Grau, M. A.; Reinhard, M. R.; Rodriguez, M. J.; Rothhaar, R. R.; Tidwell, M. W.; Victor, F.; Williams, A. C.; Zhang, D.; Boyd, S. A.; Conway, R. G.; Deo, A. S.; Lee, W.-M.; Siedem, C. S.; Singh, A. Preparation of 6-Substituted 2,3,4,5-Tetrahydro-1H-Benzo[d]azepines as 5-HT_{2c} Receptor Agonists., PCT Int. Appl, WO2005082859A1, September 9, 2005.
- (24) Liu, B.; Yu, T.; Zhang, Y.; Zhang, X.; Zhang, S.; Zheng, C.; Zhang, J. Preparation of Aromatic Heterocyclic Compounds for Treating Phosphodiesterase 4 Related Diseases. Faming Zhuanli Shenqing, CN105085429A, 2015, Pages 713-728 .
- (25) Raghavan, S.; Stelmach, J. E.; Smith, C. J.; Li, H.; Whitehead, A.; Waddell, S. T.; Chen, Y.-H.; Miao, S.; Ornoski, O. A.; Garfunkle, J.; Liao, X.; Chang, J.; Han, X.; Guo, J.; Groeper, J. A.; Brockunier, L. L.; Rosauer, K.; Parmee, E. R. Pyrrolopyrimidinone Derivatives as Soluble Guanylate Cyclase Activators and Their Preparation., PCT Int. Appl., WO2011149921A1 December 1, 2011.
- (26) Nakano, S.; Takahashi, K.; Takada, J.; Iwamoto, T.; Nagae, K.; Maruyama, Y.; Shintani, Y.; Okada, T.; Ito, Y.; Kadowaki, T.; Yamauchi, T.; Iwabu, M.; Iwabu, M. Preparation of Spiro Compounds for Activating Adiponectin Receptor., PCT Int. Appl., WO2011142359A1, November 17, 2011.
- (27) Gujjar, R.; El Mazouni, F.; White, K. L.; White, J.; Creason, S.; Shackelford, D. M.; Deng, X.; Charman, W. N.; Bathurst, I.; Burrows, J.; Floyd, D. M.; Matthews, D.; Buckner, F. S.; Charman, S. A.; Phillips, M. A.; Rathod, P. K. Lead Optimization of Aryl and Alkyl Amine-Based Triazolopyrimidine Inhibitors of Plasmodium Falciparum Dihydroorotate Dehydrogenase with Antimalarial Activity in Mice. *J. Med. Chem.* **2011**, *54* (11), 3935–3949.
- (28) Westman, J. Pyrazolo[1,5-A]pyrimidin-7-Amine Derivatives Useful in Therapy., PCT Int. Appl., WO2015110491A2, July 30, 2015.
- (29) Soares de Melo, C.; Feng, T.-S.; van der Westhuyzen, R.; Gessner, R. K.; Street, L. J.; Morgans, G. L.; Warner, D. F.; Moosa, A.; Naran, K.; Lawrence, N.; Boshoff, H. I. M.; Barry III, C. E.; Harris, C. J.; Gordon, R.; Chibale, K. Aminopyrazolo[1,5-A]pyrimidines as Potential Inhibitors of Mycobacterium Tuberculosis: Structure Activity Relationships and ADME Characterization. *Bioorg. Med. Chem.* **2015**, *23* (22), 7240–7250.
- (30) Soares de Melo, C.; Feng, T.-S.; van der Westhuyzen, R.; Gessner, R. K.; Street, L. J.; Morgans, G. L.; Warner, D. F.; Moosa, A.; Naran, K.; Lawrence, N.; Boshoff, H. I. M.; Barry, C. E.; Harris, C. J.; Gordon, R.; Chibale, K. Aminopyrazolo[1,5-A]pyrimidines as Potential Inhibitors of Mycobacterium Tuberculosis:

Structure Activity Relationships and ADME Characterization [Erratum to Document Cited in CA163:693765]. *Bioorg. Med. Chem.* **2016**, 24 (2), 314.

- (31) Gaussian 03, Revision C.02, M. J. Frisch, G. W. Trucks, H. B. Schlegel, G. E. Scuseria et al., Gaussian, Inc., Wallingford CT, 2004.
- (32) Rozas, I. On the Nature of Hydrogen Bonds: An Overview on Computational Studies and a Word about Patterns. *Phys. Chem. Chem. Phys.* 2007, 9 (22), 2782–2790.
- (33) Personal communication with Isabel Rozas, 11/30/2017.
- (34) M06-2X: Y. Zhao and D. G. Truhlar, “The M06 suite of density functionals for main group thermochemistry, thermochemical kinetics, noncovalent interactions, excited states, and transition elements: two new functionals and systematic testing of four M06-class functionals and 12 other functionals,” *Theor. Chem. Acc.*, 120 (2008) 215-41.
- (35) 6-311++G(d,p): A. D. McLean and G. S. Chandler, “Contracted Gaussian-basis sets for molecular calculations. 1. 2nd row atoms, Z=11-18,” *J. Chem. Phys.*, 72 (1980) 5639-48.
- (36) Gaussian 09: Gaussian 09, Revision A.02, M. J. Frisch, G. W. Trucks, H. B. Schlegel, G. E. Scuseria, et al., Gaussian, Inc., Wallingford CT, 2016.

Chapter 3

Pyrazolopyrimidines - R¹ exploration

Contents

Chapter 3 Pyrazolopyrimidines - R ¹ exploration	106
3.1 Early lead optimisation	106
3.2 Development of synthetic strategies for analogues with diverse R ¹ substituents	108
3.3 R ¹ Mono-substituted phenyl ring systems	110
3.4 R ¹ position biaryl ring systems	115
3.5 Small R ¹ substitutions - Aryl-Removed analogues.....	118
3.6 Bioisosteric replacement of the R ¹ phenyl ring	122
3.7 Conclusion.....	126
3.8 Experimental.....	129
3.8 References	166

Chapter 3 Pyrazolopyrimidines - R¹ exploration

3.1 Early lead optimisation

Improved template modifications as reported in Chapter 2 are summarised in **Fig 3.1**. Several modifications were tolerated at this 6-(R³) position in terms of producing compounds with acceptable *in vitro* anti-*Wolbachia* activity and so far, a methyl group was shown to provide the best balance of potency and DMPK properties. The 2-pyridyl group was essential for anti-*Wolbachia* activity and while in the analogue displayed, **AWF913** in **Fig 3.1**, methylation of the linker resulted in reduced metabolic stability within Rat hepatocyte cells; this modification seems substrate dependent as it can provide an improvement to metabolic stability and aqueous solubility when introduced into other analogues (**Chapter 2 – Fig 2.11**).

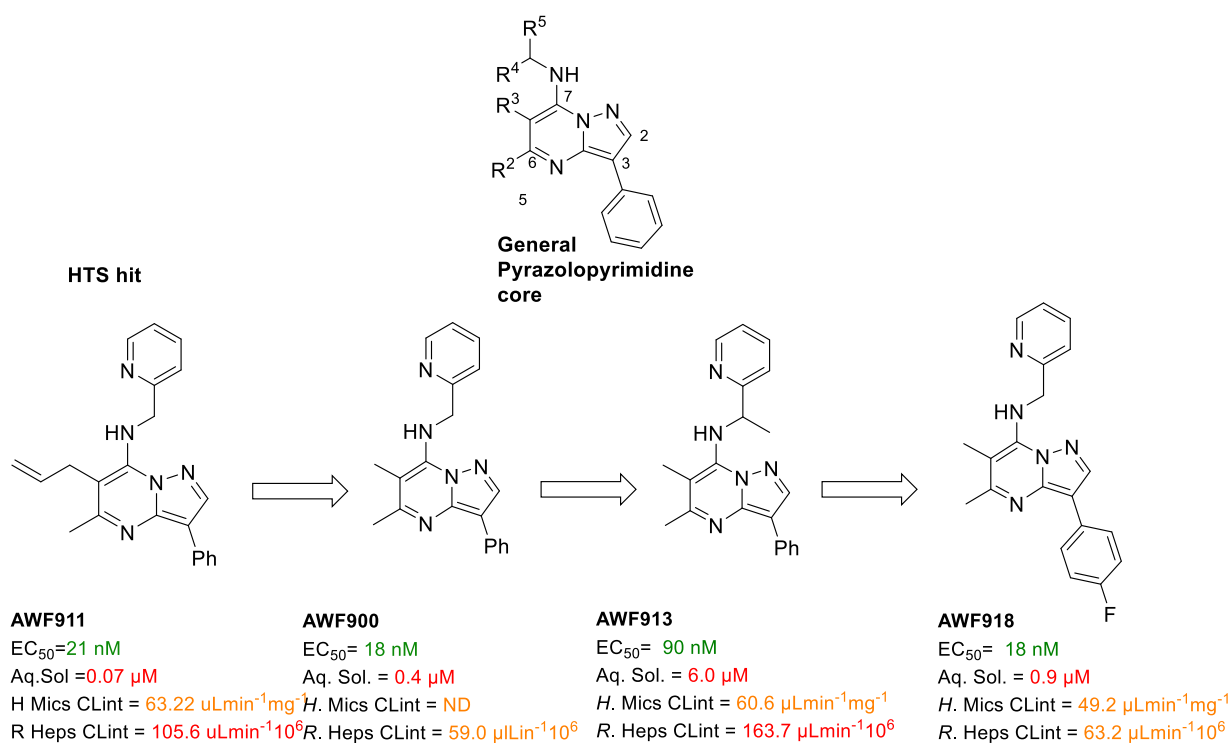


Fig 3.1 Summary of hit to early lead optimisation discussed in the previous chapter.

Compound optimisation by modification of the 6-position of the pyrazolopyrimidine core or the 2-pyridyl ring is limited; the main improvement to the pyrazolopyrimidine properties from the work carried out in the previous chapter is the over 85-fold improvement in aqueous solubility seen from the initial hit **AWF911** to **AWF913**. Despite such a notable improvement to aqueous solubility it was still necessary to enhance this property further, whilst simultaneously improving the metabolic stability profile to the target region. The desired, acceptable and poor properties as presented earlier are defined below in **Table 3.1**. The early lead **AWF918** demonstrates that modification of the lower phenyl ring is tolerated in terms of anti-*Wolbachia*

activity and has the potential to boost the aqueous solubility and metabolic stability of our pyrazolopyrimidine analogues.

	EC ₅₀ (nM)	LogD 7.4	Aq.Sol (μM)	H.M.Cl (μL/min/mg)	R.HepsCl (μL/min 10 ⁻⁶)	Human PPB (%)
Desired	<100	1-4	>50	<20	<20	<99
Acceptable	100-300	0-1,4-5	20-50	20-60	20-60	<99.5
Poor	300+	<0, >5	<20	>60	<60	>99.5

Table 3.1 A table highlighting appropriate and inappropriate potency and DMPK values.

Considering the large improvement to DMPK properties required to reach the target values as defined above, further modifications to the pyrazolopyrimidines were necessary. Molecules **1-5** displayed in **Fig 3.2** are several of the hits identified from the initial screening campaign with their activity compared to doxycycline highlighted in orange (50% activity of doxycycline) or green (90% of the activity of doxycycline). These hits demonstrate that the chemical space around the R¹ position (**Fig 3.2**) can be manipulated without complete loss of anti-*Wolbachia* activity. With the SAR restricted around the R³, R⁴, and R⁵ positions, we shifted our attention to the 3-(R¹) position of the pyrazolopyrimidine core (**Fig. 3.2**) since analysis of the HTS data suggested that this position may tolerate a wider range of modifications.

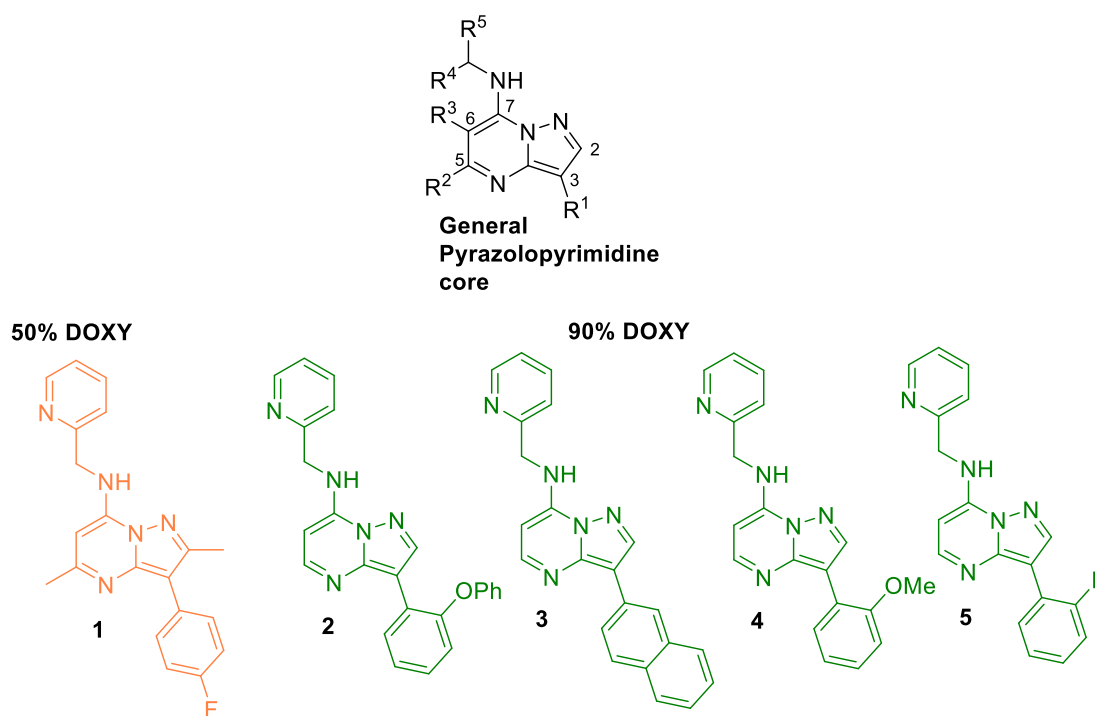
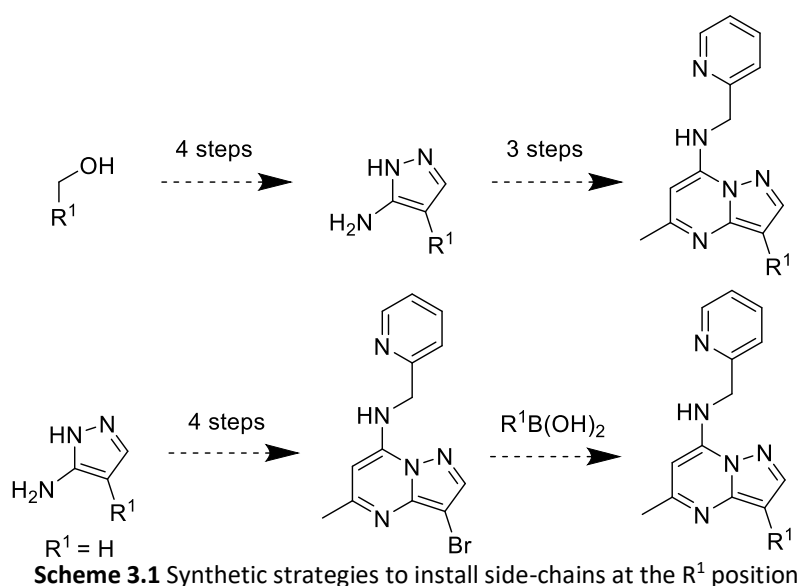


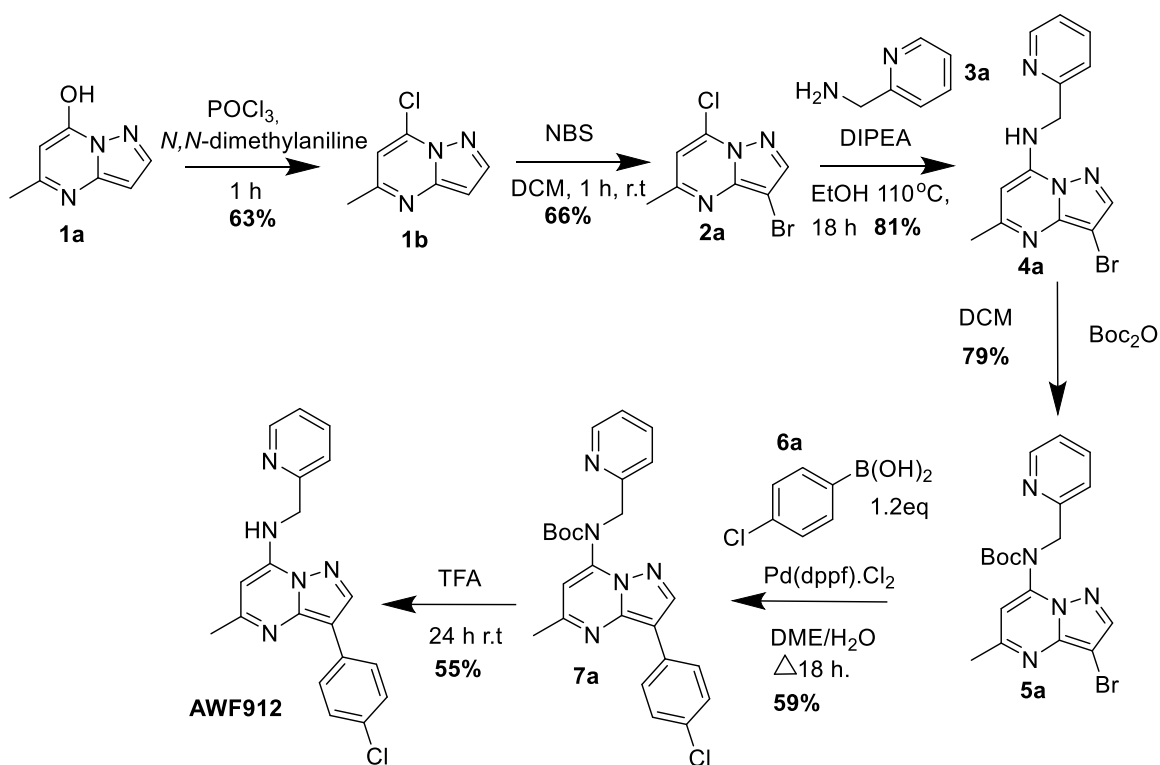
Fig 3.2 Pyrazolopyrimidine core with the general scaffold for the focus of SAR study and initial HTS hits

3.2 Development of synthetic strategies for analogues with diverse R¹ substituents

The initial synthetic route was developed to allow for the synthesis of several analogues with modified R²⁻⁵ positions around the pyrazolopyrimidine core. While it is possible to initiate synthesis with the appropriate alcohol to allow for the synthesis of compounds with diverse R¹ functionalities which requires 7 steps in total (**Fig 3.2**), a point of divergence at a later point in the synthetic pathway was desirable to produce a range of analogues from a common intermediate in fewer steps. One potential strategy to achieve this would be to couple various aryl rings at the R¹ position following halogenation as suggested in **Scheme 3.1**.



This late-stage functionalisation of the R¹ position (**Scheme 3.1**) can be achieved *via* halogenation and subsequent Suzuki coupling on the pyrazolopyrimidine core as reported by K Paruch *et al.*,¹ and was adopted to give the synthesis depicted in **Scheme 3.2**. This strategy allows for fewer steps than synthesis of the initial pyrazole (**Scheme 3.1**) to introduce various groups at the R¹ position from the common intermediate **5a**.



Scheme 3.2 Synthetic route to compound **AWF912**

Phosphoryl chloride mediated chlorination of **1a** to form the pyrazolopyrimidine intermediate **1b** (Scheme 3.1) provided poor yields using the original conditions of refluxing overnight. Modifying the reaction conditions to incorporate *N,N*-dimethylaniline as the base and by limiting the reaction time to 1 hour appeared to be optimal conditions for production of the desired product. Bromination of **1b** was performed using NBS to give **2a** and the subsequent substitution with 2-pyridyl methanamine (**3a**) afforded **4a** in moderate yields (66%) and allowed for easy purification of the intermediate. The palladium catalyst utilised for the Suzuki reaction in the production of this first in series analogue was Pd(dppf).Cl₂ (Fig 3.3) as the ferrocene ligands appear to be used quite frequently in the literature for coupling reactions at the 3-position of pyrazolopyrimidines.²⁻⁶

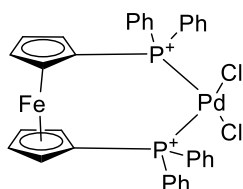


Fig. 3.3 Structure of the palladium catalyst dppf (diphenylphosphinoferrocene)

This pathway required Boc-protection of the bromide intermediate **5a** to avoid the free amine interfering with the Suzuki reaction and to allow for successful coupling to occur on **7a** in the production of the first compound in this series **AWF912** (Scheme 3.1). This analogue is the only example to be unsubstituted at the R³ position as this synthesis was performed in parallel to study of the R³ position before a 6-methyl substituent was incorporated into the pyrazolopyrimidine core.

The *in vitro* anti-*Wolbachia* potency and DMPK properties of **AWF912** are displayed below in **Fig 3.4** with the parent analogue **AWF905** containing an unsubstituted phenyl ring. **AWF912** shows enhanced *in vitro* metabolic stability over the original **AWF905**, unfortunately, this modification led to over a 4-fold drop in compound potency compared to **AWF905**. However, after acknowledging the importance of a substituted 6-(R³) position in achieving potent anti-*Wolbachia* effects, we decided to incorporate a methyl substituent at this position. With this beneficial methyl incorporated into the pyrazolopyrimidine several analogues with various aryl ring systems were designed for synthesis.

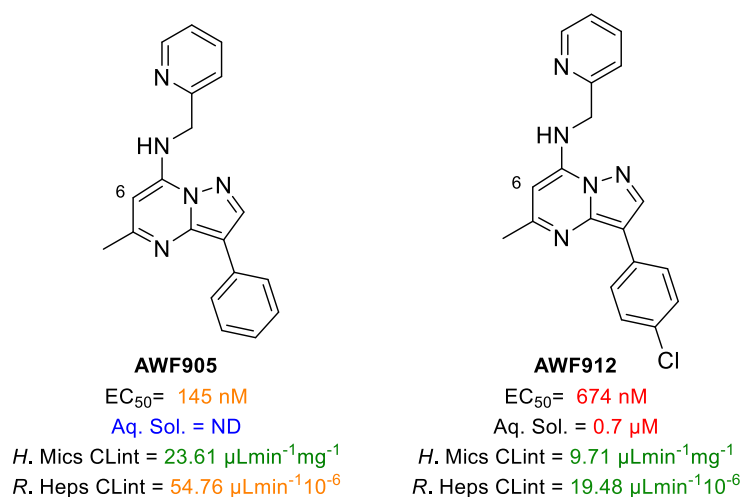


Fig 3.4 Introduction of a 4-Cl Ph at the 3-(R¹) position

3.3 R¹ Mono-substituted phenyl ring systems

A variety of substituted aryl groups were designed to probe the SAR around this position. *In silico* DMPK predictions were carried out by collaborators in AstraZeneca and are displayed in **Fig 3.5**. The predicted data suggests there will be a two-fold reduction in clearance from a metabolic system in a 4-SO₂Me Ph analogue (**AWZ9014**) in comparison to the 4-F Ph analogue (**AWF918**). Also, several alternative aromatic heterocycles were selected for synthesis following promising *in silico* DMPK predictions. These included a 2-pyridyl, 2,4,5 trimethyl pyrazole and a 3-*N*-methyl pyrazole ring system. The predicted DMPK parameters for the 3-*N*-Me pyrazole (**AWZ9030**) are displayed in **Fig 3.5** alongside the predicted properties for the 4-F Phenyl analogue, **AWF918**. These predictions suggest that **AWZ9030** will have a five-fold improvement in aqueous solubility and over a two-fold improvement in metabolic stability over **AWF918**.

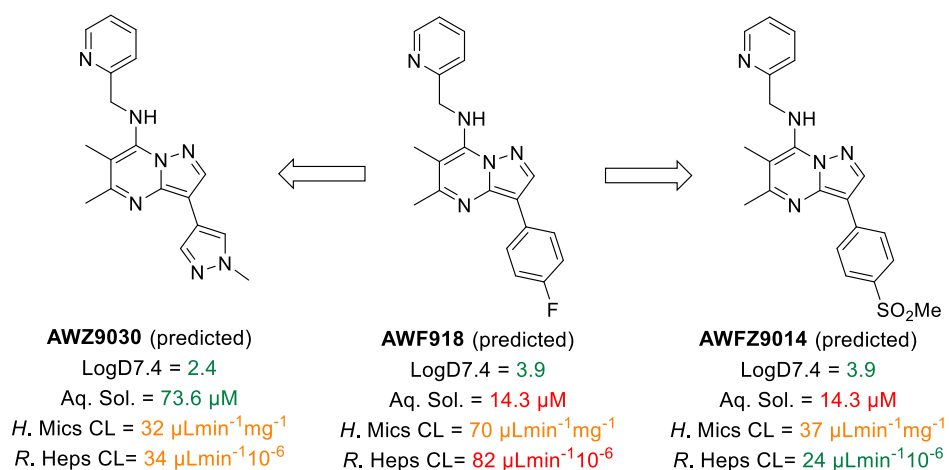


Fig 3.5 Predicted DMPK properties used in the design of a variety of aryl ring systems for the R¹ position

Ortho methylation is a common strategy to boost solubility of compounds by increasing the torsion angle between ring systems. By reducing the overall molecular planarity between two aryl ring systems crystal packing energy can be reduced and consequently aqueous solubility should increase.^{7,8} There are various examples of *ortho*-methylation which result in a significant increase in compound potency as well.⁹⁻¹²

Whilst establishing a simple synthesis to compounds containing various R¹ side-chains, our chemistry partner WuXi App Tech revealed that it is possible to synthesise these targets without Boc-protection by using a more reactive 3-iodo intermediate. However, upon attempting such reactions we observed that without Boc-protection reaction yields were poor and purification heavily relied on HPLC. The more reactive iodo intermediate **12a** (Scheme 3.3) was incorporated into our synthesis. This involved iodination of the unsubstituted analogue **11a** using the electrophilic iodinating agent NIS. The coupling reactions on **14a** were performed with the catalyst, Pd(dtbpf).Cl₂ (Fig 3.6), which upon cessation of the reaction monitored by TLC and purification of the mixture appears to result in generally higher yields for couplings performed on our substrate in comparison to using Pd(PPh₃) or Pd(dppf).Cl₂ as the catalyst.

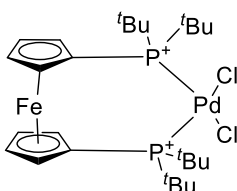
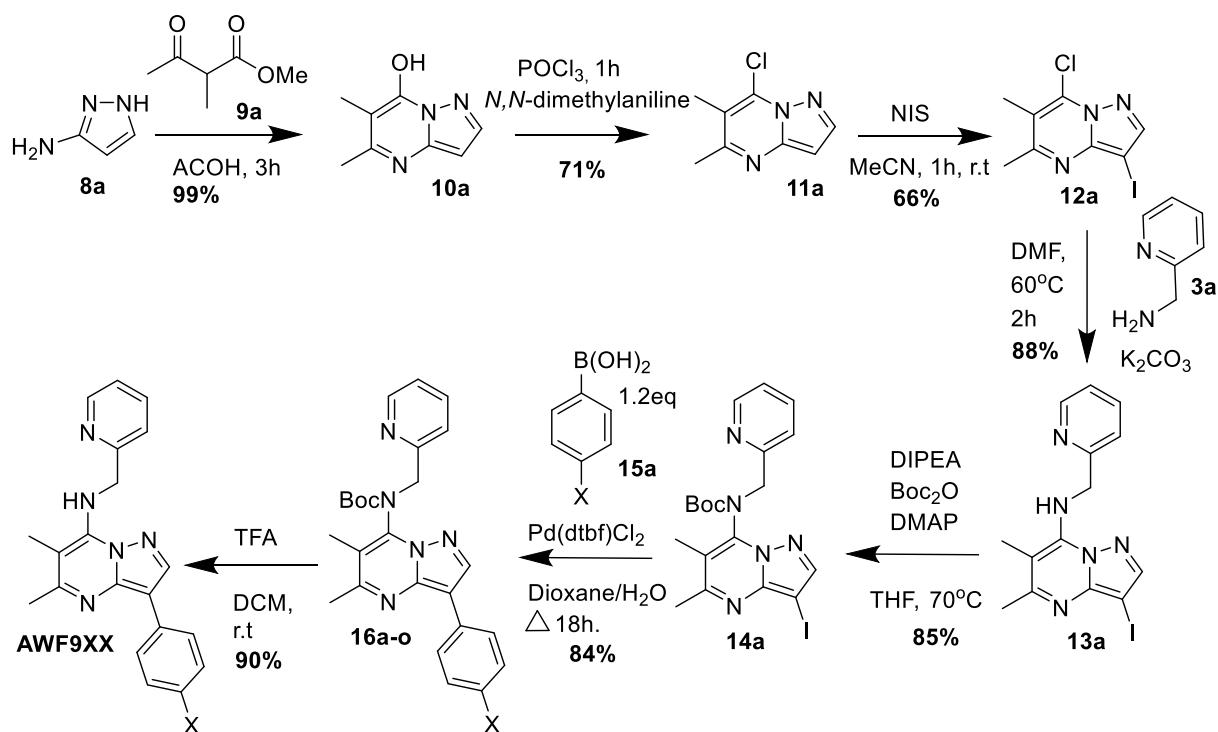


Fig 3.6 Structure of the palladium catalyst dtbpf (ditertiarybutylphosphino ferrocene).

With a consistent 2-pyridyl functionality at the R⁵ position we could perform the substitution reaction on the 7-chloro intermediate in DMF which allowed for shorter reaction times and generally superior yields allowing easier purification by recrystallization over column chromatography; the synthesis adopted for this series of analogues is shown in **Scheme.3.3**.



Scheme. 3.3 Advanced synthetic route to analogues with modified R¹ positions.

Several analogues were synthesised with various aryl rings at the R¹ position with the general scaffold depicted below in **Fig 3.7** and the measured *in vitro* anti-*Wolbachia* potency and DMPK properties displayed in **Table 3.2**

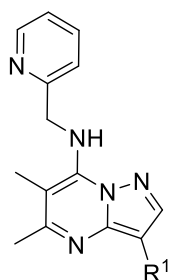
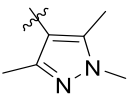
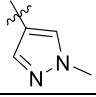
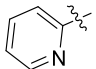
Fig.3.7 General structure for compounds with varied R¹ positions.

Table entry	Compound	R ¹	EC ₅₀ (nM)	LogD 7.4	Aq. Sol (μM)	H.MicCl (μL/min/mg)	R.HepCl (μL/min 10 ⁻⁶)	PPB (%)
1	AWF900	Ph	19	4.2	0.04	ND	59.0	99.90
2	AWZ9012	4-CF ₃ Ph	789	4.4	0.03	3.0	16.9	> 99.95
3	AWZ9013	4-OCF ₃ Ph	664	4.5	5.00	8.8	156.6	97.9
4	AWZ9014	4-SO ₂ Me Ph	143	3.3	2.00	21.8	27.6	99.81
5	AWZ9015	4-CN Ph	664	4.1	1.00	3.0	14.8	> 99.93
6	AWF917	4-Cl Ph	84	4.7	0.30	22.8	27.9	> 99.95
7	AWF918	4-F Ph	17	4.3	0.90	49.2	67.7	99.8
8	AWF945	2-SO ₂ Me Ph	>2500	2.3	11.00	74.2	>300	88
9	AWF941	3-SO ₂ Me Ph	>2500	3	2.00	12.1	147.8	96.6
10	AWF919	2-Me Ph	102	4.0	10.0	72.0	245.7	99.17
11	AWZ9009	2-Cl Ph	33	4.0	7.00	90.7	173.1	99.89
12	AWF936	2-F Ph	11	4	0.60	84.0	113.2	99.88
13	AWZ9010	3-Cl Ph	266	4.1	0.50	60.7	85.0	>99.95
14	AWF925	3-F Ph	>1000	4.1	1.00	59.3	86.2	> 99.90
15	AWF938	4-CO ₂ Me Ph	179	4.4	0.70	39.4	>300	99.8
16	AWF940	4-SO ₂ NHMe Ph	>2,500	3.5	0.50	15.1	>300	97.9
17	AWF942	4-CONH ₂ Ph	NA	ND	ND	ND	ND	ND
18	AWF943	4-SO ₂ <i>i</i> Pr Ph	175	3.8	0.70	26.7	62.1	98.7

Table entry	Compound	R ¹	EC ₅₀ (nM)	LogD 7.4	Aq. Sol (μM)	H.MicCl (μL/min/mg)	R.HepCl (μL/min 10 ⁻⁶)	PPB (%)
19	AWF944	4-SO ₂ Et Ph	131	3.4	0.20	8.2	49.1	97.8
20	AWZ9029	3-pyridyl 4-CF ₃	>2500	ND	ND	ND	ND	ND
21	AWZ9031		1479	2.9	101	14.65	80.69	85
22	AWZ9030		119	2.7	43.00	44.8	10.3	91.8
23	AWZ9033		43	2.3	30.00	243.6	144.9	97.4

NA – No activity at highest concentration (5 μM)

ND – Not determined

Table 3.2 Potency, DMPK and solubility analysis of compounds containing various aryl rings at the R¹ position.

As demonstrated by table entries **2-7** and **13-18** *para*-substitution of the phenyl ring is normally tolerated with a range of substituents. The 4-OCF₃ substituent **AWZ9013** (entry **3**) proved successful in improving aqueous solubility and reducing human microsomal clearance over the parent phenyl analogue; however, suffered over a 30-fold drop in activity (EC₅₀=664 nM). Incorporation of the polar SO₂Me group at the *para* position of the phenyl ring (entry 4 - **AWZ9014**) was successful in reducing logD, increasing aq. solubility and improving metabolic stability over the phenyl and 4-F phenyl analogue. While the 4-CN Ph analogue **AWZ9015** (entry **5**) did prove to have enhanced aqueous solubility over the parent phenyl analogue and a promising metabolic stability profile (both rat and human clearance values <20 – **Table 3.1**) this compound suffered over a 30-fold drop in anti-*Wolbachia* activity (EC₅₀ = 84 nM) compared to the phenyl parent analogue (entry **1**). The 4-Cl Ph containing analogue did possess suitable anti-*Wolbachia* activity and possessed acceptable clearance values during *in vitro* assessments however as with several of these mono-substituted phenyl rings a larger boost to aqueous solubility was necessary to reach a suitable level.

The 4-F substitution (entry **7** - **AWF918**) appears to be optimal for activity (EC₅₀=15 nM), both compounds **AWF918** and **AWZ9014** were considered early-leads resulting from this work. These compounds were both evaluated for *in vitro* potency within the *in vitro* mf study and **AWZ9014** subjected to PK and PD analysis within the *in vivo* SCID mouse model (see Chapter 4). Table entries **8** (**AWF945**) and **9** (**AWF941**) demonstrate that large groups are not tolerated in the *ortho* or *meta* positions of the phenyl ring in terms of anti-*Wolbachia* activity. Meanwhile, smaller substituents at the *ortho*-position such as methyl (entry **10**), chlorine (entry **11**) or fluorine (entry **12**), are tolerated in terms of potency. *Ortho*-methylation of the phenyl ring at the R¹ position (entry **8** - **AWF919**) provided a 250-fold improvement to aqueous solubility (Aq.sol = 10 μM) over the parent analogue **AWF900** (entry **1**, Aq.sol = 0.04 μM). Unfortunately, this analogue suffered from a 5-fold drop in potency, possessed poor metabolic stability and further improvement of solubility was still required to reach the desired solubility levels (**Table 3.2**), therefore further optimisation was necessary.

Substitution at the 3 position of the phenyl ring was not tolerated in terms of potency with any substituent studied which is demonstrated here by tables entries **13** and **14** which contain the 3-Cl Ph ring (**AWF924**) and the 3-F Ph ring (**AWF935**) respectively. The analogues **AWF938-944** (entries **15-19**) offer further evidence that a variety of substituents are tolerated in terms of activity at the *para* position. It appears that there is space within the drug binding site that tolerates an additional phenyl ring at this position (entry **15**, **18** and **19**) while incorporation of an amine at this position completely removes anti-*Wolbachia* activity.

To reduce log D further our collaborators WuXi (see appendix 1 for experimental details) prepared the analogues (table entries **20-23**) containing nitrogen heterocyclic ring systems where the CF₃ substituted pyridyl ring (**AWZ9029** – entry **20**) possessed no anti-*Wolbachia* activity as did the 2,3,4 trimethyl pyrazole analogue **AWZ9031** (entry **21**). The analogues **AWZ9030** (entry **22**) and **AWZ9033** (entry **23**) containing the 4-*N*-Me, 3,4-pyrazole and 2-pyridyl rings respectively, were both tolerated in terms of potency and greatly increased the aqueous solubility of our pyrazolopyrimidine analogues. The 4-*N*-Me, 3,4-pyrazole analogue, **AWZ9030** possessed promising stability and solubility; however, suffered from a 6-fold decrease in activity (EC₅₀ = 119 nM) compared to the phenyl analogue (entry **1** EC₅₀ = 19 nM) and while the 2-pyridyl analogue **AWZ9033** maintained most of its activity (EC₅₀ = 43 nM) it suffered from very poor metabolic stability (Human liver microsomal clearance = 244 μLmin⁻¹mg⁻¹). These results supported investigation into additional aryl ring groups bearing basic nitrogen centres to enhance solubility and allow potential formulation as amine salts.

3.4 R¹ position biaryl ring systems

After exploring the SAR around the R¹ position with several substituted aromatic ring systems we discovered that it is possible to manipulate the *para* position with various functionalities to produce compounds with acceptable anti-*Wolbachia* activities. Incorporation of saturated heterocycles as solubilising groups attached to phenyl ring systems has proven to be a successful strategy to greatly improve aqueous solubility in previous medicinal chemistry programs.¹³ Also, DMPK predictions for the two molecules **T1** and **T2** below in **Fig 3.8** demonstrate that such side-chains should possess much superior aqueous solubility than our previous analogues.

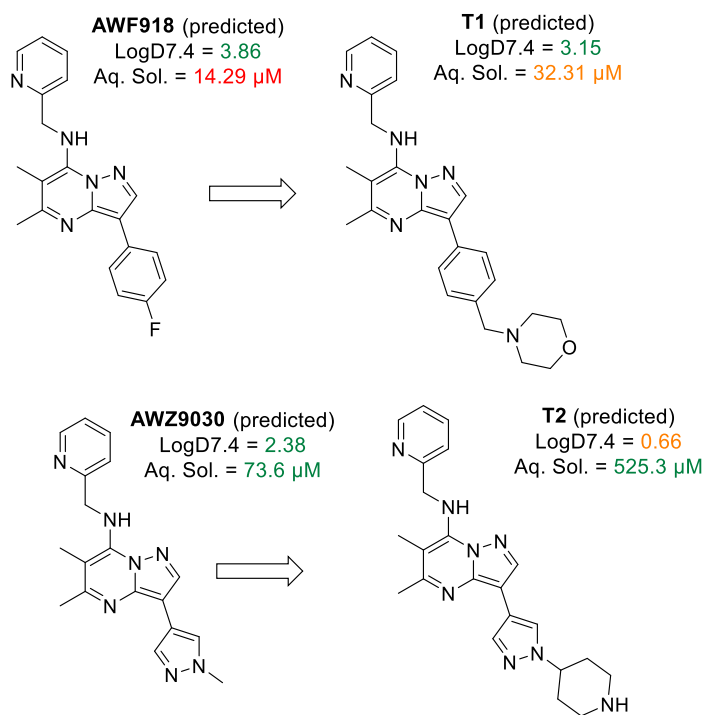
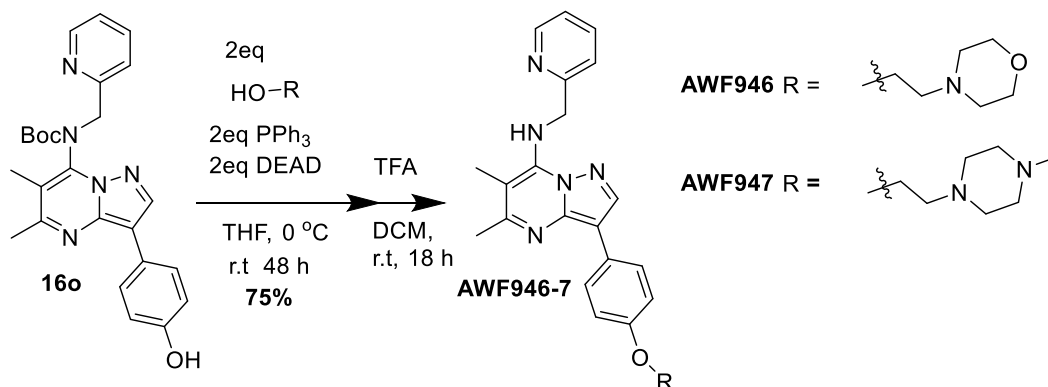


Fig. 3.8 Predicted solubility changes upon incorporation of a terminal heterocyclic ring.

Therefore, we designed compounds containing extended side-chains with terminal saturated heterocyclic ring systems like the examples above (**Fig 3.8**) containing terminal saturated nitrogen-containing heterocycles. One of these selected targets, **AWF939** (**Table 3.2**), could be synthesised *via* the previously discussed chemistry (**Scheme 3.4**), from the commercially available 4-morpholino(phenyl)methanone boronic acid. Compounds **AWF946-7** were prepared *via* Mitsunobu reactions using DEAD as an activating reagent (**Scheme.3.4**) from the phenol intermediate **16o** (**Scheme 3.4**) produced from Suzuki coupling of (4-hydroxyphenyl)boronic acid.



Scheme. 3.4 Synthetic route to **AWF946 & AWF947**

The whole-cell anti-*Wolbachia* activity and measured DMPK properties for analogues containing additional ring systems are displayed in **Table 3.3**.

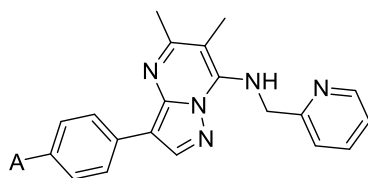


Table entry	Compound	A	EC ₅₀ (nM)	LogD 7.4	Aq. Sol (μM)	H.MicsCL (μL/min/mg)	R.HepsCL (μL/min 10 ⁻⁶)	PPB (%)
1	AWF939		680	3.2	5.00	9.8	15.6	96
2	AWF946		844	3.6	2.00	43.7	95.0	98.1
3	AWF947		1228	2.7	71.00	30.8	258.7	91.9

Table 3.3 Results for analogues containing extended side chains at the R¹ position.

These compounds possessed improved aqueous solubility over most of the mono substituted phenyl ring analogues (**Table 3.1**). The 4-morpholino phenyl methanone analogue **AWF939** (table entry 1) experienced a 6-fold improvement in metabolic stability (Clearance values <20) compared to the mono substituted phenyl analogues which is demonstrated by greatly reduced human microsomal and rat hepatocyte clearance values. The morpholine ring proved more potent than the *N*-methyl piperidine group within the ether-linked analogues in table entries 2 and 3 (**AWF946-7**) and it appears from these results that extension of the linker leads to reduced potency. Unfortunately, these analogues had greatly reduced anti-*Wolbachia* potency therefore alternative modifications to this position were deemed necessary.

Reducing the aromatic ring count within prospective drug compounds is an established strategy for the improvement of aqueous solubility.¹⁴ Therefore, we decided at this point it may be worth studying the effect that removal of the aromatic ring system all together would have in our analogues. This would allow us to determine whether the aromatic side-chain at the R¹ position is essential for potency and to potentially improve the ligand efficiency of our analogues.

3.5 Small R¹ substitutions - Aryl-Removed analogues.

These unsubstituted (R¹=H) analogues (**Fig 3.9**) can be produced *via* amination of the unsubstituted 7-Cl intermediate **11a** (**Scheme 3.3**) used in the production of the 3-iodo intermediate (**Scheme 3.3**) during study of the R¹ position. **AWF930** (**Fig 3.9**), which was unsubstituted at this position, was evaluated for biological activity to study the effect that removal of the aryl ring system induces. The potency of compound **AWF930** (EC₅₀ = 105 nM) (**Fig 3.9**) revealed that a phenyl ring at the R¹ position is not an essential functionality for pyrazolopyrimidine compounds to possess anti-*Wolbachia* activity.

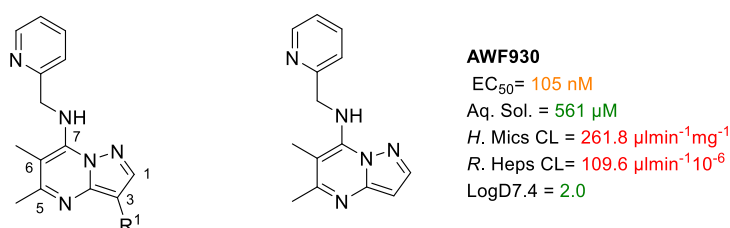


Fig. 3.9 Structure and measured biological activity for **AWF930** with an unsubstituted at the R¹ position.

Compared to the parent 4-fluoro phenyl-containing analogue **AWF918**, **AWF930** displayed greatly improved (>600 fold) aqueous solubility. **AWF930** maintained most of its potency; however, suffered from very poor metabolic stability during *in vitro* DMPK analysis. To alleviate the metabolic liability associated with this labile unsubstituted R¹ position, alternative analogues were designed with various small substitutions at the R¹ position to identify the optimal group at this position in terms of potency and DMPK properties.

During chemical modification, the 3-position of the pyrazolopyrimidine core displays both electrophilic and nucleophilic nature which will leave it exposed to both electrophilic and nucleophilic metabolising enzymes. Double bonded carbons within an aromatic ring are exposed to a range of different routes of oxidative metabolism^{15,16} such as epoxidation which can lead to addition of glutathione unit (**Fig 3.10**) or hydrogen abstraction followed by hydroxylation and subsequent conjugation to larger groups such as glucuronic acid (**Fig 3.10**).¹⁶

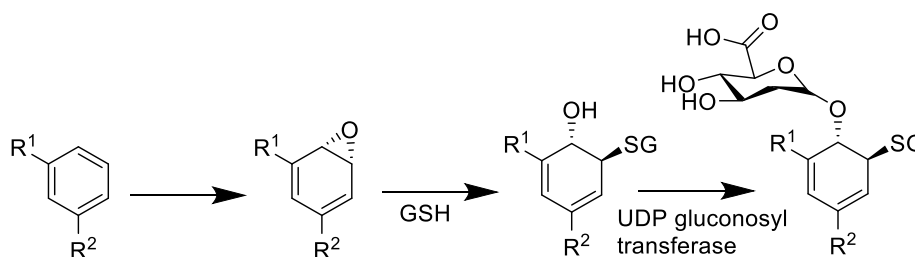


Fig 3.10 Potential metabolism pathway for drugs containing aromatic ring systems

It is quite possible that metabolism at this position is a result of hydrogen abstraction and subsequent oxidation, one of the most commonly utilised medicinal chemistry strategies for blocking this metabolism is by incorporating a fluorine atom to block metabolism. This strategy is dependent on the strength of the C-F bond, which at approximately $109 \text{ kcal mol}^{-1}$ is one of the strongest single bonds that can be made to a carbon atom,^{17–24} this allows the C-F bond to be inert under most biological conditions. Throughout the optimisation of the cholesterol absorption inhibitor ezetimibe, the introduction of two fluorine atoms into **A1** were critical steps among others during the improvement of metabolic stability (**Fig 3.11**), which allowed for a reduced dose of the resultant more-stable compound.^{19,25}

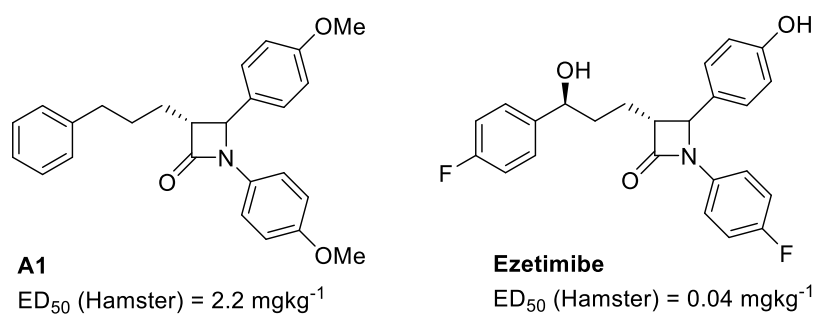


Fig 3.11 Optimization towards cholesterol absorption inhibitor ezetimibe (Zetia).

Halogenation of the R¹ position of the pyrazolopyrimidine core was achieved as previously discussed (**Scheme 3.3**) using electrophilic halogen sources, however now using NCS, NBS or selectfluor (**Fig 3.12**).^{26–28} A nitrile group was installed at the R¹ position of the pyrazolopyrimidine core by initiating synthesis from 5-amino pyrazole-4-carbonitrile **17a** (**Scheme 3.5**) using previously discussed chemistry (**Scheme 2.3 - Chapter 2**). This nitrile-containing intermediate was used to produce the 3-carboxamide 7-chloro intermediate **19a** (**Scheme 3.5**) by sulphuric acid-mediated hydrolysis of **18a** (**Scheme.3.5**), which, when subjected to substitution with 2-pyridyl methanamine afforded the carboxamide analogue **AWF953**.

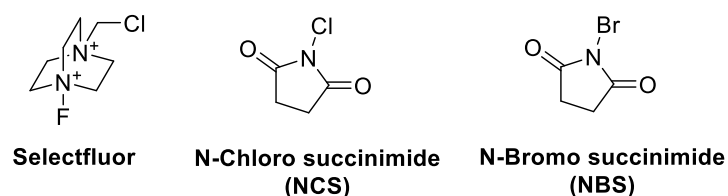
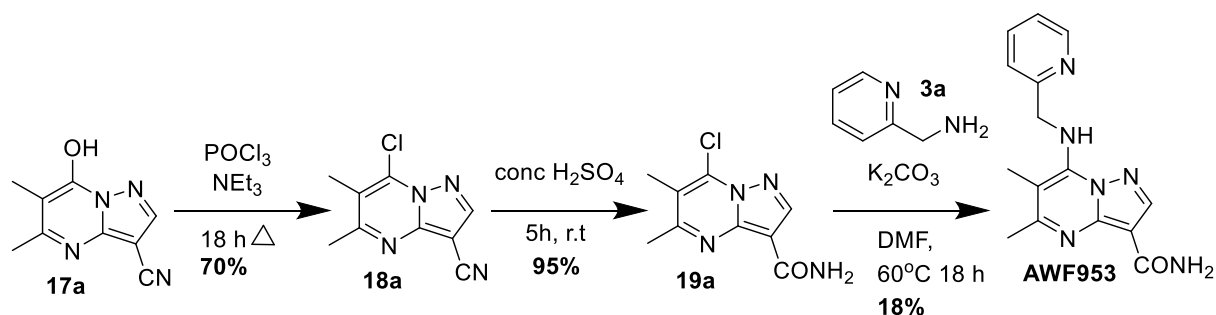


Fig 3.12 Structures of electrophilic halogenating agents, used for installing halogens at the R¹ position



Scheme. 3.5 Synthesis of R² carboxamide analogue **AWF953**

The anti-*Wolbachia* activities and measured DMPK properties for this series of analogues are displayed in **Table 3.3** with the variable groups in this study depicted in the generalised structure below.

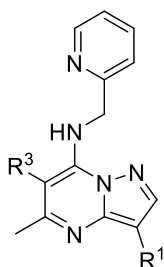


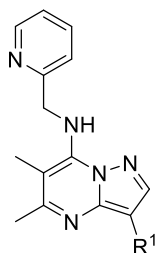
Table entry	Molecule Name	R ¹	R ³	EC ₅₀ (nM)	LogD 7.4	Aq.Sol (μM)	H.MicCL (μLmin ⁻¹ mg ⁻¹)	Rat Heps CL (μLmin ⁻¹ 10 ⁻⁶)	PPB (%)
1	AWF930	H	Me	105	2	561	261.8	109.6	ND
2	AWF931	Br	Me	176	ND	ND	ND	ND	ND
3	AWF948	Cl	Me	122	2.5	47.00	287.0	170	91.2
4	AWF951	F	Me	164	2.2	96.00	276.9	ND	ND
5	AWF932	CN	Me	NA	1.5	12.00	64.4	129.1	ND
6	AWF953	CONH ₂	Me	>2,500	1.7	9.00	18.9	63.33	65

NA – No activity at highest concentration ND – Not determined

Table 3.4 First series of analogues containing small substitutions at the R¹ position

The measured whole-cell potencies within **Table 3.4** demonstrate that a range of small groups are tolerated at the R¹ position in terms of maintaining reasonable anti-*Wolbachia* activity. Aqueous solubility is greatly enhanced upon removal of the aromatic ring system (entry **1** – **AWF930**); however, due to this modification there is an observed reduction in metabolic stability. Halogenation of the R¹ position (entries **2-4**) maintains acceptable anti-*Wolbachia* activity and aqueous solubility; however, this did not alleviate the poor metabolic stability. Introduction of a nitrile (entry **5** - **AWF932**) or an amide moiety (entry **6** - **AWF953**) at the R¹ position results in a complete loss in activity.

Further exploration of the R¹ position was conducted by our chemistry partners WuXi App Tech by the introduction of small halogenated alkyl groups. These compounds were prepared by installation of a boronic ester at the R¹ position (Appendix 1), which once treated with hydrogen peroxide and sodium hydroxide can be alkylated with the necessary alkyl halide as presented in Appendix 1.



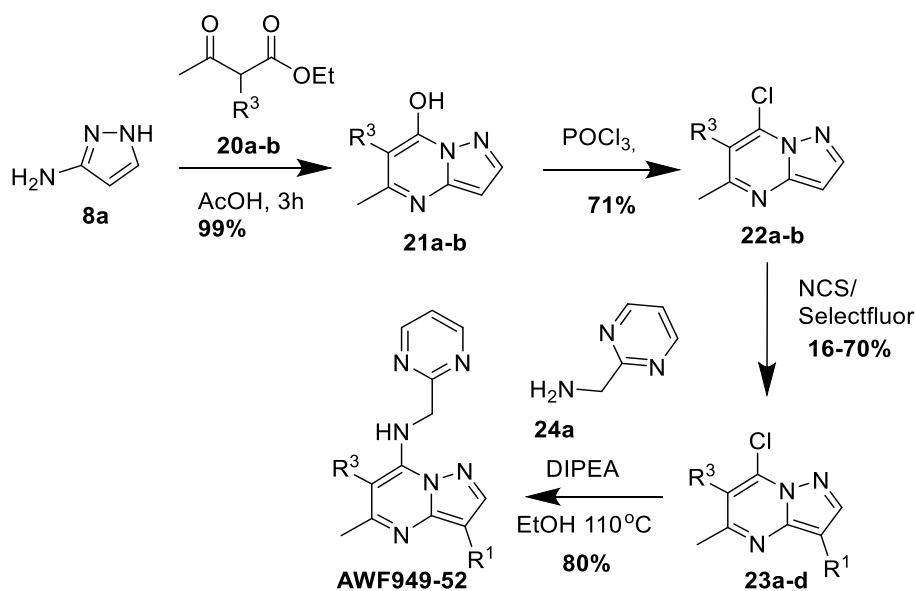
Molecule Name	R ¹	EC ₅₀ (nM)	LogD 7.4	Aq. Sol (μM)	H. Mic Cl (μL/min/mg)	R. Hep Cl (μL/min 10 ⁻⁶)	PPB (%)
AWZ9097	-OCHF ₂	251	2.6	62.00	84.3	84.3	89
AWZ9099	-OCH ₂ F	629	2.8	8.00	171.0	42.2	95

NA – No activity at highest concentration ND – Not determined

Table 3.5 Analogues containing halogenated groups chains at the R¹ position

These compounds containing small halogenated alkyl chains generally demonstrate acceptable potency however of the examples tested, none offered an improvement to the poor metabolic stability this series of analogues experienced (>80 H.Mics Cl μLmin⁻¹mg⁻¹).

Incorporation of an extra nitrogen atom into the 2-pyridyl ring system during the examination of the R⁵ position seemed tolerable in terms of anti-Wolbachia activity (**Table 2.4 – Chapter 2.3**). Therefore, several compounds with a 2,6-pyrimidine ring system at the R⁵ position were synthesised. Another modification which proved beneficial in earlier studies was the substitution of the methyl group at the R³ position for a chloride, this was also revisited in the following series of analogues. These analogues were reached by previously discussed chemistry which is summarised below in **Scheme 3.6** utilising the chlorinated β-keto ester **20a** upon formation of the pyrazolopyrimidine core and the biological activities are presented in **Table 3.6**.



Scheme 3.6 Synthesis of pyrazolopyrimidines containing varied R¹ positions. (R³ = Me/Cl)

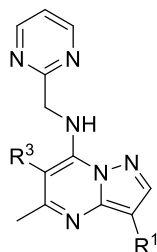


Table entry	Molecule Name	R ¹	R ³	EC ₅₀ (nM)	LogD 7.4	Aq. Sol (μM)	H. Mic Cl (μL/min/mg)	R. Hep Cl (μL/min 10 ⁻⁶)	PPB (%)
1	AWF949	Cl	Cl	311	2.5	10.00	160.5	147.6	92.3
2	AWF950	Cl	Me	>1,250	1.8	43.00	113.7	146.4	79
3	AWF952	F	Me	>1,250	1.4	107.0	129.0	146.8	73
4	AWF954	F	Cl	774	ND	ND	225.0	ND	

NA – No activity at highest concentration (5 μM) ND – Not determined

Table 3.6 Whole-cell assay *Wolbachia* activity for R³ pyrimidine compounds

This data supports previous observations that analogues containing small substitutions at the R¹ position demonstrate greatly improved solubility; however, they all suffer from poor metabolic stability. All but one analogue tested at this point containing the 2,6-pyrimidine ring displayed insufficient *in vitro* anti-*Wolbachia* activity. While **AWF937** (R¹ = 4-F Ph, R³ = Me) (**Table 2.4**) displayed acceptable potency (EC₅₀ = 33 nM), there was no increase in aqueous solubility and no sufficient increase in compound stability to justify this modification compared to the 2-pyridyl parent analogue **AWF918**. While the 2,6-pyrimidine ring-containing analogues with a chlorine at the R³ position seemed to produce some activity they still proved less potent than the parent 2-pyridyl analogues. In addition to the drop in anti-*Wolbachia* activity halogenated substituents were shown to result in undesired worm toxicity as explained earlier (**Ch. 2.4**). For this reason, it was essential to avoid such halogenated substituents at the R³ position in the design of future analogues to avoid introducing a liability for adverse effects associated with targeting the filarial nematodes directly.

3.6 Bioisosteric replacement of the R¹ phenyl ring

Following the unsuccessful incorporation of small groups at the R¹ position to improve both potency and DMPK properties we sought to identify alternative modifications. For several years, medicinal chemists have employed the strategy known as bioisosteric replacement to chemically alter compounds to modulate the biological and physicochemical properties. The rationale for this strategy is to replace a functionality with one that has some similarity in the size, shape, polarity, polarizability or lipophilicity and due to the similar chemical nature, the modified compound should possess similar biological activity to the original.²⁹

This approach was applied to our pyrazolopyrimidine compounds in our efforts to enhance aqueous solubility. One option was to replace the phenyl ring seen in the initial hit with a ring of similar size but less hydrophobic, more polar and less planar. All the suggested alterations should promote improved aq. solubility and there are several examples in the literature where saturated ring systems have been successfully installed for this purpose into drug compounds without abolishing potency.^{30,31} In the example shown below (**Fig. 3.13**) the authors Sébastien L. Degorce *et al.*,³² used a tetrahydropyran (THP) ring to replace a phenyl ring in **25a** and this served to drastically decrease the LogD which should significantly increase the aqueous solubility the resultant compound **26a** which also maintained its biological activity.

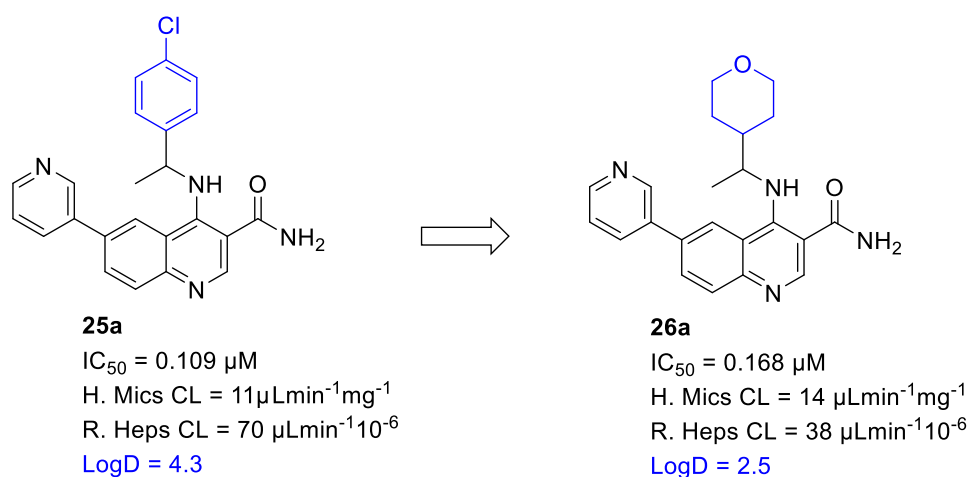


Fig 3.13 Replacement of a 4-Cl Ph ring with a THP to lower LogD

As already noted, various small groups are tolerated in terms of potency at the R¹ position, therefore reducing the size of the ring system incorporated at this position offered another viable approach to reduce the hydrophobicity caused by the aryl ring systems at this position. There are several examples within the literature where a lipophilic cyclopropyl ring has been used to replace a phenyl ring system without effecting potency.^{33,34} One of these examples is depicted in **Fig 3.14** where the authors carried out this replacement on **27a** alongside other key modifications during their optimisation of a series of selective allosteric inhibitors of mitogen/extracellular signal-regulated kinases for the development of Trametinib, approved for the treatment of metastatic melanoma.³³ Also displayed in **Fig 3.14** is the optimisation of a series of 2-amino-5-carboxamidothiazoles as novel Lymphocyte-specific protein tyrosine kinase inhibitors where the less lipophilic cyclopropyl moiety has been introduced into compound **28a** in place of a phenyl ring which also improved biological activity in the resultant analogue **29a**.³⁴ The reduction in CLogP from 2.91 in compound **28a** to 2.01 in **29a** supports that this modification may promote increased aqueous solubility.

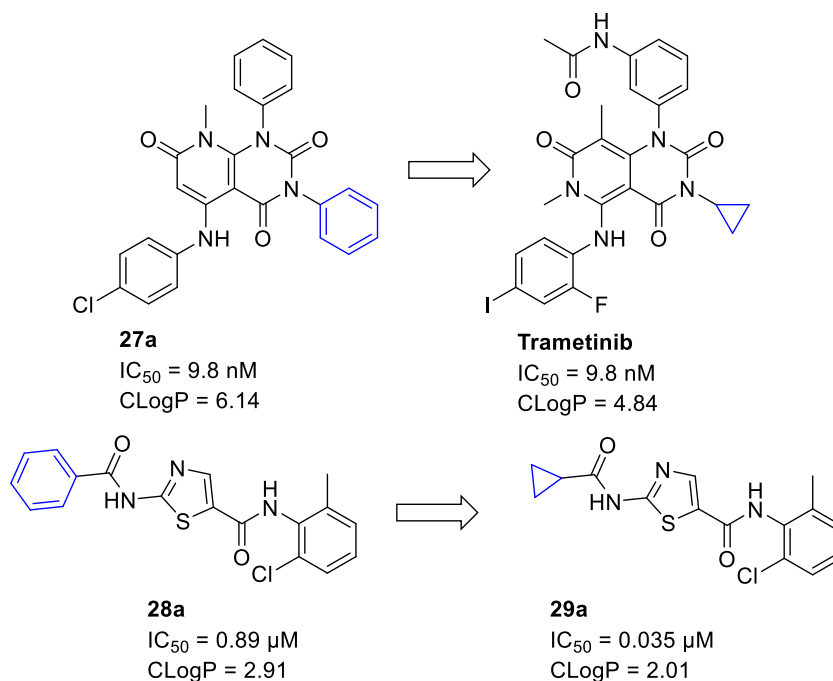


Fig 3.14 Optimisation of various compound series involving the replacement of phenyl ring with a cyclopropyl moiety.

Using the AZ DMPK predictive software, compounds containing a tetrahydropyran and cyclopropyl ring had their DMPK predictions calculated and are displayed below in **Fig 3.15**

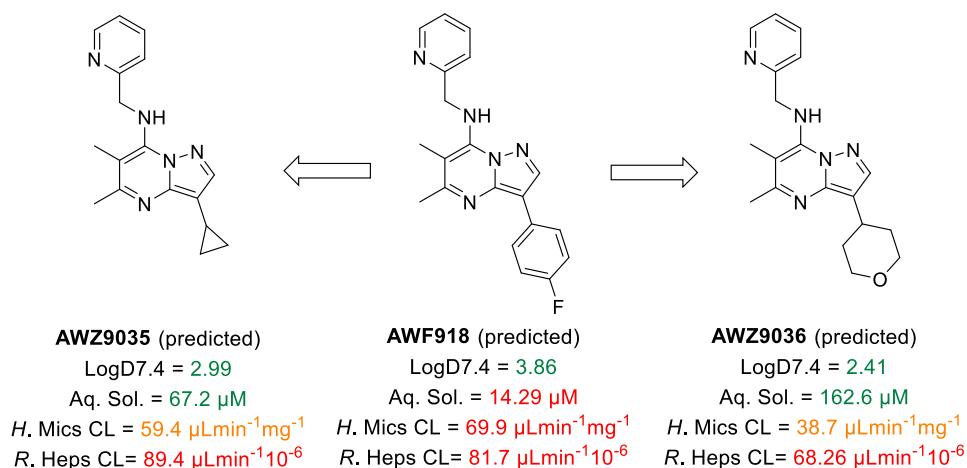
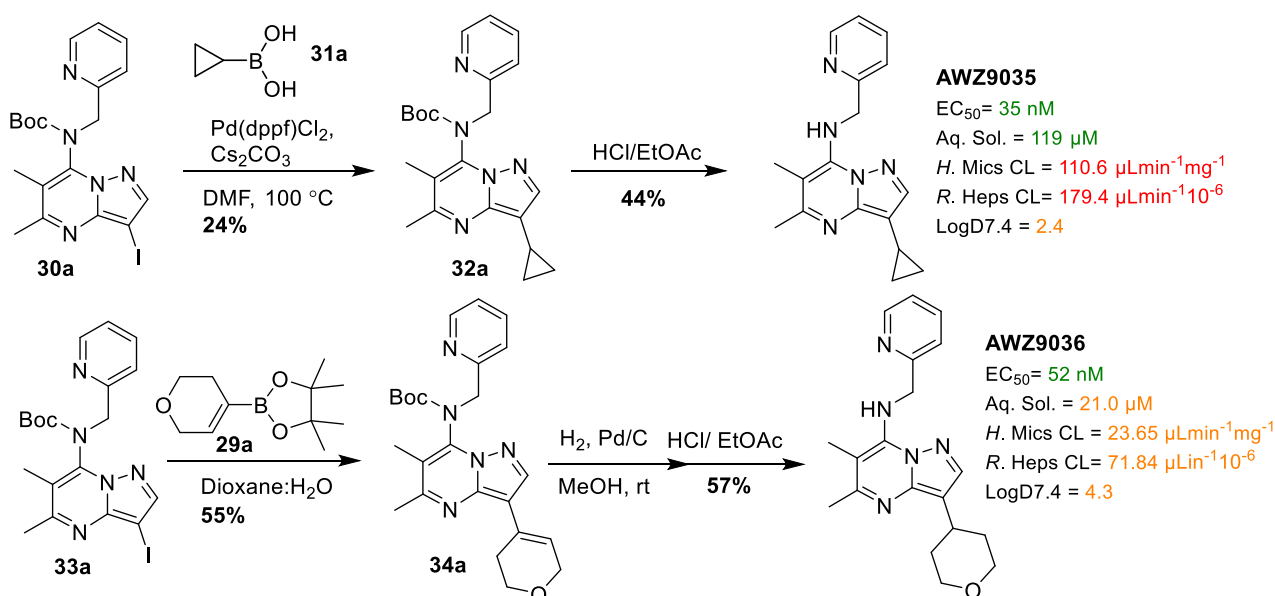


Fig 3.15 Predicted DMPK properties for analogues **AWZ9035** and **AWZ9036** containing the cyclopropyl and THP analogues respectively.

DMPK predictions for **AWZ9035** and **AWZ9036** containing the cyclopropyl and THP rings respectively demonstrate greatly improved aqueous solubility over the 4-F phenyl analogue **AWF918**. The prediction results also suggested that the THP analogue may possess improved metabolic stability compared to the 4-F Ph

analogue **AWF918**. Therefore, these analogues could positively address the poor metabolic stability seen upon removal of the phenyl ring.

These analogues were both synthesised by collaborators WuXi App Tech from chemistry previously discussed in this chapter (**Scheme 3.7**), optimised for coupling of various functionalities at the R¹ position (See appendix 1 for experimental details). The THP analogue **AWZ9036** required an extra step prior to Boc removal to hydrogenate the dihydropyran in **34a** added during the coupling reaction on **33a**. These reactions are depicted below in **Scheme 3.7**, with measured *in vitro* potency and DMPK properties displayed.



Scheme 3.7 Synthesis and biological evaluation of **AWZ9035** & **AWZ9036**

Both compounds demonstrate greatly improved aqueous solubility associated with removal of the aromatic ring system whilst maintaining potent anti-*Wolbachia* activity. **AWZ9035** suffered from poor stability like other compounds containing small substituents at this position. **AWZ9036** however, possessed the best balance of *in vitro* potency and DMPK properties seen so far in this chemotype.

3.7 Conclusion

Throughout the work conducted on this series, two of the analogues discussed in this section (**AWZ9014** and **AWZ9036**) were considered as frontrunners and were examined in further biological studies to assess their *in vitro* potency and *in vivo* efficacy against *Wolbachia* (see **Chapter 4** - biological evaluation section). The optimisation of pyrazolopyrimidine compounds described in this Chapter is briefly summarised in **Fig 3.16**.

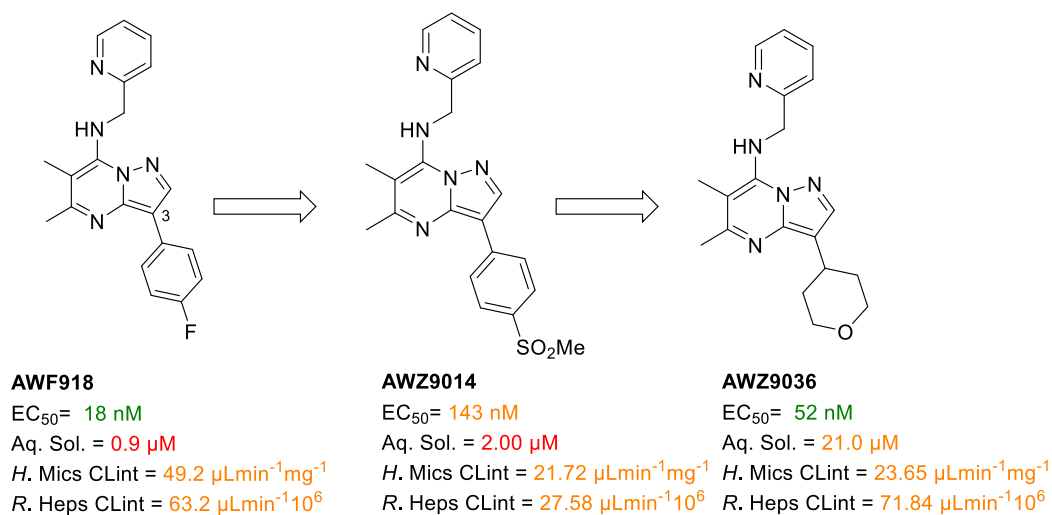


Fig 3.16 Summary of early lead optimisation discussed in this chapter.

In this Chapter, the 3 (R¹)-position has been thoroughly examined and it has been shown that a variety of substituents are tolerated in terms of anti-*Wolbachia* activity at the 4-position and whilst 4-F Ph is optimal in terms of activity, 4-SO₂Me Ph possessed the best balance of potency and DMPK properties at the time of study. Removal of the hydrophobic phenyl ring maintained most of the compound potency and resulted in compounds with greatly enhanced aqueous solubility; however, suffered from very poor metabolic stability. Study of a variety of small substituents at the R¹ position proved unsuccessful in terms of elucidating groups tolerated in terms of both potency and DMPK properties. Bioisosteric replacement of the phenyl ring seen in the initial hit with a THP group provided a compound with promising anti-*Wolbachia* potency and DMPK properties. A summary of the SAR from this body of work is displayed in **Fig 3.17**. Following lessons learnt from the introduction of heterocyclic ring systems at the R¹ position, the following series of optimisation will focus on investigation of other saturated ring systems at the R¹ position.

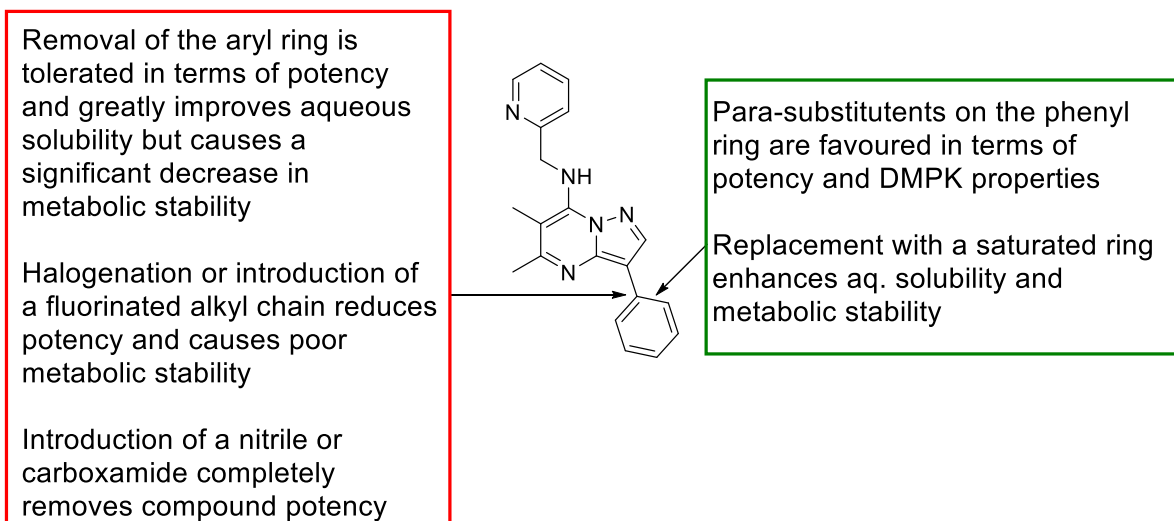


Fig 3.17 SAR summary from study of the R¹ position of the pyrazolopyrimidine core.

Finally, reviewing the analogues in this section reveals that further optimisation is still necessary to enhance specifically the aqueous solubility and metabolic stability of the next series of pyrazolopyrimidines, by doing so this will provide the greatest opportunity for our compounds to result in desirable *in vivo* efficacy. The promising potency and DMPK properties demonstrated by **AWZ9036** prompted further investigation into THP analogues and other saturated ring systems substituted at the R¹ position which will be discussed in the following chapter.

Chart 3.1 displays the logD of analogues presented within this chapter plotted against their Mw values. The Chart shows that all of our analogues within this chapter fall within promising drug space as defined by the Lipinski rule of 5 and the GlaxoSmith 4/400 rule as mentioned earlier in Chapter 1.7.2.^{35,36}

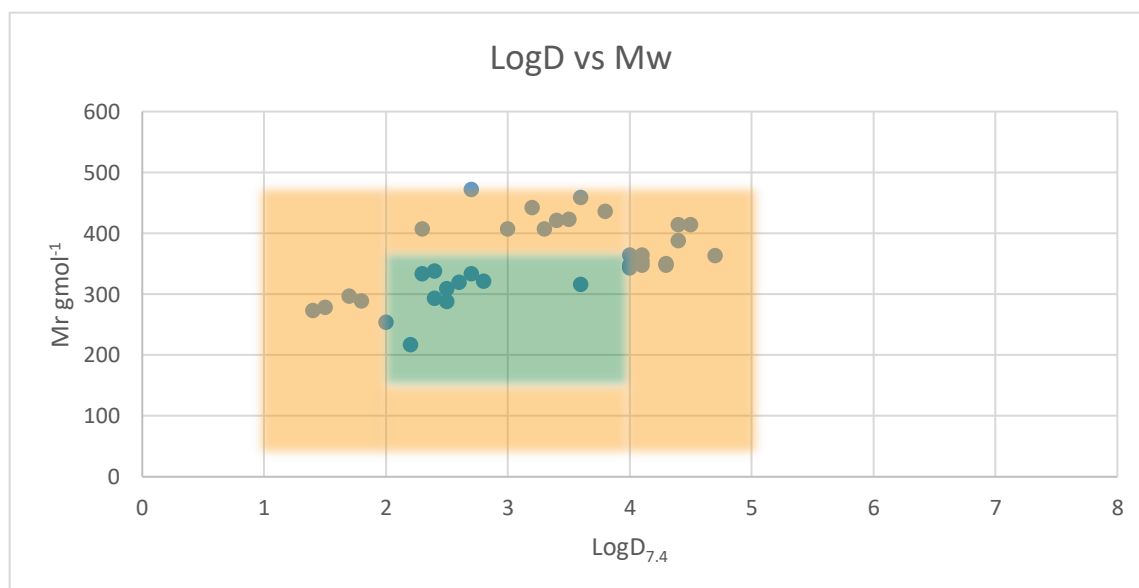


Chart 3.1 LogD values plotted against Mw (gmol⁻¹) for analogues presented within this chapter

The logD of analogues within this section also seems to be closely correlated to the aq. Solubility ($R^2 = > 0.8$, **Chart 3.2**) as seen within analogues from **Chapter 2**. Unfortunately, there does not appear to be any strong correlation between solubility/logD and any other property.

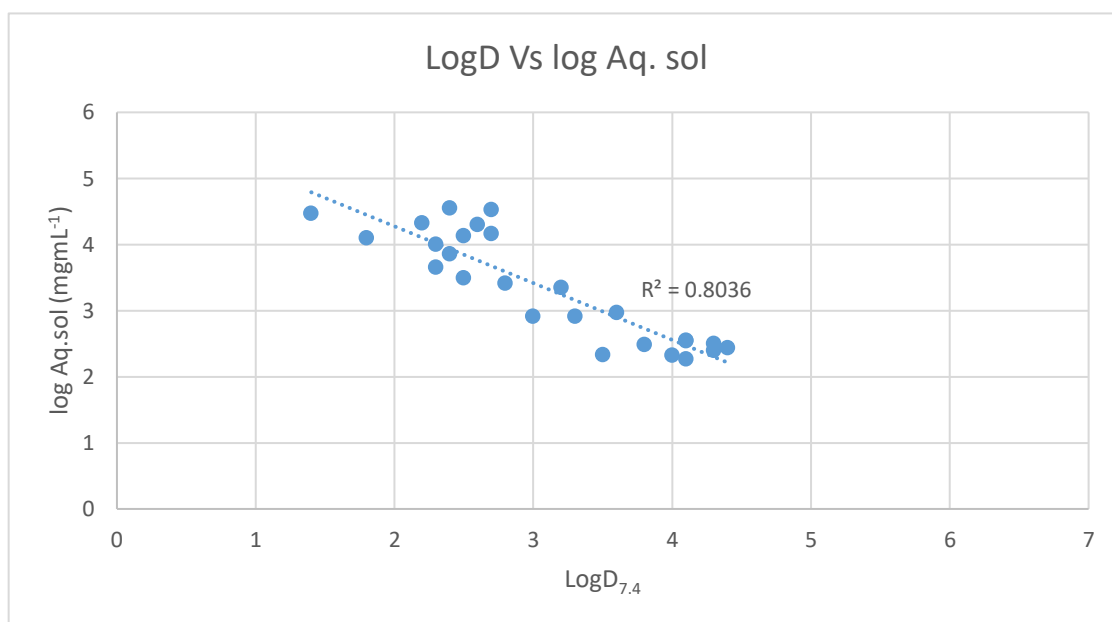


Chart 3.2 LogD values plotted against log Aq.Sol (mgmL⁻¹) for compounds within this chapter.

3.8 Experimental

Biological Evaluation (See Chapter 4 experimental for screening materials and methods)

General

Air- and moisture-sensitive reactions were performed in oven dried glassware sealed with rubber septa under an atmosphere of nitrogen from a manifold or balloon. Anhydrous solutions and sensitive liquids were transferred *via* syringe or stainless-steel cannula. Reactions were stirred using Teflon-coated magnetic stir bars. Organic solutions were concentrated using a Buchi rotary evaporator with a diaphragm vacuum pump.

Purification of solvents and reagents

Anhydrous solvents were either purchased from Sigma Aldrich or dried and distilled immediately prior to use under a constant flow of dry nitrogen. Tetrahydrofuran was distilled from Na, dichloromethane and Et₃N were distilled from CaH₂. All reagents were purchased from Sigma Aldrich, Alfa Aesar, Frontier Scientific, Apollo Scientific, Fluorochem and were used without any purification unless otherwise indicated.

Purification of products

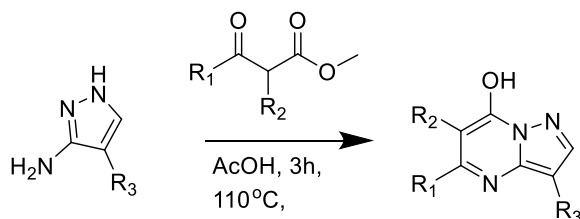
Thin layer chromatography (TLC) was performed on 0.25 mm Merck silica gel 60 F254 plates and visualised by ultraviolet light. U.V. inactive compounds were visualised using iodine, *p*-anisaldehyde solution, ninhydrin or potassium permanganate followed by gentle heating. Flash column chromatography was performed on ICN ecochrom 60 (32-63 mesh) silica gel eluting with various solvent mixtures and using an airline to apply pressure.

Analysis

Melting points were determined by a Gallenkamp apparatus and are uncorrected. ¹H NMR spectra were recorded on Bruker AMX 400 (400 MHz) spectrometer and reported as chemical shift on parts per million (ppm, δ) relative to tetramethylsilane as the internal reference, integration, multiplicity (s = singlet, br s = broad singlet, d = doublet, t = triplet, q = quartet, sex = sextet, m = multiplet), coupling constant (*J*, Hz), assignment. ¹³C NMR spectra were recorded on Bruker AMX400 (101 MHz) spectrometer and reported in terms of chemical shift (ppm, δ) relative to residual solvent peak. Mass spectra (MS) and high resolution mass spectra (HRMS) were recorded on a VG analytical 7070E machine, Fisons TRIO spectrometers using electron ionisation (EI) and chemical ionisation (CI), and Micromass LCT mass spectrometer using electron spray ionisation (ESI). All mass values are within error limits of ± 5 ppm. Elemental analyses (%C, %H, %N) were either determined by the

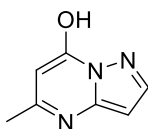
University of Liverpool Microanalysis Laboratory or the London Metropolitan University Elemental Analysis Service. Reported percentages are within error limits of $\pm 0.5\%$.

General procedure 2.1 for the synthesis of 5-Methyl pyrazolo[1,5-a]pyrimidin-7-ol³⁷



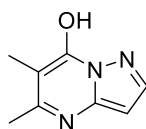
To the 3-Amino, 1,2-pyrazole (5.16 mmol) in AcOH (8 ml) was added the appropriate β -keto ester (20.64 mmol) and the reaction was allowed to stir at 110°C for 3 hours. The reaction was cooled to room temperature and diluted with Et_2O to precipitate the desired product which was filtered and washed with further Et_2O .

5-Methylpyrazolo[1,5-a]pyrimidin-7-ol³⁸ (1a)



General procedure 2.1 to give **1a** as a white solid. (5.84 g, 82%); $^1\text{H NMR}$ (400 MHz, DMSO-d_6) δ 12.27 (s, 1H), 7.82 (s, 1H), 6.09 (s, 1H), 5.57 (s, 1H), 2.29 (s, 3H); $^{13}\text{C NMR}$ (101 MHz, DMSO-d_6) δ 156.8, 150.7, 143.2, 142.1, 95.3, 88.7, 19.0; **MS (CI+ CH_4):** m/z (rel. Intensity) [M+H] 150.1 (100)

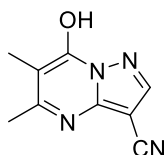
5,6-Dimethylpyrazolo[1,5-a]pyrimidin-7-ol³⁹ 10a



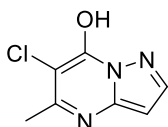
General procedure 2.1 was followed to give **10a** as an off-white solid (99%); $^1\text{H NMR}$ (400 MHz, DMSO-d_6) δ 12.11 (s, 1H), 7.80 (d, $J = 2.0$ Hz 1H), 6.04 (d, $J = 2.0$ Hz 1H), 2.30 (s, 3H), 1.96 (s, 3H); $^{13}\text{C NMR}$ (101 MHz, DMSO-d_6) δ 157.5, 146.3, 143.0, 141.2, 100.9, 87.7, 17.86, 10.8; **MS (CI+ CH_4):** m/z (rel. Intensity) [M+H] 164.1 (100) HRMS (CI+) calcd for $[(\text{C}_8\text{H}_{10}\text{N}_3\text{O})+\text{H}]$:164.0818; found: 164.0821

6-Chloro-5-methylpyrazolo[1,5-a]pyrimidin-7-ol⁴⁰ (21a)

To a solution of 1*H*-pyrazol-3-amine (2.5 g, 30.1 mmol, 1 eq) and methyl 2-chloro-3-oxo-butanoate (4.5 g, 30.1 mmol, 1 eq) in toluene (20 mL) was added TsOH.H₂O (572 mg, 3 mmol, 0.1 eq). The mixture was allowed to stir at 100 °C for 20 mins. A light-yellow solid was formed. TLC (EtOAc) showed that 1*H*-pyrazol-3-amine was consumed completely and a new spot has formed. The mixture was cooled to room temperature. The solid was filtered and was washed (Petroleum ether, 20 mL) to give **21a** (5 g, 27.2 mmol, 91% yield) as a grey solid. ¹H NMR (400MHz, DMSO-*d*₆) δ 7.91 (d, *J*=2.01 Hz, 1H), 6.18 (d, *J*=1.88 Hz, 1H), 2.45 (s, 3H); ¹³C NMR (101 MHz, DMSO-*d*₆) δ 153.4, 147.9, 144.0, 140.9, 101.5, 89.2, 18.8; MS (CI+ CH₄): *m/z* (rel. Intensity)[*M*+*H*] 150.1 (100), 184.0 (16); HRMS (CI+) calcd for [(C₇H₇ClN₃O)+H]:189.0771; found:189.0778

7-Hydroxy-5,6-dimethylpyrazolo[1,5-a]pyrimidine-3-carbonitrile (17a)

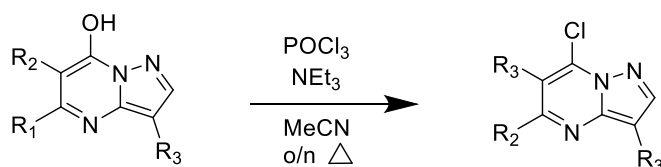
Synthesised *via* general procedure 2.1 to give **17a** as an off-white solid. (96%). ¹H NMR (400 MHz, DMSO-*d*₆) δ 13.08 (s, 1H), 8.34 (s, 1H), 2.35 (s, 3H), 1.98 (s, 3H); ¹³C NMR (101 MHz, DMSO-*d*₆) δ 156.5, 147.5, 145.2, 144.3, 113.4, 105.1, 73.9, 17.5, 10.8; MS (CI+ CH₄): *m/z* (rel. Intensity)[*M*+*H*] 189.1 (100); HRMS (CI+) calcd for [(C₉H₈N₄O)+H]:189.0771; found:189.0778

6-Chloro-5-methylpyrazolo[1,5-a]pyrimidin-7-ol⁴⁰ (21a)

To a solution of 1*H*-pyrazol-3-amine (2.5 g, 30.1 mmol, 1 eq) and methyl 2-chloro-3-oxo-butanoate (4.5 g, 30.1 mmol, 1 eq) in toluene (20 mL) was added TsOH.H₂O (572 mg, 3 mmol, 0.1 eq). The mixture was allowed to stir at 100 °C for 20 mins. A light-yellow solid was formed. TLC (EtOAc) showed that 1*H*-pyrazol-3-amine was consumed completely and a new spot. The mixture was cooled to room temperature. The solid was filtered

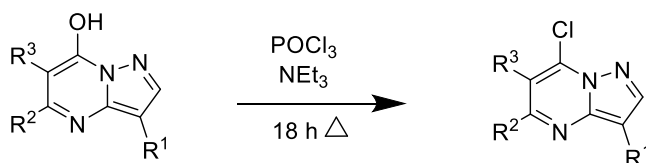
and was washed (Petroleum ether, 20 mL) to give **21a** (5 g, 27.2 mmol, 91% yield) as a grey solid. $^1\text{H NMR}$ (400MHz, DMSO- d_6) 7.91 (d, $J=2.01$ Hz, 1H), 6.18 (d, $J=1.88$ Hz, 1H), 2.45 (s, 3H).

General procedure 2.2 for the synthesis of 7-Chloro-5-Methyl-pyrazolo[1,5-a]pyrimidines²



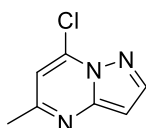
To the pyrazolo-pyrimidine compound (1 equiv) and NEt_3 (2 equiv) in MeCN was added POCl_3 (3 equiv) and the solution stirred under reflux overnight. The reaction was cooled to room temperature, volatiles removed under reduced pressure before pouring the resultant crude onto crushed ice. The mixture was basified with 2M NaOH and aqueous extracted with EtOAc, combined organic extracts washed with brine, dried with MgSO_4 and evaporated to dryness to give the product.

General procedure 3.1 - synthesis of 3-substituted 7-chloro-5-methyl-pyrazolo[1,5-a]pyrimidines¹

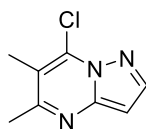


To the pyrazolo-pyrimidine compound (1 equiv) and NEt_3 was added POCl_3 (3 equiv) and the solution was allowed to stir under reflux overnight. Upon cooling to room temperature, the excess POCl_3 was quenched by diluting the reaction mixture with DCM and adding dropwise to ice-cold saturated sodium hydrogen carbonate with stirring and external cooling. The organic layer was separated and the aqueous re-extracted with DCM (3x) before washing the combined extracts with brine, drying with Na_2SO_4 , evaporating to dryness and then purifying the crude mixture by column chromatography.

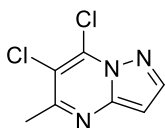
7-Chloro-5-methylpyrazolo[1,5-a]pyrimidine⁴¹ (**1b**)



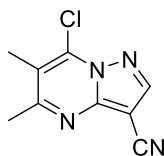
General procedure 3.1 to give **1b** as a light-yellow solid (3.55 g, 63%). $^1\text{H NMR}$ (400 MHz, MeOD) 8.10 (d, $J = 2.2$ Hz 1H), 6.97 (s, 1H), 6.54 (d, $J = 2.2$ Hz 1H), 2.49 (s, 3H); $^{13}\text{C NMR}$ (101 MHz, DMSO- d_6) δ 156.6, 155.5, 152.4, 150.7, 142.9, 142.2, 19.4; **MS (Cl+ CH₄)**: m/z (rel. Intensity) [M+H] 168.0(100)

7-Chloro-5,6-dimethylpyrazolo[1,5-a]pyrimidine³⁹ (11a)

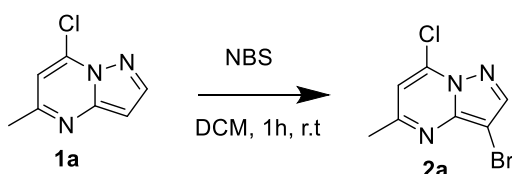
General procedure 3.1 to give **11a** as a light-yellow solid (71%). ¹H NMR(400 MHz, DMSO-d₆) δ 8.18 (d, *J* = 2.3 Hz 1H), 6.68 (d, *J* = 2.3 Hz 1H), 2.55 (s, 3H), 2.37 (s, 3H); ¹³C NMR (101 MHz, DMSO-d₆) δ 159.5, 147.6, 144.6, 135.6, 116.2, 97.0, 24.3, 14.8; **MS (Cl+ CH₄):** *m/z* (rel. Intensity) [M+H] 182.0488 (100), [M+H] 184.0488 (26) HRMS (Cl+) calcd for [(C₈H₉N₃35Cl)+H]:182.0480; found: 182.0488

6,7-Dichloro-5-methylpyrazolo[1,5-a]pyrimidine (22a)

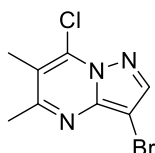
To **21a** (4.6 g, 25.95 mmol) in dimethylaniline (6.35 ml) was added to POCl₃ (6.87 ml, 75.16 mmol) in one portion at 25 °C under N₂. The mixture was heated to 110 °C and stirred for 1 hour. The reaction was quenched with ice-cold water and diluted with DCM, organic layers were washed with brine (100 mL*2), dried over Na₂SO₄ and concentrated to give **22a** (0.995 g, 19.74%). ¹H NMR (400MHz, CDCl₃-d) δ 8.18 (d, *J*=2.38 Hz, 1H), 6.73 (d, *J*=2.38 Hz, 1H), 2.75 (s, 3H).

7-Chloro-5,6-dimethylpyrazolo[1,5-a]pyrimidine-3-carbonitrile (18a)

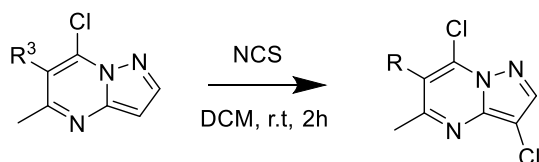
Synthesised *via* general procedure 2.2 to give **18a** as a yellow solid 70%. ¹H NMR(400 MHz, DMSO-d₆) δ 8.76 (s, 1H), 2.66 (s, 3H), 2.42 (s, 3H); ¹³C NMR (101 MHz, DMSO-d₆) δ 164.7, 149.1, 147.4, 137.7, 119.9, 113.6, 81.7, 24.6, 15.0; **MS (Cl+ CH₄):** *m/z* (rel. Intensity)[M+H] 207.0 (100), 209.0 (32); HRMS (Cl+) calcd for [(C₉H₈N₄Cl)+H]:168.0323; found: 168.0328

3-Bromo-7-chloro-5-methylpyrazolo[1,5-a]pyrimidine^{2,26} (2a)

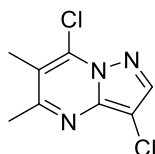
To **1a** (781 mg, 4.67 mmol) in DCM (10 ml) was added NBS (997 mg, 5.61 mmol) and the reaction was allowed to stir at room temperature for 1 hour. The reaction was evaporated to dryness and the crude product was purified by column chromatography eluting with 40% EtOAc:Hexane to give **2a**. (0.76 g, 66%). ¹H NMR (400 MHz, DMSO-*d*₆) δ 8.43 (s, 1H), 7.46 (s, 1H), 2.57 (s, 3H); ¹³C NMR (101 MHz, DMSO-*d*₆) δ 160.6, 146.0, 145.2, 138.0, 110.9, 83.5, 24.6.; MS (ES⁺): m/z (rel. Intensity) 245.9 (76), 246.9 (15), 247.9 (100), 248.9 (9), 249.9 (23)

3-Bromo-7-chloro-5,6-dimethylpyrazolo[1,5-a]pyrimidine (2b)

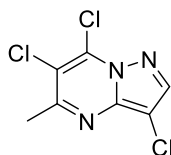
Synthesised using the procedure to give **2a**, used without any further purification (7.03 g, 89%); MS (CI+ CH₄): m/z (rel. Intensity)[M+H] 261.9 (100), 259.9 (80), 263.9 (15); HRMS (CI+) calcd for [(C₈H₈BrClN₃)+H]:259.9585; found: 259.9590

General procedure 3.2 for the synthesis of 3,7-Dichloro pyrazolo[1,5-a]pyrimidine intermediates²⁸

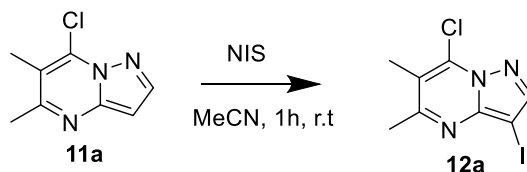
The chlorinated substrate (330 mg, 1.63 mmol) and NCS (261 mg, 1.956 mmol) were stirred in dry DCM (15 ml) at room temperature for two hours. Un-reacted NCS was quenched with water, the organic layer separated and the aqueous layer extracted with DCM (3 x 10 ml), the combined organic washed with brine (10 ml), dried with MgSO₄ and evaporated to dryness.

3,7-Dichloro-5,6-dimethylpyrazolo[1,5-a]pyrimidine (23a)

General procedure 3.2 The crude product was purified by column chromatography eluting with 20%EtOAc in Hexane to give the **23a** (0.433 g, 61%). $^1\text{H NMR}$ (400 MHz, DMSO-d_6) δ 8.34 (s, 1H), 2.59 (s, 3H), 2.38 (s, 3H); $^{13}\text{C NMR}$ (101 MHz, DMSO-d_6) δ 161.0, 143.0, 142.3, 136.2, 117.5, 98.5, 24.4, 14.8; **MS (CI+ CH_4)**: m/z (rel. Intensity) 216.0(100), 218.0 (60) HRMS (CI+) calcd for ($\text{C}_8\text{H}_7\text{Cl}_2\text{N}_3$):216.0090; found: 216.0098

3,6,7-Trichloro-5-methylpyrazolo[1,5-a]pyrimidine (23b)

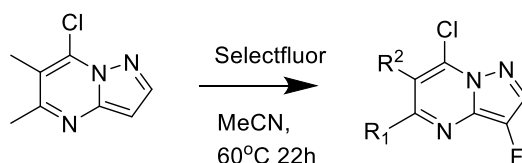
General procedure 3.2 The crude product was purified by column chromatography eluting with 20%EtOAc:Hexane to give **23b** (0.23 g, 59%). $^1\text{H NMR}$ (400 MHz, DMSO-d_6) δ 8.50 (s, 1H), 2.70 (s, 3H); $^{13}\text{C NMR}$ (101 MHz, DMSO-d_6) δ 158.1, 143.7, 142.6, 137.0, 117.5, 99.7, 24.3; **MS (CI+ CH_4)**: m/z (rel. Intensity) 236.0(100), 238.0 (97) 240.0 (27.42) HRMS (CI+) calcd for ($\text{C}_7\text{H}_4\text{Cl}_3\text{N}_3$):235.9544; found: 235.9548

Synthesis of 7-Chloro-3-iodo-5,6-dimethylpyrazolo[1,5-a]pyrimidine

Intermediate **38** (463 mg, 2.55 mmol) and NIS (573 mg, 2.55 mmol) in dry MeCN (25 ml) were stirred at room temperature for one hour. Volatiles were removed under vacuum upon completion of the reaction shown by TLC, the residue was diluted with DCM (20 ml) washed with water (10 ml) and brine (10 ml). The organic portion was dried with MgSO_4 and evaporated to dryness, the crude product was purified by column chromatography eluting with DCM. (0.54 g, 71%). $^1\text{H NMR}$ (400 MHz, DMSO-d_6) δ 8.28 (s, 1H), 2.59 (s, 3H), 2.38 (s, 3H);

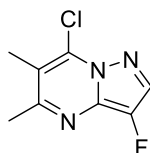
^{13}C NMR (101 MHz, DMSO- d_6) δ 148.8, 136.0, 117.2, 75.8, 62.2, 51.2, 24.0, 14.9; MS (ES+): m/z (rel. Intensity) 307.9(100), 309.9 (23) HRMS (CI+) calcd for ($\text{C}_8\text{H}_8\text{ClIN}_5$):307.9446; found: 307.9450

General procedure for the synthesis of 3-Fluoro, 7-chloro pyrazolo[1,5-a]pyrimidine intermediates ²⁷



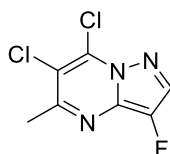
To the chlorinated substrate (450 mg, 2.23 mmol) in dry acetonitrile (20 ml) at 0°C was added selectfluor (789 mg, 2.23 mmol). The reaction was allowed to return to room temperature before warming to 60°C and stirring overnight. Volatiles were removed under reduced pressure, extracted with DCM (3 x 15ml), combined organics washed with brine (10 ml), dried with MgSO_4 and evaporated to dryness.

7-Chloro-3-fluoro-5,6-dimethylpyrazolo[1,5-a]pyrimidine (23c)



Crude product was purified by column chromatography eluting with 10%EtOAc in Hexane to afford the desired fluorinated product **23c**. (0.12 g, 13%). ^1H NMR(400 MHz, MeOD) δ 7.99 (d, J = 3.2 Hz, 1H), 2.51 (s, 3H), 2.33 (s, 3H); ^{13}C NMR (101 MHz, MeOD) δ 159.4, 141.6, 137.7 (d, J = 245.7 Hz), 134.2 (d, J = 23.7 Hz). 130.0 (d, J = 11.7 Hz), 116.7, 22.7, 13.3; MS (CI+ CH_4): m/z (rel. Intensity) 200.0(100), 202.0 (29) HRMS (CI+) calcd for ($\text{C}_8\text{H}_8\text{ClFN}_3$):200.0385; found: 200.0390

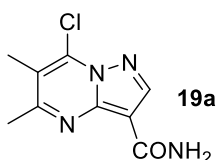
6,7-Dichloro-3-fluoro-5-methylpyrazolo[1,5-a]pyrimidine (23d)



Crude product was purified by column chromatography eluting with 10%EtOAc in Hexane to afford the desired fluorinated product **23d** (70 mg, 16%). ^1H NMR(400 MHz, MeOD) δ 8.09 (d, J = 2.8 Hz, 1H), 2.61 (s, 3H); ^{13}C

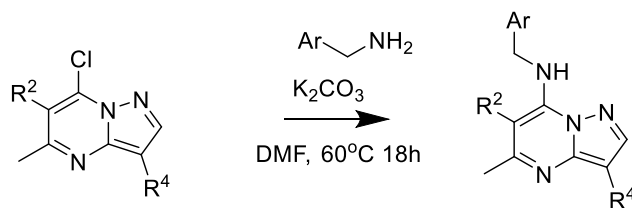
NMR (101 MHz, MeOD) δ 158.0, 156.6, 143.4 (d, $J = 203.2$ Hz), 143.0, 131.6 (d, $J = 11.9$ Hz), 117.2 (d, $J = 36.9$ Hz), 22.7; **MS (CI+ CH₄):** m/z (rel. Intensity) 220.0(98), 222.0 (62) HRMS (CI+) calcd for (C₇H₅Cl₂FN₃):219.9839; found: 219.9843

7-Chloro-5,6-dimethylpyrazolo[1,5-a]pyrimidine-3-carboxamide (**19a**)

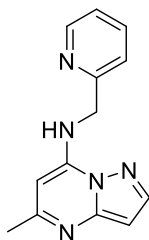


To **18a** (150 mg, 0.73 mmol) was added concentrated H₂SO₄ (7 ml) dropwise while cooling in ice. The reaction was allowed to stir for 5 hours before adding to ice-cold water dropwise and basifying to pH 7 with 30% aqueous NH₃. The solid **19a** formed was collected and dried under vacuum. (156 mg, 95%). **¹H NMR(400 MHz, DMSO-d₆) δ** 8.51 (s, 1H), 7.52 (br s, 2H), 2.68 (s, 3H), 2.43 (s, 3H); **MS (CI+ CH₄):** m/z (rel. Intensity)[M+H] 225.1 (100), 227.1 (30); **HRMS (CI+)** calcd for [(C₉H₁₀N₄ClO)+H]:225.0538; found: 225.0546; **MS (CI+ CH₄):** m/z (rel. Intensity) [M+H] 127.0 (100), [M+H] 125.1 (12)

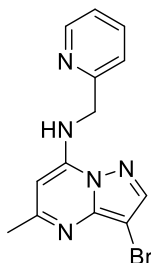
General procedure 2.5 (from Chapter 2) for the synthesis of 5,6-Dimethylpyrazolo[1,5-a]pyrimidin-7-amines³⁷



To the chlorinated pyrazolo-pyrimidine (1 equiv) in DMF was added the aryl-amine (1 equiv) and K₂CO₃ (1.2 equiv). The solutions were stirred at 60°C overnight, once completed the reactions were evaporated to dryness, diluted with EtOAc before washing with water and brine. Organics were dried using MgSO₄ before loading the crude product to silica gel and purifying by column chromatography eluting with 60% EtOAc in Hexanes.

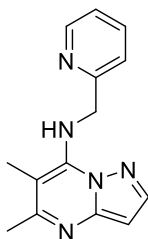
5-Methyl-N-(pyridin-2-ylmethyl)pyrazolo[1,5-a]pyrimidin-7-amine (AWF929)

General procedure 2.5 to give **AWF929** as an off-white solid 81%. $^1\text{H NMR}$ (400 MHz, DMSO-d_6) δ 8.57 (d, J = 4.0 Hz, 1H), 8.39 (t, J = 6.2 Hz, 1H), 8.06 (d, J = 2.2 Hz, 1H), 7.78 (td, J = 7.7, 1.8 Hz, 1H), 7.37 (d, J = 7.9 Hz, 1H), 7.31 (dd, J = 7.4, 4.9 Hz, 1H), 6.31 (d, J = 2.2 Hz, 1H), 5.99 (s, 1H), 4.70 (d, J = 6.2 Hz, 2H), 2.32 (s, 3H); $^{13}\text{C NMR}$ (101 MHz, DMSO-d_6) δ 159.1, 157.4, 149.5, 149.1, 146.8, 143.9, 137.5, 123.0, 121.6, 94.1, 85.8, 46.7, 25.1; **MS (ES+)**: m/z (rel. Intensity) [M+H] 240.1 (100), [M+H] 241.1 (15) HRMS (ES+) calcd for $[(\text{C}_{13}\text{H}_{14}\text{N}_5)+\text{H}]$:240.1249; found: 240.1249; **CHN analysis**: Calculated: C:65.25%, H:5.48%, N:29.27%. Found C:65.14%, H:5.45%, N:29.48%

3-Bromo-5-methyl-N-(pyridin-2-ylmethyl)pyrazolo[1,5-a]pyrimidin-7-amine² (4a)

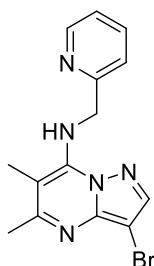
General procedure 2.5 to give **4a** as an off-white solid. (87%). $^1\text{H NMR}$ (400 MHz, DMSO-d_6) δ 8.64 – 8.50 (m, 2H), 8.22 (s, 1H), 7.79 (t, J = 7.0 Hz, 1H), 7.37 (d, J = 7.3 Hz, 1H), 7.32 (brs, 1H), 6.11 (s, 1H), 4.72 (s, 2H), 2.37 (s, 3H); $^{13}\text{C NMR}$ (101 MHz, DMSO-d_6) δ 160.6, 157.2, 149.5, 147.1, 145.7, 143.6, 137.6, 123.1, 121.6, 86.8, 80.4, 46.7, 25.1; **MS (ES+)**: m/z (rel. Intensity) [M+H] 318.0 (100), [M+H] 320.0 (99) HRMS (ES+) calcd for $[(\text{C}_{13}\text{H}_{13}\text{N}_5\text{Br})+\text{H}]$:318.0354; found: 318.0349, calcd for $(\text{C}_{13}\text{H}_{13}\text{N}_5\text{Br})$:320.0334; found: 320.0332,

5,6-Dimethyl-N-(pyridin-2-ylmethyl)pyrazolo[1,5-a]pyrimidin-7-amine (AWF930)

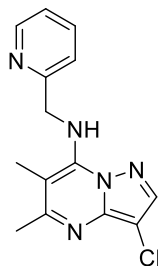


General procedure 2.5 to give **AWF930** as an off-white solid 68%. $^1\text{H NMR}$ (400 MHz, DMSO-d_6) δ 8.56 (d, J = 4.7 Hz, 1H), 7.97 (d, J = 2.2 Hz, 1H), 7.81 – 7.74 (m, 2H), 7.37 (d, J = 7.9 Hz, 1H), 7.29 (dd, J = 7.1, 5.2 Hz, 1H), 6.27 (d, J = 2.2 Hz, 1H), 5.16 (d, J = 6.1 Hz, 2H), 2.41 (s, 3H), 2.27 (s, 3H); $^{13}\text{C NMR}$ (101 MHz, DMSO-d_6) δ 159.1, 158.5, 149.3, 147.8, 145.7, 143.1, 137.4, 122.8, 121.7, 96.0, 93.6, 49.3, 24.4, 13.0; **MS (ES+)**: m/z (rel. Intensity) [M+H] 254.1 (100), [M+H] 255.1 (15) HRMS (ES+) calcd for $[(\text{C}_{14}\text{H}_{16}\text{N}_5)+\text{H}]$:254.1406; found: 254.1401; **CHN analysis**: Calculated: C:66.38%, H:5.97%, N:27.65%. Found C:66.14%, H:5.91%, N:27.81%;

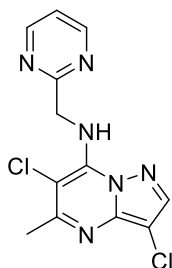
3-Bromo-5,6-dimethyl-N-(pyridin-2-ylmethyl)pyrazolo[1,5-a]pyrimidin-7-amine (AWF931)



General procedure 2.5 to give **AWF931** (0.69 g, 87%). **Melting point**: 116-118 °C $^1\text{H NMR}$ (400 MHz, DMSO-d_6) δ 8.54 (d, J = 4.7 Hz, 1H), 8.11 (s, 1H), 7.90 (t, J = 6.1 Hz, 1H), 7.78 (td, J = 7.7, 1.7 Hz, 1H), 7.36 (d, J = 7.9 Hz, 1H), 7.29 (dd, J = 6.9, 5.3 Hz, 1H), 5.18 (d, J = 6.1 Hz, 2H), 2.44 (s, 3H), 2.28 (s, 3H); $^{13}\text{C NMR}$ (101 MHz, DMSO-d_6) δ 179.8, 160.4, 158.2, 149.2, 146.0, 144.4, 142.7, 137.4, 122.8, 121.6, 97.0, 79.7, 24.4, 13.0.; **MS (ES+)**: m/z (rel. Intensity) [M+H] 332.1 (100), [M+H] 334.0 (95) HRMS (ES+) calcd for $[(\text{C}_{14}\text{H}_{15}\text{N}_5\text{79Br})+\text{H}]$:332.0511; found: 332.0503. calcd for $[(\text{C}_{14}\text{H}_{15}\text{N}_5\text{81Br})+\text{H}]$:334.0490; found: 334.0486; **CHN analysis**: Calculated: C:50.62%, H:4.25%, N:21.08%. Found C:50.63%, H:4.23%, N:20.98%;

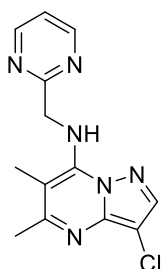
3-Chloro-5,6-dimethyl-N-(pyridin-2-ylmethyl)pyrazolo[1,5-a]pyrimidin-7-amine (AWF948)

General procedure 2.5 The crude product was washed with water and the grey precipitate triturated with Et₂O to afford **AWF948**. **Melting point:** 156-158 °C (66 mg, 33%). **¹H NMR(400 MHz, DMSO-d₆)** δ 8.54 (d, *J* = 4.6 Hz, 1H), 8.12 (s, 1H), 7.91 (t, *J* = 5.9 Hz, 1H), 7.78 (apt, *J* = 7.7 Hz, 1H), 7.36 (d, *J* = 7.8 Hz, 1H), 7.29 (t, *J* = 6.1 Hz, 1H), 5.19 (d, *J* = 6.0 Hz, 2H), 2.44 (s, 3H), 2.28 (s, 3H); **¹³C NMR (101 MHz, DMSO-d₆)** δ 160.3, 158.3, 149.3, 146.0, 143.2, 140.8, 137.4, 122.8, 121.6, 97.0, 94.9, 49.2, 24.5, 13.0; **MS (ES+):** *m/z* (rel. Intensity) 288.1 (100), 290.1 (30) **HRMS (ES+)** calcd for (C₁₄H₁₅N₅35Cl):288.1016; found: 288.1012; **CHN analysis:** Calculated: C:58.44%, H:4.90%, N:24.34%. Found C:58.20%, H:4.87%, N:24.29%.

3,6-Dichloro-5-methyl-N-(pyrimidin-2-ylmethyl)pyrazolo[1,5-a]pyrimidin-7-amine (AWF949)

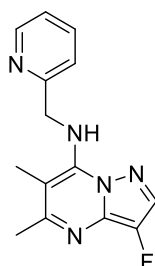
General procedure 2.5 The crude product was purified by column chromatography eluting with 60% EtOAc,NEt₃ to afford **AWF949**. **Melting point:** 175-180 °C (60 mg, 27%). **¹H NMR(400 MHz, DMSO-d₆)** δ 8.76 (d, *J* = 4.8 Hz, 2H), 8.32 (t, *J* = 6.1 Hz, 1H), 8.15 (s, 1H), 7.40 (t, *J* = 4.8 Hz, 1H), 5.44 (d, *J* = 6.2 Hz, 1H), 2.51 (s, 3H); **¹³C NMR (101 MHz, DMSO-d₆)** δ 166.7, 158.0 (2C), 157.6, 144.8, 143.1, 142.1, 120.3, 97.0, 96.0, 49.7, 24.1; **MS (ES+):** *m/z* (rel. Intensity) 309.0 (100), 311.0 (62) **HRMS (ES+)** calcd for (C₁₂H₁₁N₆F35Cl₂):309.0422; found: 309.0423; **CHN analysis:** Calculated: C:46.62%, H:3.26%, N:27.18%. Found C:45.42%, H:3.18%, N:26.33%.

Synthesis of 3-Chloro-5,6-dimethyl-N-(pyrimidin-2-ylmethyl)pyrazolo[1,5-a]pyrimidin-7-amine (AWF950)

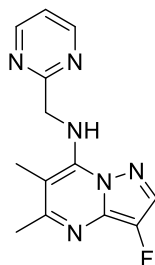


General procedure 2.5 The crude product was purified by column chromatography eluting with 60% EtOAc,NEt₃ to afford **AWF950** as an off-white product. (0.16 g, 81%). **Melting point:** 205-207 °C **¹H NMR(400 MHz, DMSO-d₆)** δ 8.78 (d, *J* = 4.8 Hz, 2H), 8.06 (s, 1H), 7.77 (t, *J* = 5.9 Hz, 1H), 7.41 (t, *J* = 4.8 Hz, 1H), 5.34 (d, *J* = 5.9 Hz, 2H), 2.46 (s, 3H), 2.28 (s, 3H); **¹³C NMR (101 MHz, DMSO-d₆)** δ 167.0, 160.0, 158.0 (2C), 146.3, 143.3, 140.8, 120.4, 97.1, 94.7, 50.1, 24.4, 12.9; **MS (ES+):** *m/z* (rel. Intensity) 289.1 (100), 291.1 (30) HRMS (ES+) calcd for (C₁₃H₁₄N₆35Cl):289.0968; found: 289.0975; **CHN analysis:** Calculated: C:54.08%, H:4.54%, N:29.11%. Found C:53.15%, H:4.42%, N:28.66%.

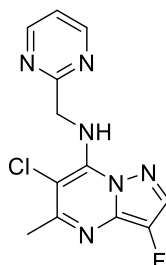
3-Fluoro-5,6-dimethyl-N-(pyridin-2-ylmethyl)pyrazolo[1,5-a]pyrimidin-7-amine (AWF951)



General procedure 2.5 The crude product was purified by column chromatography eluting with 60% EtOAc:Hexane **AWF951** as an off-white solid. (38 mg, 47%). **Melting point:** 142-144 °C **¹H NMR(400 MHz, DMSO-d₆)** δ 8.55 (d, *J* = 4.6 Hz, 1H), 8.11 (d, *J* = 3.5 Hz, 1H), 7.87 (t, *J* = 5.9 Hz, 1H), 7.78 (t, *J* = 7.7 Hz, 1H), 7.37 (d, *J* = 7.9 Hz, 1H), 7.29 (t, *J* = 6.9 Hz, 1H), 5.16 (d, *J* = 6.0 Hz, 2H), 2.43 (s, 3H), 2.27 (s, 3H); **¹³C NMR (101 MHz, DMSO-d₆)** δ 159.3, 158.3, 149.3, 145.1, 137.4, 136.3 (d, *J* = 238.2 Hz), 134.5 (d, *J* = 24.1 Hz), 129.2 (d, *J* = 10.9 Hz), 122.8, 121.7, 96.2, 49.1, 24.4, 13.0; **MS (ES+):** *m/z* (rel. Intensity) 271.1 (100), 273.1 (15) HRMS (ES+) calcd for (C₁₄H₁₅N₅F):272.1311; found: 272.1316; **CHN analysis:** Calculated: C:61.98%, H:5.20%, N:25.81%. Found C:60.98%, H:5.10%, N:25.42%.

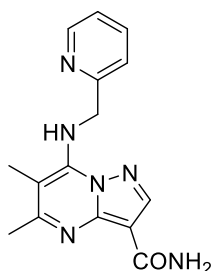
3-Fluoro-5,6-dimethyl-N-(pyrimidin-2-ylmethyl)pyrazolo[1,5-a]pyrimidin-7-amine (AWF952)

General procedure 2.5 The crude product was purified by column chromatography eluting with EtOAc to afford **AWF952** as an off-white solid. (35 mg, 43%). $^1\text{H NMR}$ (400 MHz, DMSO-d_6) δ 8.80 (d, $J = 4.7$ Hz, 2H), 8.06 (d, $J = 3.0$ Hz, 1H), 7.74 (t, $J = 5.2$ Hz, 1H), 7.42 (t, $J = 4.6$ Hz, 1H), 5.31 (d, $J = 5.7$ Hz, 2H), 2.44 (s, 3H), 2.28 (s, 3H); $^{13}\text{C NMR}$ (101 MHz, DMSO-d_6) δ 166.9, 159.1, 158.0, 145.4, 136.2 (d, $J = 238.1$ Hz), 134.6 (d, $J = 24.1$ Hz), 129.2 (d, $J = 10.9$ Hz), 120.1, 96.3, 50.0, 24.4, 12.9; **MS (ES+)**: m/z (rel. Intensity) 273.1 (100), $[\text{M}+\text{Na}]$ 295.1 (70) HRMS (ES+) calcd for ($\text{C}_{13}\text{H}_{14}\text{N}_6\text{F}$):273.1264; found: 273.1266; **CHN analysis**: Calculated: C:57.34%, H:4.81%, N:30.87%. Found C:56.80%, H:4.81%, N:30.10%.

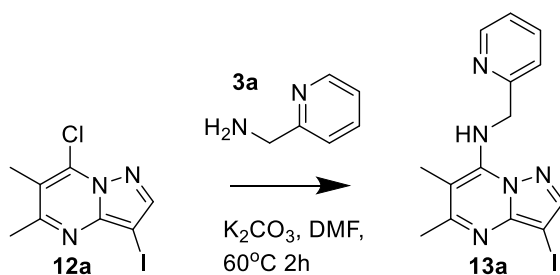
6-Chloro-3-fluoro-5-methyl-N-(pyrimidin-2-ylmethyl)pyrazolo[1,5-a]pyrimidin-7-amine (AWF954)

General procedure 2.5 The crude product was purified by column chromatography eluting with 80%EtOAc:Hex to afford **AWF954**. (31%). $^1\text{H NMR}$ (400 MHz, MeOD) δ 8.78 (d, $J = 4.2$ Hz, 2H), 7.91 (d, $J = 4.1$ Hz, 1H), 7.73 (s, 1H), 7.39 (t, $J = 4.8$ Hz, 1H), 5.53 (s, 2H), 2.57 (s, 3H); $^{13}\text{C NMR}$ (101 MHz, MeOD) δ 165.6 (s), 157.4 (s, 2C), 157.0 (s), 138.9 (d, $J = 202.7$ Hz), 133.7 (d, $J = 24.9$ Hz), 132.2 (s), 130.2 (d, $J = 11.7$ Hz), 119.9 (s), 96.3 (s), 22.4 (s), 8.1 (s); **MS (ES+)**: m/z (rel. Intensity) 293.1 (100), 295.1 (29) HRMS (ES+) calcd for ($\text{C}_{12}\text{H}_{11}\text{N}_6\text{F}_3\text{Cl}$):293.0718; found: 293.0715; **CHN analysis**: Calculated: C:49.24%, H:3.44%, N:28.71%. Found C:47.13%, H:4.25%, N:23.27%.

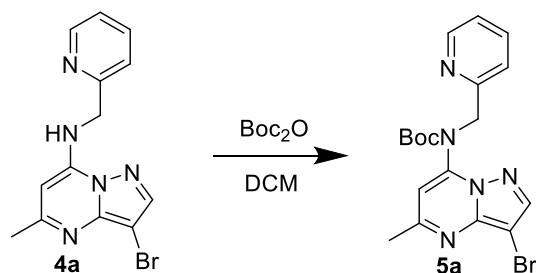
7-Chloro-5,6-dimethylpyrazolo[1,5-a]pyrimidine-3-carboxamide (AWF953)



General procedure 2.5 to give **AWF953**, (49 mg, 18%). $^1\text{H NMR}$ (400 MHz, DMSO-d_6) δ 8.54 (s, 1H), 8.29 (s, 1H), 8.07 (s, 1H), 7.84 – 7.67 (m, 2H), 7.37 (s, 1H), 7.30 (s, 1H), 7.24 (s, 1H), 5.27 (d, $J = 0.8$ Hz, 2H), 2.51 (s, 3H), 2.29 (s, 2H); $^{13}\text{C NMR}$ (101 MHz, DMSO-d_6) δ 163.9, 160.9, 158.2, 149.3, 146.8, 145.9, 144.5, 137.4, 122.8, 121.6, 102.6, 98.1, 49.2, 24.6, 13.0; **MS (ES+)**: m/z (rel. Intensity)[$\text{M}+\text{H}$] 319.1 (100), 320.1 (22); **HRMS (ES+)** calcd for $[(\text{C}_{15}\text{H}_{16}\text{N}_6\text{O}_2\text{Na})+\text{H}]$:319.1283; found: 319.1278; **CHN analysis**: Calculated: C:60.80%, H:5.44%, N:28.36%. Found C:58.03%, H:5.30%, N:27.82%.

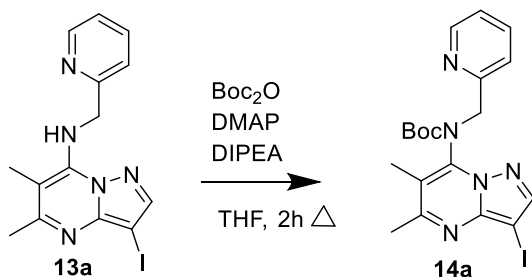
N-Benzyl-3-iodo-5,6-dimethylpyrazolo[1,5-a]pyrimidin-7-amine (13a)

To the intermediate **12a** (4.95 g, 16.1 mmol) and pyridine 2-methanamine (**3a**) (1.7 ml, 16.1 mmol) in DMF (125 ml) was added K_2CO_3 (2.67 g, 19.32 mmol) and the reaction mixture was allowed to stir at reflux under nitrogen for 2 hours. The orange mixture was allowed to cool to room temperature and the crude product precipitated out upon addition of ice-cold water with external cooling in ice. Crude solid filtered and triturated with ice cold methanol and filtered to afford the desired product **13a**. (5.92 g, 97%). $^1\text{H NMR}$ (400 MHz, DMSO-d_6) δ 8.53 (d, $J = 4.4$ Hz, 1H), 8.28 (s, 1H), 8.09 (t, $J = 6.0$, 1H), 7.76 (td, $J = 7.7, 1.5$ Hz, 1H), 7.37 (d, $J = 7.8$ Hz, 1H), 7.28 (dd, $J = 6.8, 5.3$ Hz, 1H), 5.27 (d, $J = 6.0$ 2H), 2.42 (s, 3H), 2.26 (s, 3H); $^{13}\text{C NMR}$ (101 MHz, DMSO-d_6) δ 160.4, 158.9, 149.3, 146.9, 146.9, 146.1, 137.4, 122.8, 121.6, 97.0, 49.2, 46.5, 24.5, 13.0; **MS (ES+)**: m/z (rel. Intensity) 380.0(100), 381.0 (23), 402.0, 403.0 **HRMS (CI+)** calcd for $(\text{C}_{14}\text{H}_{15}\text{N}_5\text{I})$:380.0372; found: 380.0369

Tert-butyl (3-bromo-5-methylpyrazolo[1,5-a]pyrimidin-7-yl)(pyridin-2-ylmethyl)carbamate² (**5a**)

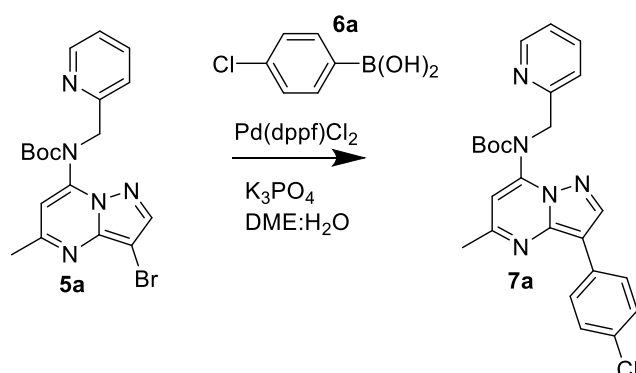
To the bromo pyrazolo-pyrimidine **4a** (1.24 g, 3.74 mmol) and DMAP (63.16 mg, 0.517 mmol) in DCM (40 ml) was added Boc_2O (1.355 g, 6.21 mmol). The reaction was allowed to stir at room temperature overnight; the DCM layer was washed with brine and dried with MgSO_4 before evaporating to dryness and purifying the crude product by column chromatography eluting with 60% EtoAc in Hexane to give the Boc-protected intermediate **5a**. (0.38 g, 85%). $^1\text{H NMR}$ (400 MHz, DMSO-d_6) δ 8.49 (br s, 1H), 8.36 (s, 1H), 7.78 (t, $J = 7.4$ Hz, 1H), 7.50 (d, $J = 7.6$ Hz, 1H), 7.28 (br s, 1H), 7.19 (s, 1H), 5.01 (s, 2H), 2.56 (s, 3H), 1.24 (s, 9H); $^{13}\text{C NMR}$ (101 MHz, DMSO-d_6) δ 157.1, 152.4, 149.6, 146.0, 144.5, 143.9, 140.5, 137.3, 123.1, 121.9, 117.2, 106.88, 8.2, 54.3, 27.9, 24.9; **MS (ES+Na)**: m/z (rel. Intensity) 440.1 (100), 442.1 (100) HRMS (ES+) calcd for $(\text{C}_{18}\text{H}_{20}\text{N}_5\text{O}_2\text{Na}79\text{Br})$:440.0698; found: 440.0707. calcd for $(\text{C}_{18}\text{H}_{20}\text{N}_5\text{O}_2\text{Na}81\text{Br})$:442.0678; found: 442.0683.

Tert-butyl (3-iodo-5,6-dimethylpyrazolo[1,5-a]pyrimidin-7-yl)(pyridin-2-ylmethyl)carbamate



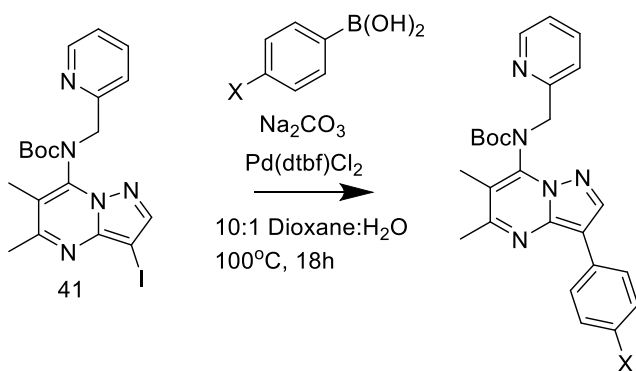
To intermediate **13a** (1.13 g, 2.97 mmol), DIPEA (1.24 ml, 5.95 mmol), and DMAP (0.182 g, 1.49 mmol) in dry THF (20 ml) was added Boc_2O (1.30 g, 5.95 mmol) and the reaction was allowed to stir at 70°C under nitrogen for 2 hours. Upon completion of the reaction volatiles were removed under pressure and purified by column chromatography eluting with 3:1 pet ether in EtoAc to isolate the desired product **14a**. (51%). $^1\text{H NMR}$ (400 MHz, DMSO-d_6) δ 8.43 (d, $J = 4.3$ Hz, 1H), 8.27 (s, 1H), 7.79 (t, $J = 7.6$ Hz, 1H), 7.48 (d, $J = 7.7$ Hz, 1H), 7.31 (dd, $J = 5.2, 1.9$ Hz, 1H), 5.60 (d, $J = 15.0$ Hz, 1H), 4.71 (d, $J = 15.0$ Hz, 1H), 2.58 (s, 3H), 2.05 (s, 3H), 1.29 (s, 9H); $^{13}\text{C NMR}$ (101 MHz, DMSO-d_6) δ 162.3, 156.2, 152.9, 149.6, 147.8, 146.9, 140.0, 137.2, 123.6, 123.2, 116.5, 82.0, 52.3, 28.0, 24.1, 13.3; **MS (ES+)**: m/z (rel. Intensity) 480.1(100) HRMS (ES+) calcd for $(\text{C}_{19}\text{H}_{23}\text{IN}_5\text{O}_2)$:480.0897; found: 480.0892

Tert-butyl(3-(4-chlorophenyl)-5-methylpyrazolo[1,5-a]pyrimidin-7-yl)(pyridin-2-ylmethyl)carbamate



To the Boc-protected **5a** (362 mg, 0.87 mmol) was added 4-chloro benzene boronic acid (**6a**) (180 mg, 10.4 mmol) and K_3PO_4 (554 mg, 2.61 mmol). A de-gassed 3:1 mixture of DME:H₂O (12 ml) was added and nitrogen bubbled through the mixture for 20 minutes before adding Pd(dppf).Cl₂ (64 mg, 0.087 mmol). The reaction was heated to reflux and was allowed to stir overnight, once completed the reaction mixture was allowed to cool to room temperature and evaporated to dryness before diluting with EtOAc. Organic layer was washed with brine, dried with MgSO₄ and evaporated to dryness to give the crude product which was purified by column eluting with 1% MeOH in DCM to give **7a**. (0.23 g, 59%). ¹H NMR (400 MHz, DMSO-d₆) δ 8.78 (s, 1H), 8.50 (s, 1H), 8.21 (d, *J* = 8.0 Hz, 2H), 7.79 (t, *J* = 6.4 Hz, 1H), 7.54 (m, 1H), 7.50 (d, *J* = 8.1 Hz, 2H), 7.29 (br s, 1H), 7.18 (s, 1H), 5.05 (s, 2H), 2.61 (s, 3H), 1.26 (s, 9H).; ¹³C NMR (101 MHz, DMSO-d₆) δ 161.0, 157.2, 152.6, 149.6, 145.7, 144.3, 142.4, 137.3, 131.6, 130.6, 129.1, 127.5, 123.0, 121.9, 107.7, 106.7, 82.4, 54.5, 27.9, 25.2; **MS (ES+Na)**: *m/z* (rel. Intensity) (35ClM+H)450.2 (83), (37Cl M+H) 452.2 (28). (35Cl, M+23Na) 472.2 (100), (37Cl, M+Na) 474.2 (32); **HRMS (ES+)** calcd for (C₂₄H₂₅N₅O₂35Cl):450.1697; found: 450.1690. calcd for (C₂₄H₂₅N₅O₂37Cl):442.0678; found: 442.0683. calcd for (C₂₄H₂₅N₅O₂³⁵Cl²³Na):472.1516; found: 472.1515. calcd for (C₂₄H₂₅N₅O₂37Cl²³Na):474.1487; found: 474.1504.

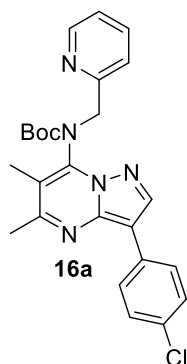
General procedure 3.3 for Suzuki couplings¹



To the Boc-protected iodo intermediate **41** (1 equiv), Na₂CO₃ (2 equiv), the necessary boronic acid (1.2 equiv) and Pd(dtbf)Cl₂ (0.1 equiv) was added a de-gassed 10:1 mixture of dioxane:H₂O. The mixture was heated to 100°C and stirred overnight. Once complete the reaction was filtered through a pad of celite washing with

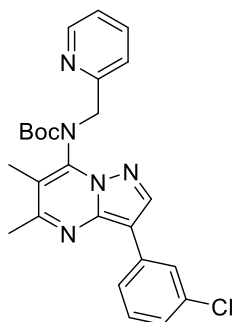
EtOAc, filtrate concentrated to dryness to give the crude product which was purified by column chromatography to afford the Boc protected product.

Tert-butyl (3-(4-chlorophenyl)-5,6-dimethylpyrazolo[1,5-a]pyrimidin-7-yl)(pyridin-2-ylmethyl)carbamate (16a)



The crude product was purified by column chromatography eluting with 50% EtOAc in Hexane to afford the Boc protected product **16a**. (69%). $^1\text{H NMR}$ (400 MHz, DMSO- d_6) δ 8.70 (s, 1H), 8.40 (d, $J = 4.7$ Hz, 1H), 8.20 (d, $J = 8.6$ Hz, 2H), 7.75 (t, $J = 7.5$ Hz, 1H), 7.70 (d, $J = 8.5$ Hz, 2H), 7.50 (m, 1H), 7.26 (m, 1H), 5.16 (d, $J = 15.2$ Hz, 1H), 4.71 (s, 1H), 2.58 (s, 3H), 2.03 (s, 3H), 1.25 (s, 9H); $^{13}\text{C NMR}$ (101 MHz, DMSO- d_6) δ 161.6, 156.3, 152.9, 149.4, 141.7, 138.1, 137.3, 133.2, 131.6, 130.5 (2C), 129.4 (2C), 128.9, 127.4, 123.2, 117.4, 107.8, 81.9, 52.4, 28.0 (2C), 24.4, 13.3; **MS (ES+)**: m/z (rel. Intensity) 464.2 (100), 466.2 (31) HRMS (ES+) calcd for (C₂₅H₂₇N₅O₂³⁵Cl):464.1853; found: 464.1840. calcd for (C₂₅H₂₇N₅O₂³⁷Cl):466.1824; found: 466.1833

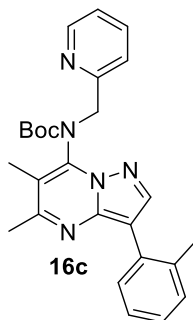
Tert-butyl (3-(3-chlorophenyl)-5,6-dimethylpyrazolo[1,5-a]pyrimidin-7-yl)(pyridin-2-ylmethyl)carbamate (16b)



A suspension of (3-chlorophenyl)boronic acid (**15b**) (39.15 mg, 250.36 μmol), compound **14a** (100.00 mg, 208.63 μmol), Na₂CO₃ (44.23 mg, 417.26 μmol), di-tert-butyl(cyclopentyl)phosphane;dichloropalladium;iron(13.60 mg, 20.86 μmol) in dioxane (10 mL) and water (2 mL) and was allowed to stir at 100°C under nitrogen atmosphere for 2 hr. TLC (petroleum ether/ethyl acetate=

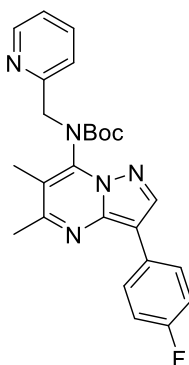
3:1) showed starting material was consumed and a new spot formed. Solvent was removed under vacuum to give a residue which used without further purification (60.00 mg, 129.32 μmol , 62% yield).

Tert-butyl (5,6-dimethyl-3-(o-tolyl)pyrazolo[1,5-a]pyrimidin-7-yl)(pyridin-2-ylmethyl)carbamate (16c)



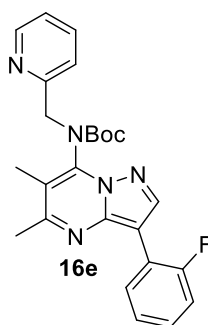
General procedure 3.3 The crude product was purified by column chromatography eluting with 50% EtOAc:Hexane to afford the Boc protected product **16c**. (295 mg, 29%). $^1\text{H NMR}$ (400 MHz, DMSO-d_6) δ 8.42 (d, $J = 3.4$ Hz, 1H), 8.27 (s, 1H), 7.76 (t, $J = 7.3$ Hz, 1H), 7.57 – 7.48 (m, 2H), 7.33 – 7.24 (m, 4H), 5.16 (d, $J = 14.7$ Hz, 1H), 4.74 (d, $J = 14.8$ Hz, 1H), 2.51 (s, 3H), 2.33 (s, 3H), 2.03 (s, 3H), 1.27 (s, 9H); $^{13}\text{C NMR}$ (101 MHz, DMSO-d_6) δ 160.7, 156.5, 153.1, 149.4, 144.4, 143.3, 139.8, 137.2, 136.6, 131.7, 130.9, 130.7, 127.3, 126.1, 123.5, 123.2, 115.7, 109.9, 81.7, 52.6, 28.0 (3C), 24.2, 21.2, 13.3; **MS (ES+)**: m/z (rel. Intensity) 466.2 (100), 467.2 (21) HRMS (ES+) calcd for $(\text{C}_{26}\text{H}_{29}\text{N}_5\text{O}_2^{23}\text{Na})$:466.2219; found: 466.2214.

Tert-butyl (3-(4-fluorophenyl)-5,6-dimethylpyrazolo[1,5-a]pyrimidin-7-yl)(pyridin-2-ylmethyl)carbamate (16d)



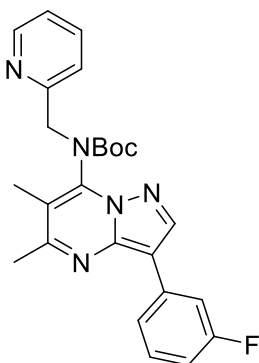
General procedure 3.3 The crude product was purified by column chromatography eluting with 50% EtOAc:Hexane to afford the Boc protected product **16d**. (80%). $^1\text{H NMR}$ (400 MHz, DMSO-d_6) δ 8.66 (s, 1H), 8.40 (d, $J = 4.5$ Hz, 1H), 8.22 – 8.17 (m, 2H), 7.75 (t, $J = 7.4$ Hz, 1H), 7.46 (d, $J = 7.8$ Hz, 1H), 7.32 – 7.22 (m, 3H), 5.16 (d, $J = 15.0$ Hz, 1H), 4.70 (d, $J = 15.0$ Hz, 1H), 2.59 (s, 3H), 2.02 (s, 3H), 1.26 (s, 9H); **MS (ES+)**: m/z (rel. Intensity) 470.2 (100), 471.22 (28) HRMS (ES+) calcd for $(\text{C}_{25}\text{H}_{26}\text{N}_5\text{O}_2\text{F}^{23}\text{Na})$:470.1968; found: 470.1964.

Tert-butyl (3-(2-fluorophenyl)-5,6-dimethylpyrazolo[1,5-a]pyrimidin-7-yl)(pyridin-2-ylmethyl)carbamate (16e)



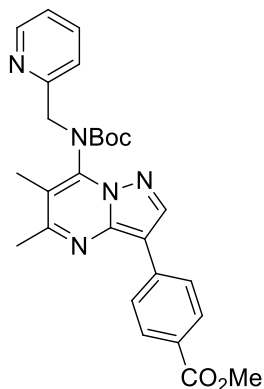
General procedure 3.3 The crude product was purified by column chromatography eluting with 50% EtOAc:Hexane to afford the Boc protected product **16e**. (79%). $^1\text{H NMR}$ (400 MHz, DMSO-d_6) δ 8.49 (m, 2H), 8.41 (d, $J = 4.6$ Hz 1H), 7.75 (t, $J = 7.7$ Hz, 1H), 7.47 (d, $J = 7.8$ Hz, 1H), 7.31 (m, 3H), 7.27 (dd, $J = 7.1, 5.1$ Hz 1H), 5.18 (d, $J = 15.1$ Hz 1H), 4.72 (d, $J = 15.1$ Hz 1H), 2.58 (s, 3H), 2.04 (s, 3H), 1.26 (s, 9H); $^{13}\text{C NMR}$ (101 MHz, DMSO-d_6) δ 161.8, 159.3 (d, $J = 245.8$ Hz), 156.3, 152.9, 149.4, 144.4, 143.4, 139.9, 137.2, 129.4 (d, $J = 4.0$ Hz), 128.1, 125.1 (d, $J = 3.2$ Hz), 123.6, 123.2 (d, $J = 1.6$ Hz), δ 120.2 (d, $J = 13.0$ Hz), 116.7, 116.3 (d, $J = 21.9$ Hz), 103.3 (d, $J = 21.9$ Hz), 81.9, 52.5, 29.0 (3C), 24.4, 13.3; **MS (ES+)**: m/z (rel. Intensity) 448.2 (100), 449.22 (22) HRMS (ES+) calcd for $(\text{C}_{25}\text{H}_{27}\text{N}_5\text{O}_2\text{F})$:448.2149; found: 448.2148.

Tert-butyl (3-(3-fluorophenyl)-5,6-dimethylpyrazolo[1,5-a]pyrimidin-7-yl)(pyridin-2-ylmethyl)carbamate (16f)



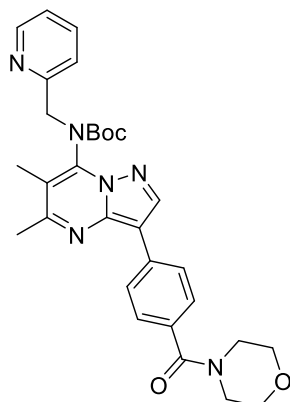
General procedure 3.3 The crude product was purified by column chromatography eluting with 50% EtOAc:Hexane to afford the Boc protected crude product **16f** which was used without further purification. (81%).

Methyl 4-(7-((tert-butoxycarbonyl)(pyridin-2-ylmethyl)amino)-5,6-dimethylpyrazolo[1,5-a]pyrimidin-3-yl)benzoate (16g)



General procedure 3.3 The crude product was purified by column chromatography eluting with 20% EtOAc:Hexane, NEt₃ to afford the Boc protected product **16g**. (75%). ¹H NMR(400 MHz, MeOD) δ 8.78 (s, 1H), 8.39 (d, *J* = 4.3 Hz, 1H), 8.32 (d, *J* = 8.4 Hz, 2H), 8.01 (d, *J* = 8.4 Hz, 2H), 7.73 (td, *J* = 7.7, 1.5 Hz, 1H), 7.45 (d, *J* = 7.8 Hz, 1H), 7.25 (m, 1H), 5.14 (d, *J* = 15.2 Hz 1H), 4.71 (d, *J* = 15.1 Hz 1H), 3.86 (s, 3H), 2.59 (s, 3H), 2.03 (s, 3H), 1.24 (s, 9H); ¹³C NMR (101 MHz, MeOD) δ 165.9, 161.6, 155.6, 152.1, 148.7, 143.6, 141.6, 139.4, 136.5, 129.4 (2C), 126.0, 124.8 (2C), 122.8, 122.5, 116.0, 107.1, 81.2, 53.1, 51.7, 27.2 (3C), 23.8, 12.6; MS (ES⁺): *m/z* (rel. Intensity) 510.2 (100), 511.2 (24) HRMS (ES⁺) calcd for (C₂₇H₂₉N₅O₄23Na) :510.2117; found: 510.2126.

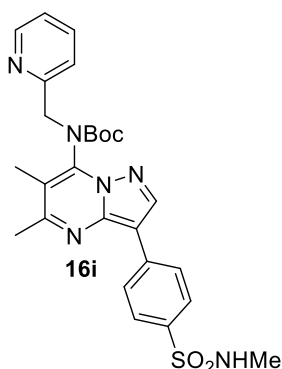
Tert-butyl (5,6-dimethyl-3-(4-(morpholine-4-carbonyl)phenyl)pyrazolo[1,5-a]pyrimidin-7-yl)(pyridin-2-ylmethyl)carbamate (16h)



General procedure 3.3 The crude product was purified by column chromatography eluting with 60% EtOAc:Hexane, NEt₃ to afford the Boc protected product (**16h**). (62%). ¹H NMR (400 MHz, DMSO-d₆) δ 8.74

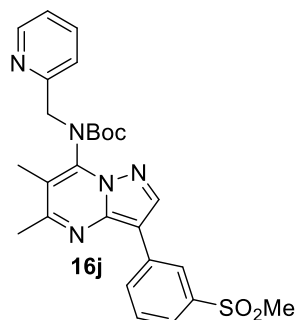
(s, 1H), 8.40 (d, $J = 4.1$ Hz, 1H), 8.24 (d, $J = 8.2$ Hz, 2H), 7.75 (td, $J = 7.7, 1.6$ Hz, 1H), 7.49 (d, $J = 8.3$ Hz, 2H), 7.27 (dd, $J = 7.3, 5.1$ Hz, 1H), 5.13 (d, $J = 15.3$ Hz, 1H), 4.70 (d, $J = 15.1$ Hz, 1H), 3.72-3.45 (br s, 8H), 2.59 (s, 3H), 2.03 (s, 3H), 1.25 (s, 9H); $^{13}\text{C NMR}$ (101 MHz, DMSO- d_6) δ 169.6, 161.8, 156.4, 152.9, 149.3, 144.2, 142.0, 139.94, 137.2, 134.1, 132.9, 128.2 (2C), 125.4 (2C), 123.5, 123.2, 116.4, 108.3, 81.9, 66.6, 53.9, 52.5, 27.7 (3C), 24.4, 13.3; **MS (ES+)**: m/z (rel. Intensity) 565.3 (100), 566.3 (30) HRMS (ES+) calcd for ($\text{C}_{30}\text{H}_{34}\text{N}_6\text{O}_4$) ^{23}Na : 565.2539; found: 565.2526.

Tert-butyl (5,6-dimethyl-3-(4-(N-methylsulfamoyl)phenyl)pyrazolo[1,5-a]pyrimidin-7-yl)(pyridin-2-ylmethyl)carbamate (16i)



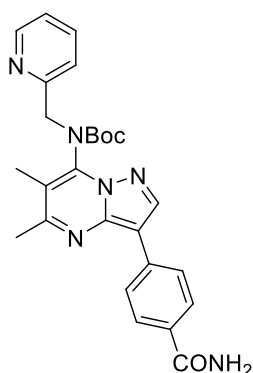
General procedure 3.3 The crude product was purified by column chromatography eluting with 60% EtOAc in Hexane, ($\sim 1\% \text{NEt}_3$) to afford the Boc protected product **16i**. (63%). $^1\text{H NMR}$ (400 MHz, DMSO- d_6) δ 8.79 (s, 1H), 8.40 (d, $J = 4.4$ Hz), 8.39 (d, $J = 8.4$ Hz, 2H), 7.82 (d, $J = 8.5$ Hz, 2H), 7.75 (td, $J = 7.7, 1.6$ Hz, 1H), 7.47 (d, $J = 7.8$ Hz, 1H), 7.42 (q, $J = 4.9$ Hz, 1H), 7.27 (m, 1H), 5.15 (d, $J = 15.2$ Hz, 1H), 4.72 (d, $J = 15.1$ Hz, 1H), 2.61 (s, 3H), 2.44 (s, 3H), 2.05 (s, 3H), 1.25 (s, 9H); $^{13}\text{C NMR}$ (101 MHz, DMSO- d_6) δ 162.4, 156.3, 152.9, 149.4, 144.4, 142.4, 140.1, 137.2, 136.8, 136.2, 127.7 (2C), 125.9 (2C), 123.6, 123.3, 116.8, 107.5, 82.0, 52.6, 29.2, 28.0 (3C), 24.5, 13.3; **MS (ES+)**: m/z (rel. Intensity) 523.2 (100), 524.4 (27) HRMS (ES+) calcd for ($\text{C}_{26}\text{H}_{31}\text{N}_6\text{O}_4\text{S}$): 523.2128; found: 523.2126.

Tert-butyl (5,6-dimethyl-3-(3-(methylsulfonyl)phenyl)pyrazolo[1,5-a]pyrimidin-7-yl)(pyridin-2-ylmethyl)carbamate 16j



General procedure 3.3 The crude product was purified by column chromatography eluting with 50% EtOAc in Hexane, (~1%NEt₃) to afford the Boc protected product **16j**. (94%). ¹H NMR(400 MHz, DMSO-d₆) δ 8.88 (s, 1H), 8.77 (m, 1H), 8.58 (dd, *J* = 7.6, 1.1 Hz, 1H), 8.45 (d, *J* = 4.1 Hz, 1H), 7.88 – 7.76 (m, 3H), 7.52 (d, *J* = 7.8 Hz, 1H), 7.32 (m, 1H), 5.21 (d, *J* = 15.0 Hz 1H), 4.78 (d, *J* = 15.1 Hz 1H), 3.34 (s, 3H) 2.66 (s, 3H), 2.10 (s, 3H), 1.30 (s, 9H); ¹³C NMR (101 MHz, DMSO-d₆) δ 162.2, 157.0, 156.3, 152.9, 149.4, 144.2, 142.2, 141.9, 140.1, 137.2, 134.0, 130.5, 130.3, 124.2, 123.6, 123.3, 116.7, 107.4, 81.9, 52.5, 44.0, 28.0 (3C), 24.6, 13.3; MS (ES⁺): *m/z* (rel. Intensity) [M+23Na] 530.2 (100), [M+23Na] 531.2 (22) HRMS (ES⁺) calcd for (C₂₆H₂₉N₅O₄23NaS):530.1838; found: 530.1845.

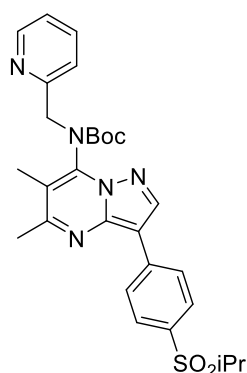
Tert-butyl (3-(4-carbamoylphenyl)-5,6-dimethylpyrazolo[1,5-a]pyrimidin-7-yl)(pyridin-2-ylmethyl)carbamate (16k)



General procedure 3.3 The crude product was purified by column chromatography eluting with 80% EtOAc in Hexane, (~1%NEt₃) to afford the Boc protected product **16k**. (18%). ¹H NMR(400 MHz, DMSO-d₆) δ 8.76 (s, 1H), 8.46 (d, *J* = 4.5 Hz, 1H), 8.26 (d, *J* = 8.3 Hz, 2H), 7.95 (d, *J* = 8.3 Hz, 2H), 7.73 (td, *J* = 7.7, 1.5 Hz, 1H), 7.50 (d, *J* = 7.8 Hz, 1H), 7.34 (s, 2H), 7.32 (m, 1H), 5.13 (d, *J* = 15.1 Hz 1H), 4.72 (d, *J* = 15.1 Hz 1H), 2.60 (s, 3H), 2.03 (s, 3H), 1.31 (s, 9H); ¹³C NMR (101 MHz, DMSO-d₆) δ 168.0, 161.9, 156.4, 152.9, 149.4, 144.3, 142.1, 140.0, 137.2,

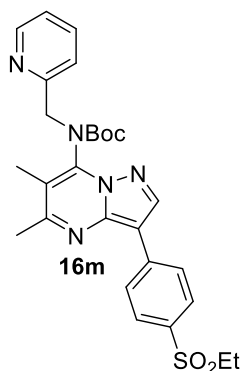
135.5, 131.6, 128.5(2C), 125.2(2C), 123.6, 123.2, 116.5, 108.2, 81.9, 52.4, 28.0 (3C), 24.6, 13.3; **MS (ES+)**: m/z (rel. Intensity) [M+23Na] 495.2 (100), [M+23Na]496.2 (24)

Tert-butyl (3-(4-(isopropylsulfonyl)phenyl)-5,6-dimethylpyrazolo[1,5-a]pyrimidin-7-yl)(pyridin-2-ylmethyl)carbamate (**16l**)



General procedure 3.3 The crude product was purified by column chromatography eluting with 60% EtOAc in Hexane, (~1%NEt₃) to afford the Boc protected product **16l**. (28%). ¹H NMR(400 MHz, DMSO-d₆) δ 8.83 (s, 1H), 8.45 (d, *J* = 8.3 Hz, 2H), 8.40 (d, *J* = 4.4 Hz, 1H), 7.89 (d, *J* = 8.2 Hz, 2H), 7.75 (t, *J* = 7.6 Hz, 1H), 7.47 (d, *J* = 7.7 Hz, 1H), 7.29 – 7.24 (m, 1H), 5.15 (d, *J* = 14.9 Hz, 1H), 4.73 (d, *J* = 14.9 Hz, 1H), 3.43 (s, *J* = 6.7Hz 1H), 2.62 (s, 3H), 2.06 (s, 3H), 1.25 (s, 9H), 1.19 (d, *J* = 6.7 Hz, 6H); ¹³C NMR (101 MHz, DMSO-d₆) δ 162.6, 158.0, 156.6, 152.8, 149.4, 142.7, 138.3, 137.3, 133.5, 132.6, 131.4, 129.6 (2C), 125.9(2C), 123.1, 107.4, 104.6, 82.0, 54.8, 52.5, 28.1 (3C), 24.6, 15.9, 13.5; **MS (ES+)**: m/z (rel. Intensity) [M+23Na] 558.2 (100), [M+23Na] 559.2 (28) HRMS (ES+) calcd for (C₂₈H₃₃N₅O₄23NaS):558.2151; found: 558.2148.

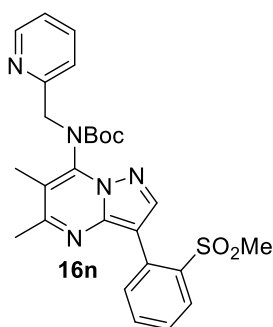
Tert-butyl (3-(4-(ethylsulfonyl)phenyl)-5,6-dimethylpyrazolo[1,5-a]pyrimidin-7-yl)(pyridin-2-ylmethyl)carbamate (**16m**)



General procedure 3.3 The crude product was purified by column chromatography eluting with 60% EtOAc in Hexane, (NEt₃) to afford the Boc protected product **16m**. (78%). ¹H NMR(400 MHz, DMSO-d₆) δ 8.86 (s, 1H),

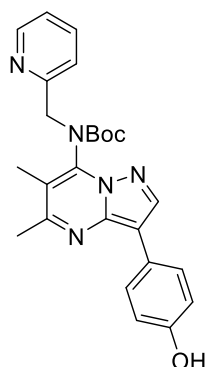
8.47 (d, $J = 8.4$ Hz, 2H), 8.43 (d, $J = 4.0$ Hz, 1H), 7.95 (d, $J = 8.4$ Hz, 2H), 7.77 (m, 1H), 7.50 (d, $J = 7.8$ Hz, 1H), 7.29 (dd, $J = 7.4, 4.8$ Hz, 1H), 5.18 (d, $J = 15.3$ Hz, 1H), 4.76 (d, $J = 15.0$ Hz, 1H), 3.34 (q, $J = 7.3$ Hz, 2H), 2.64 (s, 3H), 2.09 (s, 3H), 1.28 (s, 9H), 1.19 – 1.14 (m, 3H); ^{13}C NMR (101 MHz, DMSO- d_6) δ 162.6, 160.4, 156.3, 152.8, 149.4, 144.5, 142.5, 140.2, 138.2, 137.2, 135.2, 128.8 (2C), 126.0 (2C), 123.2, 116.9, 107.4, 82.0, 52.5, 49.8, 28.0, 24.5, 13.4, 7.7; **MS (ES+)**: m/z (rel. Intensity) [M+23Na] 544.2 (100), [M+23Na] 545.2 (31) HRMS (ES+) calcd for (C₂₇H₃₁N₅O₄²³NaS):4544.1994; found: 544.2006.

Tert-butyl (5,6-dimethyl-3-(2-(methylsulfonyl)phenyl)pyrazolo[1,5-a]pyrimidin-7-yl)(pyridin-2-ylmethyl)carbamate (16n)



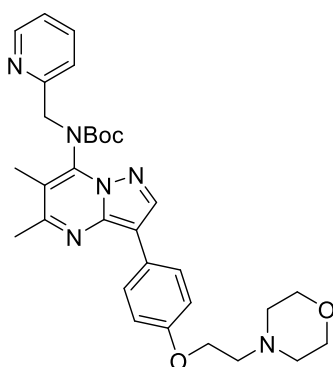
General procedure 3.3 The crude product was purified by column chromatography eluting with 60% EtOAc in Hexane, (~1%NEt₃) to afford the Boc protected product **16n**. (23%). ^1H NMR(400 MHz, MeOD) δ 8.24 (d $J = 4.6$ Hz 1H) 8.16 (s, 1H), 8.12 – 8.07 (m, 1H), 7.77 – 7.60 (m, 2H), 7.53 (m, 3H), 7.19 (dd, $J = 6.8, 5.1$ Hz 1H), 5.11 (d, $J = 14.9$ Hz 1H), 4.72 (d, $J = 14.9$ Hz 1H), 2.7 (s,3H), 2.38 (s, 3H), 1.91 (s, 3H), 1.22 (s, 9H); ^{13}C NMR (101 MHz, MeOD) δ 164.8, 162.0, 155.7, 153.1, 148.4, 145.2, 144.2, 142.0, 139.9, 139.6, 139.1, 137.5, 134.4, 133.1, 131.2, 128.7, 127.8, 124.3, 123.1, 116.4, 107.0, 82.1, 51.9, 41.9, 26.9, 22.3, 12.00; **MS (ES+)**: m/z (rel. Intensity) [M+23Na] 530.2 (100), [M+23Na] 531.2 (28) HRMS (ES+) calcd for (C₂₅H₂₇N₅O₂²³NaS):530.1838; found: 530.1838.

Tert-butyl (3-(4-hydroxyphenyl)-5,6-dimethylpyrazolo[1,5-a]pyrimidin-7-yl)(pyridin-2-ylmethyl)carbamate (16o)



General procedure 3.3 The crude product was purified by column chromatography eluting with 60% EtOAc:Hexane to afford the Boc protected product (**16o**). (84%). $^1\text{H NMR}$ (400 MHz, DMSO-d_6) δ 9.40 (s, 1H), 8.52 (s, 1H), 8.41 (d, $J = 4.4$ Hz, 1H), 7.95 (d, $J = 8.5$ Hz, 2H), 7.74 (td, $J = 7.7, 1.4$ Hz, 1H), 7.45 (d, $J = 7.8$ Hz, 1H), 7.26 (dd, $J = 7.2, 5.4$ Hz, 1H), 6.84 (d, $J = 8.6$ Hz, 2H), 2.54 (s, 3H), 1.99 (s, 3H), 1.25 (s, 9H); $^{13}\text{C NMR}$ (101 MHz, DMSO-d_6) δ 170.8, 160.3, 156.45, 156.1, 153.0, 149.4, 143.4, 140.9, 139.6, 137.2 (2C), 127.3, 123.6, 123.2, 115.9, 109.4, 81.8, 52.0, 28.0 (3C), 24.4, 13.3; **MS (ES+)**: m/z (rel. Intensity) [M+23Na] 468.2 (100), [M+23Na] 469.2 (30) HRMS (ES+) calcd for ($\text{C}_{25}\text{H}_{27}\text{N}_5\text{O}_3$) ^{23}Na :468.2012; found: 468.2012.

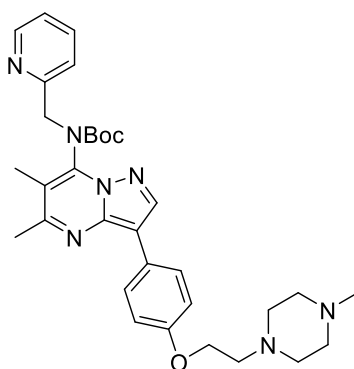
Tert-butyl (5,6-dimethyl-3-(4-(2-morpholinoethoxy)phenyl)pyrazolo[1,5-a]pyrimidin-7-yl)(pyridin-2-ylmethyl)carbamate (AWF946-Boc)



To a solution of the Boc-protected phenol intermediate **16o** (250 mg, 0.56 mmol), 2-morpholinoethan-1-ol (147 mg, 1.12 mmol) and triphenylphosphine (294 mg, 1.12 mmol) in THF (15 ml) at 0 °C was added a solution of 40% DEAD in toluene (195 mg, 1.12 mmol). The reaction was allowed to stir at room temperature for 48 h. Silica was added to the reaction and the mixture concentrated. The crude product was purified by column chromatography eluting with EtOAc to afford the Boc protected product **AWF946-Boc**. (69%). $^1\text{H NMR}$ (400 MHz, DMSO-d_6) δ 8.58 (s, 1H), 8.41 (d, $J = 4.6$ Hz, 1H), 8.06 (d, $J = 8.5$ Hz, 2H), 7.74 (t, $J = 7.6$ Hz, 1H), 7.46 (d, J

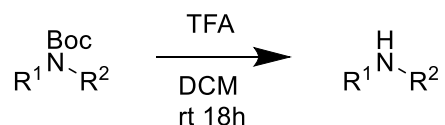
= 7.8 Hz, 1H), 7.28 – 7.24 (m, 1H), 7.03 (d, $J = 8.4$ Hz, 2H), 5.16 (d, $J = 15.1$ Hz, 1H), 4.69 (d, $J = 15.1$ Hz, 1H), 4.12 (t, $J = 5.6$ Hz, 2H), 3.61 – 3.58 (m, 4H), 2.71 (t, $J = 5.4$ Hz, 2H), 2.56 (s, 3H), 2.48 (br s, 4H), 2.00 (s, 3H), 1.26 (s, 9H); $^{13}\text{C NMR}$ (101 MHz, DMSO- d_6) δ 164.8, 160.6, 157.3, 156.5, 153.0, 149.4, 143.5, 141.1, 139.6, 137.2, 127.2 (2C), 125.2, 123.5, 123.3, 115.2 (2C), 108.9, 81.8, 66.7 (2C), 61.2, 57.5, 54.1 (2C), 52.3, 28.0, 24.4, 13.3; **MS (ES+)**: m/z (rel. Intensity) 559.3(100), 560.3 (30) HRMS (ES+) calcd for ($\text{C}_{31}\text{H}_{39}\text{N}_6\text{O}_4$):559.3033; found: 559.3024.

Tert-butyl (5,6-dimethyl-3-(4-(2-(4-methylpiperazin-1-yl)ethoxy)phenyl)pyrazolo[1,5-a]pyrimidin-7-yl)(pyridin-2-ylmethyl)carbamate (f-Boc)



To a solution of the Boc-protected phenol intermediate (250 mg, 0.56 mmol), 2-(4-methylpiperazin-1-yl)ethan-1-ol (161 mg, 1.12mmol) and triphenylphosphine (294 mg, 1.12 mmol) in THF(15ml) at 0 °C was added a solution of 40% DEAD in toluene (195 mg, 1.12 mmol). The reaction was allowed to stir at room temperature for 48 h. Silica was add to the reaction and the mixture concentrated. The crude product was purified by column chromatography eluting with EtOAc to 5% MeOH:EtOAc to afford the Boc protected product **AWF947-Boc**. (75%). $^1\text{H NMR}$ (400 MHz, DMSO- d_6) δ 8.58 (s, 1H), 8.41 (d, $J = 4.6$ Hz, 1H), 8.06 (d, $J = 8.5$ Hz, 2H), 7.75 (t, $J = 7.7$ Hz, 1H), 7.46 (d, $J = 7.8$ Hz, 1H), 7.29 – 7.23 (m, 1H), 7.02 (d, $J = 8.5$ Hz, 2H), 5.16 (d, $J = 15.1$ Hz, 1H), 4.69 (d, $J = 15.1$ Hz, 1H), 4.10 (t, $J = 5.7$ Hz, 2H), 2.70 (t, $J = 5.7$ Hz, 2H), 2.56 (s, 3H), 2.44 – 2.25 (m, 8H), 2.16 (s, 3H), 2.00 (s, 3H), 1.26 (s, 9H); $^{13}\text{C NMR}$ (101 MHz, DMSO- d_6) δ 156.4, 153.0, 149.4, 147.1, 143.4, 141.1, 139.6, 132.4, 131.8, 127.2 (2C), 125.2, 123.6, 123.2, 115.2 (2C), 108.9, 93.3, 81.8, 66.0, 57.1, 55.2 (4C), 53.5, 46.2, 28.0 (3C), 24.4, 13.3; **MS (ES+)**: m/z (rel. Intensity) 572.3(100), 573.3 (30) HRMS (ES+) calcd for ($\text{C}_{32}\text{H}_{42}\text{N}_7\text{O}_3$):572.3349; found: 572.3353.

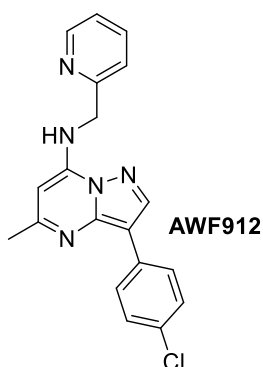
General procedure 3.4 - Boc-removal



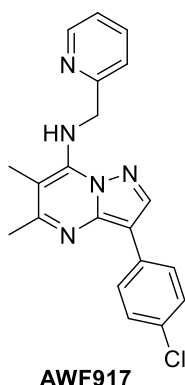
To the Boc-protected amine suspended in DCM was added TFA and the reaction was allowed to stir at room temperature for 18 hours. Upon completion of the reaction the volatiles were removed under reduced pressure, the resultant residue was diluted with EtOAc and washed with NaHCO₃ before drying and evaporating to dryness to give the crude product.

**7-Chloro-5-methylpyrazolo[1,5-a]pyrimidine
ylmethyl)pyrazolo[1,5-a]pyrimidin-7-amine² (AWF912)**

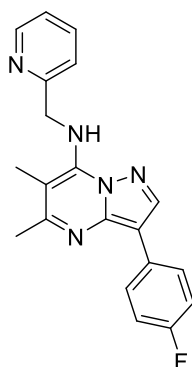
3-(4-chlorophenyl)-5-methyl-N-(pyridin-2-



General procedure 3.4 Purified eluting with 80% EtOAc in Hexanes (0.10 g, 55%). **Melting point:** 144-146 °C
¹H NMR(400 MHz, DMSO-d₆) δ 8.67 (s, 1H), 8.56 (m, 2H), 8.21 (d, *J* = 8.6 Hz, 2H), 7.79 (td, *J* = 7.7, 1.7 Hz, 1H), 7.45 (d, *J* = 8.6 Hz, 2H), 7.39 (d, *J* = 7.9 Hz, 1H), 7.32 (dd, *J* = 7.0, 5.2 Hz, 1H), 6.13 (s, 1H), 4.74 (d, *J* = 6.1 Hz, 2H), 2.43 (s, 3H); ¹³C NMR (101 MHz, DMSO-d₆) δ 160.1, 157.4, 149.6, 147.1, 145.7, 141.9, 137.6, 132.4, 129.6, 128.8, 126.9, 123.1, 121.7, 105.6, 86.9, 46.7, 25.4; **MS (ES+):** *m/z* (rel. Intensity) 350.1 (100), 352.1 (23) HRMS (ES+) calcd for (C₁₉H₁₇N₅35Cl):350.1172; found: 350.1165. calcd for (C₁₉H₁₇N₅37Cl):352.1155; found: 352.1143; **CHN analysis:** Calculated: C:65.24%, H:4.61%, N:20.02%. Found C:64.40%, H:4.66%, N:19.23%.

3-(4-Chlorophenyl)-5,6-dimethyl-N-(pyridin-2-ylmethyl)pyrazolo[1,5-a]pyrimidin-7-amine (AWF917)

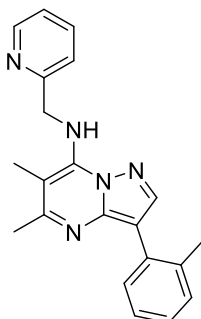
General procedure 3.4 Product was isolated from crude by column chromatography eluting with DCM to 2% MeOH:DCM giving **AWF917** in moderate yield. (53%). $^1\text{H NMR}$ (400 MHz, DMSO-d_6) δ 8.55 (d, $J = 4.8$ Hz, 1H), 8.30 (s, 1H), 8.05 (d, $J = 8.5$ Hz, 2H), 7.80 (t, $J = 7.1$ Hz, 1H), 7.45 (d, $J = 7.9$ Hz, 1H), 7.37 (d, $J = 8.5$ Hz, 2H), 7.32 (dd, $J = 7.1, 5.3$ Hz, 1H), 5.21 (s, 2H), 2.55 (s, 3H), 2.34 (s, 3H); $^{13}\text{C NMR}$ (101 MHz, DMSO-d_6) δ 160.1, 158.5, 149.24, 146.0, 144.4, 141.2, 137.6, 129.3, 128.9 (2C), 126.8 (2C), 122.8, 121.9, 105.0, 97.0, 513, 30.0, 24.8, 13.1; **MS (ES+)**: m/z (rel. Intensity) 364.1(100), 366.1 (32), 365.1 (22) HRMS (ES+) calcd for ($\text{C}_{20}\text{H}_{19}\text{N}_5\text{Cl}$):364.1329; found: 364.1320, calcd for ($\text{C}_{20}\text{H}_{19}\text{N}_5^{37}\text{Cl}$):366.1299; found: 366.1305; **CHN analysis**: Calculated: C:66.02%, H:4.99%, N:19.25%. Found C:65.07%, H:4.81%, N:19.07%.

3-(4-Fluorophenyl)-5,6-dimethyl-N-(pyridin-2-ylmethyl)pyrazolo[1,5-a]pyrimidin-7-amine (AWF918)

General procedure 3.4 The crude product was purified by column chromatography eluting with 50% EtOAc:Hexane to give **AWF918** as an off-white solid. (86%). **Melting point**: 146-148 °C $^1\text{H NMR}$ (400 MHz, DMSO-d_6) δ 8.57 (d, $J = 4.3$ Hz, 1H), 8.52 (s, 1H), 8.19 (dd, $J = 8.8, 5.6$ Hz, 2H), 7.90 (t, $J = 6.1$ Hz, 1H), 7.79 (td, $J = 7.7, 1.7$ Hz, 1H), 7.39 (d, $J = 7.9$ Hz, 1H), 7.30 (dd, $J = 6.9, 5.3$ Hz, 1H), 7.22 (t, $J = 9.0$ Hz, 2H), 5.21 (d, $J = 6.1$ Hz, 2H), 2.51 (s, 3H), 2.31 (s, 3H); $^{13}\text{C NMR}$ (101 MHz, DMSO-d_6) δ 160.5 ($J = 236.3$ Hz), 159.7, 158.5, 149.3, 145.0, 144.1, 140.9, 137.4, 130.1 (d, $J = 2.9$ Hz), 129.9, 127.1 (2C, d, $J = 7.5$ Hz), 122.2, 115.7 (2C, d, $J = 21.0$ Hz), 105.4, 96.9, 49.3, 24.8, 13.1; **MS (ES+)**: m/z (rel. Intensity) 348.2 (100), 349.2 (31) HRMS (ES+) calcd for

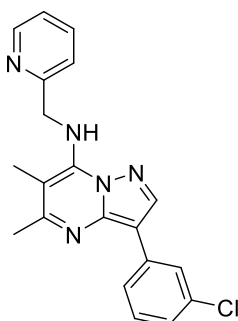
(C₂₀H₁₉N₅F):348.1624; found: 348.1620; **CHN analysis:** Calculated: C:69.15%, H:5.22%, N:20.16%. Found C:68.65%, H:5.28%, N:19.80%.

5,6-Dimethyl-N-(pyridin-2-ylmethyl)-3-(o-tolyl)pyrazolo[1,5-a]pyrimidin-7-amine (AWF919)

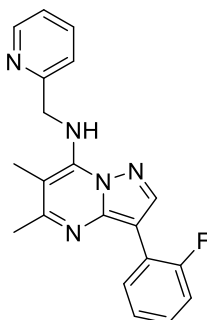


General procedure 3.4 The crude product was purified by column chromatography eluting with 50% EtOAc:Hexane to afford the product **AWF919** as an off-white solid. (126 mg, 57%). **Melting point:** 158-161 °C **¹H NMR(400 MHz, DMSO-d₆)** δ 8.59 (s, 1H), 8.14 (s, 1H), 7.89 (s, 1H), 7.81 (s, 1H), 7.53 (d, *J* = 3.0 Hz, 1H), 7.43 (d, *J* = 4.9 Hz, 1H), 7.34 – 7.26 (m, 2H), 7.21 (m, 2H), 5.20 (s, 2H), 2.42 (s, 3H), 2.34 (s, 3H), 2.32 (s, 3H); **¹³C NMR (101 MHz, DMSO-d₆)** δ 159.4, 158.4, 149.3, 145.8, 144.4, 142.8, 137.4, 136.4, 132.6, 130.8, 130.6, 126.6, 125.9, 122.8, 121.8, 107.6, 96.4, 49.3, 24.6, 21.4, 13.1; **MS (ES⁺):** *m/z* (rel. Intensity) 344.2 (100),345.2 (15) HRMS (ES⁺) calcd for (C₂₁H₂₂N₅):344.1875; found: 344.1867. **CHN analysis:** Calculated: C:73.44%, H:6.16%, N:20.39%. Found C:72.15%, H:6.07%, N:19.82%.

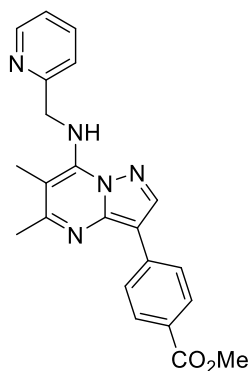
Synthesis of 3-(3-Chlorophenyl)-5,6-dimethyl-N-(pyridin-2-ylmethyl)pyrazolo[1,5-a]pyrimidin-7-amine (AWZ9010)



AWZ9010 – Synthesised by Wuxi (Experimental details in Appendix 1). **¹H NMR (400MHz, DMSO-d₆)** δ = 8.76 (d, *J*=4.8 Hz, 1H), 8.49 (s, 1H), 8.38 - 8.26 (m, 2H), 8.12 (s, 1H), 7.97 (d, *J*=7.5 Hz, 1H), 7.86 (d, *J*=8.3 Hz, 1H), 7.78 - 7.71 (m, 1H), 7.42 (t, *J*=7.9 Hz, 1H), 7.25 (d, *J*=7.7 Hz, 1H), 5.52 (br. s., 3H), 2.56 (s, 3H), 2.30 (s, 3H).

3-(2-Fluorophenyl)-5,6-dimethyl-N-(pyridin-2-ylmethyl)pyrazolo[1,5-a]pyrimidin-7-amine (AWF936)

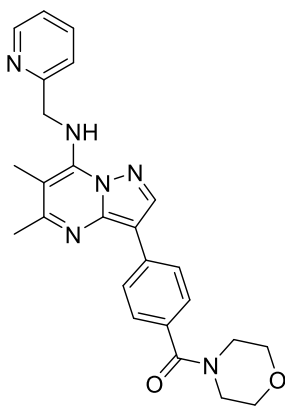
General procedure 3.4 The crude product was purified by column chromatography eluting with 50% EtOAc:Hexane, NEt_3 to afford **AWF936**. (67%). **Melting point:** 145-147 °C $^1\text{H NMR}$ (400 MHz, DMSO-d_6) δ 8.64 (td, $J = 7.7, 1.2$ Hz, 1H), 8.56 (d, $J = 4.5$ Hz, 1H), 8.38 (d, $J = 3.7$ Hz, 1H), 7.98 (t, $J = 6.0$ Hz, 1H), 7.79 (td, $J = 7.7, 1.6$ Hz, 1H), 7.39 (d, $J = 7.9$ Hz, 1H), 7.33 – 7.18 (m, 4H), 5.21 (d, $J = 6.0$ Hz, 2H), 2.49 (s, 3H), 2.31 (s, 3H); $^{13}\text{C NMR}$ (101 MHz, DMSO-d_6) δ 160.0, 159.1 (d, $J = 245.5$ Hz), 158.4, 149.3, 146.0, 144.7, 142.8 (d, $J = 13.6$ Hz), 137.5, 128.9 (d, $J = 4.2$ Hz), 126.9 (d, $J = 8.2$ Hz), 124.9 (d, $J = 3.2$ Hz), 122.8, 121.1 (d, $J = 12.6$ Hz) 121.7, 116.0 (d, $J = 22.2$ Hz), 100.3, 97.3, 49.2, 24.8, 13.2; **MS (ES+):** m/z (rel. Intensity) 348.2 (100), 349.2 (21) HRMS (ES+) calcd for $(\text{C}_{20}\text{H}_{19}\text{N}_5\text{F})$:348.1624; found: 348.1617; **CHN analysis:** Calculated: C:69.15%, H:5.22%, N:20.16%. Found C:68.44%, H:5.16%, N:19.84%.

Methyl 4-(5,6-dimethyl-7-((pyridin-2-ylmethyl)amino)pyrazolo[1,5-a]pyrimidin-3-yl)benzoate (AWF938)

General procedure 3.4 The crude product was purified by column chromatography eluting with 50% EtOAc:Hexane to give **AWF938** as an off-white solid. (41%). **Melting point:** 165-168 °C $^1\text{H NMR}$ (400 MHz, DMSO-d_6) δ 8.66 (s, 1H), 8.56 (d, $J = 4.4$ Hz, 1H), 8.32 (d, $J = 8.4$ Hz, 2H), 8.03 – 7.96 (m, 2H), 7.95 (s, 1H), 7.79 (t, $J = 7.0$ Hz, 1H), 7.39 (d, $J = 7.8$ Hz, 1H), 7.30 (d, $J = 6.8, 5.5$ Hz 1H), 5.22 (d, $J = 5.9$ Hz, 2H), 3.85 (s, 3H), 2.52 (s, 3H), 2.31 (s, 3H); $^{13}\text{C NMR}$ (101 MHz, DMSO-d_6) δ 166.7, 160.3, 158.4, 149.3, 146.2, 144.8, 141.8, 138.8, 137.4, 130.0(2C), 125.8, 124.8(2C), 122.8, 121.7, 105.2, 97.5, 52.3, 49.3, 24.9, 13.1; **MS (ES+):** m/z (rel. Intensi-

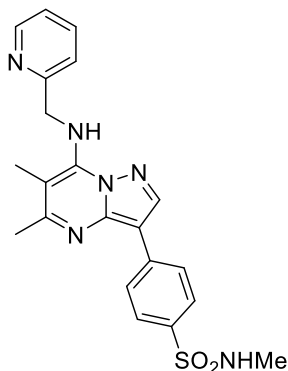
ty) 388.2 (100), 389.2 (22) HRMS (ES+) calcd for (C₂₂H₂₂N₅O₂):388.1774; found: 388.1771.; **CHN analysis:** Calculated: C:68.20%, H:5.46%, N:18.08%. Found C:67.50%, H:5.41%, N:17.70%.

(4-(5,6-Dimethyl-7-((pyridin-2-ylmethyl)amino)pyrazolo[1,5-a]pyrimidin-3-yl)phenyl)(morpholino)methanone (AWF939)



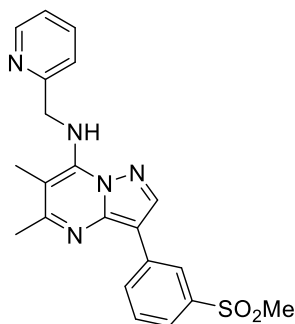
General procedure 3.4 The crude product was purified by column chromatography eluting with EtOAc (~1% NEt₃) **AWF939** (23%). **Melting point:** 206-207 °C **¹H NMR(400 MHz, DMSO-d₆)** δ 8.60 (s, 1H), 8.57 (d, *J* = 4.3 Hz, 1H), 8.23 (d, *J* = 8.2 Hz, 2H), 7.96 (t, *J* = 5.9 Hz, 1H), 7.79 (td, *J* = 7.7, 1.4 Hz, 1H), 7.44 (d, *J* = 8.2 Hz, 2H), 7.39 (d, *J* = 7.8 Hz, 1H), 7.31 (dd, *J* = 7.1, 5.3 Hz 1H), 5.21 (d, *J* = 5.9 Hz, 2H), 3.62 (br s, 4H), 3.53 (br s, 4H), 2.51 (s, 3H), 2.31 (s, 3H); **¹³C NMR (101 MHz, DMSO-d₆)** δ 169.8, 160.0, 158.4, 149.3, 146.1, 144.5, 141.4, 137.4, 135.2, 131.9, 128.1 (2C), 124.9 (2C), 122.8, 121.7, 105.5, 97.1, 66.6, 49.3 (2C), 24.9, 13.2; **MS (ES+):** *m/z* (rel. Intensity) 443.2 (100), 444.2 (26) HRMS (ES+) calcd for (C₂₅H₂₇N₆O₂):443.2195; found: 443.2191; **CHN analysis:** Calculated: C:67.86%, H:5.92%, N:18.99%. Found C:67.19%, H:5.94%, N:18.66%.

4-(5,6-Dimethyl-7-((pyridin-2-ylmethyl)amino)pyrazolo[1,5-a]pyrimidin-3-yl)-N-methylbenzenesulfonamide (AWF940)

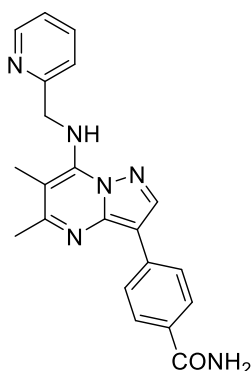


General procedure 3.4 The crude product was purified by trituration with EtOAc and Et₂O to give **AWF940** as an off-white solid (69%). **Melting point:** 181-182 °C **¹H NMR(400 MHz, DMSO-d₆) δ** 8.66 (s, 1H), 8.56 (d, *J* = 4.4 Hz, 1H), 8.37 (d, *J* = 8.4 Hz, 2H), 7.99 (t, *J* = 6.0 Hz, 1H), 7.80 (t, *J* = 7.7 Hz, 1H), 7.76 (d, *J* = 8.3 Hz, 2H), 7.39 (d, *J* = 7.7 Hz, 1H), 7.36 (q, *J* = 5.0 Hz, 1H), 7.31 (dd, *J* = 7.0, 5.4 Hz, 1H), 5.22 (d, *J* = 5.9 Hz, 2H), 2.52 (s, 3H), 2.43 (d, *J* = 5.0 Hz, 3H), 2.31 (s, 3H); **¹³C NMR (101 MHz, DMSO-d₆) δ** 160.3, 158.4, 149.3, 146.2, 144.8, 141.8, 137.9, 137.5, 135.0, 127.5(2C), 125.2(2C), 122.8, 121.6, 104.8, 97.6, 49.3, 29.2, 24.9, 13.2; **MS (ES+):** *m/z* (rel. Intensity) 423.2 (100), 424.2 (31) HRMS (ES+) calcd for (C₂₁H₂₃N₆O₂S):423.1603; found: 423.1600; **CHN analysis:** Calculated: C:59.70%, H:5.25%, N:19.89%, S:7.59%. Found C:59.40%, H:5.32%, N:19.81%, S:7.33%

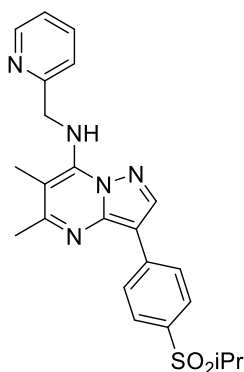
5,6-Dimethyl-3-(3-(methylsulfonyl)phenyl)-N-(pyridin-2-ylmethyl)pyrazolo[1,5-a]pyrimidin-7-amine AWF941



General procedure 3.4 The crude product was purified by trituration with Et₂O to afford **AWF941** as an off-white solid. (56%). **¹H NMR(400 MHz, DMSO-d₆) δ** 8.73 (s, 1H), 8.70 (s, 1H), 8.57 (d, *J* = 4.0 Hz, 1H), 8.53 (d, *J* = 6.9 Hz, 1H), 8.00 (t, *J* = 5.9 Hz, 1H), 7.79 (td, *J* = 7.7, 1.6 Hz, 1H), 7.71 – 7.62 (m, 2H), 7.39 (d, *J* = 7.9 Hz, 1H), 7.30 (dd, *J* = 6.8, 5.3 Hz, 1H), 5.22 (d, *J* = 6.0 Hz, 2H), 3.27 (s, 3H), 2.52 (s, 3H), 2.32 (s, 3H); **¹³C NMR (101 MHz, DMSO-d₆) δ** 160.2, 158.4, 149.3, 146.3, 144.5, 141.7, 141.5, 137.5, 135.0, 130.0, 129.7, 123.2, 123.0, 122.8, 121.7, 104.6, 97.4, 49.3, 44.0, 25.0, 13.2; **MS (ES+):** *m/z* (rel. Intensity) 408.2 (100), 409.2 (23) HRMS (ES+) calcd for (C₂₁H₂₂N₅O₂S):408.1494; found: 408.1495; **CHN analysis:** Calculated: C:61.90%, H:5.19%, N:17.19%, S:7.87. Found C:61.44%, H:5.24%, N:16.70%, S:7.62%

4-(5,6-Dimethyl-7-((pyridin-2-ylmethyl)amino)pyrazolo[1,5-a]pyrimidin-3-yl)benzamide (AWF942)

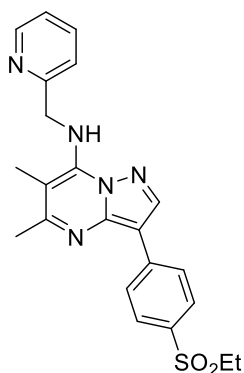
General procedure 3.4 The crude product was purified by column chromatography eluting with 50% EtOAc, (~1% NEt₃) to afford **AWF942**. **Melting point:** 212-213 °C (6%). **¹H NMR(400 MHz, DMSO-d₆)** δ 8.63 (s, 1H), 8.57 (d, *J* = 4.3 Hz, 1H), 8.24 (d, *J* = 8.4 Hz, 2H), 7.97 (t, *J* = 6.1 Hz, 1H), 7.92 (br s, 2H), 7.90 (d, *J* = 8.4 Hz, 2H), 7.79 (td, *J* = 7.7, 1.6 Hz, 1H), 7.39 (d, *J* = 7.9 Hz, 1H), 7.30 (t, *J* = 5.8 Hz, 2H), 5.22 (d, *J* = 6.0 Hz, 2H), 2.52 (s, 3H), 2.31 (s, 3H); **¹³C NMR (101 MHz, DMSO-d₆)** δ 168.2, 160.0, 158.4, 149.3, 146.1, 144.6, 141.6, 137.5, 136.7, 130.6, 128.2(2C), 124.6(2C), 122.8, 121.6, 105.5, 97.2, 49.3, 24.9, 13.2; **MS (ES+):** *m/z* (rel. Intensity) 373.2 (100), 374.2 (31) HRMS (ES+) calcd for (C₂₁H₂₁N₆O):373.1777; found: 373.1775; **CHN analysis:** Calculated: C:67.73%, H:5.41%, N:22.57%. Found C:66.62%, H:5.51%, N:21.37%.

3-(4-(Isopropylsulfonyl)phenyl)-5,6-dimethyl-N-(pyridin-2-ylmethyl)pyrazolo[1,5-a]pyrimidin-7-amine (AWF943)

General procedure 3.4 The crude product was purified by trituration with EtOAc and Et₂O to afford **AWF943** as an off-white solid. (66%). **Melting point:** 198-199 °C **¹H NMR(400 MHz, DMSO-d₆)** δ 8.69 (s, 1H), 8.56 (d, *J* = 4.3 Hz, 1H), 8.44 (d, *J* = 8.4 Hz, 2H), 8.01 (t, *J* = 5.9 Hz, 1H), 7.82 (d, *J* = 8.3 Hz, 2H), 7.78 (t, *J* = 7.7 Hz, 1H), 7.39 (d, *J* = 7.8 Hz, 1H), 7.30 (t, *J* = 6.1 Hz, 1H), 5.23 (d, *J* = 5.9 Hz, 2H), 3.42 (s, *J* = 6.8 Hz, 1H), 2.52 (s, 3H), 2.31 (s, 3H), 1.17 (d, *J* = 6.8 Hz, 6H); **¹³C NMR (101 MHz, DMSO-d₆)** δ 160.5, 158.3, 149.3, 146.3, 144.9, 142.0, 139.3, 137.5, 132.3, 129.4(2C), 125.1(2C), 122.8, 121.7, 104.6, 97.7, 54.7, 49.3, 24.9, 15.8, 13.1; **MS (ES+):** *m/z* (rel. Intensity)

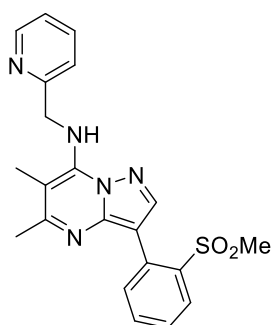
436.2 (100), 437.2 (26) HRMS (ES+) calcd for (C₂₃H₂₆N₅O₂S):436.1807; found: 436.1805; **CHN analysis:** Calculated: C:63.43%, H:5.79%, N:16.08%, S:7.36%. Found C:63.06%, H:5.74%, N:16.02%, S:7.22%.

3-(4-(Ethylsulfonyl)phenyl)-5,6-dimethyl-N-(pyridin-2-ylmethyl)pyrazolo[1,5-a]pyrimidin-7-amine (AWF944)



General procedure 3.4 The crude product was purified by trituration with EtOAc and Et₂O to afford **AWF944** as an off-white solid. (89%). **Melting point:** 175-177 °C **¹H NMR(400 MHz, DMSO-d₆)** δ 8.69 (s, 1H), 8.56 (br s, 1H), 8.43 (d, *J* = 8.3 Hz, 2H), 8.03 (t, *J* = 5.9 Hz, 1H), 7.85 (d, *J* = 8.3 Hz, 2H), 7.79 (t, *J* = 7.6 Hz, 1H), 7.39 (d, *J* = 7.7 Hz, 1H), 7.31 (t, *J* = 5.9 Hz, 1H), 5.22 (d, *J* = 5.6 Hz, 2H), 3.27 (q, *J* = 7.2 Hz, 2H), 2.51 (s, 3H), 2.30 (s, 3H), 1.12 (t, *J* = 7.4 Hz, 3H); **¹³C NMR (101 MHz, DMSO-d₆)** δ 160.5, 158.3, 149.3, 146.2, 144.9, 142.0, 139.2, 137.5, 134.1, 129.1, 128.6(2C), 125.0(2C), 122.8, 104.6, 97.7, 49.9, 49.3, 24.9, 13.1, 7.7; **MS (ES+):** *m/z* (rel. Intensity) 422.2 (100), 423.2 (22) HRMS (ES+) calcd for (C₂₂H₂₄N₅O₂S):422.1651; found: 422.1646; **CHN analysis:** Calculated: C:62.69%, H:5.50%, N:16.61%, S:7.61%. Found C:61.97%, H:5.45%, N:15.83%, S:7.81%.

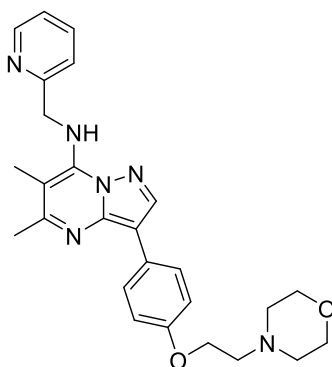
5,6-Dimethyl-3-(2-(methylsulfonyl)phenyl)-N-(pyridin-2-ylmethyl)pyrazolo[1,5-a]pyrimidin-7-amine AWF945



General procedure 3.4 The crude product was purified by trituration with EtOAc and Et₂O to afford **AWF945** (49%). **Melting point:** 116-118 °C **¹H NMR(400 MHz, DMSO-d₆)** δ 8.58 (d, *J* = 4.6 Hz, 1H), 8.24 (s, 1H), 8.10 (dd, *J* = 7.9, 0.9 Hz, 1H), 7.98 (t, *J* = 6.0 Hz, 1H), 7.81 (td, *J* = 7.7, 1.6 Hz, 1H), 7.76 (td, *J* = 7.6, 1.1 Hz, 1H), 7.43 (d, *J* =

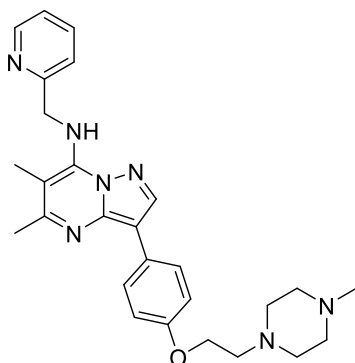
7.8 Hz, 1H), 7.32 (dd, $J = 7.0, 5.2$ Hz, 1H), 5.23 (d, $J = 6.0$ Hz, 2H), 2.95 (s, 3H), 2.39 (s, 3H), 2.31 (s, 3H); ^{13}C NMR (101 MHz, DMSO- d_6) δ 160.2, 158.4, 149.3, 146.0, 145.3, 143.8, 139.9, 137.5, 134.8, 133.6, 132.3, 129.0, 127.8, 122.9, 122.0, 104.3, 97.0, 49.2, 42.7, 24.5, 13.1; MS (ES+): m/z (rel. Intensity) 408.2 (100), 409.2 (22) HRMS (ES+) calcd for ($\text{C}_{21}\text{H}_{22}\text{N}_5\text{O}_2\text{S}$):408.1494; found: 408.1490; CHN analysis: Calculated: C:61.90%, H:5.19%, N:17.19%, S:7.87. Found C:60.94%, H:5.43%, N:15.99%, S:7.12%.

5,6-Dimethyl-3-(4-(2-morpholinoethoxy)phenyl)-N-(pyridin-2-ylmethyl)pyrazolo[1,5-a]pyrimidin-7-amine (AWF946)



General procedure 3.4 The crude product was purified by column chromatography eluting with 6% MeOH in EtOAc, (~1% NEt_3) to afford the free amine **AWF946**. (0.11 g, 62%). **Melting point:** 120-122 °C ^1H NMR(400 MHz, DMSO- d_6) δ 8.57 (d, $J = 4.3$ Hz, 1H), 8.44 (s, 1H), 8.05 (d, $J = 8.4$ Hz, 2H), 7.85 (t, $J = 5.8$ Hz, 1H), 7.78 (t, $J = 7.5$ Hz, 1H), 7.38 (d, $J = 7.8$ Hz, 1H), 7.30 (t, $J = 6.0$ Hz, 1H), 6.98 (d, $J = 8.4$ Hz, 2H), 5.19 (d, $J = 5.8$ Hz, 2H), 4.11 (t, $J = 5.1$ Hz, 2H), 3.60 (br s, 4H), 3.3 (br s, 4H) 2.71 (br s, 2H), 2.49 (s, 3H), 2.30 (s, 3H); ^{13}C NMR (101 MHz, DMSO- d_6) δ 159.3, 158.5, 156.6, 149.3, 145.8, 143.8, 140.5, 137.4, 126.7, 126.2 (2C), 122.8, 121.7, 115.0 (2C), 106.4, 96.5, 66.6 (2C), 65.7, 57.6, 54.1 (2C), 49.3, 24.8, 13.2; MS (ES+): m/z (rel. Intensity) 459.3.3(100), 460.3 (30) HRMS (ES+) calcd for ($\text{C}_{26}\text{H}_{31}\text{N}_6\text{O}_2$):459.2508; found: 459.2502; CHN analysis: Calculated: C:68.10%, H:6.59%, N:18.33%. Found C:67.43%, H:6.54%, N:17.90%.

5,6-Dimethyl-3-(4-(2-(4-methylpiperazin-1-yl)ethoxy)phenyl)-N-(pyridin-2-ylmethyl)pyrazolo[1,5-a]pyrimidin-7-amine (AWF947)



General procedure 3.4 The crude product was purified by column chromatography eluting with EtOAc to 5% MeOH:EtOAc to afford the Boc protected product. (0.10 g, 53%). **Melting point:** 102-104 °C **¹H NMR(400 MHz, DMSO-d₆)** δ 8.57 (d, J = 3.5 Hz, 1H), 8.44 (s, 1H), 8.05 (d, J = 8.1 Hz, 2H), 7.85 (s, 1H), 7.78 (t, J = 7.3 Hz, 1H), 7.38 (d, J = 7.6 Hz, 1H), 7.30 (d, J = 5.5 Hz, 1H), 6.97 (d, J = 8.1 Hz, 2H), 5.19 (d, J = 5.3 Hz, 2H), 4.08 (t, J = 4.8 Hz, 2H), 2.69 (t, J = 4.9 Hz, 2H), 2.51 (s, 4H), 2.48 (s, 3H), 2.34 (br s, 4H), 2.30 (s, 3H), 2.16 (s, 3H); **¹³C NMR (101 MHz, DMSO-d₆)** δ 159.3, 158.5, 156.6, 149.3, 145.8, 143.8, 140.5, 137.4, 126.7, 126.0, 122.8, 121.7, 115.0, 106.4, 96.5, 66.0, 57.2, 55.3, 53.5, 49.3, 46.2, 24.8, 13.2; **MS (ES⁺):** m/z (rel. Intensity) 472.3(100), 473.2 (30) HRMS (ES⁺) calcd for (C₂₇H₃₄N₇O):472.2825; found: 472.2818; **CHN analysis:** Calculated: C:67.76%, H:7.05%, N:20.79%. Found C:67.72%, H:6.98%, N:20.33%.

3.8 References

- (1) Paruch, K.; Dwyer, M. P.; Alvarez, C.; Brown, C.; Chan, T.-Y.; Doll, R. J.; Keertikar, K.; Knutson, C.; McKittrick, B.; Rivera, J.; Rossman, R.; Tucker, G.; Fischmann, T. O.; Hruza, A.; Madison, V.; Nomeir, A. A.; Wang, Y.; Lees, E.; Parry, D.; Sgambellone, N.; Seghezzi, W.; Schultz, L.; Shanahan, F.; Wiswell, D.; Xu, X.; Zhou, Q.; James, R. A.; Paradkar, V. M.; Park, H.; Rokosz, L. R.; Stauffer, T. M.; Guzi, T. J. Pyrazolo[1,5-A]pyrimidines as Orally Available Inhibitors of Cyclin-Dependent Kinase 2. *Bioorg. Med. Chem. Lett.* **2007**, *17* (22), 6220–6223.
- (2) Soares de Melo, C.; Feng, T.-S.; van der Westhuyzen, R.; Gessner, R. K.; Street, L. J.; Morgans, G. L.; Warner, D. F.; Moosa, A.; Naran, K.; Lawrence, N.; Boshoff, H. I. M.; Barry III, C. E.; Harris, C. J.; Gordon, R.; Chibale, K. Aminopyrazolo[1,5-A]pyrimidines as Potential Inhibitors of Mycobacterium Tuberculosis: Structure Activity Relationships and ADME Characterization. *Bioorg. Med. Chem.* **2015**, *23* (22), 7240–7250.
- (3) Adams, N. D.; Burgess, J. L.; Chaudhari, A. M.; Knight, S. D.; Parrish, C. A. Naphthyridine, Derivatives as p13 Kinase Inhibitors. EP2154965 (A1) — 2010-02-24
- (4) Timothy J. Guzi, Kamil Paruch, Michael P. Dwyer, David A. Parry, Lianyun Zhao, Patrick J. Curran, David B. Belanger, Blake Hamann, Panduranga Adulla P. Reddy, M. Arshad Siddiqui, Praveen K. Tadikonda Methods for Inhibiting Protein Kinases. *US2007105864 (A1)* — 2007-05-10.
- (5) Guzi Timothy J., Kamil Paruch, Dwyer Michael P., Doll Ronald J., Girijavallabhan Viyyoor M., Alvarez Carmen S., Tin-Yau Chan, Chad Knutson, Vincent Madison, Fischmann Thierry O., Dillard Lawrence W., Tran Vinh D., He Zhen Min, James Ray Anthony, Haengsoon Park, Weniger, Novel Pyrazolopyrimidines as Cyclin Dependent Kinase Inhibitors. *WO2007044401 (A2)* — 2007-04-19.
- (6) Gudmundsson, K. S.; Johns, B. A.; Weatherhead, J. Pyrazolopyrimidines and Pyrazolotriazines with Potent Activity against Herpesviruses. *Bioorg. Med. Chem. Lett.* **2009**, *19* (19), 5689–5692.
- (7) Ishikawa, M.; Hashimoto, Y. Improvement in Aqueous Solubility in Small Molecule Drug Discovery Programs by Disruption of Molecular Planarity and Symmetry. *J. Med. Chem.* **2011**, *54* (6), 1539–1554.
- (8) Schönherr, H.; Cernak, T. Profound Methyl Effects in Drug Discovery and a Call for New C-H Methylation Reactions. *Angew. Chemie Int. Ed.* **2013**, *52* (47), 12256–12267.
- (9) Schönherr, H.; Cernak, T. Profound Methyl Effects in Drug Discovery and a Call for New C-H Methylation Reactions. *Angew. Chemie Int. Ed.* **2013**, *52* (47), 12256–12267.
- (10) Berardi, F.; Abate, C.; Ferorelli, S.; de Robertis, A. F.; Leopoldo, M.; Colabufo, N. A.; Niso, M.; Perrone, R. Novel 4-(4-Aryl)cyclohexyl-1-(2-Pyridyl)piperazines as Δ^8 - Δ^7 Sterol Isomerase (Emopamil Binding

- Protein) Selective Ligands with Antiproliferative Activity. *J. Med. Chem.* **2008**, *51* (23), 7523–7531.
- (11) Kopecky, D. J.; Hao, X.; Chen, Y.; Fu, J.; Jiao, X.; Jaen, J. C.; Cardozo, M. G.; Liu, J.; Wang, Z.; Walker, N. P. C.; Wesche, H.; Li, S.; Farrelly, E.; Xiao, S.-H.; Kayser, F. Identification and Optimization of N3,N6-Diaryl-1H-pyrazolo[3,4-D]pyrimidine-3,6-Diamines as a Novel Class of ACK1 Inhibitors. *Bioorg. Med. Chem. Lett.* **2008**, *18* (24), 6352–6356.
- (12) Hwang, J. Y.; Smithson, D.; Zhu, F.; Holbrook, G.; Connelly, M. C.; Kaiser, M.; Brun, R.; Guy, R. K. Optimization of Chloronitrobenzamides (CNBs) as Therapeutic Leads for Human African Trypanosomiasis (HAT). *J. Med. Chem.* **2013**, *56* (7), 2850–2860.
- (13) Leung, S. C.; Gibbons, P.; Amewu, R.; Nixon, G. L.; Pidathala, C.; Hong, W. D.; Pacorel, B.; Berry, N. G.; Sharma, R.; Stocks, P. A.; Srivastava, A.; Shone, A. E.; Charoensutthivarakul, S.; Taylor, L.; Berger, O.; Mbekeani, A.; Hill, A.; Fisher, N. E.; Warman, A. J.; Biagini, G. A.; Ward, S. A.; O’Neill, P. M. Identification, Design and Biological Evaluation of Heterocyclic Quinolones Targeting Plasmodium Falciparum Type II NADH:Quinone Oxidoreductase (PfNDH2). *J. Med. Chem.* **2012**, *55* (5), 1844–1857.
- (14) Ritchie, T. J.; Macdonald, S. J. F. Physicochemical Descriptors of Aromatic Character and Their Use in Drug Discovery. *J. Med. Chem.* **2014**, *57* (17), 7206–7215.
- (15) Obach, R. S.; Kalgutkar, A. S.; Ryder, T. F.; Walker, G. S. In Vitro Metabolism and Covalent Binding of Enol-Carboxamide Derivatives and Anti-Inflammatory Agents Sudoxicam and Meloxicam: Insights into the Hepatotoxicity of Sudoxicam. *Chem. Res. Toxicol.* **2008**, *21* (9), 1890–1899.
- (16) St. Jean, D. J.; Fotsch, C. Mitigating Heterocycle Metabolism in Drug Discovery. *J. Med. Chem.* **2012**, *55* (13), 6002–6020.
- (17) Bégué, J.-P.; Bonnet-Delpon, D. Fluorinated Drugs. In *Bioorganic and Medicinal Chemistry of Fluorine*; John Wiley & Sons, Inc., 2008; pp 279–351.
- (18) Bégué, J.-P.; Bonnet-Delpon, D. Effects of Fluorine Substitution on Biological Properties. In *Bioorganic and Medicinal Chemistry of Fluorine*; John Wiley & Sons, Inc., 2008; pp 72–98.
- (19) Böhm, H.-J.; Banner, D.; Bendels, S.; Kansy, M.; Kuhn, B.; Müller, K.; Obst-Sander, U.; Stahl, M. Fluorine in Medicinal Chemistry. *ChemBioChem* **2004**, *5* (5), 637–643.
- (20) O’Hagan, D. Understanding Organofluorine Chemistry. An Introduction to the C-F Bond. *Chem. Soc. Rev.* **2008**, *37* (2), 308–319.
- (21) Hagmann, W. K. The Many Roles for Fluorine in Medicinal Chemistry. *J. Med. Chem.* **2008**, *51* (15), 4359–4369.
- (22) Purser, S.; Moore, P. R.; Swallow, S.; Gouverneur, V. Fluorine in Medicinal Chemistry. *Chem. Soc. Rev.*

- 2008, 37 (2), 320–330.
- (23) Muller, K.; Faeh, C.; Diederich, F. Fluorine in Pharmaceuticals: Looking beyond Intuition. *Science* **2007**, 317 (5846), 1881–1886.
- (24) Shah, P.; Westwell, A. D. The Role of Fluorine in Medicinal Chemistry. *J. Enzyme Inhib. Med. Chem.* **2007**, 22 (5), 527–540.
- (25) Clader, J. W. The Discovery of Ezetimibe: A View from Outside the Receptor. *J. Med. Chem.* **2004**, 47 (1), 1–9.
- (26) Bi, Y.; Kumi, G. Preparation of Methyloxetanyl Methoxy Pyridinyl Pyrazolopyrimidinyl Piperazine Carboxylate Derivatives for Use as Adapter Associated Kinase 1 Inhibitors., WO2015142714A1, 2015.
- (27) Bhide, R. S.; Duncia, J. V.; Hynes, J.; Nair, S. K.; Pitts, W. J.; Kumar, S. R.; Gardner, D. S.; Murugesan, N.; Paidi, V. R.; Santella III, J. B.; Sistla, R. K.; Wu, H. Substituted Pyridinecarboxamide Compounds as Kinase Modulators and Their Preparation., WO2014074657A1, 2014.
- (28) Kosugi, T.; Mitchell, D. R.; Fujino, A.; Imai, M.; Kambe, M.; Kobayashi, S.; Makino, H.; Matsueda, Y.; Oue, Y.; Komatsu, K.; Imaizumi, K.; Sakai, Y.; Sugiura, S.; Takenouchi, O.; Unoki, G.; Yamakoshi, Y.; Cunliffe, V.; Frearson, J.; Gordon, R.; Harris, C. J.; Kalloo-Hosein, H.; Le, J.; Patel, G.; Simpson, D. J.; Sherborne, B.; Thomas, P. S.; Suzuki, N.; Takimoto-Kamimura, M.; Kataoka, K. Mitogen-Activated Protein Kinase-Activated Protein Kinase 2 (MAPKAP-K2) as an Antiinflammatory Target: Discovery and in Vivo Activity of Selective Pyrazolo[1,5-A]pyrimidine Inhibitors Using a Focused Library and Structure-Based Optimization Approach. *J. Med. Chem.* **2012**, 55 (15), 6700–6715.
- (29) Meanwell, N. A. Synopsis of Some Recent Tactical Application of Bioisosteres in Drug Design. *J. Med. Chem.* **2011**, 54 (8), 2529–2591.
- (30) Lovering, F.; Bikker, J.; Humblet, C. Escape from Flatland: Increasing Saturation as an Approach to Improving Clinical Success. *J. Med. Chem.* **2009**, 52 (21), 6752–6756.
- (31) Brown, A.; Brown, T. B.; Calabrese, A.; Ellis, D.; Puhalo, N.; Ralph, M.; Watson, L. Triazole Oxytocin Antagonists: Identification of an Aryloxyazetidone Replacement for a Biaryl Substituent. *Bioorg. Med. Chem. Lett.* **2010**, 20 (2), 516–520.
- (32) Degorce, S. L.; Barlaam, B.; Cadogan, E.; Dishington, A.; Ducray, R.; Glossop, S. C.; Hassall, L. A.; Lach, F.; Lau, A.; McGuire, T. M.; Nowak, T.; Ouvry, G.; Pike, K. G.; Thomason, A. G. Discovery of Novel 3-Quinoline Carboxamides as Potent, Selective, and Orally Bioavailable Inhibitors of Ataxia Telangiectasia Mutated (ATM) Kinase. *J. Med. Chem.* **2016**, 59 (13), 6281–6292.
- (33) Abe, H.; Kikuchi, S.; Hayakawa, K.; Iida, T.; Nagahashi, N.; Maeda, K.; Sakamoto, J.; Matsumoto, N.; Miura, T.; Matsumura, K.; Seki, N.; Inaba, T.; Kawasaki, H.; Yamaguchi, T.; Kakefuda, R.; Nanayama, T.;

- Kurachi, H.; Hori, Y.; Yoshida, T.; Kakegawa, J.; Watanabe, Y.; Gilmartin, A. G.; Richter, M. C.; Moss, K. G.; Laquerre, S. G. Discovery of a Highly Potent and Selective MEK Inhibitor: GSK1120212 (JTP-74057 DMSO Solvate). *ACS Med. Chem. Lett.* **2011**, *2* (4), 320–324.
- (34) Wityak, J.; Das, J.; Moquin, R. V.; Shen, Z.; Lin, J.; Chen, P.; Doweiko, A. M.; Pitt, S.; Pang, S.; Shen, D. R.; Fang, Q.; de Fex, H. F.; Schieven, G. L.; Kanner, S. B.; Barrish, J. C. Discovery and Initial SAR of 2-Amino-5-Carboxamidothiazoles as Inhibitors of the Src-Family Kinase p56Lck. *Bioorg. Med. Chem. Lett.* **2003**, *13* (22), 4007–4010.
- (35) Lipinski, C. A.; Lombardo, F.; Dominy, B. W.; Feeney, P. J. Experimental and Computational Approaches to Estimate Solubility and Permeability in Drug Discovery and Development Settings. *Adv. Drug Deliv. Rev.* **1997**, *23* (1), 3–25.
- (36) Gleeson, M. P. Generation of a Set of Simple, Interpretable ADMET Rules of Thumb. *J. Med. Chem.* **2008**, *51* (4), 817–834.
- (37) Hwang, J. Y.; Windisch, M. P.; Jo, S.; Kim, K.; Kong, S.; Kim, H. C.; Kim, S.; Kim, H.; Lee, M. E.; Kim, Y.; Choi, J.; Park, D.-S.; Park, E.; Kwon, J.; Nam, J.; Ahn, S.; Cechetto, J.; Kim, J.; Liuzzi, M.; No, Z.; Lee, J. Discovery and Characterization of a Novel 7-aminopyrazolo[1,5-A]pyrimidine Analog as a Potent Hepatitis C Virus Inhibitor. *Bioorg. Med. Chem. Lett.* **2012**, *22* (24), 7297–7301.
- (38) Marwaha, A.; White, J.; El-Mazouni, F.; Creason, S. A.; Kokkonda, S.; Buckner, F. S.; Charman, S. A.; Phillips, M. A.; Rathod, P. K. Bioisosteric Transformations and Permutations in the Triazolopyrimidine Scaffold To Identify the Minimum Pharmacophore Required for Inhibitory Activity against Plasmodium Falciparum Dihydroorotate Dehydrogenase. *J. Med. Chem.* **2012**, *55* (17), 7425–7436.
- (39) Ni, C.; Zhang, Y.; Zhao, Y.; Zhu, L. Synthesis and Bioactivity of pyrazolo[1,5-A]pyrimidine Derivatives as Novel c-Met Inhibitors. *Youji Huaxue* **2012**, *32* (12), 2294–2299.
- (40) Wallace, E.; Seo, J.; Lyssikatos, J. P.; Yang, H. W.; Hurley, T. B.; Blake, J.; Marlow, A. L. Preparation of Pyrazolopyrimidines and Related Compounds as MEK Kinase Inhibitors for Treatment of Hyperproliferative Disorders., WO2005051906A2, June 9, 2005.
- (41) Phillips, M.; Rathod, P. K.; Gujjar, R.; Marwaha, A. S.; Charman, S. A. Dihydroorotate Dehydrogenase Inhibitors with Selective Anti-Malarial Activity., WO2009082691A1, July 2009.

Chapter 4

Lead Optimisation and Advanced Biological Evaluation

Contents

Chapter 4 Lead Optimisation and Advanced Biological Evaluation	172
4.1 Early-Lead Optimisation Summary (Chapter 3)	172
4.2 Lead optimisation	173
4.2.1 R ¹ position optimisation; saturated heterocyclic rings.....	173
4.2.2 3-(R), 5-(H), 6-(R), Pyrazolopyrimidine	179
4.3 Advanced Biological Evaluation	183
4.3.1 <i>In vitro</i> Brugia malayi microfilariae studies	183
4.3.2 Assessment of permeability, efflux ratio, <i>in vitro</i> toxicity and CYP inhibition of selected frontrunners.....	186
4.3.3 <i>In vivo</i> assays.....	191
4.4 Conclusions	196
4.5 Future Work	197
4.6 Experimental	199
4.7 References	210

Chapter 4 Lead Optimisation and Advanced Biological Evaluation

4.1 Early-Lead Optimisation Summary (Chapter 3)

The early lead development carried out in the previous chapter is depicted below in **Fig 4.1** with the DMPK properties of these important analogues displayed.

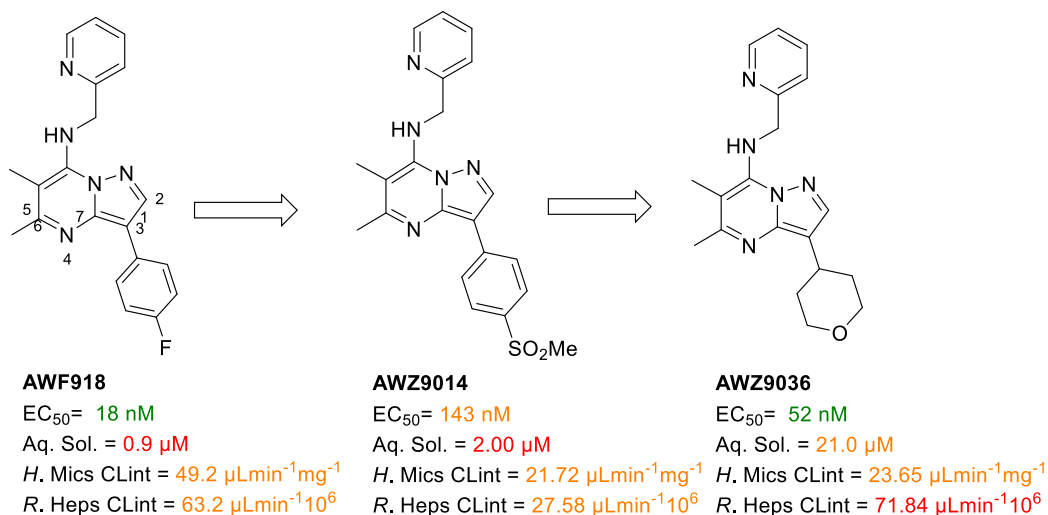


Fig 4.1 Early-lead optimisation as discussed throughout **Chapter 3**.

Removal of the unsaturated aryl ring systems at the 3-position, seen in earlier pyrazolopyrimidine analogues such as **AWZ918** or **AWZ9014** resulted in greatly improved aqueous solubility. Compounds lacking 3-position substituents or with small substituents had very poor metabolic stability. Incorporation of a tetrahydropyran (THP) ring at the 3-position produced **AWZ9036** (**Fig 4.1**); this THP analogue possessed the best balance of whole-cell anti-*Wolbachia* activity and DMPK properties seen during work on the pyrazolopyrimidine chemotype so far. It was still necessary to enhance these DMPK properties to meet the desired ranges as defined earlier in Chapter 1 Section 7.2 these are shown below in **Table 4.1**.

	EC_{50} (nM)	LogD 7.4	Aq.Sol (μM)	H.M.Cl ($\mu\text{L}/\text{min}/\text{mg}$)	R.HepsCl ($\mu\text{L}/\text{min } 10^{-6}$)	Human PPB (%)
Desired	<100	1-4	>50	<20	<20	<99
Acceptable	100-300	0-1,4-5	20-50	20-60	20-60	<99.5
Poor	300+	<0, 5+	<20	>60	>60	>99.5

Table 4.1 A table highlighting appropriate and inappropriate potency and DMPK values.

Whilst the table displays that analogues possessing EC_{50} values lower than 100 nM are considered good, a more desirable target was set at <30 nM. It was observed that analogues possessing higher potency were more likely to translate to acceptable *in vivo* efficacy.

The *in vitro* whole-cell potency and DMPK properties for the first pyrazolopyrimidines substituted with saturated ring systems (See Chapter 3) are displayed below in **Fig. 4.2**

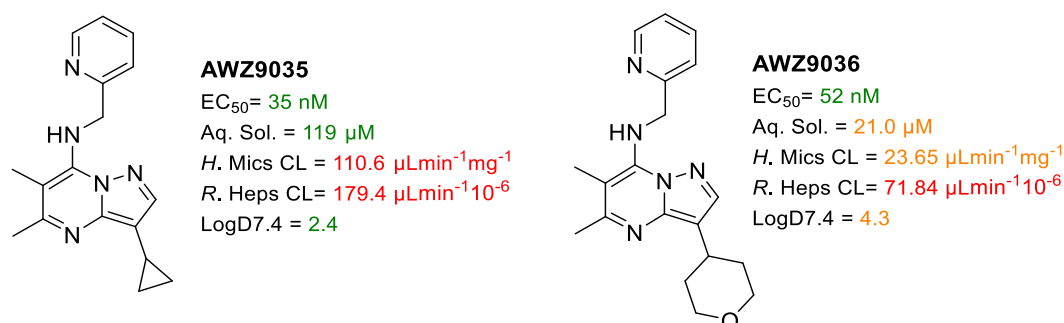


Fig 4.2 DMPK properties and whole-cell anti-*Wolbachia* activity for **AWZ9035** and **AWZ9036**.

These analogues served as the starting points for further optimisation of pyrazolopyrimidine compounds discussed below.

4.2 Lead optimisation

4.2.1 R¹ position optimisation; saturated heterocyclic rings.

As the binding site of metabolising enzymes are generally lipophilic, more polar compounds tend to undergo reduced metabolism.^{1,2} As such, reducing the overall hydrophobicity of the saturated ring system in compounds can be achieved by reducing the ring size.³⁻⁵ Reducing saturated heterocyclic ring size has successfully been employed to reduce metabolism in a variety of drug discovery programs. One example of this is seen during the optimisation of a series of γ -secretase inhibitors by Stepan *et al* is summarised below in **Fig4.3**. Within this work the THP ring in **1a** was reduced in size to give **2a** and subsequently **3a** with improved metabolic stability. The authors also acknowledged a link that reducing LogD_{7.4} results in improved metabolic stability which has previously been noted in some of our analogues (Chapter 2).⁵

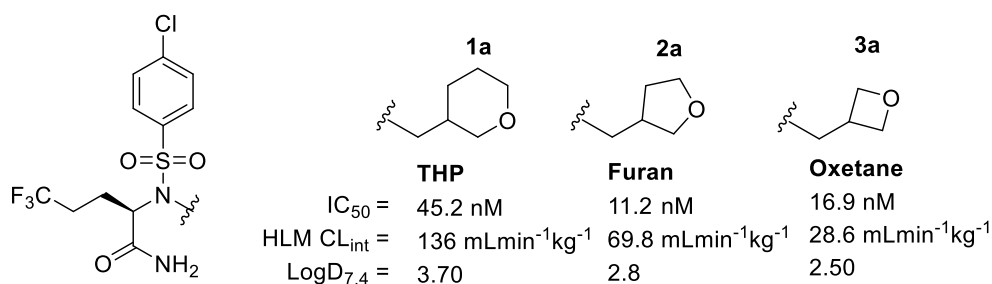


Fig 4.3 Reducing ring size from a tetrahydropyran to an oxetane ring to improve compound metabolic stability.

Another example of reducing in saturated ring size to produce more promising DMPK properties was seen during the optimisation of a series of anti-cancer aurora kinase inhibitors (**Fig 4.4**). During this work, reducing the ring size of **4a** with a 4-fluoro piperidine ring to a 3-difluoro pyrrolidine ring in **5a** served to improve the bioavailability following oral dosing during *in vivo* mouse PK studies.³

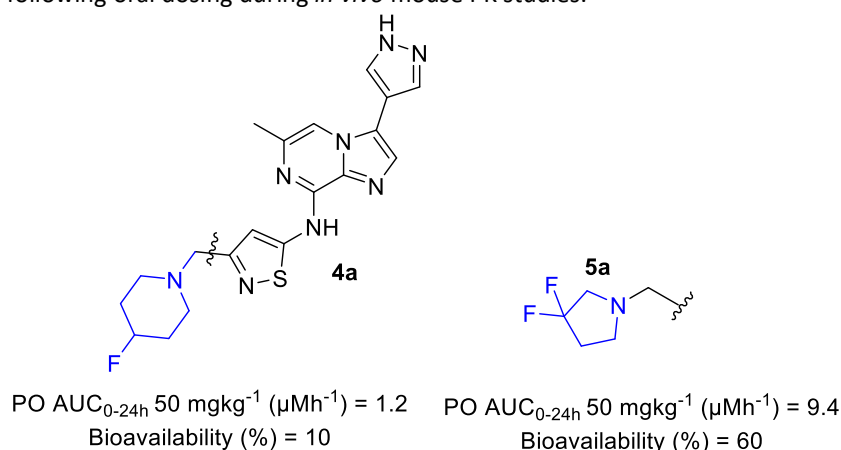


Fig 4.4 Reduction in 4-fluoro piperidine ring size to improve the oral bioavailability in a series of aurora kinase inhibitors.

These examples further support the investigation of smaller saturated heterocyclic rings during the late-stage optimisation of our pyrazolopyrimidine analogues.

Within the optimisation of compounds in other drug discovery projects, introduction of morpholine ring systems can result in improved activity.^{4,6} One example of the successful incorporation of a morpholine ring is represented in **Fig 4.5**, where a pyrrolidine ring has been replaced in **6a** for a morpholine functionality in **7a** during the optimisation of a set of hepatitis C virus NS5B inhibitors.⁶ The authors Dragovich *et al.*, reported a 6-fold increase in compound half-life when incubated with human liver microsomes upon introduction of this morpholine ring system (**Fig 4.5**).

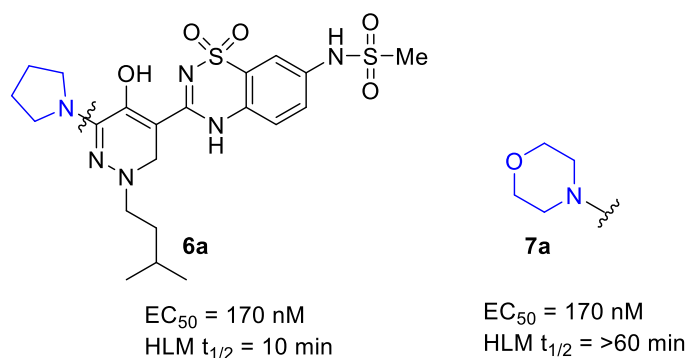


Fig 4.5 Introduction of a morpholine ring to greatly improve compound half-life when incubated with human liver microsomes.

This observed improvement in metabolic stability seems conserved upon incorporation of a morpholine ring to replace saturated nitrogen heterocycles. During a program optimising a series of cannabinoid receptor 2 agonists, both a piperidine ring (**9a**) and a 4,4-difluoro piperidine ring (**10a**) resulted in inferior stability when incubated with rat liver microsomes to the respective morpholine analogue derivative **11a** (Fig 4.6).⁴

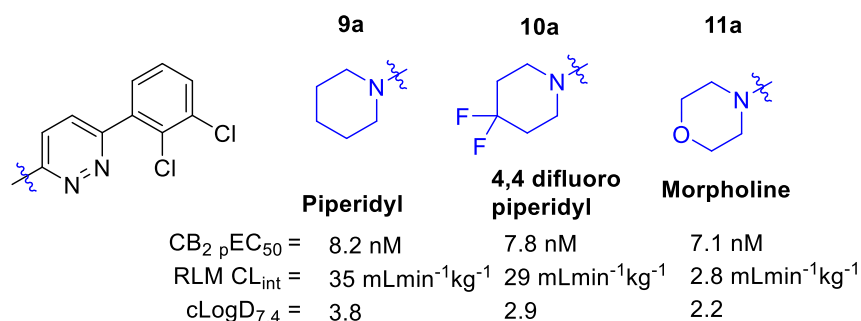


Fig. 4.6 Incorporation of various saturated nitrogen heterocycles during optimisation of cannabinoid receptor 2 agonists.

This improvement in metabolic stability also follows the trend that reduction in cLogD_{7.4} generally improves metabolic stability and should also benefit the aqueous solubility if introduced into our pyrazolopyrimidine analogues.⁴ Saturated heterocycles are also prone to metabolism at the heteroatom or at the position adjacent to the heteroatom.⁷ For this reason, we designed a number of analogues containing 4-*N*-Me piperidine at the 3- (R¹) position (Fig 4.7) and a variety of nitrogen containing heterocycles (morpholine & pyrrolidine) with the nitrogen directly attached to the pyrazolopyrimidine core.

The study of saturated heterocyclic ring systems at the 3-(R¹) position of the pyrazolopyrimidine core was carried out in parallel to further study of a chloride substituent at the 6-(R³) position (Fig 4.7). The pyrazolopyrimidine analogues designed for synthesis following the successful incorporation of various saturated heterocyclic rings in previous drug discovery projects are displayed in Fig. 4.7.

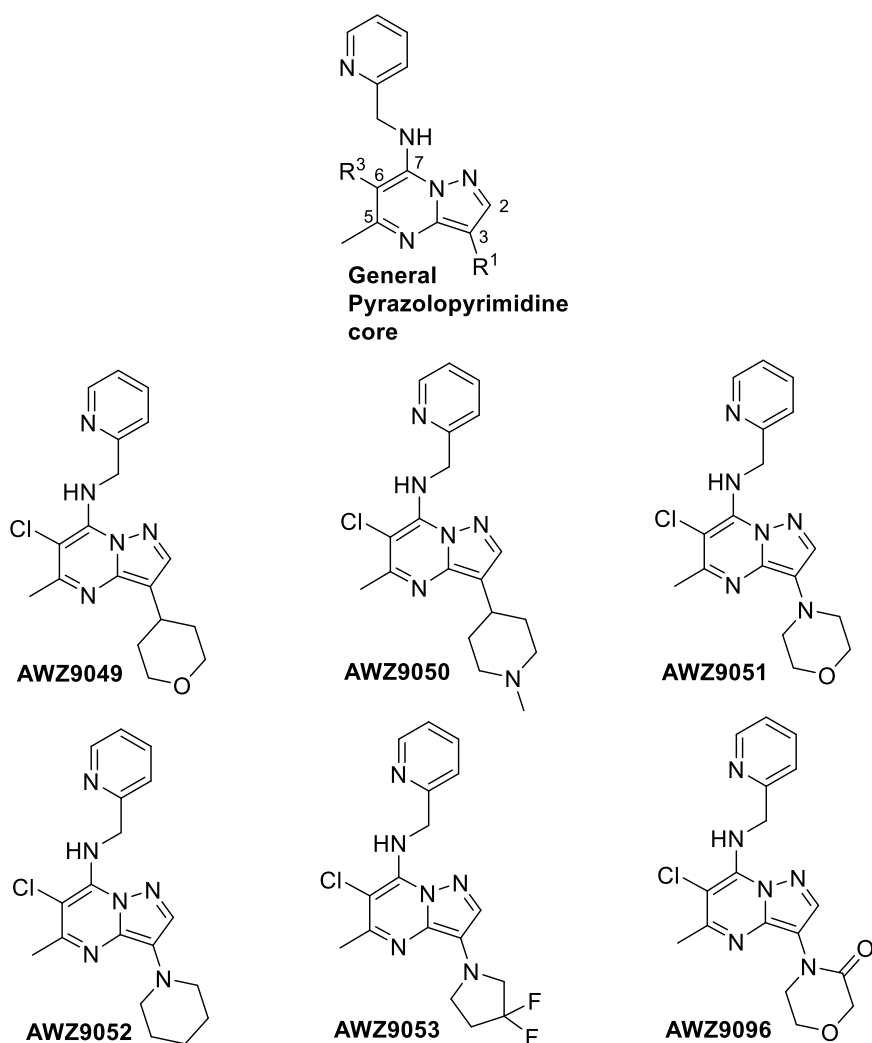
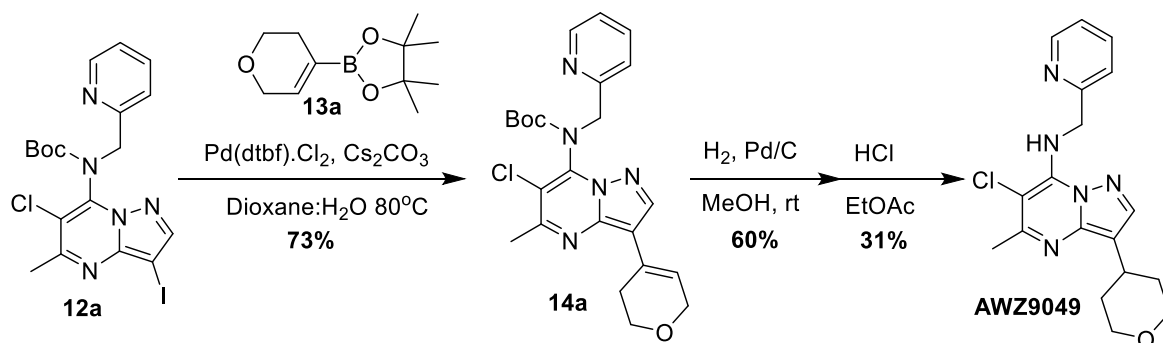


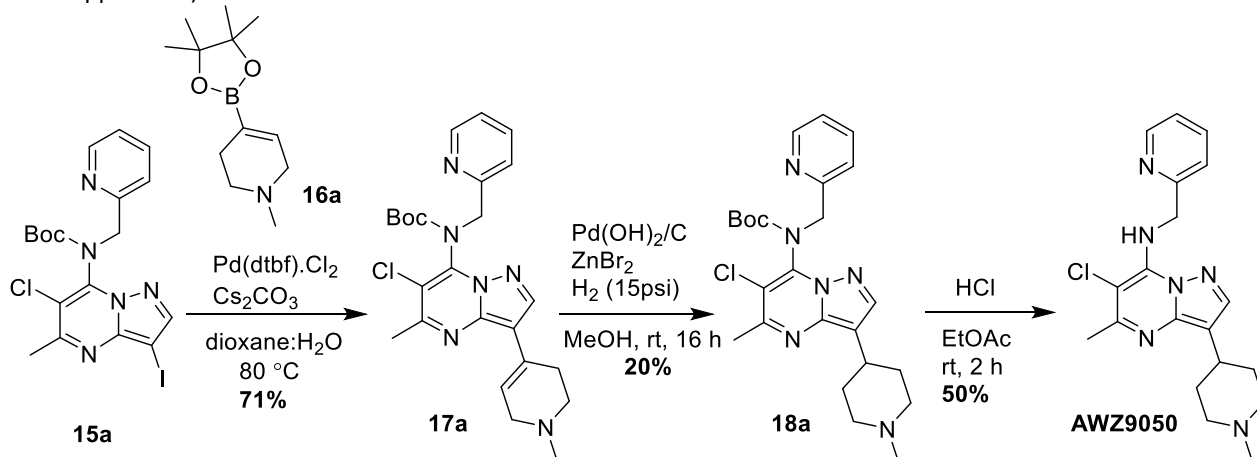
Fig 4.7 Pyrazolopyrimidines with saturated heterocycles at the R¹ position designed for synthesis.

The first in this series of analogues was **AWZ9049** (Fig 4.7) containing the tetrahydropyran ring. This target was prepared by coupling of the dihydropyran boronic ester **13a** with the iodo intermediate **12a** and subsequent hydrogenation of **14a** as depicted in **Scheme 4.1**.



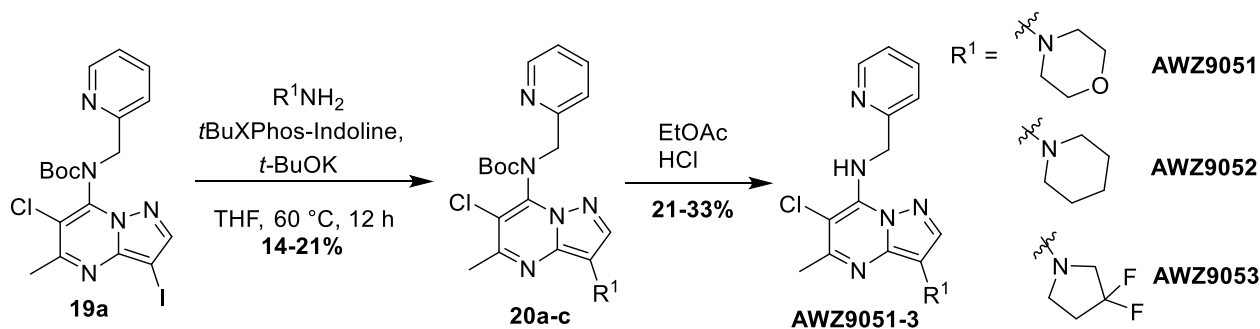
Scheme 4.1 Synthesis of **AWZ9049** via coupling of dihydropyran pinacol ester

The chosen synthesis of the 4-*N*-Me piperidiny analogue, **AWZ9050**, is depicted below in **Scheme 4.2**. This utilises similar chemistry to the synthesis of **AWZ9049**, requiring hydrogenation of the piperidyl ring intermediate **17a** which was carried out using palladium hydroxide on carbon and zinc bromide. Finally, Boc-deprotection of **18a** gave the desired 4-piperidyl pyrazolopyrimidine **AWZ9050**. (For experimental details see Appendix 1).



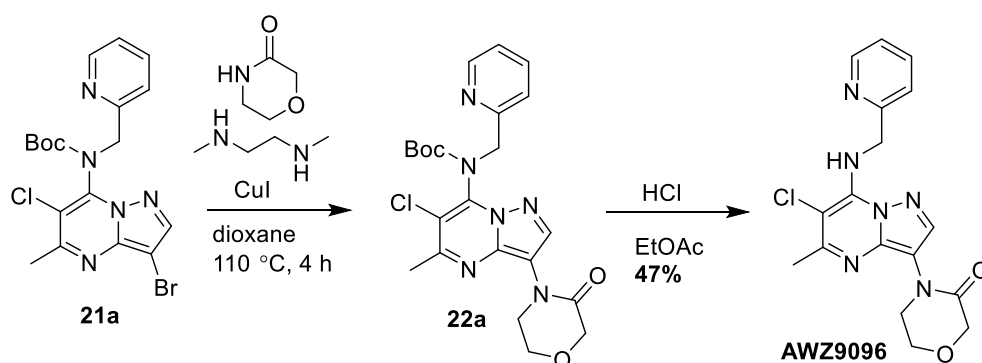
Scheme 4.2 Synthesis of 4-*N*-Methyl piperidyl analogue **AWZ9050**.

Analogues **AWZ9051-3** all possess ring systems containing a C-N bond to the pyrazolopyrimidine core at the R¹ position. These compounds were synthesised by collaborators WuXi App Tech using Buchwald-Hartwig aminations from the Boc protected iodo intermediate **19a** (**Scheme 4.3**). Boc-deprotection of the intermediates **20a-c** gave the desired products **AWZ9051-3** (See appendix 1 for experimental details).



Scheme 4.3 Synthesis of pyrazolopyrimidines with various saturated nitrogen heterocycles.

Compound **AWZ9096** (**Scheme 4.4** below) containing the 3-morpholinone ring was the final compound synthesised in this series and was prepared by a copper-mediated Goldberg reaction on **21a** as displayed below in **Scheme 4.4**.



Scheme 4.4 Goldberg reaction towards the 3-morpholinone analogue **AWZ9096**

The results from the biological evaluation of these compounds are displayed below in **Table 4.2**.

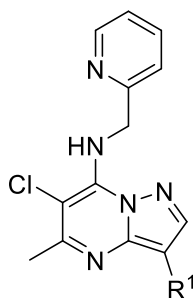


Table entry	Molecule	R ¹	EC ₅₀ (nM)	LogD 7.4	Aq. Sol (μM)	Human Mics C _{Lint} (μLmin ⁻¹ mg ⁻¹)	Rat Heps C _{Lint} (μLmin ⁻¹ 10 ⁻⁶)	PPB (%)
1	AWZ9049		73	3.4	7	83.92	108.5	96.3
2	AWZ9050		561	1.4	>1000	8.84	17.43	58
3	AWZ9051		9	2.3	49	72.89	72.90	93.8
4	AWZ9052		38	ND	ND	ND	ND	ND
5	AWZ9053		16	ND	11	116.8	>300	43
6	AWZ9096		1183	1.4	82	7.7	7.7	60

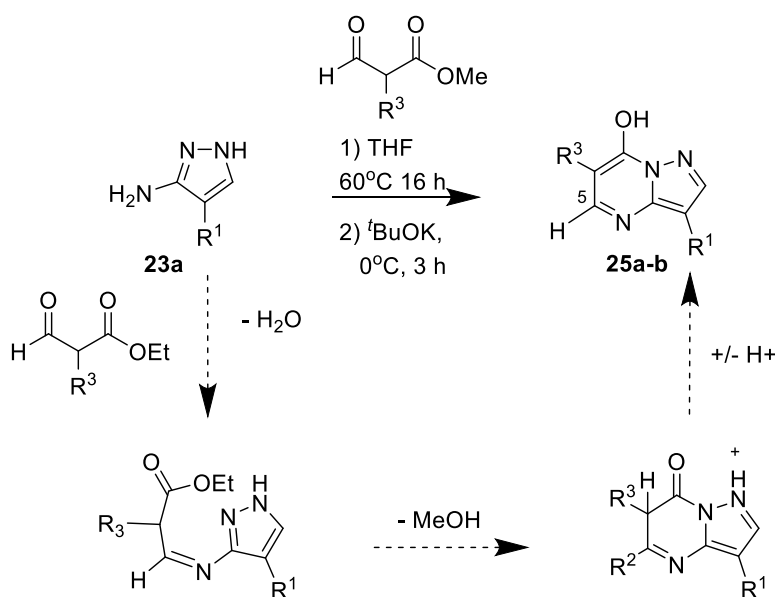
NA – No activity at highest concentration (5 μM) ND – Not determined

Table 4.2 *in vitro* whole-cell anti-*Wolbachia* and DMPK properties

AWZ9049 (table entry 1) which contained a THP ring at the R¹ position maintained high potency (EC₅₀ = 73 nM) as is seen in the first THP analogue (**AWZ9036** EC₅₀ = 52 nM). In this analogue, the chloro substituent at the R³ position did appear to negatively impact both potency and DMPK properties; the solubility and metabolic stability decreased three-fold because of this alteration compared to the 6-methyl derivative **AWZ9036** (Chapter 3.6 – Scheme 3.7). While the 4-piperidyl analogue **AWZ9050** in table entry 2 possessed an excellent DMPK profile (Aq. Sol = 1000 μM, clearance values <20), it suffered from an eight-fold drop in potency (EC₅₀ = 561 nM). The analogues **AWZ9051-3** (entries 3-5) possessed very promising anti-*Wolbachia* activity however synthesis of these compounds was difficult. The Buchwald-Hartwig aminations to **AWZ9051-3** provided very poor yields and purification proved troublesome requiring preparative-TLC in the final two steps. Also, despite promising whole-cell activity and acceptable aqueous solubility, these analogues did not possess any greatly improved metabolic stability over the THP analogue **AWZ9049**. Finally, the 3-morpholinone analogue **AWZ9096** in table entry 6 displayed greatly reduced *in vitro* whole-cell activity (EC₅₀ = 1183 nM), though significant gains were seen in aqueous solubility and metabolic stability.

4.2.2 3-(*R*), 5-(*H*), 6-(*R*), Pyrazolopyrimidine

Removal of the lipophilic methyl group at the 5-position of the pyrazolopyrimidine core could help enhance the aqueous solubility during optimisation of future analogues. A variety of pyrazolopyrimidines were designed for synthesis which were unsubstituted at the 5-position (R² = H). These analogues were prepared by the reaction of the necessary pyrazole **23a** with the desired aldehyde **24a** (Scheme 4.4). This reaction proceeds *via* an imine intermediate by reaction of the pyrazole amine and the aldehyde of the dicarbonyl. This imine intermediate then cyclises to give the pyrazolopyrimidine **25a** upon addition of base (potassium *tert*-butoxide) to give the essential 5-H 7-hydroxy pyrazolopyrimidine (**25a-b**) which can then be subjected to the various reactions discussed extensively throughout this work to produce a variety of pyrazolopyrimidines.



Scheme 4.5 Synthesis of pyrazolopyrimidines with unsubstituted R² positions (R²=H)

Several of the important analogues from this series are displayed in **Fig 4.8** alongside their respective 5-H analogues. The 3-Cl analogues were obtained by treating the R¹ analogues with NCS using chemistry discussed previously (See **Chapter 3 Scheme 3.4**). The 4-fluoro phenyl and 4-SO₂Me phenyl analogues were prepared by the Suzuki coupling synthesis discussed earlier during the study of the R¹ position (**Chapter 3 Scheme 3.3**) (See Appendix 1 for experimental details). The tetrahydropyran analogues were prepared by the introduction of a dihydropyran pinacol ester into the essential iodo-intermediate using the coupling reactions reviewed in the previous chapter (**Scheme 3.3**)

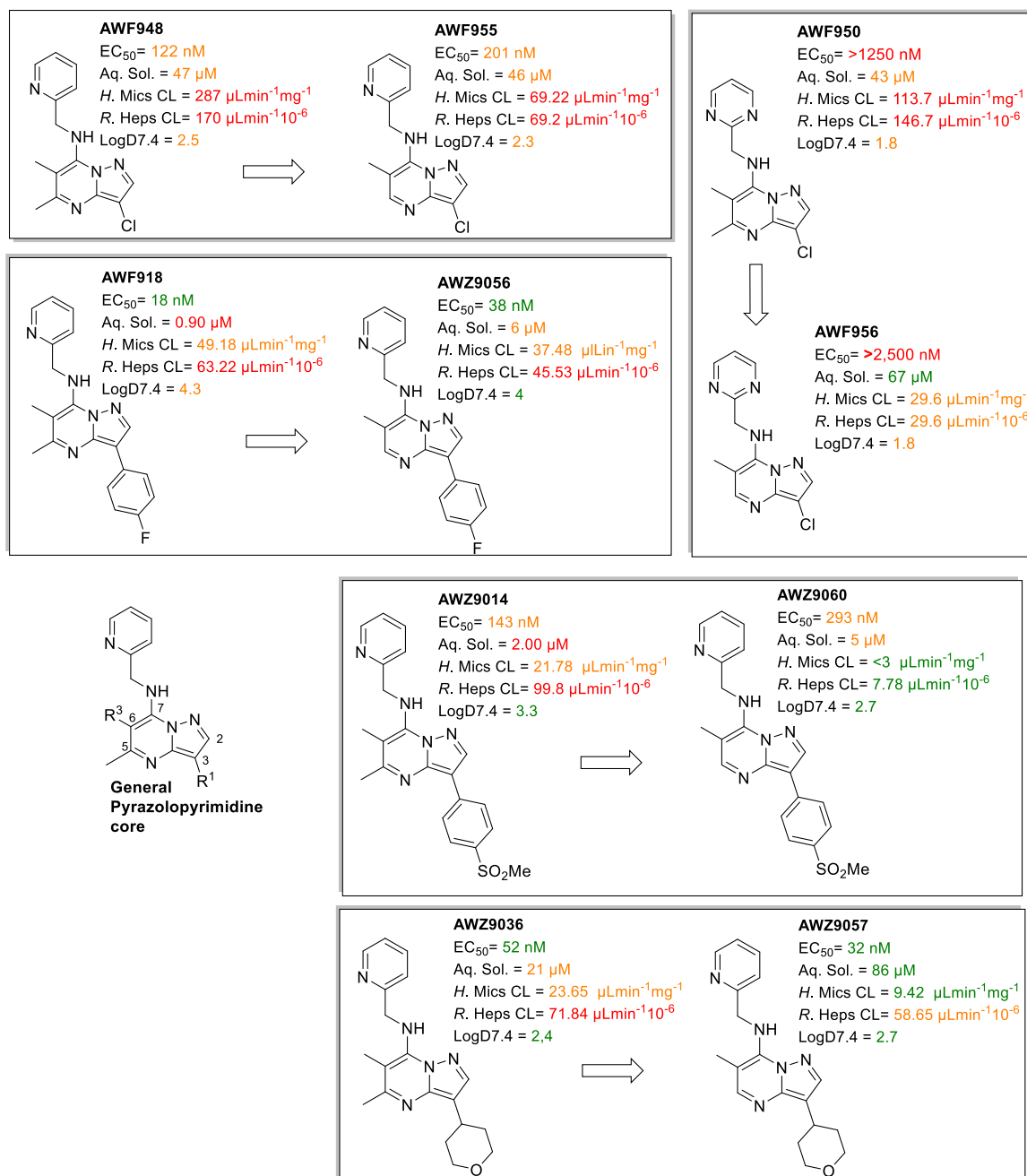
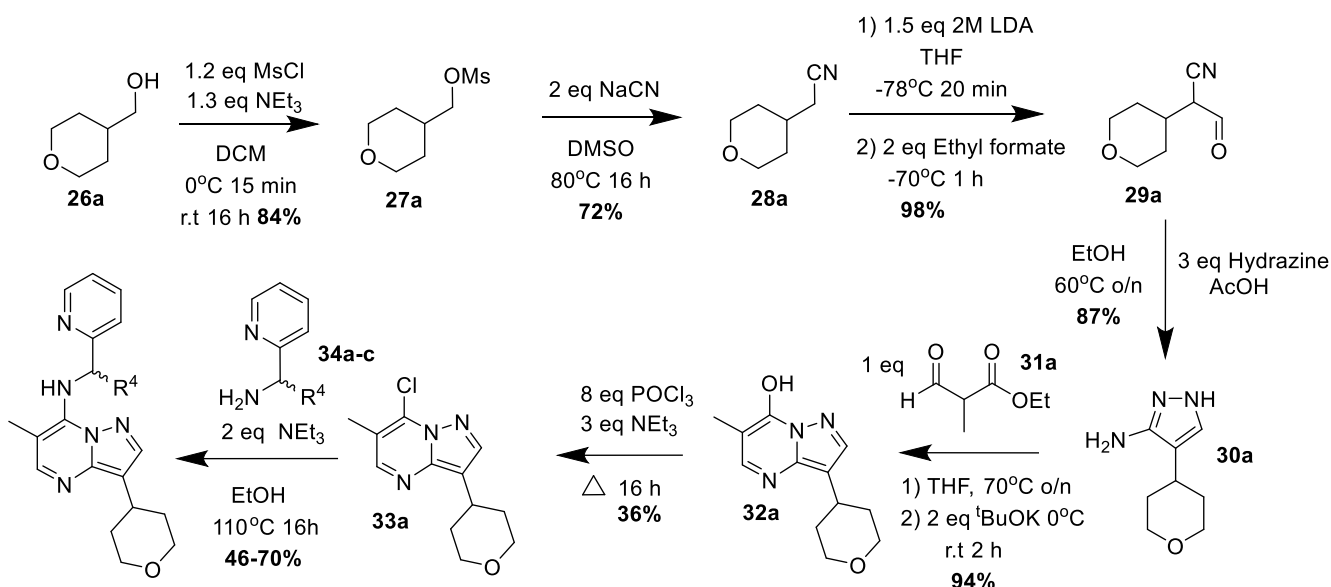


Fig 4.8 Comparison of 5-H analogues with their 6-Me parents.

The 5-H analogues in general show similar anti-*Wolbachia* activity compared to their respective 5-Me analogues, while possessing superior aqueous solubility. The 3-Cl analogue **AWF948** experienced a significant improvement in metabolic stability as shown by the reduced clearance values upon removal of the 5-methyl group of **AWF948** (>150) compared with **AWF955** (<70). The 4-fluoro phenyl analogue **AWF918** also experiences an improvement in aqueous solubility upon removal of the 5-methyl substituent giving **AWZ9056** (0.9 to 6 μM in). However, this does not result in any improvement to metabolic stability that is seen in other analogues. The 4-SO₂Me phenyl analogue **AWZ9014**, with only moderate activity relative to other analogues (EC_{50} = 143 nM), benefited from over a 2-fold improvement in aqueous solubility upon removal of the 5-Me to give **AWZ9060** (2 to 5 μM). **AWZ9060** also possessed an excellent stability profile (Human microsomal clearance <3 $\mu\text{Lmin}^{-1}\text{mg}^{-1}$, Rat Hepatocyte clearance 7.78 $\mu\text{Lmin}^{-1}\text{10}^{-6}$). Finally, the THP analogue **AWZ9036** displays an improvement to both potency and DMPK properties upon removal of this methyl group to give **AWZ9057**. This analogue was the current lead resulting from the work on the pyrazolopyrimidine chemotype at this point.

This improvement to overall DMPK properties upon removal of the methyl seemed so conserved across our analogues that we incorporated this substitution pattern into our core motif during further optimisation studies. With the tetrahydropyran analogues possessing the best balance of potency and DMPK properties examined so far it was desirable to produce a more optimised route specific for producing these analogues. This was achieved by the reactions shown in **Scheme 4.6** which involved production of the 3-THP 5-amino-pyrazole **30a**.



Scheme 4.6 Optimised pathway to tetrahydropyran analogues

This synthesis involved mesylation of the commercially available alcohol **26a** with mesyl chloride (MsCl); this proceeded with a good yield of 84%. The intermediate **27a** was then substituted using sodium cyanide in DMSO to give the necessary nitrile **28a** with a high yield of 72%. Following previously discussed chemistry the pyrazole **30a** is obtained by treating the nitrile **28a** with base (LDA) followed by ethyl formate to give the aldehyde **29a** which cyclises upon treatment with hydrazine granting nearly quantitative yields over the two steps. Formation of the pyrazolopyrimidine core was again performed using a base catalysed procedure allowing the intermediate imine to form between the amine of the pyrazole **30a** and the aldehyde of the necessary dicarbonyl compound **31a** to give **32a**. Finally, chlorination using 8 eq POCl₃ and 3 eq NEt₃ (Scheme 4.6) provided the important 7-chloro pyrazolopyrimidine **33a** in a moderate yield of 36% which could then be substituted with 2-pyridyl methanamine **34a-c** as displayed below. It was important to adopt this synthesis to produce enough of the THP analogues for advanced biological evaluation.

To improve further the metabolic stability of the current lead **AWZ9057**, the corresponding analogue with a methylated linker, **AWZ9100** (R⁴ = Me) (Fig 4.9) was prepared. Methylation of the linker was explored in earlier analogues where a small decrease in activity was seen; previously methylation was the only alteration to the linker that did not completely remove anti-*Wolbachia* activity. The two stereoisomers of **AWZ9100** (Fig 4.9) were also produced to determine any differences in activity and metabolic stability between the two enantiomers. The stereochemisomeric pure amines were purchased from Fluorochem and used as received (purity >95%); the measured *in vitro* whole cell potency and DMPK properties are shown in Fig 4.9.

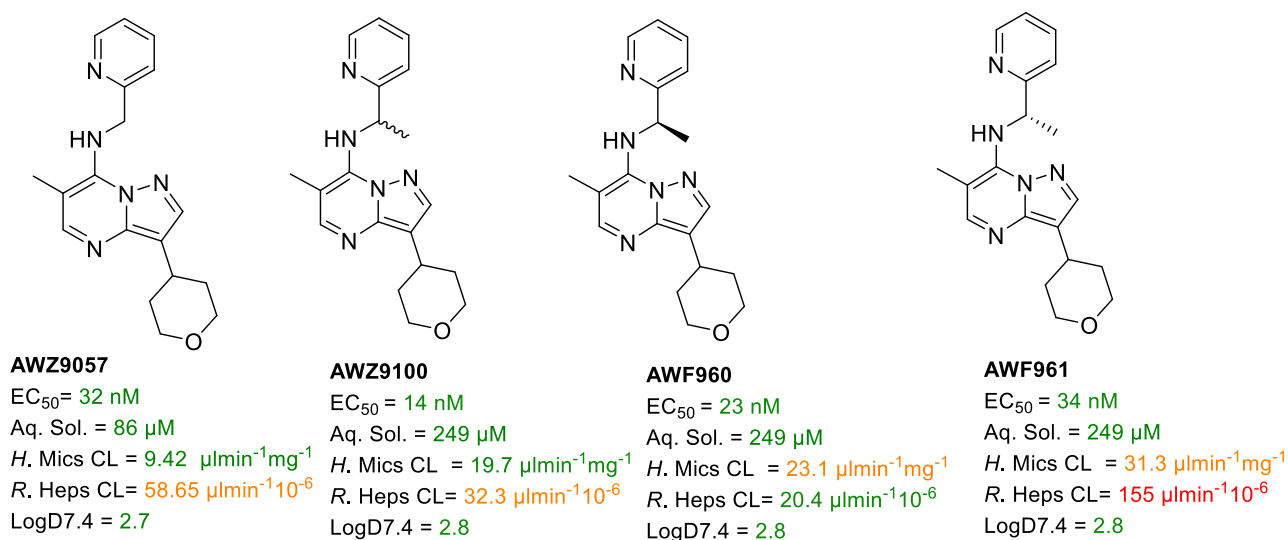
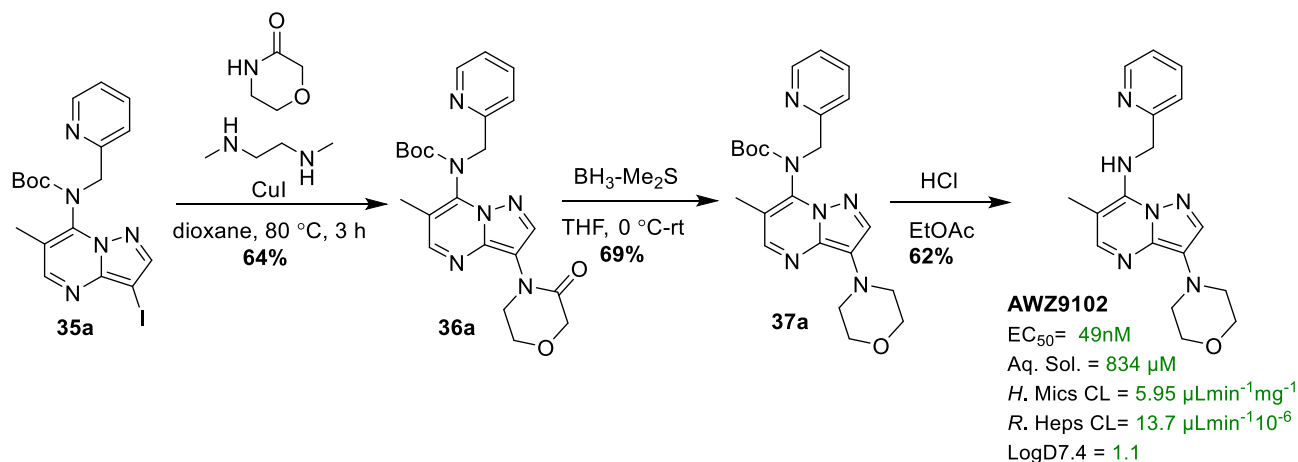


Fig 4.9 Structure of the lead tetrahydropyran analogue **AWZ9100** with the pure stereoisomers.

Within the analogues above, methylation of the linker appears to significantly boost aqueous solubility when comparing **AWZ9057** with **AWZ9100**. Considering the promising DMPK properties seen upon incorporation of a morpholine ring at the R¹ position our collaborators WuXi App Tech produced the 3-morpholine 5-H analogue (**AWZ9102** – **Scheme 4.6**). This involved another copper catalysed Goldberg reaction to form the 3-morpholinone intermediate **36a** which was reduced to give the Boc-protected 3-morpholine analogue **37a**. Compound **AWZ9102** was then reached by Boc-deprotection of **37a** as displayed in **Scheme 4.6** alongside the measured *in vitro* whole-cell potency and DMPK properties.



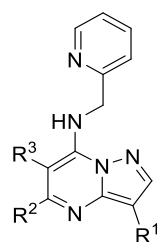
Scheme 4.7 Synthesis of the R¹ morpholino compound **AWZ9102**

Whilst the profile of **AWZ9102** looks excellent, development work will be required to optimise this synthesis. With increased pressure to select a candidate, the current lead from this work, **AWZ9100**, was taken forward for advanced biological assessment to compare with lead candidates from other small-molecule templates.

4.3 Advanced Biological Evaluation

4.3.1 *In vitro* *Brugia malayi* microfilariae studies

An *in vitro* mf assay was developed by the Liverpool School of Tropical medicine to allow for assessment of direct worm toxicity and activity against *Wolbachia* bacteria present within the mf of *B. malayi*. From observations concerning undesirable direct worm toxicity made on other templates within the programme, several important compounds containing the pyrazolopyrimidine chemotype were chosen for assessment against microfilaria (Mf) of *B. malayi* using DMSO as a negative control (**Table 4.3**). Direct worm toxicity of important compounds was assessed by using a microfilariae motility score at day 6. These values indicate the viability of the microfilariae following treatment with values ranging from 0 to 4 with scores near to zero suggesting that all microfilariae are immotile or dead (also displayed in the table below is the initial *in vitro* whole-cell potency).



Compound code	R ¹	R ²	R ³	EC ₅₀ (nM)	Mf motility score
DMSO					4.0
AWF911	Ph	Me	CH ₂ CH=CH ₂	20	3.0
AWF918	4-F Ph	Me	Me	20	2.3
AWZ9014b	4-SO ₂ Me Ph	Me	Me	100	3.3
AWZ9013	4-OCF ₃ Ph	Me	Me	664	3.0
AWF930	H	Me	Me	105	4.0
AWF920	Ph	Me	Cl	11	0.0
AWZ9031		Me	Me	873	3.0
AWZ9049		Me	Cl	73	0.0
AWZ9051		Me	Cl	9	0.0
AWZ90933		Me	Me	43	0.0
AWZ9053		Me	Cl	43	0.0
AWZ9067		H	CH ₂ CF ₃	15	0.0
AWZ9069		H	Cl	22	0.0
AWZ9055		Me	Cl	30	0.0

Table 4.3 *In vitro* cell assay EC₅₀ values for selected pyrazolopyrimidine and motility readouts describing direct Mf toxicity.

The preliminary *in vitro* mf screening results indicate that whilst some of the analogues within this template demonstrate undesired worm toxicity, this does not appear to be a template-wide issue. The direct toxicity observed during this *in vitro* mf study does not appear to be correlated to the *in vitro* potency against *Wolbachia*. Analysis of the compounds tested suggests that a chlorine or CH₂CF₃ functionality at the 6-position, although beneficial in terms of *in vitro* anti-*Wolbachia* activity, appears to increase direct toxicity to the worms. One of the desired parameters of any anti-*Wolbachia* compounds resulting from this work is that they only target the bacteria within the filarial nematodes (and not the nematode itself). For this reason, it was sensible to avoid Cl or CH₂CF₃ substitutions at the 6-position in any future target molecules.

Following the use of the *in vitro* mf assay to screen for worm toxicity, several analogues from this work were tested for *Brugia malayi* potency at 5 μ M compared to the current gold-standard, doxycycline. This potency was determined by the reduction in *Wolbachia* level in mf following treatment with our compounds in comparison to the vehicle control (DMSO) group. The results from these assays are displayed within **Fig 4.10**

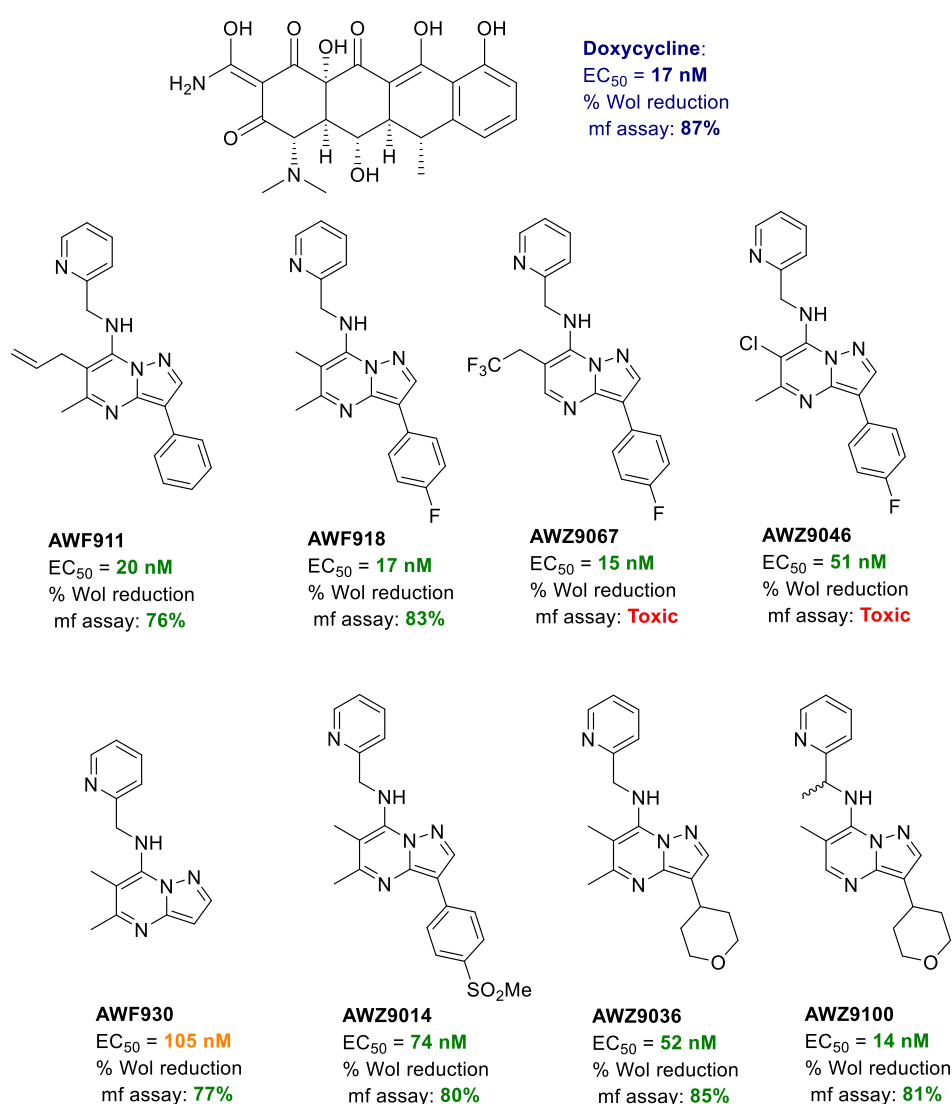


Fig 4.10 *In vitro* mf screening results for selected analogues 5 μ M

These results indicate that several compounds from this work have the capacity to reduce *Wolbachia* from infected filariae with potency comparable to the current gold-standard, doxycycline. Of these analogues, the most potent are the 4-fluoro phenyl analogue **AWF918** and the THP analogue **AWZ9057**, which demonstrated *Wolbachia* reduction comparable to doxycycline (87% of doxycycline's activity). While the optimised THP analogue **AWZ9100** had improved *in vitro* potency, this did not translate to increased *Wolbachia* reduction in the mf assay though it had similar potency to doxycycline.

During the safety assessment of a range of analogues within the AWOL III drug discovery and development program, several pyrazolopyrimidine analogues were assessed for permeability, affinity for efflux transporter p-glycoprotein, CYP inhibition, hERG and cytotoxicity measurements. In the next section these studies will be described and the assessment of the pyrazolopyrimidine series discussed.

4.3.2 Assessment of permeability, efflux ratio, *in vitro* toxicity and CYP inhibition of selected frontrunners.

The permeability of a drug is measured by its ability to cross a cell membrane. This is an important factor to determine during drug discovery and drug development as permeability can affect the intestinal absorption, oral bioavailability, blood-brain barrier penetration and entry into cells. Modification of these properties can drastically alter efficacy or toxicity within the cell and elimination by the kidney and the liver. Therefore, it is vital to measure influx into and efflux out of cells. For example, a drug that is rapidly absorbed, highly bioavailable and cleared slowly could be suitable for once-daily dosing. Whereas a drug that is rapidly absorbed, highly bioavailable and cleared quickly due to being a substrate for efflux transporters could necessitate a multiple dosing regimen.⁸

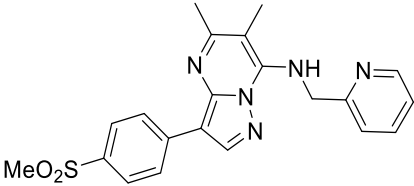
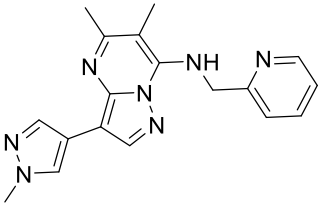
Drug compounds can enter cells transcellular (through the cells) or paracellular (between cells). Transcellular transport is the main method by which drug compounds enter cells; this can occur via passive diffusion, facilitated diffusion or active transport. Passive diffusion involves the movement of lipophilic solutes down a concentration gradient whereas charged, hydrophilic or zwitterions tend not to cross by this mechanism due to the hydrophobic nature of the phospholipid membrane. Facilitated diffusion is another form of passive diffusion across a biological membrane which is facilitated by a carrier and allows otherwise membrane impermeable molecules across. This however tends to be quite selective and in relevance to drug discovery, this method generally only favours organic molecules such as amino acids or sugars. Active transport is an energy driven process which allows the movement of a substrate against its concentration gradient. Active transport is assisted by transporters which can lead to selective efflux (removal from cells) or influx (uptake into cells) and several of these transporters are known to play a role in clinically relevant drug-drug interactions.⁸

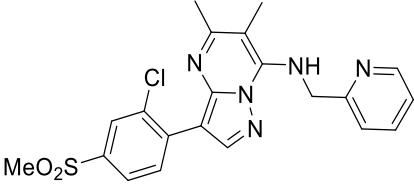
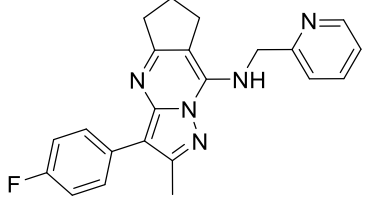
The permeability glycoprotein-1 (pgp-1) efflux transporter is encoded for by the MDR1 gene; this efflux transporter is one of the main efflux transporters in many tissues. One of the most common methods for

determining intestinal permeability and detecting substrates for efflux transporters (pgp-1 and ABCG2) which is employed in early-stage drug discovery is the Caco-2 (human colorectal adenocarcinoma cell line) assay. This assay is performed by placing the dissolved test compound into one compartment of a two-compartment chamber separated by the Caco-2 cells and a semi permeable membrane.^{9,10} The amount of compound present within each side of the chamber can then be measured following incubation and the permeability or efflux potential of the compound calculated.

By placing a compound in the compartment representing the intestinal lumen within the body (apical side) which is separated from the compartment representing the blood (basolateral side), the change in drug concentration from the apical to the basolateral side (a degree of the substrates affinity for efflux transporters) can be assessed. If the test compound is placed in the basolateral side then the change in concentration between the compartments will describe the permeability of the substrate (basolateral-apical).^{11,12} Finally, these values can be compared to determine the relative ratio of a compounds ability to permeate a cell membrane over its affinity for efflux transporters (basolateral-apical)/(apical-basolateral) with low values (CFR values) suggesting that compounds are not substrates for efflux transporters. If the efflux ratio is greater than or equal to 2 then this indicates that drug efflux is occurring.

Assessment of permeability and efflux ratio is valuable to gain a good understanding of drug efflux mechanism and to highlight any potential permeability issues. Assessment of selected pyrazolopyrimidine compounds synthesised throughout this work for permeability and human pgp-1 recognition was conducted by our collaborators Eisai. These results are displayed in **Table 4.4** alongside the structures for analogues tested.

Compound	Structure	LogD _{7.4}	Permeability (x10 ⁻⁶ cm/sec)				CFR
			LLC- PK1, A-B	LLC- PK1, B-A	LLC- MDR1, A-B	LLC- MDR1, B-A	
AWZ9014		3.3	15.6	6.8	12.1	7.3	1.4
AWZ9030		2.7	3.9	5.0	7.1	8.5	0.9

AWZ9032		3.4	20.5	7.4	17.8	9.0	1.4
AWZ9037		4.5	11.52	7.9	8.95	6.44	1.0

LLC – Lilly Laboratories Cell, **PK1** - Porcine proximal tubule kidney cell line, **MDR1** – Multi-drug resistance protein **A-B** Apical – basolateral **B-A** Basolateral - apical

Table 4.4 Permeability and efflux ratio of selected compounds.

The results indicate that all tested analogues have good permeability demonstrated by the high LLC-PK1, A-B value and none of them are substrates for P-gp transporters and have a low efflux ratio demonstrated by the low CFR value (<2). Per our guidelines for the AWOL Target Candidate Profile (TCP) the desired value for permeability (B-A) is $>10 \times 10^{-6} \text{cms}^{-1}$ and the lower acceptable value is $2 \times 10^{-6} \text{cms}^{-1}$. These early analogues demonstrate promising permeability, all within the acceptable value range ($2\text{-}10 \times 10^{-6} \text{cms}^{-1}$).

Cardiotoxicity is another considerable problem which can lead to toxicity-related drug attrition during development so it is desirable to determine any potential for cardiotoxicity early during the discovery process.^{13,14} The human ether-a-go-go gene (hERG) controls the voltage-gated potassium channel in the heart which is involved in cardiac repolarisation. Inhibition of hERG causes longer QT periods which can result in potentially fatal ventricular tachyarrhythmia with several drugs known to produce this effect.¹⁵ Various patch clamp techniques are available for a range of cells to assess the electrophysiology of cells and the effects of drugs on such cell lines.

Drug-drug interactions are another common reason for late-stage attrition of developing drug candidates due to one drug effecting the pharmacokinetics of another co-administered drug.¹⁶ This can result in toxic effects should induction of metabolising enzymes (CYPs) occur increasing the concentration of toxic metabolites or *via* CYP enzyme inhibition which can result in accumulation of a drug compound to high and harmful concentrations. For this reason, it is desirable to screen for any potential CYP inhibition that drug compounds under development may experience. Several selected analogues from the pyrazolopyrimidine chemotype were selected for CYP inhibition studies to determine any potential drug-drug interaction liability; these assays were also carried out by our collaborators Eisai.

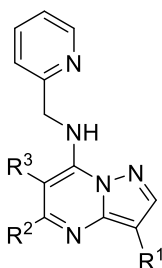
To assess the potential safety related concerns of frontrunners within this template, many compounds were chosen for *in vitro*, hERG, CYP inhibition and cytotoxicity measurements. The important analogues selected for assessment are displayed in **Table 4.5** with alongside the results from the inhibition studies.

Compound	hERG IT22938 IC ₅₀ (μM)	Cytotoxicity THP-1 IC ₅₀ (μM)	CYP Inhibitions IC ₅₀ (μM)					
			CYP1A	CYP2C8	CYP2C9	CYP2C19	CYP2D6	CYP3A
AWF918	>33.33	>50	0.4	ND	22.9	20.4	>30	>30
AWF930	>33.33	4.95	1.9	>>10μM	>>10μM	18.4	>>10μM	>>10μM
AWF937	>33.33	>50	2.9	>>10μM	18.9	>>10μM	>>10μM	>>10μM
AWZ9014	11.84	IP	19.4	>>10μM	>>10μM	14.8	>>10μM	>>10μM
AWZ9036	>33.33	IP	13.1	>>10μM	>>10μM	>>10μM	>>10μM	>>10μM
AWZ9048	>33.33	IP	0.6	>>10μM	>>10μM	30.3	>>10μM	>>10μM
AWZ9057	>33.33	15.81	>>10μM	>>10μM	>>10μM	>>10μM	>>10μM	>>10μM
AWZ9067	10.54	IP	37.8	>>10μM	>>10μM	>>10μM	>>10μM	>>10μM

THP-1 Human leukemic cell-line (acute monocytic leukaemia)

Table 4.5 *in vitro* toxicology screening results for selected analogues.

The acceptable limits for these readouts are as follows; hERG activity > 10 μM, cytotoxicity > 20 μM and CYP inhibition > 20 μM. The results from the above screen (**Table 4.5**) are all negative except for CYP1A inhibition (highlighted in red). To further probe the prevalence of this CYP1A inhibition within this template, additional analogues were chosen for *in vitro* CYP inhibition screening and the results are documented within **Table 4.6** organised by decreasing metabolic stability.



Compound	R ¹	R ²	R ³	CYP Inhibitions IC ₅₀ (μM)						
				Human Mics CLint (μL/min/mg)	CYP1A (μM)	CYP2C8 (μM)	CYP2C9 (μM)	CYP2C19 (μM)	CYP2D6 (μM)	CYP3A (μM)
AWZ9013	4-OCF ₃ Ph	Me	Me	3	20.9	>>10	>>10	>>10	>>10	>>10
AWZ9067	4-F Ph	H	CH ₂ CF ₃	5.64	37.8	>>10	>>10	>>10	>>10	>>10
AWZ9041	4-F Ph	Me	SO ₂ Me	8.76	>>10	>>10	>>10	>>10	>>10	>>10
AWZ9014	4-SO ₂ Me Ph	Me	Me	9	19.4	>>10	>>10	14.8	>>10	>>10
AWZ9057	THP	H	Me	9.42	>>10	>>10	>>10	>>10	>>10	>>10
AWF912	4-Cl Ph	Me	H	9.71	22.4	>>10	>>10	>>10	>>10	>>10
AWZ9031		Me	Me	14.65	>>10	39.4	>>10	>>10	>>10	>>10
AWZ9055		Me	Cl	28.46	>>10	>>10	>>10	>>10	>>10	>>10
AWZ9056	4-F Ph	H	Me	37.48	9.7	>>10	>>10	>>10	>>10	>>10
AWZ9059	4-F Ph	H	Me	52.94	0.9	>>10	>>10	1.8	>>10	>>10
AWF918	4-F Ph	Me	Me	55	0.4	ND	22.9	20.4	>30	>30
AWZ9048		Me	Cl	75.36	0.6	>>10	>>10	30.3	>>10	>>10
AWZ9058	2-pyridyl	H	Me	152.5	2.2	>>10	>>10	>>10	>>10	>>10
AWF930	H	Me	Me	262	1.9	>>10	>>10	18.4	>>10	>>10
AWF951	F	Me	Me	276.9	4.5	>>10	>>10	>>10	>>10	>>10
AWF948	Cl	Me	Me	287	3.9	27.6	>>10	>>10	>>10	>>10

Human Mics Clint (μL/min/mg) - Clearance of a compound from human microsomal cells

Table 4.6 CYP Inhibition studies of various pyrazolopyrimidine analogues compared to metabolic stability.

The screening results indicate that CYP1A inhibition is closely associated with metabolic stability, with compounds exhibiting high metabolic stability being weaker inhibitors of CYP1A which is shown by their higher IC_{50} values. In addition to all the safety screening studies, a variety of pyrazolopyrimidine compounds were evaluated for *in vivo* PK and PD properties during optimisation of this template, these studies are discussed in the following section.

4.3.3 *In vivo* assays.

During early lead optimisation of this chemotype, one of the analogues reported earlier, **AWZ9014** was selected as the early lead in this template. Due to its balance of *in vitro* potency and DMPK properties (**Fig 4.11**), **AWZ9014** was evaluated for *in vivo* PK and PD properties. Initially, the PK profile of **AWZ9014** was tested at 50 mg/kg and 100 mg/kg with a single oral dose to SCID mice using SSV as a dosing vehicle and the results from these studies are displayed below (**Chart 4.1** and **Table 4.7**).

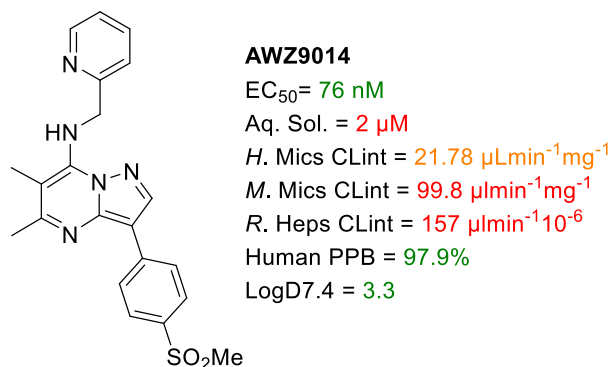


Fig 4.11 Structure of **AWZ9014** studied for *in vivo* PK PD profile with measured *in vitro* whole-cell activity and DMPK properties.

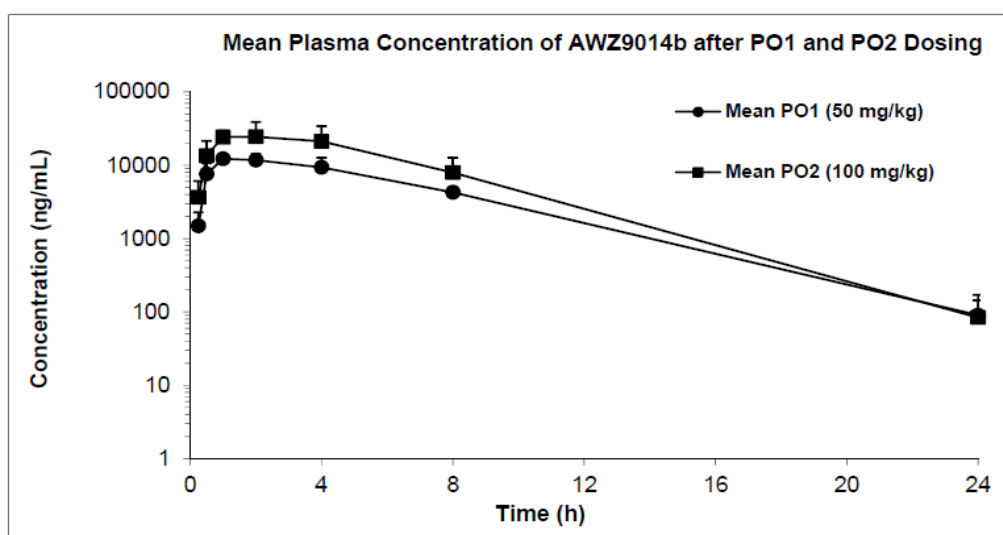


Chart 4.1 *in vivo* PK profile of **AWZ9014** using SSV as an oral dosing vehicle

Dosage (Oral)	50 mg/kg	100 mg/kg
T _{1/2} (h)	2.99	2.44
C _{max} (ng/mL)	13067	27800
T _{max} (h)	1.33	1.67
AUC _{0-t} ng.h/mL	82209	162617

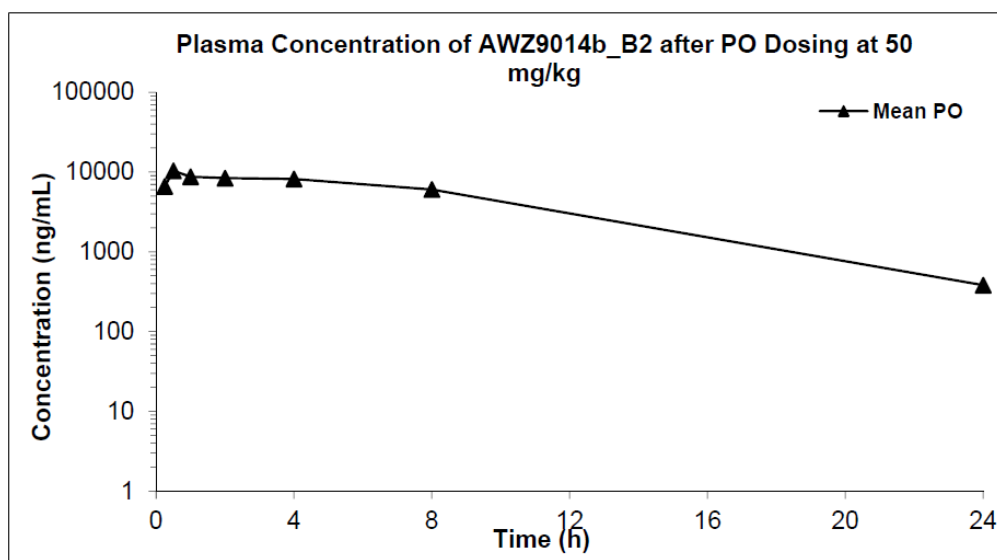
Table 4.7 *in vivo* PK profile of **AWZ9014** using SSV as an oral dosing vehicle

Despite poor aqueous solubility, **AWZ9014** demonstrated an excellent *in vivo* PK profile. This study shows that **AWZ9014** displayed high exposure, an acceptable half-life with a dose-proportional increase in AUC after doubling the dose from 50 mg/kg to 100 mg/kg. While the *in vitro* potency for **AWZ9014** was lower than several other analogues in this template it was considered that the impressive PK profile could compensate for the lower compound potency. **AWZ9014** was taken forward for assessment within the *in vivo* larval PD study. This study was limited by the amount of **AWZ9014** in stock at the time and it was only possible to dose **AWZ9014** at 50 mg/kg for 14 days and the results are displayed within **Table 4.8**. The compounds were incubated before DNA extraction and performing qPCR to calculate the reduction of *Wolbachia* Surface Protein (*wsp*) copy number to untreated controls.

Compound	Dose and duration	Wsp reduction*
DOX	50 mg/kg qd 07d	91.99%
DOX	50 mg/kg qd 14d	98.54%
AWZ9014	50 mg/kg bid 14d	52.98%
*Median % reduction of vehicle control		

Table 4.8 Results from the **AWZ9014** *in vivo* PD study using SSV

At 50 mg/kg the *Wolbachia* depletion displayed by **AWZ9014** was insufficient to reach the 90% reduction in 14 days as seen with the current gold-standard, doxycycline. However, in-house computational PK/PD studies predicted that at higher dosing levels **AWZ9014** would attain *Wolbachia* reduction levels comparable to doxycycline. Several compounds from other templates within the project were selected for PK studies using a lipid formulation consisting of 55% PEG300, 25% propylene glycol and 20% water (PEG300 formulation) as the dosing vehicle. **AWZ9014** was chosen for analysis within an *in vivo* PK study dosing at 50 mg/kg using PEG300 as the oral dosing vehicle to help improve drug exposure. The results from this study are displayed below in **Table 4.9** and **Chart 4.2** alongside the 50 mg/kg results using SSV as the dosing vehicle.



Dosage (Vehicle)	50 mg/kg (PEG300)	50 mg/kg (SSV)
T _{1/2} (h)	8.09	2.99
C _{max} (ng/mL)	10650	13067
T _{max} (h)	0.5	1.33
AUC _{0-t} ng.h/mL	93529	82209

Chart 4.2 and Table 4.9 *in vivo* PK profile for **AWZ9014b** using PEG300 as a vehicle.

In comparison with the PK profile seen when using SSV, PEG300 results in an increased half-life and slightly increased drug exposure. In the light of this study result, a further *in vivo* PD study was carried out at 50 mg/kg using the PEG300 formulation as the delivery vehicle, the results from this assay are displayed in **Table 4.10**.

Compound	Dose and duration	Wsp reduction*
DOX	50 mg/kg qd 07d	82.7%
DOX	50 mg/kg qd 14d	96.2%
AWZ9014	50 mg/kg bid 14d	46.2%
*Median % reduction of vehicle control		

Table 4.10 Results from the **AWZ9014** *in vivo* PD study using PEG300

However, the slightly improved drug exposure did not appear to result in an improved capacity of **AWZ9014** to deplete *Wolbachia* *in vivo*. The *in vivo* PD studies did not yet provide any proof-of-concept result for this template; further investigation on this template was temporarily halted until a significant breakthrough could be made in terms of analogues with superior *in vitro* efficacy and DMPK properties.

The compound **AWZ9100** (Fig 4.12) was identified following several rounds of lead optimisation from compound **AWZ9014** as depicted in Fig 4.12 and discussed earlier. Following promising improvement of **AWZ9100** (in terms of *in vitro* potency and DMPK properties) this molecule was selected for *in vivo* PK and PD evaluations.

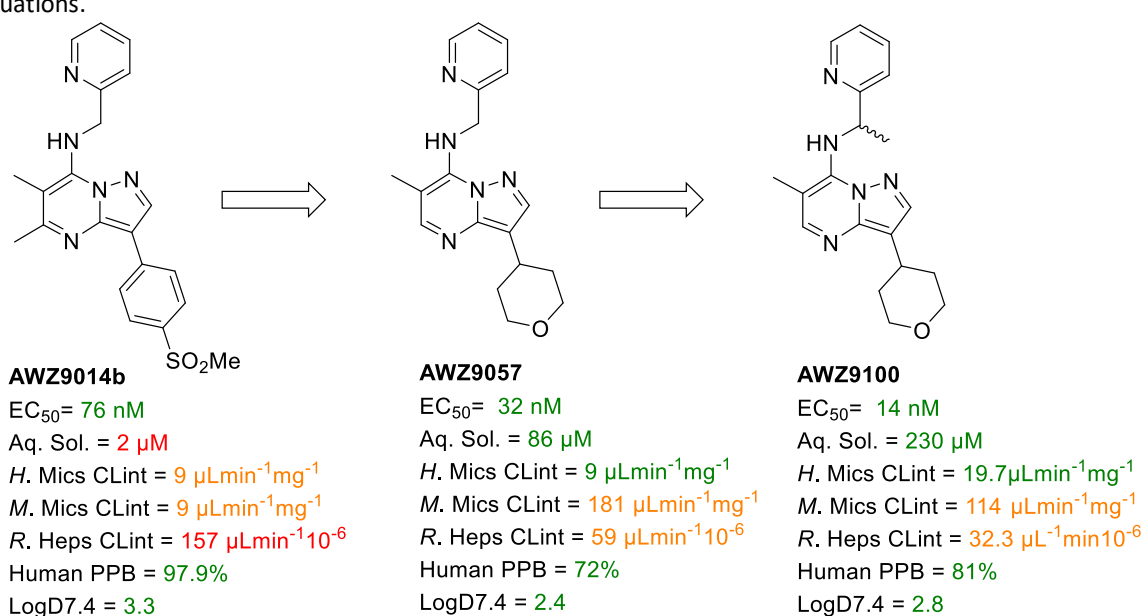


Fig 4.12 Summary of lead optimisation (Chapter 2 - 4)

The PK profiles of the new lead **AWZ9100**, was assessed within the *in vivo* SCID mouse model at 50mg/kg and 100 mg/kg using the PEG300 formulation as the oral dosing vehicle, and the PK profile is displayed in Chart 4.3 and Table 4.11 below.

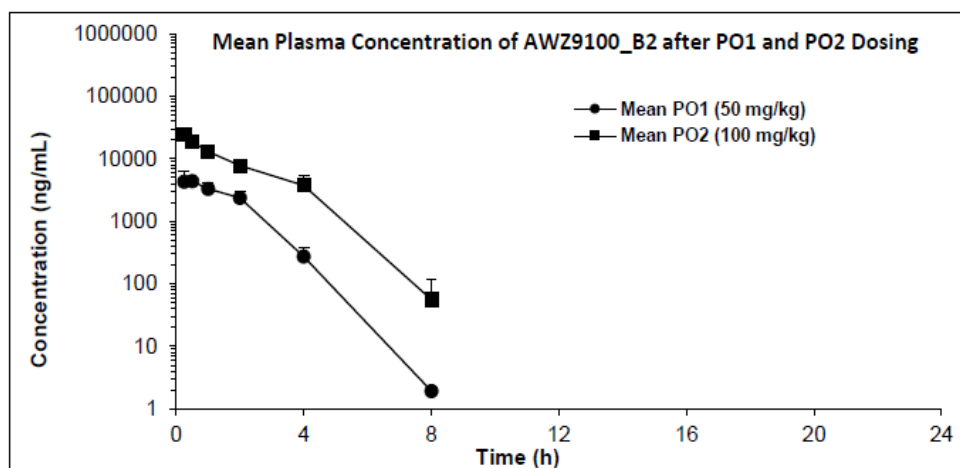


Chart 4.3 *in vivo* PK profiles of **AWZ9100** using PEG300.

Dosage (Oral)	50 mg/kg	100 mg/kg
T _{1/2} (h)	0.58	1.1
C _{max} (ng/mL)	5200	25700
T _{max} (h)	0.42	0.33
AUC _{0-t} ng.h/mL	8462	41005

Chart 4.3 and Table 4.11 *in vivo* PK profiles of **AWZ9100** using PEG300

AWZ9100 demonstrates an acceptable PK profile especially at the higher dosing level. While experiencing a short half-life, the compound is rapidly absorbed following oral dosing and the associated increase in C_{max} and AUC with increased dosing is significantly higher than expected. Although the PK profiles of **AWZ9100** were not as good as **AWZ9014**, its higher potency might compensate for the reduced exposure in the PD study. However, despite improvement of potency was made from **AWZ9014** to **AWZ9100**, it was still insufficient to provide a positive outcome when tested within the *Brugia malayi* larval model (30% reduction at 150 mgkg⁻¹ twice-daily dosing for 14 days). The *in vivo* efficacy studies carried out on various other small molecule templates within the drug discovery program demonstrated that the greatest level of *Wolbachia* reduction (>99.9%) is only observed in analogues with much superior *in vitro* potency and DMPK properties. A rough guideline of properties for analogues, which possess this superior reduction, is *in vitro* potency 0.01nM – 0.001 nM and Rat/Human clearance values <5. It would be necessary to optimise this pyrazolopyrimidine chemotype further to improve the overall properties to allow them to be successful at reducing *Wolbachia* levels *in vivo* with levels comparable to leads resulting from other small-molecule discovery projects within the program.

4.4 Conclusions

Many pyrazolopyrimidines (190) have been synthesised, many of which have demonstrated low nanomolar activity against *Wolbachia* with much superior DMPK properties over the initial hit **AWF911**. Several synthetic pathways have been explored which allow for modification of the core at key positions (R¹⁻⁵) around the pyrazolopyrimidine core. The overall hit to lead optimisation carried out during this work is summarised in **Fig 4.13**.

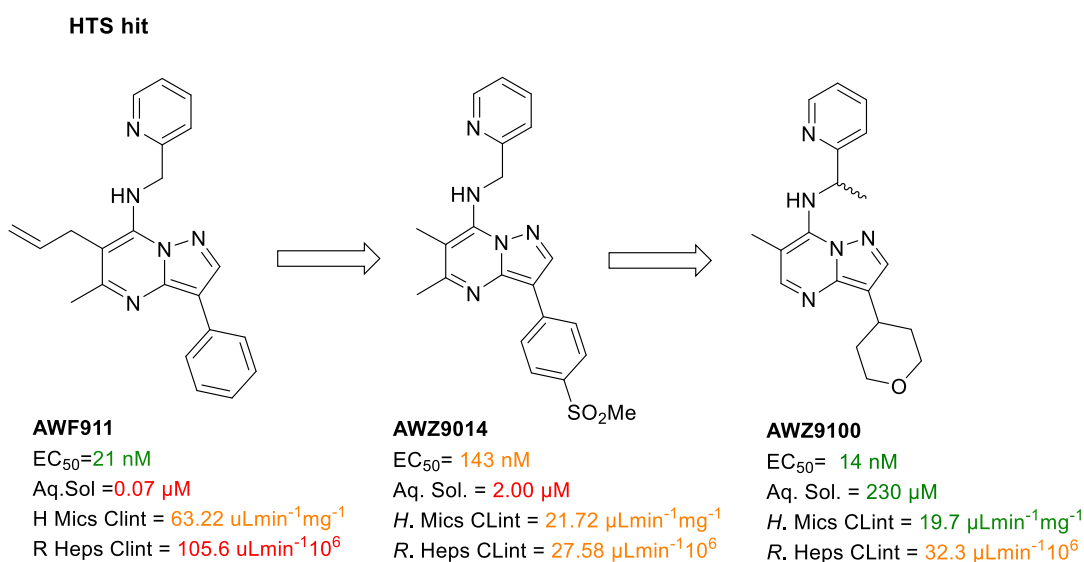


Fig 4.13 Summary of the hit to lead optimisation carried out during this work

Work on the pyrazolopyrimidine chemotype was halted during discovery efforts due to superior small-molecule templates within the AWOL III drug discovery and development project allowing all resources to be focused on the priority areas to produce a successful candidate. Should additional funding be secured for further discovery efforts, the current lead from this work **AWZ9100**, will be a very promising starting molecule for the onward late lead optimisation to deliver a suitable backup candidate for the project. There are several options for modification to both the pyrazolopyrimidine core and substituents which could allow for improvement of both metabolic stability and compound potency, these are discussed briefly below.

4.5 Future Work

Positions around the pyrazolopyrimidine core which could be further explored for additional optimisation of these compounds are highlighted in **Fig 4.14**.

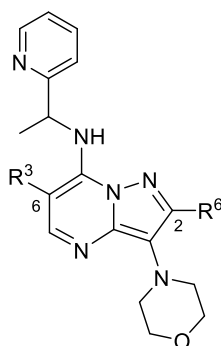
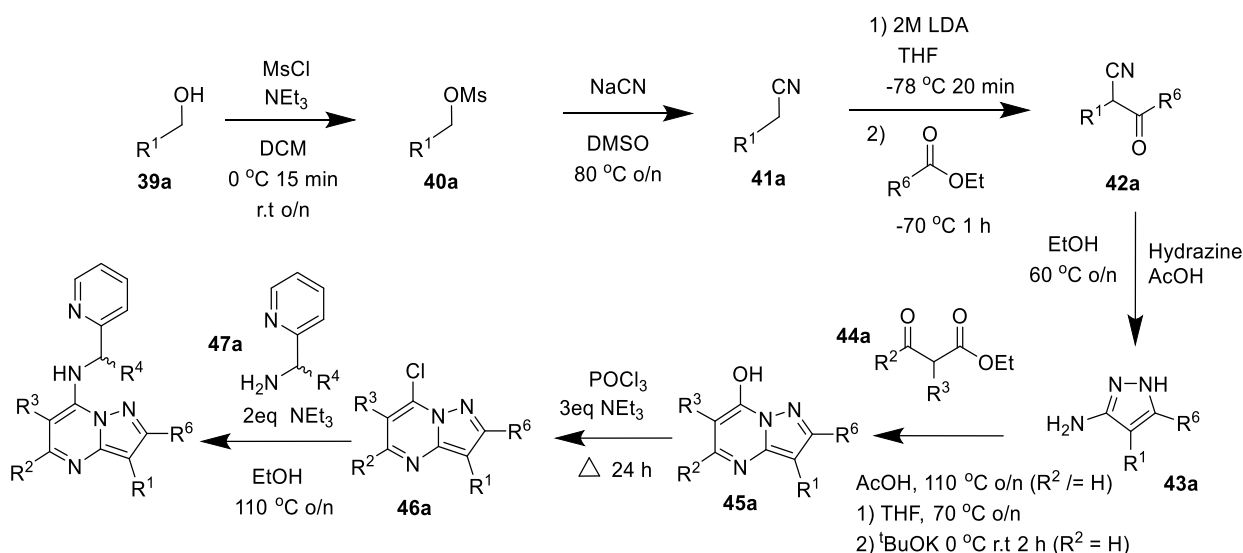


Fig 4.14 General pyrazolopyrimidine core for future optimisation.

Exploration of the 2-position (R^6) and further exploration of the 6 position (R^3) to determine the optimum substituents at these points around the pyrazolopyrimidine core. The 6-position has been successfully modified using the chemistry discussed throughout the current SAR studies (Chapter 2) as can the 2-position by synthesis of the initial pyrazole with the necessary substitution pattern (**Scheme 4.8**).

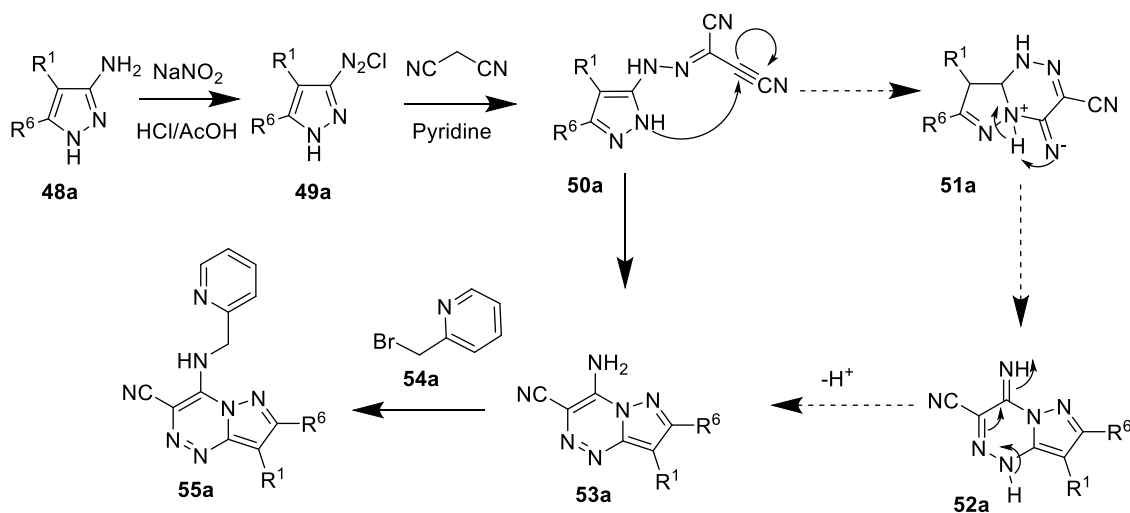


Scheme 4.8 Optimised synthesis for varying all essential positions for SAR study around the pyrazolopyrimidine core.

Optimisation of these positions may prove promising with a lipophilic substituent at the 6-position from observations made throughout this work and then offsetting this added lipophilicity with a polar group at the

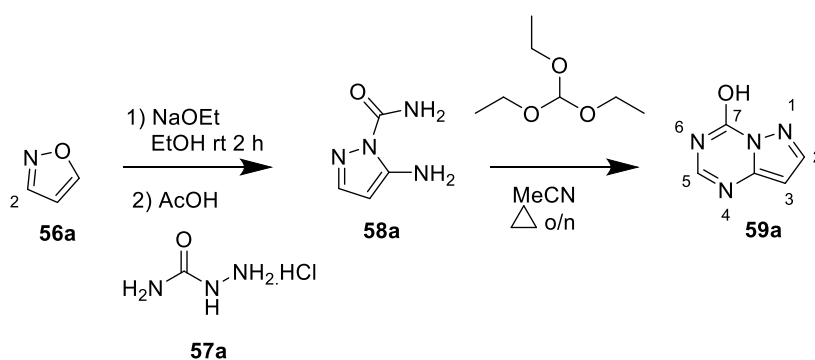
R⁶ position to maintain/improve aqueous solubility. Further to study of these positions, another potential approach for the improvement of these analogues could be a scaffold morphing strategy by inserting an additional nitrogen atom into the pyrimidine core.

Installation of the extra nitrogen can be performed following the work of Yaakov W.A *et al.*,¹⁷ as summarised in **Scheme 4.9** with the proposed mechanism for the formation of this core.¹⁷



Scheme 4.9 Formation of the pyrazolotriazine core following the work of Yaacob W.A *et al.*,¹⁷

A plausible procedure to incorporate a nitrogen at the 6-position of the pyrazolopyrimidine core to allow study of this scaffold during future work can be adapted from the work of Leifox *et al.*, and is depicted below in **Scheme 4.9**.^{18,19}



Scheme 4.10 Synthesis of the pyrazolo 1,3,5-triazine^{18,19}

4.6 Experimental

Biological Evaluation

In Vitro screening – Materials and Methods¹

Cell Culture

The C6/36 (wAlbB) cell line is a mosquito (*Aedes albopictus*) derived cell line stably infected with *Wolbachia pipientis* (wAlbB). To create this cell line, the supernatant from cultured Aa23 cells (*A. albopictus*) naturally infected with the *W. pipientis* strain wAlbB was harvested and filtered to remove whole cells. This supernatant was used to inoculate C6/36 cells (ECACC No. 89051705), resulting in a stably *Wolbachia*-infected cell line C6/36 (wAlbB).^{1,11–12} Cells were incubated at 26 °C and subpassaged every 7 days using a 1-in-4 dilution in Leibovitz media (Life Technologies, Loughborough, UK) supplemented with 20% fetal bovine serum (FBS; Fisher Scientific, Loughborough, UK), 2% tryptose phosphate broth (Sigma-Aldrich, Poole, UK), and 1% non-essential amino acids (Sigma-Aldrich).

Anti-*Wolbachia* HCS Assay Setup

C6/36 (wAlbB) cells were subpassaged 6–8 days before plating out at a density of 2000 viable cells per well in a 384-well CellCarrier plate (PerkinElmer, Llantrisant, UK), suspended in Leibovitz media with the additives described in the “Cell Culture” section. All compounds were dissolved in DMSO with each compound added to a single well at a final concentration of 5 µM (resulting in <1% final DMSO concentration). Control samples per plate consisted of 12 wells of vehicle control (DMSO) and 6 wells of the following controls: 5 µM doxycycline (positive control— the gold standard for *Wolbachia* reduction; SigmaAldrich) and a suboptimal 50 nM doxycycline concentration. Each well held a final volume of 100 µL, except for the outer wells, which contained 130 µL of phosphate-buffered saline (PBS; SigmaAldrich). After 7 days of 26 °C sterile incubation, 25 µL of staining media containing 60 µM of SYTO 11 DNA dye (Life Technologies) was added to each well. After a 15 min incubation, all media was removed from each well and replaced with fresh media (no stain). Using the Operetta high-content automated imaging system (PerkinElmer), five fields per well were imaged using a confocal 60× objective with the Fluorescein filter (excitation filter: 460–490; emission filter: 500–550). The PerkinElmer software Harmony was trained to first identify the cell nucleus and cytoplasm, followed by the spot edge ridge (SER) texture analysis, which was used to score each intact cell on the complexity of the cytoplasm.²

Anti-*Wolbachia* HCS Assay Results Analysis

Using the vehicle and positive (*Wolbachia* reduction) controls, a threshold was set to indicate if each cell was classed as infected or uninfected. *Wolbachia*-infected cells (vehicle control) have a complex cytoplasm texture

(high SER texture score), whereas *Wolbachia*-uninfected cells (doxycycline-treated positive control) have a uniform cytoplasm texture (low SER texture score). From this analysis, the following readouts were calculated per well: cell number, SER texture score, and percentage of *Wolbachia*-infected cells. Z' factor (Z') validation of each plate was calculated using the percentage of *Wolbachia*-infected cells value from the vehicle and positive controls. The 14 Vehicle controls have a high *Wolbachia* load and therefore a high percentage of cells classed as infected with *Wolbachia*. Positive control (doxycycline-treated) cells have a low *Wolbachia* load and therefore a low percentage of *Wolbachia*-infected cells. All compound sample wells were then analysed and normalized (along with the positive controls) against the vehicle (untreated) control to give a percentage reduction of *Wolbachia*-infected cells. In addition, using the cell number analysis, any compounds with a host cell number amounting to less than 50% of the vehicle control were classed as toxic and retested at a reduced compound concentration. All compounds that were >90% of the positive control's percentage reduction of *Wolbachia*-infected cells were classed as strong hits (because they were similar to or greater than the 5 μ M doxycycline positive control). Compounds that yield infection rates between 50% and 90% of the positive control were classed as moderate hits because they were similar to the suboptimal (50 nM) doxycycline control. All hit compounds were then reconfirmed in a full dose response to define their potency.

***In vitro* mf studies**

SSV – standard suspension vehicle (0.5% sodium carboxymethyl cellulose; 0.5% benzyl alcohol, 0.4% Tween 80, 0.9% NaCl)

PEG300 – 55% polyethylene glycol 300, 25% propylene glycol, 20% water

Optimisation of an *ex vivo* microfilariae (mf) *B. malayi* screen

An *ex vivo* mf assay was developed by the Liverpool School of Tropical medicine to provide a link between the insect cell based *in vitro* assay and the *in vivo* *B. malayi* screen. The validation of this new assay that enables greater throughput whilst still allowing the assessment of our compounds ability to reduce *Wolbachia* load in the targeted parasite. Since microfilariae are the more abundantly produced worm stage within our laboratory models, we can screen many more compounds using this resource in the *ex vivo* assay, allowing the resultant best performing compounds to be prioritised for screening against adult worm's *ex vivo* or *in vivo*. This reduces the use of animals, whilst allowing us to gather important information which feeds back into the drug discovery process.

Within the *ex vivo* mf assay; compounds are incubated with 8000 mf *B. malayi* per well (five wells per compound) for 6 days, before DNA is extracted and qPCR performed to compare *wsp:gst* ratio of drug treated vs control wells, full experimental details for the assay are documented below.

General biology experimental³

Animals

Male BALB/c SCID were purchased from Harlan Laboratories, UK, while male CB.17 SCID mice and BALB/c WT mice were purchased from Charles River, UK. Male *Meriones unguiculatus* (Mongolian gerbils; jirds) were purchased from either Charles River, UK or Janvier Laboratories, France. Rodents shipped to REFOTDE, Buea, Cameroon, were maintained in conventional housing with Halliday *et al.* daily cage cleaning and changing of food. Food, water and bedding were sterilised by autoclaving. For *B. malayi* experiments, animals were kept at the Biomedical Services Unit (BSU), University of Liverpool, UK in specific pathogen-free (SPF) conditions. All experiments carried out in Cameroon were approved by the Animal Care Committee, REFOTDE. All experiments on animals in the UK were approved by the ethical committees of the University of Liverpool and LSTM, and were conducted per Home Office (UK) requirements. The life cycle of *B. malayi* (Bm) was maintained in mosquitoes and susceptible *Meriones* gerbils at LSTM. To generate infective Bm larvae (BmL3) for infections, female adult *Aedes aegypti* mosquitoes were fed with Bm microfilariae (mf) collected from infected gerbils by catheterisation, as previously described, followed by mixing with human blood and feeding through an artificial membrane feeder (Hemotek®). Blood-fed mosquitoes were reared for 14 days to allow for development to L3. The L3 were collected from infected mosquitoes by crushing and concentration using a Baermann's apparatus and RPMI medium.

Implantation of adult macrofilariae

Bm macrofilariae were collected from infected SCID mice and were grouped into batches of 13 adults. Male BALB/c SCID and BALB/c WT mice were placed under surgical anaesthesia using isoflurane and were given s.c. injection of buprenorphine before 13 Bm macrofilariae were placed into the peritoneal cavity by making a small incision to the skin and abdominal cavity wall in the upper right quadrant. The incisions were re-sutured after implant and animals were individually housed after surgery. For *Onchocerca* implants, rodents were placed under surgical anaesthesia using i.p. injections of ketamine and medetomidine. *Onchocerca* comata were thoroughly cleaned of bovine tissue, washed in several changes of RPMI + PSN and small sections of the adult worms were exposed by partial rupture of the capsule. Groups of 8–15 motile *O. ochengi* male macrofilariae or 4 prepared *O. ochengi* nodules were implanted into the peritoneal cavity or to the cutaneous tissue of the upper side of the neck (for s.c nodule implants). All wounds were re-sutured after surgery and animals were individually housed and closely monitored for the recovery period (7 days post-op).

Drug treatments

Drugs were dissolved in standard suspension vehicle (0.5% sodium carboxymethyl cellulose; 0.5% benzyl alcohol; 0.4% Tween 80; 0.9% NaCl) or PEG300 (55% polyethylene glycol 300; 25% propylene glycol; 20% water).

General chemistry experimental

Air- and moisture-sensitive reactions were performed in oven dried glassware sealed with rubber septa under an atmosphere of nitrogen from a manifold or balloon. Anhydrous solutions and sensitive liquids were transferred *via* syringe or stainless-steel cannula. Reactions were stirred using Teflon-coated magnetic stir bars. Organic solutions were concentrated using a Buchi rotary evaporator with a diaphragm vacuum pump.

Purification of solvents and reagents

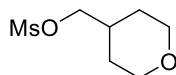
Anhydrous solvents were either purchased from Sigma Aldrich or dried and distilled immediately prior to use under a constant flow of dry nitrogen. Tetrahydrofuran was distilled from Na, dichloromethane and Et₃N were distilled from CaH₂. All reagents were purchased from Sigma Aldrich, Alfa Aesar, Frontier Scientific, Apollo Scientific, Fluorochem and were used without any purification unless otherwise indicated.

Purification of products

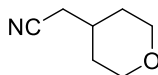
Thin layer chromatography (TLC) was performed on 0.25 mm Merck silica gel 60 F254 plates and visualised by ultraviolet light. U.V. inactive compounds were visualised using iodine, *p*-anisaldehyde solution, ninhydrin or potassium permanganate followed by gentle heating. Flash column chromatography was performed on ICN ecochrom 60 (32-63 mesh) silica gel eluting with various solvent mixtures and using an airline to apply pressure.

Analysis

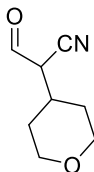
Melting points were determined by a Gallenkamp apparatus and are uncorrected. ¹H NMR spectra were recorded on Bruker AMX 400 (400 MHz) spectrometer and reported as chemical shift on parts per million (ppm, δ) relative to tetramethylsilane as the internal reference, integration, multiplicity (s = singlet, br s = broad singlet, d = doublet, t = triplet, q = quartet, sex = sextet, m = multiplet), coupling constant (*J*, Hz), assignment. ¹³C NMR spectra were recorded on Bruker AMX400 (101 MHz) spectrometer and reported in terms of chemical shift (ppm, δ) relative to residual solvent peak. Mass spectra (MS) and high resolution mass spectra (HRMS) were recorded on a VG analytical 7070E machine, Fisons TRIO spectrometers using electron ionisation (EI) and chemical ionisation (CI), and Micromass LCT mass spectrometer using electron spray ionisation (ESI). All mass values are within error limits of ± 5 ppm. Elemental analyses (%C, %H, %N) were either determined by the University of Liverpool Microanalysis Laboratory or the London Metropolitan University Elemental Analysis Service. Reported percentages are within error limits of ± 0.5 %.

(Tetrahydro-2H-pyran-4-yl)methyl methanesulfonate (27a)²⁰

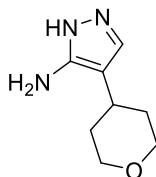
To solution of (tetrahydro-2H-pyran-4-yl)methanol (15 g, 129.0 mmol) in DCM (90 mL) was added NEt_3 (23.4 mL, 167.7 mmol). The solution was allowed to cool to 0 °C before adding MsCl (12.0 mL, 155.6 mmol) slowly over 15 minutes followed by stirring at 0 °C for 15 minutes. The reaction was allowed to stir at 25 °C overnight before removing the volatiles under reduced pressure and diluting the resultant residue with saturated Na_2CO_3 (100 mL). The crude product was extracted with EtOAc (4x80 mL), the combined organics were washed with saturated NH_4Cl (80 mL) and dried over MgSO_4 before evaporating to dryness to give crude (tetrahydro-2H-pyran-4-yl)methyl methanesulfonate as a yellow solid (21 g) which was used without further purification (21.11 g, 84%); **MS (Cl+ NH₄)**: m/z (rel. Intensity) $[\text{M}+\text{H}^+]$ 195 (46), $[\text{M}+\text{NH}_4^+]$ 212.1 (100; **HRMS (Cl+)** calcd for $[(\text{C}_7\text{H}_{18}\text{NO}_4\text{S})+\text{H}]$:212.0951; found: 212.0960

2-(Tetrahydro-2H-pyran-4-yl)acetonitrile (28a)²¹

To tetrahydro-2H-pyran-4-yl)methyl methanesulfonate (6.27 g, 32.31 mmol) in DMSO (50 mL) was added NaCN (2.69 g, 54.94 mmol). The reaction was heated to 80°C and stirred overnight. The reaction was allowed to cool to room temperature, diluted with water (100 mL), extracted with EtOAc (4x150 mL), dried over MgSO_4 and evaporated to dryness. The crude product was purified by column chromatography eluting with 60% EtOAc :Hexane to give 2-(tetrahydro-2H-pyran-4-yl)acetonitrile as a yellow oil (2.9 g). (**72%**); **¹H NMR (400 MHz, DMSO-d₆)** δ 3.85 (dd, $J = 11.0, 3.8$ Hz, 2H), 3.29 (td, $J = 11.8, 1.8$ Hz, 2H), 1.90 – 1.78 (m, 3H), 1.62 (dd, $J = 12.9, 1.8$ Hz, 2H), 1.28 (qd, $J = 12.3, 4.4$ Hz, 2H); **¹³C NMR (101 MHz, DMSO-d₆)** δ 119.7, 66.9 (2C), 31.9 (2C), 31.8, 23.5; **MS (Cl+ CH₄)**: m/z (rel. Intensity) $[\text{M}-\text{CN}]$ 99.1 (100).

3-Oxo-2-(tetrahydro-2H-pyran-4-yl)propanenitrile (29a)²²

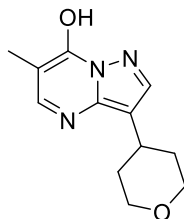
To tetrahydro-2H-pyran-4-yl)methyl methanesulfonate (3.0 g, 23.97 mmol) at -78°C was added 1M LDA in THF (28.76 mL, 28.76 mmol) and the reaction was allowed to stir at -78°C for 20 minutes. Ethyl formate (3.86 mL, 47.93 mmol) was added to the reaction which was allowed to stir for 50 minutes before diluting with NH_4Cl (30 mL). The mixture was then acidified to pH 2-3 with 1M HCl and extracted with EtOAc (5x100mL) and concentrated under vacuum to give crude PM07-75-01 as a yellow solid (3.7 g) which was used without further purification. **MS (Cl⁺ CH₄):** m/z (rel. Intensity)[M+H] 154.1 (100)

4-(Tetrahydro-2H-pyran-4-yl)-1H-pyrazol-5-amine (30a)

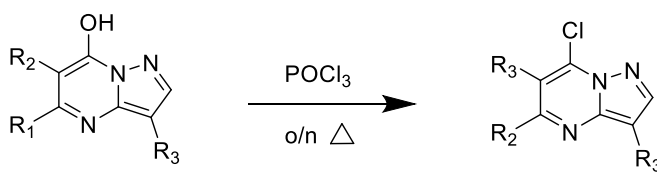
To a solution of 3-oxo-2-(tetrahydro-2H-pyran-4-yl)propanenitrile (1.81 g, 11.82 mmol) in EtOH (4 mL) was added hydrazine monohydrate (1.89 mL, 36.63 mmol) and AcOH (1.80 mL, 31.91 mmol). The reaction was allowed to stir at 60°C overnight before removing the volatiles under reduced pressure and purifying the crude product by column chromatography eluting with EtOAc to 10% MeOH in EtOAc to give 4-(tetrahydro-2H-pyran-4-yl)-1H-pyrazol-5-amine **30a** (1.86 g). **87%**; **¹H NMR (400 MHz, DMSO-*d*₆)** δ 11.46 (br s, 1H), 7.41 (s, 1H), 4.45 (br s, 2H), 4.16 (dd, $J = 11.5, 3.5$ Hz, 2H), 3.66 (td, $J = 11.5, 1.8$ Hz, 2H), 2.83 (tt, $J = 11.8, 3.5$ Hz, 1H), 2.01 (dd, $J = 12.6, 1.8$ Hz, 2H), 1.74 (qd, $J = 12.4, 4.3$ Hz, 2H); **¹³C NMR (101 MHz, DMSO-*d*₆)** δ 151.3, 127.5, 110.0, 67.9 (2C), 33.7 (2C), 30.0; **MS (Cl⁺ CH₄):** m/z (rel. Intensity)[M+H] 168.1 (100); **HRMS (Cl⁺)** calcd for [(C₈H₁₃N₃O)+H]:168.1131; found: 168.1130

General procedure 4.1 - 5-H pyrazolopyrimidine cyclisations

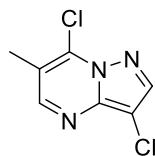
To a mixture of 1H-pyrazol-3-amine (9.87 mmol, 1.00 eq) in THF (10.00 mL) was added ethyl 2-chloro-3-oxopropanoate (9.87 mmol, 1.00 eq). The mixture was allowed to stir at 70°C for 2 h until starting material was consumed demonstrated by TLC (Petroleum ether: Ethyl acetate= 1: 1). After cooling to room temperature, *t*BuOK (14.80 mmol, 1.50 eq) was added and the mixture was allowed to stir overnight. The mixture was acidified with 4M HCl/EtOAc to adjust the pH to 5-6 and concentrated to give the crude solid

6-Methyl-3-(tetrahydro-2H-pyran-4-yl)pyrazolo[1,5-a]pyrimidin-7-ol (32a)

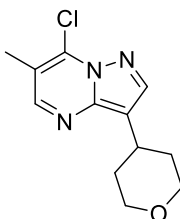
Synthesised via general procedure 4.1, reaction mixture was acidified to pH 3-4 with 4M HCl in dioxane and volatiles removed to give crude 6-methyl-3-(tetrahydro-2H-pyran-4-yl)pyrazolo[1,5-a]pyrimidin-7-ol as a yellow solid which was used without further purification; (0.52 g, 75%); **MS (Cl⁺ CH₄)**: m/z (rel. Intensity)[M+H] 234.1 (18); **HRMS (Cl⁺)** calcd for [(C₇H₆N₃Cl₂)+H]:234.1237; found: 234.1248

General procedure 4.2 for the synthesis of 7-chloro-5-methyl-pyrazolo[1,5-a]pyrimidines

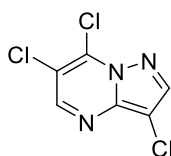
To the pyrazolo-pyrimidine compound (1 equiv) and was added POCl₃ (10 equiv) and the solution stirred under reflux overnight. The reaction was allowed to cool to room temperature, volatiles removed under reduced pressure before pouring onto crushed ice. The reaction mixture was then basified with 2M NaOH and aqueous extracted with EtOAc. The combined organic extracts were washed with brine, dried over MgSO₄ and evaporated to dryness to give the product.

3,7-Dichloro-6-methylpyrazolo[1,5-a]pyrimidine

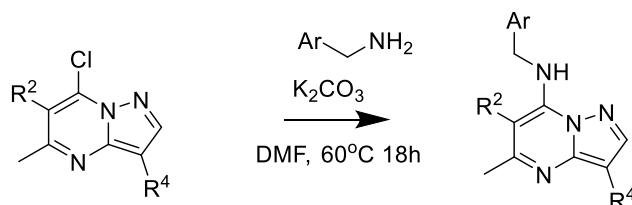
Synthesised via general procedure 4.2 as a yellow solid. (0.172 g, 36%); **¹H NMR (400 MHz, DMSO-d₆)** δ 8.61 (s, 1H), 8.45 (s, 1H), 2.43 (s, 3H); **¹³C NMR (101 MHz, DMSO-d₆)** δ 152.8, 144.2, 142.6, 137.2, 118.1, 99.8, 14.9; **MS (Cl⁺ CH₄)**: m/z (rel. Intensity)[M+H] 202.0 (100), 204.0 (65); **HRMS (Cl⁺)** calcd for [(C₇H₆N₃Cl₂)+H]:201.9933; found: 201.9943

6-Methyl-3-(tetrahydro-2H-pyran-4-yl)pyrazolo[1,5-a]pyrimidin-7-ol (33a)

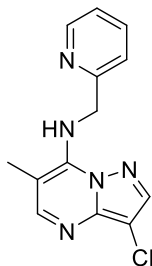
Synthesised via general procedure 4.2 to give **33a** as a yellow solid. (0.99 g, 36%); $^1\text{H NMR}$ (400 MHz, DMSO- d_6) δ 8.47 (s, 1H), 8.19 (s, 1H), 3.94 (dt, $J = 11.4, 2.9$ Hz, 2H), 3.52 – 3.45 (m, 2H), 3.19 – 3.11 (m, 1H), 2.41 (s, 3H), 1.89 – 1.76 (m, 4H); $^{13}\text{C NMR}$ (101 MHz, DMSO- d_6) δ 150.3, 145.6, 142.5, 136.1, 116.6, 116.2, 67.7, 33.4, 30.9, 14.8; **MS (CI+ CH₄)**: m/z (rel. Intensity)[M+H] 252.1 (100), 254.1 (33); **HRMS (CI+)** calcd for [(C₁₂H₁₅N₃ClO)+H]: 252.0898; found: 252.0907

3,6,7-Trichloropyrazolo[1,5-a]pyrimidine

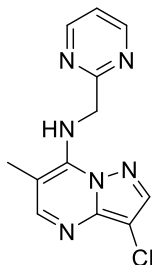
Synthesised via general procedure 4.2. (0.395 g, 66%); $^1\text{H NMR}$ (400 MHz, DMSO- d_6) δ 8.83 (s, 1H), 8.61 (s, 1H); $^{13}\text{C NMR}$ (101 MHz, DMSO- d_6) δ 149.8, 143.9, 137.5, 132.2, 117.1, 101.2; **MS (CI+ CH₄)**: m/z (rel. Intensity)[M+H] 221.9 (100), 223.9 (98); **HRMS (CI+)** calcd for [(C₆H₃N₃Cl₃)+H]: 221.9387; found: 221.9395

General procedure 4.3 for the synthesis of 5,6-dimethylpyrazolo[1,5-a]pyrimidin-7-amines²³

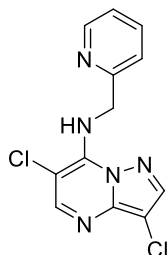
To the chlorinated pyrazolo-pyrimidine (1 equiv) in DMF was added the aryl-amine (1 equiv) and K₂CO₃ (1.2 equiv). The solutions were stirred at 60°C overnight, once completed the reactions were evaporated to dryness, diluted with EtOAc before washing with water and brine. Organics were dried using MgSO₄ before loading the crude product to silica gel and purifying by column chromatography eluting with 60% EtOAc in hexanes.

3-Chloro-6-methyl-N-(pyridin-2-ylmethyl)pyrazolo[1,5-a]pyrimidin-7-amine (AWF955)

Synthesised via general procedure 4.3 to give **AWF955** as an off-white solid. (31 mg, 29%); **Melting point:** 173-175 °C **¹H NMR (400 MHz, DMSO-*d*₆)** δ 8.56 (d, *J* = 4.2 Hz, 1H), 8.28 (t, *J* = 5.9 Hz, 1H), 8.22 (s, 1H), 8.09 (s, 1H), 7.80 (t, *J* = 7.6 Hz, 1H), 7.37 (d, *J* = 7.8 Hz, 1H), 7.31 (m, 1H), 5.17 (d, *J* = 5.9 Hz, 2H), 2.36 (s, 3H); **¹³C NMR (101 MHz, DMSO-*d*₆)** δ 158.1, 153.7, 149.4, 146.1, 144.2, 141.1, 137.6, 122.9, 121.6, 97.3, 95.9, 48.1, 14.7; **MS (ES+):** *m/z* (rel. Intensity)[*M*+*H*] 274.1 (100), 276.1 (33); **HRMS (ES+)** calcd for [(C₁₃H₁₃N₅35Cl)+*H*]:274.0859; found: 274.0862; **CHN analysis:** Calculated: C:57.04%, H:4.42%, N:25.59%. Found C:55.85%, H:4.43%, N:24.81%.

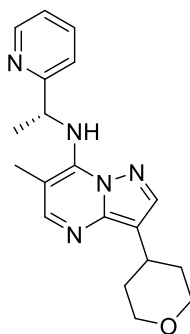
3-Chloro-6-methyl-N-(pyridin-2-ylmethyl)pyrazolo[1,5-a]pyrimidin-7-amine (AWF956)

Synthesised via general procedure 4.3 to give **AWF956** as an off-white solid. (37 mg, 35%); **Melting point:** 126-130 °C **¹H NMR (400 MHz, DMSO-*d*₆)** δ 8.86 (d, *J* = 4.8 Hz, 2H), 8.23 (s, 1H), 8.18 – 8.09 (m, 2H), 7.49 (t, *J* = 4.8 Hz, 1H) 5.36 (d, *J* = 6.0 Hz, 2H), 2.40 (s, 3H); **¹³C NMR (101 MHz, DMSO-*d*₆)** δ 166.7, 158.1, 153.4, 146.4, 144.4, 141.1, 120.5, 97.5, 95.7, 49.1, 14.5; **MS (ES+):** *m/z* (rel. Intensity)[*M*+*H*] 275.1 (100), 277.1 (30); **HRMS (ES+)** calcd for [(C₁₂H₁₂N₆35Cl)+*H*]:275.0809; found: 275.0809; **CHN analysis:** Calculated: C:52.47%, H:4.04%, N:30.59%. Found C:52.15%, H:4.24%, N:28.97%.

3,6-Dichloro-N-(pyridin-2-ylmethyl)pyrazolo[1,5-a]pyrimidin-7-amine (AWF957)

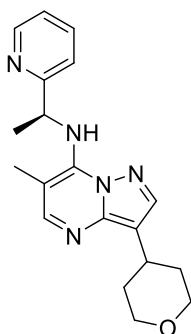
Synthesised via general procedure 4.3 (0.163 g, 83%); **Melting point:** 161-163 °C **¹H NMR (400 MHz, DMSO-*d*₆)** δ 8.69 (t, *J* = 5.9 Hz, 1H), 8.53 (d, *J* = 4.4 Hz, 1H), 8.32 (s, 1H), 8.26 (s, 1H), 7.80 (t, *J* = 7.8 Hz, 1H), 7.38 (d, *J* = 7.8 Hz, 1H), 7.30 (d, *J* = 6.1 Hz 1H), 5.31 (d, *J* = 6.2 Hz, 2H); **MS (ES+):** *m/z* (rel. Intensity)[*M*+*H*] 294.0 (100), 296.0 (50); **¹³C NMR (101 MHz, DMSO-*d*₆)** δ 157.6, 150.9, 149.2, 144.5, 143.8, 142.2, 137.5, 122.9, 121.4, 97.6, 96.3, 48.2; **HRMS (ES+)** calcd for [(C₁₂H₁₀N₅Cl₂)+H]:294.0313; found: 294.0307; **CHN analysis:** Calculated: C:49.00%, H:3.08%, N:23.81%. Found C:48.87%, H:3.12%, N:23.19%.

(R)-6-Methyl-N-(1-(pyridin-2-yl)ethyl)-3-(tetrahydro-2H-pyran-4-yl)pyrazolo[1,5-a]pyrimidin-7-amine (AWF960)



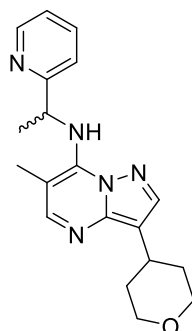
Synthesised via general procedure 4.3 to give **AWF960** as a white solid (58 mg, 14%); **Melting point:** 119-120 °C **¹H NMR (500 MHz, DMSO-*d*₆)** δ 8.61 (d, *J* = 4.5 Hz, 1H), 8.01 (s, 1H), 7.98 (s, 1H), 7.82 (td, *J* = 7.7, 1.8 Hz, 1H), 7.66 (d, *J* = 9.1 Hz, 1H), 7.50 (d, *J* = 7.9 Hz, 1H), 7.33 (ddd, *J* = 7.5, 4.5, 0.9 Hz, 1H), 5.65 (dq, *J* = 13.7, 6.8 Hz, 1H), 3.93 (dd, *J* = 10.4, 2.7 Hz, 2H), 3.46 (td, *J* = 11.3, 2.7 Hz, 2H), 3.08 – 3.01 (m, 1H), 2.37 (s, 3H), 1.89 – 1.74 (m, 4H), 1.55 (d, *J* = 6.7 Hz, 3H); **¹³C NMR (101 MHz, DMSO-*d*₆)** δ 162.0, 152.1, 149.5, 145.5, 144.6, 140.7, 137.8, 123.2, 121.4, 112.8, 96.3, 67.8(2C), 53.5, 33.5, 30.9, 24.9, 14.8; **MS (ES+):** *m/z* (rel. Intensity)[*M*+*H*] 338.2 (100), 339.2 (13); **HRMS (ES+)** calcd for [(C₁₉H₂₄N₅O)+H]:338.1981; found: 338.1968; **CHN analysis:** Calculated: C:67.63%, H:6.87%, N:20.76%. Found C:66.46%, H:6.89%, N:19.86%.

(S)-6-Methyl-N-(1-(pyridin-2-yl)ethyl)-3-(tetrahydro-2H-pyran-4-yl)pyrazolo[1,5-a]pyrimidin-7-amine (AWF961)



Synthesised via general procedure 4.3 to give **AWF961** as a white solid (45 mg, 17%); **Melting point:** 119-120 °C **¹H NMR (400 MHz, DMSO-*d*₆)** δ 8.61 (d, *J* = 4.8 Hz, 1H), 8.01 (s, 1H), 7.98 (s, 1H), 7.82 (td, *J* = 7.7, 1.5 Hz, 1H), 7.68 (d, *J* = 9.1 Hz, 1H), 7.50 (d, *J* = 7.8 Hz, 1H), 7.33 (dd, *J* = 6.8, 4.8 Hz, 1H), 5.65 (dq, *J* = 13.5, 6.6 Hz, 1H), 3.92 (d, *J* = 10.9 Hz, 1H), 3.46 (td, *J* = 11.2, 2.8 Hz, 1H), 3.09 – 2.99 (m, 1H), 2.76 (s, 3H), 1.87 – 1.73 (m, 1H), 1.55 (d, *J* = 6.6 Hz, 3H); **¹³C NMR (101 MHz, DMSO-*d*₆)** δ 162.0, 152.1, 149.5, 145.5, 144.6, 140.7, 137.8, 123.2, 121.4, 112.8, 96.3, 67.8 (2C), 53.5, 33.5, 30.9 (2C), 24.9, 14.8; **MS (ES+):** *m/z* (rel. Intensity)[M+H] 338.2 (100), 339.2 (13); **HRMS (ES+)** calcd for [(C₁₉H₂₄N₅O)+H]:338.1981; found: 338.1977; **CHN analysis:** Calculated: C:67.63%, H:6.87%, N:20.76%. Found C:66.57%, H:6.66%, N:19.90%.

6-Methyl-N-(1-(pyridin-2-yl)ethyl)-3-(tetrahydro-2H-pyran-4-yl)pyrazolo[1,5-a]pyrimidin-7-amine (AWZ9100)



Synthesised via general procedure 4.3 to give **AWZ9100** as a white solid (48 mg, 51%); **¹H NMR (400 MHz, DMSO-*d*₆)** δ 8.61 (d, *J* = 4.6 Hz, 1H), 8.01 (s, 1H), 7.98 (s, 1H), 7.81 (t, *J* = 7.1 Hz, 1H), 7.66 (d, *J* = 9.0 Hz, 1H), 7.50 (d, *J* = 7.8 Hz, 1H), 7.32 (dd, *J* = 7.1, 4.6 Hz, 1H), 5.69 – 5.60 (m, 1H), 3.92 (d, *J* = 10.8 Hz, 2H), 3.46 (td, *J* = 11.0, 2.5 Hz, 2H), 3.09 – 2.99 (m, 1H), 2.37 (s, 3H), 1.85 – 1.76 (m, 4H), 1.55 (d, *J* = 6.6 Hz, 3H); **¹³C NMR (101 MHz, DMSO-*d*₆)** δ 162.0, 152.2, 149.5, 145.5, 144.6, 140.7, 137.8, 123.2, 121.4, 112.8, 96.3, 67.8(2C), 53.5, 33.5, 30.9, 24.9, 14.8; **MS (ES+):** *m/z* (rel. Intensity)[M+H] 338.2 (100), 339.2 (13); **HRMS (ES+)** calcd for [(C₁₉H₂₄N₅O)+H]:338.1981; found: 338.1968; **CHN analysis:** Calculated: C:67.63%, H:6.87%, N:20.76%. Found C:66.92%, H:6.85%, N:20.48%.

4.7 References

- (1) St. Jean, D. J.; Fotsch, C. Mitigating Heterocycle Metabolism in Drug Discovery. *J. Med. Chem.* **2012**, *55* (13), 6002–6020.
- (2) Klebe, G. The Foundations of Protein–Ligand Interaction BT - From Molecules to Medicines: Structure of Biological Macromolecules and Its Relevance in Combating New Diseases and Bioterrorism; Sussman, J. L., Spadon, P., Eds.; Springer Netherlands: Dordrecht, 2009; pp 79–101.
- (3) Kerekes, A. D.; Esposito, S. J.; Doll, R. J.; Tagat, J. R.; Yu, T.; Xiao, Y.; Zhang, Y.; Prelusky, D. B.; Tevar, S.; Gray, K.; Terracina, G. A.; Lee, S.; Jones, J.; Liu, M.; Basso, A. D.; Smith, E. B. Aurora Kinase Inhibitors Based on the Imidazo[1,2-A]pyrazine Core: Fluorine and Deuterium Incorporation Improve Oral Absorption and Exposure. *J. Med. Chem.* **2011**, *54* (1), 201–210.
- (4) Gleave, R. J.; Beswick, P. J.; Brown, A. J.; Giblin, G. M. P.; Goldsmith, P.; Haslam, C. P.; Mitchell, W. L.; Nicholson, N. H.; Page, L. W.; Patel, S.; Roomans, S.; Slingsby, B. P.; Swarbrick, M. E. Synthesis and Evaluation of 3-Amino-6-Aryl-Pyridazines as Selective CB2 Agonists for the Treatment of Inflammatory Pain. *Bioorg. Med. Chem. Lett.* **2010**, *20* (2), 465–468.
- (5) Stepan, A. F.; Karki, K.; McDonald, W. S.; Dorff, P. H.; Dutra, J. K.; DiRico, K. J.; Won, A.; Subramanyam, C.; Efremov, I. V.; O'Donnell, C. J.; Nolan, C. E.; Becker, S. L.; Pustilnik, L. R.; Sneed, B.; Sun, H.; Lu, Y.; Robshaw, A. E.; Riddell, D.; O'Sullivan, T. J.; Sibley, E.; Capetta, S.; Atchison, K.; Hallgren, A. J.; Miller, E.; Wood, A.; Obach, R. S. Metabolism-Directed Design of Oxetane-Containing Arylsulfonamide Derivatives as γ -Secretase Inhibitors. *J. Med. Chem.* **2011**, *54* (22), 7772–7783.
- (6) Dragovich, P. S.; Blazel, J. K.; Ellis, D. A.; Han, Q.; Kamran, R.; Kissinger, C. R.; LeBrun, L. A.; Li, L.-S.; Murphy, D. E.; Noble, M.; Patel, R. A.; Ruebsam, F.; Sergeeva, M. V.; Shah, A. M.; Showalter, R. E.; Tran, C. V.; Tsan, M.; Webber, S. E.; Kirkovsky, L.; Zhou, Y. Novel HCV NS5B Polymerase Inhibitors Derived from 4-(1',1'-dioxo-1',4'-dihydro-1' λ (6)-benzo[1',2',4']thiadiazin-3'-yl)-5-Hydroxy-2H-Pyridazin-3-Ones. Part 5: Exploration of Pyridazinones Containing 6-Amino-Substituents. *Bioorg. Med. Chem. Lett.* **2008**, *18* (20), 5635–5639.
- (7) Kalgutkar, A. S.; Dalvie, D. K.; O'Donnell, J. P.; Taylor, T. J.; Sahakian, D. C. On the Diversity of Oxidative Bioactivation Reactions on Nitrogen-Containing Xenobiotics. *Curr. Drug Metab.* **2002**, *3* (4), 379–424.
- (8) Cyprotex Guide book. "Everything You Need to Know about ADME"; 2015.
- (9) Elsby, R.; Surry, D. D.; Smith, V. N.; Gray, A. J. Validation and Application of Caco-2 Assays for the in Vitro Evaluation of Development Candidate Drugs as Substrates or Inhibitors of P-Glycoprotein to Support Regulatory Submissions. *Xenobiotica* **2008**, *38* (7–8), 1140–1164.

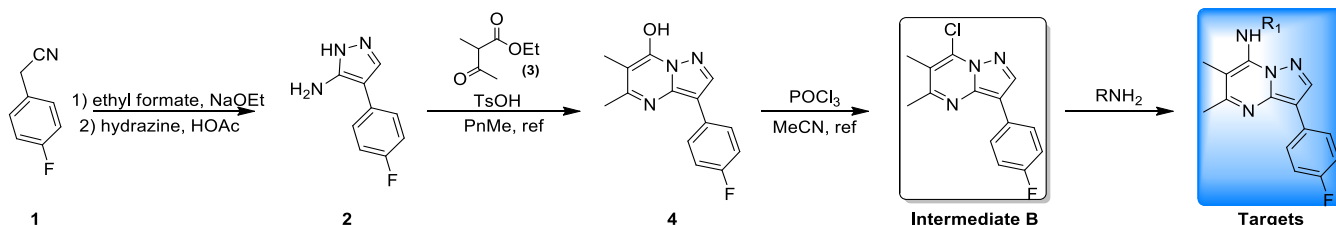
- (10) FDA. *US FDA Draft Guidance for Industry Drug Interaction Studies - Study, Design, Data, Analysis, Implications for Dosing and Labelling Recommendations*; 2012.
- (11) Japanese Ministry of Health, Labour and Welfare (JMHLW) Guideline on Drug-Drug Interactions (2014).
- (12) European Medicines Agency (EMA) Guideline on the Investigation of Drug Interactions (21 June 2012).
- (13) Hann, M. M.; Keserü, G. M. Finding the Sweet Spot: The Role of Nature and Nurture in Medicinal Chemistry. *Nat Rev Drug Discov* **2012**, *11* (5), 355–365.
- (14) Leeson, P. D.; Young, R. J. Molecular Property Design: Does Everyone Get It? *ACS Med. Chem. Lett.* **2015**, *6* (7), 722–725.
- (15) Huttunen, K. M.; Raunio, H.; Rautio, J. Prodrugs—from Serendipity to Rational Design. *Pharmacol. Rev.* **2011**, *63* (3), 750 LP-771.
- (16) Jones, C. L.; Yeung, B. K. S.; Manjunatha, U.; Shi, P.-Y.; Bodenreider, C.; Diagana, T. T. Drug Discovery for the Developing World: Progress at the Novartis Institute for Tropical Diseases. *Nat Rev Drug Discov* **2015**, *14* (6), 442–444.
- (17) Al-Adiwish, W. M.; Tahir, M. I. M.; Siti-Noor-Adnalizawati, A.; Hashim, S. F.; Ibrahim, N.; Yaacob, W. A. Synthesis, Antibacterial Activity and Cytotoxicity of New Fused pyrazolo[1,5-A]pyrimidine and pyrazolo[5,1-c][1,2,4]triazine Derivatives from New 5-Aminopyrazoles. *Eur. J. Med. Chem.* **2013**, *64*, 464–476.
- (18) Lefoix, M.; Mathis, G.; Kleinmann, T.; Truffert, J.-C.; Asseline, U. Pyrazolo[1,5-a]-1,3,5-Triazine C-Nucleoside as Deoxyadenosine Analogue: Synthesis, Pairing, and Resistance to Hydrolysis. *J. Org. Chem.* **2014**, *79* (7), 3221–3227.
- (19) Chu, C. K.; Watanabe, K. A.; Fox, J. J. Nucleosides. 117. Synthesis of 4-Oxo-8-(β -D-Ribofuranosyl)-3H-pyrazolo[1,5-a]-1,3,5-Triazine (OPTR) via 3-Amino-2N-Carbamoyl-4-(β -D-Ribofuranosyl)pyrazole (ACPR) Derivatives. *J. Heterocycl. Chem.* **1980**, *17* (7), 1435–1439.
- (20) Ryono, D. E.; Cheng, P. T. W.; Bolton, S. A.; Chen, S. S.; Shi, Y.; Meng, W.; Tino, J. A.; Zhang, H.; Sulsky, R. B. Novel N-Heterocyclic Phosphonates and Phosphinates as Glucokinase Activators for Treatment of Type II Diabetes., WO2008005964A2, January 10, 2008.
- (21) Speake, J. D.; Beck, B. C.; Fan, W. Preparation of Pyridinylthiazole Derivatives as Antiparasitic Agents., PCT Int. Appl., WO2016183173A1, November 17, 2016.
- (22) Laurent, A.; Rose, Y. Preparation of 4-aminopyrrolo[2,3-E]pyrimidine Derivatives as Btk Protein Kinase Inhibitors., PCT Int. Appl., WO2015074135A1 May 28, 2015.
- (23) Hwang, J. Y.; Windisch, M. P.; Jo, S.; Kim, K.; Kong, S.; Kim, H. C.; Kim, S.; Kim, H.; Lee, M. E.; Kim, Y.;

Choi, J.; Park, D.-S.; Park, E.; Kwon, J.; Nam, J.; Ahn, S.; Cechetto, J.; Kim, J.; Liuzzi, M.; No, Z.; Lee, J. Discovery and Characterization of a Novel 7-aminopyrazolo[1,5-A]pyrimidine Analog as a Potent Hepatitis C Virus Inhibitor. *Bioorg. Med. Chem. Lett.* **2012**, 22 (24), 7297–7301.

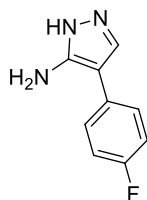
Appendix 1

WuXi App Tech Experimental

Appendix 1 WuXi App Tech Experimental

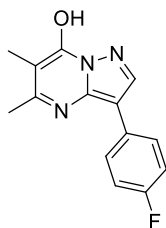


Synthesis of 4-(4-fluorophenyl)-1H-pyrazol-5-amine (2)



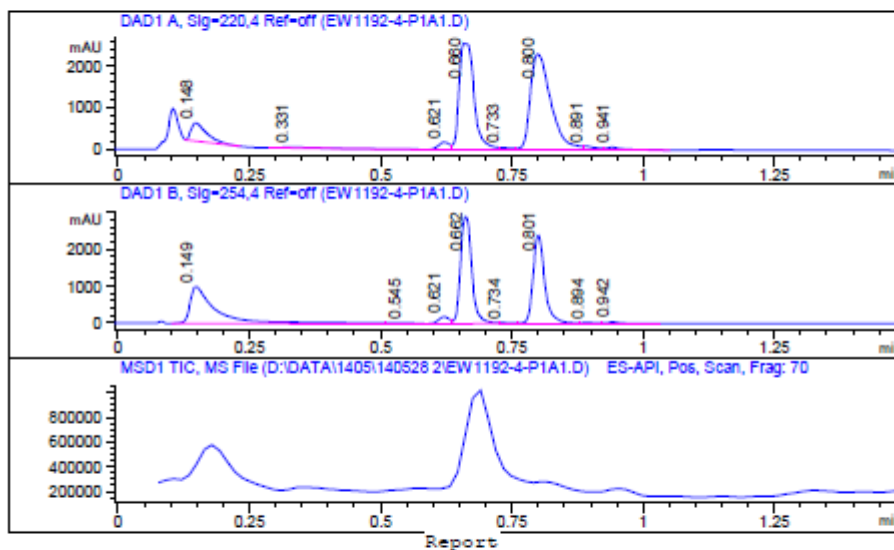
To a mixture of NaOEt (3.02 g, 44.40 mmol, 1.20 Eq) in EtOH (50 mL) at 0 °C was added 2-(4-fluorophenyl) acetonitrile (5.00 g, 37.00 mmol, 1.00 Eq). The mixture was stirred at 0 °C for 5 min. Then ethyl formate (6.85 g, 92.50 mmol, 2.50 Eq) was added. The mixture was heated to 85 °C and stirred for 1 h. TLC (Petroleum ether: EtOAc=5: 1) showed SM was consumed. The mixture was concentrated to give a residue. The residue was dissolved in H₂O (50 mL) and adjusted to pH₃~4 with HCl (aq., 2 N). Then the mixture was extracted with EtOAc (50 mL*3). The organic layer was washed with brine (50 mL*2), dried over Na₂SO₄ and concentrated to give 2-(4-fluorophenyl)-3-oxo-propanenitrile (6.00 g, crude) as a yellow solid.

NH₂-NH₂.H₂O (3.68 g, 73.56 mmol, 2.00 Eq) was added to a mixture of 2-(4-fluorophenyl)-3-oxo-propanenitrile (6.00 g, 36.78 mmol, 1.00 Eq) in EtOH (50 mL), followed by AcOH (N/A, 52.46 mmol, 1.43 Eq). After being stirred at 85 °C for 2 hr, the reaction mixture was cooled to 25 °C and concentrated to give a residue. The residue was diluted with H₂O (50 mL). The mixture was extracted with EtOAc (50 mL*3). The combined organic layer was washed with brine (50 mL*2), dried over Na₂SO₄ and concentrated to give 4-(4-fluorophenyl)-1H-pyrazol-5-amine (5.70 g, crude) as a yellow solid which was used in the next step without purification.

Synthesis of 3-(4-fluorophenyl)-5,6-dimethylpyrazolo[1,5-a]pyrimidin-7-ol (4)

A mixture of 4-(4-fluorophenyl)-1H-pyrazol-5-amine (5.50 g, 31.04 mmol, 1.00 Eq), ethyl 2-methyl-3-oxobutanoate (4.92 g, 34.14 mmol, 1.10 Eq) and TsOH (534.51 mg, 3.10 mmol, 0.10 Eq) in toluene (50 mL) was stirred at 120 °C for 2 hr. LCMS showed starting material was consumed and the major peak is the desired product. The mixture was concentrated to give a residue which was triturated with EtOAc (20 mL). The mixture was filtered and the filtrate was dried under vacuum to give 3-(4-fluorophenyl)-5,6-dimethyl-pyrazolo[1,5-a]pyrimidin-7-ol (5.20 g, 20.21 mmol, 65% yield) as a white solid.

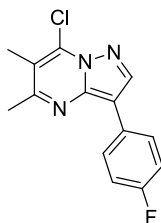
Compound ID :
 Sample ID : EW1192-4-P1A1
 Injection Date : 2014-05-28 11:53:56
 Location : P1-C-06
 Injection volume : 1.000
 Acq Method : D:\DATA\1405\140528 2\5-95AB_R_220&254.M
 Data Filename : D:\DATA\1405\140528 2\EW1192-4-P1A1.D
 Instrument : LCMS-G
 Column:Chromolith Flash RP-18e 25*2mm



Signal 1 : DAD1 A, Sig=220,4 Ref=off

#	Meas. Ret.	Height	Width	Area	Area %
1	0.148	431.731	0.032	916.317	7.052
2	0.331	20.708	0.100	154.326	1.188
3	0.621	177.199	0.023	256.135	1.971
4	0.660	2550.843	0.032	5089.151	39.167
5	0.733	50.882	0.021	77.311	0.595
6	0.800	2302.645	0.041	6231.857	47.961
7	0.891	82.572	0.024	141.846	1.092
8	0.941	61.013	0.028	126.550	0.974

Synthesis of 7-chloro-3-(4-fluorophenyl)-5,6-dimethylpyrazolo[1,5-a]pyrimidine (Intermediate B)



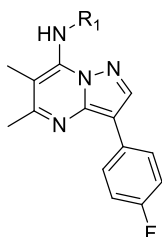
To a mixture of 3-(4-fluorophenyl)-5,6-dimethyl-pyrazolo[1,5-a]pyrimidin-7-ol (5.00 g, 19.44 mmol, 1.00 Eq) and POCl₃ (8.94 g, 58.32 mmol, 3.00 Eq) in MeCN (50 mL) was added TEA (3.93 g, 38.88 mmol, 2.00 Eq). The

mixture was stirred at 120 °C for 8 hr. LCMS showed starting material was consumed. The mixture was cooled to 25 °C, poured into water slowly and extracted with EtOAc (50 mL*3). The combined organic layer was washed with brine (50mL*2), dried over Na₂SO₄ and concentrated to give a residue which was purified by chromatography (EtOAc/Petroleum ether = 1/8) to give 7-chloro-3-(4-fluorophenyl)-5,6-dimethyl-pyrazolo[1,5-a]pyrimidine (2.70 g, 9.79 mmol, 50% yield) as a yellow solid.

¹H NMR (400 MHz, CHLOROFORM-d): δ 8.37 (s, 1 H), 7.96 - 8.07 (m, 1 H), 7.08 - 7.20 (m, 1 H), 2.68 (s, 3 H), 2.47 (s, 3 H).

LCMS (Method 5-95AB): RT =0.928 min / 1.5 min, M+H⁺ = 276.1

Synthesis of AWZ9001~9004 & AWZ9024~9026



A mixture of 7-chloro-3-(4-fluorophenyl)-5,6-dimethyl-pyrazolo[1,5-a]pyrimidine (200.00 mg, 725.40 μmol, 1.00 Eq), RNH₂ (870.48 μmol, 1.20 Eq) and TEA (146.81 mg, 1.45 mmol, 2.00 Eq) in DMF (2 mL) was stirred at 110 °C for 4 hr. LCMS showed starting material was consumed and desired mass. The mixture was diluted with water (5 mL) and the precipitate was collected by filtration and purified by prep-HPLC (FA or HCl) to give target compounds as a light yellow solid.

AWZ9001

¹H NMR (400 MHz, DMSO-d₆): δ 8.50 (s, 1 H), 8.18 (dd, J=8.72, 5.58 Hz, 2 H), 7.21 (t, J=8.91 Hz, 2 H), 6.93 (t, J=5.58 Hz, 1 H), 3.90 (q, J=6.11 Hz, 2 H), 3.48 (t, J=4.27 Hz, 4 H), 2.57 (t, J=6.09 Hz, 2 H), 2.51 - 2.53 (m, 3 H), 2.38 (br. s., 4 H), 2.29 (s, 3 H).

LCMS (Method 5-95AB): RT =0.593 min / 1.5 min, M+H⁺ = 370.3

AWZ9002

¹H NMR (400 MHz, DMSO-d₆): δ 8.49 (s, 1 H), 8.23 (s, 1 H), 8.13 - 8.20 (m, 2 H), 7.15 - 7.25 (m, 2 H), 6.90 (t, J=5.58 Hz, 1 H), 3.87 (q, J=6.02 Hz, 2 H), 2.56 (t, J=6.21 Hz, 2 H), 2.50 - 2.53 (m, 2 H), 2.48 (s, 3 H), 2.28 - 2.46 (m, 6 H), 2.27 (s, 3 H) 2.16 (s, 3 H).

LCMS (Method 5-95AB): RT =0.661 min / 1.5 min, M+H⁺ = 383.1

AWZ9003

¹H NMR (400 MHz, DMSO-d₆): δ 8.49 (s, 1H), 8.13-8.21 (m, 3H), 7.18-7.25 (m, 2H), 7.00 (t, J=5.33 Hz, 1H), 3.88 (q, J=5.90 Hz, 2H), 2.56 (t, J=6.34 Hz, 2H), 2.49 (s, 3H), 2.30 (s, 3H), 2.24 (s, 6H)

LCMS (Method 5-95AB): RT =0.676 min / 1.5 min, M+H⁺ = 328.1

AWZ9024

¹H NMR (400 MHz, DMSO-d₆) : δ 8.74 (d, J=4.89 Hz, 1H), 8.48 (s, 1H), 8.21 (br. s., 1H), 7.97-8.07 (m, 2H), 7.88 (d, J=7.78 Hz, 2H), 7.65 (br. s., 1H), 7.26 (t, J=8.97 Hz, 2H), 6.23 (br. s., 1H), 2.55 (s, 3H), 2.32 (s, 3H), 1.72 (d, J=6.78 Hz, 3H)

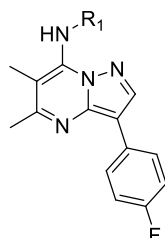
LCMS (Method 5-95AB): RT =0.787 min / 1.5 min, M+H⁺ = 362.0

AWZ9025

¹H NMR (400 MHz, DMSO-d₆) : δ 8.85 (d, J=4.89 Hz, 1H), 8.59 (s, 1H), 8.49 (t, J=7.47 Hz, 1H), 8.14-8.21 (m, 2H), 8.08 (d, J=7.78 Hz, 1H), 7.91 (t, J=6.53 Hz, 1H), 7.20-7.32 (m, 2H), 5.01 (s, 2H), 3.06 (s, 3H), 2.59 (s, 3H), 2.29 (s, 3H)

LCMS (Method 5-95AB): RT =0.808 min / 1.5 min, M+H⁺ = 362.1

Synthesis of AWZ9007-8



A mixture of 7-chloro-3-(4-fluorophenyl)-5,6-dimethyl-pyrazolo[1,5-a]pyrimidine (200.00 mg, 725.40 μmol, 1.00 Eq) , RNH₂ (797.94 μmol, 1.10 Eq) , Cs₂CO₃ (354.52 mg, 1.09 mmol, 1.50 Eq) , BINAP (90.34 mg, 145.08 μmol, 0.20 Eq) and diacetoxypalladium (16.29 mg, 72.54 μmol, 0.10 Eq) in tol. (5 mL) was stirred at 110 °C for 16 hr under N₂ protection. The color of the mixture turned brown. LCMS showed starting material consumed. The mixture was diluted with EtOAc (30 mL) and washed with brine (20 mL*2). The organic layer was dried over

Na₂SO₄ and concentrated to give a residue. The residue was purified by trituration (MeOH, 15 mL; 2 N HCl, 0.5 mL; EtOAc, 20 mL) or prep-HPLC (HCl) to give target compounds as a yellow solid.

AWZ9007

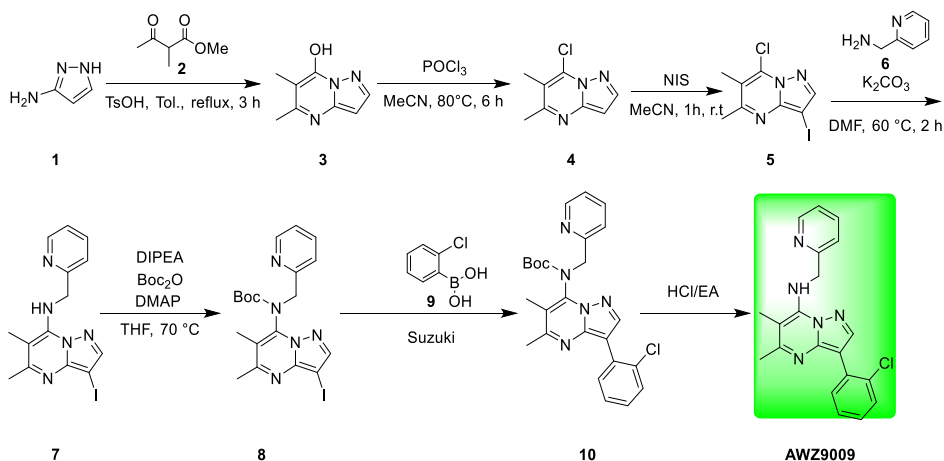
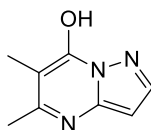
¹H NMR (400 MHz, DMSO-d₆): δ 8.53 (br. s., 1H), 8.09-8.25 (m, 3H), 7.89 (t, J=7.28 Hz, 1H), 7.20-7.30 (m, 3H), 7.04 (t, J=6.09 Hz, 1H), 2.62 (s, 3H), 2.15 (s, 3H)

LCMS (Method 5-95AB): RT = 0.811 min / 1.5 min, M+H⁺ = 334.0

AWZ9008

¹H NMR (400 MHz, DMSO-d₆): δ 9.92 (br. s., 1H), 8.55 (s, 1H), 8.16-8.23 (m, 2H), 8.13 (d, J=3.01 Hz, 1H), 7.70 (dt, J=3.07, 8.69 Hz, 1H), 7.23-7.31 (m, 2H), 7.13 (dd, J=3.70, 9.10 Hz, 1H), 2.61 (s, 3H), 2.06 (s, 3H)

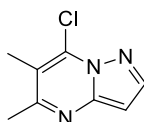
LCMS (Method 5-95AB): RT = 0.919 min / 1.5 min, M+H⁺ = 352.0

**5,6-dimethylpyrazolo[1,5-a]pyrimidin-7-ol (3).**

To a suspension of compound 1 and compound 2 (10.00 g, 76.84 mmol) in toluene (200 mL) was added 4-methylbenzenesulfonic acid hydrate (1.46 g, 7.68 mmol). The mixture was stirred at 110 °C for 3 hours. TLC

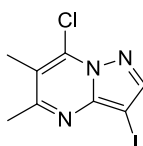
(petroleum ether: ethyl acetate = 3:1) showed the starting material disappeared. The mixture was cooled to 25 °C and water (200 mL) was added slowly. After stirred for 10 minutes, the precipitate was collected by suction filtration to give pure compound **3** (10.00 g, 61.28 mmol, 80% yield) as a white solid.

7-chloro-5,6-dimethylpyrazolo[1,5-a]pyrimidine (**4**)



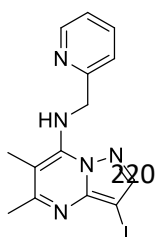
To a suspension of compound **3** (10.00 g, 61.28 mmol) in MeCN (100 mL) was added POCl₃ (82.00 g, 534.79 mmol) one portion at 25 °C. The mixture was stirred at 80 °C for 6 hours. TLC (petroleum ether: ethyl acetate = 3:1) showed the starting material disappeared. The mixture was cooled to 25 °C, then poured slowly into water (150 mL). The mixture was adjusted to pH about 7 with K₂CO₃. The mixture was extracted with ethyl acetate (100 mL*3). The combined organic layer was dried over sodium sulfate, concentrated to give crude product which was purified by chromatography (petroleum ether: ethyl acetate = 10:1 to 5:1) to give pure compound **4** (9.00 g, 49.55 mmol, 81% yield) as white solid. MS: 182.1 (M+H⁺).

7-chloro-3-iodo-5,6-dimethylpyrazolo[1,5-a]pyrimidine (**5**)



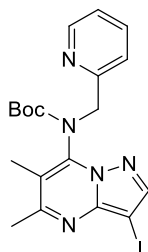
To a solution of compound **4** (1.00 g, 5.51 mmol) in MeCN (10 mL) was added NIS (1.24 g, 5.51 mmol). The mixture was stirred at 25 °C under nitrogen atmosphere for 2 hr, TLC (petroleum ether: ethyl acetate = 3:1) showed the starting material disappeared completely. The mixture was concentrated to give a residue which was purified by chromatography (petroleum ether: ethyl acetate = 10:1 to 5:1) to give compound **5** (1.20 g, 3.90 mmol, 71% yield) as a white solid. MS: 308.0 (M+H⁺)

3-iodo-5,6-dimethyl-N-(pyridin-2-ylmethyl)pyrazolo[1,5-a]pyrimidin-7-amine (**7**)



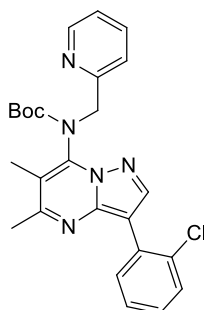
A mixture of compound **5** (1.20 g, 3.90 mmol), compound **6** (421.98 mg, 3.90 mmol) and K_2CO_3 (1.08 g, 7.80 mmol) in DMF (10 mL) was stirred at 60 °C for 2 hr. TLC (petroleum ether: ethyl acetate = 3:1) showed the starting material disappeared. After water (20 mL) was added, the precipitate was collected by suction filtration to give compound **7** (800.00 mg, 2.11 mmol, 54% yield) as a pale yellow solid. MS: 380.0 (M+H⁺)

tert-butyl(3-iodo-5,6-dimethylpyrazolo[1,5-a]pyrimidin-7-yl)(pyridin-2-ylmethyl)carbamate (8)



A mixture of compound **7** (1.00 g, 2.64 mmol), DIPEA (681.65 mg, 5.27 mmol), DMAP (161.09 mg, 1.32 mmol) and Boc_2O (1.15 g, 5.27 mmol) in THF (20 mL) was stirred at 70 °C for 2 hr. TLC (petroleum ether: ethyl acetate = 3:1) showed starting material was consumed completely and a new spot was formed. Removed the solvent under vacuum, the residue was purified by chromatography (petroleum ether/ ethyl acetate=10:1 to 3:1) to give compound **8** (1.00 g, 2.09 mmol, 79% yield) as a white solid. MS: 480.1 (M+H⁺).

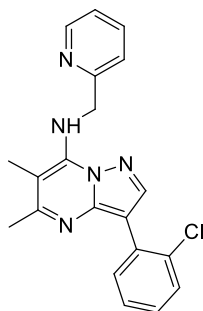
3-(2-chlorophenyl)-5,6-dimethyl-N-(pyridin-2-ylmethyl)pyrazolo[1,5-a]pyrimidin-7-amine (10)



A suspension of (2-chlorophenyl)boronic acid (39.15 mg, 250.36 μ mol), compound **8** (100.00 mg, 208.63 μ mol), Na_2CO_3 (44.23 mg, 417.26 μ mol) and ditert-butyl(cyclopentyl)phosphane;dichloropalladium;iron (13.60 mg, 20.86 μ mol) in dioxane (10 mL) and water (2 mL) was stirred at 100°C under nitrogen atmosphere for 2 hr. TLC (petroleum ether/ethyl acetate= 3:1) showed starting material was consumed and a new spot formed .

Removed solvent under vacuum to give a residue which was purified directly by chromatography (petroleum ether/ethyl acetate=10:1 to 3:1) to give compound **10** (60.00 mg, 129.32 μ mol, 62% yield) as a pale yellow oil.

3-(2-chlorophenyl)-5,6-dimethyl-N-(pyridin-2-ylmethyl)pyrazolo[1,5-a]pyrimidin-7-amine(AWZ9009)



To a solution compound (60.00 mg, 129.32 μ mol) in ethyl acetate (3 mL) was added HCl/EtOAc (4 M, 3.00 mL). The solution was stirred for 2 hr at 25 °C and a white precipitate formed. TLC (petroleum ether/ethyl acetate= 3:1) showed the starting material was consumed completely. Filtrated the precipitate by filter and washed with ethyl acetate (2 mL) to give a residue which was purified by prep-HPLC (FA) to give AWZ9009 (13.70 mg, 33.43 μ mol, 26% yield) as a gray solid.

LCMS (Method 30-90CD, ESI): RT =1.318min: 2 min, M+H⁺ =364.1

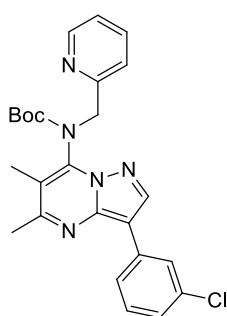
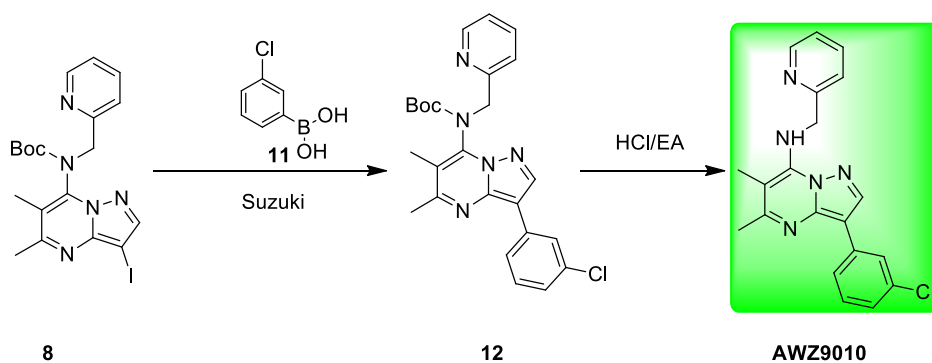
¹H NMR (400MHz, DMSO-d₆) δ = 8.58 (d, *J*=4.1 Hz, 1H), 8.40 (s, 1H), 8.00 - 7.90 (m, 2H), 7.81 (dt, *J*=1.8, 7.7 Hz, 1H), 7.53 (dd, *J*=1.1, 7.9 Hz, 1H), 7.44 - 7.37 (m, 1H), 7.34 - 7.24 (m, 1H), 5.22 (d, *J*=6.1 Hz, 1H), 2.44 (s, 1H), 2.32 (s, 1H).

The above general procedure was followed for the syntheses of **AWZ9014**.

LCMS (Method 30-90CD, ESI): RT =1.055min: 2 min, M+H⁺ =408.1

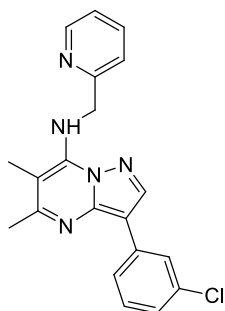
¹H NMR (400MHz, DMSO-d₆) δ = 8.69 (s, 1H), 8.56 (d, *J*=4.8 Hz, 1H), 8.42 (d, *J*=8.7 Hz, 2H), 8.00 (t, *J*=6.1 Hz, 1H), 7.90 (d, *J*=8.7 Hz, 2H), 7.79 (dt, *J*=1.8, 7.7 Hz, 1H), 7.40 (d, *J*=7.9 Hz, 1H), 7.30 (dd, *J*=5.3, 7.1 Hz, 1H), 5.24 (d, *J*=6.0 Hz, 1H), 3.20 (s, 1H), 2.54 (s, 3H), 2.33 (s, 1H)

tert-butyl(3-(3-chlorophenyl)-5,6-dimethylpyrazolo[1,5-a]pyrimidin-7-yl)(pyridin-2-ylmethyl)carbamate (12)



A suspension of (3-chlorophenyl)boronic acid (39.15 mg, 250.36 μmol), compound **8** (100.00 mg, 208.63 μmol), Na_2CO_3 (44.23 mg, 417.26 μmol), ditert-butyl(cyclopentyl)phosphane;dichloropalladium;iron(13.60 mg, 20.86 μmol) in dioxane (10 mL) and water (2 mL) was stirred at 100°C under nitrogen atmosphere for 2 hr. TLC (petroleum ether/ethyl acetate= 3:1) showed starting material was consumed and a new spot formed. Removed solvent under vacuum to give a residue which was purified directly by TLC (petroleum ether/ethyl acetate=3:1) to give compound **12** (60.00 mg, 129.32 μmol , 62% yield) as a pale yellow oil.

3-(3-chlorophenyl)-5,6-dimethyl-N-(pyridin-2-ylmethyl)pyrazolo[1,5-a]pyrimidin-7-amine(AWZ9010)



To a solution compound (60.00 mg, 129.32 μmol) in ethyl acetate (3 mL) was added HCl/EtOAc (4 M, 3.00 mL). The solution was stirred for 2 hr at 25°C and a white precipitate formed. TLC (petroleum ether/ethyl acetate= 3:1) showed

the starting material was consumed completely. Filtrated the precipitate by filter and washed with ethyl acetate (2 mL) to give AWZ9010 (42.50 mg, 106.17 μ mol, 82 % yield) as a white solid.

LCMS (Method 5-95AB, ESI): RT =0.740min: 2 min, M+H⁺ =364.1

¹H NMR (400MHz, DMSO-d₆) δ = 8.76 (d, J=4.9 Hz, 1H), 8.44 (s, 2H), 8.30 (br. s., 1H), 8.01 (d, J=8.4 Hz, 2H), 7.85 (d, J=8.2 Hz, 1H), 7.74 (br. s., 1H), 7.46 (d, J=8.4 Hz, 2H), 5.52 (br. s., 2H), 2.56 (s, 3H), 2.30 (s, 3H).

AWZ9012

LCMS (Method 5-95AB, ESI): RT =0.802min: 2 min, M+H⁺ =398.2

¹H NMR (400MHz, DMSO-d₆) δ = 8.76 (d, J=5.0 Hz, 1H), 8.54 (s, 1H), 8.28 (d, J=7.8 Hz, 4H), 7.86 (d, J=7.5 Hz, 1H), 7.73 (d, J=7.9 Hz, 1H), 5.49 (br. s., 2H), 2.56 (s, 3H), 2.30 (s, 3H).

AWZ 9013

For AWZ9014 see below

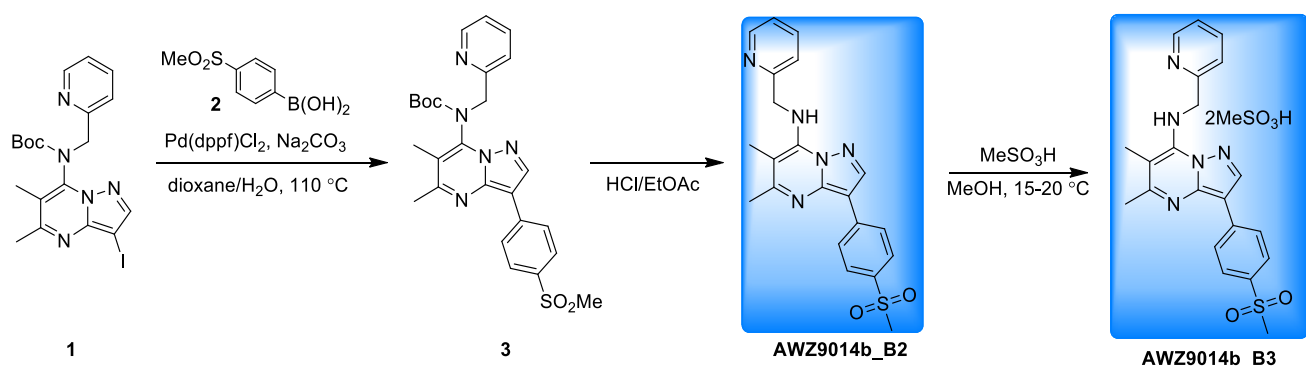
LCMS (Method 5-95AB, ESI): RT =0.797min: 2 min, M+H⁺ =414.2

¹H NMR (400MHz, DMSO-d₆) δ = 8.75 (d, J=5.1 Hz, 1H), 8.45 (s, 1H), 8.28 (t, J=7.8 Hz, 1H), 8.10 (d, J=8.4 Hz, 2H), 7.84 (d, J=7.7 Hz, 1H), 7.72 (t, J=5.6 Hz, 1H), 7.41 (d, J=8.3 Hz, 2H), 5.52 (br. s., 2H), 2.56 (s, 3H), 2.30 (s, 3H).

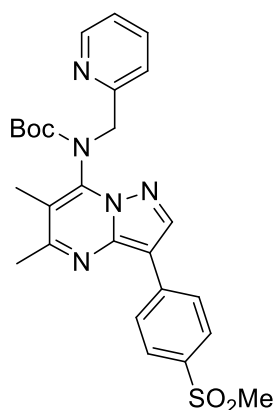
AWZ9015

LCMS (Method 5-95AB, ESI): RT =0.764min: 2 min, M+H⁺ =373.1

¹H NMR (400MHz, DMSO-d₆) δ = 8.81 (d, J=5.0 Hz, 1H), 8.54 (s, 1H), 8.42 (t, J=7.5 Hz, 1H), 8.27 (d, J=8.5 Hz, 3H), 7.96 (d, J=8.0 Hz, 1H), 7.87 - 7.76 (m, 3H), 5.55 (d, J=3.9 Hz, 2H), 2.56 (s, 3H), 2.30 (s, 3H)



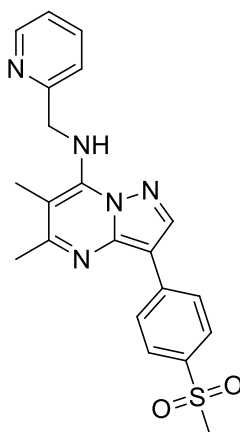
Tert-butyl (5,6-dimethyl-3-(4-(methylsulfonyl)phenyl)pyrazolo[1,5-a]pyrimidin-7-yl)(pyridin-2-yl methyl)carbamate (3)



To a mixture of tert-butyl N-(3-iodo-5,6-dimethyl-pyrazolo[1,5-a]pyrimidin-7-yl)-N-(2-pyridylmethyl)carbamate (3 g, 6.26 mmol, 1 eq), (4-methylsulfonylphenyl)boronic acid (1.5 g, 7.51 mmol, 1.2 eq), Na₂CO₃ (1.33 g, 12.5 mmol, 2 eq) in dioxane (40 mL) and H₂O (4 mL) was added ditert-butyl(cyclopentyl)phosphane;dichloropalladium;iron (408 mg, 626 μmol, 0.1 eq), the mixture was de-gassed and then heated at 110 °C for 3 hour under N₂. TLC (Petroleum ether: EtOAc=5: 1) showed that tert-butyl N-(3-iodo-5,6-dimethyl-pyrazolo[1,5-a]pyrimidin-7-yl)-N-(2-pyridylmethyl)carbamate was consumed completely. TLC (Petroleum ether: EtOAc=1: 1) showed that a major new spot. The mixture was concentrated in vacuo. The residue was purified by column chromatography on silical gel (Petroleum ether: Ethyl acetate=1: 1 to 1: 3). Compound tert-butyl N-[5,6-dimethyl-3-(4-methylsulfonylphenyl) pyrazolo[1,5-a]pyrimidin-7-yl]-N-(2-pyridylmethyl)carbamate (3 g, 5.4 mmol, 86% yield, 91% purity) was obtained as a grey solid.

¹H NMR (400MHz, CDCl₃-d) δ 8.41 (s, 2H), 8.33 (d, *J*=8.41 Hz, 2H), 7.99 (d, *J*=8.53 Hz, 2H), 7.65 (d, *J*=1.63 Hz, 1H), 7.55 (d, *J*=7.78 Hz, 1H), 7.13 - 7.23 (m, 1H), 5.16 - 5.34 (m, 1H), 4.75 - 4.85 (m, 1H), 3.09 (s, 3H), 2.58 - 2.68 (m, 3H), 2.03 - 2.15 (m, 3H), 1.50 (s, 3H), 1.32 (s, 6H).

tert-butyl 4-(4-bromo-7-chloro-1H-indazol-3-yl)piperidine-1-carboxylate (AWZ9014b_B2)

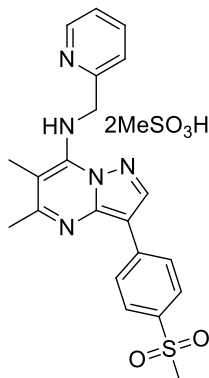


A solution of tert-butyl N-[5,6-dimethyl-3-(4-methylsulfonylphenyl)pyrazolo[1,5-a]pyrimidin-7-yl]-N-(2-pyridylmethyl)carbamate (3 g, 5.9 mmol, 1 eq) in HCl/EtOAc (40 mL) was stirred at 10-15 °C for 12 hour. TLC (EtOAc) showed that most of tert-butyl N-[5,6-dimethyl-3-(4-methylsulfonylphenyl)pyrazolo[1,5-a]pyrimidin-7-yl]-N-(2-pyridylmethyl)carbamate was consumed and a major new spot. The mixture was concentrated. The residue was dissolved in DCM/MeOH (1:1, 100 mL) and basified by strongly basic anion exchange resin, concentrated to give a crude product. The crude product was purified by trituration from (Petroleum ether: EtOAc: DCM=5: 1: 1) to give a the product (purity: 97%) which was purified by trituration from (Petroleum ether : EtOAc: DCM=3: 1: 1) for twice to give compound 5,6-dimethyl-3-(4-methylsulfonylphenyl)-N-(2-pyridylmethyl)pyrazolo[1,5-a]pyrimidin-7-amine (2.25 g, 5.44 mmol, 92% yield, 98% purity) as a light yellow solid.

LCMS (Method 5-95AB, ESI): RT =0.563 min / 1.5 min, M+H⁺ =408.0.

¹H NMR (400MHz, DMSO-d₆) δ 8.71 (d, *J*=5.15 Hz, 1H), 8.61 (s, 1H), 8.37 (d, *J*=8.53 Hz, 2H), 8.04 - 8.19 (m, 2H), 7.90 (d, *J*=8.53 Hz, 2H), 7.69 - 7.76 (m, 1H), 7.57 - 7.67 (m, 1H), 5.40 (d, *J*=4.77 Hz, 2H), 3.21 (s, 3H), 2.55 (s, 3H), 2.30 (s, 3H).

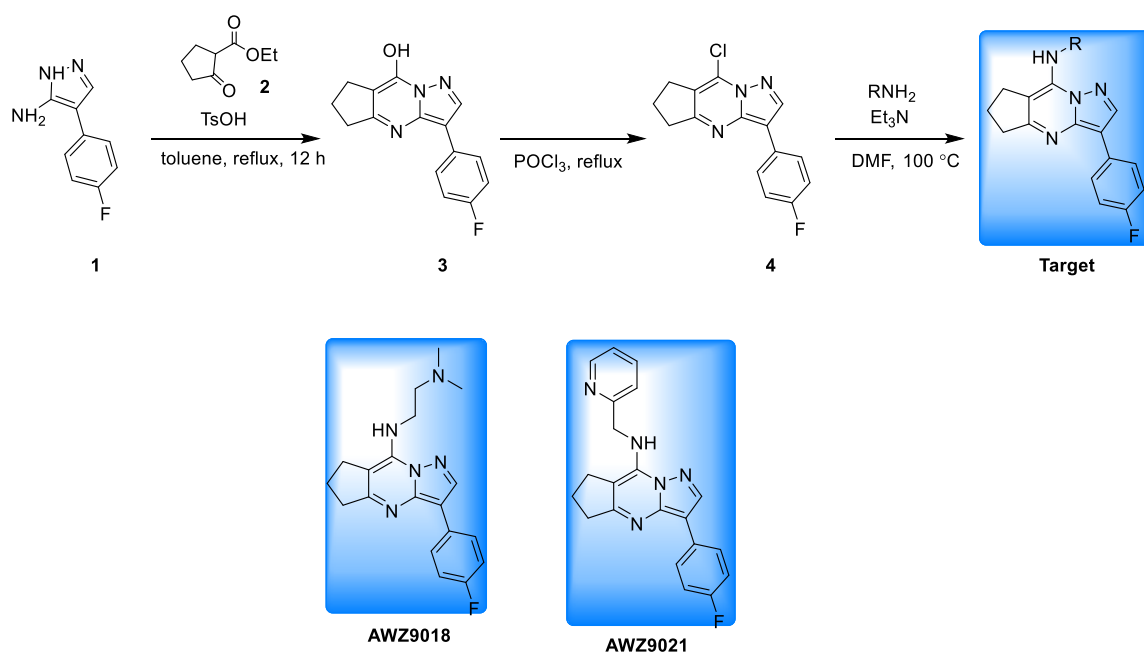
**5,6-dimethyl-3-(4-(methylsulfonyl)phenyl)-N-(pyridin-2-ylmethyl)pyrazolo[1,5-a]pyrimidin-7-amine
(AWZ9014b_B3)**



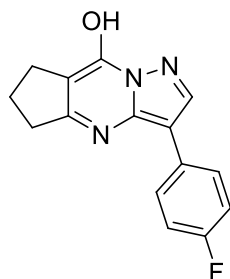
To a mixture of 5,6-dimethyl-3-(4-methylsulfonylphenyl)-N-(2-pyridylmethyl)pyrazolo[1,5-a]pyrimidin-7-amine (50.00 mg, 122.70 μmol , 1.00 eq) in MeOH (2.00 mL) was added methanesulfonic acid (35.38 mg, 368.11 μmol , 3.00 eq) in dropwise. The mixture was stirred at 15-20 $^{\circ}\text{C}$ for 12 hours. The mixture was concentrated to give a residue. The residue was triturated with EtOAc/MTBE/Petroleum ether (5 mL/5 mL/10 mL) to give 5,6-dimethyl-3-(4-methylsulfonylphenyl)-N-(2-pyridylmethyl)pyrazolo[1,5-a]pyrimidin-7-amine;methanesulfonic acid (43.40 mg, 81.01 μmol , 66% yield, 94% purity) as a grey solid.

LCMS (Method 5-95 AB): RT=0.644min/1.5 min, $[\text{M}+\text{H}]^+=408.2$

^1H NMR (400MHz, DMSO- d_6) δ 8.82 (d, $J=4.8$ Hz, 1H), 8.54 (s, 1H), 8.42 (t, $J=7.7$ Hz, 1H), 8.13-8.34 (m, 3H), 7.81-8.01 (m, 4H), 5.52 (br. s., 2H), 3.21 (s, 3H), 2.57 (s, 3H), 2.39 (s, 6H), 2.28 (s, 3H).



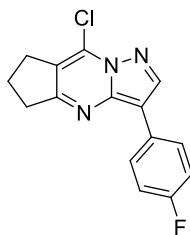
3-(4-fluorophenyl)-6,7-dihydro-5H-cyclopenta[d]pyrazolo[1,5-a]pyrimidin-8-ol (3).



To a solution of 4-(4-fluorophenyl)-1H-pyrazol-5-amine (2 g, 11.29 mmol, 1.00 Eq) and ethyl 2-oxocyclopentanecarboxylate (1.76 g, 11.29 mmol, 1.00 Eq) in toluene (20 mL) was added TsOH (194 mg, 1.13 mmol, 0.10 Eq). The mixture was stirred at 110 °C for 12 hrs. TLC (Petroleum ether: Ethyl acetate=1: 2) showed that starting material was consumed completely. The mixture was cooled to 30 °C and filtered, washed with Petroleum ether (20 mL), concentrated in vacuo to afford 3-(4-fluorophenyl)-6,7-dihydro-5H-cyclopenta[BLAH]pyrazolo[BLAH]pyrimidin-8-ol (2.3 g, 8.54 mmol, 76% yield) as a gray solid.

¹H NMR (400 MHz, DMSO-d₆): δ 12.06 - 12.40 (m, 1 H) 8.10 (s, 1 H) 7.55 - 7.64 (m, 2 H) 7.29 (t, *J*=8.85 Hz, 2 H) 2.91 - 3.00 (m, 2 H) 2.71 (t, *J*=7.25 Hz, 2 H) 2.03 - 2.15 (m, 2 H).

8-chloro-3-(4-fluorophenyl)-6,7-dihydro-5H-cyclopenta[d]pyrazolo[1,5-a]pyrimidine (4)



A solution of 3-(4-fluorophenyl)-6,7-dihydro-5H-cyclopenta[BLAH]pyrazolo [BLAH]pyrimidin-8-ol (2.3 g, 8.54 mmol, 1.00 Eq) in POCl₃ (20 mL) was stirred at 80 °C for 3 hr. TLC (Petroleum ether: Ethyl acetate=2: 1) showed that starting material was consumed completely. The mixture was cooled to 30 °C and poured into a stirring water (100 mL) slowly. The solution was extracted with EtOAc (150 mL*3). The organic layers were washed with brine (100 mL*3), dried over Na₂SO₄, concentrated to afford 8-chloro-3-(4-fluoro- phenyl)-6,7-dihydro-5H-cyclopenta[BLAH] pyrazolo[BLAH]pyrimidine (2 g, 6.95 mmol, 81% yield) as a light green solid.

¹H NMR (400 MHz, DMSO-d₆): δ 8.72 (s, 1 H) 8.12 - 8.18 (m, 2 H) 7.29 (t, *J*=8.97 Hz, 2 H) 3.10 (s, 2 H) 3.03 (t, *J*=7.40 Hz, 2 H) 2.21 (t, *J*=7.47 Hz, 2 H).

3-cyclopropyl-4-iodo-1H-pyrazolo[3,4-b]pyridine (AWZ9018)

To a solution of 8-chloro-3-(4-fluorophenyl)-6,7-dihydro-5H- cyclopenta [BLAH]pyrazolo[BLAH]pyrimidine (100 mg, 347.56 μmol, 1.00 Eq) and 2-morpholinoethanamine (45 mg, 347.56 μmol, 1.00 Eq) in DMF (2 mL) was added Et₃N (70 mg, 695.12 μmol, 2.00 Eq) . The mixture was stirred at 100 °C for 1 hr. LCMS showed that the starting material was consumed completely. The mixture was dissolved in DMSO (2 mL) and purified by prep-HPLC (Base) to AWZ9018 (24 mg, 62.92 μmol, 18% yield) as a white solid.

The above general procedure were followed for the syntheses of AWZ9021.

N1-(3-(4-fluorophenyl)-6,7-dihydro-5H-cyclopenta[d]pyrazolo[1,5-a]pyrimidin-8-yl)-N2,N2-dimethylethane-1,2-diamine (AWZ9018)

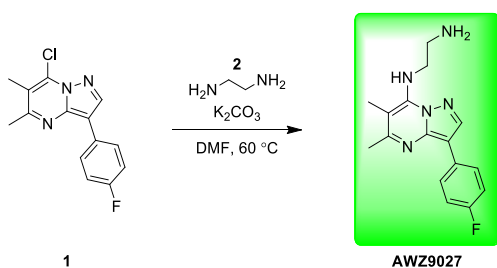
¹H NMR (400MHz, DMSO-d₆) δ 8.51 (s, 1 H) 8.24 - 8.29 (m, 1 H) 8.12 - 8.19 (m, 2 H) 7.35 - 7.41 (m, 1 H) 7.22 (s, 2 H) 3.68 - 3.77 (m, 2 H) 3.18 - 3.24 (m, 2 H) 2.89 (s, 2 H) 2.52 - 2.56 (m, 2 H) 2.23 (s, 6 H) 2.06 - 2.16 (m, 2 H).

LCMS (Method 5-95AB, ESI): RT =0.725 min / 2 min, M+H+ =340.0. yield: 25%.

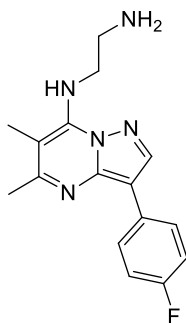
3-(4-fluorophenyl)-N-(pyridin-2-ylmethyl)-6,7-dihydro-5H-cyclopenta[d]pyrazolo[1,5-a]pyrimidin-8-amine (AWZ9021)

$^1\text{H NMR}$ (400MHz, DMSO- d_6) δ 8.55 - 8.60 (m, 1 H) 8.30 - 8.36 (m, 1 H) 8.17 (dd, $J=8.91, 5.65$ Hz, 2 H) 7.81 (d, $J=1.76$ Hz, 1 H) 7.38 (d, $J=7.91$ Hz, 1 H) 7.32 (dd, $J=7.15, 5.14$ Hz, 1 H) 7.23 (t, $J=8.97$ Hz, 2 H) 4.97 (d, $J=6.40$ Hz, 2 H) 3.03 (s, 2 H) 2.85 (s, 2 H) 1.94 - 2.05 (m, 2 H).

LCMS (Method 10-80CD, ESI): RT =1.554 min / 2 min, M+H $^+$ =360.1. yield: 42%.



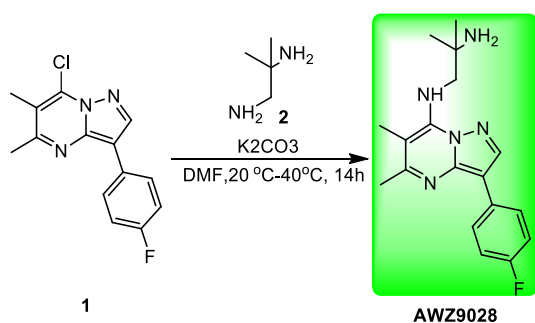
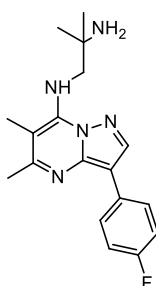
N1-(3-(4-fluorophenyl)-5,6-dimethylpyrazolo[1,5-a]pyrimidin-7-yl)ethane-1,2-diamine (AWZ9027).



A mixture of compound **1** (100.00 mg, 0.36 mmol), ethane-1,2-diamine (43.60 mg, 0.73 mmol) in DMF (6 mL) was stirred for 16 hr at 60 °C. LCMS showed the starting material was disappeared. The mixture was purified directly by prep-HPLC (FA) to **AWZ9027** (50.00 mg, 46% yield) as white solid.

LCMS (Method 0-60CDAB, ESI): RT =1.003 min / 2 min, M+H $^+$ =300.0

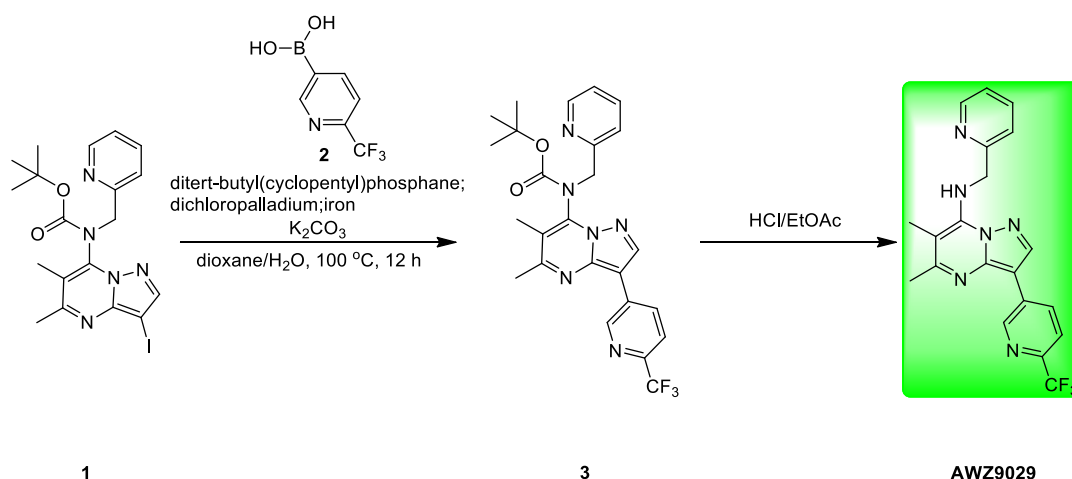
$^1\text{H NMR}$ (400MHz, DMSO- d_6) δ = 8.50 (s, 1H), 8.37 (br. s., 1H), 8.19 (dd, $J=5.6, 8.8$ Hz, 2H), 7.22 (t, $J=9.0$ Hz, 2H), 3.99 (t, $J=6.0$ Hz, 2H), 3.01 (t, $J=5.8$ Hz, 2H), 2.49 (s, 3H), 2.26 (s, 3H).

**N1-(3-(4-fluorophenyl)-5,6-dimethylpyrazolo[1,5-a]pyrimidin-7-yl)-2-methylpropane-1,2-diamine (AWZ9028)**

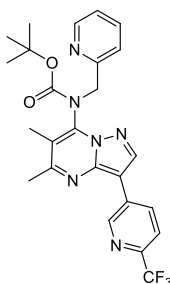
To a mixture of compound **1** (100.00 mg, 362.70 μmol , 1.00 eq) and 2-methylpropane-1,2-diamine (63.94 mg, 725.40 μmol , 2.00 eq) in DMF (6 mL) was added K_2CO_3 (100.26 mg, 725.40 μmol , 2.00 eq) in one portion at 20 °C under N_2 . The mixture was stirred at 20 °C for 12 h, then was heated to 40 °C and stirred for 2 hours. TLC (petroleum ether/ethyl acetate= 1/1) showed compound **1** was consumed completely. The mixture was concentrated in reduced pressure at 20 °C. The residue was purified by prep-HPLC (FA) to get **AWZ9028** (109.51 mg, 334.48 μmol , 92.22% yield, 100% purity) as white solid.

LCMS $\text{M}+\text{H}^+ = 328.1$, $\text{rt} = 1.081$ min, purity 100%

^1H NMR (400 MHz, CHLOROFORM-d) δ 8.38 (br. s., 1H), 8.18 (s, 1H), 8.02 (dd, $J=5.58, 8.22$ Hz, 2H), 7.12 (t, $J=8.72$ Hz, 2H), 6.36 (br. s., 1H), 3.78 (br. s., 2H), 2.55 (s, 3H), 2.29 (br. s., 3H), 1.37 (s, 6H)



tert-butyl(5,6-dimethyl-3-(6-(trifluoromethyl)pyridin-3-yl)pyrazolo[1,5-a]pyrimidin-7-yl)(pyridin-2-ylmethyl)carbamate (3)

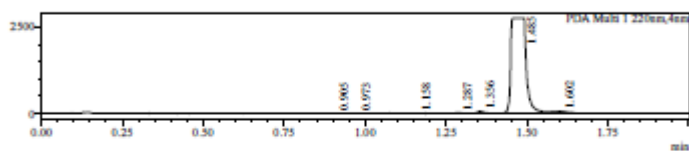


A suspension of compound **1** (150.00 mg, 312.95 μmol , 1.00 eq), [6-(trifluoromethyl)-3-pyridyl]boronic acid **2** (71.70 mg, 375.54 μmol , 1.20 eq), Na_2CO_3 (66.34 mg, 625.90 μmol , 2.00 eq) and ditert-butyl(cyclopentyl)phosphane;dichloropalladium;iron (20.40 mg, 31.30 μmol , 0.10 eq) in dioxane (10 mL) and water (2 mL) was stirred at 100 °C under nitrogen atmosphere for 12 hrs. TLC (petroleum ether/ethyl acetate= 3/1) showed compound **1** was consumed completely and a new spot was formed. Removed solvent under vacuum to give a residue which was purified directly by prep-TLC (petroleum ether/ethyl acetate= 3/1) to give compound **3** (112.00 mg, 224.67 μmol , 71.79% yield, 98.1% purity) as a yellow solid.

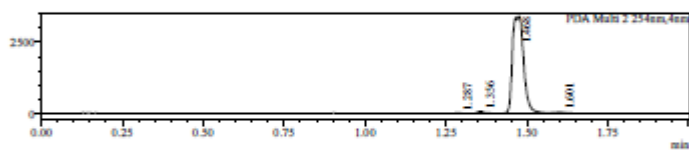
LCMS REPORT

Compound ID : 1
 Sample ID : EW1191-75-BB2
 Injection Vol : 15ul
 Location : vial35
 Acq Method : D:\method\UPLC\0-60AB_2min_2w.lcm
 Org DataFile : D:\DATA\140710\EW1191-75-BB2.lcd
 Injection Date : 2014-7-11 9:12:04
 Instrument : LCMS-A 15-105
 Column : Chromoth@Flash RP-18E 25-2MM

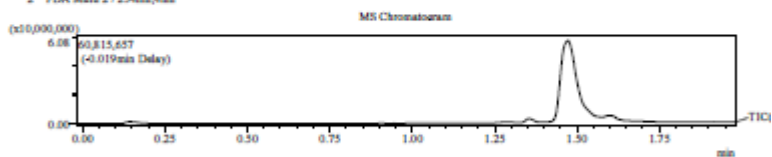
mAU Chromatogram



mAU



1 PDA Multi 1 / 220nm, 4min
 2 PDA Multi 2 / 254nm, 4min

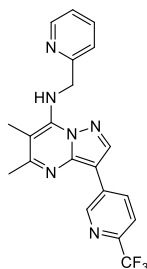


Integration Result

Peak Table						
PDA Ch1 220nm						
Peak#	Ret. Time	Height	Height%	USP Width	Area	Area%
1	0.905	3786	0.132	0.031	5178	0.057
2	0.973	3041	0.106	0.063	5680	0.062
3	1.158	3397	0.118	0.046	5253	0.058
4	1.287	14536	0.507	0.039	23412	0.257
5	1.356	53439	1.862	0.035	78236	0.860
6	1.485	2760355	96.202	0.060	8929082	98.140
7	1.602	30788	1.073	0.047	51478	0.566

Peak Table						
PDA Ch2 254nm						
Peak#	Ret. Time	Height	Height%	USP Width	Area	Area%
1	1.287	8465	0.246	0.035	11052	0.131
2	1.356	75707	2.203	0.035	104078	1.231
3	1.468	3332371	96.977	0.055	8306776	98.246

5,6-dimethyl-N-(pyridin-2-ylmethyl)-3-(6-(trifluoromethyl)pyridin-3-yl)pyrazolo[1,5-a]pyrimidin-7-amine (AWZ9029)

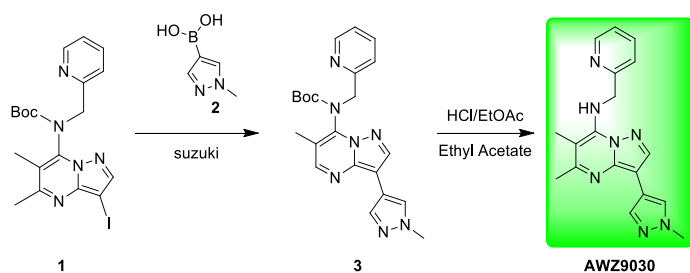


A mixture of compound **3** (113.00 mg, 226.68 μ mol, 1.00 eq) in HCl/EtOAc (6 mL) was stirred at 20 °C for 4 hrs. TLC (petroleum ether/ethyl acetate= 3/1) showed compound **3** was consumed completely. The mixture was

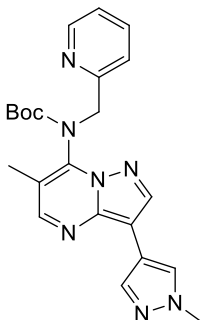
concentrated in vacuo and purified by prep-HPLC (FA) to get **AWZ9029** (33.30 mg, 83.59 μ mol, 36.88% yield, 99.7% purity) as white solid.

LCMS $M+H^+$ =399.0, $rt = 1.221$ min, purity 99.7%

1H NMR (400 MHz, METHANOL- d_4) δ 9.47 (s, 1H), 8.73 (d, $J=8.16$ Hz, 1H), 8.50-8.56 (m, 2H), 7.77-7.84 (m, 2H), 7.46 (d, $J=7.91$ Hz, 1H), 7.29-7.35 (m, 1H), 5.27 (s, 2H), 2.59 (s, 3H), 2.37 (s, 3H)

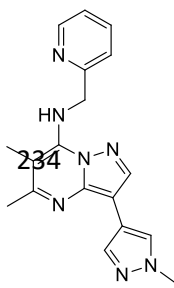


tert-butyl(6-methyl-3-(1-methyl-1H-pyrazol-4-yl)pyrazolo[1,5-a]pyrimidin-7-yl)(pyridin-2-ylmethyl)carbamate (3).



A suspension of compound 1 (150 mg, 0.3 mmol), (1-methylpyrazol-4-yl) boronic acid 2 (47.29 mg, 0.38 mmol), ditert-butyl (cyclopentyl) phosphane;dichloropalladium;iron (20.40 mg, 0.32 mmol), Na_2CO_3 (66.34 mg, 0.63 mmol) in dioxane (10 mL), water (2 mL) was stirred at $100^\circ C$ under nitrogen atmosphere for 2 hr. TLC (petroleum ether/ethyl acetate=3:1) showed starting material was consumed and a new spot formed. Removed solvent under vacuum to give a residue which was purified directly by TLC (petroleum ether/ethyl acetate=3:1) to give compound 3 (70.00 mg, 52% yield) as pale yellow oil.

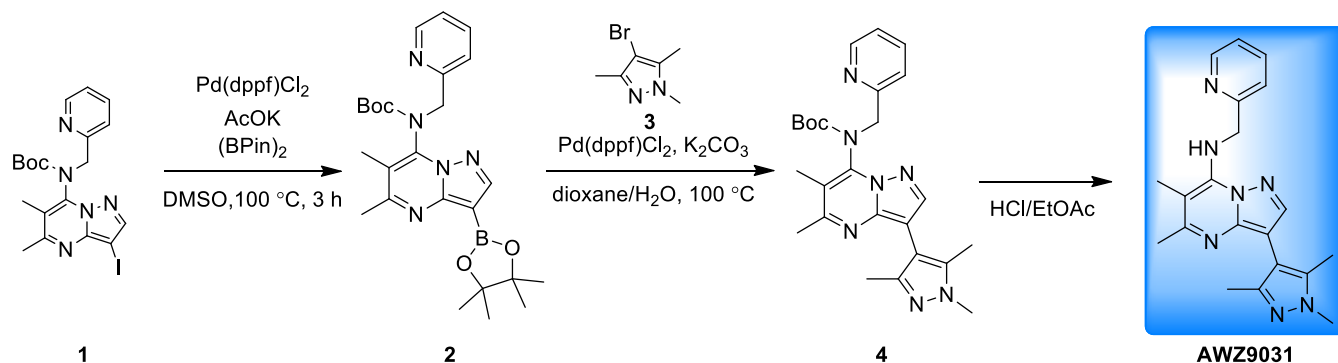
5,6-dimethyl-3-(1-methyl-1H-pyrazol-4-yl)-N-(pyridin-2-ylmethyl)pyrazolo[1,5-a]pyrimidin-7-amine (AWZ9030)



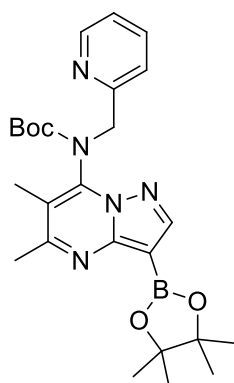
To a solution compound **3** (70.00 mg, 0.16 mmol) in EtOAc (3 mL) was added HCl/EtOAc (4 M, 3.00 mL). The solution was stirred for 2 hr at 25 °C and a white precipitate was formed. TLC (petroleum ether/ethyl acetate=3:1) showed the starting material was consumed completely. Filtrate the precipitate which was purified by prep-HPLC (FA) to give AWZ9030 (20.00 mg, 37% yield) as white solid.

LCMS (Method 5-95AB, ESI): RT=0.661 min / 2 min, M+H⁺ =334.1

¹H NMR (400MHz, DMSO-d₆) δ = 8.56 (d, J=4.8 Hz, 1H), 8.24 (s, 1H), 8.09 (s, 1H), 7.89 (s, 1H), 7.83 - 7.72 (m, 2H), 7.37 (d, J=8.2 Hz, 1H), 7.33 - 7.26 (m, 1H), 5.18 (d, J=5.8 Hz, 2H), 3.88 (s, 3H), 2.48 (s, 3H), 2.29 (s, 3H).



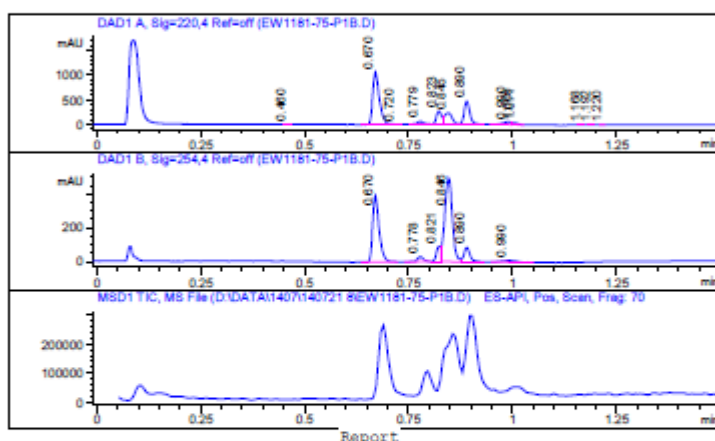
tert-butyl(5,6-dimethyl-3-(4,4,5,5-tetramethyl-1,3,2-dioxaborolan-2-yl)pyrazolo[1,5-a]pyrimidin-7-yl)(pyridin-2-ylmethyl)carbamate (2)



To a mixture of tert-butyl N-(3-iodo-5,6-dimethyl-pyrazolo[1,5-a]pyrimidin-7-yl)-N-(2-pyridylmethyl)carbamate (100 mg, 208.63 μmol , 1 eq), Pin_2B_2 (79 mg, 312.95 μmol , 1.5 eq) and KOAc (41 mg, 417.26 μmol , 2 eq) in DMSO (4 mL) was de-gassed and then heated at 100 °C for 1 hour under N_2 . LCMS showed the starting material was consumed completely and 40 % of the desired product tert-butyl N-[5,6-dimethyl-3-(4,4,5,5-tetramethyl-1,3,2-dioxaborolan-2-yl)pyrazolo[1,5-a]pyrimidin-7-yl]-N-(2-pyridylmethyl)carbamate, 30 % of the by-product tert-butyl N-[3-[7-[tert-butoxycarbonyl(2-pyridylmethyl)amino]-5,6-dimethyl-pyrazolo[1,5-a]pyrimidin-3-yl]-5,6-dimethyl-pyrazolo[1,5-a]pyrimidin-7-yl]-N-(2-pyridylmethyl)carbamate. The mixture was filtered and concentrated in vacuo to give a crude solution, which was used in the next step without purification.

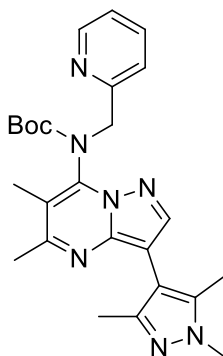
LCMS REPORT

Compound ID :
 Sample ID : EW1181-75-P1B
 Injection Date : 2014-07-21 5:02:14 PM
 Location : P1-C-07
 Injection volume : 3.000
 Acq Method : D:\DATA\1407\140721 8\5-95AB_R_220&254.M
 Data Filename : D:\DATA\1407\140721 8\EW1181-75-P1B.D
 Instrument : LCMS-B
 Column:Chromolith Flash RP-18e 25*2mm



Signal 1 : DAD1 A, Sig=220,4 Ref=off					
#	Meas. Ret.	Height	Width	Area	Area %
1	0.460	3.053	0.010	2.321	0.098
2	0.670	1063.510	0.016	1176.813	49.899
3	0.720	5.514	0.008	3.531	0.150
4	0.779	58.573	0.017	69.400	2.943
5	0.823	274.345	0.013	236.423	10.025
6	0.845	232.565	0.021	299.619	12.704
7	0.890	469.460	0.015	444.622	18.853
8	0.990	55.569	0.022	81.120	3.440
9	1.005	38.196	0.009	24.906	1.056
10	1.011	24.402	0.007	10.767	0.457
11	1.168	4.043	0.011	3.140	0.133
12	1.192	4.419	0.011	3.695	0.157
13	1.220	2.754	0.010	2.023	0.086

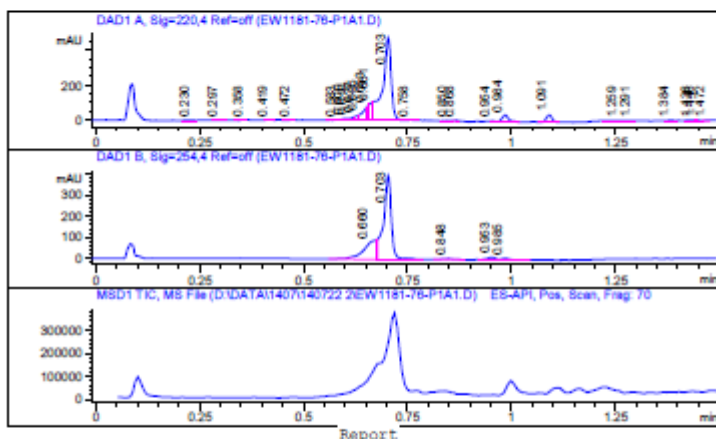
3-(3-cyclopropyl-1-methyl-1H-pyrazolo[3,4-b]pyridin-4-yl)-N-methylbenzamide (4)



To a mixture of tert-butyl N-[5,6-dimethyl-3-(4,4,5,5-tetramethyl-1,3,2-dioxaborolan-2-yl)pyrazolo[1,5-a]pyrimidin-7-yl]-N-(2-pyridylmethyl)carbamate (100 mg, 208.60 μmol , 1 eq) , 4-bromo-1,3,5-trimethylpyrazole (39 mg, 208.60 μmol , 1 eq) ,Pd(dppf)Cl₂ (15 mg, 20.86 μmol , 0.1 eq) and K₂CO₃ (57 mg, 417.20 μmol , 2 eq) in DMSO (4 mL) and H₂O (1 mL) was de-gassed and then heated at 110 °C for 1 hr under N₂. LCMS showed the starting material was consumed completely and only about 18 % of desired product. The mixture was added water (30 mL) and extracted with EtOAc (50 mL). The organic layer was washed with brine (30 mL) and dried over Na₂SO₄, concentrated in vacuo to give a residue, which was purified by prep-TLC (Petroleum ether: Ethyl acetate=1: 2) to afford the tert-butyl N-[5,6-dimethyl-3-(1,3,5-trimethylpyrazol-4-yl)pyrazolo[1,5-a]pyrimidin-7-yl]-N-(2-pyridylmethyl)carbamate (50 mg, crude) as a brown oil.

LCMS REPORT

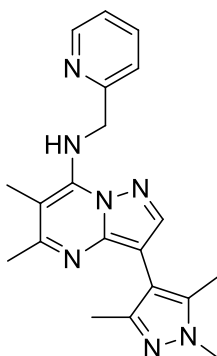
Compound ID :
 Sample ID : EW1181-76-P1A1
 Injection Date : 2014-07-22 3:08:19 PM
 Location : P1-B-07
 Injection volume : 12.000
 Acq Method : D:\DATA\1407\140722 2\5-95AB_R_2206254.M
 Data Filename : D:\DATA\1407\140722 2\EW1181-76-P1A1.D
 Instrument : LCMS-B
 Column:Chromolith Flash RP-18e 25*2mm



Signal 1 : DAD1 A, Sig=220,4 Ref-off

#	Meas.	Ret.	Height	Width	Area	Area %
1	0.230	2.431	0.016		2.835	0.289
2	0.297	3.201	0.014		3.216	0.328
3	0.358	3.777	0.011		3.082	0.314
4	0.419	3.793	0.017		4.196	0.428
5	0.472	2.279	0.013		2.320	0.236
6	0.583	3.446	0.012		3.394	0.346
7	0.600	7.331	0.014		6.338	0.646
8	0.610	9.969	0.014		10.824	1.103
9	0.627	22.627	0.008		13.371	1.363
10	0.635	32.967	0.021		55.872	5.695
11	0.653	78.262	0.006		32.886	3.352
12	0.661	97.775	0.008		49.130	5.008
13	0.703	475.633	0.020		680.434	69.353
14	0.758	4.984	0.013		4.180	0.426

5,6-dimethyl-N-(pyridin-2-ylmethyl)-3-(1,3,5-trimethyl-1H-pyrazol-4-yl)pyrazolo[1,5-a]pyrimidin-7-amine (AWZ9031)

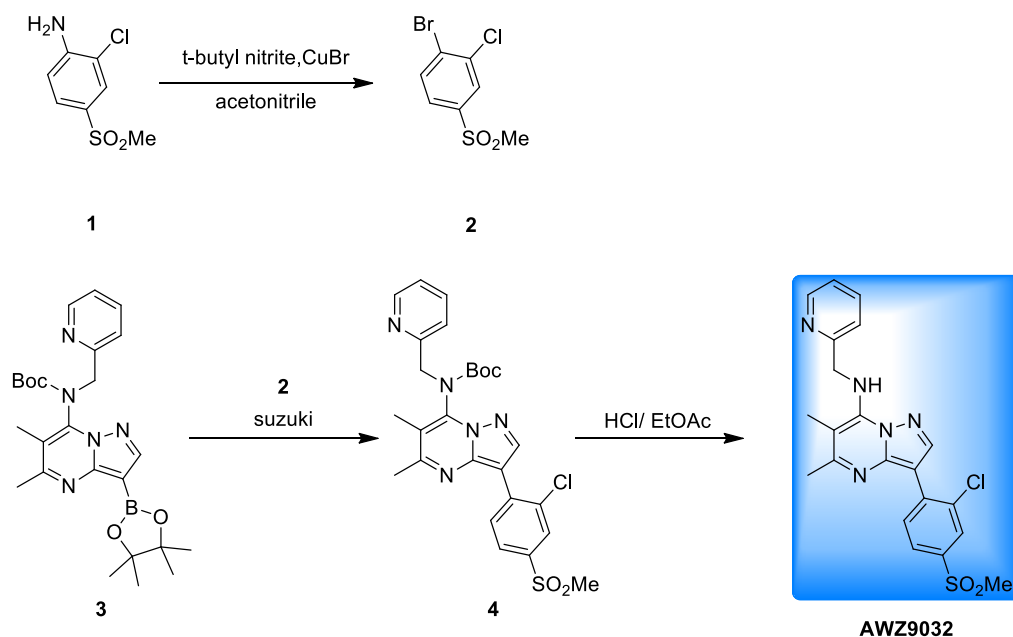


A solution of tert-butyl N-[5,6-dimethyl-3-(1,3,5-trimethylpyrazol-4-yl)pyrazolo[1,5-a]pyrimidin-7-yl]-N-(2-pyridylmethyl)carbamate (50 mg, 108.33 μmol , 1 eq) in HCl/EtOAc (5 mL) was stirred at 30 $^{\circ}\text{C}$ for 12 hour

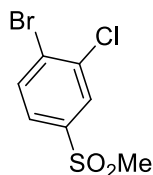
. LCMS showed that starting material was consumed completely. The mixture solution was concentrated. The residue was mixed with DMSO (3 mL) and purified by prep-HPLC (HCOOH) to afford 5,6-dimethyl-N-(2-pyridylmethyl)-3-(1,3,5-trimethylpyrazol-4-yl)pyrazolo[1,5-a]pyrimidin-7-amine (13 mg, 35.69 μ mol, 32% yield) as a white solid.

$^1\text{H NMR}$ (400MHz, DMSO- d_6) δ 8.56 - 8.60 (m, 1 H) 7.96 (s, 1 H) 7.77 - 7.84 (m, 2 H) 7.40 - 7.44 (m, 1 H) 7.28 - 7.35 (m, 1 H) 5.15 - 5.21 (m, 2 H) 3.70 (s, 3 H) 2.40 (s, 3 H) 2.30 (s, 3 H) 2.18 (s, 3 H) 2.09 (s, 3 H)

LCMS (Method 5-95AB, ESI): RT = 0.699 min / 1.5 min, M+H+ = 362.1



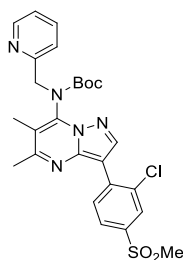
Synthesis of 1-bromo-2-chloro-4-(methylsulfonyl)benzene (2)



To a mixture of 2-chloro-4-methylsulfonyl-aniline (300.00 mg, 1.46 mmol, 1.00 eq) in ACETONITRILE (5.00 mL) was added n-butyl nitrite (225.63 mg, 2.19 mmol, 1.50 eq) in one portion at 0 °C under N₂. The mixture was stirred at 0 °C for 30 min. Then CuBr (418.51 mg, 2.92 mmol, 2.00 eq) was added to the mixture. The mixture was heated to 65 °C and stirred for 1.5 hrs. TLC (petroleum ether: ethyl acetate=3: 1) showed most of the starting material was consumed. The mixture was diluted with EtOAc (100 mL) and washed with saturated brine (20*2), dried with anhydrous Na₂SO₄, filtered and concentrated in vacuo. The residue was purified by silica gel chromatography (ethyl acetate: petroleum ether=3: 1) to afford 1-bromo-2-chloro-4-methylsulfonyl-benzene (700.00 mg, 2.60 mmol, 59% yield) as white solid.

¹H NMR (300 MHz, CHLOROFORM-d) δ 7.67 - 7.72 (m, 1 H) 7.83 - 7.89 (m, 1 H) 8.02 - 8.06 (m, 1 H)

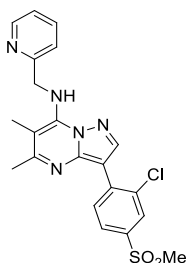
Synthesis of tert-butyl (3-(2-chloro-4-(methylsulfonyl)phenyl)-5,6-dimethylpyrazolo[1,5-a]pyrimidin-7-yl)(pyridin-2-ylmethyl)carbamate (4)



To a mixture of tert-butyl N-[5,6-dimethyl-3-(4,4,5,5-tetramethyl-1,3,2-dioxaborolan-2-yl)pyrazolo[1,5-a]pyrimidin-7-yl]-N-(2-pyridylmethyl)carbamate (120.00 mg, 250.32 μmol, 1.00 eq) and 1-bromo-2-chloro-4-methylsulfonyl-benzene (101.21 mg, 375.49 μmol, 1.50 eq) in DMF (5.00 mL) was added Pd(dppf)Cl₂ (18.32 mg, 25.03 μmol, 0.10 eq) in one portion at 25 °C under N₂. The mixture was heated to 110 °C and stirred for 1 hours. TLC (ethyl acetate: petroleum ether=3:1) showed the starting material was consumed and the MS of desired product was detected. The mixture was extracted with ethyl acetate (30 mL*2). The combined organic phase was washed with saturated brine (10 mL*5), dried with anhydrous Na₂SO₄, filtered and concentrated in vacuo. The residue was combined with EW1701-44-P1 to purify by prep-TLC (ethyl acetate:petroleum ether=3:1) to afford tert-butyl N-[3-(2-chloro-4-methylsulfonyl-phenyl)-5,6-dimethyl-pyrazolo[1,5-a]pyrimidin-7-yl]-N-(2-pyridylmethyl)carbamate (80.00 mg, 147.59 μmol, 59% yield) as white solid.

LCMS (Method 5-95AB): RT =0.791min / 1.5 min, M+H⁺ = 542.1

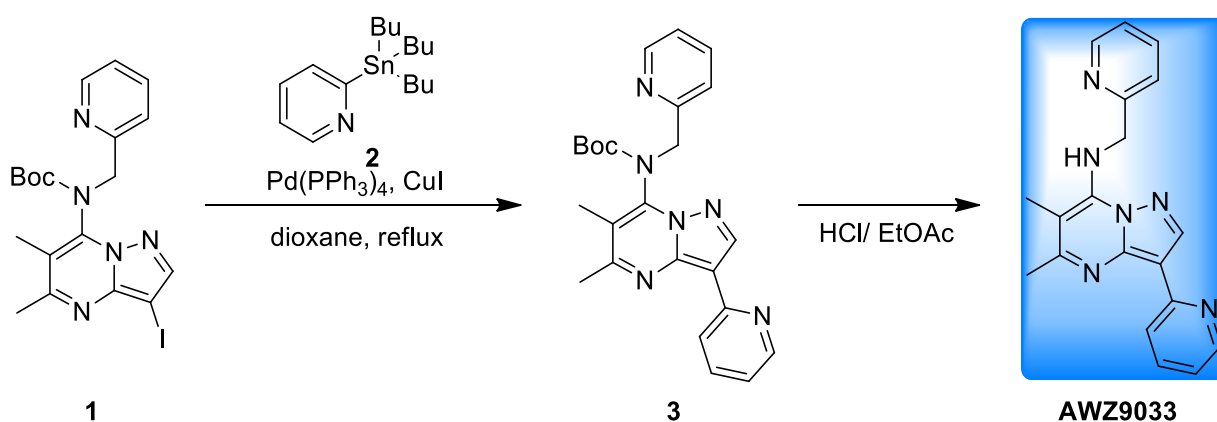
Synthesis of 3-(2-chloro-4-(methylsulfonyl)phenyl)-5,6-dimethyl-N-(pyridin-2-ylmethyl) pyrazolo[1,5-a]pyrimidin-7-amine(AWZ9032)

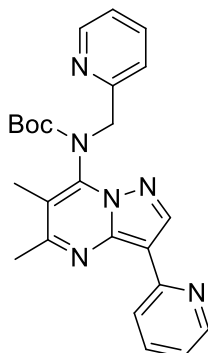


tert-butyl N-[3-(2-chloro-4-methylsulfonyl-phenyl)-5,6-dimethyl-pyrazolo[1,5-a]pyrimidin-7-yl]-N-(2-pyridylmethyl)carbamate (80.00 mg, 147.59 μmol , 1.00 eq) in HCl/EtOAc (5.00 mL) was stirred at 25 °C and stirred for 3 hours. LCMS showed the starting material was consumed and the MS of desired product was detected. The mixture was concentrated in reduced pressure. The residue was diluted with ethyl acetate (60 mL) and saturated NaHCO_3 (20 mL). The organic phase was separated and washed with saturated brine (10 mL*2), dried with anhydrous Na_2SO_4 , filtered and concentrated in vacuo. The residue was purified by prep-TLC (ethyl acetate: petroleum ether= 3: 1) to afford 3-(2-chloro-4-methylsulfonyl-phenyl)-5,6-dimethyl-N-(2-pyridylmethyl)pyrazolo[1,5-a]pyrimidin-7-amine (38.00 mg, 85.99 μmol , 58% yield) as yellow solid.

LCMS (Method 5-95AB): RT =0.720min / 1.5 min, $\text{M}+\text{H}^+ = 442.0$

$^1\text{H NMR}$ (400 MHz, DMSO-d_6) δ 2.32 (s, 3 H) 2.47 (s, 3 H) 3.31 (s, 3 H) 5.22 - 5.28 (m, 2 H) 7.28 - 7.34 (m, 1 H) 7.39 - 7.44 (m, 1 H) 7.77 - 7.84 (m, 1 H) 7.90 - 7.95 (m, 1 H) 8.01 - 8.06 (m, 2 H) 8.41 - 8.46 (m, 1 H) 8.54 - 8.58 (m, 1 H) 8.59 - 8.62 (m, 1 H)

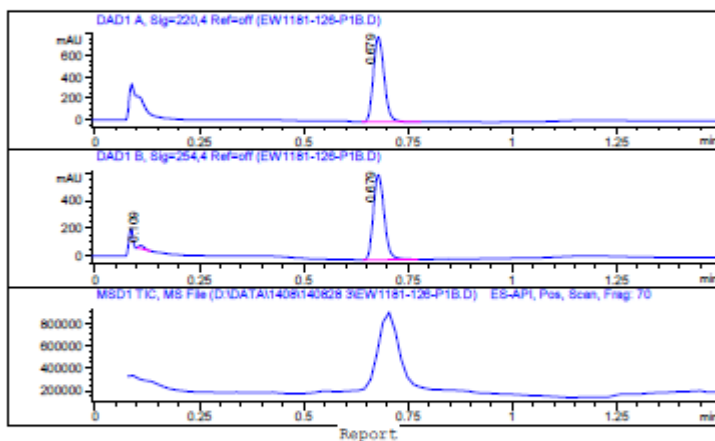


tert-butyl(5,6-dimethyl-3-(pyridin-2-yl)pyrazolo[1,5-a]pyrimidin-7-yl)(pyridin-2-ylmethyl)carbamate (3)

To a mixture of tert-butyl N-(3-iodo-5,6-dimethyl-pyrazolo[1,5-a]pyrimidin-7-yl)-N-(2-pyridylmethyl)carbamate (200 mg, 417.27 μmol , 1 eq), tributyl(2-pyridyl)stannane (215 mg, 584.18 μmol , 1.4 eq), CuI (16 mg, 83.45 μmol , 0.2 eq) in dioxane (5 mL) was added Pd(PPh₃)₄ (48.22 mg, 41.73 μmol , 0.10 eq). The mixture was degassed and then heated at 100 °C for 2 hour under N₂. TLC (Petroleum ether: Ethyl acetate=1: 1) showed that the starting material was consumed completely. The mixture was added EtOAc (40 mL) and washed with a solution of KF (10 %, 20 mL). The organic layer was washed with brine (20 mL), dried over Na₂SO₄ and concentrated in vacuo to give a residue, which was purified by chromatography on silical gel to afford the crude product (purity: 80 %). The crude was purified by prep-HPLC (FA) to afford tert-butyl N-[5,6-dimethyl-3-(2-pyridyl)pyrazolo[1,5-a]pyrimidin-7-yl]-N-(2-pyridylmethyl)carbamate (80 mg, 182.11 μmol , 44% yield, 98% purity) as a yellow solid.

LCMS REPORT

Compound ID :
 Sample ID : EW1181-126-P1B
 Injection Date : 2014-08-28 1:33:21 PM
 Location : P1-C-07
 Injection volume : 5.000
 Acq Method : D:\DATA\1408\140828 3\5-95AB_R_2204254.M
 Data Filename : D:\DATA\1408\140828 3\EW1181-126-P1B.D
 Instrument : LCMS-G
 Column:Chromolith Flash RP-18e 25*2mm

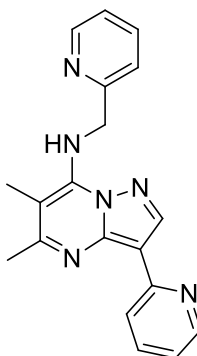


Report

Signal 1 : DAD1 A, Sig=220,4 Ref=off					
#	Meas. Ret.	Height	Width	Area	Area %
1	0.679	780.796	0.029	1417.098	100.000

Signal 2 : DAD1 B, Sig=254,4 Ref=off					
#	Meas. Ret.	Height	Width	Area	Area %
1	0.109	21.122	0.015	19.419	1.721
2	0.679	610.396	0.029	1109.170	98.279

5,6-dimethyl-3-(pyridin-2-yl)-N-(pyridin-2-ylmethyl)pyrazolo[1,5-a]pyrimidin-7-amine (AWZ9033)

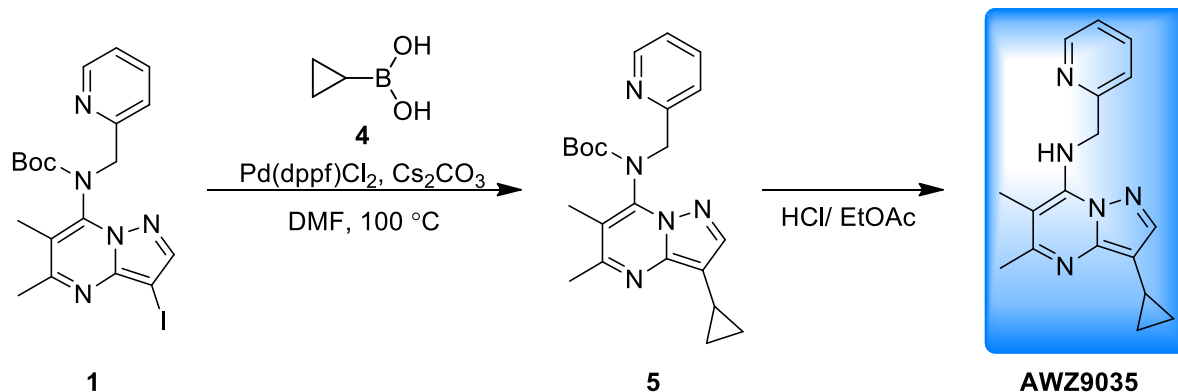


A solution of tert-butyl N-[5,6-dimethyl-3-(2-pyridyl)pyrazolo[1,5-a]pyrimidin-7-yl]-N-(2-pyridylmethyl)carbamate (90 mg, 209.06 μmol , 1 eq) in HCl/EtOAc (5 mL) was stirred at 30 °C for 12 hour. LCMS showed that starting material was consumed completely. A solid was forming. The mixture

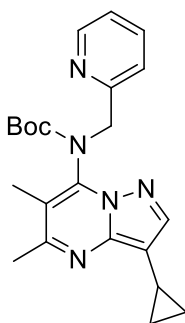
solution was concentrated. The solid was dissolved in MeOH (15 mL) and mixed with Anion exchange resin. The mixture was filtered and concentrated. The residue was added deionized water (50 mL) and lyophilized to afford 5,6-dimethyl-3-(2-pyridyl)-N-(2-pyridylmethyl)pyrazolo[1,5-a]pyrimidin-7-amine (60 mg, 181.60 μmol , 87% yield) as a yellow solid.

$^1\text{H NMR}$ (400MHz, DMSO- d_6) δ 9.08 - 9.16 (m, 1 H) 8.76 - 8.82 (m, 1 H) 8.62 - 8.72 (m, 2 H) 8.38 - 8.51 (m, 2 H) 8.10 - 8.18 (m, 1 H) 7.68 - 7.76 (m, 1 H) 7.61 (br. s., 2 H) 5.48 (d, $J=5.27$ Hz, 2 H) 2.62 (s, 3 H) 2.33 (s, 3 H)

LCMS (Method 5-95AB, ESI): RT = 0.680 min / 1.5 min, M+H $^+$ = 331.0



tert-butyl(5,6-dimethyl-3-(pyridin-2-yl)pyrazolo[1,5-a]pyrimidin-7-yl)(pyridin-2-ylmethyl)carbamate (3)

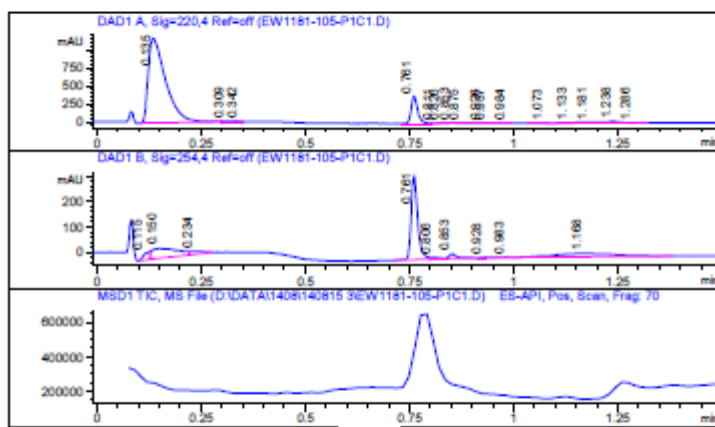


To a mixture of tert-butyl N-(3-iodo-5,6-dimethyl-pyrazolo[1,5-a]pyrimidin-7-yl)-N-(2-pyridylmethyl)carbamate (150 mg, 312.95 μmol , 1 eq), cyclopropylboronic acid (269 mg, 3.13 mmol, 10 eq), Pd(dppf)Cl $_2$ (23 mg, 31.30 μmol , 0.1 eq) in DMF (4 mL) was added Cs $_2$ CO $_3$ (204 mg, 625.90 μmol , 2 eq). The mixture was de-gassed and then heated at 100 $^\circ\text{C}$ for 12 hour under N $_2$. TLC (Petroleum ether: EtOAc=1: 1) showed the starting material

was consumed completely. The mixture was added water (20 mL) and extracted with EtOAc (40 mL). The organic layer was washed brine (20 mL*3), dried over Na₂SO₄, concentrated in vacuo to give a residue, which was purified by column chromatography on silcal gel (Petroleum ether: EtOAc=1: 1 to 1: 3, 3 % DCM) to afford the tert-butyl N-(3-cyclopropyl-5,6-dimethyl-pyrazolo[1,5-a]pyrimidin-7-yl)-N-(2-pyridylmethyl)carbamate (30 mg, 76.24 μmol, 24% yield) as a light yellow solid.

LCMS REPORT

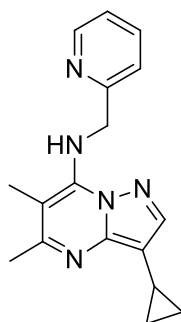
Compound ID :
 Sample ID : EW1181-105-P1C1
 Injection Date : 2014-08-15 3:27:57 PM
 Location : F1-B-06
 Injection volume : 5.000
 Acq Method : D:\DATA\1408\140815 3\5-95AB_R_2204254.M
 Data Filename : D:\DATA\1408\140815 3\EW1181-105-P1C1.D
 Instrument : LCMS-G
 Column:Chromolith Flash RP-18e 25*2mm



Report

Signal 1 : DAD1 A, Sig=220,4 Ref=off						
#	Meas.	Ret.	Height	Width	Area	Area %
1		0.135	1170.658	0.044	3449.833	85.294
2		0.309	5.206	0.021	7.653	0.189
3		0.342	2.157	0.014	2.068	0.051
4		0.761	378.558	0.017	414.035	10.237
5		0.811	8.341	0.014	8.477	0.210
6		0.826	5.665	0.010	4.246	0.105
7		0.853	13.241	0.019	17.239	0.426
8		0.875	7.413	0.017	8.818	0.218
9		0.926	5.248	0.011	3.415	0.084
10		0.937	6.245	0.020	7.755	0.192
11		0.984	2.771	0.014	2.421	0.060
12		1.073	3.158	0.017	3.593	0.089
13		1.133	9.925	0.030	23.662	0.585
14		1.181	11.481	0.049	47.052	1.163

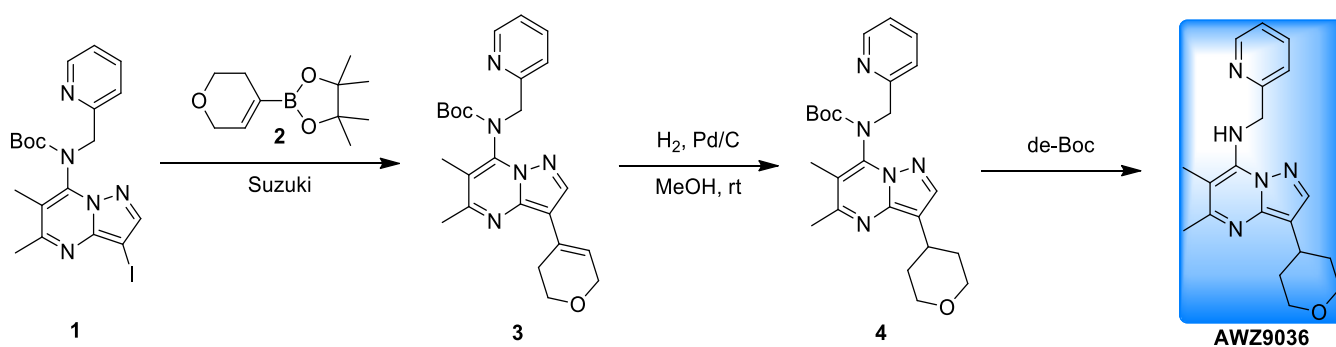
Confidential, for research only not for regulatory filing.

3-cyclopropyl-5,6-dimethyl-N-(pyridin-2-ylmethyl)pyrazolo[1,5-a]pyrimidin-7-amine (AWZ9035)

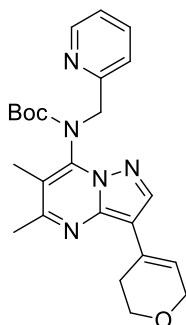
A solution of tert-butyl N-(3-cyclopropyl-5,6-dimethyl-pyrazolo[1,5-a]pyrimidin-7-yl)-N-(2-pyridylmethyl)carbamate (40 mg, 101.66 μmol , 1 eq) in HCl/EtOAc (5 mL) was stirred at 30 °C for 12 hour. LCMS showed that the reaction was completed. The mixture was concentrated to a residue. The residue was added Et₃N (0.3 mL) and DMSO (3 mL), purified by prep-HPLC (Base) to afford 3-cyclopropyl-5,6-dimethyl-N-(2-pyridylmethyl)pyrazolo[1,5-a]pyrimidin-7-amine (13 mg, 44.99 μmol , 44% yield) as a white solid.

¹H NMR (400MHz, DMSO-d₆) δ 8.53 - 8.57 (m, 1 H) 7.74 - 7.80 (m, 1 H) 7.72 (s, 1 H) 7.63 - 7.70 (m, 1 H) 7.32 - 7.37 (m, 1 H) 7.25 - 7.31 (m, 1 H) 5.12 (d, $J=5.90$ Hz, 1 H) 2.41 (s, 3 H) 2.26 (s, 3 H) 1.87 - 1.94 (m, 1 H) 0.84 (d, $J=8.28$ Hz, 2 H) 0.72 (d, $J=3.51$ Hz, 2 H).

LCMS (Method 5-95AB, ESI): RT =0.652 min / 1.5 min, M+H⁺ =294.0

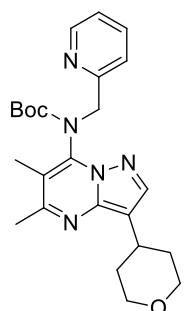


tert-butyl (3-(3,6-dihydro-2H-pyran-4-yl)-5,6-dimethylpyrazolo[1,5-a]pyrimidin-7-yl)(pyridin-2-ylmethyl)carbamate (3)



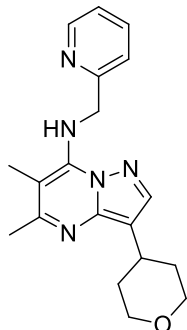
A mixture of tert-butyl N-(3-iodo-5,6-dimethyl-pyrazolo[1,5-a]pyrimidin-7-yl)-N-(2-pyridylmethyl)carbamate (200.00 mg, 417.27 μmol , 1.00 eq) , 2-(3,6-dihydro-2H-pyran-4-yl)-4,4,5,5-tetramethyl-1,3,2-dioxaborolane (131.49 mg, 625.90 μmol , 1.50 eq) , ditert-butyl(cyclopentyl)phosphane;dichloropalladium;iron (27.20 mg, 41.73 μmol , 0.10 eq) and Na_2CO_3 (88.45 mg, 834.53 μmol , 2.00 eq) in dioxane (20.00 mL) and H_2O (4.00 mL) was stirred at 100 $^\circ\text{C}$ for 4 hour under N_2 protection. The color of the mixture was turned black. TLC (Petroleum ether:EtOAc=1:1) showed starting material consumed. The mixture was concentrated to give a residue. The residue was purified by prep-TLC (Petroleum ether: EtOAc=1:1) to give tert-butyl N-[3-(3,6-dihydro-2H-pyran-4-yl)-5,6-dimethyl-pyrazolo[1,5-a]pyrimidin-7-yl]-N-(2-pyridylmethyl)carbamate (100.00 mg, 229.61 μmol , 55% yield) as a yellow solid.

tert-butyl (5,6-dimethyl-3-(tetrahydro-2H-pyran-4-yl)pyrazolo[1,5-a]pyrimidin-7-yl)(pyridin-2-ylmethyl)carbamate (4)



A mixture of tert-butyl N-[3-(3,6-dihydro-2H-pyran-4-yl)-5,6-dimethyl-pyrazolo[1,5-a]pyrimidin-7-yl]-N-(2-pyridylmethyl)carbamate (100.00 mg, 229.61 μmol , 1.00 eq) and Pd/C (10.00 mg) in MeOH (3.00 mL) was stirred at 25-35 $^\circ\text{C}$ for 1 hour under H_2 (15 psi). TLC (Petroleum ether: EtOAc=1:1) showed starting material consumed. The mixture was filtered and the filtrate was concentrated to give a residue. The residue was purified by prep-TLC (Petroleum ether: EtOAc=1:1) to give tert-butyl N-(5,6-dimethyl-3-tetrahydropyran-4-yl-pyrazolo[1,5-a]pyrimidin-7-yl)-N-(2-pyridylmethyl)carbamate (100.00 mg, crude) as a colorless oil.

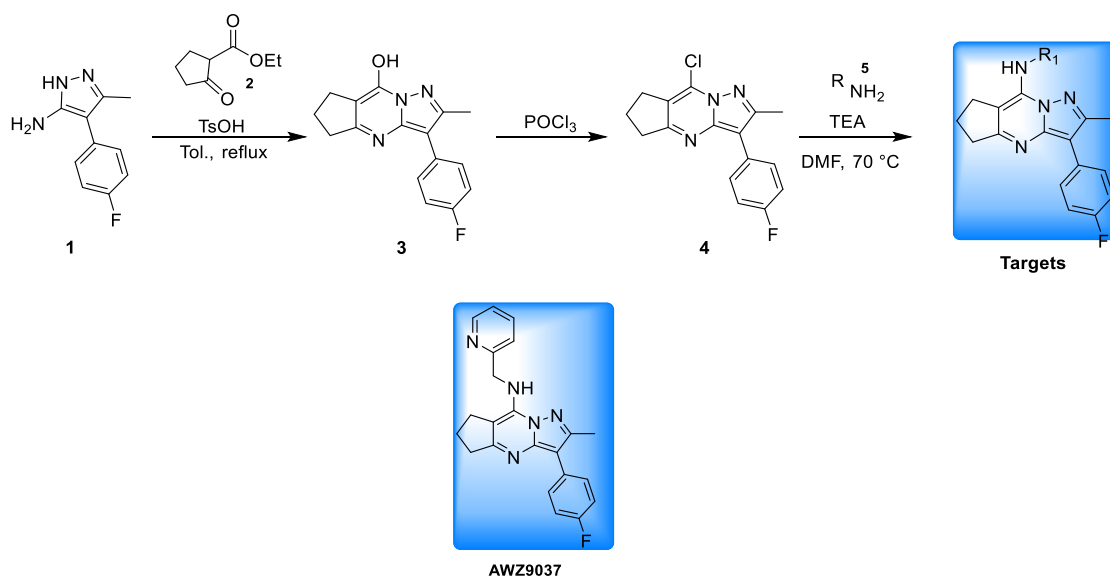
**5,6-dimethyl-N-(pyridin-2-ylmethyl)-3-(tetrahydro-2H-pyran-4-yl)pyrazolo[1,5-a]pyrimidin-7-amine
(AWZ9036)**



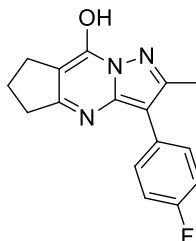
A mixture of tert-butyl N-(5,6-dimethyl-3-tetrahydropyran-4-yl-pyrazolo[1,5-a]pyrimidin-7-yl)-N-(2-pyridylmethyl)carbamate (100.00 mg, 228.56 μmol , 1.00 eq) in HCl/EtOAc (4 M, 5.00 mL) was stirred at 25-30 °C for 1 hour. LCMS showed starting material consumed and MS of desired product. The mixture was concentrated to give a residue. The residue was purified by prep-TLC (Petroleum ether:EtOAc=1:2) to give 5,6-dimethyl-N-(2-pyridylmethyl)-3-tetrahydropyran-4-yl-pyrazolo[1,5-a]pyrimidin-7-amine (45.00 mg, 132.03 μmol , 57% yield, 99% purity) as a light yellow solid.

LCMS (Method 5-95AB): RT =0.560 min / 1.5 min, M+H⁺ = 338.0

¹H NMR (400 MHz, METHANOL-d₄) : δ 8.79 (dd, J=5.71, 0.82 Hz, 1 H) 8.49 (td, J=7.94, 1.32 Hz, 1 H) 8.07 (d, J=8.16 Hz, 1 H) 7.99 (s, 1 H) 7.91 (t, J=6.53 Hz, 1 H) 5.82 (s, 2 H) 3.98 - 4.07 (m, 2 H) 3.58 (td, J=11.14, 3.58 Hz, 2 H) 3.17 (tt, J=10.49, 5.25 Hz, 1 H) 2.70 (s, 3 H) 2.37 (s, 3 H) 1.73 - 1.85 (m, 1 H).



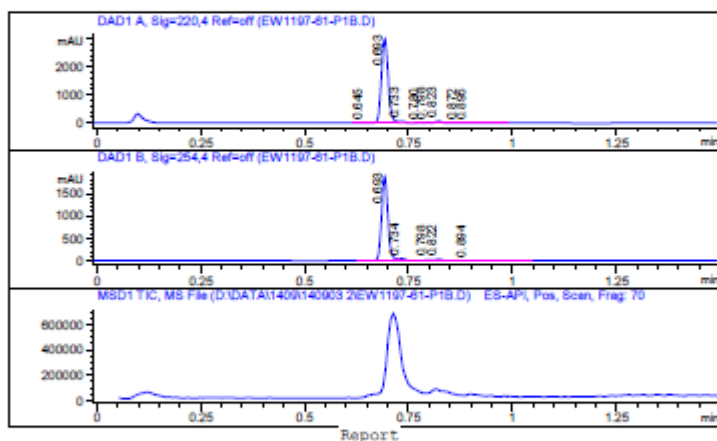
3-(4-fluorophenyl)-2-methyl-6,7-dihydro-5H-cyclopenta[d]pyrazolo[1,5-a]pyrimidin-8-ol (3).



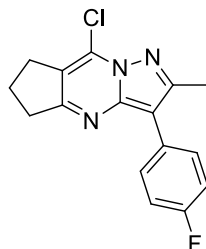
To a solution of 4-(4-fluorophenyl)-3-methyl-1H-pyrazol-5-amine (7.20 g, 37.66 mmol, 1.00 eq) and ethyl 2-oxocyclopentanecarboxylate (7.06 g, 45.19 mmol, 1.20 eq) was added TsOH.H₂O (716.31 mg, 3.77 mmol, 0.10 eq). The mixture was stirred at 110°C for 12 hrs. TLC (petroleum ether/ ethyl acetate=1:1) showed that starting material was consumed completely. The mixture was cooled to 30°C and concentrated in vacuo. The residue was triturated with petroleum ether : ethyl acetate=2 : 1 (15 mL) to afford 3-(4-fluorophenyl)-2-methyl-6,7-dihydro-5H-cyclopenta[BLAH]pyrazolo[BLAH]pyrimidin-8-ol (6.50 g, 20.65 mmol, 54% yield, 90% purity) as black brown solid

LCMS REPORT

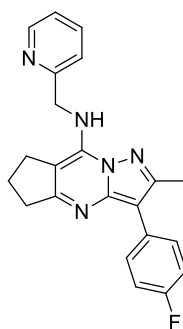
Compound ID :
 Sample ID : EW1197-61-P1B
 Injection Date : 2014-09-03 2:45:48 PM
 Location : F2-D-08
 Injection volume : 4.000
 Acq Method : D:\DATA\1409\140903 2\5-95AB_R_220&254.M
 Data Filename : D:\DATA\1409\140903 2\EW1197-61-P1B.D
 Instrument : LCMS-B
 Column:Chromolith Flash RP-18e 25*2mm



Signal 1 : DAD1 A, Sig=220,4 Ref=off					
#	Meas. Ret.	Height	Width	Area	Area %
1	0.645	9.993	0.020	12.607	0.356
2	0.693	3001.293	0.018	3381.094	95.418
3	0.733	53.992	0.016	57.276	1.616
4	0.780	5.262	0.009	3.325	0.094
5	0.798	22.097	0.014	20.782	0.587
6	0.823	58.899	0.016	59.817	1.688
7	0.872	2.813	0.018	3.268	0.092
8	0.895	3.812	0.019	5.297	0.149

8-chloro-3-(4-fluorophenyl)-2-methyl-6,7-dihydro-5H-cyclopenta[d]pyrazolo[1,5a]pyrimidine (4).

A solution of 3-(4-fluorophenyl)-2-methyl-6,7-dihydro-5H-cyclopenta[BLAH]pyrazolo[BLAH]pyrimidin-8-ol (2.00 g, 7.06 mmol, 1.00 eq) in POCl₃ (8 mL) was stirred at 110°C for 8 hr. TLC (petroleum ether : ethyl acetate=1:2) showed that starting material was consumed completely. The mixture was cooled to 30°C and poured into a stirring water (100 mL) slowly. The solution was extracted with Ethyl acetate (100 mL*3). The combined organic layer was washed with brine (50 mL*3), dried with Na₂SO₄, concentrated in vacuo, the residue was triturated with petroleum ether : ethyl acetate=20 : 1 (21 mL) to afford 8-chloro-3-(4-fluorophenyl)-2-methyl-6,7-dihydro-5H-cyclopenta[BLAH]pyrazolo[BLAH]pyrimidine (800.00 mg, 2.65 mmol, 37% yield) as dark yellow solid.

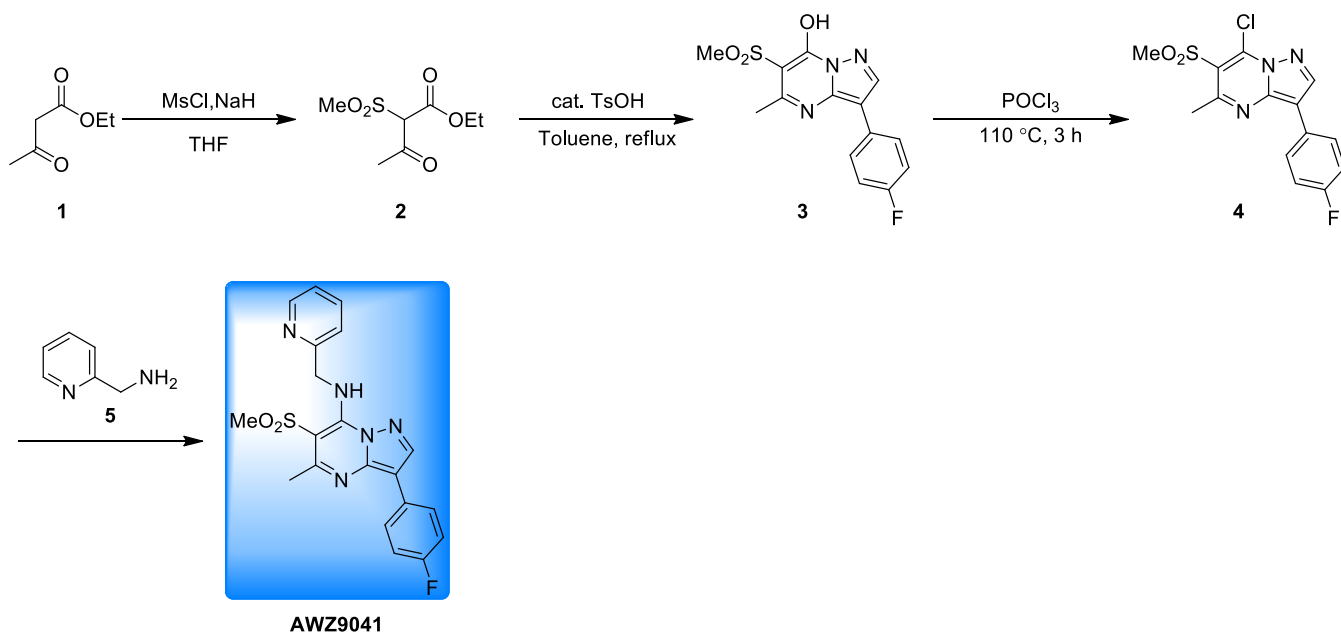
3-(4-fluorophenyl)-2-methyl-N-(pyridin-2-ylmethyl)-6,7-dihydro-5H-cyclopenta[d]pyrazolo[1,5-a]pyrimidin-8-amine (AWZ9037)

To a solution of 8-chloro-3-(4-fluorophenyl)-2-methyl-6,7-dihydro-5H-cyclopenta[BLAH]pyrazolo[BLAH]pyrimidine (100.00 mg, 331.40 μmol, 1.00 eq) and 2-pyridylmethanamine (46.59 mg, 430.82 μmol, 1.30 eq) in DMF (3.00 mL) was added Et₃N (100.60 mg, 994.20 μmol, 3.00 eq). The mixture was stirred at 70°C for 3 hrs. TLC (petroleum ether : ethyl acetate= 3 : 1) showed that starting material was consumed completely. The mixture was cooled to 30°C, then solid was precipitate after added a few drops of water. The mixture was stirred at room temperature for 1 hour. The solid was collected by filtration and triturated with ethyl acetate (3 mL) and a few drops of methanol for 1 h to afford 3-(4-fluorophenyl)-2-methyl-

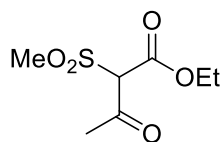
N-(2-pyridylmethyl)-6,7-dihydro-5H-cyclopenta[BLAH]pyrazolo[BLAH]pyrimidin-8-amine (54.00 mg, 140.56 μmol , 42% yield, 97.2% purity) as white solid.

LCMS (Method 5-95AB, ESI): RT = 0.828 min / 2 min, M+H+ = 374.0. yield: 42.4%

$^1\text{H NMR}$ (400MHz, DMSO- d_6) δ 8.58 - 8.57 (d, $J=4.4$ Hz, 1 H) 8.21 - 8.19 (t, $J=6.8$ Hz, 1 H) 7.80 - 7.76 (m, 3 H) 7.37 - 7.35 (d, $J=8$ Hz, 1 H) 7.28 - 7.24 (m, 3 H) 4.94 - 4.93 (d, $J=6.4$ Hz, 2 H) 2.99 - 2.96 (t, $J=7.4$ Hz, 2 H) 2.79 - 2.75 (t, $J=7.8$ Hz, 2 H) 2.55 (s, 3 H) 1.97 - 1.93 (t, $J=7.4$ Hz, 2 H)



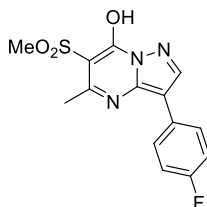
Synthesis of ethyl 2-(methylsulfonyl)-3-oxobutanoate (2)



To a mixture of ethyl 3-oxobutanoate (2.00 g, 15.37 mmol, 1.00 eq) in THF (20.00 mL) was added NaH (922.08 mg, 23.06 mmol, 1.50 eq) in portions at 0 °C under N_2 protection. The mixture was stirred at 0 °C for 30 min. Then methanesulfonyl chloride (3.89 g, 30.74 mmol, 2.00 eq) was added to the mixture and the mixture was warmed to 25 °C and stirred for 2 hrs. TLC (petroleum ether: ethyl acetate = 5: 1) showed the starting

material was consumed completely. The mixture was diluted with ethyl acetate (60 mL*2) and washed with saturated brine (40 mL*2), dried with anhydrous Na₂SO₄, filtered and concentrated in vacuo. The residue was purified by silica gel chromatography (petroleum ether: ethyl acetate = 20: 1~10:1~5: 1) to afford ethyl 2-methylsulfonyl-3-oxo-butanoate (1.00 g, crude) as yellow liquid.

Synthesis of 3-(4-fluorophenyl)-5-methyl-6-(methylsulfonyl)pyrazolo[1,5-a]pyrimidin-7-ol (3)

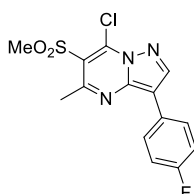


To a mixture of 4-(4-fluorophenyl)-1H-pyrazol-5-amine (1.64 g, 9.24 mmol, 1.00 eq) in toluene (20.00 mL) was added TsOH.H₂O (175.79 mg, 924.17 μmol, 0.10 eq) in portions at 25 °C under N₂. TLC (petroleum ether: ethyl acetate = 5: 1) showed the starting material was consumed completely. The mixture was concentrated in vacuo. The residue was purified by trituration (Ethyl acetate=5 mL) to afford 3-(4-fluorophenyl)-5-methyl-6-methylsulfonyl-pyrazolo[1,5-a]pyrimidin-7-ol (750.00 mg, 2.33 mmol, 25% yield) as yellow solid.

LCMS (Method 10-80CD): RT =0.702 min / 2 min, M+H⁺ = 332.1

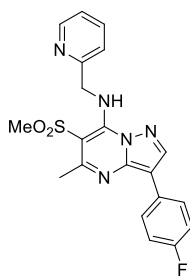
¹H NMR (400 MHz, DMSO-d₆) δ 2.73 - 2.75 (m, 3 H) 3.32 - 3.34 (m, 3 H) 7.30 - 7.37 (m, 2 H) 7.59 - 7.66 (m, 2 H) 8.21 - 8.24 (m, 1 H)

Synthesis of 3-(4-fluorophenyl)-5-methyl-6-(methylsulfonyl)pyrazolo[1,5-a]pyrimidin-7-ole (4)



3-(4-fluorophenyl)-5-methyl-6-methylsulfonyl-pyrazolo[1,5-a]pyrimidin-7-ol (200.00 mg, 622.41 μmol , 1.00 eq) and DMAC (300.00 μL) was added to POCl_3 (32.45 mg, 211.62 μmol , 0.34 eq) in one portion at 25 $^\circ\text{C}$ under N_2 . The mixture was heated to 110 $^\circ\text{C}$ and stirred for 14 hours. TLC (Dichloromethane : Methanol=10:1) showed the starting material was consumed and the desired product was detected compared with standard sample. The mixture was concentrated then azeotroped with toluene (3mL*3) in vacuo to afford 7-chloro-3-(4-fluorophenyl)-5-methyl-6-methylsulfonyl-pyrazolo[1,5-a]pyrimidine (300.00 mg, crude) as brown solid. The crude product was used directly for next step without purification.

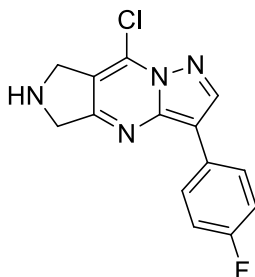
Synthesis of 3-(4-fluorophenyl)-5-methyl-6-(methylsulfonyl)-N-(pyridin-2-ylmethyl)pyrazolo[1,5-a]pyrimidin-7-amine (AWZ9041)



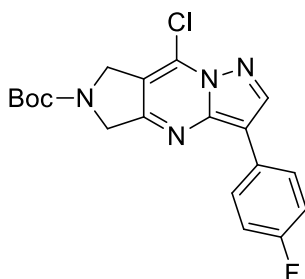
To a mixture of 7-chloro-3-(4-fluorophenyl)-5-methyl-6-methylsulfonyl-pyrazolo[1,5-a]pyrimidine (200.00 mg, 588.63 μmol , 1.00 eq) and 2-pyridylmethanamine (82.75 mg, 765.22 μmol , 1.30 eq) in DMA (5.00 mL) was added Et_3N (2.19 g, 21.64 mmol, 36.77 eq) in one portion under N_2 . The mixture was stirred at 25 $^\circ\text{C}$ for 0.5 hrs. TLC (petroleum ether: ethyl acetate=3: 1) showed the starting material was consumed and a new spot. The mixture was poured into water (20 mL). The mixture was diluted with ethyl acetate (30 mL), washed with saturated brine (10 mL*4), dried with anhydrous Na_2SO_4 , filtered and concentrated in vacuo. The residue was purified by prep-TLC (Petroleum ether: Ethyl acetate=3: 1) followed by trituration with dichloromethane (2 mL) to afford 3-(4-fluorophenyl)-5-methyl-6-methylsulfonyl-N-(2-pyridylmethyl)pyrazolo[1,5-a]pyrimidin-7-amine (48.00 mg, 116.66 μmol , 20% yield) as light yellow solid.

LCMS (Method 5-95AB): RT =0.846min / 1.5 min, $\text{M}+\text{H}^+$ = 412.0

^1H NMR (400 MHz, DMSO-d_6): δ 2.77 (s, 3 H) 3.42 - 3.43 (m, 3 H) 5.65 - 5.68 (m, 2 H) 7.23 - 7.29 (m, 2 H) 7.30 - 7.35 (m, 1 H) 7.45 - 7.49 (m, 1 H) 7.79 - 7.85 (m, 1 H) 8.14 - 8.19 (m, 2 H) 8.51 - 8.54 (m, 1 H) 8.68 (s, 1 H) 9.61 - 9.66 (m, 1 H)

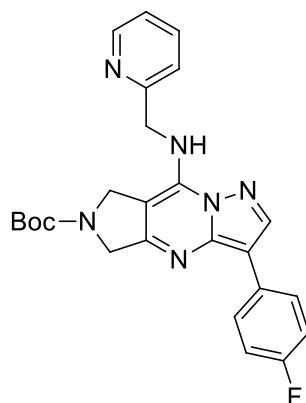
8-chloro-3-(4-fluorophenyl)-6,7-dihydro-5H-pyrazolo[1,5-a]pyrrolo[3,4-d]pyrimidine (5)

To a solution of POCl_3 (5 mL) was added tert-butyl 3-(4-fluorophenyl)-8-hydroxy-5,7-dihydropyrazolo[BLAH]pyrrolo[BLAH]pyrimidine-6-carboxylate (500 mg, 1.35 mmol, 1 eq). The mixture was stirred at 80 °C for 4 hour. TLC (Petroleum ether: EtOAc=0:1) showed that starting material was consumed completely. The mixture was added into a stirring water (50 mL) slowly and extracted with EtOAc (50 mL*2). The combined organic layers were washed with brine (50 mL), concentrated. The residue (100 mg, 346.37 μmol) was used without purification.

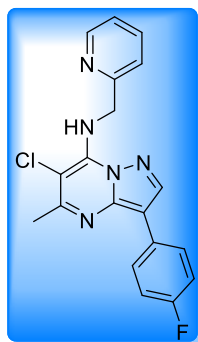
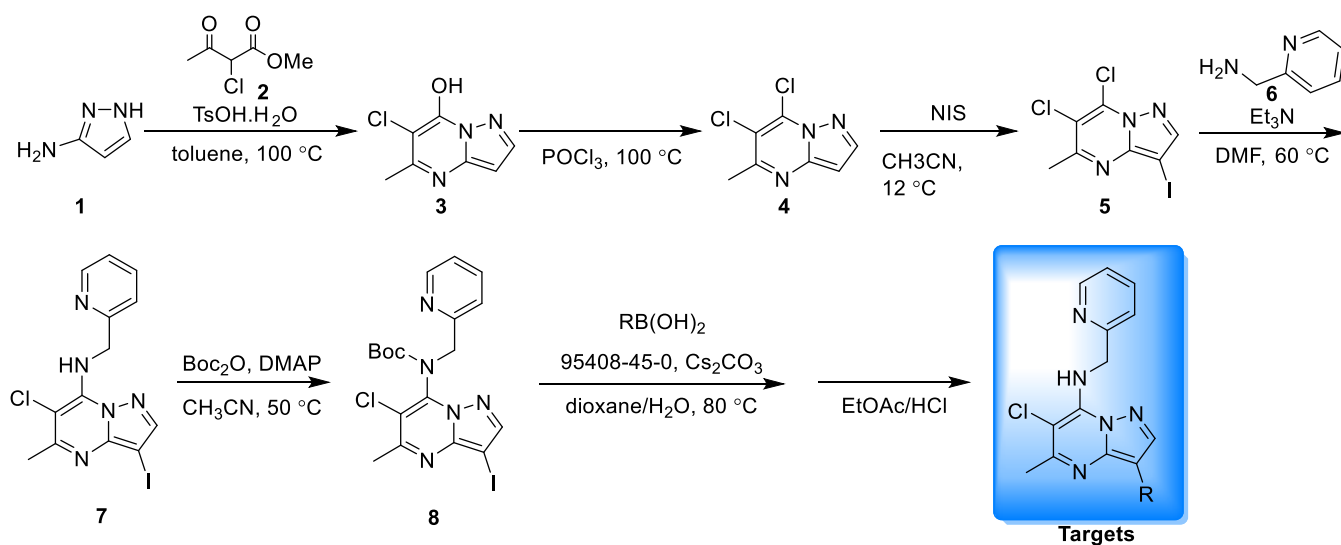
tert-butyl 8-chloro-3-(4-fluorophenyl)-5H-pyrazolo[1,5-a]pyrrolo[3,4-d]pyrimidine-6(7H)-carboxylate (6)

To a solution of 8-chloro-3-(4-fluorophenyl)-6,7-dihydro-5H-pyrazolo[BLAH]pyrrolo[BLAH]pyrimidine (100 mg, 346.37 μmol , 1 eq) in H_2O (6 mL) and THF (6 mL) was added NaHCO_3 (58 mg, 692.74 μmol , 2 eq), Boc_2O (151.19 mg, 692.74 μmol , 2 eq). The mixture was stirred at 30 °C for 12 hour. TLC (Petroleum ether: EtOAc=5: 1) showed that a new spot. The mixture was concentrated. The residue was purified by chromatography on silica gel (Petroleum ether: EtOAc=10: 1) to afford tert-butyl 8-chloro-3-(4-fluorophenyl)-5,7-dihydropyrazolo[BLAH]pyrrolo[BLAH]pyrimidine-6-carboxylate (100 mg, 257.19 μmol , 74% yield) as a yellow solid.

tert-butyl 3-(4-fluorophenyl)-8-((pyridin-2-ylmethyl)amino)-5H-pyrazolo[1,5-a]pyrrolo[3,4-d]pyrimidine-6(7H)-carboxylate (7)

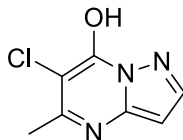


To a solution of tert-butyl 8-chloro-3-(4-fluorophenyl)-5,7-dihydropyrrolo[2,1-b]pyrimidine-6-carboxylate (80 mg, 205.75 μmol , 1 eq) in DMF (3 mL) was added phenylmethanamine (26 mg, 246.90 μmol , 1.2 eq) and Et_3N (42 mg, 411.50 μmol , 2 eq). The mixture was stirred at 80 $^\circ\text{C}$ for 1 hour. TLC (Petroleum ether: EtOAc=2: 1) showed that starting material was consumed completely. To the mixture was added water (40 mL), and the solution was extracted with EtOAc (30 mL*2). The combined organic layers were washed with brine (30 mL*2), dried over Na_2SO_4 , concentrated. The residue was purified by chromatography on silica gel (Petroleum ether: EtOAc=1: 1) to afford tert-butyl 3-(4-fluorophenyl)-8-(2-pyridylmethylamino)-5,7-dihydropyrrolo [2,1-b]pyrimidine-6-carboxylate (70 mg, 152.01 μmol , 74% yield) as a yellow solid.



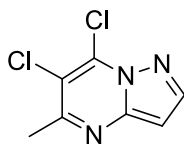
AWZ9046

6-chloro-5-methylpyrazolo[1,5-a]pyrimidin-7-ol (3)



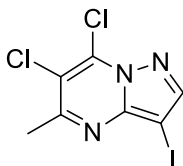
To a solution of 1H-pyrazol-3-amine (2.5 g, 30.1 mmol, 1 eq) and methyl 2-chloro-3-oxobutanoate (4.5 g, 30.1 mmol, 1 eq) in toluene (20 mL) was added TsOH.H₂O (572 mg, 3 mmol, 0.1 eq). The mixture was stirred at 100 °C for 20 mins. A light yellow solid was forming. TLC (EtOAc) showed that 1H-pyrazol-3-amine was consumed completely and a new spot. The mixture was cooled to room temperature. The solid was filtered and was washed (Petroleum ether, 20 mL) to give 6-chloro-5-methyl-pyrazolo[1,5-a]pyrimidin-7-ol (5 g, 27.2 mmol, 91% yield) as a grey solid.

¹H NMR (400MHz, DMSO-d₆) δ 7.91 (d, J=2.01 Hz, 1H), 6.18 (d, J=1.88 Hz, 1H), 2.45 (s, 3H).

6,7-dichloro-5-methylpyrazolo[1,5-a]pyrimidine (4)

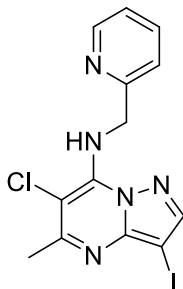
To a solution of 6-chloro-5-methyl-pyrazolo[1,5-a]pyrimidin-7-ol (3 g, 16.3 mmol, 1 *eq*) in CH₃CN (10 mL) was added POCl₃ (41 g, 267.32 mmol, 16 *eq*). The mixture was stirred at 100 °C for 16 hours. TLC (EtOAc) showed that about half of 6-chloro-5-methyl-pyrazolo[1,5-a]pyrimidin-7-ol was consumed. TLC (Petroleum ether/EtOAc=10/1) showed that three new spots. Desired product was detected by LCMS. The mixture was cooled to room temperature and added into a string water (150 mL) slowly. The mixture was extracted with EtOAc (150 mL*2). The organic layers were washed with brine (100 mL*2), dried over Na₂SO₄ and concentrated to give 6,7-dichloro-5-methyl-pyrazolo[1,5-a]pyrimidine (2 g, crude) as a brown oil.

¹H NMR (400MHz, CDCl₃-d) δ 8.18 (d, *J*=2.38 Hz, 1H), 6.73 (d, *J*=2.38 Hz, 1H), 2.75 (s, 3H).

6,7-dichloro-3-iodo-5-methylpyrazolo[1,5-a]pyrimidine (5)

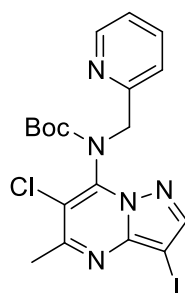
To a solution of 6,7-dichloro-5-methyl-pyrazolo[1,5-a]pyrimidine (1 g, 5 mmol, 1 *eq*) in CH₃CN (3 mL) was added NIS (1.1 g, 5 mmol, 1 *eq*). The mixture was stirred at 12 °C for 0.5 h. TLC (Petroleum ether/EtOAc=3/1) showed that 6,7-dichloro-5-methyl-pyrazolo[1,5-a]pyrimidine was consumed completely and a major spot. Desired mass was detected by LCMS. The mixture was concentrated. The residue was purified by chromatography on silica gel (Petroleum ether/EtOAc=10/1, 5/1, 2/1) to give 6,7-dichloro-3-iodo-5-methyl-pyrazolo[1,5-a]pyrimidine (900 mg, 2.7 mmol, 55% yield) as a brown solid.

¹H NMR (400MHz, CDCl₃-d) δ 8.19 (s, 1H), 2.81 (s, 3H)

6-chloro-3-iodo-5-methyl-N-(pyridin-2-ylmethyl)pyrazolo[1,5-a]pyrimidin-7-amine (7)

To a solution of 6,7-dichloro-3-iodo-5-methyl-pyrazolo[1,5-a]pyrimidine (1 g, 3 mmol, 1 *eq*) in DMF (5 mL) was added Et₃N (617 mg, 6.1 mmol, 2 *eq*) and 2-pyridylmethanamine (396 mg, 3.7 mmol, 1.2 *eq*). The mixture was stirred at 60 °C for 1.5 hours under N₂. TLC (Petroleum ether/EtOAc=2/1) showed that 6,7-dichloro-3-iodo-5-methyl-pyrazolo[1,5-a]pyrimidine was consumed completely and a major new spot. To the mixture was added water (20 mL) slowly, then a grey solid was forming. The residue was filtered and concentrated to give 6-chloro-3-iodo-5-methyl-N-(2-pyridylmethyl)pyrazolo[1,5-a]pyrimidin-7-amine (900 mg, 2.2 mmol, 74% yield) as a grey solid.

¹H NMR (400MHz, DMSO-d₆) δ 8.49-8.55 (m, 1H), 8.37-8.45 (m, 1H), 8.15 (s, 1H), 7.78 (td, *J*=7.72, 1.76 Hz, 1H), 7.35 (d, *J*=7.91 Hz, 1H), 7.28 (dd, *J*=6.90, 5.40 Hz, 1H), 5.35 (d, *J*=6.15 Hz, 2H), 2.52-2.52 (m, 3H).

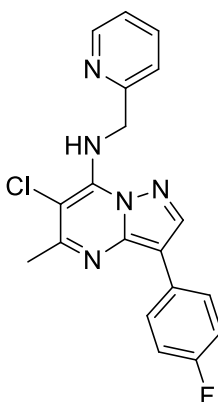
tert-butyl (6-chloro-3-iodo-5-methylpyrazolo[1,5-a]pyrimidin-7-yl)(pyridin-2-ylmethyl)carbamate (8)

To a solution of 6-chloro-3-iodo-5-methyl-N-(2-pyridylmethyl)pyrazolo[1,5-a]pyrimidin-7-amine (900 mg, 2.3 mmol, 1 *eq*) in CH₃CN (20 mL) was added Boc₂O (590 mg, 2.7 mmol, 1.2 *eq*), DMAP (28 mg, 225.2 μmol, 0.1 *eq*). The mixture was stirred at 50 °C for 1 hour. TLC (Petroleum ether/EtOAc=5/1) showed that 6-chloro-3-iodo-5-methyl-N-(2-pyridylmethyl)pyrazolo [1,5-a]pyrimidin-7-amine was consumed completely and a major new spot. The mixture was concentrated. The residue was purified by chromatography on silica gel (Petroleum ether/EtOAc=10/1, 5/1, 2/1) to give tert-butyl N-(6-chloro-3-iodo-5-methyl-pyrazolo[1,5-a]pyrimidin-7-yl)-N-(2-pyridylmethyl)carbamate (1 g, 2 mmol, 89% yield) as a light brown solid.

LCMS (Method 5-95AB, ESI): RT =0.542 min / 1.5 min, M+H+ =311.0.

¹H NMR (400MHz, DMSO-d₆) δ 8.23 (d, *J*=4.77 Hz, 1H), 7.97 (s, 1H), 7.52-7.63 (m, 2H), 7.05 (s, 1H), 4.86-5.13 (m, 2H), 2.63-2.66 (m, 3H), 1.25 (s, 9H).

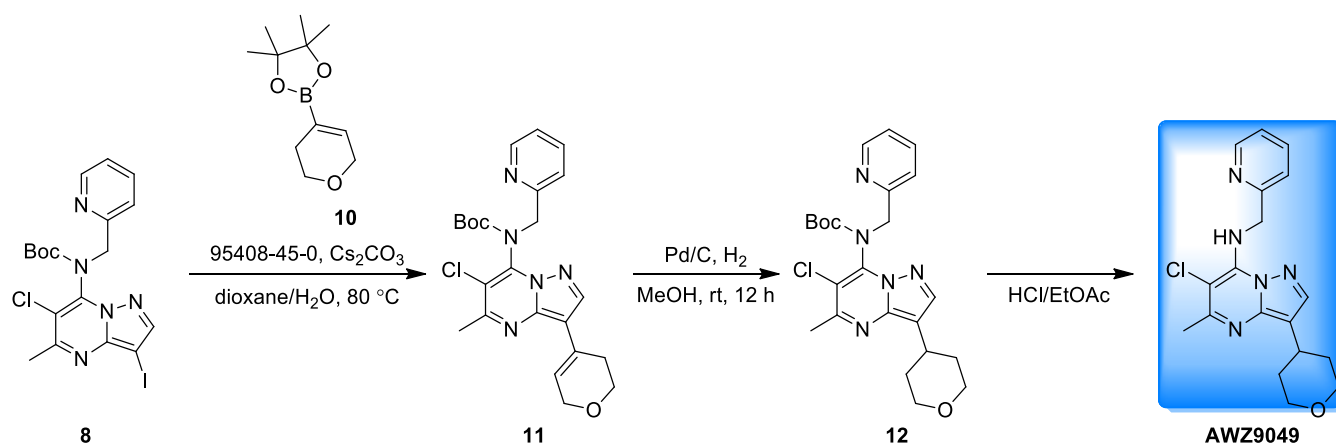
6-chloro-3-(4-fluorophenyl)-5-methyl-N-(pyridin-2-ylmethyl)pyrazolo[1,5-a]pyrimidin-7-amine (AWZ9046)



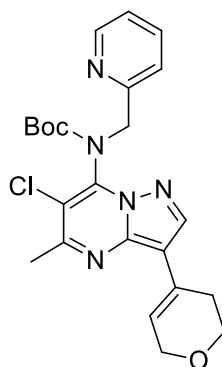
To a solution of tert-butyl N-(6-chloro-3-iodo-5-methyl-pyrazolo[1,5-a]pyrimidin-7-yl)-N-(2-pyridylmethyl)carbamate (150 mg, 300 μmol, 1 eq) and (4-fluorophenyl)boronic acid (63 mg, 450 μmol, 1.5 eq) in dioxane (5 mL) and H₂O (1 mL) was added Cs₂CO₃ (195 mg, 600 μmol, 2 eq), ditert-butyl(cyclopentyl)phosphane;dichloropalladium;iron (19 mg, 30 μmol, 0.1 eq). The mixture was stirred at 80 °C for 1.5 hours under N₂. TLC (Petroleum ether/EtOAc=5/1) showed that no new spot. LCMS showed that a major peak of desired product. The mixture was concentrated directly. The residue was purified by chromatography on silica gel (Petroleum ether/EtOAc=10/1, 2/1) to give tert-butyl N-[6-chloro-3-(4-fluorophenyl)-5-methyl-pyrazolo[1,5-a]pyrimidin-7-yl]-N-(2-pyridylmethyl)carbamate (100 mg, 213 μmol, 71% yield) as a yellow solid. A solution of tert-butyl N-[6-chloro-3-(4-fluorophenyl)-5-methyl-pyrazolo[1,5-a]pyrimidin-7-yl]-N-(2-pyridylmethyl)carbamate (100 mg, 213 μmol, 1 eq) in HCl/EtOAc (10 mL) was stirred at 15 °C for 4 hours. TLC (Petroleum ether/EtOAc=1/1) showed that tert-butyl N-[6-chloro-3-(4-fluorophenyl)-5-methyl-pyrazolo[1,5-a]pyrimidin-7-yl]-N-(2-pyridylmethyl)carbamate was consumed completely and a new spot. The mixture was concentrated. The residue was purified by trituration from (Petroleum ether/EtOAc/DCM=10/1/1, 12 mL). The solid was dissolved in MeOH (10 mL) and basified by strong basic anion exchange resin to give 6-chloro-3-(4-fluorophenyl)-5-methyl-N-(2-pyridylmethyl)pyrazolo[1,5-a]pyrimidin-7-amine (60.00 mg, 156.93 μmol, 73% yield, 96.2% purity) as a grey solid.

LCMS (Method 5-95AB, ESI): RT =0.725 min / 1.5 min, M+H+ =368.0.

¹H NMR (400MHz, DMSO-d₆) δ 8.60 (s, 1H), 8.52-8.56 (m, 1H), 8.38-8.45 (m, 1H), 8.13-8.19 (m, 2H), 7.80 (d, *J*=1.63 Hz, 1H), 7.36-7.42 (m, 1H), 7.21-7.32 (m, 3H), 5.39 (d, *J*=6.02 Hz, 2H), 2.56 (s, 3H).



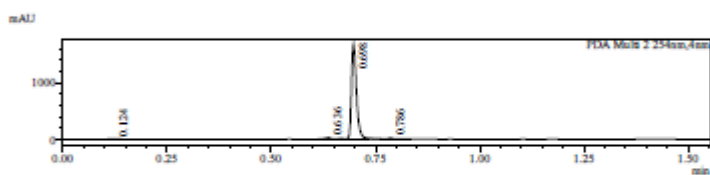
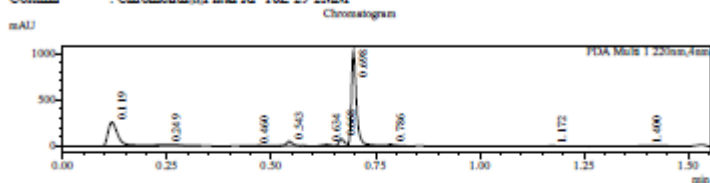
tert-butyl (6-chloro-3-(3,6-dihydro-2H-pyran-4-yl)-5-methylpyrazolo[1,5-a]pyrimidin-7-yl)(pyridin-2-ylmethyl)carbamate (11)



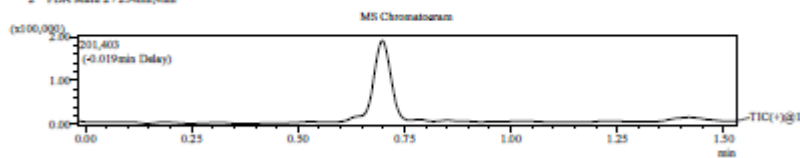
To a solution of tert-butyl N-(6-chloro-3-iodo-5-methyl-pyrazolo[1,5-a]pyrimidin-7-yl)-N-(2-pyridylmethyl)carbamate (150 mg, 300 μ mol, 1 *eq*) and 2-(3,6-dihydro-2H-pyran-4-yl)-4,4,5,5-tetramethyl-1,3,2-dioxaborolane (82 mg, 390 μ mol, 1.3 *eq*) in dioxane (10 mL) and H₂O (1 mL) was added Cs₂CO₃ (195 mg, 600 μ mol, 2 *eq*), ditert-butyl(cyclopentyl)phosphane;dichloropalladium;iron (19 mg, 30 μ mol, 0.1 *eq*). The mixture was stirred at 80 °C for 2 hours under N₂. TLC (Petroleum ether/EtOAc=1/1) showed that tert-butyl N-(6-chloro-3-iodo-5-methyl-pyrazolo[1,5-a]pyrimidin-7-yl)-N-(2-pyridylmethyl)carbamate was consumed completely and a major new spot. Desired product was detected by LCMS. The mixture was concentrated. The residue was purified by chromatography on silica gel (Petroleum ether/EtOAc=1/2) to give tert-butyl N-[6-chloro-3-(3,6-dihydro-2H-pyran-4-yl)-5-methyl-pyrazolo[1,5-a]pyrimidin-7-yl]-N-(2-pyridylmethyl)carbamate (100 mg, 219 μ mol, 73% yield) as a yellow oil.

LCMS REPORT

Compound ID : 1
 Sample ID : EW1181-447-P1A
 Injection Vol : 5ul
 Location : vial69
 Acq Method : d:\method\5-91AB_R_2W1cm
 Org DataFile : D:\data\1503\150304\EW1181-447-P1A.lcd
 Injection Date : 3/4/2015 11:07:49 AM
 Instrument : LCMS-H 16-101
 Column : Chromolith@Flash RP-18E 25-2MM



1 PDA Mobile 1 / 220nm,4nm
 2 PDA Mobile 2 / 254nm,4nm



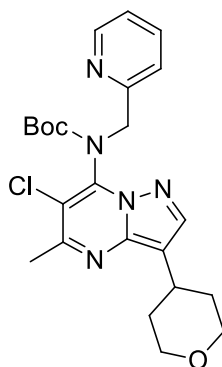
Integration Result

Peak Table						
Peak#	Ret. Time	Height	Height%	USP Width	Area	Area%
1	0.119	233945	18.171	0.042	425034	27.134
2	0.249	14654	1.040	0.099	55903	3.569
3	0.460	2967	0.211	0.077	10164	0.649
4	0.543	48487	3.442	0.029	50833	3.245
5	0.634	17280	1.227	0.039	24321	1.553
6	0.668	73794	5.239	0.028	75425	4.815
7	0.698	965324	68.535	0.024	872633	55.710
8	0.786	18171	1.290	0.028	22626	1.444
9	1.172	6511	0.462	0.031	8145	0.520
10	1.400	3375	0.382	0.105	21305	1.360

PDA Ch2 254nm

Peak Table

tert-butyl (6-chloro-5-methyl-3-(tetrahydro-2H-pyran-4-yl)pyrazolo[1,5-a]pyrimidin-7-yl)(pyridin-2-ylmethyl)carbamate (12)

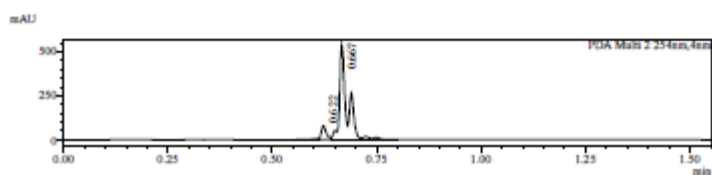
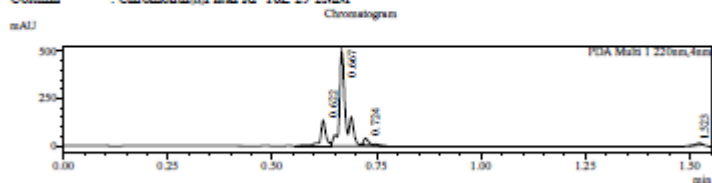


To a solution of tert-butyl N-[6-chloro-3-(3,6-dihydro-2H-pyran-4-yl)-5-methyl-pyrazolo[1,5-a]pyrimidin-7-yl]-N-(2-pyridylmethyl)carbamate (100 mg, 219 μ mol, 1 eq) in MeOH (10 mL) was added Pd/C (50 mg). The mixture

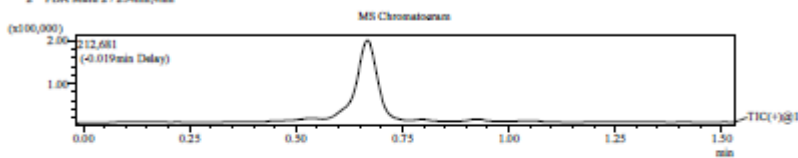
was stirred at 15 °C for 12 hours under H₂ (15 psi). TLC (Petroleum ether/EtOAc=1/1) showed that about 80% of tert-butyl N-[6-chloro-3-(3,6-dihydro-2H-pyran-4-yl)-5-methyl-pyrazolo[1,5-a]pyrimidin-7-yl]-N-(2-pyridylmethyl)carbamate was consumed and a new major spot. LCMS showed that a major peak of desired product and about 10% of by-product tert-butyl N-(5-methyl-3-tetrahydropyran-4-yl-pyrazolo[1,5-a]pyrimidin-7-yl)-N-(2-pyridylmethyl)carbamate. The mixture was filtered and concentrated. The residue was purified by prep-TLC (Petroleum ether/EtOAc=1/2) to give tert-butyl N-(6-chloro-5-methyl-3-tetrahydropyran-4-yl-pyrazolo[1,5-a]pyrimidin-7-yl)-N-(2-pyridylmethyl)carbamate (60 mg, 131 μmol, 60% yield) as a light yellow oil.

LCMS REPORT

Compound ID : 1
 Sample ID : EW1181-449-PIA
 Injection Vol : 4ul
 Location : vial71
 Acq Method : d:\method\5-95AB_R_2W1cm
 Orig Data File : D:\data\15031503T5\EW1181-449-PIA.lcd
 Injection Date : 3/5/2015 11:18:06 AM
 Instrument : LCMS-H 16-101
 Column : Chromolith@Flash RP-18E 25-2MM



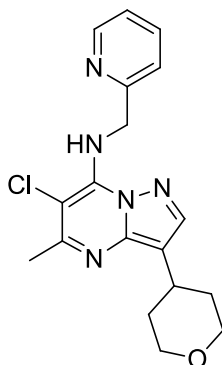
1 PDA Multi 1 / 220nm,4nm
 2 PDA Multi 2 / 254nm,4nm



Integration Result

Peak Table						
Peak#	Ret. Time	Height	Height%	USP Width	Area	Area%
PDA Ch1 220nm						
1	0.622	128827	19.477	0.022	125890	17.284
2	0.667	490048	74.089	0.023	539508	76.817
3	0.724	33475	5.061	0.024	34329	4.713
4	1.523	9077	1.372	0.026	8642	1.187
PDA Ch2 254nm						
1	0.622	76437	12.656	0.023	79083	10.399
2	0.667	527515	87.344	0.023	681477	89.601

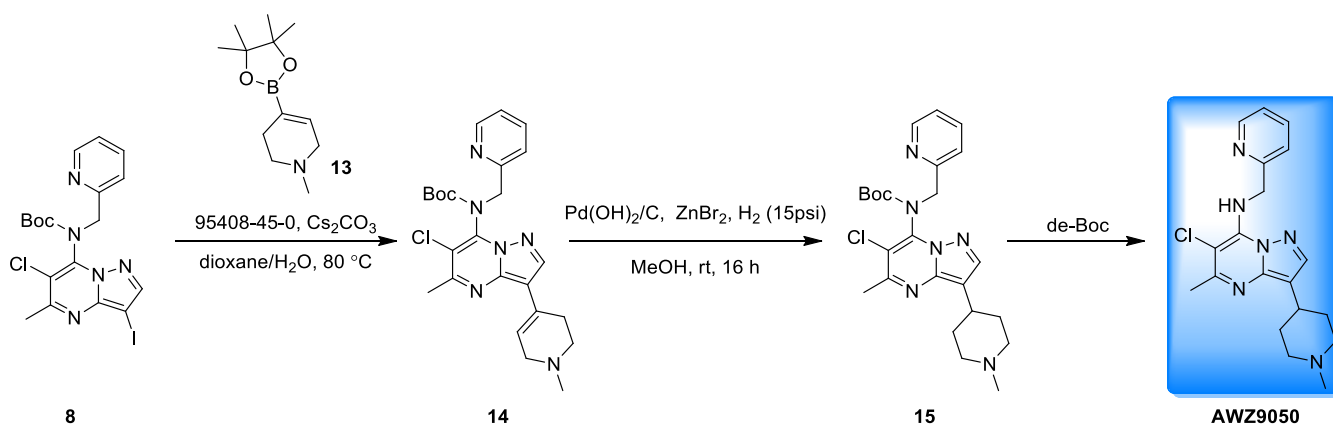
6-chloro-5-methyl-N-(pyridin-2-ylmethyl)-3-(tetrahydro-2H-pyran-4-yl)pyrazolo[1,5-a]pyrimidin-7-amine (AWZ9049)



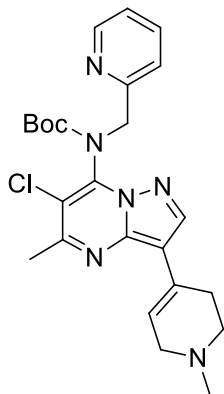
A solution of tert-butyl N-(6-chloro-5-methyl-3-tetrahydropyran-4-yl-pyrazolo[1,5-a]pyrimidin-7-yl)-N-(2-pyridylmethyl)carbamate (60 mg, 131 μmol , 1 *eq*) in HCl/EtOAc (4 M, 8 mL, 244 *eq*) was stirred at 15 °C for 1 hour. TLC (EtOAc) showed that tert-butyl N-(6-chloro-5-methyl-3-tetrahydropyran-4-yl-pyrazolo[1,5-a]pyrimidin-7-yl)-N-(2-pyridylmethyl)carbamate was consumed completely and a new major spot. The mixture was concentrated directly to remove the solvent. The residue was dissolved in MeOH (20 mL) and basified by strong basic anion exchange resin, then the mixture was filtered and concentrated, which was purified by trituration from (Petroleum ether/EtOAc/DCM=10/1/1, 12 mL) to give 6-chloro-5-methyl-N-(2-pyridylmethyl)-3-tetrahydropyran-4-yl-pyrazolo[1,5-a]pyrimidin-7-amine (15 mg, 41 μmol , 31% yield, 97% purity) as a white solid.

LCMS (Method 5-95AB, ESI): RT=0.546 min / 1.5 min, M+H⁺ =358.1.

¹H NMR (400MHz, DMSO-d₆) δ 8.64-8.68 (m, 1H), 8.01-8.08 (m, 1H), 7.86 (s, 1H), 7.62-7.67 (m, 1H), 7.55-7.60 (m, 1H), 5.48 (s, 2H), 3.90-3.97 (m, 2H), 3.43-3.51 (m, 2H), 2.53-2.56 (m, 2H), 2.44 (s, 3H), 1.73-1.89 (m, 3H).



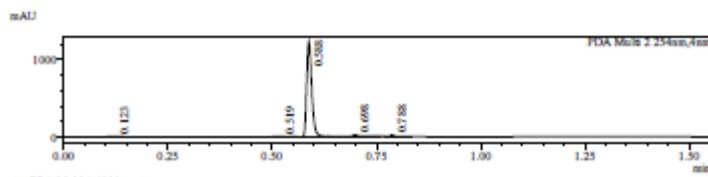
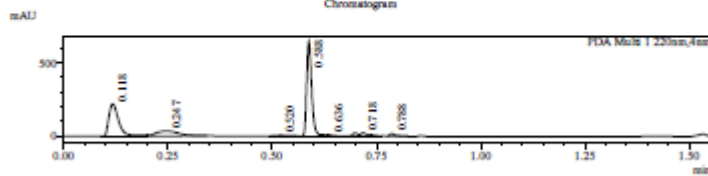
tert-butyl (6-chloro-5-methyl-3-(1-methyl-1,2,3,6-tetrahydropyridin-4-yl)pyrazolo[1,5-a]pyrimidin-7-yl)(pyridin-2-ylmethyl)carbamate (14)



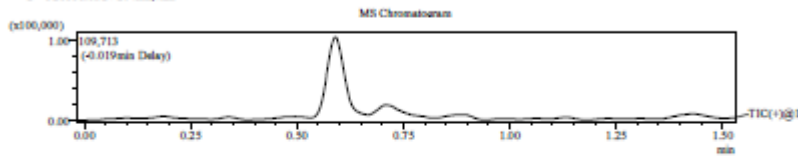
To a solution of tert-butyl N-(6-chloro-3-iodo-5-methyl-pyrazolo[1,5-a]pyrimidin-7-yl)-N-(2-pyridylmethyl)carbamate (150 mg, 300 μmol , 1 *eq*) and 1-methyl-4-(4,4,5,5-tetramethyl-1,3,2-dioxaborolan-2-yl)-3,6-dihydro-2H-pyridine (80 mg, 360 μmol , 1.2 *eq*) in dioxane (10 mL) and H₂O (1 mL) was added Cs₂CO₃ (195 mg, 600 μmol , 2 *eq*), ditert-butyl(cyclopentyl)phosphane;dichloropalladium;iron (19 mg, 30 μmol , 0.1 *eq*). The mixture was stirred at 80 °C for 2 hours under N₂. TLC (Petroleum ether/EtOAc=1/1) showed that tert-butyl N-(6-chloro-3-iodo-5-methyl-pyrazolo[1,5-a]pyrimidin-7-yl)-N-(2-pyridylmethyl)carbamate was consumed completely and TLC (Dichloromethane/Methanol=10/1) showed that a major new spot. Desired product was detected by LCMS. The mixture was concentrated. The residue was purified by chromatography on silica gel (Petroleum ether/EtOAc=1/3, Dichloromethane/Methanol=20/1, 15/1) to give tert-butyl N-[6-chloro-5-methyl-3-(1-methyl-3,6-dihydro-2H-pyridin-4-yl)pyrazolo[1,5-a]pyrimidin-7-yl]-N-(2-pyridylmethyl)carbamate (100 mg, 213 μmol , 71% yield) as a yellow oil.

LCMS REPORT

Compound ID : 1
 Sample ID : EW1181-448-P1A
 Injection Vol : 5ul
 Location : vial70
 Acq Method : d:\method\5-95AB_R_2W1cm
 Org DataFile : D:\data\1503\150304\EW1181-448-P1A.lcd
 Injection Date : 3/4/2015 11:09:49 AM
 Instrument : LCMS-H 16-101
 Column : Chromolith@Flash RP-18E 25-2MM



1 PDA Ch1 220nm,4nm
 2 PDA Ch2 254nm,4nm

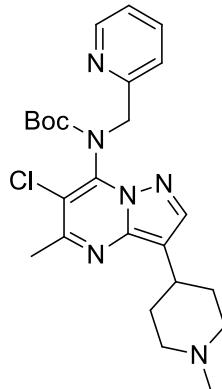


Integration Result

Peak Table						
Peak#	Ret. Time	Height	Height%	USP Width	Area	Area%
1	0.118	218532	23.322	0.042	358671	32.384
2	0.247	33007	3.552	0.095	123302	11.170
3	0.520	3841	0.629	0.080	12393	1.123
4	0.588	623449	67.101	0.024	542825	49.177
5	0.636	10658	1.147	0.037	7854	0.712
6	0.718	20587	2.216	0.032	43275	3.920
7	0.788	17028	1.833	0.021	14501	1.314

Peak Table						
Peak#	Ret. Time	Height	Height%	USP Width	Area	Area%
1	0.123	8226	0.655	0.045	13000	1.136
2	0.519	10897	0.868	0.022	10407	0.909
3	0.788	1190231	94.835	0.024	1075685	93.988

tert-butyl (6-chloro-5-methyl-3-(1-methylpiperidin-4-yl)pyrazolo[1,5-a]pyrimidin-7-yl)(pyridin-2-ylmethyl)carbamate (15)

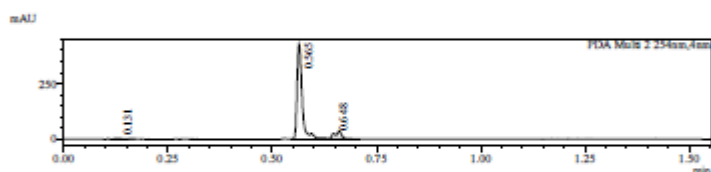
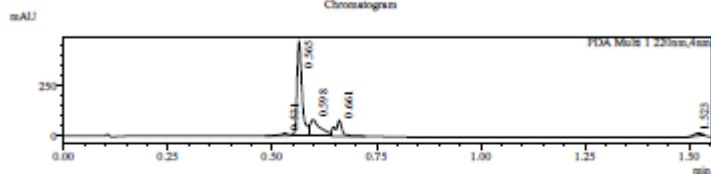


To a solution of tert-butyl N-[6-chloro-5-methyl-3-(1-methyl-3,6-dihydro-2H-pyridin-4-yl)pyrazolo[1,5-a]pyrimidin-7-yl]-N-(2-pyridylmethyl)carbamate (100 mg, 213 μ mol, 1 eq) in MeOH (8 mL) was added Pd(OH)₂ (149 mg, 1 mmol, 5 eq), ZnBr₂ (96 mg, 426 μ mol, 2 eq). The mixture was stirred at 15 °C for 16 hrs under H₂ (15 psi). TLC (Dichloromethane/Methanol=10/1) showed that most of tert-butyl N-[6-chloro-5-methyl-3-(1-methyl-3,6-dihydro-2H-pyridin-4-yl)pyrazolo [1,5-a]pyrimidin-7-yl]-N-(2-pyridylmethyl)carbamate was consumed and several spots. LCMS showed that several peaks, desired product was detected. The mixture was filtered and concentrated. The residue was purified by prep-TLC (CHCl₃/Methanol/H₂O= 30/5/1) to give tert-butyl N-[6-chloro-5-methyl-3-(1-methyl-4-piperidyl)pyrazolo[1,5-a]pyrimidin-7-yl]-N-(2-pyridylmethyl)carbamate (25 mg, 42 μ mol, 20% yield, 80% purity) as a light yellow oil.

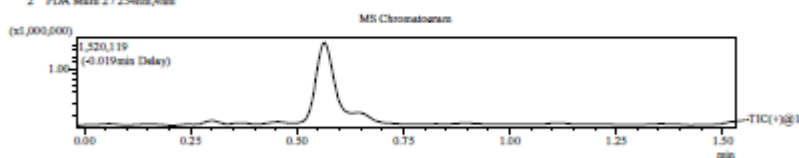
LCMS REPORT

Compound ID : 1
 Sample ID : EW1181-479-P1A1
 Injection Vol : 10ul
 Location : vial55
 Acq Method : d:\method\5-95AB_R_2W1cm
 Org DataFile : D:\data\1503\150319\EW1181-479-P1A1.lcd
 Injection Date : 3/19/2015 3:26:47 PM
 Instrument : LCMS-H 15-105
 Column : Chromolith@Flash RP-18E 25-2MM

Chromatogram



1 PDA Multi 1 / 220nm, 4nm
 2 PDA Multi 2 / 254nm, 4nm

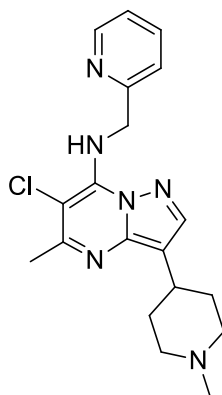


Integration Result

Peak Table						
Peak#	Ret. Time	Height	Height%	USP Width	Area	Area%
1	0.531	14233	2.328	0.034	19065	2.821
2	0.565	429223	70.199	0.024	404557	59.872
3	0.596	81836	13.384	0.048	141237	20.902
4	0.661	72675	11.886	0.027	93639	13.858
5	1.523	13470	2.203	0.034	17204	2.546

Peak Table						
Peak#	Ret. Time	Height	Height%	USP Width	Area	Area%
1	0.131	5087	1.216	0.034	6820	1.616
2	0.565	391065	93.485	0.023	377241	89.409
3	0.648	22165	5.298	0.034	37866	8.974

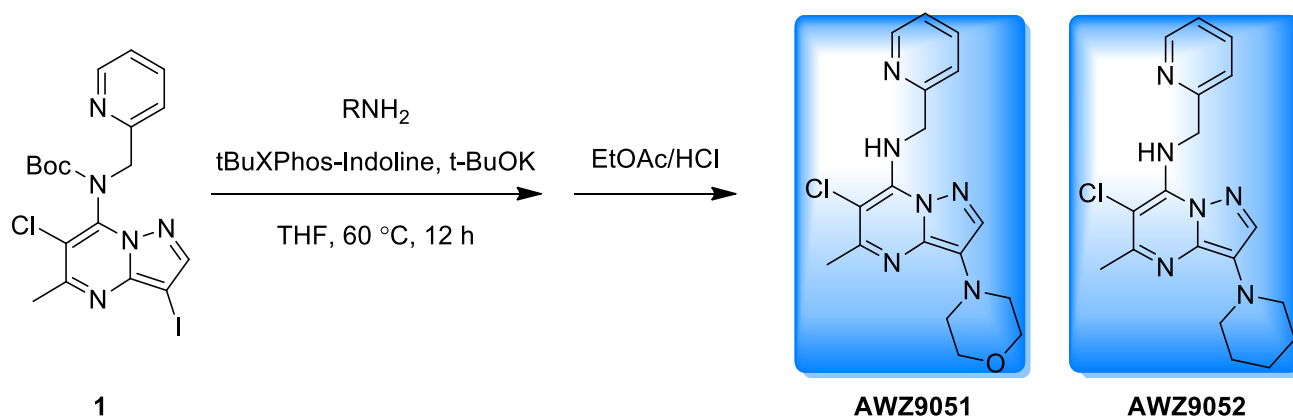
**6-chloro-5-methyl-3-(1-methylpiperidin-4-yl)-N-(pyridin-2-ylmethyl)pyrazolo[1,5-a]pyrimidin-7-amine
(AWZ9050)**



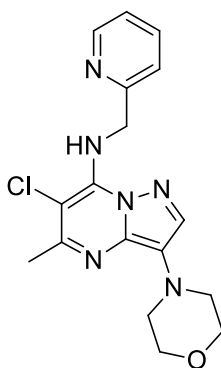
A solution of tert-butyl N-[6-chloro-5-methyl-3-(1-methyl-4-piperidyl)pyrazolo[1,5-a]pyrimidin-7-yl]-N-(2-pyridylmethyl)carbamate (25 mg, 53 μmol , 1 *eq*) in HCl/EtOAc (4 M, 5.00 mL, 377 *eq*) was stirred at 15 °C for 2 hours. LCMS showed that tert-butyl N-[6-chloro-5-methyl-3-(1-methyl-4-piperidyl)pyrazolo[1,5-a]pyrimidin-7-yl]-N-(2-pyridylmethyl)carbamate was consumed completely and a major peak of desired product. The mixture was concentrated to remove the solvent. The residue was purified by prep-HPLC (Column: Boston Green ODS 150*30 5 μ ; Condition: 0.225%FA-ACN; Gradient Time (min): 11; FlowRate(ml/min): 25) and basified by strongly basic anion exchange resin to give 6-chloro-5-methyl-3-(1-methyl-4-piperidyl)-N-(2-pyridylmethyl)pyrazolo[1,5-a]pyrimidin-7-amine (10 mg, 26 μmol , 50% yield, 98.2% purity) as a light yellow solid.

LCMS (Method 0-60AB, ESI): RT =0.690 min / 1.5 min, M+H+ =371.2.

$^1\text{H NMR}$ (400MHz, DMSO- d_6) δ 8.51 (d, $J=4.27$ Hz, 1H), 7.89 (s, 1H), 7.75-7.82 (m, 1H), 7.37-7.42 (m, 1H), 7.26-7.32 (m, 1H), 5.42 (s, 2H), 3.28-3.30 (m, 2H), 3.02-3.12 (m, 1H), 2.70-2.80 (m, 2H), 2.65 (s, 3H), 2.55 (s, 3H), 2.09-2.18 (m, 2H), 1.99 (br. s., 2H).



6-chloro-5-methyl-3-morpholino-N-(pyridin-2-ylmethyl)pyrazolo[1,5-a]pyrimidin-7-amine (AWZ9051)



To a solution of tert-butyl N-(6-chloro-3-iodo-5-methyl-pyrazolo[1,5-a]pyrimidin-7-yl)-N-(2-pyridylmethyl)carbamate (50 mg, 100.1 μmol , 1 *eq*) and morpholine (43.58 mg, 500.3 μmol , 5 *eq*) in THF (1 mL) was added [2-(2-aminoethyl)phenyl]-chloro-palladium;ditert-butyl-[2-(2,4,6-triisopropylphenyl)phenyl]phosphane (13.7 mg, 20 μmol , 0.2 *eq*). Then tBuOK (1 M, 200.1 μL , 2 *eq*) in THF was added to the mixture. The mixture was stirred at 60 $^\circ\text{C}$ for 12 h under N_2 . TLC (Petroleum ether/EtOAc=1/1) showed that most of tert-butyl N-(6-chloro-3-iodo-5-methyl-pyrazolo[1,5-a]pyrimidin-7-yl)-N-(2-pyridylmethyl)carbamate was consumed and several new spots. To the mixture was added water (20 mL) and extracted with EtOAc (20 mL*2). The organic layers were washed with brine (20 mL), dried over Na_2SO_4 and concentrated. The residue was purified by prep-TLC (Petroleum ether/EtOAc=1/1) to give tert-butyl N-(6-chloro-5-methyl-3-morpholino-pyrazolo[1,5-a]pyrimidin-7-yl)-N-(2-pyridylmethyl)carbamate (10 mg, 43.6 μmol , 21% yield) as a brown oil.

A solution of tert-butyl N-(6-chloro-5-methyl-3-morpholino-pyrazolo[1,5-a]pyrimidin-7-yl)-N-(2-pyridylmethyl)carbamate (40 mg, 87 μmol , 1 *eq*) in HCl/EtOAc (4 M, 4 mL, 183 *eq*) was stirred at 18 $^\circ\text{C}$ for 12 hours. TLC (Petroleum ether/EtOAc=1/2) showed that tert-butyl N-(6-chloro-5-methyl-3-morpholino-pyrazolo[1,5-a]pyrimidin-7-yl)-N-(2-pyridylmethyl)carbamate was consumed completely and a new major

spot. LCMS showed that a major peak of desired product. The mixture was concentrated to remove the solvent. The residue was purified by prep-HPLC (Column: Boston Green ODS 150*30 5u; Condition: 0.225% FA-ACN). The product was basified by strong basic anion exchange resin to give 6-chloro-5-methyl-3-morpholino-N-(2-pyridylmethyl)pyrazolo[1,5-a]pyrimidin-7-amine (6.5 mg, 17.6 μ mol, 20% yield, 97% purity) as a light yellow solid.

LCMS (Method 5-95AB, ESI): RT=0.615 min / 1.5 min, M+H+ =359.1.

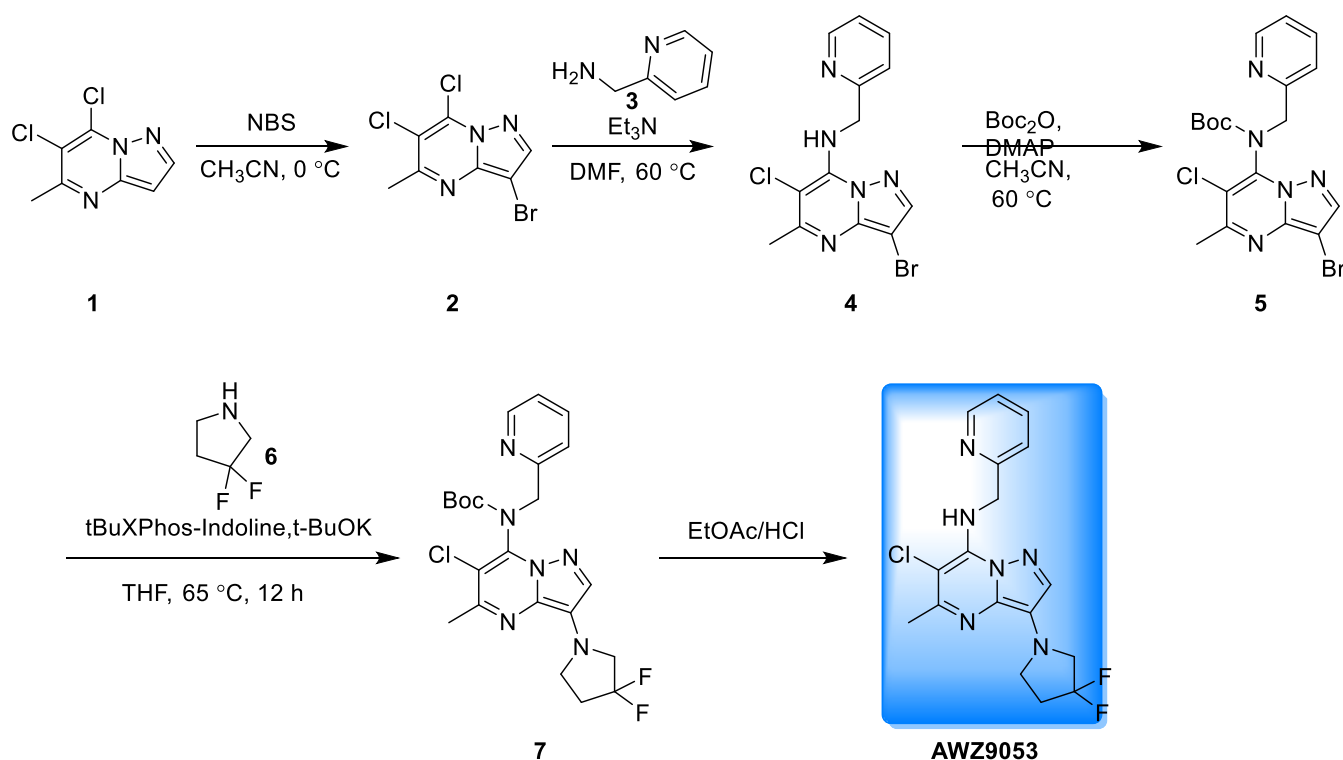
$^1\text{H NMR}$ (400MHz, DMSO-d₆) δ 8.54 (d, J =5.02 Hz, 1H), 8.18-8.27 (m, 1H), 7.75-7.85 (m, 2H), 7.35 (d, J =7.91 Hz, 1H), 7.25-7.32 (m, 1H), 5.32 (br. s., 2H), 3.73-3.79 (m, 4H), 3.15 (d, J =4.39 Hz, 4H), 2.45 (s, 3H).

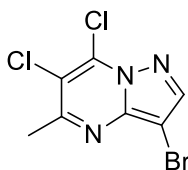
The above general procedure was followed for the syntheses of AWZ9052.

6-chloro-5-methyl-3-morpholino-N-(pyridin-2-ylmethyl)pyrazolo[1,5-a]pyrimidin-7-amine (AWZ9052)

LCMS (Method 5-95AB, ESI): RT=0.606 min / 1.5 min, M+H+ =357.1.

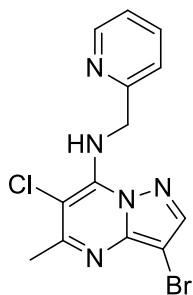
$^1\text{H NMR}$ (400MHz, DMSO-d₆) δ 8.54 (d, J =4.64 Hz, 1H), 8.16-8.24 (m, 1H), 7.76-7.83 (m, 2H), 7.36 (s, 2H), 5.26-5.35 (m, 2H), 3.08-3.15 (m, 4H), 2.46 (s, 3H), 1.62-1.68 (m, 4H), 1.49-1.54 (m, 2H).



3-bromo-6,7-dichloro-5-methylpyrazolo[1,5-a]pyrimidine (2)

To a solution of 6,7-dichloro-5-methyl-pyrazolo[1,5-a]pyrimidine (800 mg, 4 mmol, 1 *eq*) in CH₃CN (20 mL) was added NBS (940 mg, 4.8 mmol, 1.2 *eq*) at 0 °C. The mixture was stirred at 0 °C for 10 min. TLC (Petroleum ether/EtOAc=10/1) showed that starting material was consumed completely. To the mixture was added water (50 mL) and extracted with EtOAc (40 mL*2). The organic layers were washed with brine (60 mL), dried over Na₂SO₄ and concentrated. The residue was purified by chromatography on silica gel (Petroleum ether/EtOAc=10/1) to give 3-bromo-6,7-dichloro-5-methyl-pyrazolo[1,5-a]pyrimidine (1 g, 3.7 mmol, 90% yield) as a yellow solid.

¹H NMR (400MHz, CDCl₃-d) δ 8.16 (s, 1H), 2.79 (s, 3H)

6-(2,2,2-trifluoroethyl)pyrazolo[1,5-a]pyrimidin-7-ol (4)

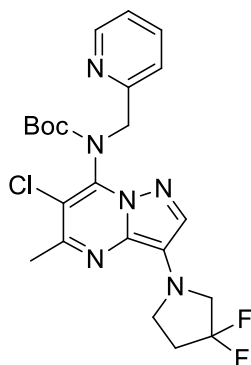
To a solution of 3-bromo-6,7-dichloro-5-methyl-pyrazolo[1,5-a]pyrimidine (400 mg, 1.4 mmol, 1 *eq*) and 2-pyridylmethanamine (184 mg, 1.7 mmol, 1.2 *eq*) in DMF (4 mL) was added Et₃N (431 mg, 4.3 mmol, 3 *eq*). The mixture was stirred at 60 °C for 0.5 hr under N₂. TLC (Petroleum ether/EtOAc=1/1) showed that 3-bromo-6,7-dichloro-5-methyl-pyrazolo[1,5-a]pyrimidine was consumed completely and a major new spot. To the mixture was added water (8 mL), a white solid was forming. Then the mixture was filtered and concentrated. The residue was used in the next step without purification to give 3-bromo-6-chloro-5-methyl-N-(2-pyridylmethyl)pyrazolo[1,5-a]pyrimidin-7-amine (400 mg, 1.1 mmol, 80% yield) as a grey solid.

¹H NMR (400MHz, DMSO-d₆) δ 8.35-8.61 (m, 2H), 8.21 (s, 1H), 7.72-7.84 (m, 1H), 7.24-7.43 (m, 2H), 5.36 (d, *J*=6.03 Hz, 2H), 2.52-2.55 (m, 3H).

Tert-butyl(3-bromo-6-chloro-5-methylpyrazolo[1,5-a]pyrimidin-7-yl)(pyridin-2-ylmethyl)carbamate (5)

To a solution of 3-bromo-6-chloro-5-methyl-N-(2-pyridylmethyl)pyrazolo[1,5-a]pyrimidin-7-amine (400 mg, 1.1 mmol, 1 eq) in THF (10 mL) was added DMAP (13 mg, 113 μ mol, 0.1 eq), Boc₂O (493 mg, 2.3 mmol, 2 eq). The mixture was stirred at 60 °C for 1 hour. TLC (Petroleum ether/EtOAc=1/1) showed that 3-bromo-6-chloro-5-methyl-N-(2-pyridylmethyl)pyrazolo[1,5-a]pyrimidin-7-amine was consumed completely and a new major spot. The mixture was concentrated. The residue was purified by chromatography on silica gel (Petroleum ether/EtOAc=5/1, 2/1) to give tert-butyl N-(3-bromo-6-chloro-5-methyl-pyrazolo[1,5-a]pyrimidin-7-yl)-N-(2-pyridylmethyl)carbamate (450 mg, 964.2 μ mol, 85% yield, 97% purity) as a yellow solid.

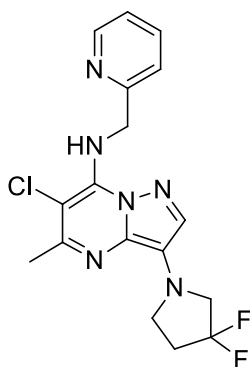
¹H NMR (400MHz, CDCl₃-d) δ 8.18-8.34 (m, 1H), 7.95 (s, 1H), 7.51-7.64 (m, 2H), 7.05 (t, *J*=5.83 Hz, 1H), 4.90-5.10 (m, 2H), 2.63 (s, 3H), 1.23-1.42 (m, 9H)

Tert-butyl(6-chloro-3-(3,3-difluoropyrrolidin-1-yl)-5-methylpyrazolo[1,5-a]pyrimidin-7-yl)(pyridin-2-ylmethyl)carbamate (7)

To a solution of tert-butyl N-(3-bromo-6-chloro-5-methyl-pyrazolo[1,5-a]pyrimidin-7-yl)-N-(2-pyridylmethyl)carbamate (50 mg, 110.4 μ mol, 1 eq) and 3,3-difluoropyrrolidine (24 mg, 220.9 μ mol, 2 eq) in THF (1 mL) was added [2-(2-aminoethyl)phenyl]-chloro-palladium;ditert-butyl-[2-(2,4,6-triisopropylphenyl)phenyl]phosphane (15 mg, 22.1 μ mol, 0.2 eq). Then tBuOK (1 M, 220.9 μ L, 2 eq) in the THF was added to the mixture. The mixture was stirred at 65 °C for 12 h under N₂. TLC (Petroleum ether/EtOAc=2/1) showed that about 80% of tert-butyl N-(6-chloro-3-iodo-5-methyl-pyrazolo[1,5-a]pyrimidin-7-yl)-N-(2-pyridylmethyl)carbamate was consumed and several spots. To the mixture was added water (20 mL) and extracted with EtOAc (20 mL*2). The organic layers were washed with brine (20 mL), dried over Na₂SO₄ and concentrated. The residue was purified by prep-TLC (Petroleum ether/EtOAc=2/1) to give tert-butyl N-[6-chloro-3-(3,3-difluoropyrrolidin-1-yl)-5-methyl-pyrazolo[1,5-a]pyrimidin-7-yl]-N-(2-pyridylmethyl)carbamate (15 mg, 62.6 μ mol, 14% yield) as a brown oil.

LCMS (Method 5-95AB, ESI): RT = 0.845 min / 1.5 min, M+H⁺ = 479.1.

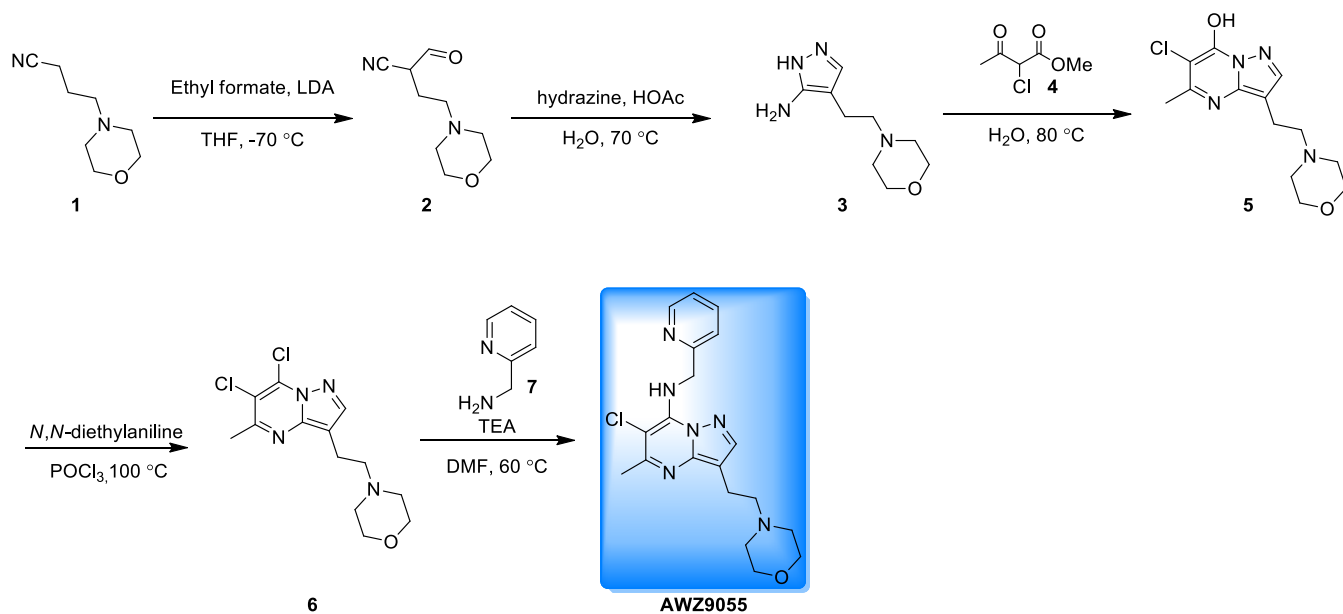
**6-chloro-3-(3,3-difluoropyrrolidin-1-yl)-5-methyl-N-(pyridin-2-ylmethyl)pyrazolo[1,5-a]pyrimidin-7-amine
(AWZ9053)**



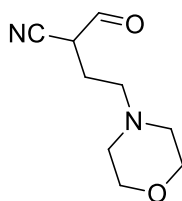
A solution of tert-butyl N-[6-chloro-3-(3,3-difluoropyrrolidin-1-yl)-5-methyl-pyrazolo[1,5-a]pyrimidin-7-yl]-N-(2-pyridylmethyl)carbamate (30 mg, 62.64 μ mol, 1 eq) in HCl/EtOAc (4 M, 8 mL, 511 eq) was stirred at 20 °C for 12 hours. LCMS showed that tert-butyl N-[6-chloro-3-(3,3-difluoropyrrolidin-1-yl)-5-methyl-pyrazolo[1,5-a]pyrimidin-7-yl]-N-(2-pyridylmethyl)carbamate was consumed completely and a major peak of desired product. The mixture was concentrated. The residue was purified by prep-HPLC (Column: Boston Green ODS 150*30 5u; Condition: 0.225%FA-ACN). The salt product was dissolved in MeOH (15 mL) and basified by strong basic anion exchange resin to give 6-chloro-3-(3,3-difluoropyrrolidin-1-yl)-5-methyl-N-(2-pyridylmethyl)pyrazolo[1,5-a]pyrimidin-7-amine (8 mg, 20.4 μ mol, 33% yield, 96.6% purity) as a light yellow solid.

LCMS (Method 5-95AB, ESI): RT =0.758 min / 1.5 min, M+H+ =379.1.

¹H NMR (400MHz, DMSO-d₆) δ 8.53 (d, *J*=4.39 Hz, 1H), 8.21 (s, 1H), 7.74-7.84 (m, 2H), 7.25-7.37 (m, 2H), 5.32 (d, *J*=6.02 Hz, 2H), 3.68 (s, 2H), 3.49 (t, *J*=7.03 Hz, 2H), 2.46 (s, 5H)

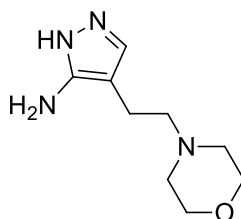


2-formyl-4-morpholinobutanenitrile (2)



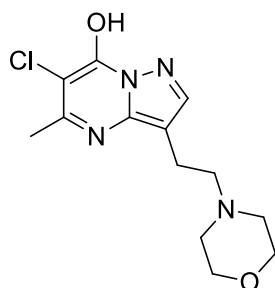
To a solution of 4-morpholinobutanenitrile (2 g, 13 mmol, 1 *eq*) in THF (20 mL) was added LDA (2 M, 13 mL, 2 *eq*) slowly at -70 °C. The mixture was stirred at -70 °C for 1 h under N₂. Then methyl formate (2 g, 32.4 mmol, 2.5 *eq*) was added to the mixture directly. The mixture was stirred at -70 °C for 0.5 h under N₂. TLC (Ethyl acetate) showed that 4-morpholinobutanenitrile was consumed completely and a major new spot at (254 nm). To the mixture was added NH₄Cl (10%, 5 mL) and water (60 mL), extracted with EtOAc (60 mL). The water layer was concentrated to give 2-formyl-4-morpholino-butanenitrile (1.5 g, crude) in water (40 mL) as a light yellow liquid. The product had a good solubility in water.

¹H NMR (400MHz, CDCl₃-d) δ 8.22 (s, 1H), 3.81 (br. s., 2H), 3.70-3.76 (m, 2H), 3.58-3.67 (m, 1H), 2.67 (d, *J*=7.65 Hz, 6H), 2.46-2.50 (m, 2H).

4-(2-morpholinoethyl)-1H-pyrazol-5-amine (3)

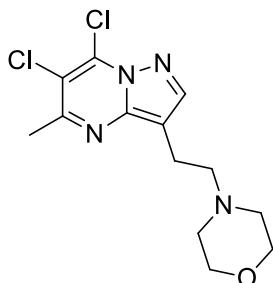
To a solution of 2-formyl-4-morpholino-butanenitrile (1.5 g, 8.2 mmol, 1 eq) in H₂O (20 mL) was added AcOH (988 mg, 16.5 mmol, 2 eq), N₂H₄·H₂O (2.1 g, 41.2 mmol, 5 eq). The mixture was stirred at 70 °C for 2 hours. TLC (CHCl₃/Methanol/H₂O=80/18/2) showed that 2-formyl-4-morpholino-butanenitrile was consumed completely and several new spots. Desired product was detected by the standard sample. To the mixture was added water (50 mL) and extracted with EtOAc (40 mL*2). The water layer was concentrated and lyophilized to give 4-(2-morpholinoethyl)-1H-pyrazol-3-amine (8 g, crude) as a grey which contained lots of salts.

LCMS (Method 0-60CD, ESI): RT=0.297 min / 4.0 min, M+H⁺ =197.2.

6-chloro-5-methyl-3-(2-morpholinoethyl)pyrazolo[1,5-a]pyrimidin-7-ol (5)

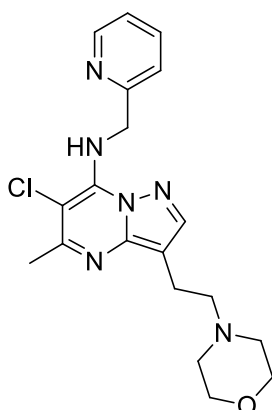
To a solution of 4-(2-morpholinoethyl)-1H-pyrazol-3-amine (7.5 g, 7.64 mmol, purity: 20%, 1 eq) and methyl 2-chloro-3-oxo-butanoate (1.2 g, 7.6 mmol, 1 eq) in H₂O (15 mL) was added TsOH·H₂O (145 mg, 764.3 μmol, 0.1 eq). The mixture was stirred at 80 °C for 2 hours under N₂. TLC (Dichloromethane/Methanol=10/1) showed that the material 4-(2-morpholinoethyl)-1H-pyrazol-3-amine was consumed completely and a major new spot. LCMS showed that a major peak of desired product. The mixture was concentrated directly. The residue was purified by chromatography on silica gel (Dichloromethane/Methanol=15/1, 10/1) to give 6-chloro-5-methyl-3-(2-morpholinoethyl)pyrazolo[1,5-a]pyrimidin-7-ol (1.2 g, crude) as a brown solid, which contained some salts.

LCMS (Method 0-60CD, ESI): RT=1.301 min / 4.0 min, M+H⁺ =297.1.

4-(2-(6,7-dichloro-5-methylpyrazolo[1,5-a]pyrimidin-3-yl)ethyl)morpholine (6)

To a solution of 6-chloro-5-methyl-3-(2-morpholinoethyl)pyrazolo[1,5-a]pyrimidin-7-ol (1 g, 3.4 mmol, 1 *eq*) in POCl_3 (20 mL) was added *N,N*-diethylaniline (1 g, 6.7 mmol, 2 *eq*). The mixture was stirred at 100 °C for 2 hours under N_2 . LCMS showed that 6-chloro-5-methyl-3-(2-morpholinoethyl)pyrazolo[1,5-a]pyrimidin-7-ol was consumed completely and a major peak of desired product. The mixture was concentrated to remove POCl_3 and mixed with EtOAc (100 mL), then added into a stirring water (150 mL). The mixture was extracted with EtOAc (100 mL*2). But only a little product in the organic layers. Most of the salt (HCl) product was in water. A grey solid was forming after 12 h. Then the solid was filtered and concentrated. The residue was used in the next step without purification to give 4-[2-(6,7-dichloro-5-methyl-pyrazolo[1,5-a]pyrimidin-3-yl)ethyl]morpholine (200 mg, 634.5 μmol , 19% yield) as a grey solid.

$^1\text{H NMR}$ (400MHz, DMSO-d_6) δ 8.26-8.32 (m, 1H), 3.95-3.99 (m, 2H), 3.84-3.89 (m, 2H), 3.32-3.35 (m, 2H), 3.26-3.29 (m, 2H), 3.00-3.06 (m, 4H), 2.67 (s, 3H)

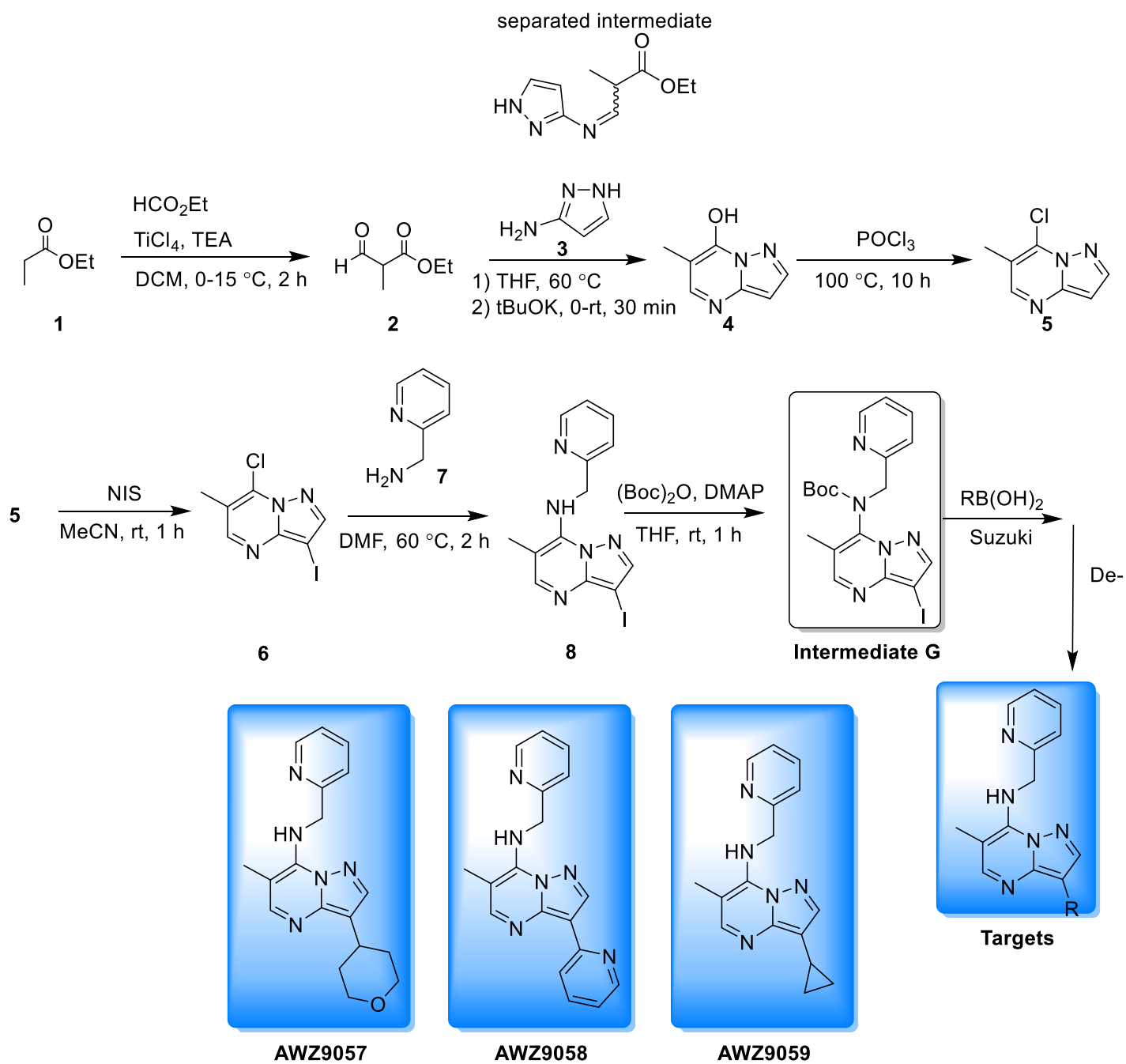
6-chloro-5-methyl-3-(2-morpholinoethyl)-*N*-(pyridin-2-ylmethyl)pyrazolo[1,5-a]pyrimidin-7-amine (AWZ9055)

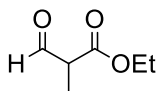
To a solution of 4-[2-(6,7-dichloro-5-methyl-pyrazolo[1,5-a]pyrimidin-3-yl)ethyl]morpholine (180 mg, 571.1 μmol , 1 *eq*) and 2-pyridylmethanamine (74 mg, 685.3 μmol , 1.2 *eq*) in DMF (8 mL) was added Et_3N (173 mg, 1.7 mmol, 3 *eq*). The mixture was stirred at 60 °C for 1 hour. LCMS showed that 4-[2-(6,7-dichloro-5-methyl-pyrazolo[1,5-a]pyrimidin-3-yl)ethyl]morpholine was consumed completely and a major peak of desired

product. The mixture was concentrated to remove TEA. The mixture was purified by prep-HPLC (Column: Boston Green ODS 150*30 5u; Condition: 0.225%FA-ACN). The product was basified by strong basic anion exchange resin to give 6-chloro-5-methyl-3-(2-morpholinoethyl)-N-(2-pyridylmethyl)pyrazolo[1,5-a]pyrimidin-7-amine (98 mg, 240.6 μ mol, 42% yield, 95% purity) as a white solid.

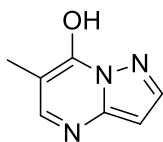
LCMS (Method 10-80CD, ESI): RT =1.263 min / 2.0 min, M+H+ =387.1.

¹H NMR (400MHz, DMSO-d6) δ 8.53 (d, J =4.27 Hz, 1H), 8.19-8.25 (m, 1H), 7.99 (s, 1H), 7.73-7.82 (m, 1H), 7.33-7.37 (m, 1H), 7.26-7.31 (m, 1H), 5.31-5.40 (m, 2H), 3.55-3.61 (m, 4H), 2.75-2.81 (m, 2H), 2.54-2.57 (m, 2H), 2.48 (s, 3H), 2.43 (br. s., 4H).



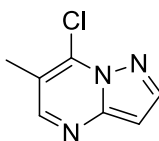
ethyl 2-methyl-3-oxopropanoate (2)

A solution of ethyl propanoate (25.00 g, 244.79 mmol, 1.00 eq) and ethyl formate (36.27 g, 489.58 mmol, 2.00 eq) in DCM (200.00 mL) at 0 °C was added TiCl₄ (92.86 g, 489.58 mmol, 2.00 eq) followed by TEA (59.45 g, 587.50 mmol, 2.40 eq) dropwise under N₂ protection. The reaction mixture was stirred at 0 °C for 1 h and at 10-15 °C for another 1 h. TLC (Petroleum ether/EtOAc=1/1) showed a new spot under 254 nm. The reaction mixture was poured into ice water and extracted with DCM (100 mL*3). The organic layer was washed with brine (100 mL*3), dried over Na₂SO₄ and concentrated to give ethyl 2-methyl-3-oxo-propanoate (50.00 g, crude) as a brown oil which used directly for next step without further purification.

6-methylpyrazolo[1,5-a]pyrimidin-7-ol (4)

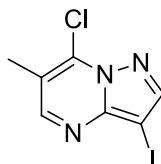
A mixture of ethyl 2-methyl-3-oxo-propanoate (35.00 g, 268.94 mmol, 1.00 eq), 1H-pyrazol-3-amine (17.88 g, 215.15 mmol, 0.80 eq) in THF (300.00 mL) was stirred at 60 °C for 1 hour. TLC (Petroleum ether/EtOAc=4/1) showed all of ethyl 2-methyl-3-oxo-propanoate was consumed and two new spots. The reaction mixture was used directly for next step without further work up and purification.

To a mixture of ethyl 3-((1H-pyrazol-3-yl)imino)-2-methylpropanoate (52.00 g, 266.37 mmol, 1.00 eq) in THF (300.00 mL) obtained from last step at 0 °C was added tBuOK (29.89 g, 266.37 mmol, 1.00 eq) in portions and the mixture was stirred at 10-15 °C for 30 mins. Solids were precipitated. TLC (DCM/MeOH=10/1) showed all of ethyl (3E)-2-methyl-3-(1H-pyrazol-3-ylimino)propanoate was consumed and a new spot. The mixture was cooled to 0 °C and acidified with HCl/EtOAc (4 M) to pH7. The mixture was concentrated to give 6-methylpyrazolo[1,5-a]pyrimidin-7-ol (60.00 g, crude) as a light yellow solid contained KCl.

7-chloro-6-methylpyrazolo[1,5-a]pyrimidine (5)

To a mixture of 6-methylpyrazolo[1,5-a]pyrimidin-7-ol (20.00 g, 67.05 mmol, 1.00 eq) in POCl_3 (246.00 g, 1.60 mol, 23.93 eq). The mixture was stirred at 100 °C for 10 hours. LCMS showed all of 6-methylpyrazolo[1,5-a]pyrimidin-7-ol was consumed and a new major peak with desired MS. The mixture was concentrated to give a residue. The reaction was quenched by slowly adding to water. The residue was dissolved in EtOAc (200 mL) and washed with brine (100 mL*2). The organic layer was dried over Na_2SO_4 and concentrated to give 7-chloro-6-methyl-pyrazolo[1,5-a]pyrimidine (7.00 g, crude) as a brown solid.

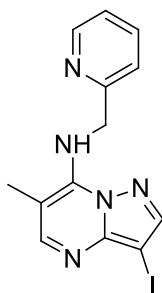
LCMS (Method 0-60 CD): RT=1.323 min/2 min, $[\text{M}+\text{H}]^+=168.1$.

7-chloro-3-iodo-6-methylpyrazolo[1,5-a]pyrimidine (6)

A mixture of 7-chloro-6-methyl-pyrazolo[1,5-a]pyrimidine (6.50 g, 38.78 mmol, 1.00 eq) and NIS (8.73 g, 38.78 mmol, 1.00 eq) in CH_3CN (60.00 mL) was stirred at 10-15 °C for 1 hour. TLC (Petroleum ether/EtOAc=3/1) showed all of 7-chloro-6-methyl-pyrazolo[1,5-a]pyrimidine was consumed and a new spot. The mixture was concentrated to give a residue. The residue was purified by chromatography (Petroleum ether/EtOAc=20/1; 10/1; 5/1) to give 7-chloro-5-iodo-6-methyl-pyrazolo[1,5-a]pyrimidine (6.00 g, 20.44 mmol, 52% yield) as a brown solid.

$^1\text{H NMR}$ (400MHz, CHCl_3 -d) δ 8.43 (s, 1H), 8.15-8.21 (m, 1H), 2.49 (s, 3H).

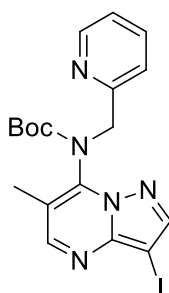
3-iodo-6-methyl-N-(pyridin-2-ylmethyl)pyrazolo[1,5-a]pyrimidin-7-amine (8)



A mixture of 7-chloro-5-iodo-6-methyl-pyrazolo[1,5-a]pyrimidine (2.00 g, 6.81 mmol, 1.00 eq), 2-pyridylmethanamine (736.92 mg, 6.81 mmol, 1.00 eq) and Et₃N (1.38 g, 13.63 mmol, 2.00 eq) in DMF (2.00 mL) was stirred at 60 °C for 2 hours. TLC (Petroleum ether/EtOAc=2/1) showed all of 7-chloro-5-iodo-6-methyl-pyrazolo[1,5-a]pyrimidine was consumed and a new spot. The mixture was diluted with EtOAc (40 mL) and washed with brine (20 mL*3). The organic layer was dried over Na₂SO₄ and concentrated to give a residue. The residue was triturated with EtOAc (20 mL) to give 3-iodo-6-methyl-N-(2-pyridylmethyl)pyrazolo[1,5-a]pyrimidin-7-amine (1.10 g, 3.01 mmol, 44% yield) as a light yellow solid.

¹H NMR (400MHz, CHLOROFORM-d) δ 8.69 (d, J=4.8 Hz, 1H), 8.15 (s, 1H), 8.04 (s, 1H), 7.73 (dt, J=1.7, 7.6 Hz, 2H), 7.27-7.32 (m, 2H), 5.17 (d, J=5.5 Hz, 2H), 2.50 (s, 3H).

tert-butyl (3-iodo-6-methylpyrazolo[1,5-a]pyrimidin-7-yl)(pyridin-2-ylmethyl)carbamate (9)

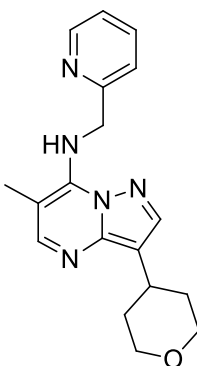


A mixture of 3-iodo-6-methyl-N-(2-pyridylmethyl)pyrazolo[1,5-a]pyrimidin-7-amine (1.10 g, 3.01 mmol, 1.00 eq), Boc₂O (1.31 g, 6.02 mmol, 2.00 eq) and DMAP (36.77 mg, 301.00 μmol, 0.10 eq) in THF (30.00 mL) was stirred at 15-20 °C for 1 hour. TLC (Petroleum ether/EtOAc=1/1) showed all of 3-iodo-6-methyl-N-(2-pyridylmethyl)pyrazolo[1,5-a]pyrimidin-7-amine was consumed and a new major spot. The mixture was concentrated to give a residue. The residue was purified by chromatography (Petroleum ether/EtOAc=10/1; 5/1; 2/1) to give tert-butyl N-(3-iodo-6-methyl-pyrazolo[1,5-a]pyrimidin-7-yl)-N-(2-pyridylmethyl)carbamate (1.20 g, 2.44 mmol, 81% yield, 94.8% purity) as a light brown solid.

LCMS (Method 10-80 CD): RT=1.467 min/2 min, [M+H]⁺=466.1.

¹H NMR (400MHz, CHLOROFORM-d) δ 8.32 (s, 1H), 8.03 (s, 1H), 7.50-7.59 (m, 1H), 7.38 (d, J=7.8 Hz, 1H), 7.04-7.13 (m, 2H), 5.16-5.26 (m, 2H), 2.02 (s, 3H), 1.24 (s, 9H).

6-methyl-N-(pyridin-2-ylmethyl)-3-(tetrahydro-2H-pyran-4-yl)pyrazolo[1,5-a]pyrimidin-7-amine (AWZ9057)



A mixture of 2-(3,6-dihydro-2H-pyran-4-yl)-4,4,5,5-tetramethyl-1,3,2-dioxaborolane (169.31 mg, 805.95 μ mol, 1.50 eq), tert-butyl N-(3-iodo-6-methyl-pyrazolo[1,5-a]pyrimidin-7-yl)-N-(2-pyridylmethyl)carbamate (250.00 mg, 537.30 μ mol, 1.00 eq), Pd(dppf)Cl₂ (78.63 mg, 107.46 μ mol, 0.20 eq) and Cs₂CO₃ (350.13 mg, 1.07 mmol, 2.00 eq) in dioxane (3.00 mL) and H₂O (500.00 μ L) was stirred at 80 °C for 12 hours under N₂ protection. LCMS showed all of tert-butyl N-(3-iodo-6-methyl-pyrazolo[1,5-a]pyrimidin-7-yl)-N-(2-pyridylmethyl)carbamate was consumed and a new major peak with desired MS. TLC (Petroleum ether/EtOAc=2/1) showed all of tert-butyl N-(3-iodo-6-methyl-pyrazolo[1,5-a]pyrimidin-7-yl)-N-(2-pyridylmethyl)carbamate was consumed and a new spot. The mixture was concentrated to give a residue. The residue was purified by chromatography (Petroleum ether/EtOAc=5/1; 3/1; 2/1) to give tert-butyl N-[3-(3,6-dihydro-2H-pyran-4-yl)-6-methyl-pyrazolo[1,5-a]pyrimidin-7-yl]-N-(2-pyridylmethyl)carbamate (150.00 mg, 355.88 μ mol, 66% yield) as a yellow solid.

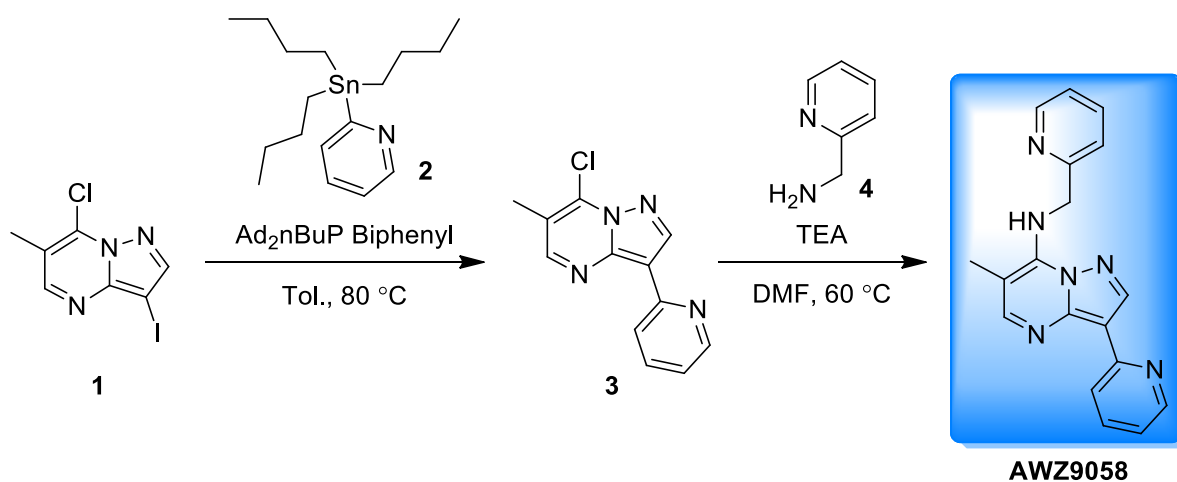
A mixture of tert-butyl N-[3-(3,6-dihydro-2H-pyran-4-yl)-6-methyl-pyrazolo[1,5-a]pyrimidin-7-yl]-N-(2-pyridylmethyl)carbamate (150.00 mg, 355.88 μ mol, 1.00 eq) in MeOH (5.00 mL) was added Pd/C (50.00 mg). The mixture was stirred at 15-20 °C for 3 hours under H₂ (15 PSI). TLC (Petroleum ether/EtOAc=1/1) showed all of tert-butyl N-[3-(3,6-dihydro-2H-pyran-4-yl)-6-methyl-pyrazolo[1,5-a]pyrimidin-7-yl]-N-(2-pyridylmethyl)carbamate was consumed and a new spot. The mixture was filtered and the filtrate was concentrated to give tert-butyl N-(6-methyl-3-tetrahydropyran-4-yl-pyrazolo[1,5-a]pyrimidin-7-yl)-N-(2-pyridylmethyl)carbamate (100.00 mg, crude) as a green solid and it was used directly for the next step.

A mixture of tert-butyl N-(6-methyl-3-tetrahydropyran-4-yl-pyrazolo[1,5-a]pyrimidin-7-yl)-N-(2-pyridylmethyl)carbamate (150.00 mg, 354.18 μ mol, 1.00 eq) in HCl/EtOAc (4 M, 4.00 mL) was stirred at 15-25 °C for 12 hours. LCMS showed all of tert-butyl N-(6-methyl-3-tetrahydropyran-4-yl-pyrazolo[1,5-a]pyrimidin-7-yl)-N-(2-pyridylmethyl)carbamate was consumed and a new peak with desired MS. The mixture was concentrated to give a residue. The residue was dissolved in MeOH (10 mL) and basified with basic resin and

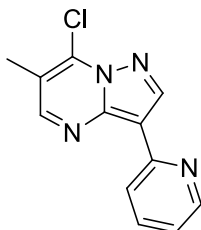
concentrated to give a residue. The residue was triturated with MeOH (2 mL) to give 6-methyl-N-(2-pyridylmethyl)-3-tetrahydropyran-4-yl-pyrazolo[1,5-a]pyrimidin-7-amine (15.80 mg, 46.41 μmol , 13% yield, 95% purity) as a light yellow solid.

LCMS (Method 5-95 AB): RT=0.572 min/1.5 min, $[\text{M}+\text{H}]^+=324.3$.

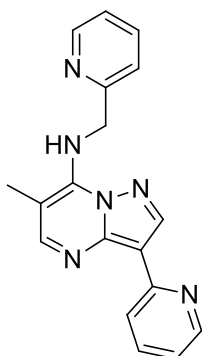
$^1\text{H NMR}$ (400MHz, DMSO- d_6) δ 8.56 (d, $J=3.5$ Hz, 1H), 8.06 (br. s., 1H), 7.95 (s, 2H), 7.79 (t, $J=7.3$ Hz, 1H), 7.23-7.43 (m, 2H), 5.13 (d, $J=5.8$ Hz, 2H), 3.92 (d, $J=10.3$ Hz, 2H), 3.46 (t, $J=10.5$ Hz, 2H), 2.95-3.10 (m, 1H), 2.33 (s, 3H), 1.72-1.91 (m, 4H).



7-chloro-6-methyl-3-(pyridin-2-yl)pyrazolo[1,5-a]pyrimidine (3)



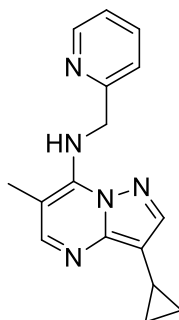
To a solution of 7-chloro-3-iodo-6-methyl-pyrazolo[1,5-a]pyrimidine (200 mg, 681 μmol , 1 *eq*) and tributyl(2-pyridyl)stannane (251 mg, 681 μmol , 1 *eq*) in toluene (8 mL) was added CATAIXIUM A-PD-G2 (45 mg, 68.2 μmol , 0.1 *eq*). The mixture was stirred at 80 °C for 12 hours under N_2 . TLC (Petroleum ether: EtOAc=2: 1) showed that about 70% of 7-chloro-3-iodo-6-methyl-pyrazolo[1,5-a]pyrimidine was consumed and a major new spot. LCMS showed that about half of 7-chloro-3-iodo-6-methyl-pyrazolo[1,5-a]pyrimidine was consumed and 20% desired product. To the mixture was added KF (30 mL, 10%) and extracted with EtOAc (30 mL*2). The organic layers were washed with brine (40 mL), dried over Na_2SO_4 and concentrated. The residue was purified by prep-TLC (Petroleum ether: EtOAc=2: 1) to obtain 7-chloro-6-methyl-3-(2-pyridyl)pyrazolo[1,5-a]pyrimidine (60 mg, 245.2 μmol , 36% yield) as a light yellow solid.

6-methyl-3-(pyridin-2-yl)-N-(pyridin-2-ylmethyl)pyrazolo[1,5-a]pyrimidin-7-amine (AWZ9058)

To a solution of 7-chloro-6-methyl-3-(2-pyridyl)pyrazolo[1,5-a]pyrimidine (60 mg, 245 μmol , 1 eq) and 2-pyridylmethanamine (32 mg, 294 μmol , 30 μL , 1.2 eq) in DMF (5 mL) was added Et_3N (74 mg, 736 μmol , 102 μL , 3 eq). The mixture was stirred at 60 $^\circ\text{C}$ for 4 hours. TLC (Petroleum ether: EtOAc=1: 1) showed that 7-chloro-6-methyl-3-(2-pyridyl)pyrazolo[1,5-a]pyrimidine was consumed completely and a new major spot. To the mixture was added water (10 mL) slowly, then a light yellow solid was forming. The solid was filtered and concentrated. The residue was purified by trituration from (Petroleum ether: EtOAc: MeOH=1: 1: 1, 6 mL) to obtain 6-methyl-3-(2-pyridyl)-N-(2-pyridylmethyl)pyrazolo[1,5-a]pyrimidin-7-amine (38 mg, 115.3 μmol , 47% yield, 96% purity) as a light yellow solid.

$^1\text{H NMR}$ (400MHz, DMSO- d_6) δ 8.69 (s, 1 H), 8.58 (d, $J=4.14$ Hz, 1 H), 8.54 (dt, $J=4.77$, 0.88 Hz, 1 H), 8.47 (d, $J=8.03$ Hz, 1 H), 8.37 (t, $J=6.15$ Hz, 1 H), 8.19 (s, 1 H), 7.81 (tdd, $J=7.69$, 7.69, 3.51, 1.82 Hz, 2 H), 7.40 (d, $J=7.78$ Hz, 1 H), 7.32 (dd, $J=6.96$, 5.33 Hz, 1 H), 7.15 (ddd, $J=7.40$, 4.83, 1.07 Hz, 1 H), 5.21 (d, $J=6.15$ Hz, 2 H), 2.41 (s, 3 H).

LCMS (Method 5-95AB, ESI): RT =0.545 min / 1.5 min, $\text{M}+\text{H}^+=317.1$.

3-cyclopropyl-6-methyl-N-(pyridin-2-ylmethyl)pyrazolo[1,5-a]pyrimidin-7-amine (AWZ9059)

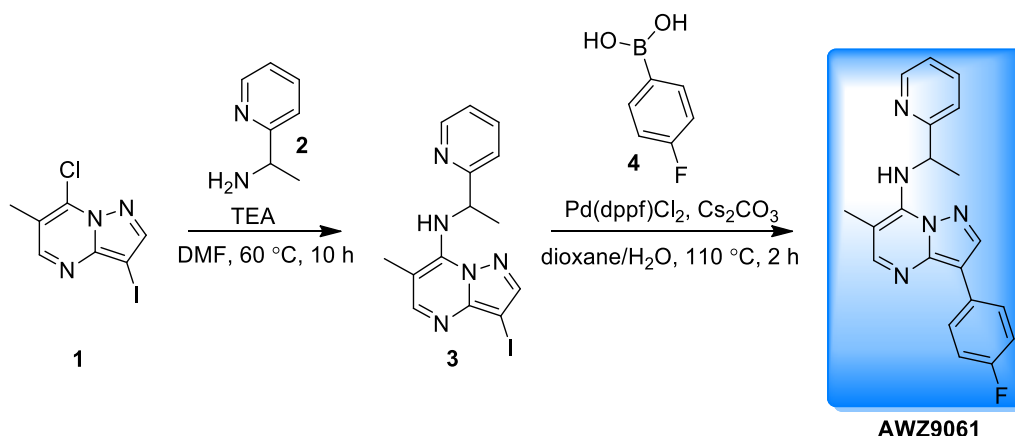
A mixture of tert-butyl N-(3-iodo-6-methyl-pyrazolo[1,5-a]pyrimidin-7-yl)-N-(2-pyridylmethyl)carbamate (250.00 mg, 537.30 μmol , 1.00 eq), cyclopropylboronic acid (923.08 mg, 10.75 mmol, 20.00 eq), $\text{Pd}(\text{dppf})\text{Cl}_2$ (58.97 mg, 80.60 μmol , 0.15 eq) and Cs_2CO_3 (350.13 mg, 1.07 mmol, 2.00 eq) in dioxane (3.00 mL) and H_2O

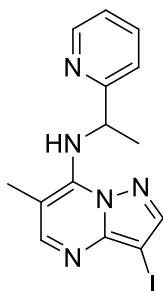
(500.00 μL) was stirred at 90 °C for 12 hours under N_2 protection. LCMS showed about all of tert-butyl N-(3-iodo-6-methyl-pyrazolo[1,5-a]pyrimidin-7-yl)-N-(2-pyridylmethyl)carbamate was consumed and a new peak with desired MS. TLC (Petroleum ether/EtOAc=1/1) showed the r_f value of tert-butyl N-(3-iodo-6-methyl-pyrazolo[1,5-a]pyrimidin-7-yl)-N-(2-pyridylmethyl)carbamate was similar with tert-butyl N-(3-cyclopropyl-6-methyl-pyrazolo[1,5-a]pyrimidin-7-yl)-N-(2-pyridylmethyl)carbamate. The mixture was diluted with EtOAc (20 mL) and washed with brine (10 mL*1). The organic layer was dried over Na_2SO_4 and concentrated to give a residue. The residue was purified by TLC (Petroleum ether/EtOAc=1/1) twice to give tert-butyl N-(3-cyclopropyl-6-methyl-pyrazolo[1,5-a]pyrimidin-7-yl)-N-(2-pyridylmethyl)carbamate (400.00 mg, 1.00 mmol, 93% yield, 95% purity) as a brown oil.

A mixture of tert-butyl N-(3-cyclopropyl-6-methyl-pyrazolo[1,5-a]pyrimidin-7-yl)-N-(2-pyridylmethyl)carbamate (100.00 mg, 263.54 μmol , 1.00 eq) in HCl/EtOAc (4 M, 2.00 mL, 30.36 eq) was stirred at 15-25 °C for 8 hours. LCMS showed all of tert-butyl N-(3-cyclopropyl-6-methyl-pyrazolo[1,5-a]pyrimidin-7-yl)-N-(2-pyridylmethyl)carbamate was consumed and desired MS. TLC (EtOAc) showed all of tert-butyl N-(3-cyclopropyl-6-methyl-pyrazolo[1,5-a]pyrimidin-7-yl)-N-(2-pyridylmethyl)carbamate and three new spot. The mixture was concentrated to give a residue. The residue was purified by prep-TLC (EtOAc/ $\text{NH}_3\cdot\text{H}_2\text{O}$ =100/1) to give 3-cyclopropyl-6-methyl-N-(2-pyridylmethyl)pyrazolo[1,5-a]pyrimidin-7-amine (10.50 mg, 35.97 μmol , 13% yield, 95.7% purity) as a light yellow solid.

LCMS (Method 5-95 AB): RT=0.608 min/1.5 min, $[\text{M}+\text{H}]^+=280.3$.

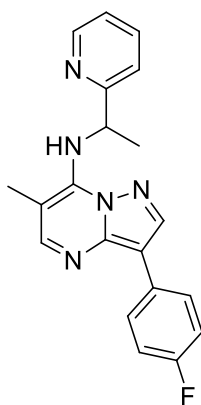
$^1\text{H NMR}$ (400MHz, DMSO-d_6) δ 8.56 (d, $J=4.4$ Hz, 1H), 8.02 (t, $J=6.2$ Hz, 1H), 7.94 (s, 1H), 7.74-7.85 (m, 2H), 7.26-7.39 (m, 2H), 5.12 (d, $J=6.3$ Hz, 2H), 2.33 (s, 3H), 1.88-1.98 (m, 1H), 0.76-0.90 (m, 4H).



3-iodo-6-methyl-N-(1-(pyridin-2-yl)ethyl)pyrazolo[1,5-a]pyrimidin-7-amine (3).

To a mixture of 7-chloro-3-iodo-6-methyl-pyrazolo[1,5-a]pyrimidine (500.00 mg, 1.70 mmol, 1.00 eq) in DMF (5.00 mL) was added 7-chloro-3-iodo-6-methyl-pyrazolo[1,5-a]pyrimidine (500.00 mg, 1.70 mmol, 1.00 eq), TEA (344.05 mg, 3.40 mmol, 2.00 eq). The mixture was stirred at 60 °C for 10 h. TLC (Petroleum ether/Ethyl acetate=2/1) showed 7-chloro-3-iodo-6-methyl-pyrazolo[1,5-a]pyrimidine was consumed completely and a new spot. The mixture was diluted with water (30 mL) and extracted with ethyl acetate (50 mL*2). The combined organic layers were washed with saturated brine (40 mL), dried with anhydrous Na₂SO₄, filtered and concentrated in vacuo. The residue was purified by chromatography (Petroleum ether/Ethyl acetate=10/1 ~1/1) to get 3-iodo-6-methyl-N-[1-(2-pyridyl)ethyl]pyrazolo[1,5-a]pyrimidin-7-amine (500.00 mg, 1.29 mmol, 76 % yield, 98% purity) as a yellow oil.

LCMS (Method 5-95AB, ESI): RT =0.594 min / 1.5 min, M⁺H⁺ =380.0.

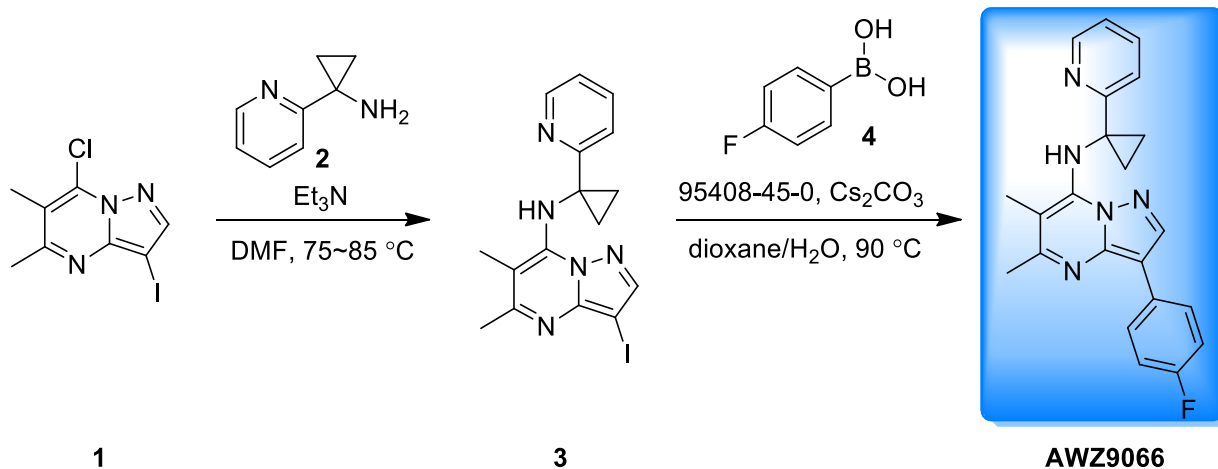
3-(4-fluorophenyl)-6-methyl-N-(1-(pyridin-2-yl)ethyl)pyrazolo[1,5-a]pyrimidin-7-amine (AWZ9061).

A mixture of 3-iodo-6-methyl-N-[1-(2-pyridyl)ethyl]pyrazolo[1,5-a]pyrimidin-7-amine (120.00 mg, 316.46 μmol, 1.00 eq), (4-fluorophenyl)boronic acid (57.56 mg, 411.39 μmol, 1.30 eq), Pd(dppf)Cl₂ (23.16 mg, 31.65 μmol, 0.10 eq), Cs₂CO₃ (206.22 mg, 632.91 μmol, 2.00 eq) in dioxane (2.00 mL) and H₂O (400.00 μL) was degassed and refilled with N₂. Then stirred at 110 °C for 2 hrs. TLC (Ethyl acetate/Petroleum ether=1/1) showed

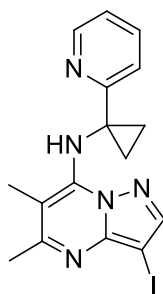
3-iodo-6-methyl-N-[1-(2-pyridyl)ethyl]pyrazolo[1,5-a]pyrimidin-7-amine was consumed completely and a new spot. LCMS showed a major peak with desired product mass. The mixture was diluted with water (50 mL) and extracted with ethyl acetate (50 mL*2). The combined organic layers were washed with saturated brine (40 mL), dried with anhydrous Na₂SO₄, filtered and concentrated in vacuo. The residue was purified by chromatography (Petroleum ether/Ethyl acetate=10/1~ 1/1) followed by prep-HPLC to get 3-(4-fluorophenyl)-6-methyl-N-[1-(2-pyridyl)ethyl]pyrazolo[1,5-a]pyrimidin-7-amine (11.40 mg, 31.77 μmol, 10% yield, 96.8% purity) as a white solid.

LCMS (Method 5-95AB, ESI): RT =0.772 min / 2 min, M⁺H⁺ =348.3.

¹H NMR (400MHz, DMSO-d₆) δ 8.62 (s, 2H), 8.15-8.18 (m, 3H), 7.80-7.86 (m, 2H), 7.51-7.53 (d, J=8.0 Hz, 1H), 7.32-7.35 (m, 1H), 7.21-7.25 (m, 2H), 5.68-5.73 (m, 2H), 2.42 (s, 3H), 1.58-1.60 (d, J=8.0 Hz, 3H).



tert-butyl 4-((methylsulfonyl)oxy)piperidine-1-carboxylate (3)

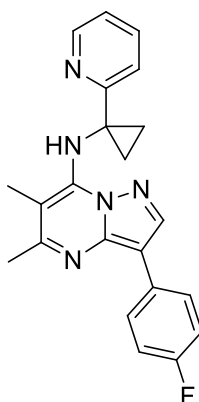


To a solution of 7-chloro-3-iodo-5,6-dimethyl-pyrazolo[1,5-a]pyrimidine (200 mg, 650 μmol, 1 eq) in DMF (5 mL) was added Et₃N (197 mg, 2 mmol, 3 eq) and 1-(2-pyridyl)cyclopropanamine (131 mg, 975 μmol, 1.5 eq). The mixture was stirred at 75 °C for 12 h. TLC (Petroleum ether/EtOAc=5/1) showed that about 30% of 6,7-

dichloro-3-iodo-5-methyl-pyrazolo[1,5-a]pyrimidine was consumed and two major new spots. LCMS showed that 34% of 6,7-dichloro-3-iodo-5-methyl-pyrazolo[1,5-a]pyrimidine was not consumed, desired mass and by-product's mass was detected. The mixture was stirred at 85 °C for another 12 h. LCMS showed that 6,7-dichloro-3-iodo-5-methyl-pyrazolo[1,5-a]pyrimidine was still remained and about 50% of desired product. To the mixture was added water (50 mL) and extracted with EtOAc (40 mL*2). The organic layers were washed with brine (60 mL), dried over Na₂SO₄ and concentrated. The residue was purified by prep-TLC (Petroleum ether/EtOAc=3/1) to give 3-iodo-5,6-dimethyl-N-[1-(2-pyridyl)cyclopropyl]pyrazolo[1,5-a]pyrimidin-7-amine (60 mg, 148 μmol, 23% yield) as a yellow solid.

¹H NMR (400MHz, CDCl₃-d) δ 8.51-8.58 (m, 1H), 7.96 (s, 1H), 7.60-7.67 (m, 1H), 7.52 (d, *J*=7.91 Hz, 1H), 7.24 (s, 1H), 7.10-7.17 (m, 1H), 2.53 (s, 3H), 2.13 (s, 3H), 1.93 (d, *J*=3.01 Hz, 2H), 1.54 (d, *J*=3.14 Hz, 2H).

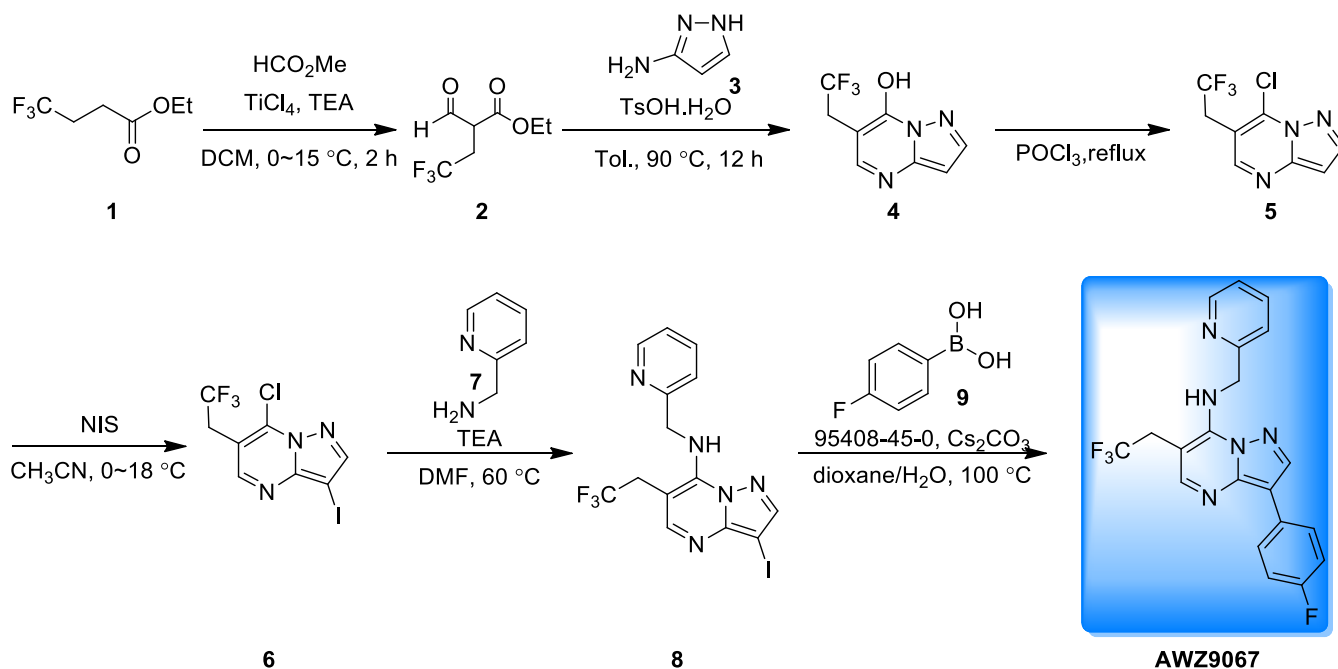
3-(4-fluorophenyl)-5,6-dimethyl-N-(1-(pyridin-2-yl)cyclopropyl)pyrazolo[1,5-a]pyrimidin-7-amine (AWZ9066)



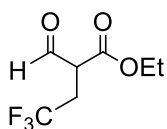
To a solution of 3-iodo-5,6-dimethyl-N-[1-(2-pyridyl)cyclopropyl]pyrazolo[1,5-a]pyrimidin-7-amine (80 mg, 197 μmol, 1 eq) and (4-fluorophenyl)boronic acid (41 mg, 296 μmol, 1.5 eq) in dioxane (4 mL) and H₂O (400 μL) was added Cs₂CO₃ (128 mg, 394 μmol, 2 eq), ditert-butyl(cyclopentyl)phosphane;dichloropalladium;iron (13 mg, 19.7 μmol, 0.1 eq). The mixture was stirred at 90 °C for 1 hour under N₂. TLC (Petroleum ether/EtOAc=5/1) showed that 3-iodo-5,6-dimethyl-N-[1-(2-pyridyl)cyclopropyl]pyrazolo[1,5-a]pyrimidin-7-amine was consumed completely and a major new spot. The mixture was concentrated directly. The residue was purified by chromatography on silica gel (Petroleum ether/EtOAc=5/1, 2/1) to give the crude product (purity: 90%), which was purified by prep-HPLC (Column: Phenomenex Gemini 150*25mm*10um; Condition: water (0.05% ammonia hydroxide v/v)-ACN; Gradient Time(min): 11; FlowRate(ml/min): 25; Injections: 5) to give 3-(4-fluorophenyl)-5,6-dimethyl-N-[1-(2-pyridyl)cyclopropyl]pyrazolo[1,5-a]pyrimidin-7-amine (10.5 mg, 26.8 μmol, 14% yield, 95.2% purity) as a white solid.

LCMS (Method 5-95AB, ESI): RT =0.666 min / 1.5 min, M+H⁺ =374.5.

$^1\text{H NMR}$ (400MHz, DMSO- d_6) δ 8.47-8.53 (m, 1H), 8.32 (s, 1H), 8.03-8.10 (m, 2H), 7.73-7.79 (m, 1H), 7.66 (s, 1H), 7.20-7.26 (m, 1H), 7.13 (t, $J=8.91$ Hz, 2H), 2.51 (s, 3H), 2.17 (s, 3H), 1.84-1.90 (m, 2H), 1.58-1.64 (m, 2H).



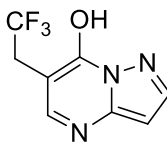
Ethyl 4,4,4-trifluoro-2-formylbutanoate (2)



To a solution of ethyl 4,4,4-trifluorobutanoate (1 g, 5.9 mmol, 1 eq) and methyl formate (530 mg, 8.8 mmol, 1.5 eq) in DCM (15 mL) was added TiCl_4 (2.2 g, 11.8 mmol, 2 eq) dropwise at 0 °C, then TEA (1.5 g, 14.7 mmol, 2.5 eq) was added to the mixture dropwise at 0 °C. The mixture was stirred at 0 °C for 1 hr under N_2 . Then the temperature was warmed to 15 °C and the mixture was stirred at 15 °C for another 1 hr. TLC (Petroleum ether/EtOAc=5/1) showed that a major spot (254 nm), and the spot of ethyl 4,4,4-trifluorobutanoate couldn't be found at 254 nm. The mixture was added into water (40 mL) and extracted with EtOAc (40 mL*2). The organic layers were washed with brine (50 mL), dried over Na_2SO_4 and concentrated to give ethyl 4,4,4-trifluoro-2-formylbutanoate (1.4 g, crude) as a light brown oil.

$^1\text{H NMR}$ (400MHz, $\text{CDCl}_3\text{-d}$) δ 11.61-11.77 (m, 1H), 3.99-4.07 (m, 2H), 3.87 (d, $J=7.16$ Hz, 1H), 2.66 (d, $J=10.36$ Hz, 2H), 1.01 (s, 3H).

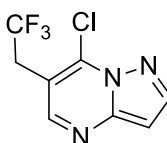
6-(2,2,2-trifluoroethyl)pyrazolo[1,5-a]pyrimidin-7-ol (4)



To a solution of 1H-pyrazol-5-amine (400 mg, 4.8 mmol, 1 *eq*) and ethyl 4,4,4-trifluoro-2-formyl-butanoate (953 mg, 4.8 mmol, 1 *eq*) in toluene (8 mL) was added $\text{TsOH}\cdot\text{H}_2\text{O}$ (91.5 mg, 481 μmol , 0.1 *eq*). The mixture was stirred at 90 °C for 12 hours. TLC (EtOAc) showed that 1H-pyrazol-5-amine was consumed completely and a new major spot (blue colour at 254 nm). The mixture was cooled to room temperature. The mixture was filtered and washed with EtOAc (3 mL) to give 6-(2,2,2-trifluoroethyl)pyrazolo[1,5-a]pyrimidin-7-ol (449.5 mg, 2.1 mmol, 43% yield) as a grey solid.

$^1\text{H NMR}$ (400MHz, DMSO-d_6) δ 8.06 (s, 1H), 7.92 (d, $J=1.88$ Hz, 1H), 6.22 (d, $J=2.01$ Hz, 1H), 3.47 (m, 2H).

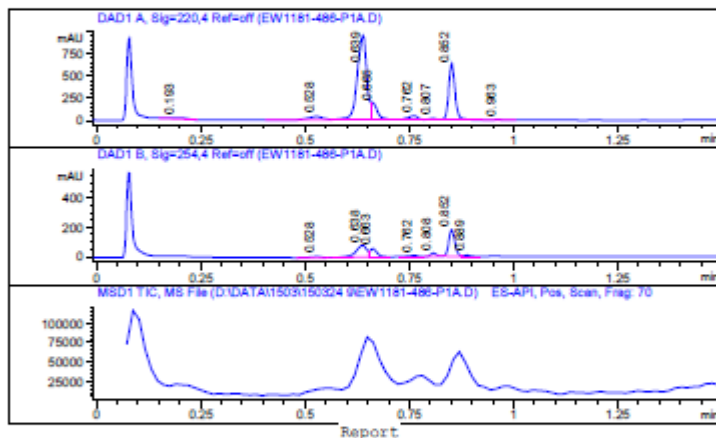
7-chloro-6-(2,2,2-trifluoroethyl)pyrazolo[1,5-a]pyrimidine (5)



A solution of 6-(2,2,2-trifluoroethyl)pyrazolo[1,5-a]pyrimidin-7-ol (450 mg, 2.1 mmol, 1 *eq*) in POCl_3 (12.7 g, 82.8 mmol, 40 *eq*) was stirred at 120 °C for 16 hours under N_2 . TLC (EtOAc) showed that more than 50% of 6-(2,2,2-trifluoroethyl)pyrazolo[1,5-a]pyrimidin-7-ol was consumed. TLC (Petroleum ether/EtOAc=1/1) showed that two new major spots. The mixture was concentrated to give 7-chloro-6-(2,2,2-trifluoroethyl)pyrazolo[1,5-a]pyrimidine (500 mg, crude) as a yellow solid.

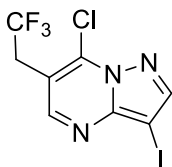
LCMS REPORT

Compound ID : 1
 Sample ID : EW1181-486-P1A
 Injection Date : 24-Mar-2015 10:28:58 AM
 Location : P2-E-04
 Injection volume : 6.000
 Acq Method : D:\DATA\1503\150324 9\5-95AB_R_220&254.M
 Data Filename : D:\DATA\1503\150324 9\EW1181-486-P1A.D
 Instrument : LCMS-G
 Column A : Chromolith Flash RP-18e 25*2mm
 Column B : XBridge C18 2.1*50mm, 5um



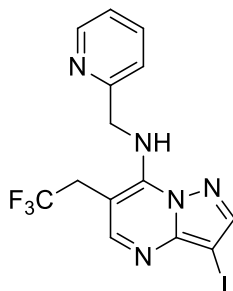
Signal 1 : DAD1 A, Sig=220,4 Ref=off					
#	Meas. Ret.	Height	Width	Area	Area %
1	0.193	11.366	0.045	32.466	1.261
2	0.528	35.743	0.040	95.023	3.690
3	0.639	950.539	0.025	1521.740	59.101
4	0.665	180.844	0.014	178.067	6.916
5	0.762	44.066	0.022	66.453	2.581
6	0.807	11.668	0.017	12.535	0.487
7	0.852	631.639	0.016	657.008	25.517
8	0.963	6.587	0.024	11.532	0.448

7-chloro-3-iodo-6-(2,2,2-trifluoroethyl)pyrazolo[1,5-a]pyrimidine (6)



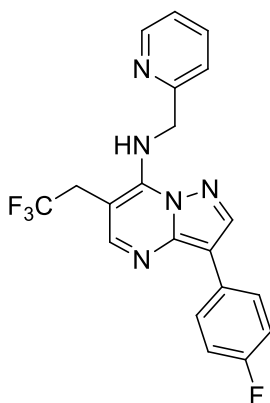
To a solution of 7-chloro-6-(2,2,2-trifluoroethyl)pyrazolo[1,5-a]pyrimidine (400 mg, 848.9 μmol , purity: 50%, 1 eq) in CH_3CN (10 mL) was added NIS (286 mg, 1.3 mmol, 1.5 eq) at 0 °C. The mixture was stirred at 18 °C for 1 hour. TLC (Petroleum ether/EtOAc=5/1) showed that 7-chloro-6-(2,2,2-trifluoroethyl)pyrazolo[1,5-a]pyrimidine was consumed completely and two major spots. The mixture was concentrated. The residue was purified by chromatography on silica gel (Petroleum ether/EtOAc=10/1, 5/1) to give 7-chloro-3-iodo-6-(2,2,2-trifluoroethyl)pyrazolo[1,5-a]pyrimidine (300 mg, 746.91 μmol , 88% yield, 90% purity) as a black brown solid.

LCMS (Method 5-95AB, ESI): RT =0.828 min / 1.5 min, M+H⁺ =362.

3-iodo-N-(pyridin-2-ylmethyl)-6-(2,2,2-trifluoroethyl)pyrazolo[1,5-a]pyrimidin-7-amine (8)

To a solution of 7-chloro-3-iodo-6-(2,2,2-trifluoroethyl)pyrazolo[1,5-a]pyrimidine (300 mg, 746.9 μmol , 1 *eq*) and 2-pyridylmethanamine (121 mg, 1.1 mmol, 1.5 *eq*) in DMF (5 mL) was added TEA (226.7 mg, 2.2 mmol, 3 *eq*). The mixture was stirred at 60 °C for 1 hour. TLC (Petroleum ether/EtOAc=5/1) showed that 7-chloro-3-iodo-6-(2,2,2-trifluoroethyl)pyrazolo[1,5-a]pyrimidine was consumed completely and a major new spot. To the mixture was added water (5 mL) and then a grey solid was forming. It was filtered and washed with water (2 mL) and concentrated to give 3-iodo-N-(2-pyridylmethyl)-6-(2,2,2-trifluoroethyl)pyrazolo[1,5-a]pyrimidin-7-amine (200 mg, 462 μmol , 62% yield) as a grey solid.

$^1\text{H NMR}$ (400MHz, $\text{CDCl}_3\text{-d}$) δ 8.70 (d, $J=4.77$ Hz, 1H), 8.26-8.34 (m, 1H), 8.20 (s, 1H), 8.08 (s, 1H), 7.75 (td, $J=7.65, 1.63$ Hz, 1H), 7.29-7.36 (m, 2H), 5.09 (d, $J=4.89$ Hz, 2H), 3.66 (q, $J=9.91$ Hz, 2H)

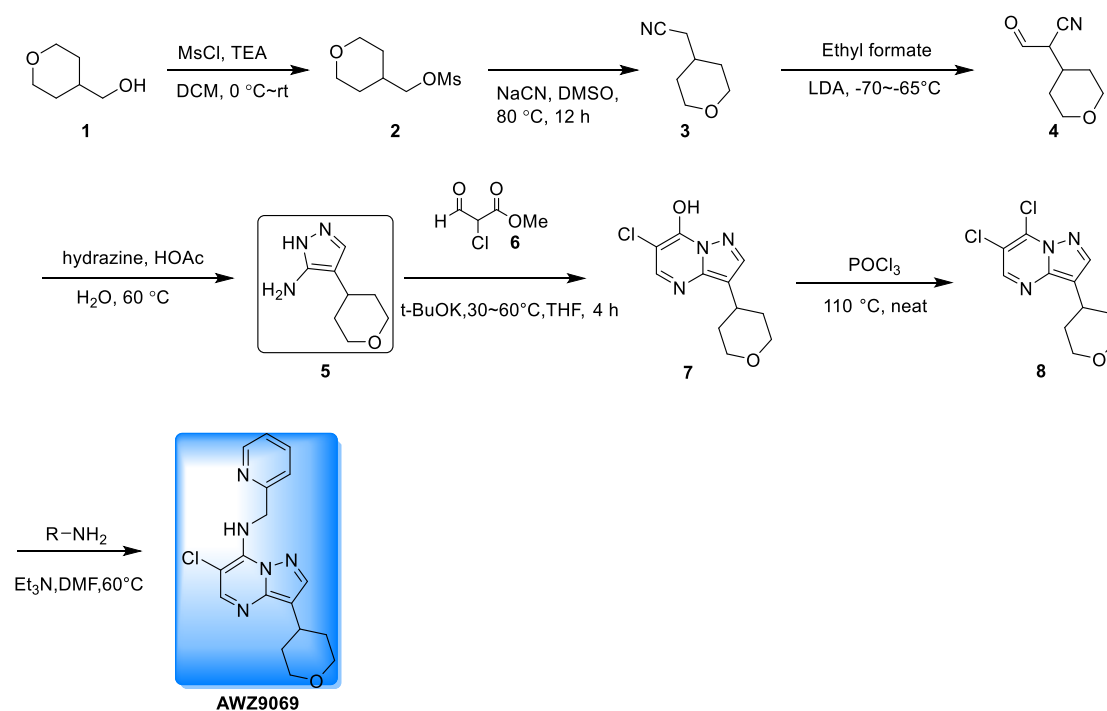
3-(4-fluorophenyl)-N-(pyridin-2-ylmethyl)-6-(2,2,2-trifluoroethyl)pyrazolo[1,5-a]pyrimidin-7-amine (AWZ9067)

To a solution of 3-iodo-N-(2-pyridylmethyl)-6-(2,2,2-trifluoroethyl)pyrazolo [1,5-a]pyrimidin-7-amine (100 mg, 231 μmol , 1 *eq*) and (4-fluorophenyl)boronic acid (64.6 mg, 461.7 μmol , 2 *eq*) in dioxane (10 mL) and H_2O (1 mL) was added ditert-butyl(cyclopentyl)phosphane;dichloropalladium;iron (15 mg, 23.1 μmol , 0.1 *eq*), Cs_2CO_3 (150 mg, 461.7 μmol , 2 *eq*). The mixture was stirred at 100 °C for 5 hours under N_2 . TLC (Petroleum ether/EtOAc=1/1) showed that about 80% of 3-iodo-N-(2-pyridylmethyl)-6-(2,2,2-trifluoroethyl)pyrazolo[1,5-a]pyri- midin-7-amine was consumed and a major new spot. Desired product's mass was detected by LCMS. The mixture was concentrated. The residue was purified by chromatography on silica gel (Petroleum

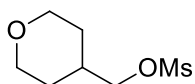
ether/EtOAc=2/1, 1/1) to give a crude product, which was purified by prep-HPLC (Column: Boston Green ODS 150*30 5u; Condition: 0.225%FA-ACN). The product was basified by strongly basic anion exchange resin to give 3-(4-fluorophenyl)-N-(2-pyridylmethyl)-6-(2,2,2-trifluoroethyl)pyrazolo[1,5-a]pyrimidin-7-amine (19 mg, 45 μ mol, 19% yield, 94.5% purity) as a white solid.

LCMS (Method 5-95AB, ESI): RT =0.794 min / 1.5 min, M+H+ =402.5.

$^1\text{H NMR}$ (400MHz, MeOD-d₄) δ 8.56-8.61 (m, 1H), 8.38 (s, 1H), 8.14-8.20 (m, 1H), 7.96-8.04 (m, 2H), 7.79-7.85 (m, 1H), 7.42-7.48 (m, 1H), 7.32-7.37 (m, 1H), 7.15 (s, 2H), 5.24 (s, 2H), 3.78 (d, J =10.42 Hz, 2H).



(tetrahydro-2H-pyran-4-yl)methyl methanesulfonate (2)

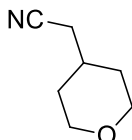


To a solution of tetrahydropyran-4-ylmethanol (5.00 g, 43.04 mmol, 1.00 eq) in DCM (30.00 mL) was added Et₃N (5.66 g, 55.95 mmol, 7.75 mL, 1.30 eq). The mixture was cooled to 0 °C and MsCl (5.92 g, 51.65 mmol, 4.00 mL, 1.20 eq) was added slowly by dropwise over 15 mins. After 15 mins, the mixture was stirred at 25 °C for 12 hrs. TLC (Petroleum ether: Ethyl acetate= 1: 1) showed tetrahydropyran-4-ylmethanol was consumed completely and a new spot with similar polarity as tetrahydropyran-4-ylmethanol. The mixture was diluted with saturated Na₂CO₃ (100 mL) and extracted with EtOAc (150 mL *3). Then the combined layers were washed

with saturated NH_4Cl (200 mL), dried with anhydrous Na_2SO_4 , filtered and concentrated in vacuo to give tetrahydropyran-4-ylmethyl methanesulfonate (7.50 g, crude) as a yellow solid.

$^1\text{H NMR}$ (400MHz, CDCl_3) δ 4.04-4.06 (d, $J=8.0$ Hz, 2H), 3.96-4.00 (dd, $J=8.0$ Hz, $J=4.0$ Hz, 2H), 3.35-3.42 (td, $J=12.0$ Hz, $J=4.0$ Hz, 2H), 3.00 (s, 3H), 1.95-2.05 (m, 2H), 1.65-1.68 (m, 2H), 1.32-1.48 (m, 2H).

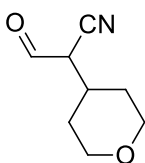
2-(tetrahydro-2H-pyran-4-yl)acetonitrile (3).



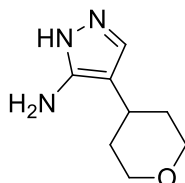
To a mixture of tetrahydropyran-4-ylmethyl methanesulfonate (6.50 g, 33.46 mmol, 1.00 *eq*) in DMSO (50.00 mL) was added NaCN (2.84 g, 57.95 mmol, 1.73 *eq*). The mixture was stirred at 80 °C for 14 h. TLC (Petroleum ether: Ethyl acetate= 3: 1) showed tetrahydropyran-4-ylmethyl methanesulfonate was consumed completely and a major new spot. The mixture was diluted with water (100 mL) and extracted with EtOAc (150 mL*5). The combined organic layers were dried with anhydrous Na_2SO_4 , filtered and concentrated in vacuo. The residue was purified by chromatography (Petroleum ether: Ethyl acetate= 10: 1~ 3: 1) to give 2-tetrahydropyran-4-ylacetonitrile (3.40 g, 27.16 mmol, 81% yield) as a yellow liquid.

$^1\text{H NMR}$ (400 MHz, CDCl_3) δ 3.98-4.02 (dd, $J=12.0$ Hz, $J=4.0$ Hz, 2H), 3.36-3.42 (td, $J=12.0$ Hz, 2H), 3.30-3.32 (d, $J=8.0$ Hz, 2H), 1.89-1.95 (m, 1H), 1.72-1.76 (dd, $J=12.0$ Hz, $J=4.0$ Hz, 2H), 1.41-1.45 (m, 2H).

3-oxo-2-(tetrahydro-2H-pyran-4-yl)propanenitrile (4).

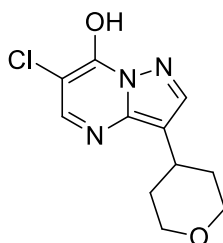


To a mixture of 2-tetrahydropyran-4-ylacetonitrile (2.40 g, 19.17 mmol, 1.00 *eq*) in THF (20.00 mL) was added LDA (2 M, 14.38 mL, 1.50 *eq*) at -70 °C~ -65 °C. After 20 mins, HCO_2Et (3.38 g, 38.35 mmol, 3.75 mL, 2.00 *eq*) was added into the mixture, then stirred at -70 °C~ -65 °C for 40 mins. TLC (Petroleum ether: Ethyl acetate= 1: 1) showed 2-tetrahydropyran-4-ylacetonitrile was consumed completely and several new spots. The mixture was diluted with saturated NH_4Cl (30 mL) and adjust pH to 3~4 with HCl (1 N), extracted with EtOAc (100 mL*5). The combined organic layers were concentrated to remove the solvents and afford give 3-oxo-2-tetrahydropyran-4-yl-propanenitrile (3.70 g, crude) as a yellow solid which was used in the next step without purification.

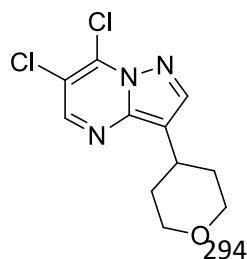
4-(tetrahydro-2H-pyran-4-yl)-1H-pyrazol-5-amine (5)

To a mixture of 3-oxo-2-tetrahydropyran-4-yl-propanenitrile (3.70 g, 24.15 mmol, 1.00 eq) in EtOH (3.00 mL) was added $\text{N}_2\text{H}_4\cdot\text{H}_2\text{O}$ (3.81 g, 76.09 mmol, 3.70 mL, 3.15 eq) and AcOH (3.89 g, 64.73 mmol, 3.70 mL, 2.68 eq). The mixture was stirred at 60 °C for 2 h. TLC (Ethyl acetate: Petroleum ether= 2: 1) showed 3-oxo-2-tetrahydropyran-4-yl-propanenitrile was consumed completely. The mixture was concentrated directly to remove the solvent. The residue was purified by chromatography (Ethyl acetate: Petroleum ether= 1: 1 to EtOAc) to give 4-tetrahydropyran-4-yl-1H-pyrazol-3-amine (3.40 g, 20.33 mmol, 84% yield) as a yellow oil.

$^1\text{H NMR}$ (400 MHz, DMSO- d_6) δ 7.11 (s, 1H), 3.85-3.88 (dd, $J=12.0$ Hz, $J=4.0$ Hz 2H), 3.39 (s, 2H), 2.53-2.57 (m, 1H), 1.68-1.71 (dd, $J=12.0$ Hz, 2H), 1.38-1.49 (m, 2H)

6-chloro-3-(tetrahydro-2H-pyran-4-yl)pyrazolo[1,5-a]pyrimidin-7-ol (7)

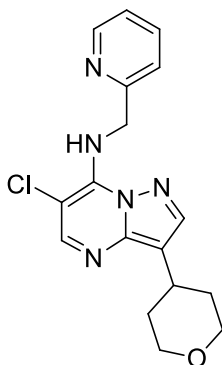
The mixture of 4-tetrahydropyran-4-yl-1H-pyrazol-3-amine (1.50 g, 8.97 mmol, 1.00 eq) and methyl 2-chloro-3-oxo-propanoate (1.35 g, 9.87 mmol, 1.10 eq) in THF (20.00 mL) was stirred at 60 °C for 2 h. Then tBuOK (1.51 g, 13.46 mmol, 1.50 eq) was added into and stirred at 30 °C for 2 h. TLC (Dichloromethane: Methanol= 10: 1) showed 4-tetrahydropyran-4-yl-1H-pyrazol-3-amine was consumed completely and a new spot. The mixture was adjust to pH=3~4 with HCl/MeOH (4 M), then was concentrated to remove the solvent to give 6-chloro-3-tetrahydropyran-4-yl-pyrazolo[1,5-a]pyrimidin-7-ol (3.00 g, crude) as a yellow solid which can used in the next step directly.

6,7-dichloro-3-(tetrahydro-2H-pyran-4-yl)pyrazolo[1,5-a]pyrimidine (8)

A mixture of 6-chloro-3-tetrahydropyran-4-yl-pyrazolo[1,5-a]pyrimidin-7-ol (3.00 g, 11.83 mmol, 1.00 eq), N,N-diethylaniline (1.77 g, 11.83 mmol, 1.90 mL, 1.00 eq) in POCl₃ (100.00 mL) was stirred at 100 °C for 16 h. TLC (Petroleum ether: Ethyl acetate= 5: 1) showed a major new spot. The mixture was concentrated to remove the POCl₃. The black residue was purified by chromatography (Petroleum ether: Ethyl acetate= 10: 1~3: 1) to give 6,7-dichloro-3-tetrahydropyran-4-yl-pyrazolo[1,5-a]pyrimidine (1.20 g, 4.23 mmol, 36% yield, 96% purity) as a yellow solid.

LCMS (Method 5-95AB, ESI): RT =0.745 min / 1.5 min, M+H⁺ =272.2

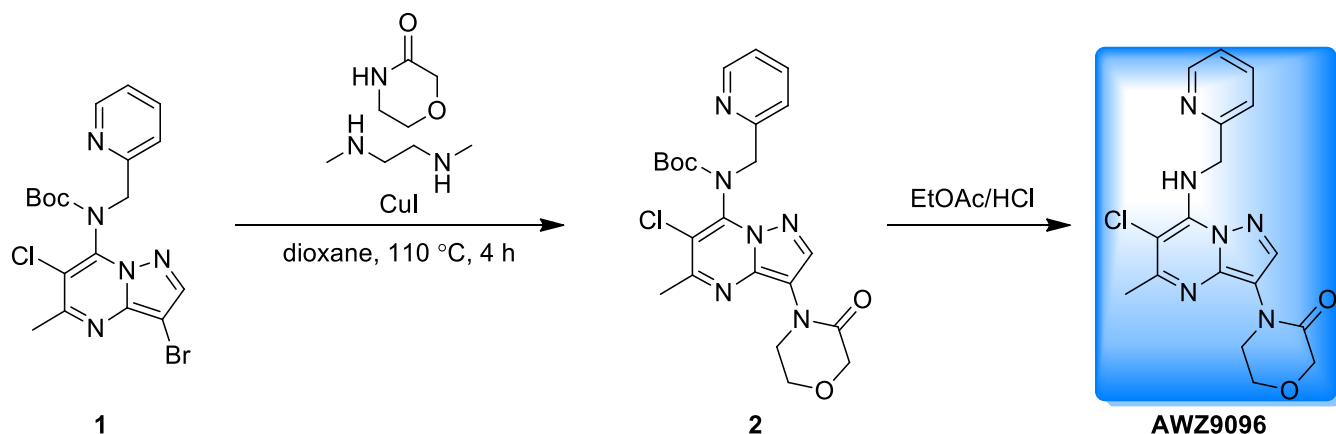
6-chloro-N-(pyridin-2-ylmethyl)-3-(tetrahydro-2H-pyran-4-yl)pyrazolo[1,5-a]pyrimidin-7-amine (AWZ9069)



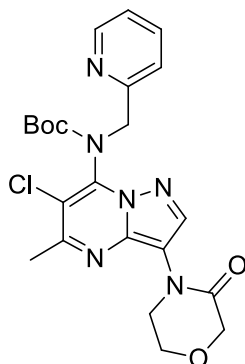
To a mixture of 6,7-dichloro-3-tetrahydropyran-4-yl-pyrazolo[1,5-a]pyrimidine (86.00 mg, 316.03 μmol, 1.00 eq) 2-pyridylmethanamine (41.01 mg, 379.24 μmol, 38.69 μL, 1.20 eq) in DMF (2.00 mL) was added Et₃N (63.96 mg, 632.06 μmol, 87.62 μL, 2.00 eq). The mixture was stirred at 60 °C for 16 h. TLC (Petroleum ether: Ethyl acetate= 2: 1) showed 6,7-dichloro-3-tetrahydropyran-4-yl-pyrazolo[1,5-a]pyrimidine was consumed completely and a new major spot. LCMS showed a major peak with desired mass. The mixture was diluted with water (15 mL), then filtered to get the filter cake which was washed with EtOAc (2 mL) and MeOH (1 mL) to afford 6-chloro-N-(2-pyridylmethyl)-3-tetrahydropyran-4-yl-pyrazolo[1,5-a]pyrimidin-7-amine (21.40 mg, 61.31 μmol, 19% yield, 98.5% purity) as a light yellow solid

LCMS (Method 5-95AB, ESI): RT =0586 min / 1.5 min, M+H⁺ =344.1.

¹H NMR (400 MHz, DMSO-d₆) δ 8.53-8.54 (d, J=4.0 Hz, 1H), 8.46-8.49 (t, J=8.0 Hz, 1H), 8.14 (s, 1H), 8.07 (s, 1H), 7.77-7.81 (td, J=8.0 Hz, 1H), 7.35-7.37 (d, J=8.0 Hz, 1H), 7.28-7.31 (m, 1H), 5.28-5.29 (d, J=4.0 Hz, 2H), 3.92-3.94 (d, J=8.0 Hz, 2H), 3.43-3.49 (m, 2H), 3.02-3.10 (m, 1H), 1.81-1.85 (m, 4H)



Tert-butyl (6-chloro-5-methyl-3-(3-oxomorpholino)pyrazolo[1,5-a]pyrimidin-7-yl)(pyridin-2-ylmethyl)carbamate (2)

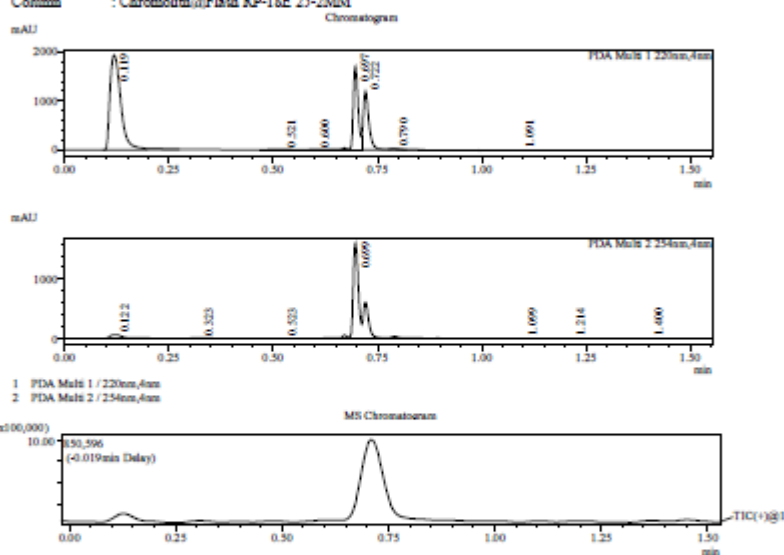


To a solution of tert-butyl N-(3-bromo-6-chloro-5-methyl-pyrazolo[1,5-a]pyrimidin-7-yl)-N-(2-pyridylmethyl)carbamate (1 g, 2.2 mmol, 1 eq) and morpholin-3-one (290 mg, 2.9 mmol, 1.3 eq) in dioxane (40 mL) was added CuI (1.7 g, 8.8 mmol, 4 eq), N,N'-dimethylethane-1,2-diamine (1.6 g, 17.7 mmol, 1.9 mL, 8 eq). The mixture was stirred at 110 °C for 4 hrs under N₂. TLC (Petroleum ether: EtOAc=2: 1) showed that about most of tert-butyl N-(3-bromo-6-chloro-5-methyl-pyrazolo[1,5-a]pyrimidin-7-yl)-N-(2-pyridylmethyl)carbamate was consumed and two new spots. The mixture was filtered and the filtrate was concentrated. The residue was purified by chromatography on silica gel (Petroleum ether: EtOAc=5: 1, 1: 1, 1: 2) to provide tert-butyl N-[6-chloro-5-methyl-3-(3-oxomorpholin-4-yl)pyrazolo[1,5-a]pyrimidin-7-yl]-N-(2-pyridylmethyl)carbamate (600 mg, crude) as a brown yellow oil.

Confidential, for research only not for regulatory filing

LCMS REPORT

Compound ID : 1
 Sample ID : EW1181-754-P1A
 Injection Vol : 5ul
 Location : vial81
 Acq Method : d:\method\5-95AB_R_220&2541cm
 Org DataFile : D:\data\1308130803\EW1181-754-P1A.lcd
 Injection Date : 8/3/2015 7:44:33 PM
 Instrument : LCMS-H 15-105
 Column : Chromolith@Flash RP-18E 25-2NDM

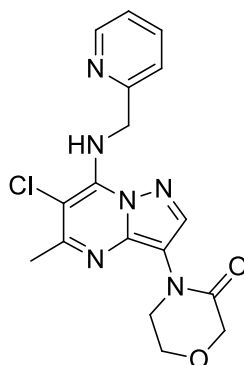


Integration Result

PDA Ch1 220nm						
Peak#	Ret. Time	Height	Height%	USP Width	Area	Area%
1	0.119	1930113	41.004	0.046	3514707	57.088
2	0.521	3881	0.125	0.074	16296	0.265
3	0.600	6013	0.128	0.079	19429	0.316
4	0.697	1603542	34.067	0.034	1413340	22.956
5	0.722	1140887	24.238	0.027	1170245	19.008
6	0.790	14751	0.313	0.030	16569	0.269
7	1.091	5903	0.125	0.028	6045	0.098

PDA Ch2 254nm						
Peak#	Ret. Time	Height	Height%	USP Width	Area	Area%
1	0.122	60357	4.333	0.050	142586	6.302
2	0.323	3170	0.228	0.220	25157	1.112
3	0.523	1707	0.123	0.088	5680	0.251

4-(6-chloro-5-methyl-7-((pyridin-2-ylmethyl)amino)pyrazolo[1,5-a]pyrimidin-3-yl)morpholin-3-one (AWZ9096)

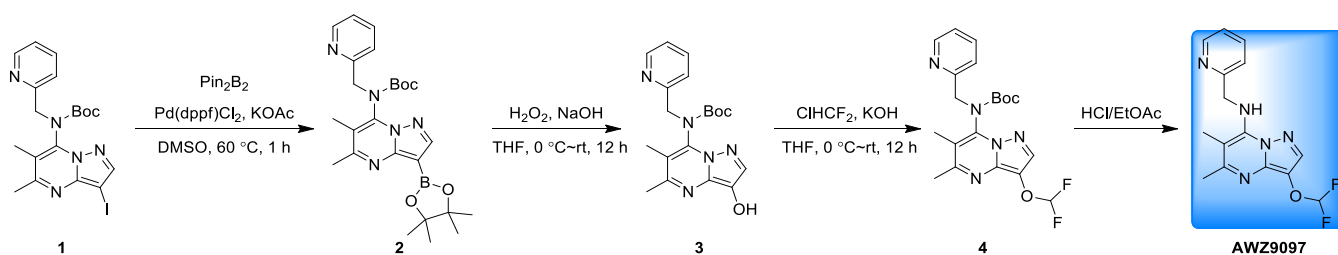


A solution of tert-butyl N-[6-chloro-5-methyl-3-(3-oxomorpholin-4-yl)pyrazolo[1,5-a]pyrimidin-7-yl]-N-(2-pyridylmethyl)carbamate (150 mg, 317 μ mol, 1 eq) in HCl/EtOAc (4 M, 10 mL, 126 eq) was stirred at 30 $^{\circ}$ C for 12 hours. LCMS showed tert-butyl N-[6-chloro-5-methyl-3-(3-oxomorpholin-4-yl)pyrazolo[1,5-a]pyrimidin-7-

yl]-N-(2-pyridylmethyl)carbamate was consumed completely and a major peak with desired mass. The mixture was concentrated. The residue was dissolved in DCM/MeOH (1: 1, 20 mL) and basified by strong basic anion exchange resin. The crude product was purified by trituration from (Petroleum ether: EtOAc: DCM=3: 3: 1, 7 mL) to provide 4-[6-chloro-5-methyl-7-(2-pyridylmethyl- amino)pyrazolo[1,5-a]pyrimidin-3-yl]morpholin-3-one (57 mg, 150 μ mol, 47% yield, 98% purity) as a light yellow solid.

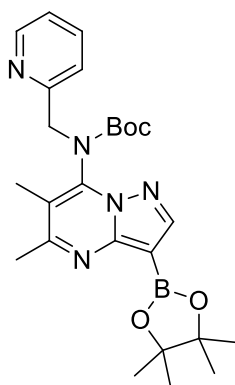
$^1\text{H NMR}$ (400MHz, DMSO- d_6) δ 8.69 (d, $J=4.5$ Hz, 1 H), 8.25 (s, 1 H), 8.01 (br. s., 1 H), 7.74 (t, $J=7.7$ Hz, 1 H), 7.34 (d, $J=7.8$ Hz, 1 H), 7.29-7.31 (m, 1 H), 5.44 (d, $J=4.9$ Hz, 2 H), 4.41 (s, 2 H), 4.07-4.13 (m, 4 H), 2.60 (s, 3 H).

LCMS (Method 5-95AB, ESI): RT =0.552 min / 1.5 min, M+H $^+$ =373.1.



Tert-butyl
ylmethyl)carbamate (2)

(6-chloro-5-methyl-3-(3-oxomorpholino)pyrazolo[1,5-a]pyrimidin-7-yl)(pyridin-2-

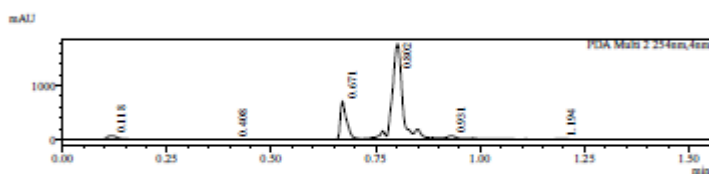
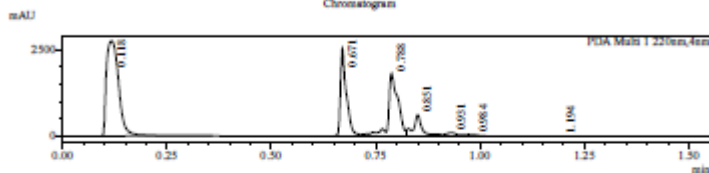


To a solution of tert-butyl N-(3-iodo-5,6-dimethyl-pyrazolo[1,5-a]pyrimidin-7-yl)-N-(2-pyridylmethyl)carbamate (2 g, 4.2 mmol, 1 *eq*) in dry DMSO (40 mL) was added KOAc (819 mg, 8.3 mmol, 2 *eq*), Pin₂B₂ (1.3 g, 5 mmol, 1.2 *eq*), Pd(dppf)Cl₂ (152 mg, 208.5 μmol, 0.05 *eq*). The mixture was stirred at 60 °C for 1 hour under N₂. TLC (Petroleum ether: EtOAc=1: 1) showed tert-butyl N-(3-iodo-5,6-dimethyl-pyrazolo[1,5-a]pyrimidin-7-yl)-N-(2-pyridylmethyl)carbamate was consumed completely and three major spots. Desired product and by-product [7-[tert-butoxycarbonyl(2-pyridylmethyl)amino]-5,6-dimethyl-pyrazolo[1,5-a]pyrimidin-3-yl]boronic acid and tert-butyl N-[2-[7-[tert-butoxycarbonyl(2-pyridylmethyl)amino]-5,6-dimethyl-pyrazolo[1,5-a]pyrimidin-3-yl]-5,6-dimethyl-pyrazolo[1,5-a]pyrimidin-7-yl]-N-(2-pyridylmethyl)carbamate was detected by LCMS. H₂O (40 mL) was added to the mixture. The aqueous layer was extracted with EtOAc (40 mL*2). The organic layer was washed brine (40 mL), dried over Na₂SO₄, concentrated. The residue was purified by chromatography on silica gel (Petroleum ether: EtOAc=5: 1, 1: 1, 1: 2) to give a mixture of tert-butyl N-[5,6-dimethyl-3-(4,4,5,5-tetramethyl-1,3,2-dioxaborolan-2-yl)pyrazolo[1,5-a]pyrimidin-7-yl]-N-(2-pyridylmethyl)carbamate and [7-[tert-butoxycarbonyl(2-pyridylmethyl)amino]-5,6-dimethyl-pyrazolo[1,5-a]pyrimidin-3-yl]boronic acid (1 g) as brown oil.

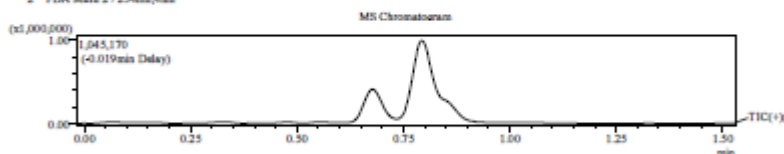
LCMS REPORT

Compound ID : 1
 Sample ID : EW1181-772-P1A
 Injection Vol : 4ul
 Location : vial78
 Acq Method : d:\method\5-95AB_R_220&2541cm
 Org DataFile : D:\data\1308150810\EW1181-772-P1A.lcd
 Injection Date : 8/10/2015 3:06:17 PM
 Instrument : LCMS-H 15-105
 Column : Chromolith@Flash RP-18E 25-2MM

Chromatogram



1 PDA Multi 1 / 220nm,4nm
 2 PDA Multi 2 / 254nm,4nm

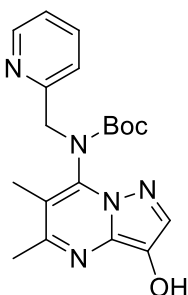


Integration Result

PDA Ch1 220nm						
Peak#	Ret. Time	Height	Height%	USP Width	Area	Area%
1	0.118	2783333	35.525	0.049	5651810	45.918
2	0.408	2455403	31.798	0.024	2489013	20.222
3	0.671	1764339	22.848	0.043	2960330	24.051
4	0.851	607451	7.867	0.029	833991	6.776
5	0.931	102821	1.332	0.052	283813	2.306
6	0.984	41247	0.534	0.065	79761	0.648
7	1.194	7420	0.096	0.035	9839	0.080

PDA Ch2 254nm						
Peak#	Ret. Time	Height	Height%	USP Width	Area	Area%
1	0.118	66370	2.746	0.043	123620	2.871
2	0.408	236	0.010	0.098	1107	0.026
3	0.671	613677	25.390	0.029	754124	17.516

Tert-butyl (3-hydroxy-5,6-dimethylpyrazolo[1,5-a]pyrimidin-7-yl)(pyridin-2-ylmethyl)carbamate (3)

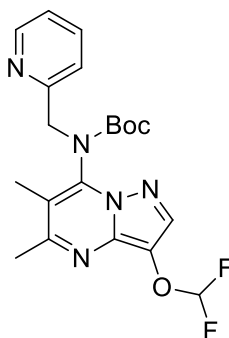


To a mixture of tert-butyl N-[5,6-dimethyl-3-(4,4,5,5-tetramethyl-1,3,2-dioxaborolan-2-yl)pyrazolo[1,5-a]pyrimidin-7-yl]-N-(2-pyridylmethyl)carbamate and [7-[tert-butoxycarbonyl(2-pyridylmethyl)amino]-5,6-dimethyl-pyrazolo[1,5-a]pyrimidin-3-yl]boronic acid (1 g) in THF (20 mL) was added NaOH (2 M, 6.3 mL, 6 eq)

and H₂O₂ (2.4 g, 21 mmol, 2 mL, 30% purity, 10 eq). The mixture was stirred at 25 °C for 12 hours. TLC (Petroleum ether: EtOAc= 1: 2) showed that two material were consumed completely and a new major spot. To the mixture was added water (50 mL) followed by HCl (1 N, 10 mL). The aqueous layer was extracted with EtOAc (50 mL*2). The organic layers were washed with brine (60 mL), dried over Na₂SO₄ and concentrated. The residue was purified by chromatography on silica gel (Petroleum ether: EtOAc=1: 1, 1: 2) to provide tert-butyl N-(3-hydroxy-5,6-dimethyl-pyrazolo[1,5-a]pyrimidin-7-yl)-N-(2-pyridylmethyl)carbamate (700 mg, 1.7 mmol, 82% yield, 90% purity) as a yellow solid.

¹H NMR (400MHz, DMSO-d₆) δ 8.9-8.93 (m, 1H), 8.40-8.47 (m, 1H), 7.70-7.94 (m, 2H), 7.40-7.49 (m, 1H), 7.24-7.27 (m, 1H), 5.03-5.18 (m, 1H), 4.56-4.62 (m, 1H), 2.43 (s, 3H), 1.91-1.99 (m, 3H), 1.24-1.16 (m, 9 H).

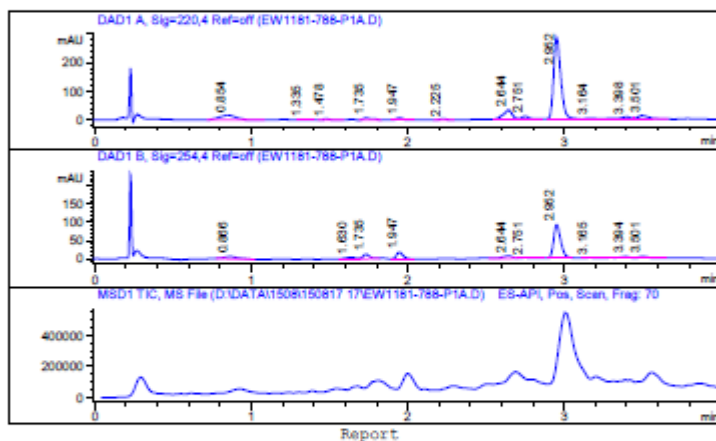
tert-butyl (3-(difluoromethoxy)-5,6-dimethylpyrazolo[1,5-a]pyrimidin-7-yl)(pyridin-2-ylmethyl)carbamate (4)



To a solution of tert-butyl N-(3-hydroxy-5,6-dimethyl-pyrazolo[1,5-a]pyrimidin-7-yl)-N-(2-pyridylmethyl)carbamate (300 mg, 812 μmol, 1 eq) in THF (10 mL) was added KOH (3.5 M, 2.3 mL, 10 eq). The mixture was stirred at 25 °C for 12 hours under chloro(difluoro)methane (15 psi). TLC (Petroleum ether: EtOAc=1: 1) showed that around half of tert-butyl N-(3-hydroxy-5,6-dimethyl-pyrazolo[1,5-a]pyrimidin-7-yl)-N-(2-pyridylmethyl)carbamate was consumed and a new major spot. To the mixture was added water (30 mL) and the resultant mixture was extracted with EtOAc (40 mL*2). The organic layers were washed with brine (40 mL), dried over Na₂SO₄ and concentrated. The residue was purified by chromatography on silica gel (Petroleum ether: EtOAc=1: 1) to give tert-butyl N-[3-(difluoromethoxy)-5,6-dimethyl-pyrazolo[1,5-a]pyrimidin-7-yl]-N-(2-pyridylmethyl)carbamate (80 mg, 191 μmol, 23% yield) as light yellow oil.

LCMS REPORT

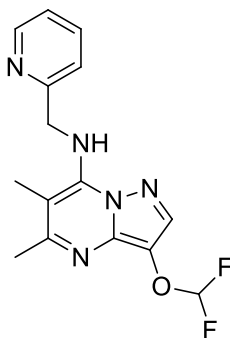
Compound ID : 1
 Sample ID : EW1181-788-P1A
 Injection Date : 17-Aug-2015 19:06:43
 Location : P1-D-06
 Injection volume : 5.000
 Acq Method : D:\DATA\1508\150817 17\10-80CD_4MIN_220&25
 Data Filename : D:\DATA\1508\150817 17\EW1181-788-P1A.D
 Instrument : LCMS-G
 Column A : Chromolith Flash RP-18e 25*2mm
 Column B : XBridge C18 2.1*50mm, 5um



Signal 1 : DAD1 A, Sig=220,4 Ref-off

#	Meas.	Ret.	Height	Width	Area	Area %
1	0.854	15.221	0.120		111.128	7.814
2	1.335	1.986	0.032		4.182	0.294
3	1.478	4.118	0.044		12.759	0.897
4	1.735	7.373	0.053		27.347	1.923
5	1.947	8.365	0.042		22.729	1.598
6	2.225	3.740	0.048		11.899	0.837
7	2.644	33.235	0.059		138.165	9.715
8	2.751	11.527	0.053		41.918	2.948
9	2.952	285.603	0.049		925.056	65.046
10	3.164	4.862	0.072		24.908	1.751
11	3.398	8.162	0.069		39.973	2.811
12	3.501	12.455	0.075		62.083	4.365

3-(difluoromethoxy)-5,6-dimethyl-N-(pyridin-2-ylmethyl)pyrazolo[1,5-a]pyrimidin-7-amine (AWZ9097)

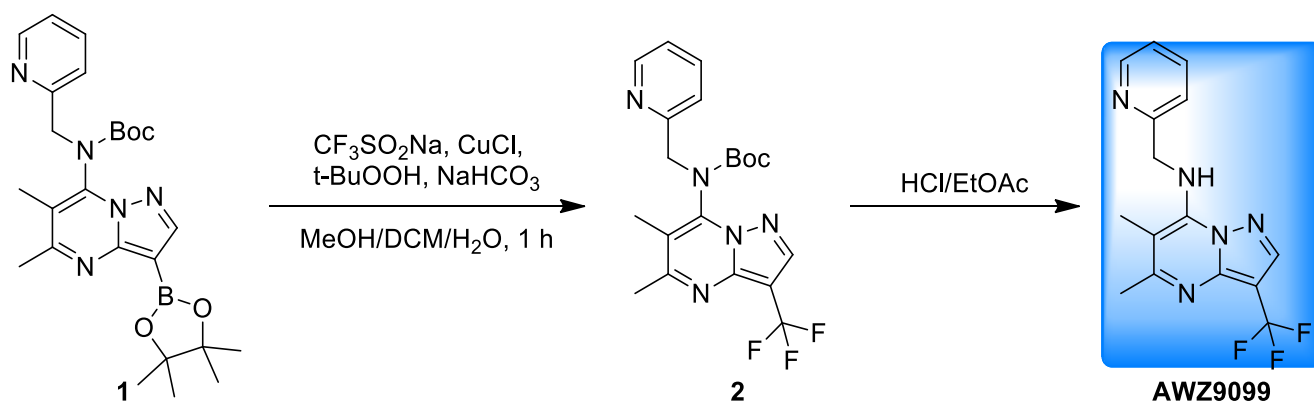


A solution of tert-butyl N-[3-(difluoromethoxy)-5,6-dimethyl-pyrazolo[1,5-a]pyrimidin-7-yl]-N-(2-pyridylmethyl)carbamate (80 mg, 191 μ mol, 1 eq) in HCl/EtOAc (4 M, 5 mL, 105 eq) was stirred at 30 $^{\circ}$ C for 2

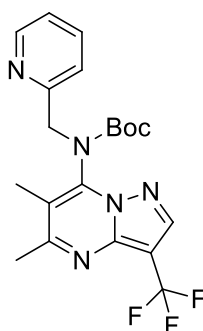
hours. LCMS showed most of tert-butyl N-[3-(difluoromethoxy)-5,6-dimethyl-pyrazolo[1,5-a]pyrimidin-7-yl]-N-(2-pyridylmethyl)carbamate was consumed and a major peak with desired mass. The mixture was concentrated. The residue was basified with two drops of TEA and then purified by prep-HPLC (FA, Column: Phenomenex Synergi C18 150*30mm*4um; Condition: water(0.225%FA)-ACN) to give 3-(difluoromethoxy)-5,6-dimethyl-N-(2-pyridylmethyl)pyrazolo[1,5-a]pyrimidin-7-amine (27 mg, 83 μ mol, 43% yield, 98% purity) as a light grey solid.

$^1\text{H NMR}$ (400MHz, DMSO- d_6) δ 8.68-8.69 (d, $J=4.8$ Hz, 1H), 7.95 (s, 1H), 7.71-7.75 (td, $J=7.6, 2.0$ Hz, 1H), 7.46 (br. s., 1H), 7.32-7.34 (d, $J=7.6$ Hz, 1H), 7.26 (m, 1H), 6.51-6.88 (t, $J=148.4$, 1H), 5.12-5.14 (d, $J=5.2$ Hz, 2H), 2.55 (s, 3H), 2.38 (s, 3 H).

LCMS (Method 10-80CD, ESI): RT =1.275 min / 2.0 min, M+H+ =320.1.



Tert-butyl (5,6-dimethyl-3-(trifluoromethyl)pyrazolo[1,5-a]pyrimidin-7-yl)(pyridin-2-ylmethyl)carbamate (2)

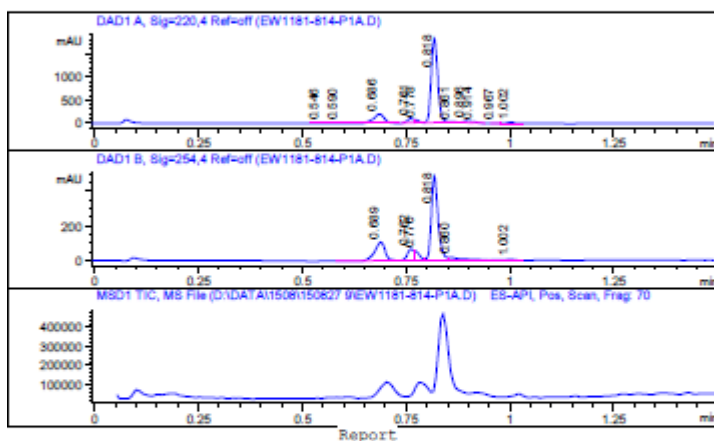


To a solution of tert-butyl N-[5,6-dimethyl-3-(4,4,5,5-tetramethyl-1,3,2-dioxaborolan-2-yl)pyrazolo[1,5-a]pyrimidin-7-yl]-N-(2-pyridylmethyl)carbamate (200 mg, 417 μ mol, 1 eq) in MeOH (3 mL) and DCM (3 mL),

H₂O (500 µL) was added sodium;trifluoromethanesulfinate (130 mg, 834 µmol, 130 µL, 2 eq), CuCl (83 mg, 834 µmol, 20 µL, 2 eq), NaHCO₃ (30%, 0.1 mL, 2 eq). Then to the mixture was added 2-hydroperoxy-2-methylpropane (752 mg, 8.3 mmol, 800 µL, 20 eq) dropwise. The mixture was stirred at 25 °C for 1 hour. TLC (Petroleum ether: EtOAc=1: 1) showed tert-butyl N-[5,6-dimethyl-3-(4,4,5,5-tetramethyl-1,3,2-dioxaborolan-2-yl)pyrazolo[1,5-a]pyrimidin-7-yl]-N-(2-pyridylmethyl)carbamate was consumed completely and a new major spot. The mixture was filtered and the filtrate was concentrated. The residue was purified by chromatography on silica gel (Petroleum ether: EtOAc=5: 1, 2: 1) to give tert-butyl N-[5,6-dimethyl-3-(trifluoromethyl)pyrazolo[1,5-a]pyrimidin-7-yl]-N-(2-pyridylmethyl)carbamate (100 mg, 237 µmol, 57% yield) as a light yellow oil.

LCMS REPORT

Compound ID : 1
 Sample ID : EW1181-814-P1A
 Injection Date : 27-Aug-2015 13:18:43
 Location : P1-F-08
 Injection volume : 5.000
 Acq Method : D:\DATA\1508\150827 9\5-95AB_R_2204254.M
 Data Filename : D:\DATA\1508\150827 9\EW1181-814-P1A.D
 Instrument : LCMS-B
 Column : Chromolith Flash RP-18e 25*2mm

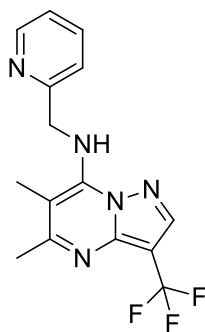


Signal 1 : DAD1 A, Sig=220,4 Ref=off

#	Meas. Ret.	Height	Width	Area	Area %
1	0.546	2.877	0.022	3.971	0.154
2	0.590	3.894	0.017	4.159	0.161
3	0.686	194.812	0.027	350.319	13.543
4	0.761	94.703	0.016	100.931	3.902
5	0.778	49.632	0.012	41.921	1.621
6	0.818	1806.402	0.017	1984.355	76.715
7	0.861	14.079	0.014	13.269	0.513
8	0.896	36.652	0.016	37.410	1.446
9	0.914	17.571	0.015	18.832	0.728
10	0.967	2.401	0.014	2.403	0.093
11	1.002	23.781	0.019	29.075	1.124

Signal 2 : DAD1 B, Sig=254,4 Ref=off

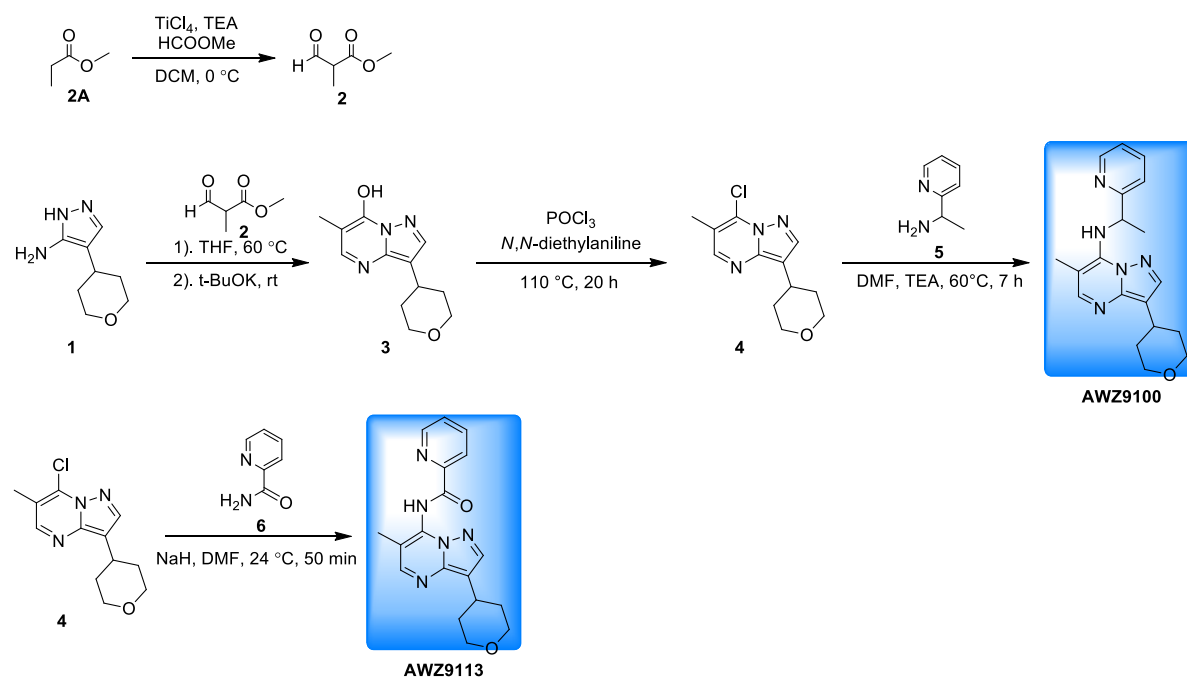
5,6-dimethyl-N-(pyridin-2-ylmethyl)-3-(trifluoromethyl)pyrazolo[1,5-a]pyrimidin-7-amine (AWZ9099)

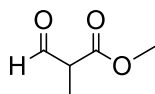


A solution of tert-butyl N-[5,6-dimethyl-3-(trifluoromethyl)pyrazolo[1,5-a]pyrimidin-7-yl]-N-(2-pyridylmethyl)carbamate (80 mg, 189.83 μmol , 1.00 eq) in HCl/EtOAc (4 M, 4 mL, 84 eq) was stirred at 28 $^{\circ}\text{C}$ for 3 hours. LCMS showed tert-butyl N-[5,6-dimethyl-3-(trifluoromethyl)pyrazolo[1,5-a]pyrimidin-7-yl]-N-(2-pyridylmethyl)carbamate was consumed completely and a major peak with desired mass. The mixture was concentrated. The residue was dissolved in MeOH and basified with three drops of Et_3N , then it was purified by prep-HPLC (Column: Phenomenex Synergi Max-RP 250*50mm*10 μm ; Condition: water(0.225%FA)-ACN) to get crude product which was purified by prep-TLC (Petroleum ether: Ethyl acetate=1: 1) to give 5,6-dimethyl-N-(2-pyridylmethyl)-3-(trifluoromethyl)pyrazolo[1,5-a]pyrimidin-7-amine (15 mg, 45 μmol , 24% yield, 97% purity) as a white solid.

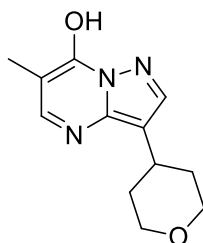
$^1\text{H NMR}$ (400MHz, DMSO- d_6) δ 8.68 (d, $J=4.64$ Hz, 1 H), 8.15 (s, 1 H), 7.74 (td, $J=7.65$, 1.76 Hz, 1 H), 7.59 (br. s., 1 H), 7.29 - 7.36 (m, 2 H), 5.18 (d, $J=5.14$ Hz, 2 H), 2.59 (s, 3 H), 2.41 (s, 3 H).

LCMS (Method 5-95CD, ESI): RT =0.635 min / 1.5 min, M+H $^+$ =322.1.



methyl 2-methyl-3-oxopropanoate (2)

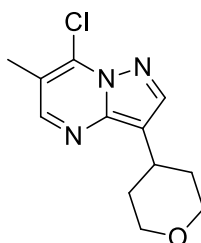
A solution of methyl propanoate (20.00 g, 227.01 mmol, 21.74 mL, 1.00 eq) and ethyl formate (25.23 g, 340.52 mmol, 27.42 mL, 1.50 eq) in DCM (200.00 mL) was degassed and purged with N₂ for 3 times. TiCl₄ (86.99 g, 454.02 mmol, 50.28 mL, 99% purity, 2.00 eq) and TEA (57.43 g, 567.53 mmol, 78.67 mL, 2.50 eq) was added dropwise to above mixture at 0 °C successively. The mixture was stirred at 0 °C for 1 h under N₂ atmosphere. Then the temperature was warmed to 20 °C and the mixture was stirred at 20 °C for another 1 h. TLC (Petroleum ether: Ethyl acetate=10: 1) showed a major spot at UV 254 nm (the starting materials methyl propanoate and ethyl formate couldn't be observed at 254 nm). The mixture was diluted with water (500 mL) and the resultant mixture was extracted with DCM (400mL*2). The organic layers were washed with brine (200mL*2), dried over Na₂SO₄ and concentrated. The crude product purified by column chromatography (SiO₂, Petroleum ether: Ethyl acetate=100: 1 to 10: 1) to give methyl 2-methyl-3-oxo-propanoate (18.00 g, crude) as a yellow oil.

6-methyl-3-(tetrahydro-2H-pyran-4-yl)pyrazolo[1,5-a]pyrimidin-7-ol (3).

A mixture of 4-tetrahydropyran-4-yl-1H-pyrazol-5-amine (300.00 mg, 1.79 mmol, 1.00 eq) and ethyl 2-methyl-3-oxo-propanoate (279.54 mg, 2.15 mmol, 1.20 eq) in THF (10.00 mL) was stirred at 60 °C for 2 h. Then the mixture was cooled to 28 °C, t-BuOK (241.03 mg, 2.15 mmol, 1.20 eq) was added into the reaction mixture. The mixture was stirred at 26 °C for 13 h. TLC (Dichloromethane: Methanol=10: 1) indicated 4-tetrahydropyran-4-yl-1H-pyrazol-5-amine was consumed completely and two new spots were formed. The reaction mixture was concentrated under reduced pressure to remove THF to give a residue. The residue was diluted with EtOAc (10 mL). The mixture was acidified with HCl/EtOAc to pH=3. The resulting solution was

concentrated under reduced pressure to give the crude product 6-methyl-3-tetrahydropyran-4-yl-pyrazolo[1,5-a]pyrimidin-7-ol (428.60 mg, crude) as a yellow solid which was used next step without purification.

7-chloro-6-methyl-3-(tetrahydro-2H-pyran-4-yl)pyrazolo[1,5-a]pyrimidine (4).



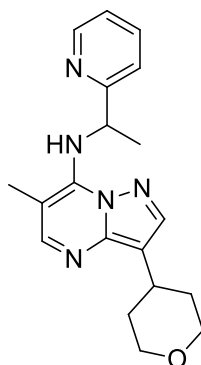
To a mixture of 6-methyl-3-tetrahydropyran-4-yl-pyrazolo[1,5-a] pyrimidin-7-ol (500.00 mg, 2.14 mmol, 1.00 eq) in POCl₃ (25.00 mL) was added N,N-DIETHYLANILINE (479.03 mg, 3.21 mmol, 515.09 μ L, 1.50 eq). The mixture was stirred at 110 °C for 20 h. TLC (Petroleum ether: Ethyl acetate=5: 1) indicated 6-methyl-3-tetrahydropyran-4-yl-pyrazolo[1,5-a]pyrimidin-7-ol was consumed completely, a new spot was formed. The reaction mixture was evaporated to dryness and azeotroped with toluene to remove residue POCl₃ to give a residue. The residue was purified by column chromatography (Petroleum ether: Ethyl acetate=20: 1 to 5: 1) to give 7-chloro-6-methyl-3-tetrahydropyran-4-yl-pyrazolo[1,5-a]pyrimidine (183.00 mg, 727.03 μ mol, 33.97% yield) as a yellow solid.

LCMS (Method 0-60 AB, ESI): RT =0.855 min / 1.5 min, M+H⁺ =252.1.

¹H NMR (400 MHz, CHLOROFORM-d) δ ppm 8.31 (s, 1H), 8.04 (s, 1H), 4.07 - 4.13 (m, 2H), 3.56 - 3.69 (m, 3H), 3.26 (tt, J=10.51, 5.30 Hz, 1H), 2.48 (s, 3H), 1.98 (dd, J=9.54, 3.64 Hz, 4H).

6-methyl-N-(1-(pyridin-2-yl)ethyl)-3-(tetrahydro-2H-pyran-4-yl)pyrazolo[1,5-a]pyrimidin-7-amine (AWZ9100)

Batch 1:

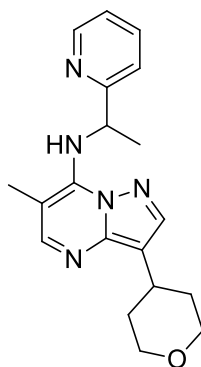


To a solution of 7-chloro-6-methyl-3-tetrahydropyran-4-yl-pyrazolo[1,5-a]pyrimidine (80.00 mg, 317.83 μmol , 1.00 *eq*) in DMF (3.00 mL) were added TEA (160.81 mg, 1.59 mmol, 220.28 μL , 5.00 *eq*) and 1-(2-pyridyl)ethanamine (38.83 mg, 317.83 μmol , 1.00 *eq*). The mixture was stirred at 65 °C for 20 h. TLC (Petroleum ether: Ethyl acetate=2: 1) showed 7-chloro-6-methyl-3-tetrahydropyran-4-yl-pyrazolo[1,5-a]pyrimidine was consumed completely and a new spot. The reaction mixture was diluted with water (10 mL) and extracted with EtOAc (10 mL*3). The combined organic layers were washed with brine (10 mL * 2), dried over anhydrous NaSO_4 , filtered and concentrated under reduced pressure to give a residue. The residue was purified by prep-HPLC (Condition: water(0.05% HCl)-ACN; Column: Phenomenex Synergi C18 150*30mm*4 μm), and alkalinized with strong-base anion exchange resin to give 6-methyl-N-[1-(2-pyridyl)ethyl]-3-tetrahydropyran-4-yl-pyrazolo[1,5-a]pyrimidin-7-amine (32.00 mg, 93.79 μmol , 29.51% yield, 98.9% purity) as a white solid.

LCMS (Method 5-95 AB, ESI): RT =0.629 min / 1.5 min, $\text{M}+\text{H}^+$ =338.1.

$^1\text{H NMR}$ (400 MHz, CHLOROFORM-d) ppm 8.65 (d, $J=4.77$ Hz, 1H), 7.99 (s, 1H), 7.91 (s, 1H), 7.67 (td, $J=7.65$, 1.76 Hz, 1H), 7.34 - 7.36 (d, $J=8.00$ Hz, 1H), 7.29 - 7.28 (t, $J=4.00$ Hz, 1H), 7.20 - 7.25 (m, 1H), 5.48 - 5.62 (m, 1H), 4.08 (dd, $J=10.92$, 3.14 Hz, 2H), 3.62 (td, $J=11.61$, 2.26 Hz, 2H), 3.21 (tt, $J=11.62$, 4.13 Hz, 1H), 2.35 (s, 3H), 1.88 - 2.02 (m, 4H), 1.68 - 1.69 (d, $J=6.65$ Hz, 3H).

Batch 2:

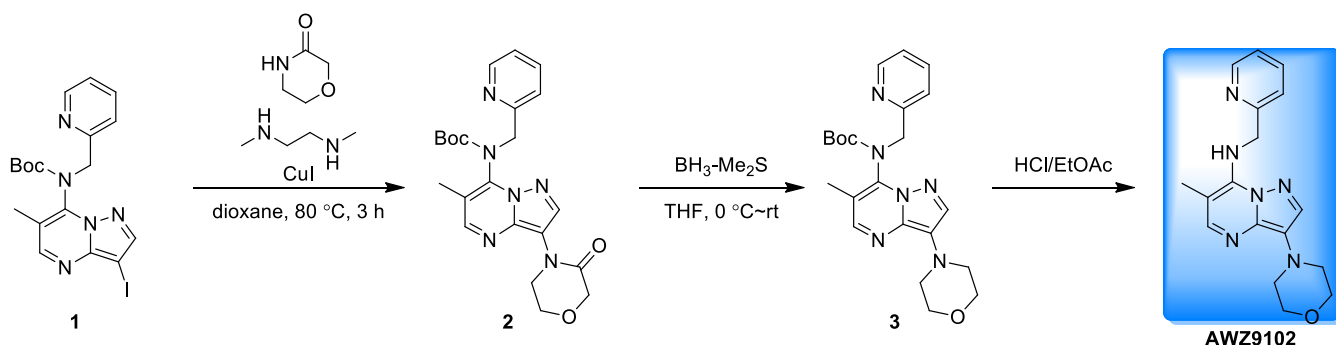


To a mixture of 7-chloro-6-methyl-3-tetrahydropyran-4-yl-pyrazolo[1,5-a]pyrimidine (200.00 mg, 794.57 μmol , 1.00 *eq*) in DMF (3.00 mL) was added 1-(2-pyridyl)ethanamine (145.61 mg, 1.19 mmol, 1.50 *eq*) and TEA (160.80 mg, 1.59 mmol, 220.28 μL , 2.00 *eq*). The mixture was stirred at 65 °C for 12 h. TLC (Ethyl acetate: Petroleum ether= 2: 1) showed the 7-chloro-6-methyl-3-tetrahydropyran-4-yl-pyrazolo[1,5-a]pyrimidine was consumed completely and three new spots were formed. The mixture was diluted with water (40 mL) and the resultant mixture was extracted with ethyl acetate (100 mL*3). The combined organic layers were washed with saturated brine (40 mL), dried with anhydrous Na_2SO_4 , filtered and concentrated in vacuo. The crude product was purified by chromatography (Petroleum ether: Ethyl acetate= 5: 1 to 1: 2) to give 6-methyl-N-[1-

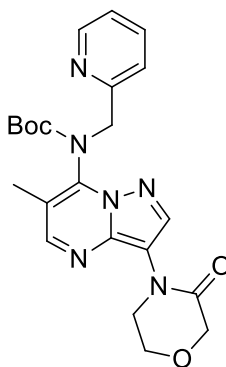
(2-pyridyl)ethyl]-3-tetrahydropyran-4-yl-pyrazolo[1,5-a]pyrimidin-7-amine (71.20 mg, 206.79 μmol , 26% yield, 98% purity) as a light yellow solid.

$^1\text{H NMR}$ (400 MHz, DMSO-d_6) δ ppm 8.59-8.60 (d, $J=4.0$ Hz, 1H), 8.00 (s, 1H), 7.97 (s, 1H), 7.79-7.83 (td, $J=8.0$ Hz, 1H), 7.65-7.67 (d, $J=8.0$ Hz, 1H), 7.48-7.50 (d, $J=8.0$ Hz, 1H), 7.31-7.34 (d, $J=8.0$ Hz, $J=4.0$ Hz, 1H), 5.62-5.66 (m, 1H), 3.90-3.93 (m, 2H), 3.42-3.48 (td, $J=12.0$ Hz, $J=4.0$ Hz, 2H), 3.01-3.06 (m, 1H), 2.36 (s, 3H), 1.17-1.83 (m, 4H), 1.54-1.55 (d, $J=4.0$ Hz, 3H).

LCMS (Method 5-95 AB, ESI): RT = 0.616 min / 1.5 min, $\text{M}+\text{H}^+$ = 338.2.



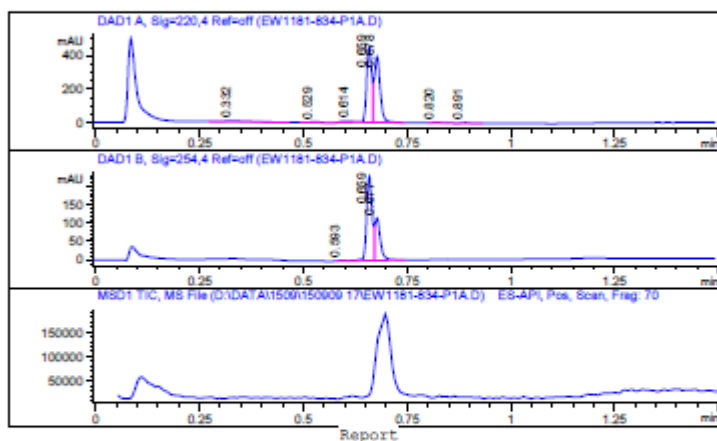
Tert-butyl (6-methyl-3-(3-oxomorpholino)pyrazolo[1,5-a]pyrimidin-7-yl)(pyridin-2-ylmethyl)carbamate (2)



To a solution of tert-butyl N-(3-iodo-6-methyl-pyrazolo[1,5-a]pyrimidin-7-yl)-N-(2-pyridylmethyl)carbamate (250 mg, 537 μmol , 1 *eq*) and morpholin-3-one (81 mg, 806 μmol , 1.5 *eq*) in dioxane (15 mL) was added N,N'-dimethylethane-1,2-diamine (189 mg, 2.1 mmol, 231 μL , 4 *eq*), CuI (205 mg, 1.1 mmol, 2 *eq*). The mixture was stirred at 80 $^{\circ}\text{C}$ for 3 hours under N_2 . TLC (EtOAc) showed most of tert-butyl N-(3-iodo-6-methyl-pyrazolo[1,5-a]pyrimidin-7-yl)-N-(2-pyridylmethyl)carbamate was consumed and a new major spot. The mixture was filtered and concentrated. The residue was purified by chromatography on silica gel (Petroleum ether: EtOAc=1: 1, DCM: MeOH=15: 1) to give tert-butyl N-[6-methyl-3-(3-oxomorpholin-4-yl)pyrazolo[1,5-a]pyrimidin-7-yl]-N-(2-pyridylmethyl)carbamate (150 mg, 342 μmol , 64% yield) as a yellow oil.

LCMS REPORT

Compound ID : 1
 Sample ID : EW1181-834-P1A
 Injection Date : 9-Sep-2015 16:32:37
 Location : F2-E-01
 Injection volume : 4.000
 Acq Method : D:\DATA\1509\150909 17\5-95AB_R_2204254.M
 Data Filename : D:\DATA\1509\150909 17\EW1181-834-P1A.D
 Instrument : LCMS-B
 Column : Chromolith Flash RP-18e 25*2mm



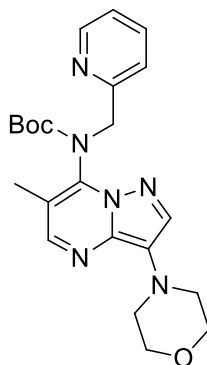
 Signal 1 : DAD1 A, Sig=220,4 Ref=off

#	Meas. Ret.	Height	Width	Area	Area %
1	0.332	7.543	0.054	31.685	3.784
2	0.529	4.018	0.027	8.015	0.957
3	0.614	4.578	0.031	10.834	1.294
4	0.659	449.378	0.013	382.365	45.661
5	0.678	394.522	0.015	389.030	46.457
6	0.820	4.754	0.026	8.762	1.046
7	0.891	4.311	0.023	6.712	0.802

 Signal 2 : DAD1 B, Sig=254,4 Ref=off

#	Meas. Ret.	Height	Width	Area	Area %
1	0.593	1.950	0.030	4.099	1.262
2	0.659	230.244	0.014	208.520	64.197
3	0.677	115.971	0.014	112.195	34.541

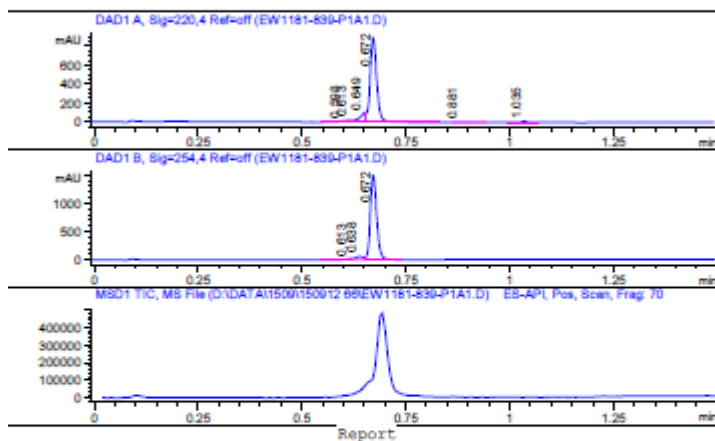
Tert-butyl (6-methyl-3-morpholinopyrazolo[1,5-a]pyrimidin-7-yl)(pyridin-2-ylmethyl)carbamate (3)



To a solution of tert-butyl N-[6-methyl-3-(3-oxomorpholin-4-yl)pyrazolo[1,5-a]pyrimidin-7-yl]-N-(2-pyridylmethyl)carbamate (150 mg, 342 μmol , 1 eq) in THF (5 mL) was added $\text{BH}_3\text{-Me}_2\text{S}$ (10 M, 342 μL , 10 eq) at 0 °C. The mixture was stirred at 25 °C for 12 hours under N_2 . TLC (EtOAc) showed tert-butyl N-[6-methyl-3-(3-oxomorpholin-4-yl)pyrazolo[1,5-a]pyrimidin-7-yl]-N-(2-pyridylmethyl)carbamate was consumed completely and a new major spot. To the mixture was added MeOH (5 mL) slowly at 0 °C and glycerunum (3 mL). The mixture was stirred at 25 °C for 12 h. LCMS showed that a major peak with desired mass. Then to the mixture was added water (40 mL) and extracted with EtOAc (30 mL*2). The organic layers were combined and washed with brine (30*3 mL), dried over Na_2SO_4 and concentrated. The residue was purified by chromatography on silica gel (Petroleum ether: EtOAc=1: 1, DCM: MeOH=25: 1) to give tert-butyl N-(6-methyl-3-morpholino-pyrazolo[1,5-a]pyrimidin-7-yl)-N-(2-pyridylmethyl)carbamate (100 mg, 235 μmol , 69% yield) as brown oil.

LCMS REPORT

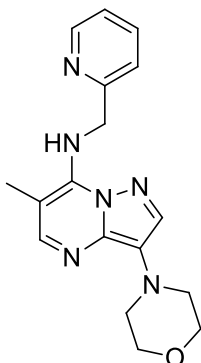
Compound ID : 1
 Sample ID : EW1181-839-P1A1
 Injection Date : 13-Sep-2015 09:27:19
 Location : F1-E-08
 Injection volume : 3.000
 Acq Method : D:\DATA\1509\150912 66\5-95AB_R_2204254.M
 Data Filename : D:\DATA\1509\150912 66\EW1181-839-P1A1.D
 Instrument : LCMS-B
 Column : Chromolith Flash RP-18e 25*2mm



Signal 1 : DAD1 A, Sig=220,4 Ref=off					
#	Meas. Ret.	Height	Width	Area	Area %
1	0.598	9.982	0.017	12.305	1.084
2	0.613	15.531	0.016	17.668	1.556
3	0.649	92.636	0.016	105.903	9.329
4	0.672	896.855	0.017	979.712	86.307
5	0.881	2.653	0.021	3.936	0.347
6	1.035	11.722	0.020	15.624	1.376

Signal 2 : DAD1 B, Sig=254,4 Ref=off					
#	Meas. Ret.	Height	Width	Area	Area %
1	0.613	19.026	0.020	29.305	1.700
2	0.638	57.334	0.020	79.473	4.610
3	0.672	1502.571	0.017	1615.094	93.690

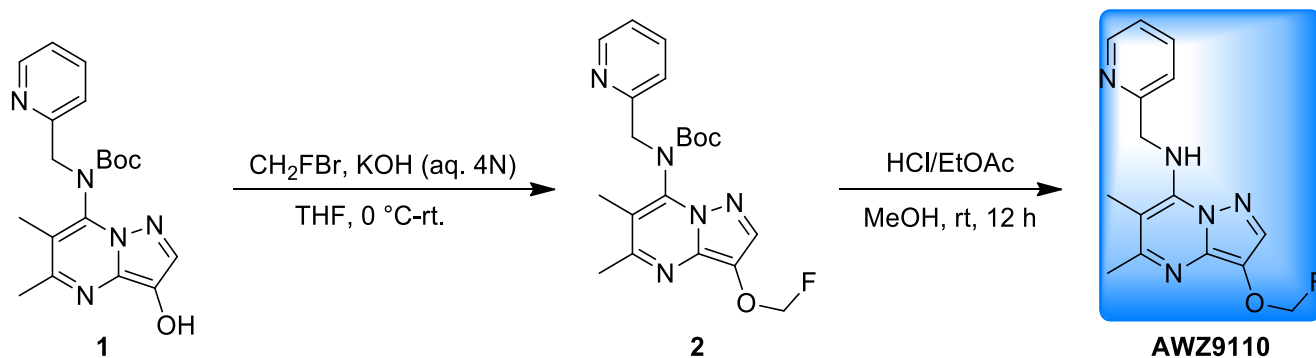
6-methyl-3-morpholino-N-(pyridin-2-ylmethyl)pyrazolo[1,5-a]pyrimidin-7-amine (AWZ9102)

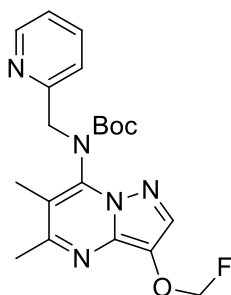


A solution of tert-butyl N-(6-methyl-3-morpholino-pyrazolo[1,5-a]pyrimidin-7-yl)-N-(2-pyridylmethyl)carbamate (120 mg, 282 μmol , 1 *eq*) in HCl/EtOAc (4 M, 10 mL, 141 *eq*) was stirred at 25 °C for 12 hours. LCMS showed starting material was consumed completely and a major peak of desired product. The mixture was concentrated directly and basified by TEA. The residue was purified by prep-HPLC (Column: Boston Green ODS 150*30 5 μ ; Condition: water (0.225%FA)-ACN). The FA salt of product was basified by strong base anion exchange resin to give 6-methyl-3-morpholino-N-(2-pyridylmethyl)pyrazolo[1,5-a]pyrimidin-7-amine (58 mg, 176 μmol , 62% yield, 98% purity) as a light yellow solid.

$^1\text{H NMR}$ (400MHz, $\text{CDCl}_3\text{-d}$) δ 8.66 (d, $J=4.27$ Hz, 1 H), 7.96 (s, 1 H), 7.75 (s, 1 H), 7.70 (td, $J=7.65, 1.76$ Hz, 1 H), 7.56 (t, $J=5.58$ Hz, 1 H), 7.30 (d, $J=7.91$ Hz, 1 H), 7.22 - 7.27 (m, 1 H), 5.11 (d, $J=5.90$ Hz, 2 H), 3.90 - 3.97 (m, 4 H), 3.22 - 3.29 (m, 4 H), 2.44 (s, 3 H).

LCMS (Method 10-80CD, ESI): RT =1.019 min / 2.0 min, M+H+ =325.1.

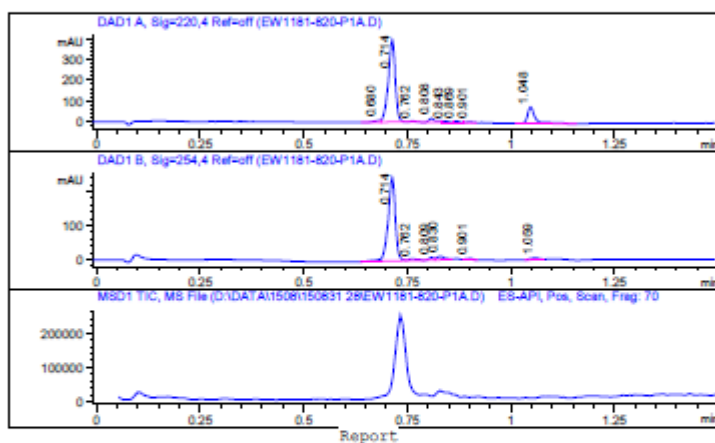


Tert-butyl (3-(fluoromethoxy)-5,6-dimethylpyrazolo[1,5-a]pyrimidin-7-yl)(pyridin-2-ylmethyl)carbamate (2)

To a solution of tert-butyl N-(3-hydroxy-5,6-dimethyl-pyrazolo[1,5-a]pyrimidin-7-yl)-N-(2-pyridylmethyl)carbamate (150 mg, 406 μmol , 1 *eq*) in THF (8 mL) was added KOH (3.5 M, 464 μL , 4 *eq*), then bromo(fluoro)methane (458 mg, 4.1 mmol, 10 *eq*) at 0 $^{\circ}\text{C}$ was added in one portion. The mixture was stirred at 26 $^{\circ}\text{C}$ for 1 hour under N_2 . TLC (Petroleum ether: EtOAc=1: 1) showed tert-butyl N-(3-hydroxy-5,6-dimethyl-pyrazolo[1,5-a]pyrimidin-7-yl)-N-(2-pyridylmethyl)carbamate was consumed completely and a major new spot. The reaction mixture was concentrated. The residue was purified by chromatography on silica gel (Petroleum ether: EtOAc=2: 1, 1: 2) to give tert-butyl N-[3-(fluoromethoxy)-5,6-dimethyl-pyrazolo[1,5-a]pyrimidin-7-yl]-N-(2-pyridylmethyl)carbamate (100 mg, 249 μmol , 61% yield) as a light yellow oil.

LCMS REPORT

Compound ID : 1
 Sample ID : EW1181-820-P1A
 Injection Date : 31-Aug-2015 16:48:41
 Location : P2-D-04
 Injection volume : 5.000
 Acq Method : D:\DATA\1508\150831 28\5-95AB_R_2204254.M
 Data Filename : D:\DATA\1508\150831 28\EW1181-820-P1A.D
 Instrument : LCMS-B
 Column : Chromolith Flash RP-18e 25*2mm



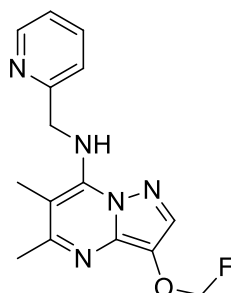
Signal 1 : DAD1 A, Sig=220,4 Ref=off

#	Meas. Ret.	Height	Width	Area	Area %
1	0.680	9.171	0.016	11.555	1.849
2	0.714	397.010	0.018	464.735	74.377
3	0.762	4.049	0.017	4.744	0.759
4	0.808	18.646	0.017	21.874	3.501
5	0.843	5.466	0.016	6.097	0.976
6	0.869	5.914	0.015	6.183	0.989
7	0.901	4.623	0.015	4.679	0.749
8	1.048	79.237	0.019	104.969	16.799

Signal 2 : DAD1 B, Sig=254,4 Ref=off

#	Meas. Ret.	Height	Width	Area	Area %
1	0.714	243.601	0.018	295.715	89.324
2	0.762	4.134	0.021	6.457	1.951
3	0.809	6.876	0.013	5.711	1.725

3-(fluoromethoxy)-5,6-dimethyl-N-(pyridin-2-ylmethyl)pyrazolo[1,5-a]pyrimidin-7-amine (AWZ9110)

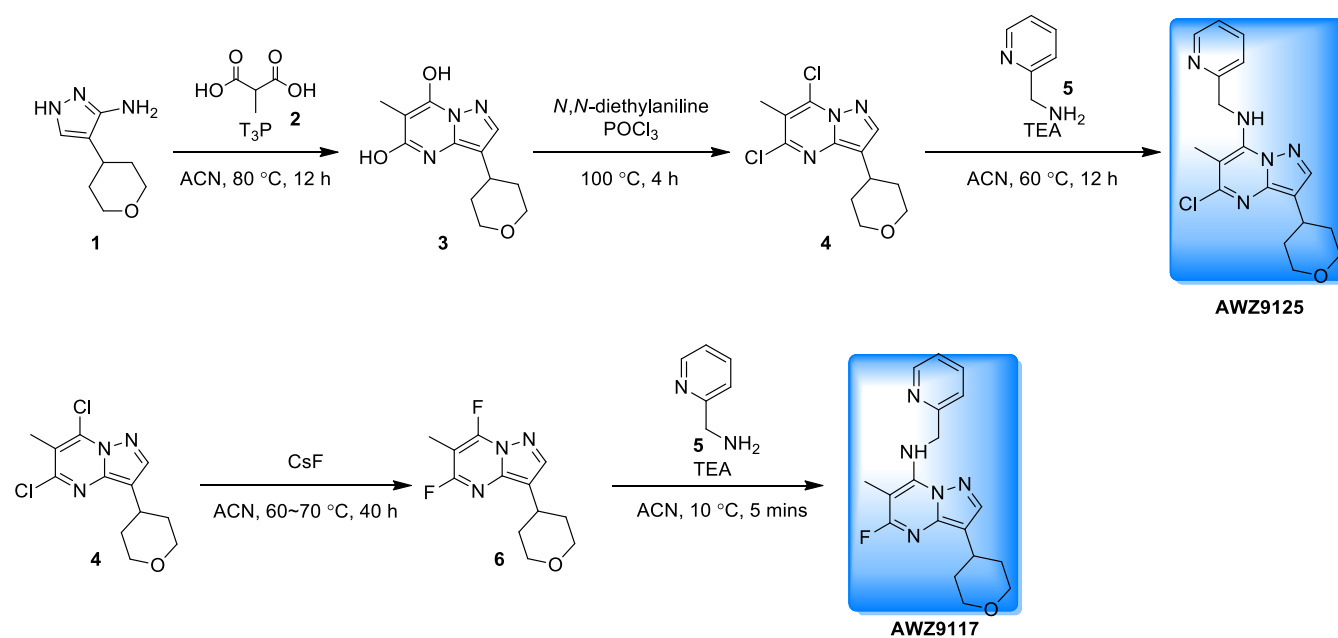


To a solution of tert-butyl N-[3-(fluoromethoxy)-5,6-dimethyl-pyrazolo[1,5-a]pyrimidin-7-yl]-N-(2-pyridylmethyl)carbamate (100 mg, 249 μ mol, 1 eq) in MeOH (5 mL) was added HCl/EtOAc (4 M, 5 mL, 80 eq).

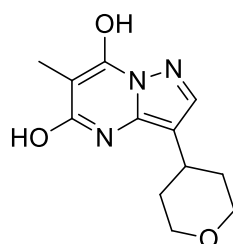
The mixture was stirred at 26 °C for 12 hours. LCMS showed tert-butyl N-[3-(fluoromethoxy)-5,6-dimethyl-pyrazolo[1,5-a]pyrimidin-7-yl]-N-(2-pyridylmethyl)carbamate was consumed completely and two major peaks of desired product and by-product 3-(methoxymethoxy)-5,6-dimethyl-N-(2-pyridylmethyl)pyrazolo[1,5-a]pyrimidin-7-amine. The mixture was concentrated directly. The residue was purified by prep-HPLC (Column: Phenomenex Synergi C18 150*30mm*4um; Condition: water (0.05%HCl)-ACN) followed by basification by strong basic anion exchange resin to give 3-(fluoromethoxy)-5,6-dimethyl-N-(2-pyridylmethyl)pyrazolo[1,5-a]pyrimidin-7-amine (14 mg, 43 μmol, 17% yield, 93% purity) as a light yellow solid.

¹H NMR (400MHz, CDCl₃-d) δ 8.66 (d, *J*=4.77 Hz, 1 H), 7.94 (d, *J*=1.76 Hz, 1 H), 7.71 (td, *J*=7.65, 1.76 Hz, 1 H), 7.38 (br. s., 1 H), 7.32 (d, *J*=7.78 Hz, 1 H), 7.22-7.27 (m, 1 H), 5.62-5.80 (m, 2 H), 5.10 (d, *J*=5.65 Hz, 2 H), 2.53 (s, 3 H), 2.36 (s, 3 H).

LCMS (Method 10-80CD, ESI): RT =1.378 min / 2.0 min, M+H⁺ =302.0.



6-methyl-3-(tetrahydro-2H-pyran-4-yl)pyrazolo[1,5-a]pyrimidine-5,7-diol (3)

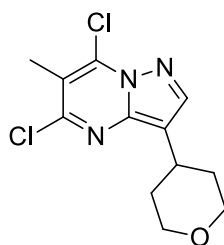


To a solution of 4-tetrahydropyran-4-yl-1H-pyrazol-3-amine (1 g, 6 mmol, 1 eq) and 2-methylpropanedioic acid (706 mg, 6 mmol, 1 eq) in CH₃CN (10.00 mL) was added T₃P (7.6 g, 24 mmol, 7 mL, 4 eq). The mixture was stirred at 80 °C for 12 hrs. TLC (EtOAc) showed starting material was consumed completely. The mixture was filtered and the filter cake was concentrated. The residue was purified by trituration from H₂O/EtOH (1/1, 20 mL) to provide 6-methyl-3-tetrahydropyran-4-yl-pyrazolo[1,5-a]pyrimidine-5,7-diol (1 g, 4 mmol, 67% yield) as a grey solid.

¹H NMR (400MHz, DMSO-d₆) δ 11.41 (br. s., 1H), 7.79 (br. s., 1H), 3.91 (d, *J*=10.3 Hz, 4H), 2.88-2.96 (m, 1H), 1.86 (s, 3H), 1.71-1.76 (m, 2H), 1.60-1.62 (m, 2 H).

LCMS: M+H⁺ =250.1.

5,7-dichloro-6-methyl-3-(tetrahydro-2H-pyran-4-yl)pyrazolo[1,5-a]pyrimidine (4)

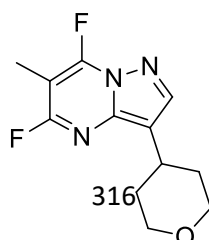


To a solution of 6-methyl-3-tetrahydropyran-4-yl-pyrazolo[1,5-a]pyrimidine-5,7-diol (1 g, 4 mmol, 1 eq) in POCl₃ (33 g, 215 mmol, 20 mL, 54 eq) was added N,N-diethylaniline (1.2 g, 8 mmol, 1.3 mL, 2 eq). The mixture was stirred at 100 °C for 4 hours under N₂. TLC (Petroleum ether: EtOAc=3: 1) indicated that a new major spot. Desired product was detected by LCMS. The mixture was concentrated directly. The residue was purified by chromatography on silica gel (Petroleum ether: EtOAc=5: 1, 3: 1, 2: 1) to afford 5,7-dichloro-6-methyl-3-tetrahydropyran-4-yl-pyrazolo[1,5-a]pyrimidine (1 g, crude) as a grey solid.

¹H NMR (400MHz, CDCl₃-d) δ 8.03 (s, 1H), 4.07 (dd, *J*=10.4, 2.4 Hz, 2H), 3.59 (td, *J*=11.2, 3.3 Hz, 2H), 3.14-3.29 (m, 1H), 2.54 (s, 3H), 1.87-2.00 (m, 4 H).

LCMS: M+H⁺ =286.0.

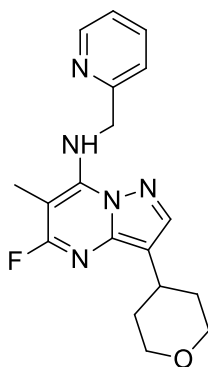
5,7-difluoro-6-methyl-3-(tetrahydro-2H-pyran-4-yl)pyrazolo[1,5-a]pyrimidine (6)



To a solution of 5,7-dichloro-6-methyl-3-tetrahydropyran-4-yl-pyrazolo[1,5-a]pyrimidine (400 mg, 1.4 mmol, 1 eq) in ACN (20 mL) was added CsF (1.1 g, 7 mmol, 5 eq). The mixture was stirred at 60 °C for 16 hrs in a sealed tube. TLC (Petroleum ether: EtOAc=3: 1) several new spots. LCMS showed 31% of by-product 5-chloro-6-methyl-3-tetrahydropyran-4-yl-pyrazolo[1,5-a]pyrimidin-7-ol, 40% of by-product 5-chloro-7-fluoro-6-methyl-3-tetrahydropyran-4-yl-pyrazolo[1,5-a]pyrimidine and 16% of desired product. Then the mixture was stirred at 70 °C for 24 hrs. LCMS showed 31% of by-product 5-chloro-6-methyl-3-tetrahydropyran-4-yl-pyrazolo[1,5-a]pyrimidin-7-ol, 16% of by-product 5-chloro-7-fluoro-6-methyl-3-tetrahydropyran-4-yl-pyrazolo[1,5-a]pyrimidine and 40% of desired product. The mixture was filtered and the filtrate was concentrated. The residue was purified by chromatography on silica gel (Petroleum ether: EtOAc=5: 1, 3: 1) to give 5,7-difluoro-6-methyl-3-tetrahydropyran-4-yl-pyrazolo[1,5-a]pyrimidine (70 mg, crude) as a light yellow oil which was used in the next step without further purification..

LCMS: $M+H^+ = 254.2$.

5-fluoro-6-methyl-N-(pyridin-2-ylmethyl)-3-(tetrahydro-2H-pyran-4-yl)pyrazolo[1,5-a]pyrimidin-7-amine (AWZ9117)



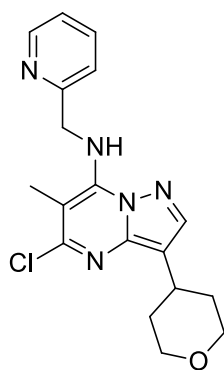
To a solution of 5,7-difluoro-6-methyl-3-tetrahydropyran-4-yl-pyrazolo[1,5-a]pyrimidine (50 mg, 197 μ mol, 1 eq) and 2-pyridylmethanamine (21 mg, 197 μ mol, 20 μ L, 1 eq) in ACN (3 mL) was added TEA (40 mg, 395 μ mol, 55 μ L, 2 eq). The mixture was stirred at 10 °C for 5 mins. Light yellow solid was formed. LCMS showed starting material was consumed completely and a major peak with desired mass. The mixture was filtered. The filter cake was dissolved in ACN. One drop of HCl (1N) was added to the mixture. The solution was purified by prep-HPLC (column: Agela ASB 150*25mm*5 μ m; mobile phase: [water (0.225%TFA)-ACN];B%: 15%-

45%, 11 min). The fraction was basified with NaHCO_3 (5%, 10 mL). The basified mixture was extracted with DCM (20 mL*2). The organic layers were concentrated. The residue was purified by chromatography on silica gel (DCM: MeOH=20: 1) to afford 5-fluoro-6-methyl-N-(2-pyridylmethyl)-3-tetrahydropyran-4-yl-pyrazolo[1,5-a]pyrimidin-7-amine (16 mg, 46 μmol , 23% yield, 99.3% purity) as a light yellow solid.

$^1\text{H NMR}$ (400 MHz, CDCl_3 -d) δ 8.68 (d, $J=4.8$ Hz, 1H), 7.87 (s, 1H), 7.81 (br. s., 1H), 7.73 (td, $J=7.7, 1.7$ Hz, 1H), 7.27-7.34 (m, 2H), 5.15 (d, $J=5.5$ Hz, 2H), 4.06 (dd, $J=11.6, 2.8$ Hz, 2H), 3.58 (td, $J=11.6, 2.2$ Hz, 2H), 3.11 (tt, $J=11.6, 4.2$ Hz, 1H), 2.36 (s, 3H), 1.80-1.97 (m, 4 H).

LCMS (Method: 5-95AB, ESI): RT = 0.692 min / 1.5 min, $\text{M}+\text{H}^+ = 342.1$.

5-chloro-6-methyl-N-(pyridin-2-ylmethyl)-3-(tetrahydro-2H-pyran-4-yl)pyrazolo[1,5-a]pyrimidin-7-amine (AWZ9125)



To a solution of 5,7-dichloro-6-methyl-3-tetrahydropyran-4-yl-pyrazolo[1,5-a]pyrimidine (50 mg, 174 μmol , 1 eq) and 2-pyridylmethanamine (23 mg, 230 μmol , 21 μL , 1.2 eq) in ACN (4 mL) was added TEA (35 mg, 349 μmol , 48 μL , 2 eq). The mixture was stirred at 60 °C for 12 hours. TLC (Petroleum ether: EtOAc=1: 2) showed all of starting material was consumed and a major spot. To the mixture was added H_2O (1 mL). Then the suspension was stirred at 20 °C for 2 h and filtered. The filter cake was dried in vacuo to afford 5-chloro-6-methyl-N-(2-pyridylmethyl)-3-tetrahydropyran-4-yl-pyrazolo[1,5-a]pyrimidin-7-amine (36 mg, 96 μmol , 55% yield, 94.8% purity) as a white solid.

$^1\text{H NMR}$ (400 MHz, CDCl_3 -d) δ 8.67 (d, $J=4.6$ Hz, 1H), 7.89 (s, 1H), 7.65-7.79 (m, 2H), 7.26-7.34 (m, 2H), 5.16 (d, $J=5.3$ Hz, 2H), 4.05 (dd, $J=11.2, 3.1$ Hz, 2H), 3.54-3.64 (m, 2H), 3.19 (m, 4.0 Hz, 1H), 2.50 (s, 3H), 1.79-1.98 (m, 4 H).

LCMS (Method: 5-95CD, ESI): RT = 0.954 min / 1.5 min, $\text{M}+\text{H}^+ = 358.1$.